FTD-HC-23-18-70

AD719774

FOREIGN TECHNOLOGY DIVISION

DYNAMICS OF LIQUID ROCKET ENGINES

by

V. A. Makhin, V. F. Prisnyakov,
N. P. Belik

FTD - HC-23-18-70

EDITED TRANSLATION

DYNAMICS OF LIQUID ROCKET ENGINES

By: V. A. Makhin, V. F. Prisnyakov, N. P. Belik

English pages: 465

Source: Dinamika Zhidkostnykh Raketnykh Dvigateley 1969, 1-384

Translated under: F33657-70-D-0607

PREPARED BY:

TRANSLATION DIVISION
FOREIGN TECHNOLOGY DIVISION
WP-AFB, OHIO.

TABLE OF CONTENTS

ABSTRACT

UDC 629.7.036.5.015.3.03

This book discusses questions of the theory and calculation of certain dynamic processes which take place with variable parameters in liquid rocket engines and their major components. Primary attention is devoted to the description of the dynamic processes and the study of methods for the engineering calculation of these processes.

The differential equations of motion of the working medium and of the moving parts of the individual components are used to describe the dynamic processes of liquid rocket engines (LRE). Theoretical LRE arrangements and their static characteristics are examined. Assuming the LRE to be potentially a dynamic system, the authors derive the equations of the dynamics of the powerplant primary components.

The dynamics of the LRE automation elements are analyzed and the questions of automatic regulation, trimming, and retrimming of engines using the results of firing tests are studied. The oscillatory processes in the tubing lines are examined in detail; the influence of oscillations in the pneumatic and hydraulic lines on the stability of the LRE working process is determined.

An analysis is given of the LRE startup processes and the effect of the thrust tailoff impulse (TTI) on the scatter of ballistic rockets. Original material used in the analysis of several engine elements and their control systems is presented.

The book will be of interest for a wide range of specialists in rocket and aircraft engineering. It may also be useful to teachers and students in advanced technical school courses.

There are 5 Tables, 138 Illustrations, and 195 References.

FOREWORD

The last 10 - 15 years have seen tremendous advances in rocket engineering, particularly in the creation of high-power liquid rocket engines (LRE). These engines have reached such a high degree of structural efficiency and operational reliability in their development that it has been possible not only to provide unlimited rocket flight ranges, but also to accomplish the launch of piloted flight vehicles into outer space.

The hundreds of successfully launched artificial earth satellites, launches of space rockets, flights of cosmonauts aboard space flight vehicles have initiated a new era — the era of direct emergence of man into space.

This has excited great interest in rocket engines and has led to the appearance of several books by Soviet and foreign authors devoted to rocket engines, in particular questions of the theory and computation of the working processes in these engines.

However, at the present stage of rocket technology development we can no longer restrict ourselves to the study of only the steady operating regimes and static characteristics of the engine. The study of the dynamics of the engine working processes is becoming increasingly important and necessary in practice. Knowledge of engine dynamic characteristics is of paramount importance in the preliminary design process and particularly in the engine experimental development stage.

The accumulated scientific and practical experience in the field of LRE dynamics has obviously not been presented adequately in the technical literature, the published data are scattered in individual articles and monographs devoted to particular problems. For example, the well known monograph by Crocco and Cheng [78] covers only the questions of instability, while the recently published book of Moshkin

[102] does not cover the entire range of questions relating to LRE dynamics.

An impressive study by Shevyakov has recently appeared ("Automatic Control of Aircraft and Rocket Powerplants") [150]; however this book devotes only a single chapter to certain questions of LRE dynamics.

As far as we know the present book is the first attempt to write a monograph covering the theory and calculation of the basic dynamic processes in an engine and its individual components, which are processes which proceed with time-variable parameters. Such processes include LRE startup, shutdown, wave processes in the fuel lines, transient regulation processes, unstable (pulsative) engine operating regimes, and so on.

The liquid rocket powerplant is a dynamic system. To describe the dynamic processes in a LRE we use the differential equations of motion of the working medium (liquid fuel or its combustion products) and the moving parts of the individual components (turbopump assembly rotor, valve disks, and so on).

In presenting the fundamentals of LRE dynamics it is more profitable to first examine the pneumo-hydraulic arrangements and the engine static characteristics, and also to derive the equations of the dynamic components of the LRE. Then we examine in sequence the questions which constitute the principal content of the book: automatic regulation, wave processes and hydraulic hammer in pneumo-hydraulic systems, damping, stability of the working process, LRE shutdown, questions of test stand dynamics, and certain other problems.

Among these questions are some which should be considered problems or questions which have received insufficient study. For example, at the present time many questions of the stability of the LRE process have not been entirely solved or have not been studied at all. In the analysis of such questions the authors do not pretend to present a complete or exhaustive discussion of these questions; their objective is to introduce the reader to the problem and describe

briefly its present status.

The rapid development of rocketry makes it impossible to cover all the latest advances in the field in question. However the material covered in the book is sufficient for the reader to obtain the fundamental information on the dynamic processes in the LRE.

Professor Makhin wrote Sections 1 - 3 of Chapter 2, Chapters 6 and 9, Sections 1 and 2 (subsection 3) of Chapter 10; Assistant Professor Prisnyakov, Candidate of Tech. Sci., wrote Sections 4 - 7 of Chapter 2, Chapters 3, 4, 5, and 10; Assistant Professor Belik, Candidate of Tech. Sci., prepared Chapters 7 and 8. All the authors cooperated in the writing of Chapter 1.

The authors wish to thank A.A. Shevyakov for his kind and helpful advice given in the course of the manuscript review.

CHAPTER I

SCHEMATIC DIAGRAMS OF LRE

The schematic diagram of the LRE is a simplified graphical representation of the interaction of its major components and assemblies. This diagram gives a graphical picture of the sequence of the action and interaction of these components and assemblies in the process of the performance of the entire cycle of all the engine operating regimes, beginning from startup and terminating with shutdown. This diagram also defines the path which the components of the basic working medium follow from the tanks to the combustion chamber, and also indicates the lines for the auxiliary working media used to pressurize the fuel tanks, supply the turbines and the engine pyropneumatics.

Thus the present-day liquid rocket powerplant is a complex system of inter-related assemblies and systems which make it possible to obtain certain basic parameters in the process of its functioning on the flight vehicle. Therefore the choice of the optimal arrangement for a new LRE design is not a simple task. Here we see the influence of many different factors, beginning with the particular mission of the engine, its power characteristics, and terminating with operational reliability, manufacturing cost, and so on.

However, concerning several fundamentally different arrangements we can express quite definite ideas on the advisability of their use in a particular case. For example, with regard to feed systems the LRE are divided into engines with pressure-fed and turbopump-fed propellant systems. We know that the former are sometimes preferable for short-range rockets (anti-aircraft guided missiles), for which the structural weight increase resulting from the thick-walled tanks is offset by the relative simplicity of the powerplant pneumatic and hydraulic systems. But in most cases the pump-fed LRE is more efficient. In the following we examine the most typical LRE arrangements, both those in use and future designs, which have been described in the technical literature.

§ 1. Pressure-Fed LRE

In the pressure-fed propellant supply system, the pressure in the rocket tanks is higher than that in the combustion chamber. To ensure tank strength they are thick-walled and therefore have considerable weight.

Let us examine some LRE arrangements with pressure feed.

A schematic diagram of a monopropellant LRE with gaseous pressure accumulator is shown in Figure 1.1. The monopropellant is forced from the tank 10 into the combustion chamber 7 by the compressed gas in the bottle 1 (gas pressure accumulator).

The engine thrust is regulated by the combustion chamber pressure. When the chamber pressure deviates from the set value, an electric signal from the pressure sensor 6 travels to the amplifier 5 and the servomotor 4, which readjusts the gas pressure reducer to a new regime. This is accompanied by a change of the pressure in the propellant tank and therefore a change of the pressure in the combustion chamber.

Engine startup and shutdown are accomplished by actuation of the valves 2 and 8. The membrane 11 is used to separate the tank chamber and the expulsion system.

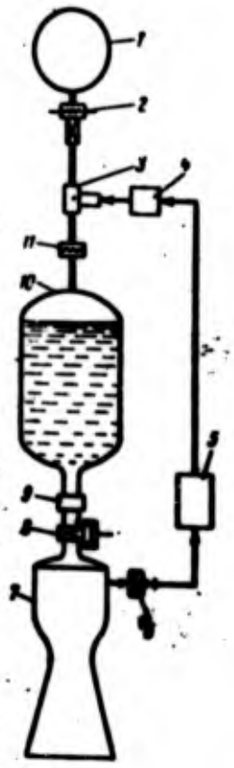

Figure 1.1. Monopropellant LRE with pressurized propellant feed system:

1) gas pressure accumulator; 2) electropneumatic valve; 3) gas pressure reducer; 4) servomotor; 5) amplifier; 6) pressure sensor; 7) combustion chamber; 8) main propellant valve; 9) orifice; 10) propellant tank 11) membrane

The bipropellant LRE arrangement (Figure 1.2) does not differ fundamentally from the monopropellant scheme just discussed. Here the thrust is also regulated by the combustion chamber pressure, but the ratio of the propellant components is maintained within set limits by the (flow control) orifices 13 and 7 in the oxidizer and fuel lines. Engine startup and shutdown are accomplished by the valves 2, 9, and 12. The separating membranes 5 are used to avoid mixing of the propellent components during rocket transportation and storage in the fuelled condition.

We note that in certain cases thrust regulation is not accomplished by varying the combustion chamber pressure, rather it is accomplished by varying the pressure in the tanks, which is maintained by a nonadjustable pressure regulator. In this case the propellant feed system is simplified somewhat, since there is no need for the amplifier, servomotor, and the adjustable pressure reducer. The engine thrust varies over a considerable range, since the pressure ahead of the orifices depends on the flight load factor and the pressure reducer characteristics.

The efficiency of the pressure-fed system can be improved by preheating the working medium by means of a heat exchanger which uses

the thermal energy of the exhaust gases [66].

The presence of the gas pressure accumulator on board the rocket is not always justified, since it has considerable weight and volume. Therefore, in place of the gas pressure accumulator, use is often made of a solid pressure accumulator (SPA), which has definite weight and structural advantages. A serious drawback of the pressure-fed propellant system using the SPA is that it is very difficult to organize a stable process for the combustion of the solid grain in the accumulator combustion chamber. This can be avoided if the propellant is expelled from the tanks using a liquid pressure accumulator (LPA) in which the working medium are the products of combustion of the liquid propellant components.

A schematic diagram of a LRE with LPA is shown in Figure 1.3. Air flows from the high-pressure bottle (accumulator) 1 through the valve 2, pressure reducer 3, and check valves 4 into the tanks 5 and 13 with the liquid propellants. After the membranes 6 and 12 burst, the liquid component enters the propellant tanks, where it burns as a result of mixing with the vapor and liquid phases of the components in tanks 7 and 11. We note that considerable pressure pulsations in the tanks may be observed in this arrangement.

Moreover, for the realization of this scheme it is necessary that the oxidizer and fuel be hypergolic.

More successful is the LPA arrangement in which the liquid components are burned in special gas generators mounted on the tanks. In this case a stable tank pressure and combustion products with the required temperature can be obtained.

§ 2. Turbopump-Fed LRE

The LRE schemes with turbopump feed system have been widely used for rockets with various missions. These schemes are divided into two basic types:

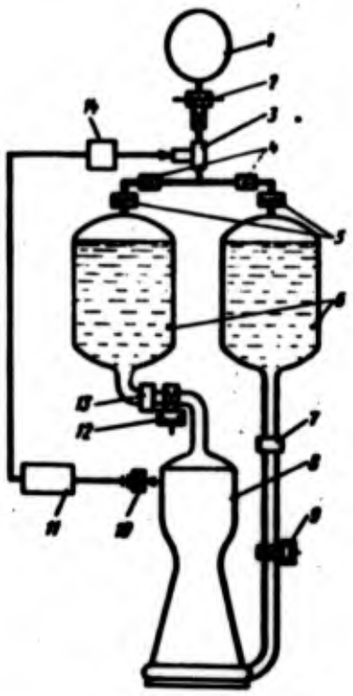

Figure 1.2. Bipropellant LRE with pressurized propellant feed system:

1) gas pressure accumulator; 2) electropneumatic valve; 3) main pressure reducer; 4) check valve; 5) membrane; 6) propellant tanks; 7 and 13) orifices; 8) combustion chamber; 9) main fuel valve; 10) pressure sensor; 11) amplifier; 12) main oxidizer valve; 14) servomotor

Figure 1.3. LRE with liquid pressure accumulator:

1) gas pressure accumulator; 2) electropneumatic valve; 3) gas pressure reducer; 4) check valve; 5) small oxidizer tank; 6 and 12) membranes; 7) fuel tank; 8) main fuel valve; 9) combustion chamber 10) main oxidizer valve; 11) oxidizer tank; 13) small fuel tank; 14) restrictors

1) open schemes, in which the used generator gas is exhausted into the atmosphere downstream of the turbine;

2) closed schemes, in which provision is made for afterburning the generator gas downstream of the turbine in the thrust combustion chamber.

From the energetic viewpoint the closed systems are preferable to the open systems, since a definite gain in the powerplant specific thrust is achieved as a result of the utilization of the generator gas energy in the propulsor (thrust chamber).

The pump-fed engines may be regulated or unregulated, depending on whether or not there are regulating organs in the system for varying (regulating) the LRE operating regime. Let us examine some typical LRE arrangements with a turbopump system for feeding the propellant components.

Figure 1.4 shows a LRE in which the turbine working medium are the products of decomposition of H_2O_2. To create the required pressure ahead of the pumps the oxidizer and fuel tanks 5 and 7, and also the hydrogen peroxide tank 19 are pressurized by the compressed air in the bottle (accumulator) 1.

Prestart spinup of the turbine 16 is accomplished by the pyrostarter 9. After the turbopump assembly (TPA) has reached its nominal operating regime, the turbine is fed by the products of combustion of the hydrogen peroxide, which is fed by the pump 15 into the steam gas generator 8. Engine shutdown is accomplished by actuating the cutoff valves 12 and 13 and the steam gas generator valve 17.

The H_2O_2 decomposition products have a comparatively low temperature; therefore the use of steam-gas as the working medium is advantageous from the viewpoint of reducing the thermal loads on the turbine blades. It is true that this scheme results in a reduction of the engine specific thrust and complication of the fuel feed system.

These drawbacks may be avoided if we use as the working medium for the turbine the combustion products of the main propellant components, which can be bled from the combustion chamber or obtained from a specially provided gas generator. A schematic of such a LRE is shown in Figure 1.5.

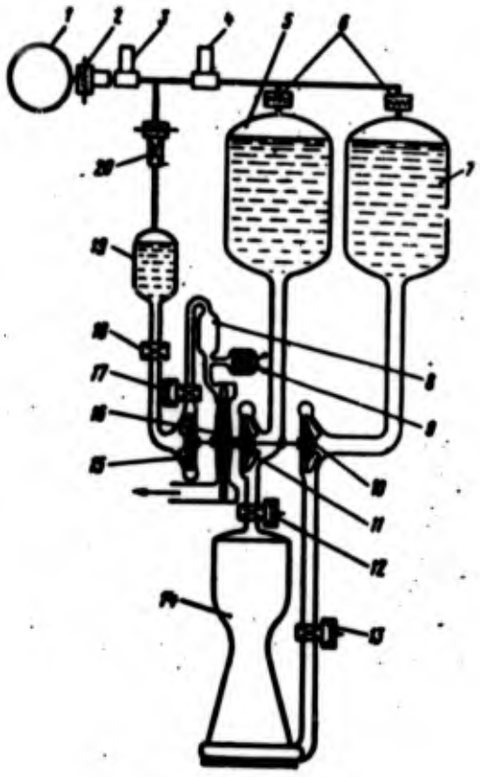

Figure 1.4. LRE with turbopump assembly:

1) gas pressure accumulator; 2 and 20) electropneumatic valves; 3) high pressure reducer; 4) low pressure reducer 5) oxidizer tank; 6) membranes; 7) fuel tank; 8) gas generator; 9) pyrostarter; 10) fuel pump; 11) oxidizer pump; 12) main oxidizer valve; 13) main fuel valve; 14) combustion chamber; 15) H_2O_2 pump; 16) turbine; 17) H_2O_2 valve; 18) control valve 19) H_2O_2 tank

The oxidizer and fuel are bled from the pump outlets and flow through the valve 15 to the gas-generator combustion chamber. The engine thrust is regulated by varying the TPA rpm, which depends on the

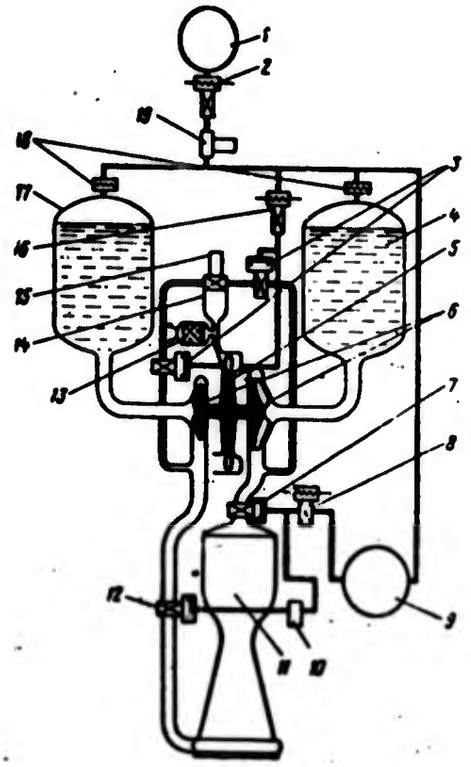

Figure 1.5. LRE with turbopump assembly operating on the products of combustion of the main propellants:

1) gas pressure accumulator; 2, 8, and 16) electropneumatic valves; 3) pneumatic valves; 4) oxidizer tank; 5) turbine; 6) oxidizer and fuel pumps; 7) main oxidizer valve; 9) low pressure accumulator; 10) injector; 11) combustion chamber; 12) main fuel valve; 13) pyrostarter; 14) liquid gas generator LGG; 15) LGG valve; 17) fuel tank; 18) membranes; 19) gas pressure reducer

fuel flowrate through the the valve 15. Engine startup and shutdown is accomplished by the valves 3, 7, and 12, which are supplied from the pressure accumulators 1 and 9.

In this arrangement the propellant tanks are pressurized by compressed gas from the accumulator 1. The propellant combustion products used in the turbine are dumped overboard, which naturally reduces somewhat the engine specific thrust. Therefore the LRE with afterburning of the propellants (Figure 1.6) is more economical. Here the used gases are directed into the combustion chamber, where they are afterburned. Additionally, the propellant tanks are pressurized by the gas generators 1 and 2, operating on the main propellant components, which makes it possible to eliminate the gas pressure accumulator and thereby improve the powerplant weight characteristics.

Of definite interest is the LRE arrangement (Figure 1.7) using liquid hydrogen and oxygen [180]. In this scheme the turbine is installed directly in the combustion chamber and its working medium is the hydrogen which has been preheated in the combustion chamber cooling passages.

§ 3. Some Present-Day LRE Arrangements

The rapid development of rocketry, resulting from its use in military operations and in the study of outer space, has been accompanied by intensive research and preliminary design development in the direction of new, more reliable, and more economical LRE. The majority of the engine schemes which only recently were considered to be designs of the future have now been developed or are in the process of experimental and test development. In the following we examine briefly some of the present-day LRE which the authors believe to be of definite methodological and practical interest.

RZ-2 Engine. This engine (Figure 1.8) is the powerplant of the Blue Streak medium-range rocket, which operates on kerosene and liquid oxygen [179]. The sealevel engine thrust is 602,000 N (62 T), combustion chamber pressure is 37.5 bar (38 at), propellant component ratio $k = 2.16$, nozzle exit to throat area ratio is 8:1.

The engine has a tubular combustion chamber which is kerosene cooled. The propellant components are fed to the combustion chamber

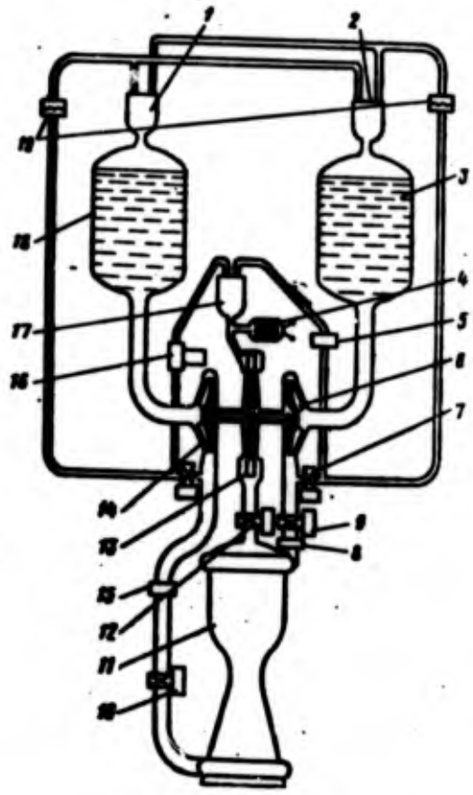

Figure 1.6. LRE with afterburning:

1 and 2) LGG for tank pressurization; 3) oxidizer tank; 4) pyrostarter; 5, 8, and 15) orifices 6) oxidizer pump; 7 and 12) valves; 9 and 10) main oxidizer and fuel valves; 11) combustion chamber; 13) turbine; 14) fuel pump; 15) regulator; 17) gas generator; 18) fuel tank; 19) membrane

by the centrifugal pumps 1 and 3, which are coupled with the turbine through a spur-gear speed reducer. The turbine working medium are the combustion products of the main components in the gas generator with $k = 0.35$.

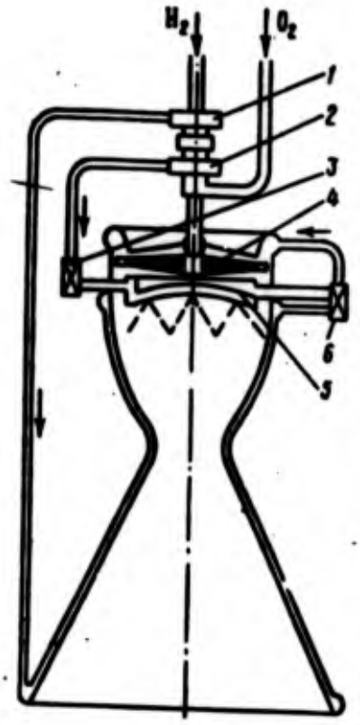

Figure 1.7. LRE with turbine in combustion chamber:

1 and 2) hydrogen and oxygen valves; 3) main oxygen valve; 4) turbine; 5) injector head; 6) main hydrogen valve

The engine is controlled by an electropneumatic system operating on the principle of a strict actuation sequence: each process takes place after the controlling organ receives an impulse from the preceding actuator which has completed its function.

Propellant ignition in both the liquid gas generator (LGG) and the main combustion chamber takes place with the aid of pyrotechnic igniters. The sequence of activation of the various assemblies during start is accomplished automatically from the ground station.

The engine starting sequence is as follows.

1) Depressing the start button pressurizes the ground propellant tanks and the tank with oil to lubricate the planetary reducer and the bearings.

2) The pyrotechnic squib igniter in the combustion chamber is ignited.

3) After the electrical contact in the squib burns through, the main oxidizer valve and the starting fuel valve open. The liquid oxygen and kerosine flow from the ground tanks to the combustion chamber and are ignited.

4) The flame burns through the contact wire stretched across the nozzle exit, which then sends a signal to start the LGG.

5) The pyrotechnic squib ignites, after which a signal is sent to open the main fuel valve.

6) When the main fuel valve opens it sends a signal to open the LGG valve.

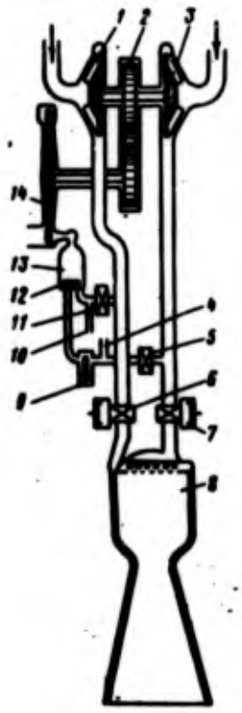

Figure 1.8. RZ-2 engine:

1) fuel pump; 2) reduction gearing; 3) oxidizer pump; 4) oxidizer supply line from ground tank; 5) and 11) check valves; 6) main fuel valve; 7) main oxidizer valve; 8) combustion chamber; 9) LGG valve; 10) fuel supply line from ground tank; 12) igniter squib; 13) liquid gas generator; 14) turbine

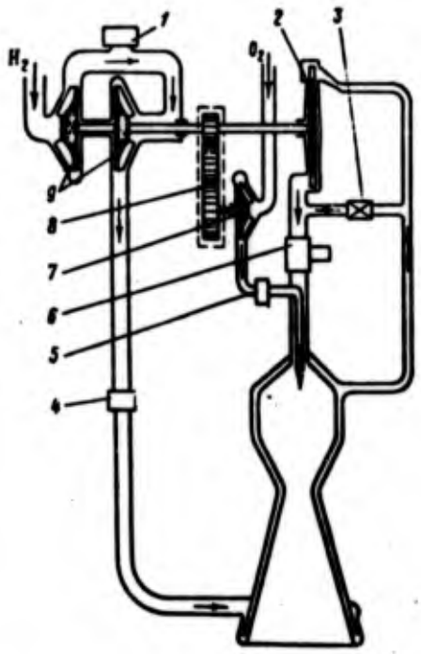

Figure 1.9. LR-115 engine:

1) H_2 valve; 2) turbine; 3) turbine power regulator; 4 and 5) main fuel propellant valves; 6) regulating valve; 7) O_2 pump; 8) reduction gearing; 9) two-stage H_2 pump

7) The turbine starts up and the centrifugal pumps begin to deliver the propellant components to the combustion chamber and the LGG.

8) When the pressure in the fuel feed system and in the rocket tanks reaches the operating values, i.e., when the engine has stabilized, the inlet valves from the ground start tanks are closed.

It is interesting to note that the start is aborted automatically if a particular parameter, for example the turbine speed or the liquid oxygen pump temperature, deviates from its value, and also if strong vibrations develop. The acceleration time is about 4 seconds. Engine shutdown is accomplished on command from the rocket range control system. The LGG valve is first closed, then the main oxygen valve, and then 0.2 seconds later the main fuel valve is closed.

LR-115 Engine. This engine is used for the upper stage of the Saturn rocket [188]. The propellant components are liquid hydrogen and oxygen, which provide an increase of about a third in the specific thrust in comparison with engines operating on oxygen and kerosene. The engine develops a thrust of 66,600 N (6.8 T) with a combustion product exhaust velocity of 4100 m/sec. The nominal pressure in the combustion chamber is 20.6 bar, the nozzle expansion ratio is 40.

The use of liquid hydrogen as the fuel made it possible to simplify the engine arrangement considerably (Figure 1.9). We see from the schematic that the hydrogen flows from the tank through the two-stage centrifugal pump to the combustion chamber cooling passage. As a result of the low critical temperature and pressure of hydrogen, the heat added is sufficient to obtain the energy of the working medium for driving the TPA. Thus, in this arrangement there is no need for the gas generator, which complicates the control system and creates a problem in getting rid of the combustion products downstream of the turbine. Additionally, this cycle is more efficient, since all the fuel is burned in the main combustion chamber under conditions which provide the maximal specific thrust.

In this arrangement no additional energy source is required for starting, since the available initial energy of the propellant stream flow is sufficient to accelerate the TPA.

Simultaneously with the initiation of turbopump rotor rotation, the first portion of the propellant components is ignited in the combustion chamber and the engine accelerates.

The liquid oxygen pump is driven from the shaft of the turbine 2 through the reducer 8. After the pump, the oxygen flows ghrough the throttling valve 5 which is used to trim the engine with respect to the component flow ratio during acceptance testing. The bypass line and regulator 3 in the turbine line make it possible to change the TPA power, which determines the required pressure in the combustion chamber and provides the possibility of regulating the engine thrust.

X-405 Engine. This engine is used for the first stage of the Vanguard three-stage rocket, which is used to launch artificial earth satellites [169, 187, 156, 164]. The engine thrust is $12 \cdot 10^4$ N; the propellants are kerosene and liquid oxygen.

Figure 1.10 shows the pneumatic and hydraulic system. The propellant tanks of the rocket first stage are pressurized by compressed helium in the accumlator 1. The propellant components are fed by the two centrifugal pumps 11 and 13, which are driven by a single-stage turbine operating on the products of decomposition of 90% hydrogen peroxide. The used steam-gas is fed to movable nozzles, which are rotated by a special system used to eliminate the possibility of rocket rotation about the longitudinal axis.

The propellant flow rate into the combustion chamber is regulated by pneumatic valves. The component mass flow rate ratio is varied in accordance with a special program by a valve installed in the oxidizer line.

Pyrotechnic ignition of the propellant components is used. Melting of the corresponding element of an electrical circuit (after a definite delay) sends a signal which opens the main fuel valve fully and opens the main oxidizer valve partially. The propellant components under pressure enter the chamber and ignite, with the combustion taking place at a relatively low temperature because of the excess fuel. The appearance of a flame downstream of the nozzle is detected by a sensor located in the nozzle exit plane. The sensor signal travels to the hydrogen peroxide valve 4, after which the TPA turbine accelerates, the chamber inlet pressure rises, and engine operation stabilizes.

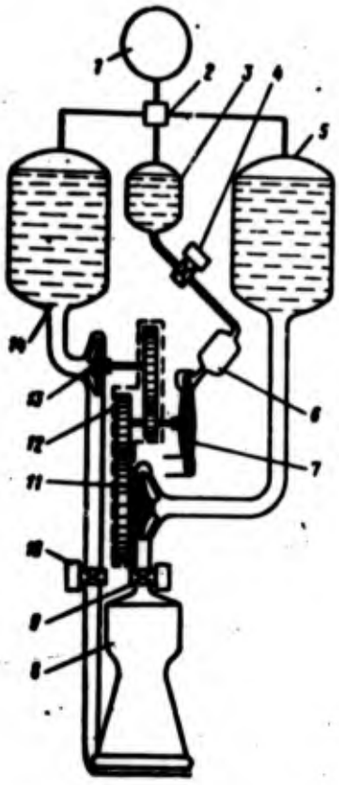

Figure 1.10. X-405 engine:

1) gas pressure accumulator; 2) pressure reducer; 3) H_2O_2 tank; 4) valve; 5) oxidizer tank; 6) gas generator; 7) turbine; 8) combustion chamber; 9) main oxidizer valve; 10) main fuel valve; 11) oxidizer pump; 12) reduction gearing; 13) fuel pump; 14) fuel tank

During the startup process the oxygen flow rate and the chamber pressure are regulated in accordance with a set program by the spring-loaded pneumatic oxidizer valve, which opens in proportion to the pump outlet pressure. The engine startup and acceleration is controlled by a special device located outside the rocket which automatically records the powerplant parameters and controls the sequence of startup operations and also shuts the engine down if any problems arise. Shutdown is accomplished by sending a signal to close the main propellant valves 9 and 10 and the valve 4.

A pneumatic relay which anticipates valve closure is installed in the main propellant valve to prevent hydraulic shock in the fuel line.

RL 20P-3 Engine. This engine is built by Pratt and Whitney and operates on liquid oxygen and hydrogen [170]. The unusual arrangement of this engine is shown in Figure 1.11. The combustion chamber consists of two segments: one operates with sweat cooling, the other (nozzle adapter) operates with regenerative cooling. The combustion chamber is divided into two approximately equal volumes which have a series of radial tubes with the oxidizer injectors. A flat type head for atomization of the fuel is located in the upper part of the combustion chamber.

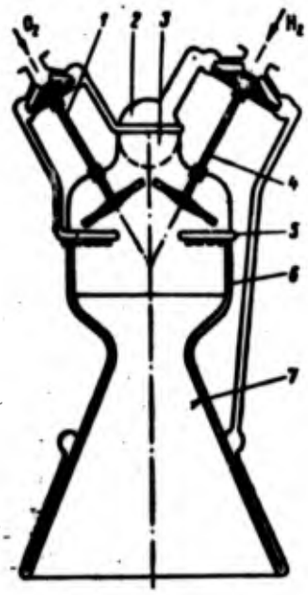

Figure 1.11. RL-20P3 engine:

1) oxidizer turbopump; 2) fuel injector head; 3) forechamber; 4) fuel turbopump; 5) oxidizer injector tubes; 6) porous sleeve; 7) combustion chamber

The oxidizer and fuel pumps have their own turbines, located in the upper part of the combustion chamber. The turbine working medium are the products of incomplete combustion of hydrogen and oxygen. During startup the expansion energy of the hydrogen flowing through the supply system lines is sufficient to rotate the pumps. A small amount of fluorine is added to the oxidizer for ignition. Combustion begins in the forechamber 3, then the flow continues through the turbine blades and enters the main combustion chamber.

AJ-10-104 Engine. The AJ-10-104 engine, installed on the second stage of the Thor-Able-Star rocket [28], is a typical LRE with pressure-fed LRE. The engine operates on inhibited RFNA and asymmetric DMH (k = 2.8) and develops a thrust of $3.5 \cdot 10^4$ N with a chamber pressure of 14 bar.

The pneumatic and hydraulic system is shown in Figure 1.12. The propellant is forced from the tanks by compressed helium and the oxidizer is the cooling component. The propellant flow rate is regulated by the main propellant pneumatic valves 9 and 11. The thrust is regulated by the oxidizer 15 and fuel 10 flowmeters.

Oerlikon Rocket Engine. A LRE (Figure 1.13) with 9800 N thrust which operates on kerosene and nitric acid is installed on the Oerlikon guided anti-aircraft rocket [171], [94].

The propellant is located in concentric tanks. The pistons 4, which expel the oxidizer and fuel under compressed nitrogen pressure,

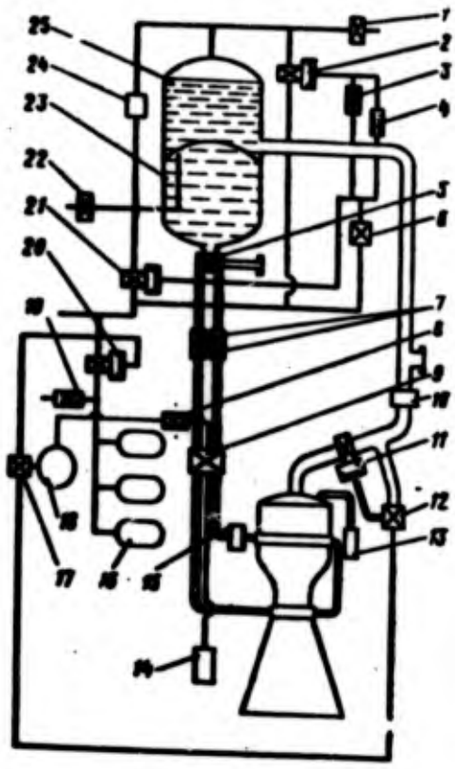

Figure 1.12. AJ-10-104 engine:

1) fuel tank vent valve; 2 and 21) pneumatic valves; 3 and 5) filters; 4, 7, 8, and 19) check valves; 6, 12, and 17) servovalves; 9) main oxidizer valve; 10) fuel flowmeter; 11) main fuel valve; 13) combustion chamber pneumatic valve; 14) valve switch; 15) oxidizer flowmeter; 16) compressed helium bottles; 18) accumulator for valve 9; 20) pressure regulator; 22) oxidizer tank vent valve; 23) oxidizer tank; 24) pneumatic switch; 25) fuel tank

travel inside the tanks.

Starting fuel (a mixture of triethylaminol and xylidine) is used for ignition during startup. The propellant flow rate is regulated by the valves 10 and 12. A smooth start is ensured by gradual opening of the valves 10 and 12, with the oxidizer flowing through the bypass line

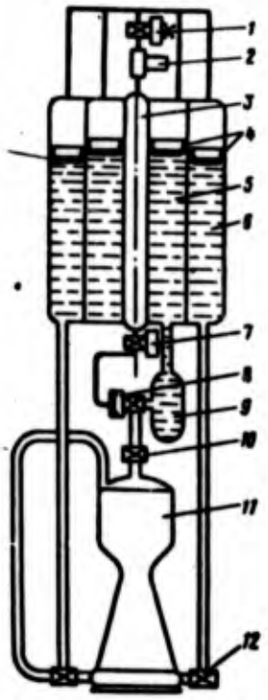

Figure 1.13. LRE for Oerlikon rocket:

1) pyrovalve; 2) pressure reducer; 3) compressed nitrogen bottle; 4) pistons; 5) oxidizer tank; 6) fuel tank; 7) pyrovalve; 8) pneumatic valve; 9) starting tank; 10) main fuel valve; 11) combustion chamber; 12) main oxidizer valve

directly into the head of the combustion chamber. To shut the engine down a signal is sent to the valve 7; after this valve actuates, gas from the bottle 3 flows to the cutoff valve and closes it.

XL-99 Airplane Engine. This engine was used for the high-speed X-15 experimental airplane [53], [27], [118]. The LRE develops a vacuum thrust of $248 \cdot 10^3$ N, the combustion chamber pressure is 41 bar, the combustion product velocity at the nozzle exit is 2780 m/sec. The fuel is liquid oxygen and anhydrous liquid ammonia. A turbopump system is used for propellant feed. The thrust throttling range is 100 - 30%.

The pneumatic and hydraulic system of this LRE is shown in Figure 1.14. The propellant components are fed by the pumps 11 and 12 from the tanks 7 and 9 through lines to the combustion chamber, with the fuel first being used to cool the combustion chamber walls and then flowing through the oil heat exchanger 21 of the hydraulic system, while the part of the oxidizer which flows to the igniter passes through the vaporizer 13.

The hydrogen peroxide is forced by compressed helium from the tank 1 into the steam-gas generator 5, from which the products of H_2O_2 decomposition flow to the turbine 6. The heat of the exhaust steam-gas is used in the vaporizer 13 to preheat the liquid oxygen.

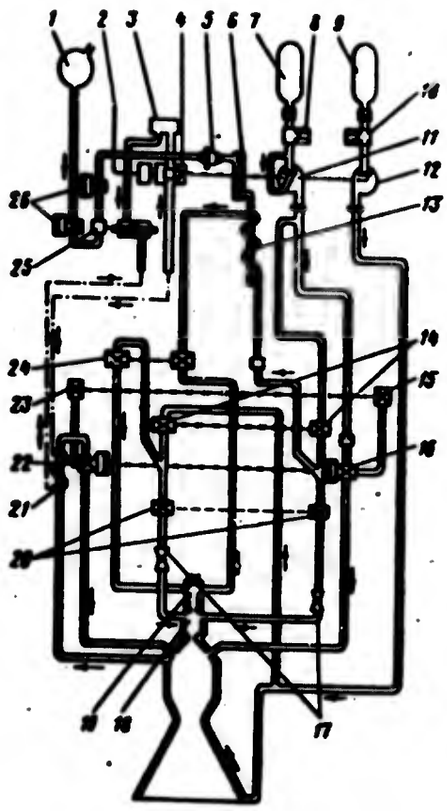

Figure 1.14. XL-99 airplane engine:

1) H_2O_2 tank; 2) throttling signal transmission channel; 3) hydraulic power source; 4) turbine speed regulator; 5) steam gas generator; 6) turbine; 7) liquid oxygen tank; 8) safety valve; 9) NH_3 tank; 10) safety valve; 11) liquid oxygen tank; 12) NH_3 pump; 13) liquid oxygen evaporator; 14 and 20) second stage ignition propellant valves; 15) liquid oxygen scavenge valve; 16) liquid oxygen cutoff valve; 17) Venturi tube; 18) igniter; 19) sparking plug; 21) hydraulic system oil heat exchanger; 22) NH_3 cutoff valve; 23) NH_3 scavenge valve; 24) first stage ignition propellant valve; 25) H_2O_2 regulating valve; 26) H_2O_2 cutoff valve

Engine throttling is accomplished by means of the controllable regulating valve 25, which changes the hydrogen peroxide flow rate,

which in turn leads to a change of the turbine speed and therefore a change of the propellant component flowrates.

The engine startup sequence is as follows.

1) When the launch airplane reaches a given altitude, the X-15 engine is scavenged for 75 seconds to bring the metal parts of the TPA, lines, and valves down to cryogenic conditions.

2) The combustion chamber is cleared by scavenging with compressed helium.

3) Prior to X-15 separation from the launch plane a signal is sent to start the hydrogen peroxide flow, the TPA starts up, and the igniter is turned on. This is the so-called "idle" engine operating cycle.

4) After separation from the launch airplane a signal is transmitted to open the main propellant valves 14 and 24. Ignition of the components in the combustion chamber is provided by the already operating igniter. Since airplane control is in the hands of the pilot, the possibility exists for engine throttling, shutdown, and restart.

The engine is shut down by closing the main propellant valves with a subsequent helium scavenge. The engine is shut down automatically after complete exhaustion of the propellant when cavitation takes place in the pumps.

Armstrong Siddeley "Screamer" Airplane LRE. This engine operates on liquid oxygen and aviation gasoline, developing a sea-level thrust from 4450 to 35,500 N [178], [33], [192], [193]. The pneumatic and hydraulic system of the engine is shown in Figure 1.15.

The pumps 13, 14, and 27 feed the propellants from the tanks 7 and 8 and the cooling water into the combustion chamber and the cooling passage. The pumps are driven by a turbine whose working mediums are the combustion products of the propellants in the gas generator 29

Water is injected into the gas generator to reduce the temperature. The igniter and the wall of the gas generator are also water cooled.

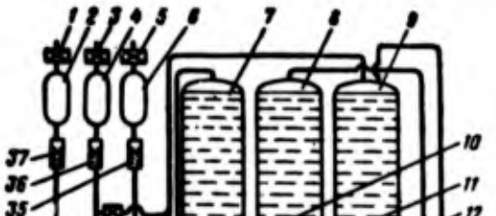

Figure 1.15. Armstrong Siddeley "Screamer" airplane LRE:

1) oxidizer tank nitrogen inlet valve; 2) oxidizer starting tank; 3) fuel tank nitrogen inlet valve; 4) starting fuel tank; 5) H_2O tank nitrogen inlet valve; 6) starting H_2O tank; 7) oxidizer tank; 8) fuel tank; 9) H_2O tank; 10) oxidizer shutoff valve; 11) fuel shutoff valve; 12) H_2O shutoff valve; 13) fuel pump; 14) H_2O pump; 15) fuel flow regulator; 16) H_2O flow regulator; 17 and 18) filters; 19) main fuel valve; 20) igniter; 21) combustion chamber; 22) main H_2O valve; 23) main oxidizer valve; 24) fuel check valve; 25) oxidizer flow regulator; 26) oxidizer check valve; 27) oxidizer pump; 28) turbine; 29) LGG; 30) H_2O regulating valve in LGG line; 31) LGG igniter; 32) oxidizer pneumatic regulating valve in LGG line; 33) fuel pneumatic regulating valve in LGG line; 34) throttling valve; 35, 36, and 37) check valves

The main combustion chamber is also cooled by water, which after passing through the entire passage is sprayed into the chamber at the head end.

Thrust regulation is accomplished by the throttling valve 34 in the oxygen line.

Since the system for starting and controlling the Screamer engine is quite complex, we shall examine only the general description of the transient regimes. To start the engine a signal is sent to the EPV (electropneumatic valves) shutoff valves 10, 11, and 12, after which the propellants and water enter the starting tanks 2, 4, and 6, filling the main engine lines up to the cutoff and bypass valves 19, 22, and 23. Then a signal is sent to feed nitrogen into the starting tanks, as a result of which liquid oxygen flows to the LGG igniter valves and fuel and water flow to the LGG igniter and its valves. The pressure in the ignition chamber rises, the valves open, and the components enter the LGG. Simultaneously the pneumatic valve transfers the ignition to the main chamber.

The LGG combustion products accelerate the turbine, and until the moment the turbine reaches its nominal speed the pumps force the liquid through the bypass lines back to the tanks.

After the LGG stabilizes, the propellants enter the ignition chamber. Here the propellants are ignited by high-voltage sparking plugs and the increasing pressure opens the main water valve. Then after the pressure increases in the cooling slot the main oxygen valve is opened. The main fuel valve opens upon increase of the pressure in the oxygen line. The entire acceleration requires 2-3 seconds.

Downstream of the pumps the propellants are partly diverted to the LGG, with the water and fuel flowing through control valves, while the liquid oxygen flows through a selector control valve and a remotely controlled flow regulator, which consists of a spring-loaded reducer valve which regulates the turbine speed and therefore the engine thrust. To obtain a variable thrust the pilot can change the spring tension.

In case of excessive increase of the turbine speed an emergency switch shuts the engine down. During engine shutdown the main operating valves are closed, and prior to complete turbine stoppage the propellants are returned to the main tanks through the bypass valves. The lines are scavenged with nitrogen to prevent a subsequent hard start.

§ 4. Trends in Development of LRE Arrangements

The requirement for high reliability during startup, shutdown, and continuous operation leads to ever increasing simplification of the engine arrangements.

In the early powerplant designs the low reliability of the LRE was to a considerable degree due to the complex starting and regulating systems. Therefore, at the present time we see a trend toward maximal simplification of the starting, shutdown, and interlock systems, toward reduction of the number of elements of the engine automatic control systems, and so on. These simplifications are accompanied by the rapid introduction of various sorts of inventions, the latest developments in chemistry and physics, and also intensive scientific research investigations.

At one time, for example, special tanks with fuel and oxidizer or a monopropellant H_2O_2 were installed on board the rocket for starting and operating the TPA. The propellants were pressure fed from the tanks into the LGG (SGG) (solid gas generator), which required additional system complexity.

Valve operation was provided by an electrical interlock system which controlled the pneumatic actuators in the required sequence. A complex pyrotechnic system was used to ignite the propellant components in the combustion chamber, and TPA lubrication was accomplished by pressure feed of the lubricant from the tank.

The technique and methods for starting and control techniques and methods were later simplified considerably. As a rule, the turbopump assembly is accelerated by a pyrostarter or using the head in the propellant tanks.

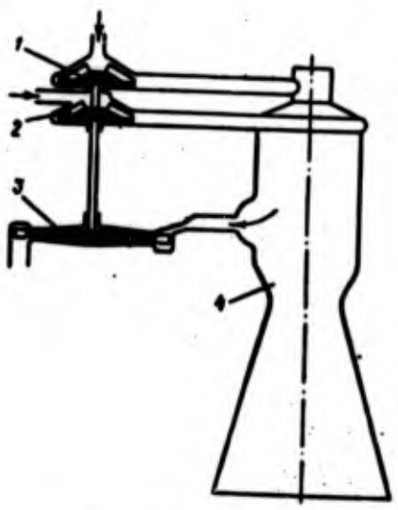

Figure 1.16. LRE with combustion product bleed from chamber:

1 and 2) fuel and oxidizer pumps; 3) turbine; 4) combustion chamber

The main fuel valves are opened by the propellant component itself upon reaching a given pump outlet pressure. This has made it possible to eliminate the electrical and pneumatic control system.

Ignition in the LRE is accomplished either by the pyrostarter combustion products or an electric plug igniter. Ignition in the combustion chamber is provided by preinjecting hypergolic components. Shutdown is accomplished using fast-acting and structurally simple pyrovalves, which permit a considerable reduction of the thrust tail-off impulse. Control of the rocket is provided by a pivoting nozzle installed at the end of the turbine exit duct rather than with the use of special engines.

The gas generator system can be eliminated if we locate the turbine in the upper part of the combustion chamber (see RL 20P-3 LRE in Figure 1.11) or if we use the arrangement with combustion product bleed from the main chamber (Figure 1.16). The trend toward simpli-

fication of the engine system has led to elimination of most of the requirements for servo control. The system simplification has culminated in the combining of several engine functions into a single servosystem.

Still another characteristic of the present trend is the simplification of the systems for prestart servicing, fueling, and prestart checkout of the engine.

§ 1. Cl

The
only for
developme
gine oper

The
parameter
combustio
these par
as the ch
pellant f
tional to

Figu
time. In
unsteady
steady (s
time. Th
final 5 s

The
of LRE op

CHAPTER 2

STATIC CHARACTERISTICS OF POWER PLANTS AND THEIR MAIN COMPONENTS

§ 1. Classification of Operational Regimes and LRE Characteristics

The basic engine parameters are determined by thermal calculation only for a few (basic) design conditions. However, in the experimental development process and under test stand and flight conditions the engine operates in various flight regimes, including off-design regimes.

The engine operating regime is characterized by a whole series of parameters: flow rates of the propellent components, pressure in the combustion chamber, absolute thrust, specific thrust, and so on. All these parameters are interrelated and any one of them may be selected as the characteristic of the LRE operating regime. Usually the propellant flow rate or the combustion chamber pressure, which is proportional to the flow rate, is taken as the operating condition parameter.

Figure 2.1 shows a typical plot of the LRE thrust variation with time. In accordance with this graph we differentiate the steady and unsteady engine operating regimes. The engine operating regime is steady (stationary) if its operating regime parameters are constant in time. The engine operating regimes in the preliminary 1,main 3, and firal 5 stages are steady.

The preliminary stage is provided to ensure higher reliability of LRE operation, particularly to organize a smoother acceleration of

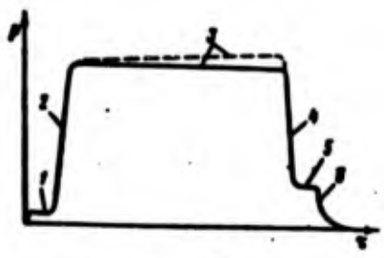

Figure 2.1. Nature of LRE thrust variation with time for long-range ballistic rocket:

1) preliminary stage; 2) launch; 3) main stage; 4) transition regime; 5) final stage; 6) engine shutdown

the engine to the main stage regime, to make possible simultaneous control of startup of all the chambers of a multichamber power plant, to prevent combustion chamber explosion if a large amount of the propellent components accumulates at the initial moment, and so on.

Transition to the main stage regime is accomplished when a pump outlet pressure is reached by transmitting a command for complete valve opening, or by automatic triggering of a valve when reaching a specified fluid pressure in the line. Such a startup is sometimes called a two-stage start. It is provided by installing in one of the lines (most often in the oxidizer line) a two-position valve, which is initially only partially opened to a position corresponding to the preliminary stage and then is opened fully, which corresponds to the main stage.

The main stage regime, in which the engine operates for a long time period, is the basic stage. In Figure 2.1 the dashed line reflects the thrust increase with the engine operating in the steady regime due to reduction of atmospheric pressure during the flight time. The solid horizontal line corresponds to engine operation on the test stand in the steady main stage regime.

For the proper determination of the moment of engine shutdown it is necessary to maintain with a high degree of precision the specified flight vehicle velocity and the coordinate of the end of the powered portion of the trajectory. This is achieved more easily in the case of a lower acceleration and, thus, lower thrust. Therefore, prior to engine shutdown in flight it is first switched from the main stage regime to the final stage regime. This shutdown technique reduces the magnitude and scatter of the tailoff thrust impulse (see Chapter 11), which is the primary reason for down-range scatter distance for

long-range ballistic rockets.

The engine operating time in the final stage regime is about 2 - 5 seconds, and the thrust is 10 - 20% of the main stage regime thrust.

The LRE engine operating regime with time varying parameters is termed the unsteady regime. The unsteady regime is characterized by the corresponding transient process. The transient processes include startup, transition from the main stage regime to the final stage regime, shutdown, and engine regulation.

The above classification of the steady regimes is applicable only to the autonomous engines of guided rockets. Launch boosters have only a single operating regime, while experimental engines may have a more extensive classification of the regimes.

Thrust control in flight during transition from one regime to another is usually accomplished in two ways.

In the single chamber engine the transition from the main stage to the final stage is accomplished by varying the component supply pressure. This technique is characterized by simplicity of the power plant arrangement, but its capabilities are limited, since extensive throttling usually leads to a pulsative engine operating regime which is accompanied by marked oscillations of the chamber pressure and the pressure in the hydraulic lines. Moreover, the mixture formation and combustion processes deteriorate at the low flow rates and low chamber pressures and this results in some decrease of the specific thrust.

In the multichamber power plants the transition from main stage to final stage is accomplished by shutting down one or more chambers. This technique does not lead to any deterioration of the working process and, most importantly, it yields the possibility of obtaining a smaller thrust in the final stage. The power plant installation often includes a group of steering chambers in addition to the main engines.

In this case only the steering chambers are operated in the final stage, and their total thrust amounts to no more than 10% of the overall power plant thrust.

The most important factor which influences the operation of the LRE is the pressure of the surrounding medium, which varies with altitude. Therefore, even with a constant engine operating regime the thrust and specific thrust will change along the flight trajectory from the sea level to the space values. These changes are taken into account in calculating the flight characteristics.

The dependence of the main LRE parameters — absolute and specific thrust — on the operating conditions is called the engine characteristic. Two characteristics — throttling and altitude — are most important for the LRE.

The throttling (regulating) characteristic is the dependence of the absolute and specific thrust on the propellent flow rate or the combustion chamber pressure for constant ambient pressure or, equivalently, constant flight altitude.

The dependence of the absolute and specific thrust on flight altitude (or ambient pressure) for a constant flow rate (or constant combustion chamber pressure) is termed the altitude characteristic.

The propellent composition characteristics are calculated for research purposes or are sometimes obtained experimentally. These characteristics are the dependence of the absolute or specific thrust on the mass ratio of the component flow rates or the oxidizer excess coefficient, other conditions remaining the same. The experimental variation of the thrust and specific thrust as a function of the engine design (spray injector head, combustion chamber, nozzle, and so on) is often obtained for these same reasons.

In studying LRE regulation processes the need frequently arises to use the static characteristics of the individual engine components — pumps, turbines, hydraulic lines. Therefore, in the following, we

shall examine the characteristics of the major engine components in addition to the basic characteristics of the engine as a whole.

§ 2. LRE Throttling Characteristics

The throttling characteristics can be calculated only approximately under the assumption that the efficiency of the working process remains constant (constant efficiency of the mixture formation and combustion processes). Account for the change of the working process efficiency with change of the engine operating regime and the associated change of the combustion products temperature, gas constant, and polytrope exponent is not yet possible at the present time.

If the efficiency of the process in the chamber is assumed to be the same in the different regimes, then the relationship between the flow rate and the combustion chamber pressure will be linear [6]. Therefore, the throttling characteristics are plotted either as a function of the value of the flow rate G, or as a function of the chamber pressure p_K. Since the quantities G and p_K are proportional, the form of these characteristics will be the same; they will differ only with respect to the scale used. In practice it is more convenient to use the thrust and specific thrust characteristics:

$$P=P(p_H),\ P_1=P_1(p_H)$$

We note that in the low-altitude low-power regimes with the engine operating at sea level or underwater a diamond compression shock pattern forms inside the nozzle, and the usual thrust formula becomes invalid. The study of LRE dynamics is usually conducted only for the shock free regime.

1. Absolute thrust throttling characteristics.

The engine absolute thrust at the altitude H will be

$$P_H=\varphi_c G w_c+F_c(p_c-p_H) \qquad (2.1)$$

where φ_a is the coefficient of exit velocity loss due to spreading, which is a function of the nozzle exit divergence angle:

G is the propellent mass flow rate;

w_c is the velocity of the combustion products at the nozzle exit;

F_c is the nozzle exit area;

p_H is the ambient atmospheric pressure at the altitude H (for sea level $H = 0$, $p_H = p_0$).

Setting $p_H = 0$, we obtain the expression for the vacuum thrust:

$$P_\infty = \varphi_a G w_c + F_c p_c. \tag{2.2}$$

The thrust at the altitude H is related with the vacuum thrust by the formula

$$P_H = P_\infty - F_c p_H. \tag{2.3}$$

We express the specific thrust in a vacuum and at the altitude H in the form

$$P_{1\infty} = \varphi_a w_c + \frac{F_c p_c}{G};$$

$$P_{1H} = P_{1\infty} - \frac{F_c p_H}{G}.$$

To obtain the equation for the throttling characteristics of a given engine (with fixed nozzle) for vacuum and altitude conditions in the form $P_\infty, P_{1\infty}, P_H; P_{1H} = f(p_K)$ we must obviously replace all the parameters in these formulas which depend on the chamber pressure by p_K. These parameters include the flow rate and the nozzle exit pressure p_c. For fixed nozzle dimensions and constant working process efficiency the discharge velocity is independent of the combustion chamber pressure.

For a given engine operating with a given fuel the flow rate depends only on the chamber pressure and they are connected by the linear relation

$$G = C p_K, \tag{2.4}$$

where

$$C=\sqrt{n\left(\frac{2}{n+1}\right)^{\frac{n+1}{n-1}}}\frac{F_{cr}}{\sqrt{R_K T_K}};$$

n is the polytropic exponent for the combustion products;

F_{cr} is the chamber critical area;

R_K, T_K are, respectively, the gas constant and the temperature of the combustion products in the chamber.

The value of the coefficient C is easily found from the parameters in the design regime (denoted by asterisk):

$$C=\frac{G^*}{P_K^*}.$$

Replacing p_n by p_k in (2.2), we obtain

$$P_\infty=C_1 p_K \qquad (2.5)$$

where C_1 combines the quantities which are independent of p_k.

$$C_1=\eta_K C\cdot w_c+\frac{F_c}{\delta}$$

Here δ is the gas expansion ratio in the nozzle, equal to p_K/p_c. The coefficient C_1 can also be defined in terms of the design regime parameters:

$$C_1=\frac{P_\infty^*}{P_K^*}.$$

Equation (2.5) shows that the absolute thrust is directly proportional to the combustion chamber pressure. This is then the equation of the throttling characteristic for the vacuum absolute thrust. It is represented graphically by a straight line passing through the coordinate origin (Figure 2.2).

Replacing the quantity P_∞ in (2.3) by (2.5), we obtain the equation for the throttling characteristic at the altitude H

$$P = C_1 p_k - F_c p_H. \qquad (2.6)$$

This characteristic is a straight line parallel to the first line, but shifted downward by a distance equal to the quantity $F_c p_H$ (see Figure 2.2).

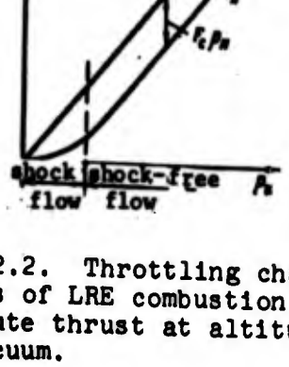

Figure 2.2. Throttling characteristics of LRE combustion chamber absolute thrust at altitude H and in vacuum.

2. Specific thrust throttling characteristics.

The vacuum specific thrust equals the ratio of the vacuum thrust to the flow rate

$$P_{1\text{-}} = \frac{P_-}{G}.$$

Taking account of (2.4) and (2.5), we obtain

$$P_{1\text{-}} = \frac{C_1}{C} = \text{const}. \qquad (2.7)$$

This means that under those assumptions used in constructing the throttling characteristics, the vacuum specific thrust of a given engine is independent of the operating regime, i.e., independent of the chamber pressure and flow rate. Thus the vacuum specific thrust characteristic is represented in the figure by a horizontal line (Figure 2.3). In reality, at small flow rates, (for low chamber pressures) some reduction of the vacuum specific thrust is noted due to deterioration of the working process efficiency and increase of the degree of dissociation of the combustion products.

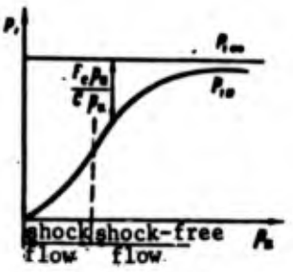

Figure 2.3. Throttling characteristics of LRE combustion chamber specific thrust at altitude H and in vacuum.

We obtain the equation of the specific thrust throttling characteristic at the altitude H for the shock free flow regime in the nozzle by dividing (2.6) by (2.4)

$$P_{1H}=\frac{C_1}{C}-\frac{F_c p_H}{C p_K},$$

or, using (2.7),

$$P_{1H}=P_{1\infty}-\frac{F_c p_H}{C}\frac{1}{p_K}$$

Hence we see that the sealevel specific thrust increases with increase of the chamber pressure p_K (or the flow rate G). The difference between $P_{1\infty}$ and P_{1H} equals $\frac{F_c p_H}{C p_K}$ and depends on p_K; this difference is larger for small values of p_K and vice versa. For very large p_H (in the limit as $p_K \to \infty$) P_{1H} approaches $P_{1\infty}$ asymptotically.

§ 3. LRE Altitude Characteristics

While the throttling characteristics can be recorded during engine test stand runs, the altitude characteristics are usually plotted on the basis of calculation, since their experimental determination involves serious difficulties.

The altitude characteristics can be plotted for different but specific values of the chamber pressure p_K. For example, if the altitude characteristic is plotted for the nominal values of p_K it shows the nature of the variation of the nominal values of the absolute and specific thrust as a function of flight altitude. The usual formulas may be used as the equations of the altitude characteristics

$$P_H=P_\infty-F_c p_H; \tag{2.8}$$

$$P_{1H}=P_{1\infty}-\frac{F_c}{C p_K}p_H=P_{1\infty}-\frac{F_c}{G}p_H. \tag{2.9}$$

Since in the case of supersonic shock free gas flow in the nozzle, the ambient conditions do not affect the discharge velocity w_c, the factor which affects directly the basic parameters of the chamber is the ambient pressure p_H, which changes as a function of the flight altitude. The variation of atmospheric pressure with flight altitude is presented graphically or in tabular form. Calculations show that when the ISA tables are used we can set $p_H = 0$ at altitudes greater than 25 km. The error of this assumption is less than 1%; therefore, the ISA tables can be used in constructing the altitude characteristics.

The altitude characteristics are plotted as a function of the altitude H or the ambient pressure p_H. Figure 2.4 shows the LRE altitude characteristics as a function of flight altitude H and ambient pressure. The characteristics of the form $P_H = P_H(H)$ are simpler and more convenient, particularly in the case in which they must be constructed for the underwater engine operation.

We see from Figure 2.4 that the absolute and specific thrust of the LRE increase with altitude, approaching the limiting values which are reached in vacuum (for $p_H = 0$). The difference between like parameters in vacuum and at the altitude H is determined on the curves by the segments $F_c p_H$ and $\frac{F_c p_H}{G}$ which are larger, the larger the nozzle exit area and the lower the flight altitude. The greatest difference, representing the change of the absolute and specific thrusts from sea level to vacuum conditions, amounts to 18 - 20% of the same parameters in vacuum.

Figure 2.5 shows the altitude characteristics of a LRE operating in two different regimes. The first regime is characterized by the flow rate G_I, the second by G_{II}, where $G_I < G_{II}$. The thrust characteristics for operation in the second regime lie below the corresponding values for the first regime. The thrust increase with climb due to the reduction of the ambient pressure is the same for both regimes and equals $F_c p_H$. The vacuum specific thrust is independent of the engine operating regime: $P_{1-II} = P_{1-I}$. The specific thrust increase with climb for the engine operating in the second regime will be greater than for operation in the first regime, since $\frac{F_c p_H}{G_{II}} > \frac{F_c p_H}{G_I}$

Figure 2.4.
istics of
ambient pr
altitude H

Therefore th
the first at
thrust is lo

§ 4. Cha

Let us
pellant comp
what is the
α. The chan
position) du
the gas capa
products in
thrust.

Figure
ture, and ga
cient for a

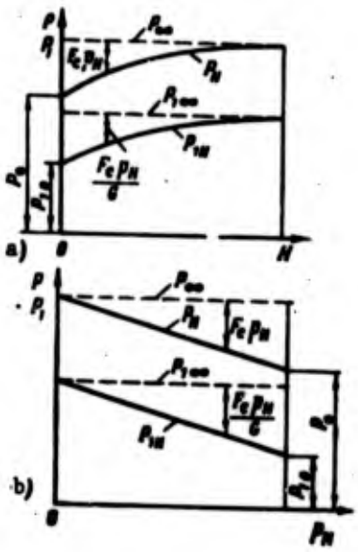

Figure 2.4. Altitude characteristics of LRE as a function of ambient pressure p_H and flight altitude H.

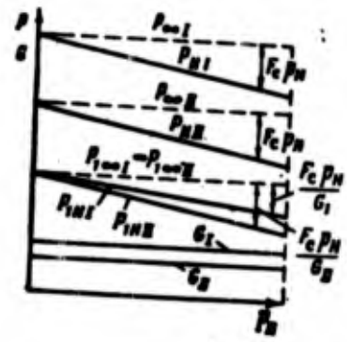

Figure 2.5. Altitude characteristics of LRE operating in two different regimes.

Therefore the specific thrust is lower in the second regime than in the first at all altitudes. In particular the sealevel specific thrust is lower in the second regime than in the first ($P_{0II} < P_{0I}$).

§ 4. Characteristics as a Function of Propellant Composition

Let us examine the characteristics of a LRE with variable propellant composition, caused by a change of the component ratio k, or what is the same thing, by a change of the excess oxidizer coefficient α. The change of the propellant composition (combustion product composition) due to a change of the component ratio leads to a change of the gas capacity for work $R_K T_K$ (R_K is the gas constant of the combustion products in the chamber, T_K is the temperature) and the specific thrust.

Figure 2.6a shows curves of the vacuum specific thrust, temperature, and gas constant as a function of the excess oxidizer coefficient for a liquid fluorine plus liquid ammonia propellant, while

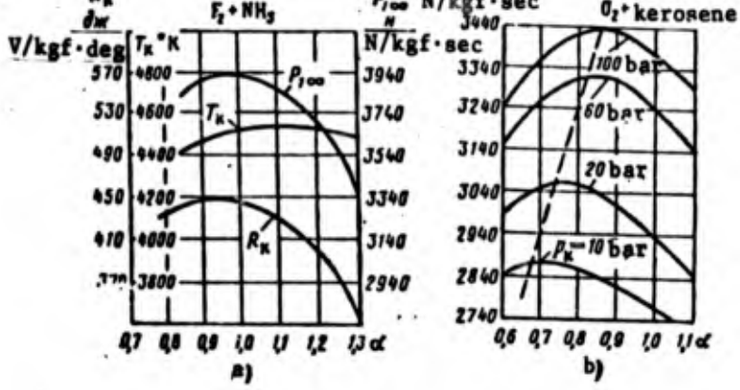

Figure 2.6. LRE characteristics as a function of propellant composition: (a) fluorine and ammonia; (b) and oxygen and kerosene.

Figure 2.6b shows the vacuum specific thrust as a function of α for different chamber pressures for a kerosene plus liquid oxygen propellant. We see that in the first case the specific thrust maximum occurs at the stoichiometric component ratio ($\alpha = 1$), in the second case, the optimal value of $\alpha < 1$. This is not just a random situation. Thermodynamic calculations and experiments show that the maximal specific thrusts of rocket engines using carbon-oxygen propellants are reached not for the stoichiometric component ratio but for some oxidizer deficiency ($\alpha < 1$). The fact that the optimal α is less than one for the carbon-oxygen fuels is due to the high content in the combustion product composition of carbon monoxide (CO) which, even though it is the product of incomplete combustion, is relatively resistant to dissociation and leads to loss of part of the heat. Therefore, T_K may be higher than for complete combustion, i.e., for $\alpha = 1$. Moreover, the high content of CO, which has lower molecular weight than CO_2, leads to an increase of R_K. Therefore the product $R_K T_K$, which is proportional to the specific thrust, will be maximal for $\alpha < 1$ for the carbon-based propellants.

Thus, a change of the propellant component ratio k (or the coefficient α) leads to a change of the combustion product composition

which, other conditions being the same, causes a change of the combustion chamber thrust characteristics.

§ 5. Pump Characteristics

The basic parameters characterizing the operation of centrifugal pumps are the mass flow rate G or the volume flow rate Q (output), the pressure rise Δp (head), efficiency η, angular velocity (or rpm n), power N (or shaft torque M). The interdependences of these quantities then yield the pump characteristics. Usually the output and the angular velocity $\omega = 2\pi n$.

Then the characteristics may be written as follows:

$$\left.\begin{array}{ll} \text{pressure rise} & \Delta p = \Delta p(G, \omega) \\ \text{power} & N = N(G, \omega) \\ \text{torque} & M = M(G, \omega) \\ \text{efficiency} & \eta = \eta(G, \omega) \end{array}\right\} \tag{2.10}$$

The connection between these mutually dependent parameters is defined by the relations

$$\eta = \frac{\Delta p G}{\rho N}, \tag{2.11}$$

$$N = M\omega, \tag{2.12}$$

where ρ is the density of the fluid being pumped.

These expressions can be used to find the remaining quantities from any two which are known. The Relations (2.10) are represented by characteristic surfaces in three-dimensional coordinates. Since the use of these surfaces is difficult in practice, some one parameter ω or G is fixed and characteristic curves are obtained. Pump characteristics constructed for ω = const. are widely used in practice. This is due basically to the fact that these characteristics are sufficient for examining steady processes taking place in pump-fed propellant lines.

In studying the dynamic phenomena in propellant lines, particularly in studying LRE regulation, it is necessary to know the partial

derivatives of the various parameters with respect to the angular velocity. For example, to determine these derivatives at a point of a known regime (usually the rated condition) we must know the dependences of these parameters on ω for a fixed flow rate, i.e., the pump characteristics which are defined by (2.10) with G = const.

1. Head characteristic.

Let us examine the head characteristic of a centrifugal pump, expressing the head as a function of the flow rate for ω = const. or the head as a function of impeller angular velocity for G = const.

The theoretical head characteristic is easily obtained from the equation for the pump theoretical head (Euler equation) under the assumption of an infinite number of blades

$$\Delta p'_\infty = \rho(u_2 c_2 \cos\alpha_2 - u_1 c_1 \cos\alpha_1),$$

where $\Delta p'_\infty$ is the theoretical pump head;
- u is the circumferential velocity;
- n is the absolute fluid velocity;
- ρ is the fluid density;
- α is the angle between the absolute and circumferential velocities.

The subscript «1» applies to the rotor inlet, the subscript «2» applies to the rotor outlet.

Usually the pump impellers are designed so that $\alpha_1 = \frac{\pi}{2}$. Therefore, we can write

$$\Delta p'_\infty = \rho u_2 c_2 \cos\alpha_2. \tag{2.13}$$

As is known (see, for example, [104]), the projection of the absolute velocity on the circumferential velocity will be

$$c_2 \cos\alpha_2 = u_2 - c_{2m} \operatorname{ctg}\beta_2, \tag{2.14}$$

where β_2
cities at
velocity.

In a

where

Subs
$u_2 = r_2\omega$,

Let
obtained
fore, the
2.7). Si
for a fin

where Ψ_b
the charac
intercepts
Figure 2.7

The
magnitude

where β_2 is the angle between the relative and circumferential velocities at the blade exit; c_{2m} is the radial component of the absolute velocity.

In accordance with the discharge formula the radial component is

$$c_{2m} = \frac{G'}{2\varphi_2 \rho \pi r_2 b_{K2}}, \tag{2.15}$$

where $2\pi r_2 b_{K2}$ is the rotor exit section area without account for the thickness of the blades; it is defined as the lateral surface of a cylinder of radius r_2 and height equal to the rotor exit width b_{K2};

G' is the theoretical mass flow rate;

φ_2 is a coefficient accounting for the blade thickness at the rotor exit.

Substituting (2.14) into (2.15) and (2.13) and assuming that $u_2 = r_2\omega$, we obtain the theoretical head characteristic

$$\Delta p'_\infty = \rho r_2^2 \omega^2 - \frac{\operatorname{ctg}\beta_2}{2\varphi_2 \pi b_{K2}} G'\omega. \tag{2.16}$$

Let us first examine the case in which ω= const. In the equation obtained all the quantities other than G' will be constants. Therefore, the characteristic will have the form of a straight line (Figure 2.7). Since the connection between $\Delta p'_\infty$ and the theoretical head $\Delta p'$ for a finite number of blades is defined by the expression

$$\Delta p' = \varphi_b \Delta p'_\infty,$$

where φ_b is the coefficient accounting for the finite number of blades, the characteristic for $\Delta p'$ will have the form of a straight line which intercepts on the coordinate axis a distance equal to $\varphi \pi \rho r_2^2 \omega^2$ (see Figure 2.7).

The real characteristic differs from the theoretical one by the magnitude of the hydraulic losses in the pump rotor and scroll

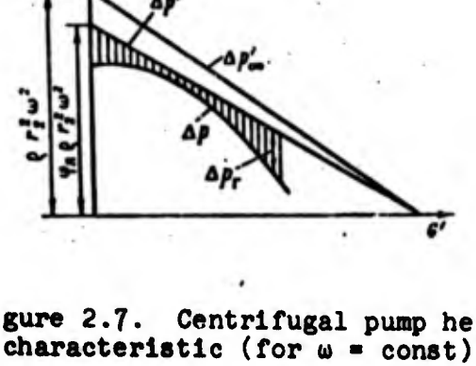

Figure 2.7. Centrifugal pump head characteristic (for ω = const)

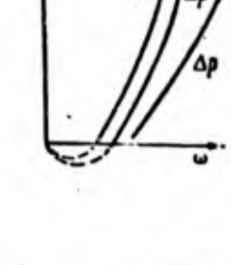

Figure 2.8. Centrifugal pump head characteristic (for G = const)

$$\Delta p = \Delta p' - \Delta p_r.$$

In practice the losses in overcoming the viscous forces are evaluated with the aid of the so-called hydraulic efficiency

$$\eta_r = \frac{\Delta p}{\Delta p'}.$$

As a result of the nonlinear dependence of the hydraulic losses Δp_h on the output, the actual head characteristic has the form of a curve lying somewhat below the straight line $\Delta p' = \Delta p'(G)$ (see Figure 2.7).

Now let us examine the case in which ω = var for G = const. The characteristic has the form of a second-order curve passing through the coordinate origin and crossing the abscissa axis twice (Figure 2.8).

$$\Delta p' = a_1\omega^2 - a_2' G'\omega,$$

where

$$a_1 = \varphi_2 r_2^2, \quad a_2' = \frac{\varphi_2 \operatorname{ctg} \beta_2}{2\pi\varphi_2 b_{a2}}.$$

The falloff of the theoretical head to zero for some value of ω is explained by the fact that after the circumferential velocity reaches the value of the projection of the relative velocity on the circumferential velocity the pump begins to operate as a turbine, i.e., while providing the flow rate G' = const the required rpm is provided by the fluid head at the pump inlet.

The actual characteristic must obviously lie somewhat below the theoretical curve.

2. Power characteristic.

The theoretical pump power characteristic can be obtained from the known relation

$$N'_{\infty} = \frac{\Delta p'_{\infty} G'}{\varrho}$$

Taking (2.16) into account, we obtain easily

$$N'_{\infty} = r_2^2 \omega^2 G' - \frac{c \lg \beta_2}{2\pi r_2 b_{\omega 2} \varrho} \omega G'^2$$

and

$$N' = \eta_r r_2^2 \omega^2 G' - \frac{\eta_r}{\eta_2} \frac{c \lg \beta_2}{2\pi b_{\omega 2} \varrho} \omega G'^2 .$$

As a result of losses of various forms the actual pump power must always be greater than the theoretical value. Therefore the actual power characteristic, equal to $N = \frac{N'}{\eta}$ lies above the theoretical curve.

The power characteristics constructed using these formulas for centrifugal pumps with ω = const and G = const are shown in Figure 2.9.

3. Pump efficiency characteristic.

Now let us examine the dependence of the pump efficiency η on the output (for ω = const) and on the angular velocity (for G = const).

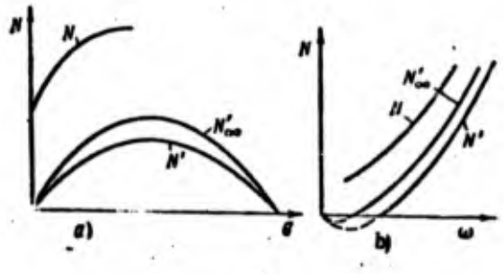

Figure 2.9. Pump power characteristic:
a) for ω = const; b) for G = const

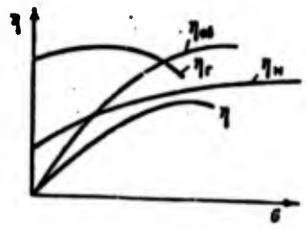

Figure 2.10. Pump efficiency versus component flow rate G (for ω = const)

We have mentioned previously that the head losses in overcoming viscous forces are characterized by the hydraulic efficiency η_h. Its dependence on the flow rate is shown in Figure 2.10. The losses associated with fluid cross flow resulting from circulation within the pump due to the presence of clearances are accounted for by the volumetric efficiency

$$\eta_{об} = \frac{G}{G'},$$

where G is the actual mass flow rate of the component through the pump;

G' is the theoretical flow rate.

Additional power is expended on overcoming friction forces in the bearings and seals and also friction of the fluid on the rotor disk, and these losses are accounted for by the mechanical efficiency

$$\eta_M = \frac{N_s - \Delta N}{N_s},$$

where N_s, ΔN are respectively the pump shaft power and the power losses overcoming mechanical resistances.

Curves of η_v and η_M versus pump output are shown in Figure 2.10. The overall efficiency, which defines the degree of perfection of the pump design from the mechanical and hydraulic viewpoint, is equal to the product of all the efficiencies mentioned above

$$\eta_H = \eta_r \eta_M \eta_{0б}.$$

The pump characteristic $\eta_H = f(\omega)$ is shown in Figure 2.11. We note that the function $\eta_H = \eta_H(\omega, G)$ can be approximated by the following relation [153]

$$\eta_H = \left(B_1 - B_2 \frac{G}{\omega}\right) \frac{G}{\omega},$$

where B_1, B_2 are coefficients which are constant for a given pump.

4. Pump torque characteristic.

The torque characteristic of the centrifugal pump, i.e., the variation of the torsional or rotational moment M as a function of the output and angular velocity, is easily found with the aid of the obvious expression

$$M' = \varphi_n G' r_2 c_2 \cos \alpha_2$$

As before, the prime denotes theoretical values of the parameters. Actually, substituting in place of $c_2 \cos \alpha_2$ its value from (2.14) with account for (2.5) it is easy to obtain

$$M' = \varphi_n r_2^2 \omega G' - \frac{\varphi_n c (g \lambda_2}{2\pi r_2 0 b_{\lambda 2}} G'^2.$$

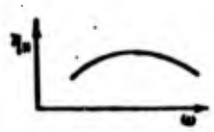

Figure 2.11. Pump efficiency versus angular rotation rate ω (for G = const).

Figure 2.12. Pump torque M versus output G (for ω = const)

Figure 2.13. Pump torque versus speed (for G = const)

The torque pump characteristics plotted using this equation with ω = const and G = const are shown in Figures 2.12 and 2.13.

5. Universal characteristic.

Let us examine the universal characteristic of a centrifugal pump, which consists of a network of characteristics plotted for different shaft angular velocities or different component flow rates (Figure 2.14). On this network are plotted the curves of constant efficiency, which are curves of similar regimes and are parabolas passing through the zero value

$$\frac{\Delta p}{G^2} = \text{const} \text{ and } \frac{\Delta p}{\omega^2} = \text{const}.$$

The actual parabolas of the similar regimes join near the coordinate origin (due to the existence of mechanical losses) and for high angular velocities and high flow rates (due to the onset of cavitation), transforming the constant efficiency curves into ellipses[1]. This figure also shows the families of characteristics N(G) and N(ω).

We note that when the LRE is regulated by varying the pump rpm the operating point on the characteristic in the general case does not move along a curve of constant efficiency, rather it moves along some line AB.

Footnote (1) appears on page 62.

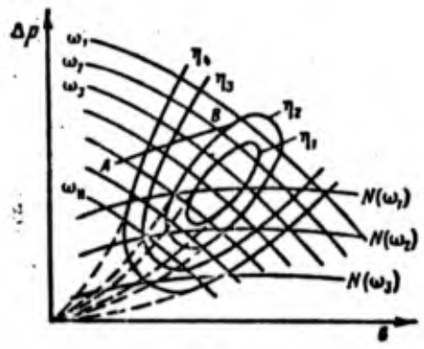

Figure 2.14. Universal pump characteristic.

6. Approximate dependences of pump head, output, power, and torque on angular velocity.

In practical calculations, for small variations of the pump shaft angular velocity, use is made of the approximate dependences of the head Δp, flow rate G, power N, and torque M of the centrifugal pump on the angular velocity ω. In this case we can assume with adequate accuracy that the pump overall efficiency η_p is constant. Using this assumption, the computational formulas are found to be quite simple and convenient and still yield adequate accuracy.

Let us examine first the approximate relation $\Delta p = \Delta p(\omega)$. To this end we use the obvious equation

$$\Delta p = \eta_r \eta_z \varrho u_2 c_2 \cos u_2. \tag{2.17}$$

Considering that (see [122])

$$c_2 = u_2 \frac{\sin \beta_2}{\sin (u_2 + \beta_2)}, \tag{2.18}$$

we obtain

$$\Delta p = c_1 \varrho \omega^2, \tag{2.19}$$

where

$$c_{\Delta p} = 2\eta_c \varphi_2 r_2^2 \frac{\sin\beta_2 \cos\alpha_2}{\sin(\alpha_2+\beta_2)},$$

For LRE pumps we can assume approximately [9] that the complex

$$\varphi_2 \frac{\sin\beta_2 \cos\alpha_2}{\sin(\alpha_2+\beta_2)} \approx 1.$$

Then we obtain the evaluative formula

$$\Delta p \approx \eta_c \rho r_2^2 u_2^2.$$

Formula (2.19) makes it possible to calculate the head for transition from one regime (index *) to another quite closeby regime

$$\Delta p = \Delta p^* \frac{\omega^2}{\omega_*^2}. \qquad (2.20)$$

Now let us turn to the output G, which may be defined by the formula

$$G = 2\pi\eta_v \rho r_2 b_{t2} \varphi_2 Q c_2 \sin\alpha_2.$$

Using (2.18), we obtain easily

$$G = c_G Q\omega, \qquad (2.21)$$

where

$$c_G = 2\pi\varphi_2 \eta_v \rho r_2^2 b_{t2} \frac{\sin\beta_2 \sin\alpha_2}{\sin(\alpha_2+\beta_2)}.$$

Similarly, it is not difficult to find from (2.21) the pump output in a different regime

$$G = \frac{\omega}{\omega_*} G^*.$$

These Expressions (2.20) and (2.21) make it possible to find the dependence of the power N on ω . In fact, since

$$N=\frac{\Delta pG}{\varrho\eta},$$

then

complex

$$N=c_N\varrho\omega^3,$$

where

$$c_N=\frac{c_{\Delta p}c_Q}{\eta}.$$

Similarly

or tran-
egime

$$N=\frac{\omega^3}{\omega^{*3}}N^*.$$

(2.20)

The connection between the torque M and the angular velocity ω is obviously defined by the formula (see [2.12])

y the

$$M=c_N\varrho\omega^2, \tag{2.22}$$

hence,

$$M=\frac{\omega^2}{\omega^{*2}}M^*.$$

(2.21)

§ 6. Turbine Characteristics

The turbines used as the power drives in the TPA of rocket engines are usually designed as active turbines with velocity stages. Therefore, we shall restrict ourselves to an examination of the characteristics of turbines of this type only. Additionally, we shall assume that the gas generator which generates the working medium provides the critical pressure differential.

pump output

Let us examine the relationships between the basic parameters which characterize the turbine ooperating regime [9], [57], [129]: power N, torque M, angular velocity ω, efficiency η, gas flow rate G,

find the

gas work capacity $R_K T_K$, and the back pressure p_2. These relationships are necessary in order to calculate the variable turbine operating regimes which occur both when regulating the design regime and during engine startup and shutdown.

The turbine power, torque, and efficiency vary as a function of the working medium parameters ahead of the turbine — temperature, gas constant, expansion polytropic exponent n, and the turbine angular velocity. If we take $R_K T_K$ and ω as the independent variables (neglecting the change of the polytropic exponent) the turbine characteristics will be defined by the following functional relationships.(2)

$$\left.\begin{aligned}\eta &= \eta(G, R_г T_г, \omega);\\ M &= M(G, R_г T_г, \omega);\\ N &= N(G, R_г T_г, \omega).\end{aligned}\right\} \tag{2.23}$$

The connection between these quantities is defined by the known formulas

$$N = M\omega; \tag{2.24}$$

$$\eta = \frac{N}{GL'}. \tag{2.25}$$

Here L' is the adiabatic work of expansion per kilogram of gas, which is defined by the known relation

$$L' = \frac{c_1''}{2}, \tag{2.26}$$

where the theoretical gas discharge velocity is

$$c_1' = \sqrt{2\frac{n}{(n-1)} R_г T_г \left[1 - \left(\frac{p_2}{p_г}\right)^{\frac{n-1}{n}}\right]}. \tag{2.27}$$

Thus, the turbine operating regime can be changed by changing G or the propellant component ratio k, on which the gas work capacity $R_K T_K$ [183] depends (we neglect the influence of the pressure change

Footnote (2) appears on page 62.

in the gas generator on $R_K T_K$). In a particular case, engine regulation may be accomplished by changing only the flow rate G (with constant k, i.e., with $R_K T_K$ = const) or by changing the propellant composition (with G = const)[3]. Therefore we shall examine separately the turbine characteristics plotted for $R_K T_K$ = const and G = const, which are also necessary for determining the partial derivatives when studying regulation in the general case.

Now let us find the analytic relationships between the basic turbine parameters, i.e., let us determine the form of the Functions (2.23).

We examine the efficiency, which characterizes the magnitude of the various losses which occur in gas turbines: losses in the stator ring, in the blades, with the exit velocity, leakage, gas cooling, windage, and disk friction in the gas, and mechanical losses.

The losses in the stator ring are defined by the following expression [129]

$$z_c = \xi_c \frac{c_1''^2}{2},$$

where $\xi_c = 1 - \varphi_1^2$ is the stator ring loss coefficient;

$\varphi_1 = \frac{c_1}{c_1'}$ is a coefficient accounting for the difference between the actual velocity c_1 and the theoretical velocity c_1'.

The losses in the turbine rotor are found from the formula

$$z_л = \xi_л \frac{c_1''^2}{2},$$

where

$$\xi_л = \left(\frac{1}{\varphi_3^2} - 1\right) \varphi_3^2 \varphi_1^2 \left[\left(\cos\alpha_1 - \frac{u}{c_1}\right)^2 + \sin^2\alpha_1\right];$$

Footnote (3) appears on page 62.

$\varphi_3 = \frac{w_2}{w_1}$ is a coefficient accounting for the decrease of the relative velocity in the interblade channel (found from charts as a function of the sum of the inclination angles of the relative gas velocity at the inlet and outlet $\beta_1 + \beta_2$);

w_2, w_1 are respectively the relative gas velocities in the interblade channel at the outlet and inlet;

u is the circumferential velocity;

α_1 is the inclination of the absolute gas velocity vector to the plane of rotation at the blade inlet.

The outlet losses are determined by the exit velocity

$$z_в = \frac{c_2^2}{2},$$

or in relative units

$$\xi_в = \varphi_1^2 \operatorname{tg}^2 \beta_2 \left(\frac{u}{c_1}\right)^2.$$

The losses discussed above are characterized by the so-called blading efficiency

where

$$\eta_л = 1 - \xi_с - \xi_з - \xi_в$$

Substituting into this expression the values presented above for the coefficients ξ, after transformation (see, for example, [129]) we can obtain for the active turbine

$$\eta_л = 2\varphi_1^2 \left(1 + \varphi_3 \frac{\cos\beta_2}{\cos\beta_1}\right)\left(\cos\alpha_1 - \frac{u}{c_1}\right)\frac{u}{c_1}. \qquad (2.28)$$

For the two-stage active turbine the formula for the blading efficiency can be obtained without account for the exit losses [57]

$$\eta_л = \frac{2\varphi_1 u}{c_1^2}\left\{\left(1 + \varphi_3 \frac{\cos\beta_2}{\cos\beta_1}\left[1 + \varphi_3' \frac{\cos\alpha_1'}{\cos\alpha_2}\left(1 + \varphi_3' \frac{\cos\beta_2'}{\cos\beta_1'}\right)\right]\right)\cos\alpha_1 c_1 -\right.$$

$$-u\left(2+\varphi_3\frac{\cos\beta_2}{\cos\beta_1}\left[1+\varphi_3''\frac{\cos\alpha_1'}{\cos\alpha_2}\left(1+\varphi_3'\frac{\cos\beta_2'}{\cos\beta_1'}\right)\right]+\right.$$
$$\left.+\varphi_3''\frac{\cos\alpha_1'}{\cos\alpha_2}\left(1+\varphi_3'\frac{\cos\beta_2'}{\cos\beta_1'}\right)+\varphi_3'\frac{\cos\beta_2'}{\cos\beta_1'}\right).$$

The friction and windage losses can be found using the formula

$$\xi_{\tau.в}=a_{\tau.в}\frac{\varphi_1^2}{\varphi_2^2\sin\alpha_1}\left(\frac{u}{c_1}\right)^3, \tag{2.29}$$

where φ_2 is the constriction coefficient, equal to the ratio of the width of the interblade channel to the blade pitch;

ε is the degree of turbine partiality;

$a_{f.w.}$ is a coefficient which depends on the number of rows of motor blades (for a disk with a single blade row $a_{f.w.}=7.74\cdot10^{-2}$, for a disk with two rows $a_{f.w.}=9.17\cdot10^{-2}$, with three rows $a_{f.w.}=12.46\cdot10^{-2}$).

The relative gas leakage losses are defined by the formula

$$\xi_{\gamma\tau}=\frac{G_{\gamma\tau.к}}{G}+3{,}1\frac{\delta_в}{h_л}, \tag{2.30}$$

where $G_{le.K}$ is the amount of gas leaking through the labyrinth tip seals, determined by the geometric dimensions of the gaps;

δ_b is the blade clearance;

h_b is the blade height.

These losses make it possible to determine the internal efficiency

$$\eta_i=\eta_u-\xi_{\tau.в}-\xi_{\gamma\tau}. \tag{2.31}$$

The magnitude of the overall effective turbine efficiency is defined as the product

$$\eta=\eta_i\eta_м. \tag{2.32}$$

where η_M is the mechanical efficiency.

Hereafter, we shall assume that the quantities ξ_{le} and η_M are independent of the turbine operating regime (which is very close to reality). Using (2.28) — (2.32) it is easy to find the dependence of the effective turbine efficiency on its independent parameters

$$\eta = a_1 \frac{\omega}{\sqrt{R_к T_к}} - a_2 \frac{\omega^2}{R_к T_к} - a_3 \frac{\omega^3}{(\sqrt{R_к T_к})^3} - \xi_{le}, \tag{2.33}$$

where

$$a_1 = \frac{}{\sqrt{2\frac{n}{n-1}\left[1-\left(\frac{p_2}{p_к}\right)^{\frac{n-1}{n}}\right]}};$$

$$a_2 = \frac{\eta_M\left(1+\gamma_3\frac{\cos\beta_2}{\cos\beta_1}\right)r^2}{\frac{n}{n-1}\left[1-\left(\frac{p_2}{p_к}\right)^{\frac{n-1}{n}}\right]};$$

$$a_3 = \frac{}{\left(\sqrt{2\frac{n}{n-1}\left[1-\left(\frac{p_2}{p_к}\right)^{\frac{n-1}{n}}\right]}\right)^3};$$

The value of the effective turbine torque is defined by the expression

$$M = \frac{GL'\eta}{\omega}. \tag{2.34}$$

Substituting into this formula the values of L' from (2.26) with account for (2.27) and the value of the efficiency from (2.33), after transformations we obtain

$$M = G\left[a_4\sqrt{R_к T_к} - a_5 - a_6\frac{\omega^2}{\sqrt{R_к T_к}} - a_7\frac{R_к T_к}{\omega}\right], \tag{2.35}$$

where

are inde-
to reality).
the effec-

(2.33)

$$a_4=\eta_{\text{м}}\bar{\tau}_1\left(1+\bar{\tau}_2\frac{\cos\beta_2}{\cos\beta_1}\right)\cos\alpha_1\cdot r\sqrt{2\frac{n}{n-1}\left[1-\left(\frac{p_2}{p_{\text{к}}}\right)^{\frac{n-1}{n}}\right]};$$

$$a_5=\eta_{\text{м}}\left(1+\bar{\tau}_2\frac{\cos\beta_2}{\cos\beta_1}\right)r^2;$$

$$a_6=\frac{\eta_{\text{м}}r^2a_{1,0}}{2\eta_{\text{г}}\varphi\sin\alpha_1\cdot\bar{\tau}_1\sqrt{2\frac{n}{n-1}\left[1-\left(\frac{p_2}{p_{\text{к}}}\right)^{\frac{n-1}{n}}\right]}};$$

$$a_7=\eta_{\text{м}}k_{\text{г}}\frac{n}{(n-1)}\left[1-\left(\frac{p_2}{p_{\text{к}}}\right)^{\frac{n-1}{n}}\right].$$

This expression makes it easy to find the form of the turbine power characteristic

$$N=G\left[a_4\sqrt{R_{\text{к}}T_{\text{к}}}\cdot\omega-a_5\omega^2-a_6\frac{\omega^2}{\sqrt{R_{\text{к}}T_{\text{к}}}}-a_7R_{\text{к}}T_{\text{к}}\right]. \tag{2.36}$$

Let us study these relations in more detail. We see from (2.33) that η depends on the angular velocity and on the gas work capacity R_KT_K. We first obtain the turbine efficiency characteristic constructed for R_KT_K = const. In this case the characteristic is defined by a parabola of third order in terms of the angular velocity ω. The form of the characteristic is shown in Figure 2.15. All the forms of losses considered above are also shown in this figure. The curve $\eta = \eta(\omega)$ has a maximum at the optimal regime point[4] and crosses the abscissa axis twice.

the ex-

(2.34)

Now let us construct the turbine characteristic as a function of the working medium work capacity for a constant angular velocity (Figure 2.16). We see that the curve $\eta = \eta(R_KT_K)$ also has a single maximum.

26) with
), after

For practical use it is convenient to plot a network of curves $\eta = \eta(\omega)$, each of which corresponds to a constant value of R_KT_K (Figure 2.17). We note that with increase of the quantity R_KT_K the efficiency peak is shifted toward higher angular velocities.

(2.35)

Footnote (4) appears on page 62.

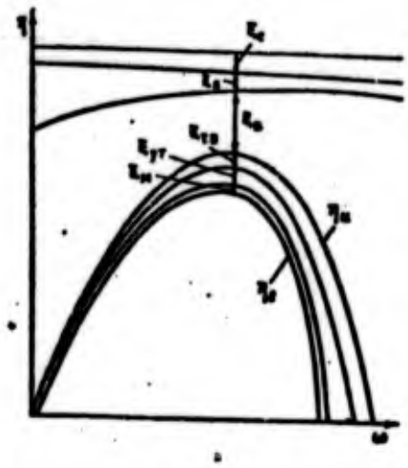

Figure 2.15. Turbine efficiency characteristic (for $R_K T_K$ = const)

The turbine torque characteristic is defined by (2.35). Since M is a function of the three independent variables G, ω and $R_K T_K$, for convenience we plot the characteristics for a fixed value of some two variables. Figure 2.18 shows the relation $M = M(\omega)$ for G = const, $R_K T_K$ = const, $M = M(G)$ with ω = const and $R_K T_K$ = const and $M = M(R_K T_K)$ with ω = const and G = const, also shown are the power characteristics constructed in a similar fashion.

§ 7. Hydraulic Line Characteristics

The engine hydraulic system includes a considerable number of lines, whose characteristics (both static and dynamic) have a significant effect on the characteristics of the entire system. Of particular importance are the main lines through which the components flow to the combustion chamber from the pumps. The line static characteristics show the dependence of the pressure drop on the component flow rate, i.e., they are determined by the hydraulic resistance. The line characteristic can be expressed analytically by a relation of the form

$$G = G(\Delta p).$$

The line losses Δp are made up of the length-dependent distributed losses and local losses. The distributed losses are determined by the formula

$$\Delta p_{l_p} = \lambda \frac{l}{d_0} \frac{\rho w^2}{2}, \qquad (2.37)$$

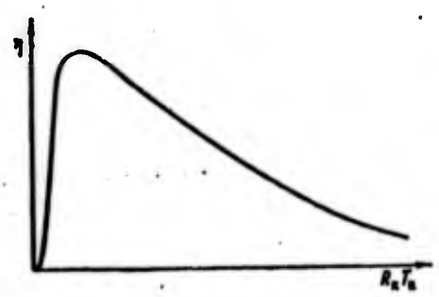

Figure 2.16. Turbine efficiency versus gas energy (for ω = const)

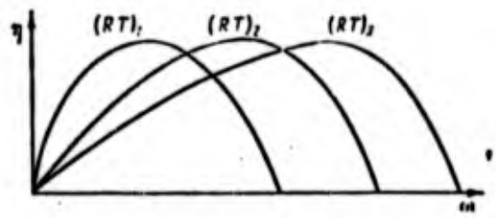

Figure 2.17. Turbine efficiency curves for different values of $R_K T_K$.

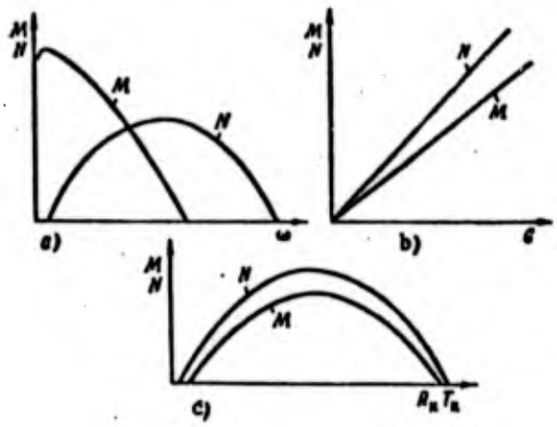

Figure 2.18. Turbine torque M versus speed , output G, and working fluid energy $R_K T_K$.

where λ is the coefficient accounting for fluid friction on the line wall;

w is the fluid velocity;

l, d_e are respectively the line length and equivalent diameter.

The pressure losses in overcoming local resistances, as is known, are proportional to the velocity head

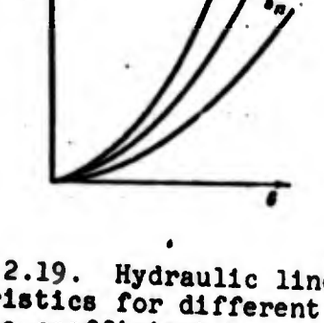

Figure 2.19. Hydraulic line characteristics for different values of the coefficient b_l.

$$\Delta p_{м} = \xi \frac{\rho w^2}{2}, \tag{2.38}$$

where ξ is the local resistance coefficient.

Assuming that

$$w = \frac{G}{\rho F},$$

we obtain from (2.37) and (2.38)

after transformations

$$\Delta p = b_l G^2, \tag{2.39}$$

where $b_l = \frac{1}{2} \frac{\lambda \frac{l}{d_э} + \xi}{\rho F^2}$ is the hydraulic line characteristic coefficient $[\text{kgf}\cdot\text{m})^{-1}$.

The Characteristic (2.39) is represented graphically as a second-order parabola passing through the coordinate origin (Figure 2.19). Assuming that $\Delta p = p_{in} - p_{out}$, (2.39) may be rewritten as

$$p_{вх} = p_{вых} + b_l G^2. \tag{2.40}$$

The curve of the outlet pressure versus flow rate (for constant p_{in}) obviously has the same quadratic parabola form, shifted relative to the coordinate origin by the amount p_{in}. If the hydraulic line consists of several line segments connected in series, then its characteristic will have the same form,but the coefficient g is defined by summation of all b_{li}.

(2.38)

stance

(2.38)

(2.39)

cient

a second-
2.19).

(2.40)

onstant
relative
line
ts charac-
ined by

Footnotes

1. on page 41 — In practice, the form of the angular velocity universal characteristic differs very little from that of the flow rate characteristic.

2. on page 53 — In view of the assumption made above that the gas generator operates with the critical pressure differential, we can assume that the ratio p_K/p_2 is constant, which provides a basis for ignoring the effect of p_2 on the quantities in question.

3. on page 54 — Usually the gas generator operates with a large excess of one of the components. Therefore, by increasing (or decreasing) the supply of the component with the smaller flow rate we can alter $k(R_K T_K)$ without any essential change of the overall flow rate, since the relative increase (decrease) of G is very slight.

4. on page 58 — Actually (2.33), which yields the dependence of the efficiency on the angular velocity, has three roots. However there is no need to examine the third point of intersection of the curve $\eta = \eta(\omega)$ with the axis, since the value of η is negative in the region of the third root of our equation.

CHAPTER 3

LRE MAJOR COMPONENT DYNAMIC EQUATIONS

The equations of the dynamics of both the individual elements of the LRE and of the entire power plant as a whole express the time dependences of thier basic parameters, i.e., the parameter dependences in the transient regimes. We shall examine the equations of the dynamic of the major engine components.

§ 1. Combustion Chamber Dynamic Equations

The equation of LRE combustion chamber dynamics describes the variation of the combustion product pressure and temperature in time as a function of the input of the basic propellant components. The combustion chamber can be considered as an element having mass capacity and thermal capacity, i.e., an element in which accumulation of the working medium and heat is possible in the transient regimes.

The exact mathematical description of the phenomena taking place in the combustion chamber involves serious mathematical difficulties associated with the complexity of the processes taking place. Therefore, we first make several assumptions which simplify the mathematical arguments [78]. We assume that the propellant entering the chamber is transformed instantaneously rather than gradually into the final combustion products, but that this transformation does not take place

immediately upon entry into the chamber, rather it takes place after some time interval in the course of which no energy is released and the volume of the components does not change. We term the time from the moment of propellant injection until its instantaneous transformation into the combustion products the lag time τ_K, assuming it to be constant. This approximation makes it possible to consider the combustion chamber as a volume filled with gas in which the injected components are present in the form of droplets in the course of the time τ_K. We also assume that the products of combustion of the propellant components are an ideal gas whose temperature, pressure, and gas constant are constant, both along the chamber and radially.

We write the balance equation for the mass in the chamber at each moment of time

$$\frac{dm_к}{d\tau} = G_{inf} - G_к, \tag{3.1}$$

i.e., the rate of accumulation m_K of the mass of gaseous combustion products is determined by the difference between the gas mass inflow rate G_{inf} and its outflow rate G_K.

Let us examine individually each term of (3.1).

The mass of the gaseous combustion products can clearly be found from the equation of state

$$m_к = \frac{p_к V_к}{R_к T_к}, \tag{3.2}$$

where p_K is the combustion chamber pressure in N/m^2;
R_K, T_K are respectively the gas constant in J/kgf·deg and the temperature of the combustion products in ^0K;
V_K is the chamber volume in m^3.

Hence it is easy to find the derivative $\frac{dm_к}{d\tau}$:

$$\frac{dm_к}{d\tau} = \frac{V_к}{R_к T_к}\frac{dp_к}{d\tau} - \frac{V_к}{(R_к T_к)^2}\frac{d(R_к T_к)}{d\tau}p_к. \tag{3.3}$$

In view of the assumption made above concerning the instantaneous nature of the propellant combustion, the gas input at the moment τ is determined by the amount of liquid components sprayed through the injectors at the moment $\tau - \tau_K$.

$$G_{вх}(\tau) = G_{ф}(\tau - \tau_к). \tag{3.4}$$

This means that the component ratio k (or the oxidizer excess coefficient α) in the incoming combustion products at the moment τ is determined by the relationship between the flow rate of the liquid oxidizer and fuel through the injectors at the moment $\tau - \tau_K$, i.e.,

$$k = k(\tau - \tau_к). \tag{3.5}$$

As is known [70], the work capacity of the combustion products R_KT_K is a function of k and p_K. Therefore the value of the derivative $\frac{d(R_кT_к)}{d\tau}$ can be found as follows

$$\frac{d(R_кT_к)}{d\tau} = \frac{\partial(R_кT_к)}{\partial p_к}\frac{dp_к}{d\tau} + \frac{\partial(R_кT_к)}{\partial k}\frac{dk(\tau-\tau_к)}{d\tau}. \tag{3.6}$$

The gas flow rate from the chamber is defined by the known gas dynamic relation

$$G_к = A_к\frac{p_к f_{кр}}{\sqrt{R_кT_к}}, \tag{3.7}$$

where $A_к = \sqrt{n\left(\frac{2}{n+1}\right)^{\frac{n+1}{n-1}}}$.

n is the polytropic expansion exponent.

Expressions (3.3), (3.4), (3.6) and (3.7) with account for the equality

$$G = G_в + G_т \tag{3.8}$$

make it possible to obtain the combustion chamber equation in the form

$$\frac{V_к}{R_кT_к}\left[1-\frac{1}{R_кT_к}\frac{\partial(R_кT_к)}{\partial p_к}p_к\right]\frac{dp_к}{d\tau}+\left[\frac{A_кF_{кр}}{\sqrt{R_кT_к}}-\right.$$
$$\left.-\frac{V_к}{(R_кT_к)^2}\frac{\partial(R_кT_к)}{\partial k}\frac{dk(\tau-\tau_к)}{d\tau}\right]p_к=G_в(\tau-\tau_к)+G_г(\tau-\tau_к). \qquad (3.9)$$

The propellant component ratio

$$k=\frac{G_в}{G_г}. \qquad (3.10)$$

Hence it is easy to find the time derivative of k

$$\frac{dk}{d\tau}=\frac{1}{G_г}\left(\frac{dG_в}{d\tau}-\frac{G_в}{G_г}\frac{dG_г}{d\tau}\right). \qquad (3.11)$$

Thus (3.9) together with (3.11) makes it possible to find, generally speaking, the value of the combustion chamber pressure p_K at any instant of time, provided the time dependences of the component flow rates are known.

To determine the partial derivatives $\frac{\partial(R_кT_к)}{\partial p_к}$ and $\frac{\partial(R_кT_к)}{\partial k}$ which appear in (3.9) we need to know the function $R_KT_K = f(p_K,k)$, which is usually represented by a series of curves $R_KT_K = p(k)$ for fixed values of p_K for the given propellant. These curves may be approximated by functions of the type

$$R_кT_к=\frac{1}{a_1(p_к)k^2+a_2(p_к)k+a_3(p_к)} \qquad (3.12)$$

Since the coefficients a_1, a_2, a_3 for many pairs of components depend very weakly on p_K they are usually taken to be constants. In practice, in most cases we use the combustion chamber equation obtained for R_KT_K = const:

$$\frac{V_к}{R_кT_к}\frac{dp_к}{d\tau}+\frac{A_кF_{кр}}{\sqrt{R_кT_к}}p_к=$$
$$=G_в(\tau-\tau_к)+G_г(\tau-\tau_к). \qquad (3.13)$$

Multiplying both sides of this equation by the ratio p_K/G_K after simple transformations we obtain

$$\theta_к \frac{dp_к}{d\tau} + p_к = K[G_o(\tau - \tau_к) + G_г(\tau - \tau_г)]. \tag{3.14}$$

where $\theta_к = \frac{p_к V_к}{G_к R_к T_к}$ is the so-called chamber constant in seconds;

$K = \frac{\sqrt{R_к T_к}}{\lambda_к F_{кр}}$ is the gain with respect to the overall propellant component flow rate in 1/m·sec.

The constant θ_K is one of the basic quantities which characterize the dynamic processes in the chamber. If we introduce the widely used concepts of characteristic (equivalent) length $L^* = \frac{V_к}{F_{кр}}$ and specific pressure impulse $J = \frac{p_к F_{кр}}{G_к}$ we obtain the following expression for θ_K:

$$\theta_к = \frac{JL^*}{R_к T_к} \tag{3.15}$$

If the delay time is variable the mass balance equation for the chamber will have the form

$$\frac{dm_к}{d\tau} = \left(1 - \frac{d\tau_к}{d\tau}\right)[G_o(\tau - \tau_к) + G_г(\tau - \tau_г)] - G_к. \tag{3.16}$$

In this case the combustion chamber equation for k = const will be

$$\theta_к \frac{dp_к}{d\tau} + p_к = K\left(1 - \frac{d\tau_к}{d\tau}\right)[G_o(\tau - \tau_к) + G_г(\tau - \tau_г)]. \tag{3.17}$$

In conclusion we note that the combustion chamber equation obtained above can obviously also be used to study the dynamic processes which take place in liquid gas generators.

§ 2. Equations of Unsteady Fluid Motion in Hydraulic Lines

1. Derivation of basic equations.

We shall derive the differential equations of unsteady fluid motion in hydraulic lines, with the presentation being based primarily on the known works of Ginzburg [47] and Charnyy[145].

We isolate a line segment of length dx (Figure 3.1). Let the cross-section at the initial section be F and the section-average fluid pressure be p.

At the second section the area is $F+\frac{\partial F}{\partial x}dx$, and the pressure is $p+\frac{\partial p}{\partial x}dx$. We assume that the hydraulic line material obeys the elastic deformation laws. Therefore, the cross-section area is a function, not only of the x coordinate, but also of the time τ:

$$F=F(x,\tau)$$

We apply the momentum change law to the isolated fluid mass: the increment of the momentum of the mass over an elementary displacement is equal to the impulse of all the external forces acting during the time of the displacement in question. This is written mathematically as follows

$$\frac{d\vec{K}}{d\tau}=\sum\vec{P}_i, \tag{3.18}$$

where $\vec{K}=\iiint_V \rho\vec{\omega}\,dV$

$\vec{K}$ is the momentum vector of the given fluid mass;
$\vec{P}_i$ is the vector of the i^{th} external force;
V is the volume of the isolated part of the fluid;
ρ is the density;
$\vec{\omega}$ is the velocity.

Since in the fluid motion the change of the mass per unit time (due to the change of the density ρ) is $\iiint_V \frac{\partial\rho}{\partial\tau}dV$, and since (due to the change of volume) — $\iint_{S_V}\rho w_n dS$, where S_V is the surface bounding the volume V, w_n is the normal component of the velocity at a given point of the surface — the velocity along the normal to the surface — then the change of the momentum of the fluid mass in question obviously can be written as follows

$$\frac{d\vec{K}}{d\tau}=\iiint_V\frac{\partial(\rho\vec{\omega})}{\partial\tau}dV+\iint_{S_V}\rho\vec{\omega}\omega_n dS. \tag{3.19}$$

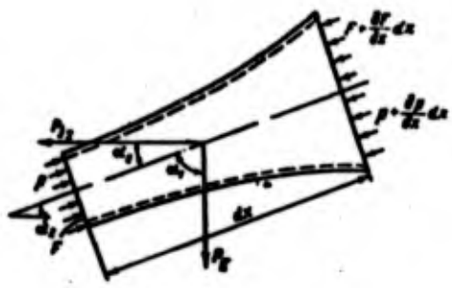

Figure 3.1. Diagram for derivation of equation of unsteady fluid motion in hydraulic lines.

The external forces acting on the isolated fluid volume include:

<u>mass forces</u> - for example, such as the gravity force, centrifugal force, and so on, defined in the general case by the triple integral

$$\vec{P}_j = \iiint_V \rho \vec{j}\, dV, \tag{3.20}$$

where $\vec{j}$ is the mass force (referred to unit mass);

<u>pressure forces</u> - equal to

$$\vec{P}_p = \iint_{S_V} p\vec{n}\, dS, \tag{3.21}$$

where $\vec{n}$ is the outward normal to the surface element dS;

p is the pressure at the given point — a force which is independent of the orientation of the surface to which it is applied;

<u>friction force</u> - which can be expressed in terms of the friction stress $\vec{\tau}_n$ as follows

$$\vec{P}_\tau = \iint_{S_V} \vec{\tau}_n\, dS; \tag{3.22}$$

<u>reaction force</u> - $\vec{P}_R$ of the solid bodies (if there are any) with which the surface S_V comes into contact.

Considering the expressions obtained above, we write the fluid momentum change law in the form

$$\iiint_V \frac{\partial(\rho\vec{w})}{\partial t}\, dV + \iint_{S_V} \rho\vec{w}w_n\, dS = -\iiint_V \rho\vec{j}\, dV - \iint_{S_V} p\vec{n}\, dS + \iint_{S_V} \vec{\tau}_n\, dS + \vec{P}_R. \tag{3.23}$$

Let us transform somewhat the integrals over the surface S_V. Since S_V can be represented as the sum of the lateral surface and the cross section area

$$S_V = S + 2F + \frac{\partial F}{\partial x} dx,$$

the double integrals in (3.23) will be

$$\left.\begin{aligned}
\iint_{S_V} \rho \vec{w} w_n dS &= \iint_F \rho \vec{w} w_n dF + \iint_{F+\frac{\partial F}{\partial x} dx} \rho \vec{w} w_n dF + \iint_S \rho \vec{w} w_n dS; \\
\iint_{S_V} \vec{p} n dS &= \iint_F \vec{p} n dF + \iint_{F+\frac{\partial F}{\partial x} dx} \vec{p} n dF + \iint_S \vec{p} n dS; \\
\iint_{S_V} \vec{\tau}_n dS &= \iint_F \vec{\tau}_n dF + \iint_{F+\frac{\partial F}{\partial x} dx} \vec{\tau}_n dF + \iint_S \vec{\tau}_n dS.
\end{aligned}\right\} \quad (3.24)$$

Considering that at the first section $w_n = -w_x$, $p = +p$, $\tau_n = -\tau_{xx}$, at the second section $w_n = w_x$, $p = -p$, $\tau_n = \tau_{xx}$, we project (3.23) onto the x-axis

$$\begin{aligned}
&\iiint_V \frac{\partial (\rho w_x)}{\partial \tau} dV + \iint_S \rho w_x w_n dS + \iint_{\frac{\partial F}{\partial x} dx} \rho w_x^2 dF = \\
&= \iiint_V \rho j_x dV - \iint_S p \cos(n, x) dS - \iint_{\frac{\partial F}{\partial x} dx} p \cos 0 dF + \\
&+ \iint_S \tau_{nx} dS + \iint_{\frac{\partial F}{\partial x} dx} \tau_{xx} dF.
\end{aligned} \quad (3.25)$$

Under the assumption that the area and the shape of the line section change sufficiently smoothly along the axis, the differential of the lateral surface of the isolated volume may be calculated as

$$dS = d\Pi dx, \quad (3.26)$$

where Π is the perimeter of the flow section; and the differential volume will be

$$dV = dF dx.$$

We divide both sides of (3.25) by dx and find the limits of each term as dx → 0:

$$\left.\begin{aligned}
&\lim_{dx\to 0}\frac{\iiint_V \varphi\, dF\, dx}{dx}=\iint_F \varphi\, dF;\\
&\lim_{dx\to 0}\frac{\iint_\Pi \varphi\, d\Pi\, dx}{dx}=\int_\Pi \varphi\, d\Pi;\\
&\lim_{dx\to 0}\frac{\iint_F \frac{\partial\varphi}{\partial x}dx\, dF}{dx}=\frac{\partial}{\partial x}\iint_F \varphi\, dF,
\end{aligned}\right\} \qquad (3.27)$$

where φ is the integrand.

Now (3.25) may be written as follows

$$\begin{aligned}
&\iint_F \frac{\partial(\rho w_x)}{\partial\tau}dF+\int_\Pi \rho w_x w_n\, d\Pi+\frac{\partial}{\partial x}\iint_F \rho w_x^2\, dF=\\
&=-\int_\Pi p\cos(\hat{n},x)\,d\Pi-\frac{\partial}{\partial x}\iint_F p\, dF+\int_\Pi \tau_{nx}\, d\Pi+\frac{\partial}{\partial x}\iint_F \tau_{xx}\, dF+\\
&+\iint_F \rho f_x\, dF.
\end{aligned} \qquad (3.28)$$

Let us transform some terms. We first calculate the partial derivative $\frac{\partial}{\partial\tau}\iint_F \rho w_x dF$. The change of $\iint_F \rho w_x dF$ with time can take place both due to the product ρw_x and as a result of a change of the cross section per unit time. The influence of the first factor is determined by the term $\iint_F \frac{\partial}{\partial\tau}(\rho w_x)dF$. Since the increment of the line flow area is expressed in terms of the projection of the velocity on the outward normal n' to the section contour by the expression (Figure 3.2)

$$dF=\int_\Pi w_n\cdot d\tau\, d\Pi,$$

then the second term will be equal to $\int_\Pi \rho w_x w_n\cdot d\Pi$.

We are considering the flow of viscous fluids. Therefore, on

the side surface S the tangential component $w_\tau = 0$ and the normal component $w_n = \pm|\vec{w}|$. The normal n' is drawn in the plane of the contour Π, i.e., it lies in the plane perpendicular to the Ox axis, while the normal n applies to the surface S. On the basis of the previously made assumption on the smoothness of the channel transition, we hypothesize that

$$w_{n'} \cong w_n. \tag{3.27}$$

Therefore, we can finally write that the first two terms of $(3.28)^{(1)}$ are equal to the partial derivative in question

$$\frac{\partial}{\partial \tau}\iint_F \rho w_x dF = \iint_F \frac{\partial}{\partial \tau}(\rho w_x) dF + \int_\Pi \rho w_x w_{n'} d\Pi. \tag{3.29}$$

Let us now examine the integral $\int_\Pi p\cos(n, x)d\Pi$. With a good degree of accuracy we can assume that the magnitude of the pressure varies little across the section, i.e., we can refer p to the center of the section. Then

$$\frac{\partial}{\partial x}\iint_F p dF = \frac{\partial}{\partial x}(pF) \tag{3.28}$$

(3.30)

and

$$\int_\Pi p\cos(n,x)d\Pi = p\int_\Pi \cos(n,x)d\Pi.$$

The integral $\int_\Pi \cos(n,x)d\Pi$ equals $-\frac{\partial F}{\partial x}$ to within small quantities of second order. Therefore, we finally obtain

$$\int_\Pi p\cos(n,x)d\Pi = -p\frac{\partial F}{\partial x}. \tag{3.31}$$

Footnote (1) appears on page 101

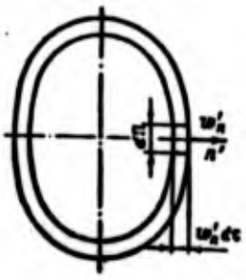

Figure 3.2. Line cross section.

Let us examine the integral $\int_{\Pi} \tau_{nx} d\Pi$. We denote the magnitude of the friction force acting per unit area of the lateral surface by Φ. Then, considering the fact that the direction of Φ is always opposing the direction of the mean velocity w and also considering the assumption made above that cos(n, x), is small, we obtain

$$\int_{\Pi} \tau_{nx} d\Pi = -\Phi\Pi. \tag{3.32}$$

Since $\tau_{xx} \ll p$, we neglect the term $\frac{\partial}{\partial x} \iint_F \tau_{xx} dF$ in comparison with the other terms of (3.28) i.e., we assume that

$$\frac{\partial}{\partial x} \iint_F \tau_{xx} dF = 0. \tag{3.33}$$

Let us turn to the last term of (3.28). The projection of the acceleration $\vec{j}$ on the x axis will be

$$j_x = -j \sin \alpha.$$

Averaging the fluid density across the section, we obtain

$$\iint_F \varrho j_x dF = -\varrho j \sin \alpha F. \tag{3.34}$$

Expressions (3.29) - (3.34) permit us to write (3.28) as follows

$$\frac{\partial}{\partial \tau} \iint_F \varrho w_x dF + \frac{\partial}{\partial x} \iint_F \varrho w_x^2 dF = -F \frac{\partial p}{\partial x} - \Phi\Pi - \varrho j \sin \alpha F. \tag{3.35}$$

Since the fluid mass flow rate

$$G=\iint_F \rho w_x dF, \tag{3.36}$$

and the projection of the momentum K on the x axis is defined by the expression

$$K=\iint_F \rho w_x^2 dF, \tag{3.37}$$

with the aid of the known formula

$$\Delta=\frac{\zeta}{g}\rho w^2, \tag{3.38}$$

we can reduce (3.35) to the form

$$\frac{\partial K}{\partial x}+\frac{\partial Q}{\partial t}=-F\frac{\partial p}{\partial x}-\frac{\zeta}{g}\rho\Pi w^2-\rho F j\sin\alpha, \tag{A}$$

where ζ is the hydraulic resistance coefficient, which is a function of the channel dimensions and shape, degree of roughness, fluid physical parameters, and the flow regime.

The resulting equation of fluid motion is most often used in this form in studying unsteady flows. We note that the flow rate G and the momentum K appearing in (A) are defined by the formulas

$$G=\rho wF; \tag{3.39}$$

$$K=\varepsilon Gw, \tag{3.40}$$

where ε is the Coriolis coefficient, accounting for the nonuniformity of the velocity distribution across the flow section (for a uniform velocity distribution $\varepsilon = 1$, for turbulent flow $\varepsilon = 1.02 - 1.03$, for laminar flow $\varepsilon = 1\frac{1}{3}$, for unsteady motion ε is, generally speaking, variable).

Equation (A) is not sufficient for the solution of many problems. Therefore, we also use the continuity equation, obtained from the con-

dition of conservation of the mass contained in the isolated fluid volume

$$\frac{d}{d\tau}\iiint_V \rho dV = 0.$$

The mass change with time for fluid motion takes place both as a result of density change (the term $\iiint_V \frac{\partial \rho}{\partial \tau} dV$), and volume change (the term $\iint_{S_V} \rho w_n dS$):

$$\iiint_V \frac{\partial \rho}{\partial \tau} dV + \iint_{S_V} \rho w_n dS = 0.$$

Hence, after familiar transformation we can obtain the conservation equation in the form

$$\frac{\partial G}{\partial x} + \frac{\partial (\rho F)}{\partial \tau} = 0. \qquad (B)$$

Equations (A) and (B) are quite general. They contain four unknowns: p, ρ , w or G and F. Therefore, in order to close the system, we must add to the above equations the equation of state of the fluid and the tubing wall deformation elastic law, i.e., the dependence of the area F on the pressure p.

The fluid density is a function of both the fluid pressure and temperature. But since we are examining isothermal flow of liquids, their equation of state is represented by Hooke's law

$$\rho = \rho^* \left(1 + \frac{p - p^*}{E'}\right), \qquad (C)$$

where ρ^* is the density at the pressure p^*;

E' is the liquid bulk modulus of elasticity, which depends in general case on pressure and temperature.

In the study of transient processes in LRE hydraulic lines the pressure changes are relatively small. Therefore, we shall assume the liquid bulk modulus of elasticity to be constant. The numerical values of E' for various liquids are shown in Table 1.

TABLE 1

Values of the Bulk Elastic Modulus,
Speed of Sound in an Infinite Fluid Volume, and Temperature
Coefficient for Several Liquids

Liquid	Temperature T°K	Bulk Elastic Modulus $E' \cdot 10^{-5}$ N/m^2	Speed of sound in infinite volume a_∞, m/sec	Temp. coefficient β_T, m/sec·deg
Nitric acid	289	31577	1425	—
Nitric tetroxide	289	30500	1465	—
Ammonia (aqueous solution)	289	—	1660	—
Aniline	293	27565	1659	-4.6
Benzene	293	15030	1324	-5.2
ADMH	277	18397	1502	—
Hydrogen (liquid)	20.3	4419	1127	-1.5
Kerosene	288	—	1330	
Oxygen (liquid)	307	11830	1295	-2
Nitromethane	89.4	9296	911	—
Methyl Alcohol	298	19586	1330	-4.8
Ethyl alcohol (95%)	293	9408	1123	-3.3
Toluene	293.5	8918	1213	-3.6
Tetranitromethane	293	14740	1320	-3.2
Water	293	17315	1039	-4
	293	21360	1483	+1.6

Assuming that the tubing wall material operates in the elastic deformation region and also obeys Hooke's law, in accordance with which

$$\frac{d - d^\circ}{d^\circ} = \frac{\chi}{2} \frac{p - p^\circ}{E}, \qquad (3.41)$$

and considering that $\Delta d = d - d^\circ \approx \frac{\Delta F}{2} = \frac{F - F^\circ}{2}$

$$\frac{F - F^\circ}{F^\circ} = \chi \frac{p - p^\circ}{E}$$

hence

$$F = F^{*}\left(1 + \chi \frac{p - p^{*}}{E}\right). \qquad (D)$$

where E is the tubing wall material elastic deformation modulus;
d,d* are respectively the tubing diameters for the liquid pressures p and p*.

The dimensionless coefficient χ depends on the wall thickness and the cross section shape. We shall show how χ is determined for thin-walled circular tubing of length l and thickness σ. With increase of the pressure by $\Delta p = p - p^{*}$, the increase of the force tending to burst the tubing is obviously $dl\Delta p$. Therefore, the increase of the tensile stresses in the wall longitudinal section will be

$$\Delta\sigma = \frac{dl\Delta p}{2l\delta} = \frac{\Delta p d}{2\delta}$$

In accordance with Hooke's law the relative elongation is

$$\frac{\Delta d}{d} = \frac{\Delta\sigma}{E} = \frac{d}{2\delta}\frac{(p - p^{*})}{E}$$

Comparing this expression with (3.41), we obtain $\chi = \frac{d}{\delta}$.

For thick-walled circular tubes

$$\chi = 2\mu + \frac{\frac{d}{\delta} + 2\mu + \frac{2\mu^{2}}{\frac{d}{\delta}}}{\frac{d}{\delta} + \frac{2\mu}{\frac{d}{\delta}}},$$

where μ is Poisson's ratio.

The value of the coefficient χ for polygonal and oval tubes was obtained by Dvukhsherstov [52]

$$\chi = (1 - \mu^{2})(1 + \chi_{2}l^{2})\chi_{1}l,$$

where x_1, x_2 are dimensionless form factors of the tube cross section, shown in Table 2;

$$\bar{s} = \frac{s}{b};$$

l_0 is the characteristic linear dimension, whose values are also shown in Table 2.

TABLE 2

Values of the Quantities l_0, x_1 and for Tubes of Different Cross Sections

Tube cross section shape	x_1	l_0	x_2
Circle of diameter d	2	d	0
Rectangle with ratio of short to long side equal to α (larger side is c)	$1+\alpha$	c	$\frac{5(1+\alpha^2)(1+\alpha^3)-3(1+\alpha^5)-15\alpha^2(1+\alpha)}{60\alpha(1+\alpha)}$
Regular triangle with side c	$\frac{2}{\sqrt{3}}$	c	0,2
Regular 2n-gon with circumscribed circle of diameter d	$2\cos\frac{\pi}{2n}$	d	$\frac{1}{15}\sin^2\frac{\pi}{2n}\operatorname{tg}^2\frac{\pi}{2n}$
Oval with ratio of short and long axes equal to α (long axis equals c)	$\frac{(1+\alpha)(5-2\alpha+5\alpha^2)}{(-1+10\alpha-\alpha^2)}$	c	$\frac{81}{128}\frac{1}{Z}(1-\alpha)^4(-65+194\alpha-65\alpha^2)\times$ $\times\sqrt{(2-\alpha)(2\alpha-1)}$, where $Z=(5-2\alpha+5\alpha^2)[(2-5\alpha+2\alpha^2)5(1+\alpha)+$ $+2(-1+7\alpha-\alpha^2)\sqrt{(2-\alpha)(2\alpha-1)}]$

The following formulas were obtained in [113] for the coefficient χ for the cooling passage of a LRE combustion chamber with corrugated spacers

$$\chi=\frac{b^2}{h_1(b-2\delta_r)}\left\{0{,}0142\,b^3\left(\frac{1}{\delta_1^3}+\frac{1}{\delta_2^3}\right)+\frac{1}{h_r}\left[\frac{h_1}{2}+\right.\right.$$
$$\left.\left.+0{,}785\,r\left(1+5{,}44\,\frac{r^2}{\delta_r^2}\right)\right]\right\}+\frac{h_1 d_{cp}}{d_1\delta_1+d_2\delta_2},$$

where b is the corrugation pitch;

$$h_1=h-\delta_r;$$

δ_{corr} and h are respectively the corrugation thickness and height;
δ_1, δ_2, d_1, d_2 are respectively the thickness and diameter of the inner and outer walls of the combustion chamber;
r is the corrugation radius.

We can also use the following formula of [113] to find the coefficient χ of the chamber head

$$\chi=\frac{3(1-\mu)r^3}{8\delta(3R-h)},$$

where r and δ are respectively the radius and thickness of the combustion chamber head;
h is the height of the spherical segment formed by the head.

2. Transformations of the basic equations

We shall make some transformations of the basic equations (A) - (D) which describe unsteady fluid flow.

Since we have considered pressure changes such that Hooke's law is applicable for the liquid and the line wall,

$$p-p^0\ll E' \quad \text{and} \quad \chi(p-p^0)\ll E.$$

Therefore, Equations (C) and (D) can be written as follows to within small quantities of second order(1)

Footnote (1) appears on page 101.

$$\left.\begin{aligned} \rho &= \rho^{\circ} \exp \frac{p-p^{\circ}}{E'}; \\ F &= F^{\circ} \exp \chi \frac{p-p^{\circ}}{E}. \end{aligned}\right\} \tag{3.42}$$

Multiplying these expressions and differentiating with respect to τ, we obtain

$$\frac{\partial(\rho F)}{\partial \tau} = \rho F \frac{\left(1+\chi\frac{E'}{E}\right)}{E'} \frac{\partial p}{\partial \tau} \tag{3.43}$$

Zhukovskey showed [59] that for circular lines the speed of sound in a flowing liquid is defined by the formula

$$a = \frac{a_{\infty}}{\sqrt{1+\chi\frac{E'}{E}}} \tag{3.44}$$

This was also shown by Dvukhsherstov [52] for lines of complex cross section.

The quantity $a_{\infty} = \sqrt{\frac{E'}{\rho}}$ defines the so-called sound speed in an infinite fluid volume. The values of a_{∞} for various liquids are shown in Table 1. The temperature dependence of a_{∞} obeys the law

$$a_{T\infty} = a^{\circ}_{\infty} + \beta_T (T - T^{\circ}),$$

where a°_{∞} is the sound speed at the temperature T°;
T is the temperature for which the quantity a is calculated;
β_T is the temperature coefficient, whose value is shown in Table 1.

Expression (3.44) makes it possible to write the derivative (3.43) as follows

$$\frac{\partial(\rho F)}{\partial \tau} = \frac{F}{a^2} \frac{\partial p}{\partial \tau} \tag{3.45}$$

As is known, the sound speed for a gas can be written in the form

$$a^2 = \frac{dp}{d\rho} \tag{3.46}$$

Therefore

$$\frac{\partial \rho}{\partial \tau} d\tau + \frac{\partial \rho}{\partial x} dx = \frac{1}{a^2}\left(\frac{\partial p}{\partial \tau} d\tau + \frac{\partial p}{\partial x} dx\right).$$

Since d^{τ} and dx are arbitrary increments,

$$\frac{\partial \rho}{\partial \tau} = \frac{1}{a^2} \frac{\partial p}{\partial \tau}.$$

If we take $\frac{\partial F}{\partial \tau} = 0$, for a gas, which is very close to reality, the result obtained is analogous to the Expression (3.45) for a liquid.

Replacing the momentum in (A), using (3.40), and substituting (3.45) into (B), we obtain the differential equations of unsteady motion for both liquid and gas

$$\left.\begin{aligned} -F\frac{\partial p}{\partial x} &= \frac{\partial G}{\partial \tau} + \frac{\partial (GG\omega)}{\partial x} + \frac{\zeta}{2}\frac{G}{d_0}\omega + \rho g \sin\alpha \cdot F; \\ -F\frac{\partial p}{\partial \tau} &= a^2 \frac{\partial G}{\partial x}. \end{aligned}\right\} \tag{E}$$

These first order partial differential equations are nonlinear equations of the hyperbolic type.. Their solution has been obtained under various simplifications for specific problems (see [47] and [145]). If we consider liquid flows at subsonic velocities, then both the dynamic head and its change, and the change of the flow rate due to density changes can be neglected. Then we can write

$$F\frac{\partial}{\partial x}(\rho\omega^2) = 0; \quad F\omega\frac{\partial \rho}{\partial x} = 0; \quad F\omega\frac{\partial \rho}{\partial \tau} = 0.$$

In this case the Equations (E) are written as

$$\left.\begin{aligned} -F\frac{\partial p}{\partial x} &= \rho\frac{\partial (F\omega)}{\partial \tau} + \rho\omega^2\left(\pm\frac{\partial F}{\partial x} + \frac{\zeta}{2d_0}F\right) + \rho g \sin\alpha \cdot F; \\ -F\frac{\partial p}{\partial \tau} &= \rho a^2 \frac{\partial (F\omega)}{\partial x}. \end{aligned}\right\} \tag{F}$$

In the case of a rigid line with very slight change of the cross section, i.e., for F = const, the differential Equations (E) can be reduced to the form

$$\left.\begin{aligned} -\frac{\partial p}{\partial x} &= \varrho\left(\frac{\partial w}{\partial \tau}+\frac{\zeta}{2d_{\text{э}}}\varrho w^2+\varrho j\sin\alpha;\right.\\ -\frac{\partial p}{\partial \tau} &= \varrho a^2\frac{\partial w}{\partial x}. \end{aligned}\right\} \qquad (G)$$

(3.46)

3. Equation of motion of components in hydraulic lines

We shall obtain the equation of motion of the components in LRE hydraulic lines under the following simplifying assumptions [148], [184]: 1) the liquid motion is one-dimensional, i.e., $w_x = w$, $w_y = 0$, $w_z = 0$, $\frac{\partial w_y}{\partial \tau} = 0$, $\frac{\partial w_z}{\partial \tau} = 0$; 2) the liquid is incompressible; 3) the line walls are rigid; 4) the motion of the components in the injectors, head, and cooling passage of the combustion chamber is inertialess; 5) the local losses and friction losses are referred to the dynamic head $\varrho\frac{w^2}{2}$, in the line, i.e., all losses are essentially concentrated at a single section, for example, at the line exit — just upstream of the head or the collector manifold.

(E)

Under these assumptions the equation of unsteady motion of the component will have the form [73]

$$\left[z_{\text{н}}\varrho(g\sin\alpha_1+j_x\cos\alpha_2)+p_{\text{н}}+\varrho\frac{w_{\text{н}}^2}{2}\right]-\left[\varrho(g\sin\alpha_1+j_x\cos\alpha_2)+\right.$$
$$\left.+p_{\text{к}}+\varrho\frac{w_{\phi}^2}{2}\right]=\varrho\frac{dw}{d\tau}l+\left(\zeta_{\text{н}}+\zeta_{\text{тр}}\frac{l}{d_{\text{э}}}\right)\frac{\varrho w^2}{2}, \qquad (3.47)$$

(F)

where $w_{\text{н}}, w_{\phi}, w$ are respectively the component velocity at the line inlet, in the injectors, and at the end of the line (just upstream of the head or collector), in m/sec;

$z_{\text{Н}}, z_{\text{К}}$ are the locations of the initial line section and the injector head, measured from an arbitrary level, in m;

α_1, α_2 are the inclinations of the line axis to the horizontal and to the direction of the flight vehicle acceleration;

p_H, p_K are the pressures at the line entrance section and in the combustion chamber, in N/m^2;

ζ are the local loss and friction loss coefficients;

j_z is the vehicle axial acceleration, in m/sec^2;

d_e is the equivalent line diameter, in meters.

From the continuity equation for different sections of the line it is easy to obtain

$$F_H w_H = F w = F_\Phi w_\Phi.$$

With the aid of these Equalities (3.47) may be written as

$$p_H - p_K = \frac{G^2}{2\rho F^2}\left[\zeta_{in} + \zeta_{tr}\frac{l}{d_e} + \frac{F^2}{F_\Phi^2}\left(1 - \frac{F_\Phi^2}{F_H^2}\right)\right] + \frac{l}{F}\frac{dG}{dt} - \rho(z_H - z_K)(g\sin\alpha_1 + j_z\cos\alpha_1). \tag{3.48}$$

The difference of the geometric levels of the sections "H" and "K" can be expressed as follows:

1) if the component flows through the combustion chamber cooling passage, then

$$z_H - z_K = (l - l_{cool})\sin\alpha_1,$$

where l_{cool} is the length of the cooled segment along the chamber axis;

2) if the component flows directly to the head, then

$$z_H - z_K = l\sin\alpha_1.$$

We introduce the notations

$$\left.\begin{aligned} b_1 &= \frac{1}{2\rho F^2}\left[\zeta_{in} + \zeta_{tr}\frac{l}{d_e} + \frac{F^2}{F_\Phi^2}\left(1 - \frac{F_\Phi^2}{F_H^2}\right)\right]; \\ b_2 &= \frac{l}{F}; \\ p_z &= \rho(l - l_{cool})\sin\alpha_1(g\sin\alpha_1 + j_z\cos\alpha_1). \end{aligned}\right\} \tag{3.49}$$

Then the equation of motion of the components in the hydraulic line can be written as follows

$$p_1 = p_2 - p_3 + b_1 G^2 + b_2 \frac{dG}{d\tau} \qquad (3.50)$$

This expression is sometimes termed the equation of motion of a liquid with lumped parameters.

If the inertial forces in the head and in the cooling passage are large and the dynamic head losses in the line lead to large errors, then we must break the line down into individual segments and write (3.50) for each segment. In this case the influence of the liquid column can be neglected and the coefficient ε can be taken equal to some average value. Under these assumptions (E) is written in the form

(3.48)

$$-F\frac{dp}{dx} = \frac{dG}{d\tau} + \frac{\varepsilon G^2}{\varrho}\frac{d\left(\frac{1}{F}\right)}{dx} + \frac{\zeta G^2}{2\varrho d_3 F}$$

We integrate in the limits from one section to the other

$$p_1 - p_2 = \frac{dG}{d\tau}\int_0^l \frac{dx}{F} + \frac{\varepsilon G^2}{\varrho}\int_0^l \frac{1}{F}\frac{d}{dx}\left(\frac{1}{F}\right)dx + \frac{G^2}{8\varrho}\int_0^l \frac{\zeta\Pi}{F^3}dx.$$

Denoting

$$\int_0^l \frac{dx}{F} = b_2,$$

we obtain

$$p_1 = p_2 + \left[\varepsilon\left(\frac{1}{F_2^2} - \frac{1}{F_1^2}\right) + \frac{1}{4}\int_0^l \frac{\Pi}{F^3}\zeta\, dx\right]\frac{G^2}{2\varrho} + b_2\frac{dG}{d\tau}.$$

(3.49)

Hence

$$p_1 = p_2 + b_1 G^2 + b_2\frac{dG}{d\tau}, \qquad (3.51)$$

where

$$b_1=\frac{1}{2g}\left[\zeta\left(\frac{1}{F_2^2}-\frac{1}{F_1^2}\right)+\frac{1}{4}\int_0^l\frac{\Pi\zeta}{F^3}\,dx\right];$$

$$b_2=\int_0^l\frac{dx}{F}\cong\sum_{i=1}^{m}\frac{\Delta x_i}{F_i}.$$

We represent the loss coefficient ζ by the formula

$$\zeta=\zeta_1+\frac{\zeta_2}{\mathrm{Re}^{n_1}},$$

where ζ_1, ζ_2, n_1 are known constant coefficients;

$$\mathrm{Re}=\frac{4Q}{\Pi\eta_{liq}};$$

η_{liq} is the fluid dynamic viscosity.

Then

$$\int_l^l\frac{\Pi\zeta}{F^3}\,dx=\zeta_1\int_0^l\frac{\Pi}{F^3}dx+\frac{\zeta_2}{Q^{n_1}}\int_0^l\frac{\Pi}{F^3}\left(\frac{\Pi\eta_{liq}}{4}\right)^{n_1}dx=c_1+c_2Q^{-n_1}.$$

For the line of constant section and for ζ = const we have

$$b_1=\frac{\zeta}{2gF^2d_0};$$

$$b_2=\frac{l}{F}.$$

§ 3. Equations of Pump Dynamics

We shall derive the equation for unsteady liquid motion in a centrifugal pump. We break the entire pump passage into three segments (Figure 3.3): 1) the inlet duct; 2) the impeller channels; 3) the outlet arrangement, i.e., spiral and conical diffusers, and we follow the movement of the component from the inlet duct to the exit from the diffuser.

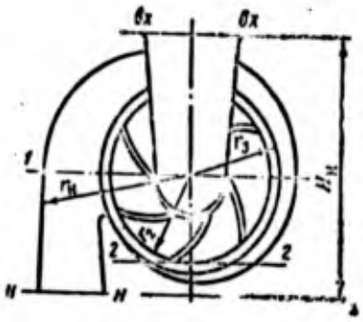

Figure 3.3. Diagram for derivation of pump dynamic equation.

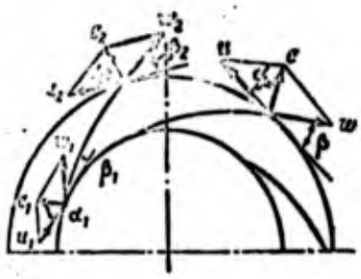

Figure 3.4. Diagram of velocities in pump blades.

We write the Bernoulli equation for the unsteady fluid motion in the inlet duct in the form

$$\rho z_{вх}(g\sin\alpha_1 + j_x\cos\alpha_2) + p_{вх} + \frac{\rho c_{1x}^2}{2} = \rho z_1(g\sin\alpha_1 + j_x\cos\alpha_2) +$$

$$+ p_1 + \frac{\rho c_1^2}{2} + \Delta p_{пот} + \frac{dG}{d\tau}\int_{(вх)}^{(1)} \frac{dx}{F(x)},$$

where Δp_{loss} — are the hydraulic losses;
c — is the absolute fluid motion velocity.

Neglecting the difference of the levels of the sections in question, with account for the transformations made in the preceding section we can write

$$p_{вх} - p_1 = \frac{\rho}{2}(c_1^2 - c_{1x}^2) + b_{1вх}G^2 + b_{2вх}\frac{dG}{d\tau}. \qquad (3.52)$$

Now let us examine the motion of the component in the impeller channel (Figure 3.4). The angular momentum of the fluid flowing in the blades relative to the axis of rotation may be expressed as follows with the aid of the known theorem of mechanics

$$M = \frac{d}{d\tau}\int_{(1)}^{(2)} rc\,dm,$$

where d_m is the elementary mass, equal to $\rho F dx$;

c_u is the projection of the absolute velocity on the circumferential component, equal to

$$u - w\cos\beta,$$

u and w are the circumferential and relative velocities;

r is the instantaneous radius;

β is the angle between the relative and circumferential velocity vectors.

We substitute in place of dm and c_u their values and with account for the fact that $\frac{dx}{d\tau} = w$, we find

$$M = r(u - w\cos\beta)\rho F w \Big|_{(1)}^{(2)} + \int_{(1)}^{(2)} r\rho F\left(\frac{du}{d\tau} - \frac{dw}{d\tau}\cos\beta\right) dx. \tag{3.53}$$

We know from theoretical mechanics that the power N is equal to the time rate of change of the kinetic energy. Therefore, we can write for the fluid flowing through the pump impeller channels

$$N = \frac{d}{d\tau}\int_{(1)}^{(2)} \frac{c^2}{2} dm$$

Since

$$dm = \rho F dx$$

and $c^2 = w^2 + u^2 - 2wu\cos\beta$,
then

$$N = \frac{1}{2}(w^2 - 2wu\cos\beta + u^2)\rho F w \Big|_{(1)}^{(2)} + \int_{(1)}^{(2)}\left[w\frac{dw}{d\tau} + u\frac{du}{d\tau} - \left(w\frac{du}{d\tau} + u\frac{dw}{d\tau}\right)\cos\beta\right]\rho F dx. \tag{3.54}$$

On the other hand, the power of the flowing fluid is defined by the formula

Equat
and at the

Since
that wF =
pression w

For r
losses in
formation
These loss
of the flo

where

ζ_{fr}

$$N = M\omega + p_1 F_1 w_1 - p_2 F_2 w_2. \tag{3.55}$$

Equating (3.54) and (3.55) with account for (3.53) for the torque and at the same time replacing $r\omega$ by u, we obtain

$$p_1 F_1 w_1 - p_2 F_2 w_2 = \frac{1}{2}(w^2 - 2wu\cos\beta + u^2)\varrho F w \Big|_{(1)}^{(2)} +$$
$$+ \int_{(1)}^{(2)} \left[w\frac{dw}{d\tau} + u\frac{du}{d\tau} - \left(w\frac{du}{d\tau} + u\frac{dw}{d\tau} \right)\cos\beta \right] \varrho F dx -$$
$$- u(u - w\cos\beta)\varrho F w \Big|_{(1)}^{(2)} + \int_{(1)}^{(2)} u\varrho F \frac{dw}{d\tau}\cos\beta dx -$$
$$- \int_{(1)}^{(2)} u\varrho F \frac{du}{d\tau} dx.$$

Since for an incompressible fluid the continuity equation implies that wF = const, after some transformations we can obtain from the expression written above

$$p_1 - p_2 = \frac{\varrho}{2}\left[(u_1^2 - w_1^2) - (u_2^2 - w_2^2)\right] + \varrho \int_{(1)}^{(2)} \left(\frac{dw}{d\tau} - \frac{du}{d\tau}\cos\beta \right) dx. \tag{3.56}$$

For real fluid flows it is necessary to take into account the losses in the blades, which are made up from the friction loss, eddy formation loss, separation zone formation loss, and so on (see [104]). These losses $\Delta_{b\pi}$ may be considered to be proportional to the square of the flow rate, i.e.,

$$\Delta p_{1,2} = b_{1,2} G^2, \tag{3.57}$$

where

$$b_{1,2} = \zeta_{fr.b,2}\frac{l_2}{2\varrho d_e \tilde{F}^2} + \frac{\zeta_{vf.b,2}}{2\varrho F_1^2}$$

$\zeta_{fr.b}$ and $\zeta_{vf.b}$ are respectively the blade friction and eddy formation coefficients;

$\tilde{d}_e$ and $\tilde{F}$ are the mean equivalent diameter and the mean flow area of the blade channel;

F_1 is the inlet section area;

l_b is the length of the fluid motion path in the pump blades.

Thus, with account for the losses (3.56) is written as:

$$p_1 - p_2 = \frac{\varrho}{2}\left[(u_1^2 - w_1^2) - (u_2^2 - w_2^2)\right] + \varrho \int_{(1)}^{(2)} \left(-\frac{dw}{d\tau} - \right.$$
$$\left. - \frac{du}{d\tau}\cos\beta\right) dx + b_{1\text{в}} G^2. \qquad (3.58)$$

The pressure rise in the diffuser is determined from the Bernoulli equation for unsteady motion in a fashion analogous to the procedure for the inlet duct

$$p_2 - p_{\text{н}} = \frac{1}{2}\varrho(c_{\text{н}}^2 - c_2^2) + b_{1\text{д}} G^2 + b_{2\text{д}} \frac{dG}{d\tau}. \qquad (3.59)$$

The resulting equations (3.52), (3.58) and (3.59) make it possible to determine the pressure change in the pump from the inlet duct to the outlet

$$p_{\text{н}} - p_{\text{вх}} = \frac{1}{2}\varrho(c_2^2 - c_{\text{н}}^2 + u_2^2 - w_2^2 - u_1^2 + w_1^2 - c_1^2 + c_{\text{вх}}^2) -$$
$$- (b_{1\text{к}} + b_{1\text{д}} + b_{1\text{вх}}) G^2 - \left[b_{2\text{д}} + b_{2\text{вх}} - \varrho \int_{(1)}^{(2)} \left(\frac{dw}{d\tau} - \right.\right.$$
$$\left.\left. - \frac{du}{d\tau}\cos\beta\right) dx\right] \frac{dG}{d\tau}. \qquad (3.60)$$

From this it is not difficult to find the pump head in the steady regime, when $\frac{dG}{d\tau} = 0$:

$$p_{\text{н}}^*(G, w) = \frac{1}{2}\varrho\left[(c_2^2 - c_{\text{н}}^2) + (u_2^2 - w_2^2) - (u_1^2 - w_1^2) - (c_1^2 - c_{\text{вх}}^2)\right] -$$
$$- b_{1\text{н}} G^2, \qquad (3.61)$$

where $$b_{1\text{н}} = b_{1\text{к}} + b_{1\text{д}} + b_{1\text{вх}}.$$

With account for this expression, the equation of the pump dynamics will have the form

$$p_{\text{н}} - p_{\text{вх}} = p_{\text{н}}^*(G, w) - (b_{2\text{д}} + b_{2\text{вх}}) \frac{dG}{d\tau} - \varrho \int_{(1)}^{(2)} \left(\frac{dw}{d\tau} - \right.$$
$$\left. - \frac{du}{d\tau}\cos\beta\right) dx. \qquad (3.62)$$

in the

The coefficients b_{2d} and b_{2in} are calculated similarly to the preceding calculation:

$$b_{2вх}=\int_{(вх)}^{(1)}\frac{dx}{F}\approx\sum_{i=1}^{m_1}\frac{\Delta x_{i вх}}{F_{i вх}};$$

(3.58)

$$b_{2i}\approx\sum_{i=1}^{m_1}\frac{\Delta x_{i1}}{F_{i1}}+\sum_{i=1}^{m_2}\frac{\Delta x_{i сп}}{F_{i сп}}\approx\sum_{i=1}^{m_1}\frac{\Delta x_{i1}}{F_{i1}}+\frac{l_{сп}}{\bar{F}_{сп}},$$

ernoulli
edure

where l_{sp} is the length of the spiral middle line;
F_{sp} is the average value of the spiral flow area.

(3.59)

Now we calculate the integral of (3.62)

$$\int_{(1)}^{(2)}\varrho\left(\frac{dw}{d\tau}-\frac{du}{d\tau}\cos\beta\right)dx=\int_{(1)}^{(2)}\varrho\frac{dw}{d\tau}dx-\int_{(1)}^{(2)}\varrho r\cos\beta\frac{d\omega}{d\tau}dx.$$

possible
ct to the

Since the velocity in the impeller channel is defined by the formula

(3.60)

$$w=\frac{Q}{2\pi r b_{2K}\sin\beta\varphi\varrho}$$

where b_{2K} is the blade width;
φ is the constriction factor, equal to $1-\frac{\delta_K i}{2\pi r\sin\beta}$;
σ_K is the rotor blade thickness;
i is the number of blades,

e steady

(3.61)

then the first integral of the expression written above will be

$$\int_{(1)}^{(2)}\varrho\frac{dw}{d\tau}dx=\sum_{i=1}^{m_1}\frac{\Delta x_i}{2\pi r_i b_{2i}\sin\beta_i\cdot\varphi_i}\frac{dQ}{d\tau}.$$

dynamics

The second integral is easily found:

$$\int_{(1)}^{(2)}\varrho r\cos\beta\cdot\frac{d\omega}{d\tau}dx=\varrho\sum_{i=1}^{m_1}r_i\cos\beta_i\cdot\Delta x_i\frac{d\omega}{d\tau}.$$

(3.62)

These formulas make it possible to write (3.62) for the pump head in the transient regimes in the form

$$p_н - p_{нх} = p_н^*(G, \omega) - b_{2н}\frac{dG}{d\tau} + b_{3н}\frac{d\omega}{d\tau} \qquad (3.63)$$

where

$$b_{2н} = \sum_{i=1}^{m_1}\frac{\Delta x_{i\,вх}}{F_{i\,вх}} + \sum_{i=1}^{m_2}\frac{\Delta x_{i\,л}}{F_{i\,л}} + \sum_{i=1}^{m_3}\frac{\Delta x_{i\,сн}}{F_{i\,сн}} + \sum_{i=1}^{m_4}\frac{\Delta x_i}{2\pi r_i b_{2ni}\sin\beta_i \cdot \eta_i},$$

$$b_{3н} = \varrho\sum_{i=1}^{m_5} r_i\cos\beta_i \cdot \Delta x_i.$$

Assuming that the losses in the pump are proportional to the square of the flow rate and using (2.16), it is not difficult to obtain the approximate equation for the pump dynamics in a somewhat different form (for constant volumetric efficiency)

$$p_н - p_{нх} = a_{1н}\omega^2 - a_{2н}\omega G - b_{1н}G^2 - b_{2н}\frac{dG}{d\tau} + b_{3н}\frac{d\omega}{d\tau} \qquad (3.64)$$

where $a_{1н} = \eta_л r_2^2\varrho + a_{1y.т}$;

$$a_{2н} = \frac{\eta_л \operatorname{ctg}\beta_2}{2\pi\eta_2 b_{н2}\eta_{об}} + a_{2y.т};$$

$$b_{1н} = b_{1нг} + b_{1л} + b'_{1сн} + b_{1н.п} + b_{1y.т}.$$

The coefficient $b_{1\,b}$ is found from the formulas

$$b_{1нг} = \frac{1}{2\varrho}\left[\varrho\left(\frac{1}{F_1^2} - \frac{1}{F_{вх}^2}\right) + \frac{\rho_{вх}}{4}\sum_{i=1}^{m_1}\frac{\Pi_{i\,вх}}{F_{i\,вх}^2}\Delta x_{i\,вх}\right].$$

The coefficient $b_{1\,in}$ can be found from an approximate formula (see [3.57]) or from the following more exact formula

$$b_{1л} = \sum_{i=1}^{m_6}\zeta_{i\,p.л}\frac{\Delta x_{i\,л}}{d_{э\,i}F_i\varrho} + \frac{\zeta_{в.л}}{2\varrho F_1^2}.$$

mp head

The friction loss coefficient $b'_{1\ sp}$ in the spiral diffuser is found from the formula

(3.63)

$$b'_{1\,sp}=\sum_{i=1}^{m_3}\zeta_{fr.sp}\frac{\Delta x_i}{2gd_{e\,i}F_i^2}.$$

The coefficient accounting for the losses in the conical diffuser is defined by the expression

$$b_{1\,sh}=\frac{\zeta_{con}\varepsilon_{con}^2}{2gF_{in}^2},$$

where ε_{con} is the coefficient of nonuniformity of the velocity field at the entrance to the conical diffuser;

F_{in} is the conical diffuser inlet area;

ζ_{con} is the loss coefficient, equal to [104]

ne
o obtain
fferent

$$\zeta_{con}=\frac{\zeta_{fr}}{8\sin\gamma/2}\left(1-\frac{F_{in}^2}{F_{out}^2}\right)+\sin\gamma\left(1-\frac{F_{in}^2}{F_{out}^2}\right)^2;$$

(3.64)

where γ is the diffuser cone angle;

F_{out} is the diffuser outlet area.

Now let us examine the losses associated with the sudden velocity change, which are termed shock losses [104]

$$\Delta p_{y.s}=\zeta_{y.s}\left(1-\frac{r_3^2}{r_4^2}\right)\rho\frac{c_{3u}^2}{2}$$

We substitute here $c_{3u}^2=\frac{1}{\rho^2r_3^2}(a_1\omega-a_2G)^2$:

mula

$$\Delta p_{y.s}=\frac{\zeta_{y.s}}{2gr_3^2}\left(1-\frac{r_3^2}{r_4^2}\right)(a_1^2\omega^2+a_2^2G^2-2a_1a_2\omega G).$$

This expression makes it possible to find the values of the coefficients $a_{1\ sh}$, $a_{2\ sh}$, and $b_{1\ sh}$

$$a_{1\gamma\kappa}=\frac{\zeta_{\gamma\kappa}}{2}\left(1-\frac{r_3^2}{r_4^2}\right)\varphi_\kappa^2 r_2^2\omega;$$

$$a_{2\gamma\kappa}=\frac{\zeta_{\gamma\kappa}\left(1-\frac{r_3^2}{r_4^2}\right)\varphi_\kappa^2 \operatorname{ctg}\beta_2}{2\pi\varphi_2\eta_{0\kappa}b_{\kappa 2}};$$

$$b_{1\gamma\kappa}=\frac{\zeta_{\gamma\kappa}\left(1-\frac{r_3^2}{r_4^2}\right)\varphi_\kappa^2 \operatorname{ctg}^2\beta_2}{8\pi^2\varphi_2^2\eta_{0\kappa}^2 r_2^2 b_{\kappa 2}^2 Q}.$$

Now we obtain the equation for the pump power in the unsteady flow case. To do this we use (3.53) and (3.55)

$$N=G\left[\omega^2\left(r_2^2-r_1^2\right)-\omega\left(w_2 r_2\cos\beta_2-w_1 r_1\cos\beta_1\right)+\frac{p_1-p_2}{\varrho}\right]+$$
$$+\omega\varrho\int_{(1)}^{(2)} rF\left(r\frac{d\omega}{d\tau}-\frac{dw}{d\tau}\cos\beta\right)dx. \qquad (3.65)$$

The first term is the expression for the pump power in the steady regime $N'(G,\omega)$. The integral of the dynamic component of the power is expressed analogously

$$\int_{(1)}^{(2)} rF\left(r\frac{d\omega}{d\tau}-\frac{dw}{d\tau}\cos\beta\right)dx=\frac{d\omega}{d\tau}\sum_{i=1}^{m_i} r_i^2 F_i\Delta x_i-$$
$$-\frac{1}{\varrho}\frac{dG}{d\tau}\sum_{i=1}^{m_i} r_i\cos\beta_i\Delta x_i.$$

Denoting the sums appearing in this equality by A_1/ϱ and A_2, we obtain the dynamic pump power equation in final form

$$N(G,\omega)=N^*(G,\omega)+\left(A_1\frac{d\omega}{d\tau}-A_2\frac{dG}{d\tau}\right)\omega. \qquad (3.66)$$

Hence, with the aid of the known relation $N=M\omega$ it is not difficult to write the equation for the pump torque in the variable regimes

$$M(G,\omega)=M^*(G,\omega)+A_1\frac{d\omega}{d\tau}-A_2\frac{dG}{d\tau}. \qquad (3.67)$$

Let
tank to t
the forci
exit at t

where
w_t
a_{1t}

If t
F_t = cons

and

The
the inert
the pressu

§ 4. Equation of Motion of the Components From the Tank to the Combustion Chamber

Let us examine the motion of the propellant components from the tank to the combustion chamber (see the schematic in Figure 3.5). If the forcing pressure in the tank is p_t then the pressure at the tank exit at the section "1t - 1t" is determined by the expression

$$p_{1t}=p_t+\frac{1}{2}\rho(w_t^2-w_{1t}^2)+\rho H_t(g\sin\alpha_{1t}+j_x\cos\alpha_{2t})-$$
$$-\rho\int_{x_t}^{x_{1t}}\frac{dw}{d\tau}dx-\Delta p_t. \qquad (3.68)$$

where Δp_t are the hydraulic pressure losses in the tank;

w_t and w_{1t} are the component velocities in the tank at the sections "t - t" and "1t - 1t";

α_{1t} and α_{2t} are the inclinations of the tank longitudinal axis to the horizon and the rocket axis;

x is the coordinate along the axis;

H_t is the liquid level in the tank, which is a function of engine operating time

$$H_t=H_t^0-\int_0^\tau\frac{G}{\rho F_t}d\tau.$$

If the component flow rate is constant and the cross section area F_t = const, then

$$H_t=H_t^0-\frac{G\tau}{\rho F_t}$$

and

$$\frac{1}{2}\rho(w_t^2-w_{1t}^2)=0.$$

The liquid velocity in the tank is low and therefore we can ignore the inertia forces and the losses in the tank [Equation [3.8]). Then the pressure variation in the tank will be

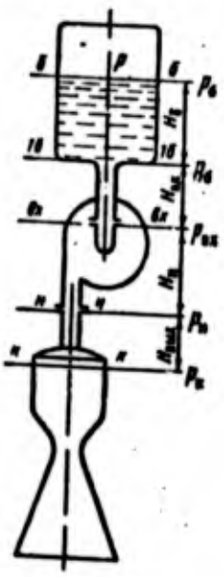

Figure 3.5. Diagram for derivation of flow equation for propellant from tank into combustion chamber.

$$p_{16} - p_6 = \varrho H_6(\tau)(g \sin\alpha_{16} + j_x \cos\alpha_{26}).$$

(3.69)

We write the equation for the unsteady motion of the component along the segment from the tank exit to the pump inlet

$$p_{ex} - p_{16} = \varrho H_{ex}(g \sin\alpha_{1ex} + j_x \cos\alpha_{2ex}) + \frac{1}{2}\varrho(w_{16}^2 - w_{ex}^2) - \varrho\int_{x_{16}}^{x} \frac{dw}{d\tau} dx - \Delta p_{ex},$$

where Δp_{in} are the hydraulic losses along the segment "lt" - "in";

H_{in} is the difference of the heights of the initial and final sections;

α_{1in} and α_{2in} are respectively the inclinations of the line to the horizon and to the rocket axis.

Considering that $w = \frac{G}{\varrho F}$ and the losses are proportional to the velocity head, we obtain

$$p_{ex} - p_{16} = \varrho H_{ex}(g \sin\alpha_{1ex} + j_x \cos\alpha_{2ex}) - b_{1ex} G^2 - b_{2ex} \frac{dG}{d\tau}. \quad (3.70)$$

Here

$$b_{1ex} \cong \frac{1}{2\varrho}\left[\left(\sum_{i=1}^{m_3} \frac{\zeta_{wi}}{F_i^2} + \sum_{i=1}^{m_3} \frac{\zeta_{tpi}\Delta x_i}{d_{hi}F_i^2}\right) + \frac{1}{F_{ex}^2}\left(1 - \frac{F_{ex}^2}{F_{16}^2}\right)\right]; \quad (3.71)$$

$$b_{2ex}=\int_{x_{16}}^{x_{ex}}\frac{dx}{F}\cong\sum_{i=1}^{m_5}\frac{\Delta x_i}{F_i};\qquad(3.72)$$

m_5 is the number of local resistances;

m_6 is the number of line segments with constant cross section.

For a cylindrical line of constant section the formulas for the coefficients b_{1in} and b_{2in} are considerably simplified

$$b_{1ex}=\frac{1}{2\varrho F_{ex}^2}\left(\zeta_{in}+\zeta_{tp}\frac{l_{ex}\pi d}{4F_{ex}}\right);$$

$$b_{2ex}=\frac{l_{ex}}{F_{ex}}.$$

where l_{in} is the line length;

d is the diameter.

We use the equation of steady motion of the liquid in the pump in the Form (3.63)

$$p_{in}-p_{ex}=p_{in}^{*}-b_{2in}\frac{dG_{in}}{d\tau}+b_{1in}\frac{dw}{d\tau}.\qquad(3.73)$$

Regulating organs may be located along the segment from the pump to the combustion chamber(2). Therefore, we shall divide the line losses into losses in the regulating organs and other losses, both of which will be considered to be proportional to the square of the flow rate. Therefore we can write for the "pump-chamber" segment

$$p_k-p_{in}=\varrho l_{1ex}(g\sin\alpha_{1ex}+j_x\cos\alpha_{2ex})-b_{1ex}G^2-$$
$$-b_{1p.o}G^2-b_{2ex}\frac{dG}{d\tau},\qquad(3.74)$$

where

$$b_{1ex}=\frac{1}{2\varrho}\left[\sum_{i=1}^{m_5}\frac{\zeta_{in\,i}}{F_i^2}+\sum_{i=1}^{m_5}\frac{\zeta_{tp}\Delta x_i}{d_{3i}F_i^2}+\right.$$

Footnote (2) appears on page 101

$$+\frac{1}{F_\phi^2}\left(1-\frac{F_\phi^2}{F_{reg}^2}\right)\Bigg];$$

$$b_{1p.o}=\frac{\zeta_{reg}}{2\rho F_{reg}^2};$$

ζ_{reg} is the loss coefficient in the regulating organ;

F_{reg} is the flow area, which depends on the position of the regulating organ;

F_ϕ is the flow section of the injectors for the given component.

Combining Equations (3.69), (3.70), (3.63) and (3.74), we finally have[3]

$$p_k=p_0(\tau)+p_n^*(G,\omega)+p_s(\tau)-(b_{1p.o}+b_{1m})G^2-$$
$$-b_2\frac{dG}{d\tau}+b_{2m}\frac{d\omega}{d\tau}. \qquad (3.75)$$

Here

$$b_{1p.o}=\sum_{i=1}^{n_1} b_{1i\,p.o};$$

$$b_{1m}=\sum_{i=1}^{n_1} b_{1im};$$

$$b_2=b_{2m}+b_{2n}+b_{2m_{1i}};$$

n_1 and n_2 are respectively the number of regulating organs and the number of hydraulic lines

$$p_s(\tau)=\rho\sum_{i=1}^{n_2} H_i(g\sin\alpha_{1i}+j_s\cos\alpha_{2i});$$

$$j_s=j_s(\tau);\ \alpha_{1i}=\alpha_{1i}(\tau);\ \alpha_{2i}=\alpha_{2i}(\tau).$$

If the axes of the tank and the hydraulic lines up to the combustion chamber do not change direction, i.e., $\alpha_{1i}=\alpha_1$ and $\alpha_{2i}=\alpha_2$, then

---

Footnote (3) appears on page 101

$$p_z = \varrho\left(H_0^0 + H_{\text{вх}} + H_{\text{н}} + \dot{H}_{\text{вых}} - \int_0^t \frac{Q dt}{\omega F_0}\right)(g\sin\alpha_1 + j_x\cos\alpha_2).$$

§ 5. Equation of Turbopump Assembly Dynamics

In studying the operation of the TPA we must usually examine rotational motion rather than translational. We know from theoretical mechanics that in this case the translational velocity is replaced by the rotational velocity and the body mass is replaced by the moment of inertia relative to the axis of rotation. In accordance with the basic law of rotary motion dynamics, the time derivative of the TPA angular momentum about the axis of rotation equals the moment of the external forces applied to the TPA rotor

$$\frac{dK}{d\tau} = M. \tag{3.76}$$

The moment of the external forces equals the difference between the turbine and pump torques, i.e.,

$$M = M_{\text{т}} - \sum_{i=1}^{n} M_{\text{н}i}, \tag{3.77}$$

where n is the number of pumps per shaft;
M_T is the turbine torque;
M_H is the pump torque.

The angular momentum about the TPA axis is equal to the product of the angular velocity or rotation ω and the moment of inertia J of the material points of the system about the axis of the rotating system

$$K = J\omega. \tag{3.78}$$

Substituting (3.77) and (3.78) into (3.76), we obtain

$$\frac{d(J\omega)}{d\tau} = M_{\text{т}} - \sum_{i=1}^{n} M_{\text{н}i}. \tag{3.79}$$

The moment of inertia J about the axis of rotation is defined in the general case by a triple integral

$$J=\iiint_{\rho}\varrho(x^2+y^2)\,dx\,dy\,dz,$$

where the z-axis is directed along the axis of rotation while the x and y-axes are perpendicular to the z-axis.

This integral may be split into two integrals, which define the moments of inertia of the metallic rotating parts and the liquid respectively

$$J=\iiint_{V_p}\varrho_p(x^2+y^2)\,dx\,dy\,dz+\iiint_{V_{liq}}\varrho_{liq}(x^2+y^2)\,d.\,dy\,dz, \tag{3.80}$$

where the subscript "r" denotes parameters of the TPA rotor assembly, and the subscript "liq" denotes those of the liquid.

The first term can be found by numerical integration, summing the products of the elementary masses of the TPA rotor by the squares of their distances from the axis of rotation

$$J_p=\iiint_{V_p}\varrho_p(x^2+y^2)\,dx\,dy\,dz\cong\sum_{i=1}^{n}\Delta m_i r_i^2, \tag{3.81}$$

It is obvious that the magnitude of the rotor moment of inertia is independent of the time.

The second term of (3.80), which is the moment of inertia of the component filling the pump, can also be determined by numerical integration. But the magnitude of this moment of inertia depends on time in the general case. Therefore, using the relations described above, we can obtain from (3.79)

$$(J_p+J_{liq})\frac{d\omega}{d\tau}+\omega\frac{dJ_{liq}}{d\tau}=M_r-\sum_{i=1}M_{ai}, \tag{3.82}$$

where J_{liq} is the sum of the moments of inertia of all the propellant components filling the pumps located on a single shaft.

The derivative $dJ_{liq}/d\tau$ is nonzero during the pump filling or emptying period. If J_{liq} changes only slightly i.e., J_{liq} = conts, then the term $\omega \frac{dJ_{liq}}{d\tau}$ may be neglected, which simplifies (3.82) considerably. Therefore, the equation of TPA dynamics can finally be written as follows

$$J_a \frac{d\omega}{d\tau} = M_T - \sum_{i=1}^{n} M_{ai}, \tag{3.83}$$

where J_a is the moment of inertia of all the rotating masses.

Footnotes

1. on page 72 — We recall that we are considering lines of small curvature. Therefore, the projection of the vector $(\omega_y\vec{j}+\omega_z\vec{k})$ on the x axis is negligibly small in comparison with the other terms.

1'. on page 79 — We recall that $e^x \approx 1+x$ for $x \approx 0$.

2. on page 96 — Generally speaking, there must also be a regulating organ in the segment from the tank to the pump inlet.

3. on page 97 — In the present case we assume for simplicity that all the component flows from the pump to the combustion chamber.

In
power pl
particul

In
the pneu
take pla
volume.
dynamics

is not v
of energ

The
with a v
practica

small
e vector
in com-

gulating
ump inlet.

y that
e

CHAPTER 4

DYNAMICS OF LRE AUTOMATIC CONTROL COMPONENTS

In order to study the dynamic processes which take place in a power plant we must know the dynamics of its individual elements and particularly the automatic control system elements.

§ 1. The Equation of Unsteady Thermodynamics

In the variable engine operating regimes there are processes in the pneumatic drives for the LRE automatic control components which take place with change of the amount of gas in a chamber of variable volume. For such processes the equation of the first law of thermodynamics in the form

$$dQ=dU+dL$$

is not valid, since it does not take into account the influx and efflux of energy with the incoming and outgoing gas.

The development of techniques for calculating the working processes with a variable quantity of gas is of significant theoretical and practical importance for the dynamics of LRE pneumatic automatic

control components. In examining unsteady thermodynamics and its applications, we will utilize the studies of Mamontov [88] [89], Morozov [98], Bezhanov [10], Gerts and Kreynin [42] [43].

Let us examine the energy balance of the gas in the working space of the system shown in Figure 4.1. If the amount of energy entering the chamber with the incoming gas is denoted by $i_s dm_s$, and the amount of energy contained in the outgoing gas is denoted by idm, then the energy balance equation for the variable quantity of gas will have the form

$$dU = dQ + i_s dm_s - (dL + i dm), \tag{4.1}$$

where U is the internal energy of the working medium;
Q is the amount of heat supplied to the gas from outside;
L is the work of expansion of the gas;
i is the gas enthalpy.

Figure 4.1. Diagram for derivation of equation of unsteady thermodynamics.

The subscript "s" refers to parameters of the supply system. In other words, the heat supplied to the working medium from outside together with the energy of the incoming gas is expended on changing the internal energy and performing external work, with account for the fact that part of the energy is carried away with the outgoing gas. With the aid of the obvious equality

$$dm = G d\tau,$$

where G is the rate of change of the gas mass, (4.1) may be written in the form

$$dQ + (i_s G_s - iG) d\tau = dU + dL.$$

It is more convenient to write this expression, which is the mathematical formulation of the first law of thermodynamics for processes with a variable quantity of gas, as follows

$$\frac{dU}{d\tau} = i_s G_s - iG + \frac{dQ}{d\tau} - \frac{dL}{d\tau}. \qquad (4.2)$$

In practice we usually use the pressure p and the chamber volume V rather than the internal energy U and the work of expansion L of the working medium.

Therefore, it is advisable to transform (4.2) somewhat. With the aid of the known relations

$$dU = c_v m dT,$$
$$pV = mRT$$

and

$$c_v = \frac{R}{k-1}$$

it is not difficult to obtain the value of the time derivative of the internal energy in the form

$$\frac{dU}{d\tau} = \frac{1}{k-1}\left(V\frac{dp}{d\tau} + p\frac{dV}{d\tau}\right).$$

Substituting this expression into (4.2) and considering that

$$dL = pdV,$$

we finally obtain

$$\frac{dp}{d\tau} = \frac{k-1}{V}\left(i_s G_s - iG - \frac{k}{k-1} p\frac{dV}{d\tau} + \frac{dQ}{d\tau}\right) \qquad (4.3)$$

This equation, which describes the rate of change of the pressure in the gas vessel, is the most convenient relation for studying the dynamics of LRE automatic control components.

For the solution of certain problems we need to know the derivative dp/dρ, which is obtained easily from (4.3). In fact, since

$$\rho=\frac{m}{V}$$

and

$$\frac{dp}{d\rho}=\frac{dp}{d\tau}\Big/\frac{d\rho}{d\tau}, \tag{4.4}$$

then

$$\frac{dp}{d\rho}=(k-1)\frac{\left(l_s G_s-lG-\frac{k}{k-1}p\frac{dV}{d\tau}+\frac{dQ}{d\tau}\right)}{\frac{dm}{d\tau}-\rho\frac{dV}{d\tau}}. \tag{4.5}$$

The magnitude of the change of the amount of gas in the vessel will obviously be

$$\frac{dm}{d\tau}=G_s-G. \tag{4.6}$$

Therefore, we can finally write

$$\frac{dp}{d\rho}=(k-1)\frac{l_s G_s-lG-\frac{k}{k-1}p\frac{dV}{d\tau}+\frac{dQ}{d\tau}}{G_s-G-\rho\frac{dV}{d\tau}}. \tag{4.7}$$

§ 2. LRE Pneumohydraulic Valves

LRE startup and shutdown, and also regulation of their operation, is usually accomplished by various valves, located both in the main propellant lines and in the auxiliary lines which supply the gas generator. Because of the high component flow rates the valve disk dimensions are quite large. The present-day pressure level in the hydraulic lines is also quite high. Therefore, large operating forces are required to control the valves.

The use of an electromagnet to obtain these forces is not feasible, since a large amount of electric energy would have to be expended. Moreover, the use of an electromagnet causes considerable weight increase of the entire system. The best results are obtained by developing the operating force on the hydraulic valve disk with the aid of a servopiston which displaces under the influence of high-pressure control gas. The gas is supplied to the control chamber of the electropneumatic valve (EPV) (Figure 4.2). This type of valve, usually termed pneumohydraulic valves (PHV), has been used extensively on several flight vehicles [94], [34], [30], [160], [158], [161], [152]. In the following we will examine PHV of two types: normally-closed and normally-open, i.e. valves which are respectively closed and open without any input control pressure (Figure 4.3).

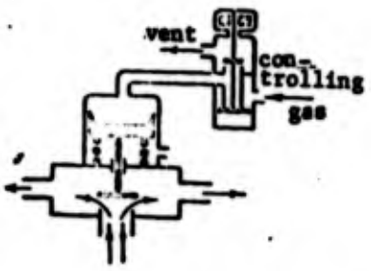

Figure 4.2. Control of pneudraulic valve by EPV.

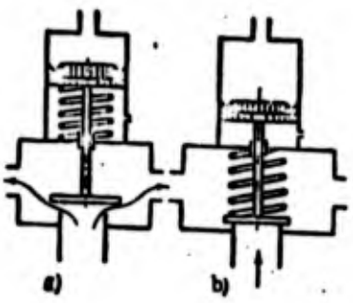

Figure 4.3. Pneudraulic valves: a) normally open; b) normally closed.

1. Control of PHV Disk Movement

Let us formulate the equation of motion of the PHV disk, which moves together with several other parts — rod, piston, spring. To this end we examine the forces acting on the moving parts. We direct the x-axis along the piston rod axis (Figure 4.4) and we locate the coordinate origin on the plane passing through the valve seat.

The primary forces acting on the PHV moving parts will be: a) the component pressure force P_{liq} valve disk; b) the control gas

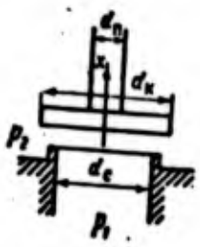

Figure 4.4. Diagram for determining forces acting on PHV disk.

pressure force on the piston P_y; c) the spring force P_c; d) the friction force P_f in the seals; e) the inertial force P_j of the moving parts.

We neglect the other forces. Let us examine in more detail each of these forces.

The liquid pressure force on the valve disk is determined by the component pressure on the inlet and back sides of the disk.

If we neglect the magnitude of the velocity head in comparison with the static pressure and assume that the pressure between the valve disk on the inlet side and the valve housing equals the pressure downstream of the valve ($p \cong p_2$), then the liquid pressure force on the valve disk will be

$$P_ж = p_1 F_1 - p_2 F_2, \tag{4.8}$$

where

$$F_2 = F_1 - F_3; \qquad F_1 = \frac{\pi d_c^2}{4}; \qquad F_3 = \frac{\pi d_n^2}{4}. \tag{4.9}$$

The force of the control gas pressure on the piston can be found without any difficulty

$$P_y = -(p_y - p_н) F_y, \tag{4.10}$$

where p_y, p_H are respectively the control gas pressure and the ambient (atmospheric) pressure; F_y is the piston area.

The spring force may be written as follows [10]:

$$P_c = \pm P_{co} - cx, \tag{4.11}$$

where c is the spring stiffness; P_{co} is the spring force with the valve closed (for the normally closed valve it equals the initial compression, for the normally open valve it equals the initial compression plus ch_1, where h_1 is the disk travel).

The symbol "+" applies to the normally open valve and "-" applies to the normally closed valve.

The friction force in the piston and rod seals is defined by the expression [10]

$$P_f = \pm |f_y [S_y (p_y - p_н) + P_{fy}] + f_w [S_w (p_2 - p_н) + P_{fw}]|, \qquad (4.12)$$

where f_y, f_r are respectively the sliding friction coefficients between the piston seal and the cylinder walls and between the seal packing and the rod; S_y, S_r are the contact areas of the seals with the cylinder and the rod; P_{fy}, P_{fr} are the seal preload forces.

The symbol "+" applies to valve opening closure, the symbol "-" applies to valve opening.

Generally speaking, the friction coefficient is a function of the sliding velocity [76]

$$f = (f_1 + f_2 \omega) \exp(-f_3 \omega) + f_4,$$

where f_1, f_2, f_3, f_4 are constants which depend on the nature of the bodies and the friction conditions.

The nature of the variation of the friction coefficient f is determined to a considerable degree by the magnitude of the specific loading between the contacting surfaces. If the specific load increases, the friction coefficient decreases (Figure 4.5). The specific loads which occur in various pneumatic mechanisms make it possible to consider that [10]

$$f = c_f \omega. \qquad (4.13)$$

Considering the friction coefficients of the seals with the cylinder and the rod to be the same, which is close to the real situation, we can transform the expression for the friction force to the form

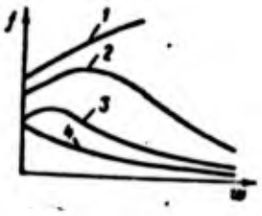

Figure 4.5. Friction coefficient f versus sliding velocity w for different specific loads [76]: 1) low specific load; 2,3) intermediate specific load; 4) high specific load

$$P_f = \pm c_f w (p_y S_y + p_2 S_m + P_{f0} - P_a), \quad (4.14)$$

where $w = \frac{dx}{dt}$;

$$P_{f0} = P_{fy} + P_{fm};$$
$$P_a = p_H (S_y + S_m).$$

If the plate movement velocity changes in a small range, we can assume the friction coefficient to be constant

$$P_f = \pm f (p_y S_y + p_2 S_m + P_{f0} - P_a). \quad (4.15)$$

The inertia force of the moving parts of the PHV will obviously be

$$P_j = m_1 \frac{d^2x}{dt^2} \quad (4.16)$$

where the mass m_1 consists of the mass of the disk, rod, piston, and the equivalent mass of the spring, which is defined with adequate accuracy as follows [92]

$$\bar{m}_c = \zeta m_c,$$

where ζ is a reduction factor which depends on the spring construction.

The Expressions (4.9), (4.10), (4.11), (4.14), (4.16) make it possible to write the differential equation of the valve disk motion

$$m_1 \ddot{x} \pm [c_f (P_a - P_{f0} - p_y S_y - p_2 S_m)] \dot{x} + cx = \\ = p_1 F_1 - p_2 F_2 - (p_y - p_H) F_y \pm P_{c0}. \quad (4.17)$$

In this equation there are two dependent variables — the pressures p_1 and p_2. The connection between them is defined by the Bernoulli equation

4.14)

$$p_1 = p_2 + \zeta(x)\varrho\frac{w_1^2}{2},$$

where ζ is the coefficient of the hydraulic losses across the valve disk, which is a function of the disk displacement; w_1 is the velocity of the component at the valve inlet.

Replacing w_1 by the component flow rate G using formula

velocity
e can
ient

$$w_1 = \frac{G}{\varrho F_1 \mu_1}$$

we obtain

(4.15)

$$p_1 = p_2 + \zeta(x)\frac{G^2}{2\varrho F_1^2\mu_1^2}, \qquad (4.18)$$

ously be

where μ_1 is the flow coefficient for the inlet section.

(4.16)

The function $\zeta=\zeta(x)$ has the following form for the valve in question [137]

, and
te

$$\zeta = \zeta_1 + \zeta_2\frac{d_c}{x}, \qquad (4.19)$$

where

ruction.

$$\zeta_1 = 0{,}55 + \frac{2(d_x - 1{,}2d_c)}{d_c};$$
$$\zeta_2 = 0{,}15 + 0{,}16.$$

it
otion

(4.17)

2. Determining PHV Opening Delay Time

pressures
ulli

After an electrical command is sent to the EPV, the disk of the PHV does not begin to move immediately; the movement begins after a time which is usually called the triggering delay time. This time consists of two parts: the EPV delay time (τ_e) and the PHV delay time (τ_1).

The first delay is determined by the parameters of the electrical circuit with account for the EPV disk triggering time, and if an EPV with unloading is used, by the parameters of its gas chambers. The second delay is considerably longer and is determined by the parameters of the pneumatic line connecting the EPV and the hydraulic valve. In the present section we shall examine only the triggering delay of the PHV itself, i.e., the quantity τ_1.

The delay τ_1 is defined as the time from initiation of the pressure decrease in the pneumatic line (see Figure 4.2) to the beginning of the valve disk motion, i.e., until the moment when the inequality

$$p_1F_1-p_2F_2-(p_y-p_H)F_y\pm P_{c0}<0 \qquad (4.20)$$

becomes an equality(1).

Here the magnitude of the resultant force is negative, i.e., it is directed opposite the x-axis, since the valve will be closed if the force of the control gas pressure exceeds the force of the component pressure on the valve disk.

In (4.20) only the magnitude of the control pressure is variable. Therefore, this inequality can become an equality only as a result of a decrease of p_y from the initial value p_{y0} to the final value $p_{y\,\tau_1}$, which can be obtained from the formula

$$(p_{y\tau_1}-p_H)F_y=p_1F_1-p_2F_2\pm P_{c0}. \qquad (4.21)$$

To determine the actuation lag time we must find the time dependence of the pressure in the chamber as it empties [13].

In studies devoted to the calculation of the emptying of gas vessels [10, 88, 90, 99, 124], the process is assumed to be polytropic with some average polytropic exponent n, whose determination involves serious difficulties. Let us examine the emptying of a gas vessel without determining the average polytropic exponent, assuming that the pressure differential between the vessel and the surrounding medium is supercritical.

Footnote (1) appears on page 147.

For this case (V=const, i,G, 0) (4.3) and (4.4) simplify considerably

$$\frac{dp}{d\tau}=\frac{k-1}{V}\left(\frac{dQ}{d\tau}-iG\right); \tag{4.22}$$

$$\frac{dp}{dQ}=-\frac{k-1}{G}\left(\frac{dQ}{d\tau}-iG\right). \tag{4.23}$$

We have omitted the subscripts in these expressions for simplicity. As is known, the formulas for the enthalpy and gas flow rate have the form

$$i=\frac{k}{k-1}RT;$$

$$G=A_k\frac{\mu F_{kr}p}{\sqrt{RT}},$$

where

$$A_k=\sqrt{k\left(\frac{2}{k+1}\right)^{\frac{k+1}{k-1}}};$$

F_{cr} is the area of the section which determines the gas flow rate;
μ is the discharge coefficient.

Substituting these expressions into (4.22) and (4.23), we obtain the values of the derivatives $dp/d\tau$ and $dp/d\tau$:

$$\frac{dp}{d\tau}=\frac{k-1}{V}\left(\frac{dQ}{d\tau}-\frac{k}{k-1}A_k\mu F_{kp}p\sqrt{RT}\right); \tag{4.24}$$

$$\frac{dQ}{d\tau}=-\frac{A_k\mu F_{kp}}{V\sqrt{RT}}p. \tag{4.25}$$

We now differentiate the equation of state with respect to time

$$\frac{dp}{d\tau}=\rho R\frac{dT}{d\tau}+RT\frac{d\rho}{d\tau}.$$

After substituting in place of the derivatives their values from (4.24) and (4.25), we find the expression for the time derivative of the gas temperature

$$\frac{dT}{d\tau}=\frac{(k-1)A_{ад}\mu F_{вр}\sqrt{RT}}{V}\left(\frac{\sqrt{T}}{A_{ад}\mu F_{вр}\sqrt{R}\rho}\frac{dQ}{d\tau}-T\right). \qquad (4.26)$$

The magnitude of the heat flux from the vessel wall to the gas may be determined as follows

$$\frac{dQ}{d\tau}=\alpha(T_0-T)S,$$

where T_0 is the wall temperature;
S is the heat transfer surface area;
α is the heat transfer coefficient.

Assuming that the heat transfer between the vessel walls and the gas is due to free convection [99], we use the formula for the heat transfer coefficient in the form (for [82]):

$$\alpha=\chi_*(T_0-T)^{1/3},$$

where

$$\chi_*=\frac{\chi}{\sqrt{T}}\rho^{2/3},$$

x is a constant coefficient which depends on the sort of gas.

The walls of high pressure gas vessels are quite thick. Therefore, the mass of the vessel is many times greater than the mass of the gas enclosed in the vessel. Considering this, and also the high thermal conductivity of the wall material and the addition of heat from the surrounding medium, we can assume that the inner wall temperature T_0 remains practically constant over the quite long duration of the emptying process This has been confirmed by several experiments which have been made [99]. Thus, taking T_0 = const, we obtain the following expression for the thermal flux

$$\frac{dQ}{d\tau}=\chi T^{-\frac{1}{2}}\rho^{2/3}(T_0-T)^{4/3}S. \qquad (4.27)$$

(4.26)

the gas

Using the method of least squares to approximate the pressure and temperature head over the range of their possible variation by means of linear relations, we obtain

$$p^{2/3} = \frac{9}{8} p_0^{-\frac{1}{3}} p;$$

$$(T_0 - T)^{1/3} = \frac{9}{10} T_0^{1/3} (T_0 - T),$$

where p_0 is the initial pressure in the vessel.

Equation (4.27) can be transformed to the form

$$\frac{dQ}{d\tau} = 1{,}01\chi \left(\frac{T_0}{p_0}\right)^{1/3} \frac{p(T_0 - T)}{\sqrt{T}} S.$$

ls and the
the heat

Substituting this value of the derivative dQ/dτ into (4.26), after some transformations we obtain the following differential equation

$$\frac{dt}{\sigma^2 - t^2} = \frac{\omega}{\sigma} d\tau, \tag{4.28}$$

where

s.

. There-
mass of the
high thermal
from the
rature T_0
f the empty-
which have
lowing ex-

$$t = \sqrt{\frac{T}{T_0}};$$

$$\sigma = \sqrt{\frac{\theta}{1+\theta}};$$

$$\omega = \frac{1}{2} \sigma \gamma (1+\theta) \sqrt{T_0};$$

$$\gamma = \frac{(k-1) A_k \mu F_{kp} \sqrt{R}}{V};$$

$$\theta = \frac{1{,}01 \chi F}{A_k \mu F_{kp} \sqrt{R}} \sqrt[3]{\frac{T_0}{p_0}}.$$

The solution of (4.28) can be written in the form

(4.27)

$$\frac{T}{T_0} = \sigma^2 \operatorname{cth}^2 (\omega\tau + \varepsilon), \tag{4.29}$$

where $\varepsilon = \operatorname{arth} \sigma$.

To determine the time dependence ρ of the gas density we use (4.25), in which we substitute in place of p its value from the equation of state, and in place of T the Expression (4.29)

$$\frac{d\rho}{\rho} = -\frac{\gamma \sqrt{T_0}\, e}{k-1} \operatorname{cth}(\omega\tau + \varepsilon)\, d\tau. \tag{4.30}$$

Integrating this equation from 0 to τ and from ρ_0 to ρ, we obtain

$$\frac{\rho}{\rho_0} = \frac{\operatorname{sh}^{\delta}(\varepsilon + \omega\tau)}{\theta^{\delta/2}}, \tag{4.31}$$

where

$$\delta = -\frac{2}{(k-1)(1+\theta)}.$$

After determining T and ρ, we obtain with the aid of the equation of state the formula for calculating the time dependence of the gas pressure p in the vessel

$$\frac{p}{p_0} = \frac{\theta^2}{\theta^{\delta/2}} \operatorname{cth}^2(\varepsilon + \omega\tau) \operatorname{sh}^{\delta}(\varepsilon + \omega\tau). \tag{4.32}$$

Formulas (4.29) and (4.32) also make it possible to find the law for the variation of the gas flow rate from the vessel

$$\frac{G}{G_0} = \frac{\theta}{\theta^{\delta/2}} \operatorname{cth}(\varepsilon + \omega\tau) \operatorname{sh}^{\delta}(\varepsilon + \omega\tau), \tag{4.33}$$

where $G_0 = \frac{A_{kr} F_{kr} p_0}{\sqrt{RT_0}}$ is the gas flow rate at the initial instant.

Excluding time from (4.29) and (4.31), we obtain the thermodynamic relation for the parameters

Hence
process wi
$\frac{T}{T_0} = \left(\frac{\rho}{\rho_0}\right)^{k-1}$

In th
form [99]

where

As 0
equation fo
calculating

where

These
delay. To

use (4.25),
on of

$$\frac{T}{T_0}=\frac{1}{1+\theta}\left[\theta+\left(\frac{\varrho}{\varrho_0}\right)^{(k-1)(1+\theta)}\right]. \tag{4.34}$$

Hence it is not difficult to see that for $\theta=0$ (or for $\chi=0$ — the process without heat addition) the vessel emptying process is adiabatic

(4.30) $\frac{T}{T_0}=\left(\frac{\varrho}{\varrho_0}\right)^{k-1}$

e obtain

In this case the functions $T=T(\tau)$, $p=p(\tau)$ and $G=G(\tau)$ have the form [99]

(4.31)

$$\left.\begin{aligned}\frac{T}{T_0}&=(1+\omega_1\tau)^{-2};\quad \frac{p}{p_0}=(1+\omega_1\tau)^{\frac{2k}{1-k}};\\ \frac{G}{G_0}&=\frac{(1+\omega_1\tau)^{\frac{k+1}{1-k}}}{\sqrt{R}},\end{aligned}\right\} \tag{4.35}$$

equation
e gas

where

$$\omega_1=\frac{(k-1)\mu_{ex}F_{ex}\sqrt{RT_0}}{2V}.$$

(4.32)

As $\theta\to\infty$ (i.e., as $\chi\to\infty$) the Expression (4.34) becomes the equation for the isothermal process $T/T_0 = 1$, and the formulas for calculating the vessel emptying process are written in the form [141]

the law

$$\frac{p}{p_0}=\frac{G}{G_0}=\exp\left(-\frac{\tau}{\theta}\right), \tag{4.36}$$

(4.33)

where

$$\theta=\frac{\mu_{ex}F_{ex}\sqrt{RT_0}}{V}$$

nodynamic

These formulas make it possible to calculate the PHV opening time delay. To this end we use (4.21) to find $p_y = \tau_1$:

$$p_{y\tau_1} = \frac{F_1}{F_y} p_1 - \frac{F_2}{F_y} p_2 + p_H \pm \frac{P}{F_y} \tag{4.37}$$

On the other hand, in accordance with (4.32) the pressure in the control chamber at the time equal to the opening delay τ_1, will be

$$p_{y\tau_1} = \frac{\sigma^2}{\theta^{1/2}} \frac{\mathrm{sh}^{\frac{1}{2}}(\varepsilon + \omega\tau_1)}{\mathrm{sh}^2(\varepsilon + \omega\tau_1)} p_{y0}. \tag{4.38}$$

Equating (4.37) and (4.38), we obtain

$$\frac{\mathrm{sh}^{1/2}(\varepsilon + \omega\tau_1)}{\mathrm{sh}(\varepsilon + \omega\tau_1)} = \varkappa_1, \tag{4.39}$$

where

$$\varkappa_1 = \frac{\theta^{1/4}}{\sigma} \sqrt{\left(\frac{F_1}{F_y} p_1 - \frac{F_2}{F_y} p_2 + p_H \pm \frac{P_{c.n}}{F_y}\right) \frac{1}{p_{y0}}}.$$

This transcendental equation in τ_1 is easily solved graphically with the aid of the time dependences of the numerator and denominator, multiplied by $\varkappa_1$. A somewhat simpler but less exact expression for determining τ_1 can be obtained with the aid of (4.35)

$$\tau_1 = \frac{1}{\omega_1} \left[\left(\frac{p_{y0}}{p_{y\tau_1}} \right)^{\frac{n-1}{2n}} - 1 \right]. \tag{4.40}$$

For preliminary calculations it is convenient to use the formula obtained from (4.36)

$$\tau_1 = \frac{1}{\theta} \ln \frac{p_{y0}}{p_{y\tau_1}}. \tag{4.41}$$

3. Determining PHV Closing Time Delay

After transmission of a command for closure of the PHV, its disk begins to travel after the time τ_3, termed the PHV closing delay time. The time τ_3 consists of the EPV triggering delay and the delay of the PHV itself. The actuation delay τ_2 of the PHV itself is determined by the time for the pressure to rise in the control chamber up to the beginning of the motion of the valve disk, when the inequality

$$p_1F_1 - p_2F_2 - (p_y - p_{II})F_y \pm P_{c0} > 0 \tag{4.42}$$

becomes an equality.

It is obvious that in order to calculate τ_2 we must know the law governing the gas pressure rise in the control chamber as it fills. Therefore, we first integrate the differential equations obtained from (4.3) and (4.4) which describe the change of the parameters in the PHV control chamber as it fills

$$\frac{dp}{d\tau} = \frac{k-1}{V}\left(l_3G_s + \frac{dQ}{d\tau}\right); \tag{4.43}$$

$$\frac{dQ}{d\tau} = \frac{G_s}{V}. \tag{4.44}$$

Usually the gas enters the valve chamber from a pressure accumulator in which all the parameters vary in accordance with (4.29), (4.31), (4.32) and (4.33) as the accumulator empties. Therefore, substituting into (4.44) in place of G_s its value from (4.33), we obtain

$$dQ = \frac{G_{s0}\vartheta^3}{\vartheta^{k/2}V}\,\frac{\mathrm{sh}^2(\varepsilon + \omega\tau)}{\mathrm{th}(\varepsilon + \omega\tau)}\,d\tau. \tag{4.45}$$

We integrate this equation in the limits from 0 to τ and from ρ_0 to ρ

$$\varrho = \varrho^* + \vartheta_1 \mathrm{sh}^2(\varepsilon + \omega\tau), \tag{4.46}$$

where

$$Q^* = Q_0 - \frac{G_{s0}\sigma^{1+\delta}}{\vartheta^{\delta/2}V\omega\delta\,(1-\sigma^2)^{\delta/2}};$$

$$\beta_1 = \frac{G_{s0}\sigma}{\vartheta^{\delta/2}V\omega\delta}.$$

We note that the constants σ, ϑ, ω, δ, ε are found from the parameters of the incoming gas. Neglecting the heat transfer to the gas $\left(\frac{dQ}{d\tau}=0\right)$ and taking (4.29) and (4.33) into account, we reduce (4.43) to the form

$$dp = \frac{kR_sT_{s0}\sigma^3G_{s0}}{V\vartheta^{\delta/2}}\cdot\frac{\mathrm{sh}^{\delta}(\varepsilon+\omega\tau)}{\mathrm{th}^3(\varepsilon+\omega\tau)}\,d\tau, \qquad (4.47)$$

where R_s, T_{s0} are the gas constant of the incoming gas and the temperature of the supply system walls.

After integrating (4.47) from p_0 to p, we obtain

$$p = p^* + \beta_2\,\mathrm{sh}^{\delta-2}(\varepsilon+\omega\tau)\left[\mathrm{sh}^2(\varepsilon+\omega\tau)+\frac{\delta}{\delta-2}\right], \qquad (4.48)$$

where

$$p^* = p_0 - \frac{kR_sT_{s0}\sigma^{\delta+1}G_{s0}(\delta-2\sigma^2)}{V\vartheta^{\delta/2}\omega\delta\,(1-\sigma^2)^{\delta/2}(\delta-2)};$$

$$\beta_2 = \frac{kR_sT_{s0}\sigma^3G_{s0}}{V\vartheta^{\delta/2}\omega\delta}.$$

Formulas (4.46) and (4.48) make it possible to determine the time dependence of the temperature in the control chamber

$$T = \frac{p^* + \beta_2\,\mathrm{sh}^{\delta-2}(\varepsilon+\omega\tau)\left[\mathrm{sh}^2(\varepsilon+\omega\tau)+\frac{\delta}{\delta-2}\right]}{R\left[Q^* + \beta_1\,\mathrm{sh}^{\delta}(\varepsilon+\omega\tau)\right]} \qquad (4.49)$$

Now le
disk begins

At the

Equatir

where

The mag
ically from

If we n
the solution

where

Hence, it
delay

Now let us find the pressure corresponding to the moment the valve disk begins to move toward closure

$$p_{y\tau_1} = p^* + \beta_2 \operatorname{sh}^{\delta-2}(\varepsilon + \omega\tau_2)\left[\operatorname{sh}^2(\varepsilon + \omega\tau_2) + \frac{\delta}{\delta-2}\right]. \tag{4.50}$$

param-
gas

At the moment of equilibrium we obtain from (4.42)

$$p_{y\tau_1} = \frac{F_1}{F_y} p_1 - \frac{F_2}{F_y} p_2 + p_H \pm \frac{P_{r0}}{F_y}. \tag{4.51}$$

Equating (4.50) and (4.51), we obtain

(4.47)

$$\operatorname{sh}^{\delta}(\varepsilon + \omega\tau_2) = x_2 - \frac{\delta}{(\delta-2)\operatorname{sh}^2(\varepsilon + \omega\tau_2)}, \tag{4.52}$$

temp-

where

$$x_2 = \frac{1}{\beta_2}\left(\frac{F_1}{F_y} p_1 - \frac{F_2}{F_y} p_2 + p_H \pm \frac{P_{r0}}{F_y} - p^*\right).$$

(4.48)

The magnitude of the PHV opening delay τ_2 is easily found graphically from the transcendental Equation (4.52).

If we neglect the variation of the incoming gas parameters, then the solution of (4.43) is simplified considerably

$$p = p_0 + \omega_2 \tau,$$

where

he time

$$\omega_2 = \frac{\chi A_{\text{ш}} F_{\text{кр}} p_{s0} \sqrt{R_s T_{s0}}}{V}.$$

Hence, it is not difficult to obtain the approximate PHV closure

(4.49)

delay

$$\tau_2 = \frac{1}{\omega_2}\left(\frac{F_1}{F_y} p_1 - \frac{F_2}{F_y} p_2 + p_H - p_0 \pm \frac{P_{r0}}{F_y}\right) \tag{4.53}$$

4. Calculation of the PHV Opening Process

In calculating the transient processes in LRE we must know the time dependence of the component flow rates in the period of PHV opening and closing. It is obvious that the flow rate through the valve will be determined primarily by the position of the valve disk at each instant of time. To determine the disk coordinate function as a function of time $x(\tau)$, we must integrate the equation of motion (4.17) of the valve disk and the equation of the pneumatic-hydraulic line (4.3) for the case of PHV opening

$$\begin{aligned} m_1\ddot{x} \pm [c_f(P_0 - P_{f0} - p_y S_y - p_2 S_m)]\dot{x} + cx = \\ = p_1 F_1 - p_2 F_2 - (p_y - p_{II}) F_y \pm P_{c0}; \\ \frac{dp_y}{d\tau} = \frac{k-1}{V}\left(-iG - \frac{k}{k-1} p_y \frac{dV}{d\tau} + \frac{dQ}{d\tau}\right). \end{aligned} \tag{4.54}$$

In the general case this equation can not be integrated. Therefore, we seek the solution under the following simplifying assumptions: 1) the inertia and friction forces are negligibly small in comparison with the other forces; 2) the pressure p_2 downstream of the valve disk is constant and equal to the atmospheric pressure during valve opening; 3) there is no heat transfer between the walls of the valve chamber and the control gas; 4) $T = T_0$. Under these assumptions, (4.17) and (4.54) will have the form

$$p_y = p_{y\tau_1} - b_1 x; \tag{4.55}$$

$$\frac{dp_y}{d\tau} = -\frac{b_2}{V} p_y - \frac{k}{V} p_y \frac{dV}{d\tau}, \tag{4.56}$$

where

$$b_1 = \frac{c}{F_y}; \quad b_2 = k\sqrt{RT_0} A_{2\max} F_{y\max}.$$

The v
be
where V_0 i
Hence
Differ
(4.56) with
equation o
We int
to τ
The valve o
stituting x
5. Ca
We see
simplificat
ligibly sma
stream of t
the control
scribing the

The volume of the gas space under the valve piston will obviously be

$$V = V_0 - F_y x, \tag{4.57}$$

where V_0 is the volume with the valve closed.

Hence, considering that $\frac{dV}{d\tau} = \frac{dV}{dx}\frac{dx}{d\tau}$, we obtain

$$\frac{dV}{d\tau} = -F_y \frac{dx}{d\tau}. \tag{4.58}$$

Differentiating (4.55) with respect to τ and substituting it into (4.56) with account for (4.58) and (4.55), we obtain the differential equation of motion of the valve disk in the form

$$\left[F_y + \frac{b_1(V_0 - F_y x_1)}{p_{y x_1} - b_1 x}\right] dx = b_2 d\tau. \tag{4.59}$$

We integrate this equation in the limits from 0 to x and from 0 to τ

$$\tau = (k+1)\frac{F_y}{b_2}x + \frac{(p_{y x_1} F_y - V_0 b_1)}{b_2 b_1} \ln\left(1 - \frac{b_1}{p_{y x_1}} x\right). \tag{4.60}$$

The valve opening time is determined from this expression after substituting x = h, where h is the valve disk travel.

5. Calculation of PHV Closing Process

We seek the relation $x = x(\tau)$ for PHV closure under the following simplifications; 1) the inertia, friction, and damping forces are negligibly small; 2) during the valve closure period the pressure p_2 downstream of the disk is constant; 3) there is no heat transfer between the control chamber walls and the gas. In this case the equations describing the valve dynamics during closure may be written as follows

$$\frac{dp_y}{d\tau}=\frac{k-1}{V}\left(l_2G_2-\frac{k}{k-1}p_y\frac{dV}{d\tau}\right);$$

$$p_y=p_{y\tau_0}-b_1x. \tag{4.61}$$

(4.62)

Hen

where

$$V=V_0-F_y(h-x).$$

$$\frac{dV}{d\tau}=F_y\frac{dx}{d\tau}.$$

where

With the aid of (4.29), (4.32) and (4.33), which account for the change of the incoming gas parameters, these equations can be transformed into the following differential equation describing the PHV closure process

If

chamber

$$[b_4-c(k+1)x]dx=b_3\frac{\sin^k(\tau+\omega\tau)}{\cos^3(\tau+\omega\tau)}d\tau, \tag{4.63}$$

where

where

$$b_3=kA_{k2}F_{x_2}\pi^{(k-1)/2}\sqrt{R_1T_{\tau_0}}p_{\tau_0};$$

$$b_4=kF_yp_{y\tau_0}-\frac{c(V_0-F_yh)}{F_y}.$$

We recall that the constants σ, θ, δ, ε, ω are determined by the parameters of the pressure accumulator.

Ele

power pl

actuatio

is deter

We integrate (4.63) in the limits from 0 to τ and from h to x

Let

action E

τ_{el} is d

until th

force in

$$\frac{b_3}{\omega\theta}\sin^{k-1}(\tau+\omega\tau)\left[\sin^2(\tau+\omega\tau)+\frac{k-1}{3}\cos^2\right]+$$

$$+b_4x-\frac{1}{2}(k+1)cx^2,$$

where

(4.61) $$b_3 = -\frac{1}{2}(k+1)c h^2 - b_1 h + \frac{b_1}{\omega^3}\cdot\frac{\tau^2}{(1-\omega\tau)^{\delta-2}}\cdot\frac{(k-2)^2}{(\delta-2)}.$$

(4.62) Hence, we find desired relation $x = x(\tau)$

$$x = \frac{1}{c(k+1)}\left[\sqrt{b_4^2 + 2c(k+1)[b_3 - \varphi(\tau)]} - b_4\right], \tag{4.64}$$

where

$$\varphi(\tau) = \frac{b_1}{\omega^3}\operatorname{sh}^{\delta-2}(\varepsilon+\omega\tau)\left[\operatorname{sh}^2(\varepsilon+\omega\tau) + \frac{\delta}{\delta-2}\right].$$

t for the
e trans-
ne PHV

If we consider the parameters of the gas entering the control chamber to be constant, then the function $x(\tau)$ is simplified

(4.63) $$x = b_6 \pm \sqrt{b_6^2 - 2hb_6 + h^2 + 2b_7\tau}, \tag{4.65}$$

where

$$b_6 = \frac{kF_y p_{y\tau_0} - b_1 V_3}{(k+1)b_1 F_y};$$
$$b_7 = \frac{(k-1)l_0 G_3}{b_1 F_y (1+k)}.$$

the param-

to x

§ 3. LRE Electropneumatic Valves

Electropneumatic valves (EPV) are used for remote control of various power plant regulating elements. We have mentioned previously that the actuation delay of LRE AUTOMATIC CONTROL ELEMENTS (including the PHV) is determined to some degree by the triggering delay of the EPV.

Let us examine the opening delay of the normally closed EPV direct-action EPV shown schematically in Figure 4.6. The opening delay time τ_{el} is determined from the instant of closure of the electrical circuit until the beginning of motion of the EPV disk. If the electromotive force in the circuit is E, the coil inductance is L, and the resistance

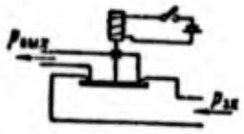

Figure 4.6. Direct action electropneumatic valve.

R, then the law governing the variation of the current intensity I during making and breaking of the circuit is defined by the Expression [166]

$$I=I_0\exp\left(-\frac{R}{L}\tau\right)+\frac{E}{R}\left[1-\exp\left(-\frac{R}{L}\tau\right)\right], \quad (4.66)$$

where I_0 is the current intensity at the initial moment of time (it is obvious that $I_0 = 0$ for closure).

The electromagnet pull force is defined by the formula [87]

$$P_{эм}=\frac{B^2F_a}{8\pi\sin\alpha}10^7, \quad (4.67)$$

where B is the magnetic induction between the planes of the electromagnet core and the armature; F_a is the armature area; α is the electromagnet apex cone halfangle (for a magnet with conical armature end).

Assuming that

$$B\sim\frac{Ii(1-\zeta)}{h},$$

where i is the number of winding turns; ζ is the magnetomotive force leakage factor; h is the air gap between the armature and the magnet yoke along the magnet axis, we obtain

$$P_{эм}=6{,}4\cdot10^{-4}\frac{F_a(1-\zeta)^2i^2I^2}{h^2\sin\alpha}. \quad (4.68)$$

At the instant of opening the magnet force must be

$$P_{эм1}=(p_{вх}-p_н)F_c,$$

which corresponds to the current intensity

$$I_1=\sqrt{\frac{(p_{вх}-p_н)F_c}{\ldots}}.$$

Here F_s i

Subs
the openi

Now
disk begi

which cor

This
the aid o

In th
delay cons
obtained u

Gas p
flow rates
some gas p

Here F_s is the EPV seat area

$$x_0 = 6{,}4 \cdot 10^{-4} \frac{F_s}{\sin\alpha} \frac{(1-\zeta)^2 l^2}{A^2}$$

Substituting the value of I_1 in place of I into (4.66), we obtain the opening delay of the direct-action EPV

$$\tau_{o1} = \frac{L}{R} \ln\left[\frac{1}{1-\frac{I_1 R}{E}}\right]. \qquad (4.69)$$

Now let us find the EPV closing delay. At the instant the valve disk begins to move the magnet force is

$$P_{эм2} = (p_{вх} - p_{вых}) F_c,$$

which corresponds to the current intensity

$$I_2 = \sqrt{\frac{(p_{вх} - p_{вых}) F_c}{x_0}}$$

This value of the current intensity makes it possible to find with the aid of (4.66) the EPV closure delay

$$\tau_{o2} = \frac{L}{R} \ln \frac{I_0}{I_2}. \qquad (4.70)$$

In the case of the EPV with unloading (Figure 4.7) the triggering delay consists of the electric and pneumatic delays, which are easily obtained using the formulas presented above.

§ 4. Gas Pressure Reducers

Gas pressure reducers are used to maintain the working medium flow rates and pressures within a definite range. Let us examine some gas pressure reducers.

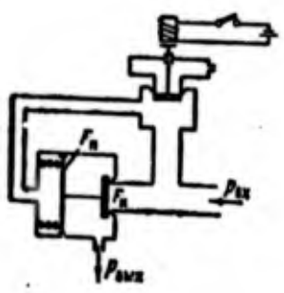

Figure 4.7. Electropneumatic valve with unloading.

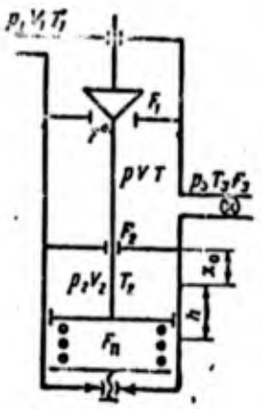

Figure 4.8. Gas pressure reducer.

We shall first derive the equation of the dynamics of the gas pressure reducer shown schematically in Figure 4.8 [140].

In the steady state regime, the flow rate through the reducer equals the flow rate through the control valve, with the valve disk stationary and the inlet pressure p equals the pressure p_2 (see Figure 4.8). The disk equilibrium position is determined by equality of the forces acting on the disk: the spring force and the force of the pressure p acting on the valve disk in the upward direction, and the forces of the pressures p_1 and p_2 acting downward.

Since the force acting on the piston changes with change of the pressure in the volume V, the valve is established in a new position in which the magnitude of the flow section provides a flow rate such that the pressure does not change. During steady state or very slow change of the reducer operating regime, the flow rate oscillations lead to the appearance of an additional force which can always be equilibrated by the force acting on the piston, which plays the role of a feedback. During transient processes there appears an inertia force which reaches significant magnitudes. Moreover, the pressure p_2 cannot follow the variation of p. These factors can lead to the appearance of oscillations in the reducer, which are obviously undesirable.

We shall assume the gasdynamic processes in the reducer to be adiabatic and quasisteady (without pressure oscillations).

The mass flow rate through the area F_1 is defined by the familiar formula of Saint-Venant and Wentzel [144]

$$G_1 = \mu_1 \sqrt{\frac{k}{RT_1}} F_1 p_1 \pi_1\left(\frac{p}{p_1}\right), \tag{4.71}$$

where p, p_1 are respectively the pressures in the volumes V and V_1 (see Figure 4.8); μ_1 is the coefficient of discharge through the area F_1

$$\pi_1\left(\frac{p}{p_1}\right) = \sqrt{\frac{2}{k-1}\left[\left(\frac{p}{p_1}\right)^{\frac{2}{k}} - \left(\frac{p}{p_1}\right)^{\frac{k+1}{k}}\right]}.$$

For $\frac{p}{p_1} = \left(\frac{2}{k+1}\right)^{\frac{k}{k-1}}$ the function $\pi_1\left(\frac{p}{p_1}\right)$ has a maximal value equal to

$\sqrt{\frac{2}{k-1}\left(\frac{2}{k+1}\right)^{\frac{2}{k-1}}\left[1-\left(\frac{2}{k+1}\right)^{\frac{k+1}{2}}\right]}$ (for air $\pi_1\left(\frac{p}{p_1}\right) = 0{,}579$). In this case the critical velocity is reached in the section F_1 and further reduction of the ratio p/p_1 does not yield any increase of the flow rate, i.e., the function $\pi_1\left(\frac{p}{p_1}\right) = \text{const}$.

The gas flow rate formulas for sections F_2 and F_3 are written similarly to (4.71).

Now we write the equation of state for the mass of gas located in the volume V

$$pV = mRT. \tag{4.72}$$

Since the sound velocity is defined by the formula

$$a^2 = kRT, \tag{4.73}$$

the equation of state can be rewritten in the form

$$kVp = a^2 m. \tag{4.74}$$

Hence, after differentiating we obtain

$$dm = \frac{kV}{a^2}\,dp - \frac{2kV\rho}{a^3}\,da.$$

At the initial moment the gas mass will obviously be

$$m^* = \frac{kVp^*}{a^{*2}}. \tag{4.75}$$

Here and hereafter, the superscript "*" denotes parameters at the initial time. Therefore,

$$\frac{dm}{m^*} = \left(\frac{a^*}{a}\right)^2 \left(\frac{dp}{p^*} - 2\frac{\rho}{p^*}\frac{da}{a}\right). \tag{4.76}$$

On the other hand,

$$\frac{dm}{m^*} = \frac{G_1 + G_2 + G_3}{m^*}\,d\tau. \tag{4.77}$$

These expressions make it possible to find the quantity $\frac{G_1 d\tau}{m^*}$:

$$\frac{G_1 d\tau}{m^*} = \frac{p_1 F_1}{p^*}\frac{p_1}{p^*}\frac{a^*}{a_1}\pi_1\frac{a^* F^*}{V}\,d\tau, \tag{4.78}$$

where F^* is the initial area (see Figure 4.8).

We introduce the notations

Then

Simi

We s
that in t
and (4.77
have the

The
follows

Now
V_2. If we
change in
section F_2
using the

we obtain

(4.73)
$$\bar{F}_1=\frac{F_1}{F^*};\quad \bar{p}_1=\frac{p_1}{p^*};\quad \bar{a}_1=\frac{a_1}{a^*};\quad \bar{\tau}=\frac{a^*F^*}{V}\tau.$$

Then

(4.74)
$$\frac{G_1}{m^*}d\tau=\frac{\mu_1\bar{F}_1\bar{p}_1}{\bar{a}_1}\pi_1 d\bar{\tau}. \tag{4.79}$$

Similar expressions can be written for sections F_2 and F_3.

We shall denote the gas flow from V into V_2 by the symbol "2e" and that in the reverse direction by "2s" . Then with account for (4.76) and (4.77) the continuity equation for the flow from V into V_2 will
(4.75) have the form

at the
$$\frac{d\bar{p}}{d\bar{\tau}}-2\frac{\bar{p}}{\bar{a}}\frac{d\bar{a}}{d\bar{\tau}}=\bar{a}^2\left(\frac{\mu_1\bar{F}_1\bar{p}_1\pi_1}{\bar{a}_1}+\frac{\mu_2\bar{F}_2\bar{p}_2\pi_{2e}}{\bar{a}}-\frac{\mu_3\bar{F}_3\bar{p}_3\pi_3}{\bar{a}}\right) \tag{4.80}$$

The continuity equation for the flow from V_2 into V is written as
(4.76) follows

$$\frac{d\bar{p}}{d\bar{\tau}}-2\frac{\bar{p}}{\bar{a}}\frac{d\bar{a}}{d\bar{\tau}}=\bar{a}^2\left(\frac{\mu_1\bar{F}_1\bar{p}_1\pi_1}{\bar{a}_1}+\frac{\mu_2\bar{F}_2\bar{p}_2\pi_{2s}}{\bar{a}_2}-\frac{\mu_3\bar{F}_3\bar{p}_3\pi_3}{\bar{a}}\right) \tag{4.81}$$

(4.77) Now let us obtain the energy equation for the gas in the volume V_2. If we neglect the heat input, we can assume the internal energy change in this volume takes place as a result of gas outflow through section F_2 and as a result of the work done by the piston. Therefore, using the expression for the enthalpy

$\frac{G_1 d\tau}{m^*}$:

(4.78)
$$i=\frac{k}{k-1}RT,$$

we obtain from (4.3) the expression for the volume V_2

$$V_2\frac{dp_2}{d\tau}=kRTG_{2e}-kp_2\frac{dV_2}{d\tau}. \tag{4.82}$$

We take the coordinate origin at the point corresponding to the piston position with the spring unloaded. Then at the instant τ the instantaneous volume of the chanber above the piston will be

$$V_2=(x+x_0)F_p.$$

With the valve fully closed, i.e., when $F_1 = 0$, the volume is defined by the formula

$$V_{20}=(x_0+h)F_p,$$

where x is the instantaneous piston location coordinate;

x_0 is the distance between the piston and the wall diaphragm with the piston free;

h is the maximal spring contraction, corresponding to the instant when $F_1 = 0$.

F_p is the piston area.

Using the notations

$$\bar{x}=\frac{x}{h+x_0};\quad \bar{x}_0=\frac{x_0}{h+x_0};\quad \bar{V}_2=\frac{V_2}{V_{20}}=\bar{x}+\bar{x}_0,$$

we transform (4.82) to the following form

$$(\bar{x}+\bar{x}_0)\frac{d\bar{p}_2}{d\bar{\tau}}+k\bar{p}_2\frac{d\bar{x}}{d\bar{\tau}}=k\bar{V}\mu_{2e}\bar{F}_2\bar{a}\bar{p}\pi_{2e}, \qquad (4.83)$$

since

$$G_{2e}=\frac{\bar{F}_2\bar{p}\pi_{2e}F^*p^*}{aa^*}$$

We obtain similarly for the flow from V_2 into V

$$(\bar{x}+\bar{x}_0)\frac{d\bar{p}_2}{d\bar{\tau}}+k\bar{p}_2\frac{d\bar{x}}{d\bar{\tau}}=-k\mu_{1e}\bar{V}\bar{F}_1\bar{a}_1\bar{p}_1\pi_{1e}. \qquad (4.84)$$

Let u
neglecting
due to val
internal e
(efflux) t
also negle

for t

for t

The sp
formulas.

We obt
with the ai
follows

We tra

Then, a

Let us write the energy equation for the gas in the volume V, neglecting the work done on the gas by the piston and the volume change due to valve displacement. In this case the increase (decrease) of the internal energy in the volume V occurs as a result of the gas influx (efflux) through the sections F_1, F_2, F_3 (provided heat transfer is also neglected). Then:

for the flux from volume V into V_2

$$\frac{d\bar{p}}{d\bar{\tau}} = k\left[\mu_1 \bar{F}_1 \bar{a}_1 \bar{p}_1 \pi_1 - \mu_{2\epsilon} \bar{F}_2 \bar{a} \bar{p} \pi_{2\epsilon} - \mu_3 \bar{F}_3 \bar{a} \bar{p} \pi_3\right]; \tag{4.85}$$

for the flux from volume V_2 into V

$$\frac{d\bar{p}}{d\bar{\tau}} = k\left[\mu_1 \bar{F}_1 \bar{a}_1 \bar{p}_1 \pi_1 + \mu_{2\epsilon} \bar{F}_2 \bar{a}_2 \bar{p}_2 \pi_{2\epsilon} - \mu_3 \bar{F}_3 \bar{a} \bar{p} \pi_3\right] \tag{4.86}$$

The speed of sound in the gas in the volume V_2 appears in these formulas. Therefore let us find the dependence of $\bar{a}_2$ on $\bar{\tau}$.

We obtain the equation for $\bar{a}_2$ for the gas flow in the volume V with the aid of (4.74), (4.75), and (4.83). We first write (4.83) as follows

$$(\bar{x} + \bar{x}_0)\frac{d\bar{p}_2}{d\bar{\tau}} + \bar{p}_2 \frac{d\bar{x}}{d\bar{\tau}} + (k-1)\bar{p}_2 \frac{d\bar{x}}{d\bar{\tau}} = kV\mu_{2\epsilon} \bar{F}_2 \bar{a} \bar{p} \pi_{2\epsilon}. \tag{4.87}$$

(4.83)

We transform the equation of state (4.74) to the form

$$\bar{p}_2 \bar{V}_2 = \frac{\bar{a}_2^2 a^{*2} m_2}{k V_{0\Sigma} p^*}. \tag{4.88}$$

Then, assuming that $V_2 = \bar{x} + \bar{x}_0$ and

$$G_{2\epsilon} = \frac{dm_2}{d\tau} = \frac{a^* F^*}{V} \frac{dm_2}{d\bar{\tau}},$$

(4.84)

we obtain

$$(\bar{x}+\bar{x}_0)\frac{d\bar{p}_2}{d\bar{\tau}}+\bar{p}_2\frac{d\bar{x}}{d\bar{\tau}}=\frac{2\bar{p}_2(\bar{x}+\bar{x}_0)}{\bar{a}_2}\frac{d\bar{a}_2}{d\bar{\tau}}+$$
$$+\frac{1}{2}\mu_{2c}\bar{F}_2\bar{V}\bar{a}\bar{p}\pi_{2c}\frac{\bar{a}_2^2}{\bar{a}^2}.$$

Substituting this expression into (4.87), we find

$$\frac{2(\bar{x}+\bar{x}_0)}{\bar{a}_2}\frac{d\bar{a}_2}{d\bar{\tau}}=\left(k-\frac{\bar{a}_2^2}{\bar{a}^2}\right)\frac{\mu_{2c}\bar{F}_2\bar{V}\pi_{2c}\bar{a}\bar{p}}{\bar{p}_2}-(k-1)\frac{d\bar{x}}{d\bar{\tau}}. \qquad (4.89)$$

Assuming the process in the chamber V_2 to be isentropic, we can write the equation for $\bar{a}_2$ in the case of gas flow from the chamber above the piston into the volume V:

$$\bar{p}_2=\bar{a}_2^{\frac{2k}{k-1}}. \qquad (4.90)$$

We obtain the equation of the reducer dynamics by equating the inertia force to the sum of all the forces acting on the valve disk (pressure, aerodynamic, elasticity, and damping).

The aerodynamic forces are determined by the action of the flowing gas stream on the valve disk. Since it is difficult to calculate the aerodynamic forces theoretically, we usually use experimental data. Analyses of these data for valves of different construction have made it possible to obtain an empirical formula of the form [140]

$$P_L=F^*\bar{p}_x\bar{p}_r(p_1-p) \qquad (4.91)$$

where $\bar{p}_x=\frac{P_L}{P_{0L}}$ is the function which describes the change of the aerodynamic forces with a change of the valve position coordinate x;

$\bar{p}_r=\frac{P_{0L}}{F^*(p_1-p)}=\frac{P_c}{F^*}$ is the function describing the change of P_L with a change of the pressure difference $(p_1 - p)$;

F_c

P_{0L}

The

as a func

Figure 4.

It is

The e

as follows

where m_1 i

c_f i

c i

With

formed to

F_c is the seat area;

P_{0L} is the aerodynamic force corresponding to liftoff from the seat.

The values of $\bar{P}_x$ and $\bar{P}_r$ are found from the experimental results as a function of $\bar{F}_1$ and p/p_1 respectively (Figure 4.9).

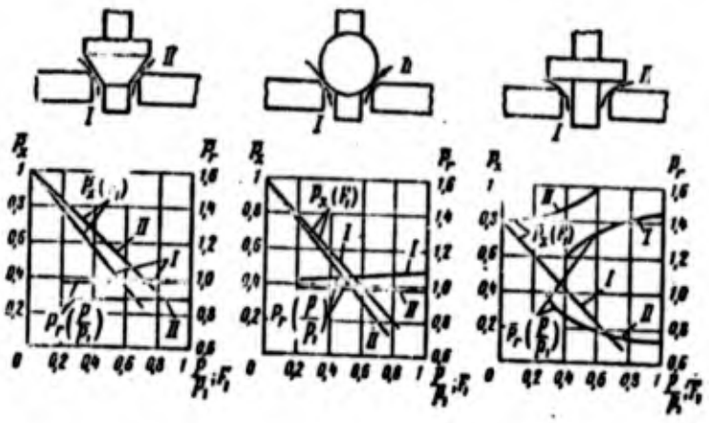

Figure 4.9. Dimensionless aerodynamic forces versus $\bar{F}_1$ and p/p_1.

It is not difficult to write (4.91) in dimensionless form

$$\frac{P_{0L}}{F^* p^*} = \bar{P}_x \bar{P}_r (\bar{p}_1 - \bar{p}). \tag{4.92}$$

The equation of motion of the valve disk can obviously be written as follows

$$m_1 \frac{d^2x}{dt^2} + c_f \frac{dx}{dt} - p_1 F_n + cx - F^* \bar{P}_x \bar{P}_r (p_1 - p) = 0, \tag{4.93}$$

where m_1 is the mass of all the moving parts;

c_f is a coefficient of proportionality;

c is the spring stiffness.

With account for the adopted notations this equation may be transformed to the form

$$\frac{d^2\bar{x}}{d\bar{\tau}^2}+\zeta_1\frac{d\bar{x}}{d\bar{\tau}}+\omega^2\bar{x}-\zeta_2\bar{p}_2-\zeta_3\bar{p}_*\bar{P}_r(\bar{p}_1-\bar{p})=0. \qquad (4.94)$$

where $\zeta_1=\frac{c_f V}{m_1F^*a^*}$ is the damping coefficient;

$\omega=\frac{V}{a^*F^*}\sqrt{\frac{c}{m_1}}$; is the real oscillation frequency of the inertial-elastic system in the reducer;

$\zeta_2=\frac{F_n p^*V^2}{m_1(h+x_0)a^{*2}F^{*2}}$ is the force coefficient for F_p;

$\zeta_3=\frac{V^2p^*}{m_1(h+x_0)a^{*2}F^*}$ is the force coefficient for F*.

The resulting Equations (4.80), (4.83), (4.85), (4.89), (4.90), and (4.94) describe the reducer dynamics for the gas flow through the section F_2 from the volume V into V_2

$$\left.\begin{aligned}
&\frac{d\bar{p}}{d\bar{\tau}}-2\frac{\bar{p}}{\bar{a}}\frac{d\bar{a}}{d\bar{\tau}}=\bar{a}^2\left(\frac{\mu_1\bar{F}_1\bar{p}_1\pi_1}{\bar{a}_1}-\frac{\mu_{2c}\bar{F}_2\bar{p}\pi_{2c}}{\bar{a}}-\frac{\mu_3\bar{F}_3\bar{p}\pi_3}{\bar{a}}\right);\\
&(\bar{x}+\bar{x}_0)\frac{d\bar{p}}{d\bar{\tau}}+k\bar{p}_2\frac{d\bar{x}}{d\bar{\tau}}=k\bar{V}\mu_{2c}\bar{F}_2\bar{a}\bar{p}\pi_{2c};\\
&\frac{d\bar{p}}{d\bar{\tau}}=k\left(\mu_1\bar{F}_1\bar{a}_1\bar{p}_1\pi_1-\mu_{2c}\bar{F}_2\bar{a}\bar{p}\pi_{2c}-\mu_3\bar{F}_3\bar{a}\bar{p}\pi_3\right);\\
&\frac{2(\bar{\tau}+\bar{\tau}_0)}{\bar{a}_2}\frac{d\bar{a}_2}{d\bar{\tau}}=\left(k-\frac{\bar{a}_2^2}{\bar{a}^2}\right)\frac{\mu_{2c}\bar{V}\bar{F}_2\pi_{2c}\bar{a}\bar{p}}{\bar{p}_2}-(k-1)\frac{d\bar{\tau}}{d\bar{\tau}};\\
&\frac{d^2\bar{\tau}}{d\bar{\tau}^2}+\zeta_1\frac{d\bar{x}}{d\bar{\tau}}+\omega^2\bar{x}-\zeta_2\bar{p}_2-\zeta_3\bar{p}_*\bar{P}_r(\bar{p}_1-\bar{p})=0.
\end{aligned}\right\} \qquad (A)$$

We have the following system of equations for the gas flow from volume V_2 into V

(4.94)

$$\left.\begin{aligned}
&\frac{d\bar{p}}{d\tau} = -2\frac{\bar{p}}{\bar{a}}\frac{d\bar{a}}{d\tau} - \frac{\kappa}{\bar{V}}\left(\frac{\bar{F}_1\bar{a}_1}{a_1} + \frac{\bar{F}_2\bar{a}_2}{a_2} - \frac{\bar{F}_3\bar{a}_3}{\bar{a}}\right);\\
&(\bar{x}+\bar{h})\frac{d\bar{p}_2}{d\tau} + \kappa\bar{p}_2\frac{d\bar{x}}{d\tau} = \kappa\bar{V}_{20}\bar{F}_2\bar{a}_2\bar{p}_2\tau_2;\\
&\frac{d\bar{p}}{d\tau} = \kappa\left(\bar{F}_1\bar{a}_1\bar{p}_1\tau_1 + \bar{F}_2\bar{a}_2\bar{p}_2\tau_2 - \bar{F}_3\bar{a}_3\bar{p}\tau_3\right);\\
&\bar{p}_2 = \bar{a}_2^{\frac{2\kappa}{\kappa-1}};\\
&\frac{d^2\bar{x}}{d\tau^2} + \zeta_1\frac{d\bar{x}}{d\tau} + \omega^2\bar{x} - \zeta_2\bar{p}_2 - \zeta_3\bar{p}_x\bar{p}_r(\bar{p}_1 - \bar{p}) = 0
\end{aligned}\right\} \quad (B)$$

inertial-

The first equation of the systems (A) and (B) is the continuity equation for the gas in the volume V, the second and third are the equations of energy conservation in the volumes V_2 and V respectively, the fourth defines the state of the gas in volume V_2, which relates the quantities $\bar{a}_2$ and $\bar{p}_2$, and the fifth is the equation of motion of the reducer valve disk.

4.90),
ugh the

We see that each of the resulting systems of five equations contains five unknowns ($\bar{p}$, $\bar{p}_2$, $\bar{a}$, $\bar{a}_2$, $\bar{x}$) and therefore can be solved for the parameter $\bar{\tau}$.

The boundary conditions of the posed problem are written as follows:

(A)

1) for $\bar{x}=\bar{h}$ $\frac{d\bar{x}}{d\bar{\tau}}=0$, since in this case the reducer is closed ($\bar{F}_1 = 0$) and there is no further motion of the valve disk, i.e., $\bar{x}\leqslant\bar{h}$ always;

2) the equalities always hold

$$\bar{p}_1 < \bar{p} < \bar{p}_1';$$

m volume

3) the system (A) is solved when $\bar{p}_2<\bar{p}$; system (B) is solved when $\bar{p}<\bar{p}_1$.

This system of five nonlinear differential equations cannot be solved by analytic methods. Various numerical methods, the Runge-Kutta

method, for example, must be used for its solution. But the numerical methods do not permit obtaining the stability criteria for this system in general form. Therefore, we must linearize the equations of the system by making some simplifications. We shall assume that

1) $\bar{p}_1 = \text{const}$;

2) $\bar{p}_3 = \text{const}$;

3) $\mu_1 = \text{const}$; $\mu_{2e} = \mu_{2s} = \text{const}$; $\mu_3 = \text{const}$;

4) $\bar{F}_1' = \frac{d\bar{F}_1}{d\bar{x}} = -\frac{\bar{F}_1}{\bar{h}-\bar{x}} = \text{const}$;

5) $\bar{a} = \bar{a}_2 = \bar{a}_1 = \text{const}$ which confirms the numerical solutions of our problem, obtained using the simplifications 1-4;

6) $\pi_2 = \varkappa \frac{\bar{p}-\bar{p}_2}{\bar{p}}$ where $\varkappa$ is a coefficient of proportionality;

7) since for $\bar{p}_2 < \bar{p}$ $\pi_2 \approx \pi_{2e} > 0$ and for $\bar{p}_2 > \bar{p}$ $\pi_2 = \pi_{2s} < 0$, then we shall represent π_{2e} and π_{2s} by the single function π_2.

Assumption 5) makes it possible to eliminate two unknowns, and therefore we can eliminate two equations — the first and fourth equations of the systems (A) and (B)[2]. The last assumption makes it possible to reduce the two systems of equations to a single system

$$\frac{d\bar{w}}{d\bar{\tau}} + \zeta_1 \bar{w} + \omega^2 \bar{x} - \zeta_2 \bar{p} - \zeta_3 \bar{p}_x \bar{p}_r (\bar{p}_1 - \bar{p}) = 0; \tag{4.95}$$

$$\frac{d\bar{p}}{d\bar{\tau}} = k\bar{a}\left[\mu_1 \bar{F}_1 \bar{p}_1 \pi_1 - \mu_2 \bar{F}_2 \varkappa (\bar{p} - \bar{p}_2) - \mu_3 \bar{F}_3 \pi_3 \bar{p}\right]; \tag{4.96}$$

$$(\bar{x} + \bar{x}_0)\frac{d\bar{p}_2}{d\bar{\tau}} = k\left[\mu_2 \bar{F}_2 \sqrt{\bar{a}} \varkappa (\bar{p} - \bar{p}_2) - \bar{p}_2 \frac{d\bar{x}}{d\bar{\tau}}\right]; \tag{4.97}$$

$$\frac{d\bar{x}}{d\bar{\tau}} = \bar{w}. \tag{4.98}$$

Footnote (2) appears on page 147.

merical
s sys-
s of the

In the linearization the deviations of the parameters are much smaller than their nominal values, i.e., $\delta\bar{x} \ll \bar{x}^\circ$, $\delta\bar{p} \ll \bar{p}^\circ$, $\delta\bar{p}_2 \ll \bar{p}_2^\circ$. Therefore, we assume, as usual, that

$$\left.\begin{aligned} \bar{x} &= \bar{x}^\circ + \delta\bar{x}; \\ \bar{p} &= 1 + \delta\bar{p}; \\ \bar{p}_2 &= 1 + \delta\bar{p}_2; \\ \bar{w} &= \bar{w}^\circ + \delta\bar{w}, \end{aligned}\right\} \tag{4.99}$$

since

$$\bar{p}^\circ = 1 \text{ and } \bar{p}_2^\circ = 1.$$

tions of

We can also write in the vicinity of the point of linearization

$$\left.\begin{aligned} \bar{P}_x &= 1 - \bar{P}'_x(\bar{h} - \bar{x}^\circ - \delta\bar{x}); \\ \bar{F}_1 &= -\bar{F}'_1(\bar{h} - \bar{x}^\circ - \delta\bar{x}), \end{aligned}\right\} \tag{4.100}$$

y;

shall

where

$$\bar{P}'_x = -\frac{d\bar{P}_x}{d\bar{x}} = \text{const};$$

$$\bar{F}'_1 = -\frac{d\bar{F}_1}{d\bar{x}} = \text{const}.$$

, and
th equa-
s it
stem

We can assume with satisfactory accuracy that $\bar{P}_x \approx \text{const}$, $\pi_1 \approx \text{const}$, $\pi_3 \approx \text{const}$. Differentiating (4.99), we also obtain

(4.95)
(4.96)
(4.97)
(4.98)

$$\left.\begin{aligned} \frac{d\bar{x}}{d\bar{\tau}} &= \frac{d\delta\bar{x}}{d\bar{\tau}} = \delta\dot{\bar{x}}; \\ \frac{d\bar{w}}{d\bar{\tau}} &= \frac{d\delta\bar{w}}{d\bar{\tau}} = \delta\dot{\bar{w}}; \\ \frac{d\bar{p}}{d\bar{\tau}} &= \frac{d\delta\bar{p}}{d\bar{\tau}} = \delta\dot{\bar{p}}; \\ \frac{d\bar{p}_2}{d\bar{\tau}} &= \frac{d\delta\bar{p}_2}{d\bar{\tau}} = \delta\dot{\bar{p}}_2 \end{aligned}\right\} \tag{4.101}$$

Expressions (4.99), (4.100) and (4.101) make it possible to reduce (4.95) - (4.98) to the linearized form

$$\dot{\delta\bar{w}} = -\zeta_1\delta\bar{w} - (\omega^2 - K_1)\delta\bar{x} - K_2\delta\bar{p} + \zeta_2\delta\bar{p}_2; \tag{4.102}$$

$$\dot{\delta\bar{x}} = \delta\bar{w}, \tag{4.103}$$

$$\dot{\delta\bar{p}} = K_3\delta\bar{x} - (K_4 + K_5)\delta\bar{p} + K_4\delta\bar{p}_2; \tag{4.104}$$

$$\dot{\delta\bar{p}}_2 = -K_6\delta\bar{w} + K_7\delta\bar{p} - K_7\delta\bar{p}_2. \tag{4.105}$$

Here

$$K_1 = \zeta_3\bar{P}_r(\bar{p}_1 - 1)\bar{P}'_x;$$
$$K_2 = \zeta_3\bar{P}_r[1 - \bar{P}'_x(\bar{h} - \bar{x}^*)];$$
$$K_3 = k\bar{a}_{p_1}\bar{F}_1\bar{p}_1\pi_1;$$
$$K_4 = k\bar{a}_{p_2}\bar{F}_2\pi;$$
$$K_5 = k\bar{a}_{p_3}\bar{F}_3\pi_3;$$

$$K_6 = \frac{k}{\bar{x}^* + \bar{x}_0},$$

$$K_7 = -\frac{k\bar{V}\mu_r\bar{F}_2\bar{a}_x}{(\bar{x}^* + \bar{x}_0)}.$$

We form a determinate from the coefficients of the right side of (4.102) – (4.105):

$$\begin{vmatrix} (-\zeta_1 - \lambda) & -(\omega^2 - K_1) & -K_2 & \zeta_2 \\ 1 & -\lambda & 0 & 0 \\ 0 & -K_3 & -(K_4 + K_5) - \lambda & K_4 \\ -K_6 & 0 & K_7 & (-K_7 - \lambda) \end{vmatrix} = 0. \tag{4.106}$$

Expanding this determinant, we obtain the characteristic equation

$$\lambda^4 + a_3\lambda^3 + a_2\lambda^2 + a_1\lambda + a_0 = 0 \tag{4.107}$$

where

$$a_3 = \zeta_1 + K_4 + K_5 + K_7;$$
$$a_2 = \omega^2 - K_1 + \zeta_1(K_4 + K_5 + K_7) + K_5K_7 + \zeta_2K_6;$$
$$a_1 = (\omega^2 - K_1)(K_4 + K_5 + K_7) + \zeta_1K_5K_7 - K_2K_4K_6 + \zeta_2K_6(K_4 + K_5) - K_2K_3;$$
$$a_0 = (\omega^2 - K_1)K_5K_7 + K_3K_7(\zeta_2 - K_2).$$

Studies of Hurwitz and Routh [36] showed that satisfaction of the following conditions is necessary and sufficient for stability of a fourth order system

$$\left.\begin{aligned} &1)\ a_1>0;\ \ a_2>0;\ \ a_3>0;\ a_0=0;\\ &2)\ a_1a_2a_3>a_0a_3^2+a_1^2;\\ &3)\ a_2^2>4a_0. \end{aligned}\right\} \tag{4.108}$$

Various constructional and operating conditions determine the magnitudes of the coefficients K_1 and a_1. Therefore, we can evaluate the stability of reducer operation by studying the influence of the various parameters on these coefficients.

If the natural frequency of the inertial-elastic system in the reducer is increased, the coefficients a_0, a_1 and a_2 also increase, which strengthens the first condition, i.e., the stability region is expanded. An increase of the damping coefficient ζ_1 has a similar effect, since a_1, a_2, a_3 are increased. Conversely, we see that increase of the inlet pressure $\bar{p}_1$ reduces the system stability region, since the coefficients a_0, a_1, a_2 decrease.

The study of the quantitative effect of the various parameters on reducer stability involves the necessity for repeated solution of (4.107), which leads to serious difficulties. Therefore, the solution of (4.107) was obtained by conventional algebraic methods, with the solution results being expressed in terms of the coefficients ω_{n1}/ω and ω_{n2}/ω, which are connected with the roots of (4.107) as follows

$$\left.\begin{aligned} \lambda_1&=-\zeta_1'\omega_{n1}-\omega_{n1}\sqrt{\zeta_1'^2-1};\\ \lambda_2&=-\zeta_1'\omega_{n1}+\omega_{n1}\sqrt{\zeta_1'^2-1};\\ \lambda_3&=-\zeta_1'\omega_{n2}+\omega_{n2}\sqrt{\zeta_1'^2-1};\\ \lambda_4&=-\zeta_1'\omega_{n2}-\omega_{n2}\sqrt{\zeta_1'^2-1}. \end{aligned}\right\} \tag{4.109}$$

We see that for $|\zeta_1'|<1$ and $|\zeta_1'|<1$ we have complex roots and ω_{n1} and ω_{n2} are the natural frequencies of the reducer oscillations. For $|\zeta_1'|<1$ and $|\zeta_1'|\geq 1$ we have only the natural frequency ω_{n1}, and ω_{n2} has

no physical meaning. The reducer is stable "in the small" if $\zeta_1' > 0$ and $\zeta_1'' > 0$. The stability boundary corresponds to the case in which one (or both) of the component coefficients equals zero while the other is positive.

The nonlinear solution of the equations of the dynamics of a gas pressure reducer were examined in [140]. However, the complexity of these solutions makes it impossible to evaluate the effect of the various design and operating parameters on the stability. Solutions of the linearized characteristic Equation (4.107) for variable parameters $\bar{F}_2$ and $\bar{\omega} = \omega/\omega^*$, where ω^* is the initial value of the real oscillation frequency of the inertial-elastic system in the reducer and ω is the current value, are shown in Figure 4.10. In the calculation we assumed:

$$F_* = 19{,}4 \cdot 10^{-4}\ м^2;\quad x_0 + h = 0{,}0254\ м;\quad \bar{p}_1 = 3;$$
$$F^* = 1{,}94 \cdot 10^{-3}\ м^2;$$
$$\bar{F}_1' = -4{,}82;\quad \bar{p}_2 = 0{,}5;\quad \bar{F}_3 = 0{,}2;$$
$$\bar{V} = 120;\quad c_f = 1{,}5\ \frac{\text{N}\cdot\text{sec}}{м};\quad \bar{a} = 1;\quad \zeta_1 = 0;$$
$$d_c = 0{,}0159\ м;\quad \bar{p}_1 = 0{,}8;\quad \bar{p}_2 = \bar{p}_3 = 1;\quad a^* = 335\ \text{м/sec};\quad \zeta_2 = 1904;$$
$$\zeta_3 = 190{,}4;\quad c = 5650\ \text{N/м};\quad m_1 = 0{,}227\ \text{kg};\quad \bar{P}_r = 1{,}07;$$
$$p^* = 70{,}31\ \text{bar};\quad \bar{P}' = 4{,}93;\quad \omega^{*'} = 2007;\quad V = 5{,}9 \cdot 10^{-3}\ м^3;$$
$$\bar{p} = \bar{p}_2 = 1;\quad \varkappa = 9{,}3.$$

Since two types of curves $\bar{F}_2 = \text{const}$ (dashed) and $\bar{\omega}^{-2} = \text{const}$ (continuous) are presented in the figure, the solution for each pair of values $\bar{F}_2$ and $\bar{\omega}^{-2}$ is given by a pair of points representing the corresponding solutions with the coordinates $(\zeta_1', \omega_{n1}/\omega)$ and $(\zeta_1'', \omega_{n2}/\omega)$.

The shaded region in Figure 4.10 represents one component of the oscillatory process and one component of the nonoscillatory process; the unshaded region represents both components of the oscillatory process. It is not difficult to see from the figure that increase of $\bar{F}_2$ above 3 has very little effect on the damping coefficients ζ_1' and ζ_1'' and on the frequency coefficients, since these values of $\bar{F}_2$ represent very low resistance to flow between V and V_2.

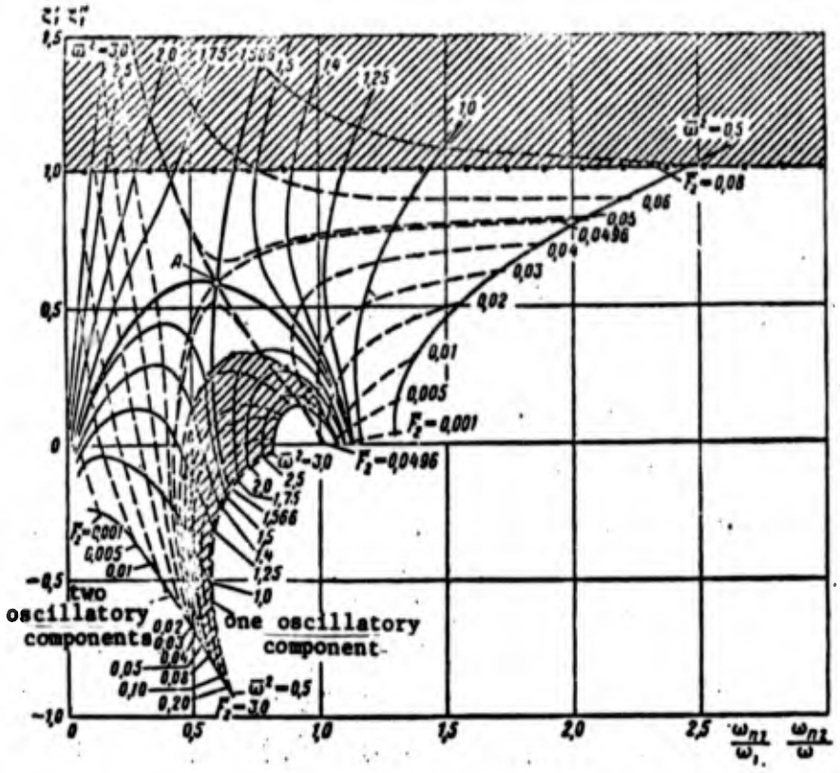

Figure 4.10. Effect of $\bar{F}_2$ and $\bar{\omega}^{-2}$ on damping coefficients ζ_1' amd ζ_1'' and frequency ω_{n1}/ω, ω_{n2}/ω for the linearized solution [140].

It is also not difficult to show that as $\bar{\omega} \to \infty$ one component approaches $\zeta_1' = 0$, $\omega_{n1}/\omega = 1$ while the other approaches the limit in which $\omega_{2n}/\omega = 0$, while ζ_1'' becomes indeterminate. The curves $\bar{F}_2 = 0.0496$ and $\bar{\omega}^{-2} = 1.566$ at the intersection point of A have $\zeta_1' = \zeta_1''$ and $\omega_{n1} = \omega_{n2}$. These curves are useful in that they separate regions in each of which it is not difficult to find the general nature of the variation of the intermediate curves. In these regions $\bar{F}_2$ and $\bar{\omega}^{-2}$ cross (ζ_1', ω_{n1}) and (ζ_1'', ω_{n2}) at different points.

In fact, let us assume that the operating and design parameters of the reducer, which enter into the coefficients a_3, a_2, a_1, a_0 in various combinations, change. Then we can see from Figure 4.10 that the theoretical solutions yield a stable process for many combinations of the parameters $\bar{F}_2$ and $\bar{\omega}^{-2}$, for example, for zero damping coefficient. With increase of the coefficients ζ_1' and ζ_1'' the point A shifts upward along

the vertical and has no effect on ω_{n1}, ω_{n2}. For small $\bar{F}_2$ or large $\bar{\omega}^2$ the curves (dashed and continuous) change only slightly. This indicates that in these regions the coefficients ζ_1' and ζ_1'' change the reducer damping very little. Thus, we can with a certain approximation classify the design and operating parameters of the reducer in accordance with their effect on ζ_1 and ω_n.

5. Component Pressure and Flow Rate Regulators

The maintenance of a definite LRE operating regime depends on the operation of various regulation systems, whose primary elements are regulators serving various purposes.

The most important parameter of a power plant is its thrust, which depends on the pressure in the combustion chamber and the ratio of the propellant components entering the chamber. It is obvious, therefore, that the primary LRE regulators will be the regulator for the combustion chamber pressure and the regulator for the component flow rate ratio.

Let us examine a combustion chamber pressure regulator, which can be, for example, a conventional pressure reducing valve [46]. A possible schematic pressure regulator is shown in Figure 4.11. We see from the schematic that increase of the combustion chamber pressure leads to displacement of the slide valve such that the flow section is reduced, and the flow rate of one of the components decreases. If the regulator is installed in the LGG line, then the power of the TPA decreases, the flow rates of the primary components decrease, and the pressure in the combustion chamber is reduced.

Let us write the equation of motion of the regulator disk, neglecting reactive forces; we direct the x-axis upward along the regulator axis and locate the coordinate origin in the plane of the seat

$$m_1\frac{d^2x}{dt^2}+c_f\frac{dx}{dt}=(p_2-p_1)F_k-p_2F_{c\phi}+p_kF_{c\phi}+P_{c0}-cx, \qquad (4.110)$$

where p_1 and p_2 are respectively the inlet and outlet pressures;

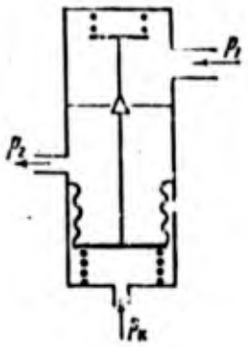

Figure 4.11. Schematic of combustion chamber pressure regulator.

F_K is the valve seat area;

F_b is the so-called effective bellows area, equal to the area of a piston which under the action of the differential pressure Δp equalizes the force applied to it.

The effective bellows area is related with its stiffness and sensitivity as follows

$$F_{c\phi}=c_{c\phi}A_{c\phi}. \qquad (4.111)$$

where A_b is the bellows sensitivity, equal to

$$A_{c\phi}=\frac{\Delta x}{\Delta p};$$

P_{c0} is the overall force of the spring and bellows for x = 0;

c is the overall stiffness of the spring and bellows.

Equation (4.110) can be rewritten in a somewhat different form

$$m_t\frac{d^2x}{dt^2}+c_f\frac{dx}{dt}-(p_2-p_1)F_K-(p_K-p_2)F_{c\phi}-$$
$$-P_{c0}+cx=0. \qquad (4.112)$$

If the TPA is driven by the products of decomposition of hydrogen peroxide, regulation of the pressure in the combustion chamber can be accomplished by varying the hydrogen peroxide flow rate into the steam gas generator.

When using an expulsion system for feeding the hydrogen peroxide to the reactor, the magnitude of the pressure p_K is determined by the pressurization pressure in the hydrogen perioxide tank. In this case the gaseous pressurization reducer acts as the p_K regulator.

In the LRE scheme with steam gas generation, a liquid pressure reducer in which the regulating force is created by the pressure of a

gas supplied through a pressure reducer from another vessel can be used in the hydrogen perioxide line as the regulator for p_K. A possible arrangement of a liquid pressure regulator with a slide valve of the knife-edge type is shown in Figure 4.12 (see [46]).

Figure 4.12. Schematic of liquid pressure reducer.

If there is a change of the peroxide flow rate, the force of its pressure on the slide valve changes and under the action of the difference of the forces the flow openings are increased (or decreased), restoring the liquid pressure to the predetermined value. A change of the engine operating regime can also be accomplished by resetting the gas pressure reducer, which leads to a new equilibrium position of the slide valve and therefore to a new hydrogen peroxide flow rate.

The equation of motion of the slide valve can be written as follows

$$m_1\frac{d^2x}{d\tau^2}+c_f\frac{dx}{d\tau}=p_yF_м-p_1F_м+p_1F_з-$$
$$-p_2F_з-c_мx-Gw, \qquad (4.113)$$

where p_y is the gas reducer exit pressure;
F_M is the effective membrane area;
F_s is the slide valve area;
p_1, p_2 are respectively the pressures at the inlet to and outlet from the liquid pressure reducer;
c_M is the membrane stiffness;
G is the liquid mass flow rate through the reducer;
w is the velocity of the liquid discharge from the slide valve body;
c_f is the friction force coefficient;
x is the coordinate measured from the inoperative position of the slide valve.

The value of the propellant component flow rate ratio in the engine combustion chamber determines the maximal specific thrust, and in the

liquid gas
the working
stant value
tion chambe

The pr
ventional
parameter
rate is not

A poss
Figure 4.13
one of the
ponent line
regulator
the degree

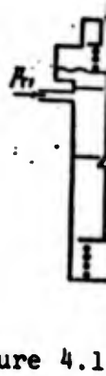

Figure 4.1
matic of
componen
regulato

c is
F_M is

$F_м$
diamet

liquid gas generator k is chosen so as to obtain constant parameters of the working medium for the turbine. Therefore, maintenance of a constant value of the propellant component ratio in both the main combustion chamber and the LGG takes on particular importance.

The propellant component flow rate ratio regulator can be a conventional flow rate limiter [46], which uses as the external regulating parameter the pressure in the line of the other component, whose flow rate is not regulated.

A possible propellant component ratio regulator scheme is shown in Figure 4.13. We see from the schematic that the resulting pressure of one of the components is compared with the pressure in the other component line. If the prescribed equilibrium position is disturbed, the regulator valve moves in the direction required to increase or decrease the degree of throttling.

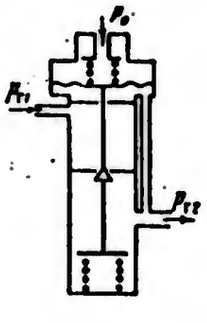

Figure 4.13. Schematic of propellant component ratio regulator.

The equation of the dynamics of this propellant component ratio regulator has the form (for the fuel line)

$$m_1\frac{d^2x}{dt^2}+c_f\frac{dx}{dt}=(p_{r1}-p_{r2})F_к+(p_{r2}-p_{II})F_{c\phi}-$$
$$-P_{r0}-cx+(p_0-p_{r2})F_м, \tag{4.114}$$

where p_{r1}, p_{r2} are respectively the fuel pressures at the regulator inlet and outlet;

F_K is the valve area;

p_0 is the oxidizer pressure, which is used in this case as the external regulating parameter;

c is the overall stiffness of the spring, bellows, and membrane;

F_M is the effective membrane area, equal to approximately

$$F_м=\frac{\pi}{4}\frac{(D'_м+D''_м)^2}{4}$$

D'_M and D''_M are respectively the outer membrane diameter and the inner diameter of the retainer.

FOOTNOTES

Footnote (1), page 111 — Here and hereafter, the static resting friction force is arbitrarily referred to the spring force p_{c0}.

Footnote (2), page 137 — Actually, for $d\bar{a}/d\bar{\tau} = 0$ the first and third equations of Systems (A) and (B) become analogous to one another; however, we retain the third equation (energy), since it also includes the first (continuity) equation, being at the same time more exact.

The obj
creation of
dynamic elem
meter of the
with other p
mines the pr
of space.

In calcu
thrust force
a given progr
tors the actu
programmed va
more accurate
produced.(1)

The exis
cult to obtai
quires the us
conditions sy

Footnote (1)

friction
ring

hird
e
retain
lso
on,

CHAPTER 5

AUTOMATIC REGULATION OF LRE

The objective of the power plant of any flight vehicle is the creation of a thrust force, which is the output parameter of the given dynamic element. The thrust force is at the same time the input parameter of the entire rocket as a dynamic system and determines along with other parameters the rocket flight trajectory, i.e., it determines the precision with which the payload is delivered to a given point of space.

In calculating the rocket trajectory, in the general case the thrust force is specified as some known time function corresponding to a given program. As a result of the action of various disturbing factors the actual value of the power plant thrust force differs from the programmed value. It is obvious that the mission will be accomplished more accurately, the more precisely the engine operating regime is reproduced.(1)

The existence of various disturbing factors which make it difficult to obtain the design parameters of the power plant components requires the use of special measures to ensure under various operating conditions synchronization in magnitude and time of the individual

---

Footnote (1) appears on page 189.

parameters of all the operating components and, in the final analysis, the proper value of the principal LRE parameter — the thrust force. In other words, in view of the fact that it is not possible to account theoretically for all the possible disturbing influences on the engine (for example, those associated with variation of meteorological conditions), it is necessary to regulate continuously the plower plant so that the disturbing deviations of the thrust force from its programmed value will approach zero in a definite fashion in the course of time. The engine automatic regulation system performs this function.

In addition to the thrust, the rocket engine is also characterized by the magnitude of the specific thrust, which defines the effectiveness of the utilization of 1 kg of propellant, i.e., the engine efficiency.

In view of the fact that the absolute and specific thrusts depend on the combustion chamber pressure and the propellant component ratio in both the main chamber and the LGG, usually the combustion chamber pressure p_K and the component ratio k are selected as the regulating parameters. Therefore, we shall examine systems for regulating the combustion chamber pressure and the propellant component ratio.

Other automatic regulation systems are also provided in addition to those just mentioned, for example, systems for maintaining a definite pressure at the inlet to the centrifugal pumps, for reducing the residual quantities of the components in the tanks, for synchronizing the operation of multichamber power plants, and so on.

The LRE is a complex dynamic system consisting of a group of elements combined in a definite fashion, which have various feedforward and feedback connections with one another. The main elements of the controllable liquid rocket engine are: combustion chamber, turbopump assembly, gas generator, hydraulic lines, automatic regulation and control elements, and so on, which constitute the structural block diagram of the engine.

The system of differential equations of all the system elements is formulated with the aid of the LRE block diagram. It is obvious that for the correct mathematical description of such a complex dynamic system as the LRE we must first obtain the equations describing the operation of its individual components.

In view of the fact that the deviations of the parameters from their nominal values which are considered in the study of the automatic regulation processes are much smaller than the nominal values themselves, usually we use the linearized equations, obtained by the method of small deviations. In this case the instantaneous value of any parameter can be represented as follows

$$\varphi=\varphi^{*}+\delta\varphi. \tag{5.1}$$

where φ^{*} is the nominal value of the parameter in question;
$\delta\varphi$ is its deviation from the nominal value.

Hereafter, we shall use the symbol "*" to denote the parameters which are defined by the nominal engine operating regime, or any other regime which is maintained at a constant level by the automatic regulation system. If the quantity is a function of several parameters its deviation is defined as follows

$$\delta\varphi(x_1, x_2, x_3, \ldots)=\left(\frac{\partial\varphi}{\partial x_1}\right)^{*}\delta x_1+\left(\frac{\partial\varphi}{\partial x_2}\right)^{*}\delta x_2+ +\left(\frac{\partial\varphi}{\partial x_3}\right)^{*}\delta x_3+\ldots. \tag{5.2}$$

where the partial derivatives are determined at the nominal operating regime point.

Usually we do not consider the absolute deviation $\delta\varphi$ but the relative deviation, represented by the ratio of the absolute deviation to the nominal value (or any other constant value) of the parameter in question

$$\bar{\delta\varphi}=\frac{\delta\varphi}{\varphi^{*}}.$$

Differentiating (5.1), we obtain a relation which will be used frequently

$$\frac{dq}{d\tau}=\frac{d\ln p}{d\tau}. \tag{5.3}$$

Now we shall derive the linearized equations of the individual LRE components and use them to obtain and study the dynamic characteristics: transfer function, amplitude-phase and transient characteristics, and so on, which are used in analyzing the automatic regulation systems for LRE.

§ 1. Combustion Chamber as a Dynamic Element of the Regulation System

We shall examine the dynamic properties of the combustion chamber in the LRE automatic regulation system, which are defined by the time variation of its basic parameters during unsteady processes. We first obtain the linearized equation of the chamber which is used to derive its basic characteristics and also to analyze the quality and stability of the regulation processes. For the derivation we use the differential Equation (3.9)

$$\begin{aligned}&\frac{V_к}{R_кT_к}\left[1-\frac{1}{R_кT_к}\frac{\partial(R_кT_к)}{\partial p_к}p_к\right]\frac{dp_к}{d\tau}+\\&+\left[\frac{A_кF_{кр}}{\sqrt{R_кT_к}}-\frac{V_к}{(R_кT_к)^2}\frac{\partial(R_кT_к)}{\partial k}\frac{dk(\tau-\tau_к)}{d\tau}\right]p_к=\\&=G_0(\tau-\tau_к)+G_г(\tau-\tau_к).\end{aligned} \tag{5.4}$$

We write this equation in terms of deviations

$$\begin{aligned}&\frac{V_к}{R_к^*T_к^*}\left[1-\frac{p_к^*}{R_к^*T_к^*}\left(\frac{\partial(R_кT_к)}{\partial p_к}\right)^*\right]\frac{d\delta p_к}{d\tau}+\frac{A_к^*F_{кр}}{\sqrt{R_к^*T_к^*}}\delta p_к+\\&+\frac{F_{кр}p_к^*}{\sqrt{R_к^*T_к^*}}\delta A_к-\frac{A_к^*F_{кр}p_к^*}{2\sqrt{(R_кT_к)^3}}\delta(R_кT_к)-\\&-\frac{p_к^*V_к}{(R_к^*T_к^*)^2}\left(\frac{\partial(R_кT_к)}{\partial k}\right)^*\frac{d\delta k(\tau-\tau_к)}{d\tau}=\\&=\delta G_0(\tau-\tau_к)+\delta G_г(\tau-\tau_к).\end{aligned} \tag{5.5}$$

We know from LRE theory that the product R_KT_K depends on the initial enthalpies l_0 and l_f of the propellant components, the component ratio k, and the chamber pressure p_K, i.e.,

$$R_{\text{к}}T_{\text{к}}=f(I_0,\ I_{\text{г}},\ k,\ p_{\text{к}}),\qquad (5.6)$$

and the complex A_n, defined by the expansion polytrope exponent n, can be considered a function of the component ratio.

Therefore, the deviations of these quantities are defined by the relations

$$\delta(R_{\text{к}}T_{\text{к}})=\left(\frac{\partial(R_{\text{к}}T_{\text{к}})}{\partial k}\right)^{*}\delta k+\left(\frac{\partial(R_{\text{к}}T_{\text{к}})}{\partial I_0}\right)^{*}\delta I_0+ \qquad (5.7)$$
$$+\left(\frac{\partial(R_{\text{к}}T_{\text{к}})}{\partial I_{\text{г}}}\right)^{*}\delta I_{\text{г}}+\left(\frac{\partial(R_{\text{к}}T_{\text{к}})}{\partial p_{\text{к}}}\right)^{*}\delta p_{\text{к}}.$$

$$\delta A_n=\left(\frac{\partial A_n}{\partial k}\right)^{*}\delta k. \qquad (5.8)$$

The deviations of the oxidizer I_0 and fuel I_f enthalpies are functions of the deviations of the component composition and the component temperature, which we shall not consider. We write (5.5) in terms of relative deviations with account for (5.7) and (5.8)

$$\frac{V_{\text{к}}p_{\text{к}}^{*}}{R_{\text{к}}^{*}T_{\text{к}}^{*}}\left[1-\frac{p_{\text{к}}^{*}}{R_{\text{к}}^{*}T_{\text{к}}^{*}}\left(\frac{\partial(R_{\text{к}}T_{\text{к}})}{\partial p_{\text{к}}}\right)^{*}\right]\frac{d\bar{\delta p}_{\text{к}}}{d\tau}+$$
$$+G^{*}\left[1-\frac{p_{\text{к}}^{*}}{2R_{\text{к}}^{*}T_{\text{к}}^{*}}\left(\frac{\partial(R_{\text{к}}T_{\text{к}})}{\partial p_{\text{к}}}\right)^{*}\right]\bar{\delta p}_{\text{к}}=$$
$$=\frac{k^{*}G^{*}}{A_n^{*}}\left[\frac{A_n^{*}}{2R_{\text{к}}^{*}T_{\text{к}}^{*}}\left(\frac{\partial(R_{\text{к}}T_{\text{к}})}{\partial k}\right)^{*}-\left(\frac{\partial A_n}{\partial k}\right)^{*}\right]\bar{\delta k}(\tau-\tau_{\text{к}})+ \qquad (5.9)$$
$$+\frac{k^{*}p_{\text{к}}^{*}V_{\text{к}}}{(R_{\text{к}}^{*}T_{\text{к}}^{*})^{2}}\left(\frac{\partial(R_{\text{к}}T_{\text{к}})}{\partial k}\right)^{*}\frac{d\bar{\delta k}(\tau-\tau_{\text{к}})}{d\tau}+G_0^{*}\bar{\delta G}_0(\tau-\tau_{\text{к}})+$$
$$+G_{\text{г}}^{*}\bar{\delta G}_{\text{г}}(\tau-\tau_{\text{к}}).$$

where the value of the overall propellant component flow rate G^{*} is defined by the known gas dynamic relation

$$G^{*}=\frac{A_{\text{кр}}^{*}p_{\text{кр}}^{*}}{\sqrt{R_{\text{к}}^{*}T_{\text{к}}^{*}}}. \qquad (5.10)$$

We introduce the following notations for the constants in (5.9):

$$\theta_{1\kappa}=\frac{p_\kappa^\circ V_\kappa}{R_\kappa^\circ T_\kappa^\circ G^\circ}\frac{\left[1-p_\kappa^\circ\left(\frac{\partial\ln(R_\kappa T_\kappa)}{\partial p_\kappa}\right)^\circ\right]}{\left[1-\frac{p_\kappa^\circ}{2}\left(\frac{\partial\ln(R_\kappa T_\kappa)}{\partial p_\kappa}\right)^\circ\right]};$$

$$\theta_{2\kappa}=\frac{k^\circ\left(\frac{\partial\ln(R_\kappa T_\kappa)}{\partial k}\right)^\circ}{\left[1-p_\kappa^\circ\left(\frac{\partial\ln(R_\kappa T_\kappa)}{\partial p_\kappa}\right)^\circ\right]}\theta_{1\kappa};$$

$$K_{\kappa k}=\frac{\left[\frac{1}{2}\left(\frac{\partial\ln(R_\kappa T_\kappa)}{\partial k}\right)^\circ-\left(\frac{\partial\ln\Lambda_\kappa}{\partial k}\right)^\circ\right]}{\left[1-\frac{p_\kappa^\circ}{2}\left(\frac{\partial\ln(R_\kappa T_\kappa)}{\partial p_\kappa}\right)^\circ\right]}k^\circ;$$

$$K_{\kappa,\sigma}=\frac{k^\circ}{(1+k^\circ)\left[1-\frac{p_\kappa^\circ}{2}\left(\frac{\partial\ln(R_\kappa T_\kappa)}{\partial p_\kappa}\right)^\circ\right]};$$

$$K_{\kappa,\tau}=\frac{1}{(1+k^\circ)\left[1-\frac{p_\kappa^\circ}{2}\left(\frac{\partial\ln(R_\kappa T_\kappa)}{\partial p_\kappa}\right)^\circ\right]}.$$

With the aid of these notations (5.9) can be easily transformed to the form

$$\theta_{2\kappa}\frac{d\bar{p}_\kappa}{d\tau}+\bar{p}_\kappa=\theta_{2\kappa}\frac{d\bar{k}(\tau-\tau_\kappa)}{d\tau}+K_{\kappa k}\bar{k}(\tau-\tau_\kappa)+$$
$$+K_{\kappa,\sigma}\bar{G}_\sigma(\tau-\tau_\kappa)+K_{\kappa,\tau}\bar{G}_\tau(\tau-\tau_\kappa). \qquad (5.11)$$

If we introduce into consideration the overall propellant liquid component flow rate, equal to $G_\tau=G_\sigma+G_\zeta$ then (5.11) will have the form

$$\theta_{2\kappa}\frac{d\bar{p}_\kappa}{d\tau}+\bar{p}_\kappa=\theta_{2\kappa}\frac{d\bar{k}(\tau-\tau_\kappa)}{d\tau}+K_{\kappa k}\bar{k}(\tau-\tau_\kappa)+$$
$$+K_\kappa^\tau\bar{G}_\tau(\tau-\tau_\kappa),$$

where $K_\kappa^\tau=\frac{1}{\left[1-\frac{p_\kappa^\circ}{2}\left(\frac{\partial\ln(R_\kappa T_\kappa)}{\partial p_\kappa}\right)^\circ\right]}$. (5.12)

The product $R_K T_K$ depends very weakly on the combustion chamber pressure. Therefore, we can assume that $\frac{\partial\ln(R_\kappa T_\kappa)}{\partial p_\kappa}=0$. In this case the expression for the coefficients presented above are simplified

The qu
We recall t

since the p

and the cha
ratio

We see
the chamber

To dete
use precompu
of the quant
as follows

Here th
of propellan

$$\theta_{1\kappa}=\frac{p_\kappa^\circ V_\kappa}{G^\circ R_\kappa^\circ T_\kappa^\circ}=\theta_\kappa;\quad \theta_{2\kappa}=k^\circ\left(\frac{\partial\ln(R_\kappa T_\kappa)}{\partial k}\right)^\circ\theta_{1\kappa};$$

$$K_{\kappa\,\beta}=k^\circ\left[\frac{1}{2}\left(\frac{\partial\ln(R_\kappa T_\kappa)}{\partial k}\right)^\circ-\left(\frac{\partial\ln A_n}{\partial k}\right)^\circ\right];$$

$$K_{\kappa\,\kappa}=\frac{k^\circ}{1+k^\circ};\quad K_{\kappa\,r}=\frac{1}{1+k^\circ};\quad K_\kappa^0=1.$$

The quantity θ_{1K} has been termed the combustion chamber constant. We recall that it is sometimes written in the form

$$\theta_{1\kappa}=\frac{p^\circ}{R_\kappa^\circ T_\kappa^\circ}L^\circ \tag{5.13}$$

since the pressure specific impulse is

$$p=\frac{P_\kappa F_{kp}}{G}, \tag{5.14}$$

and the characteristic combustion chamber length L* is defined by the ratio

$$L^\circ=\frac{V_\kappa}{F_{kp}}. \tag{5.11}$$

We see from (5.13) that for engines with similar values of $\frac{p^\circ}{R_\kappa^\circ T_\kappa^\circ}$ the chamber constant is proportional to its characteristic length.

To determine the partial derivatives $\frac{\partial\ln(R_\kappa T_\kappa)}{\partial k}$ and $\frac{\partial\ln A_n}{\partial k}$ we can use precomputed graphs or approximate formulas describing the variation of the quantities $R_K T_K$ and A_n in the vicinity of the regulation regime as follows

$$\left.\begin{aligned}\ln(R_\kappa T_\kappa)&=B_1k^2+B_2k+B_3;\\ \ln A_n&=A_1+A_2k.\end{aligned}\right\} \tag{5.12}$$

Here the coefficients A_1, A_2, B_2, B_1, and B_3 depend on the sort of propellant components.

Then it is not difficult to obtain

$$\frac{\partial \ln (R_{\kappa} T_{\kappa})}{\partial k} = 2B_1 k + B_2;$$

$$\frac{\partial \ln A_{\kappa}}{\partial k} = A_1.$$

In the case k = const (5.12) will have the form

$$\theta_{\kappa} \frac{d\delta \bar{p}_{\kappa}}{d\tau} + \delta \bar{p}_{\kappa} = \delta \bar{G}_{\tau}(\tau - \tau_{\kappa}) K_{\kappa}^{0}, \tag{5.16}$$

or

$$\theta_{\kappa} \frac{d\delta \bar{p}_{\kappa}}{d\tau} + \delta \bar{p}_{\kappa} = K_{\kappa.o} \delta \bar{G}_{o}(\tau - \tau_{\kappa}) + K_{\kappa.r} \delta \bar{G}_{r}(\tau - \tau_{\kappa}), \tag{5.17}$$

where for simplification the subscript "1", in the combustion chamber constant θ_{1K}, is dropped.

Let us find the combustion chamber transfer function. To do this we first perform Laplace transform of (5.16) and (5.17)

$$(1 + s\theta_{\kappa}) L[\delta \bar{p}_{\kappa}] = e^{-s\tau_{\kappa}} L[\delta \bar{G}_{\tau}] K_{\kappa}^{0}; \tag{5.18}$$

$$(1 + s\theta_{\kappa}) L[\delta \bar{p}_{\kappa}] = e^{-s\tau_{\kappa}} [K_{\kappa.o} L[\delta \bar{G}_{o}] + K_{\kappa.r} L[\delta \bar{G}_{r}]]. \tag{5.19}$$

We see from these equations that the combustion chamber inputs are the flow rates $\delta \bar{G}_o$ and $\delta \bar{G}_f$ and the output is the combustion chamber pressure $\delta \bar{p}_K$. Therefore, the block diagram of the combustion chamber may be represented as shown in Figure 5.1.

Now let us calculate the chamber transfer function as a dynamic element of the regulation system. In acccrdance with the definition of the transfer function, given in the preceding chapter, we can write

$$W_{\kappa}(s) = \frac{L[\delta \bar{p}_{\kappa}]}{L[\delta \bar{G}_{\tau}]} = \frac{e^{-s\tau_{\kappa}}}{1 + s\theta_{\kappa}}. \tag{5.20}$$

Replacing the complex number s by the imaginary number iω, we obtain the expression for the combustion chamber amplitude-phase characteristic

$$W_к(i\omega)=\frac{e^{-i\omega\tau_к}}{1+i\omega\theta_к}. \tag{5.21}$$

Hence we can obtain the expression for the amplitude and phase characteristics. To do this we must first determine the amplitude and phase of the complex Function (5.21). Since when dividing, the moduli are divided while the arguments are subtracted, we can obviously write

$$\overline{B}_к=\operatorname{mod}W_к(i\omega)=\frac{1}{\sqrt{1+\omega^2\theta_к^2}}; \tag{5.22}$$

$$\varphi_к=\arg W_к(i\omega)=-\tau_к\omega-\operatorname{arc\,tg}(\theta_к\omega). \tag{5.23}$$

Thus we have obtained the Amplitude (5.22) and Phase (5.23) characteristics.

Using the familiar Euler formula

$$e^{-i\tau_к\omega}=\cos\omega\tau_к-i\sin\omega\tau_к \tag{5.24}$$

it is not difficult to obatin from (5.21) the real and imaginary combustion chamber characteristics

$$u_к(\omega)=\frac{\cos\omega\tau_к-\omega\theta_к\sin\omega\tau_к}{1+\omega^2\theta_к^2}; \tag{5.25}$$

$$v_к(\omega)=-\frac{\sin\omega\tau_к+\omega\theta_к\cos\omega\tau_к}{1+\omega^2\theta_к^2}. \tag{5.26}$$

Graphs of the amplitude, phase, amplitude-phase, real and imaginary combustion chamber characteristics, constructed for θ_K = 0.0045 sec and τ_K = 0.005 sec, are shown in Figures 5.2 - 5.4.

We note that an approximate relation is sometimes used in place of the Expression (5.20) obtained for the transfer function. To do this we substitute in place of the exponential function $e^{-\cdot}$ its series expansion

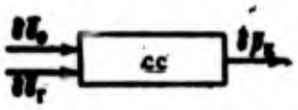

Figure 5.1. Combustion chamber block diagram.

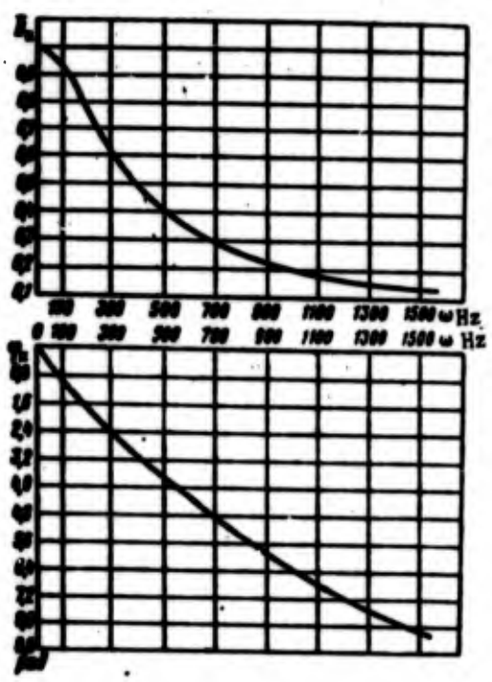

Figure 5.2. Amplitude and phase characteristics of combustion chamber.

$$e^{-s\tau_k} = 1 - s\tau_k + \frac{1}{2!}s^2\tau_k^2 - \frac{1}{3!}s^3\tau_k^3 + \ldots, \tag{5.27}$$

limited to the first two terms

$$W_k(s) = \frac{1 - s\tau_k}{1 + s\tau_k}. \tag{5.28}$$

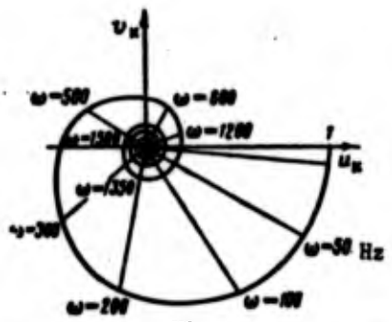

Figure 5.3. Amplitude-phse characteristic of combustion chamber.

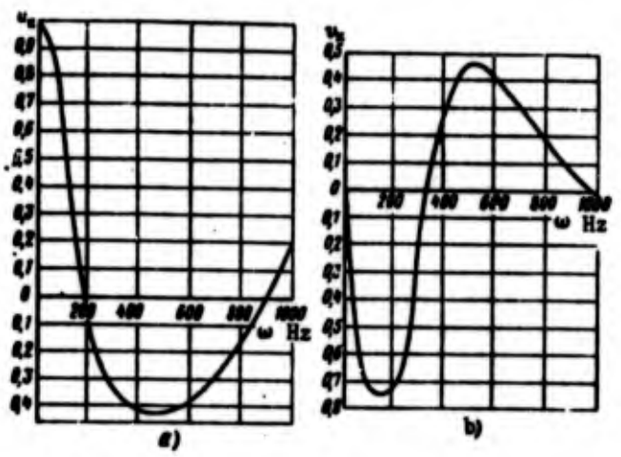

Figure 5.4. Real and imaginary characteristics of combustion chamber.

ion chamber.

From this it is easy to obtain the approximate expression for the amplitude-phase characteristic

$$W_{\text{к}}(i\omega)=\frac{1-i\omega\tau_{\text{к}}}{1+i\omega\theta_{\text{к}}} \tag{5.27}$$

Now let us examine the combustion chamber transient characteristic. In view of the fact that the root of the transfer function denominator equals $-\frac{1}{\theta_{\text{к}}}$ in accordance with the Heaviside theorem for a step function we obtain (5.28)

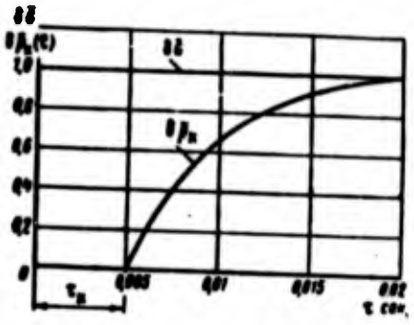

Figure 5.5. Combustion chamber transient characteristics and graph of input curve.

$$\delta\bar{p}_{\kappa}(\tau)=1-\exp\left(\frac{\tau_{\kappa}-\tau}{\theta_{\kappa}}\right)$$

A plot of the transient characteristic for a step input signal is shown in Figure 5.5.

It is not difficult to obtain the combustion chamber frequency characteristic for k = var from (5.12) after a Laplace transformation

$$W_{\kappa\beta}(i\omega)=\frac{e^{-i\omega\tau_{\kappa}}(K_{\kappa\beta}+i\omega\theta_{2\kappa})}{1+i\omega\theta_{1\kappa}};$$

$$a_{\kappa\beta}(\omega)=\frac{(K_{\kappa\beta}+\omega^2\theta_{1\kappa}\theta_{2\kappa})\cos\omega\tau_{\kappa}+\omega(\theta_{2\kappa}-K_{\kappa\beta}\theta_{1\kappa})\sin\omega\tau_{\kappa}}{1+\omega^2\theta_{1\kappa}^2};$$

$$\varphi_{\kappa\beta}(\omega)=\frac{\omega(\theta_{2\kappa}-K_{\kappa\beta}\theta_{1\kappa})\cos\omega\tau_{\kappa}-(K_{\kappa\beta}+\omega^2\theta_{1\kappa}\theta_{2\kappa})\sin\omega\tau_{\kappa}}{1+\omega^2\theta_{1\kappa}^2};$$

$$\operatorname{mod}W_{\kappa\beta}(i\omega)=\frac{1}{1+\omega^2\theta_{1\kappa}^2}\sqrt{\omega^2(\theta_{2\kappa}-K_{\kappa\beta}\theta_{1\kappa})^2+(K_{\kappa\beta}+\omega^2\theta_{1\kappa}\theta_{2\kappa})^2}\times$$

$$\sqrt{\times(\cos^2\omega\tau_{\kappa}-\sin^2\omega\tau_{\kappa})};$$

$$\arg W_{\kappa\beta}(i\omega)=\operatorname{arc\,tg}\frac{\omega(\theta_{2\kappa}-K_{\kappa\beta}\theta_{1\kappa})\cos\omega\tau_{\kappa}-(K_{\kappa\beta}+\omega^2\theta_{1\kappa}\theta_{2\kappa})\sin\omega\tau_{\kappa}}{\omega(\theta_{2\kappa}-K_{\kappa\beta}\theta_{1\kappa})\sin\omega\tau_{\kappa}+(K_{\kappa\beta}+\omega^2\theta_{1\kappa}\theta_{2\kappa})\cos\omega\tau_{\kappa}}.$$

§ 2. Equation of Centrifugal Pump as a Dynamic Element of the Regulation System

In view of the fact that the TPA of a LRE is a combination of centrifugal pumps and turbine drive, it is advisable to examine their dynamic properties separately. To derive the pump equation in terms of deviations we use the expression obtained in Chapter 3

$$p_{\kappa}=p_{\kappa x}+a_{1\kappa}\omega^2-a_{2\kappa}\omega G-b_{1\kappa}G^2-b_{2\kappa}\frac{dG}{d\tau}+b_{3\kappa}\frac{d^2\omega}{d\tau^2}. \qquad (5.29)$$

We see from this differential equation that the pump input parameters are the pumped liquid flow rate G, the angular velocity of rotation ω, and the pump inlet pressure p_{in}; the output parameter is the pressure p_H developed by the pump. The block diagram of the pump as a dynamic element is shown in Figure 5.6. We write (5.29) in terms of deviations

$$\delta(p_н - p_{вх}) = (2a_{1н}\omega^\circ - a_{2н}G^\circ)\delta\omega - \\ -(a_{2н}\omega^\circ + 2b_{1н}G^\circ)\delta G - b_{2н}\frac{d\delta G}{d\tau} + b_{1н}\frac{d\delta\omega}{d\tau}. \qquad (5.30)$$

(Here and hereafter all the parameters denoted by the symbol ° apply to the nominal regime.)

We introduce the notations

$$\delta\bar{p}_н = \frac{\delta(p_н - p_{вх})}{p_н^\circ}; \quad \delta\bar{\omega} = \frac{\delta\omega}{\omega^\circ}; \quad \delta\bar{G} = \frac{\delta G}{G^\circ}.$$

With the aid of these notations it is not difficult to obtain from (5.30) the equation of the pump dynamics in terms of linear deviations

$$\delta\bar{p}_н = \theta_{1н}\frac{d\delta\bar{\omega}}{d\tau} + K_{1н}\delta\bar{\omega} - \theta_{2н}\frac{d\delta\bar{G}}{d\tau} - K_{2н}\delta\bar{G}, \qquad (5.31)$$

where $\theta_{1н} = \frac{b_{1н}\omega^\circ}{p_н^\circ}$

$$K_{1н} = (2a_{1н}\omega^\circ - a_{2н}G^\circ)\frac{\omega^\circ}{p_н^\circ};$$

$$\theta_{2н} = \frac{b_{2н}G^\circ}{p_н^\circ};$$

$$K_{2н} = \frac{G^\circ}{p_н^\circ}(a_{2н}\omega^\circ + 2b_{1н}G^\circ).$$

Usually the terms with θ_{1H} and θ_{2H} are neglected and the pumps are considered as inertialess elements, i.e., we assume

$$\delta\bar{p}_н = K_{1н}\delta\bar{\omega} - K_{2н}\delta\bar{G}. \qquad (5.32)$$

Equations (5.31) and (5.32), Laplace transformed, have the form

$$L[\delta\bar{p}_н] = (\theta_{1н}s + K_{1н})L[\delta\bar{\omega}] - (\theta_{2н}s + K_{2н})L[\delta\bar{G}], \qquad (5.33)$$

Figure 5.6. Block diagram of centrifugal pump.

$$L[\delta\bar{p}_{\text{н}}] = K_{1\text{н}} L[\delta\bar{\omega}] - K_{2\text{н}} L[\delta\bar{G}]. \tag{5.34}$$

It is not difficult to obtain from these equations the transfer functions of the pump with respect to angular velocity and flow rate

$$W_{\text{н}\omega}(s) = \frac{L[\delta\bar{p}_{\text{н}}]}{L[\delta\bar{G}]} = -[K_{2\text{н}} + s\theta_{2\text{н}}];$$

$$W_{\text{н}\omega}(s) = \frac{L[\delta\bar{p}_{\text{н}}]}{L[\delta\bar{\omega}]} = K_{1\text{н}} + s\theta_{1\text{н}},$$

or approximately

$$W_{\text{н}\omega}(s) = K_{1\text{н}};$$
$$W_{\text{н}G}(s) = -K_{2\text{н}}.$$

We see that the construction of the amplitude characteristic corresponding to the actual characteristic does not offer any difficulty when using these formulas. The pump transient characteristic for step flow rate and angular velocity inputs can be obtained from the inverse Laplace transform formulas

$$\delta\bar{p}_{\text{н}\omega}(\tau) = L^{-1}\left[\frac{K_{1\text{н}}}{s}\right] = K_{1\text{н}};$$
$$\delta\bar{p}_{\text{н}G}(\tau) = L^{-1}\left[-\frac{K_{2\text{н}}}{s}\right] = -K_{2\text{н}}.$$

Expressions (5.31) and (5.32) can also be obtained from the pump head Equation (3.63)

$$p_{\text{н}} - p_{\text{вх}} = p_{\text{н}}^{*}(G, \omega) - b_{2\text{н}}\frac{dG}{d\tau} + b_{3\text{н}}\frac{d\omega}{d\tau}. \tag{5.35}$$

In this case the coefficients K_{1H} and K_{2H} are defined by the expressions

$$K_{1\text{н}} = \left(\frac{\partial p_{\text{н}}}{\partial \omega}\right)^{*}\frac{\omega^{*}}{p_{\text{н}}^{*}}; \tag{5.36}$$

$$K_{2H}=\left(\frac{\partial p_H}{\partial G}\right)^{*}\frac{G^{*}}{p_H^{*}}. \qquad (5.37)$$

If the pump characteristics are known, the partial derivatives are easily determined graphically at the nominal regime point as the slope of the tangent to the curves $p_H = p_H(\omega)$ and $p_H = p_H(G)$, plotted for the nominal values of ω^* and G^*.

In the preliminary design stage, when the pump characteristics are not known, the coefficients K_{1H} and K_{2H} are defined by the formulas obtained previously.

In addition to the pump head equation, in studying the regulation of LRE we also use the pump torque equation, written in linearized form. To obtain this equation we use the expression derived in Chapter 3 for M_H

$$M_H(G,\omega)=M_H^{*}(G,\omega)+A_{1H}\frac{d\omega}{d\tau}-A_{2H}\frac{dG}{d\tau}. \qquad (5.38)$$

We write this equation in terms of deviations and after making the usual transformations we obtain

$$\delta\bar{M}_H=K_{3H}\delta\bar{\omega}+K_{4H}\delta\bar{G}+\theta_{3H}\frac{d\delta\bar{\omega}}{d\tau}-\theta_{4H}\frac{d\delta\bar{G}}{d\tau} \qquad (5.39)$$

where $\delta\bar{M}_H=\frac{\delta M_H}{M_H^{*}}$;

$$K_{3H}=\left(\frac{\partial M_H}{\partial\omega}\right)^{*}\frac{\omega^{*}}{M_H^{*}};\quad K_{4H}=\left(\frac{\partial M_H}{\partial G}\right)^{*}\frac{G^{*}}{M_H^{*}};$$
$$\theta_{3H}=\frac{A_{1H}\omega^{*}}{M_H^{*}};\quad \theta_{4H}=\frac{A_{2H}G^{*}}{M_H^{*}}.$$

Neglecting the inertial terms in (5.39), we obtain

$$\delta\bar{M}_H=K_{3H}\delta\bar{\omega}+K_{4H}\delta\bar{G}. \qquad (5.40)$$

The partial derivatives appearing in the gains K_{3H} and K_{4H} and constants θ_{3H} and θ_{4H} written out above can be determined from the known relationship between the pump parameters

$$M_{\text{в}} = \frac{p_{\text{в}} - p_{\text{вх}}}{\omega \eta_{\text{в}}} G. \tag{5.41}$$

We write this expression in terms of deviations

$$\delta M_{\text{в}} = \frac{(p_{\text{в}}^{\circ} - p_{\text{вх}}^{\circ})}{\omega^{\circ} \eta_{\text{в}}^{\circ}} \delta G + \frac{G^{\circ}}{\omega^{\circ} \eta_{\text{в}}^{\circ}} \delta (p_{\text{в}} - p_{\text{вх}}) - \frac{(p_{\text{в}}^{\circ} - p_{\text{вх}}^{\circ}) G^{\circ}}{\omega^{\circ} \eta_{\text{в}}^{\circ}} \delta \omega - \frac{(p_{\text{в}}^{\circ} - p_{\text{вх}}^{\circ}) G^{\circ}}{\omega^{\circ} \eta_{\text{в}}^{\circ}} \delta \eta_{\text{в}}. \tag{5.42}$$

Assuming that

$$\eta_{\text{в}} = \eta_{\text{в}}(G, \omega),$$

we find the quantity

$$\delta \eta_{\text{в}} = \left(\frac{\partial \eta_{\text{в}}}{\partial G}\right)^{\circ} \delta G + \left(\frac{\partial \eta_{\text{в}}}{\partial \omega}\right)^{\circ} \delta \omega. \tag{5.43}$$

Substituting (5.32) and (5.43) into (5.42), after transformation we obtain

$$\delta M_{\text{в}} = \frac{(p_{\text{в}}^{\circ} - p_{\text{вх}}^{\circ}) G^{\circ}}{\omega^{\circ} \eta_{\text{в}}^{\circ}} \left[\left(\frac{\partial (p_{\text{в}} - p_{\text{вх}})}{\partial G}\right)^{\circ} \frac{1}{(p_{\text{в}}^{\circ} - p_{\text{вх}}^{\circ})} + \frac{1}{G^{\circ}} - \frac{1}{\eta_{\text{в}}^{\circ}} \left(\frac{\partial \eta_{\text{в}}}{\partial G}\right)^{\circ}\right] \delta G + \frac{(p_{\text{в}}^{\circ} - p_{\text{вх}}^{\circ}) G^{\circ}}{\omega^{\circ} \eta_{\text{в}}^{\circ}} \left[\frac{1}{(p_{\text{в}}^{\circ} - p_{\text{вх}}^{\circ})} \left(\frac{\partial (p_{\text{в}} - p_{\text{вх}})}{\partial \omega}\right)^{\circ} - \frac{1}{\omega^{\circ}} - \frac{1}{\eta_{\text{в}}^{\circ}} \left(\frac{\partial \eta_{\text{в}}}{\partial \omega}\right)^{\circ}\right] \delta \omega. \tag{5.44}$$

Since

$$\delta M_{\text{в}} = \left(\frac{\partial M_{\text{в}}}{\partial G}\right)^{\circ} \delta G + \left(\frac{\partial M_{\text{в}}}{\partial \omega}\right)^{\circ} \delta \omega, \tag{5.45}$$

it is not difficult to see from comparison of (5.44) and (5.45) that

$$\left(\frac{\partial M_{\text{в}}}{\partial G}\right)^{\circ} = \frac{(p_{\text{в}}^{\circ} - p_{\text{вх}}^{\circ}) G^{\circ}}{\omega^{\circ} \eta_{\text{в}}^{\circ}} \left[\frac{1}{(p_{\text{в}}^{\circ} - p_{\text{вх}}^{\circ})} \left(\frac{\partial (p_{\text{в}} - p_{\text{вх}})}{\partial G}\right)^{\circ} + \frac{1}{G^{\circ}} - \frac{1}{\eta_{\text{в}}^{\circ}} \left(\frac{\partial \eta_{\text{в}}}{\partial G}\right)^{\circ}\right]; \tag{5.46}$$

(5.41)

$$\left(\frac{\partial M_н}{\partial \omega}\right)^{\circ} = \frac{(p_н^{\circ} - p_{вх}^{\circ})G^{\circ}}{\omega^{\circ}\eta_н^{\circ}}\left[\frac{1}{(p_н^{\circ} - p_{вх}^{\circ})}\left(\frac{\partial(p_н - p_{вх})}{\partial \omega}\right)^{\circ} - \right.$$

$$\left. - \frac{1}{\omega^{\circ}} - \frac{1}{\eta_н^{\circ}}\left(\frac{\partial \eta_н}{\partial \omega}\right)^{\circ}\right]. \qquad (5.47)$$

(5.42) Neglecting the variation of the efficiency for small linear deviations from the regulated regime, we finally obtain

$$\left(\frac{\partial M_н}{\partial G}\right)^{\circ} = \frac{(p_н^{\circ} - p_{вх}^{\circ})G^{\circ}}{\omega^{\circ}\eta_н^{\circ}}\left[\frac{1}{p_н^{\circ} - p_{вх}^{\circ}}\left(\frac{\partial(p_н - p_{вх})}{\partial G}\right)^{\circ} + \frac{1}{G^{\circ}}\right]. \qquad (5.48)$$

$$\left(\frac{\partial M_н}{\partial \omega}\right)^{\circ} = \frac{(p_н^{\circ} - p_{вх}^{\circ})G^{\circ}}{\omega^{\circ}\eta_н^{\circ}}\left[\frac{1}{p_н^{\circ} - p_{вх}^{\circ}}\left(\frac{\partial(p_н - p_{вх})}{\partial \omega}\right)^{\circ} - \frac{1}{\omega^{\circ}}\right]. \qquad (5.49)$$

The partial derivatives $\left(\frac{\partial(p_н - p_{вх})}{\partial G}\right)^{\circ}$ and $\left(\frac{\partial(p_н - p_{вх})}{\partial \omega}\right)^{\circ}$ appearing in these formulas are determined, as shown above, graphically.

(5.43) If the pump characteristics are not known, then the partial derivatives appearing in the constant quantities $K_{3н}$, $K_{4н}$, $0_{3н}$, $0_{4н}$ are

nsformation determined as approximately as follows. Assuming

$$M_н \approx K\omega G,$$

where the constant of proportionality is determined by the nominal regime parameters

(5.44)

$$K = \frac{M_н^{\circ}}{\omega^{\circ}G^{\circ}}$$

we obtain

(5.45)

$$\left(\frac{\partial M_н}{\partial \omega}\right)^{\circ} = \frac{M_н^{\circ}}{\omega^{\circ}};$$

$$\left(\frac{\partial M_н}{\partial G}\right)^{\circ} = \frac{M_н^{\circ}}{G^{\circ}}.$$

5.45) that

(5.46)

§ 3. TPA Rotor as a Dynamic Element of the Regulation System

To derive the equation of TPA rotor dynamics in linearized form we use (3.83)

$$J_a \frac{d\omega}{dt} = M_T - M_{a.c} - M_{a.r}, \tag{5.50}$$

written in terms of deviations

$$J_a \frac{d\delta\omega}{dt} = \delta M_T - \delta M_{a.c} - \delta M_{a.r}. \tag{5.51}$$

Let us determine the deviation of the turbine torque. We know from turbine theory that M_T is a function of the working medium flow rate G' through the turbine, angular velocity of rotation ω, gas work capacity $R'_K T'_K$, and turbine backpressure or, more precisely, the ratio of the pressure downstream of the turbine to the pressure in the gas generator p_2/p'_K [(2)]:

$$M_T = M_T\left(G', \omega, R'_g T'_g, \frac{p_2}{p'_g}\right). \tag{5.52}$$

We find the turbine torque deviation

$$\delta M_T = \left(\frac{\partial M_T}{\partial G'}\right)^* \delta G' + \left(\frac{\partial M_T}{\partial \omega}\right)^* \delta\omega + \left(\frac{\partial M_T}{\partial R'_g}\right)^* \delta R'_g + \left(\frac{\partial M_T}{\partial \pi_2}\right)^* \delta\pi_2, \tag{5.53}$$

where $\pi_2 = \frac{p_2}{p'_g}$

$$l'_g = \sqrt{R'_g T'_g}.$$

Substituting (5.53) into (5.51) and taking account of (5.45), we obtain

---

Footnote (2) appears on page 189.

$$J_a \frac{d\omega}{d\tau} = \left(\frac{\partial M_T}{\partial \omega} - \frac{\partial M_{a.n}}{\partial \omega} - \frac{\partial M_{a.r}}{\partial \omega}\right)^\circ \delta\omega - \left(\frac{\partial M_T}{\partial G'}\right)^\circ \delta G' + \\ + \left(\frac{\partial M_T}{\partial l_K'}\right)^\circ \delta l_K' + \left(\frac{\partial M_T}{\partial \pi_2}\right)^\circ \delta\pi_2 - \left(\frac{\partial M_{a.n}}{\partial G_0}\right)^\circ \delta G_0 - \left(\frac{\partial M_{a.r}}{\partial G_r}\right)^\circ \delta G_r. \quad (5.54)$$

We convert to dimensionless parameters

$$\theta_a \frac{d\bar{\omega}}{d\tau} + \delta\bar{\omega} = K_{1a}\delta\bar{G}' + K_{2a}\delta\bar{l}_K' + K_{3a}\delta\pi_2 - K_{4a}\delta\bar{G}_0 - K_{5a}\delta\bar{G}_r. \quad (5.55)$$

Here

$$\theta_a = \frac{J_a}{\left(\frac{\partial M_{a.a}}{\partial \omega}\right)^\circ + \left(\frac{\partial M_{a.r}}{\partial \omega}\right)^\circ - \left(\frac{\partial M_T}{\partial \omega}\right)^\circ},$$

$$K_{1a} = \frac{G_*'\left(\frac{\partial M_T}{\partial G'}\right)^\circ}{\omega^\circ\left[\left(\frac{\partial M_{a.a}}{\partial \omega}\right)^\circ + \left(\frac{\partial M_{a.r}}{\partial \omega}\right)^\circ - \left(\frac{\partial M_T}{\partial \omega}\right)^\circ\right]};$$

$$K_{2a} = \frac{l_K^{a'}}{\omega^\circ} \frac{\left(\frac{\partial M_T}{\partial l_K'}\right)^\circ}{\left[\left(\frac{\partial M_{a.a}}{\partial \omega}\right)^\circ + \left(\frac{\partial M_{a.r}}{\partial \omega}\right)^\circ - \left(\frac{\partial M_T}{\partial \omega}\right)^\circ\right]};$$

$$K_{3a} = \frac{p_2^\circ\left(\frac{\partial M_T}{\partial \pi_2}\right)^\circ}{p_*^{a'}\omega^\circ\left[\left(\frac{\partial M_{a.n}}{\partial \omega}\right)^\circ + \left(\frac{\partial M_{a.r}}{\partial \omega}\right)^\circ - \left(\frac{\partial M_T}{\partial \omega}\right)^\circ\right]};$$

$$K_{4a} = \frac{G_0^\circ}{\omega^\circ} \frac{\left(\frac{\partial M_{a.a}}{\partial G_0}\right)^\circ}{\left[\left(\frac{\partial M_{a.n}}{\partial \omega}\right)^\circ + \left(\frac{\partial M_{a.r}}{\partial \omega}\right)^\circ - \left(\frac{\partial M_T}{\partial \omega}\right)^\circ\right]};$$

$$K_{5a} = \frac{G_r^\circ}{\omega^\circ} \frac{\left(\frac{\partial M_{a.r}}{\partial G_r}\right)^\circ}{\left[\left(\frac{\partial M_{a.a}}{\partial \omega}\right)^\circ + \left(\frac{\partial M_{a.r}}{\partial \omega}\right)^\circ - \left(\frac{\partial M_T}{\partial \omega}\right)^\circ\right]}.$$

If the pressure differential across the tribune is critical, then the back pressure has no effect on the turbine characteristics and then[3] $K_{3a} = 0$. If we neglect the change of the working medium work capacity, i.e., if we assume $l_K' = \text{const}$, then the coefficient $K_{2a} = 0$. With these assumptions (5.55) is simplified

---

Footnote (3) appears on page 189.

$$T_a \frac{d\bar{\omega}}{d\tau} + \bar{\omega} = K_{\omega G'} \bar{G}' - K_{\omega G_0} \bar{G}_0 - K_{\omega l_K'} \bar{l}_{K'}. \qquad (5.56)$$

Equations (5.55) and (5.56) make it possible to represent the block diagram of the TPA rotor as a dynamic element of the automatic regulation system (Figure 5.7).

To determine the partial derivatives $\frac{\partial M_T}{\partial \omega}$, $\frac{\partial M_T}{\partial G'}$, $\frac{\partial M_T}{\partial l_K'}$ and $\frac{\partial M_T}{\partial \pi_2}$ we use (2.35)

$$M_T = G' \left[a_4(\pi_2) l_K' - a_5 \omega - \frac{a_6(\pi_2)\omega^2}{l_K'} - a_7(\pi_2) \frac{(l_K')^2}{\omega} \right]. \qquad (5.57)$$

We differentiate this expression with respect to ω, G', l_K', π_2:

$$\left(\frac{\partial M_T}{\partial \omega}\right)^0 = -G_0' \left[a_5 + 2\frac{a_6(\pi_2^0)\omega^0}{l_K'^0} - a_7(\pi_2^0)\frac{(l_K'^0)^2}{\omega^{02}} \right]; \qquad (5.58)$$

$$\left(\frac{\partial M_T}{\partial G'}\right)^0 = a_4(\pi_2^0) l_K'^0 - a_5\omega^0 - \frac{a_6(\pi_2^0)\omega^{02}}{l_K'^0} - a_7(\pi_2^0)\frac{(l_K'^0)^2}{\omega^0}; \qquad (5.59)$$

$$\left(\frac{\partial M_T}{\partial l_K'}\right)^0 = G^{0\prime} \left[a_4(\pi_2^0) + \frac{a_6(\pi_2^0)\omega^{02}}{l'^{02}_K} - 2\frac{a_7(\pi_2^0) l_K'^0}{\omega^0} \right]; \qquad (5.60)$$

$$\left(\frac{\partial M_T}{\partial \pi_2}\right)^0 = G^{0\prime} \left[l_K'^0 \left(\frac{\partial a_4}{\partial \pi_2}\right)^0 - \frac{(\omega^0)^2}{l_K'^0} \left(\frac{\partial a_6}{\partial \pi_2}\right)^0 - \frac{(l_K'^0)^2}{\omega^0} \left(\frac{\partial a_7}{\partial \pi_2}\right)^0 \right]. \qquad (5.61)$$

Since the coefficients a_4, a_6, a_7 are defined by the formulas (see Chapter 2)

$$\left.\begin{aligned} a_4 &= a_4' \sqrt{1 - \pi_2^{\frac{n-1}{n}}}; \\ a_6 &= a_6' \left(1 - \pi_2^{\frac{n-1}{n}}\right)^{\frac{1}{2}}; \\ a_7 &= a_7' \left(1 - \pi_2^{\frac{n-1}{n}}\right), \end{aligned}\right\} \qquad (5.62)$$

where a_4', a_6', a_7' are constants for a given turbine, it is not difficult to find the partial derivatives $\frac{\partial a_4}{\partial \pi_2}$, $\frac{\partial a_6}{\partial \pi_2}$ and $\frac{\partial a_7}{\partial \pi_2}$

(5.56)

ent the
automatic

$\frac{\partial M_T}{\partial n_2}$ we use

(5.57)

, l'_K, π_2:

(5.58)

(5.59)

(5.60)

(5.61)

ormulas

(5.62)

not diffi-

$$\left.\begin{aligned}
\left(\frac{\partial a_4}{\partial n_2}\right)^\circ &= -\frac{(n-1)\,a'_4}{2n\sqrt[n]{\pi_2^\circ}\sqrt{1-(\pi_2^\circ)^{\frac{n-1}{n}}}};\\
\left(\frac{\partial a_6}{\partial n_2}\right)^\circ &= \frac{(n-1)\,a'_6}{2n\left(1-\pi_2^{\circ\frac{n-1}{n}}\right)^{1/2}\sqrt[n]{\pi_2^\circ}};\\
\left(\frac{\partial a_7}{\partial n_2}\right)^\circ &= -\left(\frac{n-1}{n}\right)a'_7\sqrt[n]{\pi_2^\circ}.
\end{aligned}\right\} \qquad (5.63)$$

In the general case the quantity $l'_\kappa=\sqrt{R'_\kappa T'_\kappa}$ depends on the component ratio k' in the gas generator, the enthalpy of the components, and the pressure p'_K. Usually the propellant component ratio k' has the greatest influence on the parameter l'_K. Therefore we can assume that

$$\delta l'_\kappa=\frac{\partial l'_\kappa}{\partial k'}\delta k'. \qquad (5.64)$$

Then the equation of the TPA rotor dynamics (5.55) can with sufficient accuracy be written as follows

$$\theta_\omega\frac{d\bar{\omega}}{d\tau}+\bar{\omega}=K_{1\omega}\delta\bar{G}'+K_{2\omega}\delta\bar{n}_2-K_{4\omega}\delta\bar{G}_0-K_{5\omega}\delta\bar{G}_T+K_{6\omega}\delta\bar{k}', \qquad (5.65)$$

where

$$K_{6\omega}=\frac{k^{\circ\prime}}{\omega^\circ}\frac{\left(\frac{\partial M_T}{\partial l'_\kappa}\right)^\circ}{\left(\frac{\partial M_{\kappa.n}}{\partial\omega}\right)^\circ+\left(\frac{\partial M_{\kappa.r}}{\partial\omega}\right)^\circ-\left(\frac{\partial M_T}{\partial\omega}\right)^\circ}\left(\frac{\partial l'_\kappa}{\partial k'}\right)^\circ. \qquad (5.66)$$

The partial derivative $\frac{\partial l'_\kappa}{\partial k'}$ is determined from the graph of the relation $l'_K = l_K(k)$ in the nominal regime or with the aid of the approximate formula

$$l'_\kappa=\frac{1}{\sqrt{a_1k'^2+a_2k'+a_3}} \qquad (5.67)$$

hence

$$\frac{\partial l'_\kappa}{\partial k'}=-\frac{2a_1k^{\circ\prime}+a_2}{(l'_\kappa)^3} \qquad (5.68)$$

We now perform the Laplace transform (5.65)

$$(1+s\theta_a)L[\bar{\omega}]=K_{1a}L[\bar{\delta U}']+K_{2a}L[\bar{z_1 z_2}]-K_{3a}L[\bar{\delta U_0}]-$$
$$-K_{4a}L[\bar{\delta U_r}]+K_{5a}L[\bar{\delta k'}]. \tag{5.69}$$

We find the TPA rotor transfer functions

$$W_{a\delta U'}=\frac{L[\bar{\omega}]}{L[\bar{\delta U'}]}=\frac{K_{1a}}{1+s\theta_a}; \tag{5.70}$$

$$W_{a\delta k'}=\frac{L[\bar{\omega}]}{L[\bar{\delta k'}]}=\frac{K_{5a}}{1+s\theta_a}; \tag{5.71}$$

$$W_{az_1z_2}=\frac{L[\bar{\omega}]}{L[\bar{z_1 z_2}]}=\frac{K_{2a}}{1+s\theta_a}; \tag{5.72}$$

$$W_{a\delta U_{0,r}}=\frac{L[\bar{\omega}]}{L[\bar{\delta U_{0,r}}]}=-\frac{K_{3,4a}}{1+s\theta_a}, \tag{5.73}$$

i.e., in the general form the transfer function for all the inputs can be written as

$$W_a=\frac{K_a}{1+s\theta_a}. \tag{5.74}$$

The amplitude-phase characteristic of the TPA rotor will obviously be[4]

$$W_a=\frac{K_a}{1+i\omega\theta_a}. \tag{5.75}$$

We can easily obtain the real and imaginary TPA rotor characteristics from (5.75)

$$u_a(\omega)=\frac{K_a}{1+\omega^2\theta_a^2}; \tag{5.76}$$

$$v_a(\omega)=-\frac{K_a\theta_a\omega}{1+\omega^2\theta_a^2}. \tag{5.77}$$

and also the amplitude and phase characteristics

Footnote (4) appears on page 169.

$$\bar{B}_a = \operatorname{mod} W_a(i\omega) = \frac{K_a}{\sqrt{1+\omega^2\theta_a^2}}, \tag{5.78}$$

(5.69)

$$\varphi_a = \arg W_a(i\omega) = -\operatorname{arctg}\omega\theta_a. \tag{5.79}$$

Now let us find the TPA rotor transient process. In view of the fact that the root of the transfer function denominator is $s = -\frac{1}{\theta_a}$ in accordance with the Heaviside theorem for a step input we obtain

(5.70)

$$\bar{h}_\omega(\tau) = K_a\left[1-\exp\left(-\frac{\tau}{\theta_a}\right)\right]. \tag{5.71}$$

(5.72)

§ 4. Equation of the Hydraulic Line as a Dynamic Element of the Regulation System

(5.73)

In view of the fact that the deviations of the parameters during regulation from the steady state regime are very small, we use the approximate equation for the hydraulic line dynamics in the form

nputs can

$$p_1 = p_2 + b_1 G^2 + b_2\frac{dG}{d\tau} - p_z. \tag{5.81}$$

(5.74)

We write this equation in terms of deviations for p_z = const:

obviously

$$\delta(p_1-p_2) = 2b_1G^*\delta G + b_2\frac{d\delta G}{d\tau}. \tag{5.82}$$

(5.75)

Converting to relative quantities, we obtain

$$\theta_m\frac{d\bar{G}}{d\tau} + \bar{G} = K_m\delta\Delta\bar{p}_m, \tag{5.83}$$

aracter-

(5.76)

where

(5.77)

$$\delta\Delta\bar{p}_m = \frac{\delta(p_1-p_2)}{p_1^*-p_2^*};$$

$$K_m = \frac{p_1^*-p_2^*}{2b_1G^{*2}};$$

$$\theta_m = \frac{b_2}{2b_1G^*}.$$

The block diagram of the hydraulic line as a dynamic element is shown in Figure 5.8. We perform the Laplace transform (5.83)

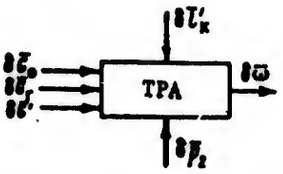

Figure 5.7. Block diagram of turbopump assembly rotor.

Figure 5.8. Block diagram of hydraulic line.

$$(1+s\theta_{\text{н}})L[\delta\bar{G}]=K_{\text{н}}L[\delta\Delta\bar{p}_{\text{н}}]. \tag{5.84}$$

Hence it is easy to find the transfer function of the hydraulic line

$$W_{\text{н}}(s)=\frac{L[\delta\bar{G}]}{L[\delta\Delta\bar{p}]}=\frac{K_{\text{н}}}{1+s\theta_{\text{н}}} \tag{5.85}$$

and this means we can also find the amplitude-phase, real, imaginary, amplitude, and phase characterisitcs

$$W_{\text{н}}(i\omega)=\frac{K_{\text{н}}}{1+i\omega\theta_{\text{н}}}; \tag{5.86}$$

$$u_{\text{н}}(\omega)=\frac{K_{\text{н}}}{1+\omega^2\theta_{\text{н}}^2}; \tag{5.87}$$

$$v_{\text{н}}(\omega)=-\frac{K_{\text{н}}\omega\theta_{\text{н}}}{1+\omega^2\theta_{\text{н}}^2}; \tag{5.88}$$

$$\bar{B}_{\text{н}}=\operatorname{mod}W(i\omega)=\frac{K_{\text{н}}}{\sqrt{1+\omega^2\theta_{\text{н}}^2}}; \tag{5.89}$$

$$\varphi_{\text{н}}=\arg W(i\omega)=-\operatorname{arctg}\theta_{\text{н}}\omega. \tag{5.90}$$

The graphs of these characteristics do not differ from those of the TPA rotor. The transient process in the hydraulic line is determined similarly

$$\delta\bar{G}(\tau)=K_{\text{н}}(1-e^{-\tau/\theta_{\text{н}}}). \tag{5.91}$$

We note that the inertial term in (5.82) is frequently neglected and then the equation for the hydraulic line is simplified considerably

$$\delta\bar{G} = K_{\text{л}}\delta\Delta\bar{p}_{\text{л}}. \tag{5.92}$$

§ 5. Equation of Combustion Chamber Pressure Regulator as a Dynamic Element of the Regulation System

The various engine automatic control elements do not differ significantly from one another. Therefore, it is advisable to examine the dynamic properties of some one regulator in the regulation system, for example the combustion chamber pressure regulator, whose dynamic equation is written in accordance with (4.110)

$$m_1\frac{d^2x}{d\tau^2} + c_f\frac{dx}{d\tau} + cx = -p_1F_{\text{к}} + (F_{\text{к}} - F_{\text{с}\phi})p_2 + F_{\text{с}\phi}p_{\text{к}} + P_{\text{с}0}. \tag{5.93}$$

For the sake of simplicity we consider the case in which $F_{be} = F_K$. Then, assuming that P_{c0} depends in the general case on the adjusting screw rotation angle Ψ, in terms of deviations we can write

$$m_1\frac{d^2\delta x}{d\tau^2} + c_f\frac{d\delta x}{d\tau} + c\delta x = -F_{\text{к}}\delta p_1 + F_{\text{к}}\delta p_{\text{к}} + \frac{\partial P_{\text{с}0}(\psi)}{\partial\psi}\delta\psi. \tag{5.94}$$

We convert to dimensionless quantities and after transformations obtain

$$\theta_{2p}\frac{d^2\delta\bar{x}}{d\tau^2} + \theta_{1p}\frac{d\delta\bar{x}}{d\tau} + \delta\bar{x} = K_{1p}\delta\bar{p}_{\text{к}} + K_{2p}\delta\bar{p}_1 + K_{3p}\delta\bar{\psi}, \tag{5.95}$$

where

$$\theta_{1p} = \frac{c_f}{c};\quad \theta_{2p} = \frac{m_1}{c};$$

$$K_{1p} = \frac{p_{\text{к}}^{\circ}F_{\text{к}}}{x^{\circ}c};$$

$$K_{2p} = -\frac{p_1^{\circ}F_{\text{к}}}{x^{\circ}c};$$

$$K_{3p} = \frac{\partial P_{\text{с}0}(\psi)}{\partial\psi}\frac{\psi^{\circ}}{x^{\circ}c}.$$

This equation makes it possible to construct the block diagram of the combustion chamber pressure regulator as shown in Figure 5.9. We see that the output coordinate — the displacement $\delta\bar{x}$ which determines the component flow rate into the chamber — is determined by the pressure p_K, the regulator inlet pressure p_1 and the spring adjusting screw angular rotation.

Now we Laplace transform (5.95)

$$(1+\theta_{1p}s+\theta_{2p}s^2)L[\delta\bar{x}]=K_{1p}L[\delta\bar{p}_K]+K_{2p}L[\delta\bar{p}_1]+K_{3p}L[\delta\bar{\gamma}]. \tag{5.96}$$

Hence the regulator transfer functions will be

$$W_{1p}=\frac{L[\delta\bar{x}]}{L[\delta\bar{p}_K]}=\frac{K_{1p}}{1+\theta_{1p}s+\theta_{2p}s^2}; \tag{5.97}$$

$$W_{2p}=\frac{L[\delta\bar{x}]}{L[\delta\bar{p}_1]}=\frac{K_{2p}}{1+\theta_{1p}s+\theta_{2p}s^2}; \tag{5.98}$$

$$W_{3p}=\frac{L[\delta\bar{x}]}{L[\delta\bar{\gamma}]}=\frac{K_{3p}}{1+\theta_{1p}s+\theta_{2p}s^2}. \tag{5.99}$$

The amplitude-phase characteristic of the regulator for any j^{th} parameter is defined by the obvious expression

$$W_{jp}(i\omega)=\frac{K_{jp}}{1+i\omega\theta_{1p}-\theta_{2p}\omega^2}.$$

Hence it is not difficult to find all the remaining characteristics — real, imaginary, amplitude, and phase

$$u_p(\omega)=\frac{K_{jp}(1-\theta_{2p}\omega^2)}{1+(\theta_{1p}^2-2\theta_{2p})\omega^2+\theta_{2p}^2\omega^4};$$

$$v_p(\omega)=-\frac{K_{jp}\theta_{1p}\omega}{1+(\theta_{1p}^2-2\theta_{2p})\omega^2+\theta_{2p}^2\omega^4};$$

$$\bar{B}_p=\operatorname{mod}W_{jp}(i\omega)=\frac{K_{jp}}{\sqrt{1+(\theta_{1p}^2-2\theta_{2p})\omega^2+\theta_{2p}^2\omega^4}};$$

$$\varphi_p=\arg W_{jp}(i\omega)=-\operatorname{arctg}\frac{\theta_{1p}\omega}{1-\theta_{2p}\omega^2}.$$

The regulator transient characteristic can be obtained easily using (5.98)

Figure 5.
bustion
tor.

The
of the dy
the speci
in practi
particula
studying
another p
possible
position p
matic is s

For t
effects du
We see fro
the automa
justing sc
determines
result of
across the
the steam
causes a d
quired dir
regime of
rates, and

diagram
ure 5.9.
ch deter-
ned by the
adjusting

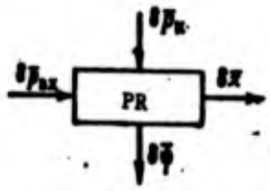

Figure 5.9. Block diagram of combustion chamber pressure regulator.

$$\delta\bar{x}(\tau)=1+\frac{\exp(s_1\tau)}{s_1(\theta_{1p}+2\theta_{2p}s_1)}+\frac{\exp(s_2\tau)}{s_2(\theta_{1p}+2\theta_{2p}s_2)}$$

where

$$s_{1,2}=\frac{-\theta_{1p}\pm\sqrt{\theta_{1p}^2-4\theta_{2p}}}{2\theta_{2p}}.$$

(5.96)

§ 6. The LRE as a Controlled Plant

(5.97)

(5.98)

(5.99)

any j^{th}

The results obtained above make it possible to approach the study of the dynamic properties of the rocket engine as a whole. In view of the specific peculiarities of the various types of LRE it is difficult in practice to study all possible engine schemes. But there is no particular advantage in doing this, since the principles involved in studying one power plant do not differ in any way from those used with another power plant. Therefore, as an example we shall examine a possible LRE scheme with a turbopump assembly operating on the decomposition products of hydrogen peroxide (see [150], [9]) whose schematic is shown in Figure 5.10.

racteristics

For the sake of simplicity we shall not take into account the effects due to the change of the propellant component inlet pressures. We see from Figure 5.10 that the flight vehicle velocity signal causes the automatic regulation system to turn the gas pressure reducer adjusting screw in the required direction (through the angle $\delta\psi$) and this determines the hydrogen peroxide tank pressurization pressure. As a result of this there is a change of the pressure differential $p'_H - p'_K$ across the peroxide line and a change of the component flow rate into the steam gas generator (SGG). The SGG operating regime changes and causes a deviation of the turbine rotor angular velocity in the required direction. The deviation $\delta\omega$ causes a change of the operating regime of the oxidizer and fuel pumps, a change of the component flow rates, and in the final analysis a change of the combustion chamber

easily

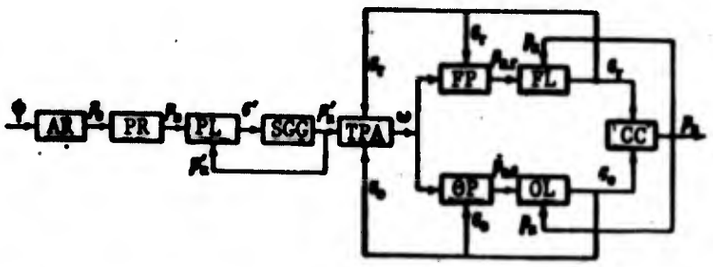

Figure 5.10. Block diagram of LRE with turbopump and with gas generation.

1) air pressure reducer (AR); 2) hydrogen peroxide pressure reducer (PR); 3) peroxide line (PL); 4) gas generator (SGG); 5) turbopump (TPA); 6) fuel pump (FP); 7) oxidizer pump (OP); 8) fuel line (FL); 9) oxidizer line (OL); 10) combustion chamber (CC).

pressure (and this means a change of the power plant thrust, which determines the flight vehicle velocity).

We shall construct a mathematical model of this particular LRE, i.e., we shall formulate the system of equations describing the operation of the individual elements of the engine. On the basis of the results obtained previously it is obvious that this system will include the following equations:

a) equation of the combustion chamber in transform form

$$(1+\vartheta\theta_{\kappa})L[\delta\bar{p}_{\kappa}]=e^{-\tau_{\kappa}s}[K_{\kappa.o}L[\delta\bar{G}_{0}]+K_{\kappa.r}L[\delta\bar{G}_{r}]]; \qquad (5.100)$$

b) equation of the lines (without regulating organs)

$$(1+\vartheta\theta_{\pi.o})L[\delta\bar{G}_{0}]=K_{\pi.o}L[\delta\Delta\bar{p}_{\pi.o}]; \qquad (5.101)$$

$$(1+\vartheta\theta_{\pi.r})L[\delta\bar{G}_{r}]=K_{\pi.r}L[\delta\Delta\bar{p}_{\pi.r}]; \qquad (5.102)$$

c) equation of the pumps

$$L[\delta\bar{p}_{\text{н.о}}]=(K_{\text{н.о}}+\theta_{\text{н.о}}s)L[\delta\bar{\omega}]-(K_{\text{н.о}}+\theta_{\text{н.о}}s)L[\delta\bar{G}_{0}]; \qquad (5.103)$$

d) eq
the assumpt
critical,(5

e) eq

f) eq

g) co

We neg
we set the
equations a

Footnote (5)

$$L[\delta\bar{p}_{\text{н.г}}]=(K_{1\text{н.г}}+\theta_{1\text{н.г}}s)L[\delta\bar{\omega}]-(K_{2\text{н.г}}+\theta_{2\text{н.г}}s)L[\delta\bar{G}_{\text{г}}];\qquad(5.104)$$

d) equation of the TPA rotor in transform form, obtained under the assumption that the pressure drop across the turbine is supercritical,[5] i.e., for $K_{3a} = 0$

$$(1+s\theta_{\text{н}})L[\delta\bar{\omega}]=K_{1\text{н}}L[\delta\bar{G}']-K_{4\text{н}}L[\delta\bar{G}_0]-K_{5\text{н}}L[\delta\bar{G}_{\text{г}}];\qquad(5.105)$$

e) equation of the steam gas generator

$$(1+s\theta'_{\text{г}})L[\delta\bar{p}'_{\text{г}}]=e^{-s\tau'_{\text{г}}}K'_{\text{г}}L[\delta\bar{G}'];\qquad(5.106)$$

f) equation of the hydrogen peroxide line

$$(1+s\theta'_{\text{м}})L[\delta\bar{G}']=K'_{\text{м}}L[\delta\Delta\bar{p}'_{\text{м}}];\qquad(5.107)$$

g) combined equation of the gas and liquid pressure reducers

$$L[\delta\bar{p}'_{\text{м}}]=K'_{\phi}L[\delta\bar{\varphi}].\qquad(5.108)$$

We neglect the effect of the pump and hydraulic line inertia, i.e., we set the terms with θ_H and θ_M equal to zero. Then the system of equations above (5.100) - (5.108) can be written in the form

$$(1+s\theta_{\text{г}})L[\delta\bar{p}_{\text{г}}]=e^{-s\tau_{\text{г}}}K_{\text{г.0}}L[\delta\bar{G}_0]+e^{-s\tau_{\text{г}}}K_{\text{г.г}}L[\delta\bar{G}_{\text{г}}];\qquad(5.109)$$

$$L[\delta\bar{G}_0]=K_{1\text{н.0}}L[\delta\bar{p}_{\text{н.0}}]-K_{2\text{н.0}}L[\delta\bar{p}_{\text{г}}];\qquad(5.110)$$

$$L[\delta\bar{G}_{\text{г}}]=K_{1\text{н.г}}L[\delta\bar{p}_{\text{н.г}}]-K_{2\text{н.г}}L[\delta\bar{p}_{\text{г}}];\qquad(5.111)$$

$$L[\delta\bar{p}_{\text{н.0}}]=K_{1\text{н.0}}L[\delta\bar{\omega}]-K_{2\text{н.0}}L[\delta\bar{G}_0];\qquad(5.112)$$

$$L[\delta\bar{p}_{\text{н.г}}]=K_{1\text{н.г}}L[\delta\bar{\omega}]-K_{2\text{н.г}}L[\delta\bar{G}_{\text{г}}];\qquad(5.113)$$

$$(1+s\theta_{\text{н}})L[\delta\bar{\omega}]=K_{3\text{н}}L[\delta\bar{p}'_{\text{м}}]-K_{4\text{н}}L[\delta\bar{G}_0]-K_{5\text{н}}L[\delta\bar{G}_{\text{г}}];\qquad(5.114)$$

$$(1+s\theta'_{\text{г}})L[\delta\bar{p}'_{\text{г}}]=e^{-s\tau'_{\text{г}}}K'_{\text{г}}L[\delta\bar{G}'];\qquad(5.115)$$

$$L[\delta\bar{G}']=K'_{1\text{м}}L[\delta\bar{p}'_{\text{м}}]-K'_{2\text{м}}L[\delta\bar{p}'_{\text{г}}];\qquad(5.116)$$

Footnote (5) appears on page 189.

$$L[\delta\bar{p}_{\kappa}] = K_{\psi} L[\delta\bar{\psi}]. \tag{5.117}$$

Here

$$K_{\kappa\psi} = \frac{p_{\kappa}^{\circ}}{2G_{1}^{\circ}G^{\circ}}; \quad K_{\kappa n} = \frac{p_{\kappa}^{\circ}}{2n_{1}^{\circ}(G^{\circ})^{2}};$$

$$K_{\kappa n} = CK_{\kappa\psi}.$$

since for a supercritical pressure drop the working medium flow rate G' through the turbine is proportional to the pressure in the steam gas generator, i.e.,

$$G' = Cp_{\kappa}'.$$

The transfer function of the power plant in question shows the mathematical connection between the input action, represented by the reducer set screw rotation angle $\delta\bar{\psi}$ and the output action — the combustion chamber pressure $\delta\bar{p}_K$. We see from Figure 5.10 that it is advisable to separate the block diagram of the engine being studied into two elements connected in series: one element having the input coordinate $\delta\bar{\psi}$ and the output coordinate the gas generator pressure $\delta\bar{p}_K'$, and the other having the corresponding input $\delta\bar{p}_K'$ and output $\delta\bar{p}_K$. Therefore, the transfer function of the power plant can be written as follows

$$W_{\kappa\psi} = W_{p_{\kappa}p_{\kappa}'} = W_{p_{\kappa}'n} W_{p_{\kappa}n/p_{\kappa}'}. \tag{5.118}$$

To determine the transfer function $W_{p_{\kappa}'n}$ we must examine the system of equations (5.115) - (5.117); to determine $W_{p_{\kappa}p_{\kappa}'}$ we must examine the system (5.109) - (5.114).

We know from automatic control theory that the transfer function is calculated with the aid of the determinant of the system of equations being examined. Let us formulate the fundamental determinants of the systems (5.115) - (5.117),and (5.109) - (5.114), respectively.

(5.117)

$$\Delta_1=\begin{vmatrix} -(1+s\vartheta_{\text{д}}^{\cdot})e^{-\tau_{\text{д}}s}K_{\text{д}}^{\cdot} & 0 \\ K_{2\text{т}}^{\cdot} & 1 & -K_{2\text{т}}^{\cdot} \\ 0 & 0 & 1 \end{vmatrix}$$

$$\Delta_{11}=\begin{vmatrix} -(1+s\vartheta_{\text{д}})e^{-\tau_{\text{д}}s} & K_{\text{д.о}}^{\cdot} & K_{\text{д.г}} & 0 & 0 & 0 \\ K_{2\text{т.о}}^{\cdot} & 1 & 0 & -K_{1\text{т.о}}^{\cdot} & 0 & 0 \\ K_{2\text{т.г}} & 0 & 1 & 0 & -K_{1\text{т.г}} & 0 \\ 0 & K_{2\text{т.о}}^{\cdot} & 0 & 1 & 0 & -K_{1\text{т.о}}^{\cdot} \\ 0 & 0 & K_{2\text{т.г}} & 0 & 1 & -K_{1\text{т.г}} \\ 0 & K_{\text{ст}} & K_{\text{ст}} & 0 & 0 & (1+s\vartheta_{\text{д}}) \end{vmatrix}$$

low rate
e steam

ows the
d by the
the com-
t is ad-
dded into
out coor-
re $\delta\bar{P}_K'$,
$\delta\bar{P}_K$.
ritten as

We also formulate the determinants as a function of the action in question, which are obtained from the fundamental determinants written out above by replacing the column of the coefficients corresponding to the output signal by the column of coefficients corresponding to the input action

$$\Delta_\phi=\begin{vmatrix} 0 & K_{\text{д}}^{\cdot} & 0 \\ 0 & 1 & -K_{1\text{т}}^{\cdot} \\ K_\phi & 0 & 1 \end{vmatrix}$$

(5.118)

$$\Delta_{p_{\text{д}}}=\begin{vmatrix} 0 & K_{\text{д.о}}^{\cdot} & K_{\text{д.г}} & 0 & 0 & 0 \\ 0 & 1 & 0 & -K_{1\text{т.о}}^{\cdot} & 0 & 0 \\ 0 & 0 & 1 & 0 & -K_{1\text{т.г}} & 0 \\ 0 & K_{2\text{т.о}}^{\cdot} & 0 & 1 & 0 & -K_{1\text{т.о}}^{\cdot} \\ 0 & 0 & K_{2\text{т.г}} & 0 & 1 & -K_{1\text{т.г}} \\ K_{2\text{т}} & K_{\text{ст}} & K_{\text{ст}} & 0 & 0 & (1+s\vartheta_{\text{д}}) \end{vmatrix}.$$

the
must ex-

Expanding these determinants by the usual methods, after some transformations we obtain

function
f equa-
minants
ctively.

$$\Delta_1=-[(1+s\vartheta_{\text{д}}^{\cdot})e^{-\tau_{\text{д}}s}+K_{2\text{т}}^{\cdot}K_{\text{д}}^{\cdot}];$$

$$\Delta_\phi=-K_{\text{д}}^{\cdot}K_{1\text{т}}^{\cdot}K_\phi=-A_{\text{д}}^{\cdot};$$

$$\Delta_{11}=-(1+s\vartheta_{\text{д}})e^{-\tau_{\text{д}}s}(K_1\vartheta_{\text{ст}}s+K_3)-K_3\vartheta_{\text{ст}}s-K_4;$$

$$\Delta_{p_{\text{д}}}^{\cdot}=-K_{2\text{т}}[K_{\text{д.г}}K_{1\text{т.г}}K_{2\text{т.г}}+K_{1\text{т.о}}^{\cdot}[K_{\text{д.г}}K_{1\text{т.г}}K_{1\text{т.г}}K_{2\text{т}}^{\cdot}+$$

$$+K_{\text{д.о}}K_{1\text{т.о}}^{\cdot}(1+K_{1\text{т.г}}K_{2\text{т.г}})]]=-A_{\text{д}}.$$

where

$$K_1=1+K_{1u.r}K_{2u.r}+K_{1u.e}K_{2u.e}(1+K_{2u.r}K_{1u.r});$$
$$K_2=K_1+K_{1u.r}K_{1u.r}K_{6e}+K_{1u.e}[K_{1u.e}K_{4e}+$$
$$+K_{1u.r}(K_{4e}K_{2u.r}K_{1u.e}+K_{2u.e}K_{6e}K_{1u.r})];$$

$$K_3=K_{2u.e}K_{u.e}(1+K_{1u.r}K_{2u.r})+K_{2u.r}K_{u.r}(1+K_{1u.e}K_{2u.e});$$
$$K_4=K_3-(K_{4e}K_{u.r}-K_{u.e}K_{6e})(K_{2u.e}K_{1u.r}K_{1u.r}-$$
$$-K_{2u.r}K_{1u.e}K_{1u.e}).$$

We determine the desired transfer functions for the first element — the steam gas generator, and the second element — the combustion chamber

$$W_{p_u'/p_0}(s)=\frac{A_u'}{(1+s\theta_u')e^{s\tau_u'}+K_5}; \tag{5.119}$$

$$W_{p_u'/p_u'}(s)=\frac{A_u}{(1+s\theta_u)e^{s\tau_u}(K_1\theta_e s+K_2)+K_3\theta_e s+K_4}, \tag{5.120}$$

where

$$K_5'=K_{2u}'K_u'.$$

Hence it is easy to find the amplitude-phase characteristics of the steam gas generator and the combustion chamber

$$W_u'(j\omega)=\frac{A_u'}{(1+j\omega\theta_u')\exp(j\omega\tau_u')+K_5}; \tag{5.121}$$

$$W_u(j\omega)=\frac{A_u}{(1+j\omega\theta_u)\exp(j\omega\tau_u)(j\omega K_1\theta_e+K_2)+j\omega K_3\theta_e+K_4}. \tag{5.122}$$

The Expression (5.121) for the amplitude-phase characteristics of the gas steam gas generator makes it possible to use the standard techniques to find all its remaining characteristics — amplitude, phase, real, and imaginary

$$B'_{\kappa} = \operatorname{mod} W'_{\kappa}(i\omega) = \frac{A'_{\kappa}}{\sqrt{\Psi'_{\kappa}(\omega)}}; \tag{5.123}$$

$$\varphi'_{\kappa} = \arg W'_{\kappa}(i\omega) = -\operatorname{arctg}\left(\frac{\sin\omega\tau'_{\kappa} + \omega\theta'_{\kappa}\cos\omega\tau'_{\kappa}}{\cos\omega\tau'_{\kappa} - \omega\theta'_{\kappa}\sin\omega\tau'_{\kappa} + K_5}\right) \tag{5.124}$$

$$\alpha'_{\kappa}(\omega) = \frac{A'_{\kappa}(\cos\omega\tau'_{\kappa} - \omega\theta'_{\kappa}\sin\omega\tau'_{\kappa} + K_5)}{\Psi'_{\kappa}(\omega)}; \tag{5.125}$$

$$\sigma'_{\kappa}(\omega) = -\frac{A'_{\kappa}(\sin\omega\tau'_{\kappa} + \omega\theta'_{\kappa}\cos\omega\tau'_{\kappa})}{\Psi'_{\kappa}(\omega)}, \tag{5.126}$$

where

$$\Psi'_{\kappa}(\omega) = 1 + K_5^2 + \theta'^2_{\kappa}\omega^2 + 2K_5(\cos\omega\tau'_{\kappa} - \omega\theta'_{\kappa}\sin\omega\tau'_{\kappa}).$$

rst element
ombustion

All the combustion chamber characteristics are found similarly

(5.119)

$$B_{\kappa} = \operatorname{mod} W_{\kappa}(i\omega) = \frac{A_{\kappa}}{\sqrt{\Psi_{\kappa}(\omega)}}; \tag{5.127}$$

(5.120)

$$\varphi_{\kappa} = \arg W_{\kappa}(i\omega) = -\operatorname{arctg}\frac{\beta(\omega)}{\alpha(\omega)}; \tag{5.128}$$

$$\alpha_{\kappa}(\omega) = \frac{A_{\kappa}\alpha(\omega)}{\Psi_{\kappa}(\omega)}; \tag{5.129}$$

$$\sigma_{\kappa}(\omega) = -\frac{A_{\kappa}\beta(\omega)}{\Psi_{\kappa}(\omega)}, \tag{5.130}$$

where

stics of

$$\alpha(\omega) = (K_2 - K_1\theta_{\kappa}\theta'_{\kappa}\omega^2)\cos\omega\tau_{\kappa} + K_4 - (K_1\theta_{\kappa} + K_2\theta'_{\kappa})\omega\sin\omega\tau_{\kappa};$$
$$\beta(\omega) = (K_1\theta_{\kappa} + K_2\theta'_{\kappa})\omega\cos\omega\tau_{\kappa} + (K_3 - K_1\theta_{\kappa}\theta'_{\kappa}\omega^2)\sin\omega\tau_{\kappa} + K_3\theta_{\kappa}\omega;$$
$$\Psi_{\kappa}(\omega) = \alpha^2(\omega) + \beta^2(\omega).$$

(5.121)

(5.122)

These expressions for the characteristics of the individual power plant elements make it possible to use the familiar techniques of automatic control theory to study the regulation stability of the engine as a whole, the quality of its transient process, and so on.

ristics of
ndard
itude,

Figure 5.11 shows the amplitude-phase characteristic of a LRE with TPA and steam gas generation, plotted using the formulas presented above with the aid of (5.118) for the following values of the parameters

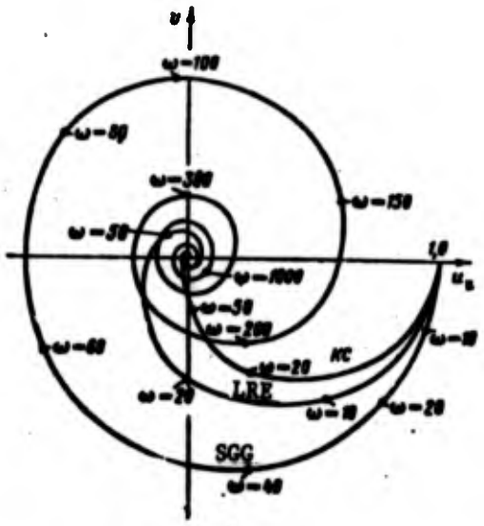

Figure 5.11. Amplitude-phase characteristic of LRE with turbopump and with gas generation.

$$K_{\text{г.г}}=0{,}4;\ K_{\text{г.о}}=0{,}6;\ \theta_{\text{г}}=0{,}005\ \text{sec}$$
$$\tau_{\text{г}}=0{,}005\ \text{sec}\quad \theta_{\text{в}}=0{,}2\ \text{sec}\quad K_{\text{вн}}=0{,}15;$$
$$K_{\text{вн}}=0{,}2;\ K_{\text{вн}}=0{,}3;\ K'_{\text{г}}=0{,}6;$$
$$\theta'_{\text{г}}=0{,}003\ \text{sec}\quad \tau'_{\text{г}}=0{,}03\ \text{sec}$$
$$K_{\text{вн.о}}=3{,}2;\ K_{\text{вн.г}}=2;\ K_{\text{вн.о}}=2{,}75;$$
$$K_{\text{вн.г}}=1{,}43;\ K_{\text{вн.}\tau}=-0{,}2;$$
$$K_{\text{вн.г}}=-0{,}22;\ K'_{\text{вн}}=2;\ K'_{\text{ин}}=2{,}5;$$
$$K_{\phi}=1;\ K_{\text{ин.о}}=2{,}2;\ K_{\text{ин.г}}=1{,}9.$$

We see that the hodograph of the amplitude-phase characteristic does not enclose the point (- 1, i0), which indicates stability of the automatic control system in question.

§ 7. Some LRE Automatic Regulation Systems

The determination of the various characteristics of the systems for regulating power plants obviously depends on the regulation schemes used. Therefore, we need to examine the possible LRE automatic control systems [6], [150], [149].

We know that the LRE operation is determined by a whole complex of various different parameters which characterize its stability, reliability, and efficiency. The requirements on these parameters depend on the missions performed by the flight vehicle. These requirements usually involve variation of the parameters during the period of engine operation in accordance with a specified law or in maintaining these parameters at a fixed level.

As a rule a power plant has several automatic control systems.

Usually the absolute and specific thrusts are considered as the basic LRE parameters (see Chapter 2)

$$P = Gw_c + F_c(p_c - p_H);$$
$$P_1 = w_c + \frac{F_c}{G}(p_c - p_H).$$

Both the propellant component flow rate and the combustion product exhaust velocity w_c are functions of the combustion chamber pressure p_K and the mixture ratio k. In view of the fact that the pressure ratio p_K/p_c does not change in the course of LRE operation, we can obviously write

$$P = P(p_H, k, p_H);$$
$$P_1 = P_1(p_H, k, p_H).$$

The magnitude of the ambient pressure p_H is an independent parameter. Therefore, we usually consider systems for automatic regulation of the combustion chamber pressure p_K and the mixture ratio k, with the latter also being used frequently for the liquid gas generator as well. This is explained by the fact that in the region of nominal combustion chamber operation the primary thermodynamic characteristics (temperature, gas constant) of the combustion products change very little. Therefore, quite large deviations of k from the nominal value do not lead to a marked change of T_K and R_K. The opposite picture is observed in the LGG, which operates with an excess of one of the components. Therefore, the requirements on the accuracy of the value of the propellant mixture ratio in the LGG are more severe, since a small

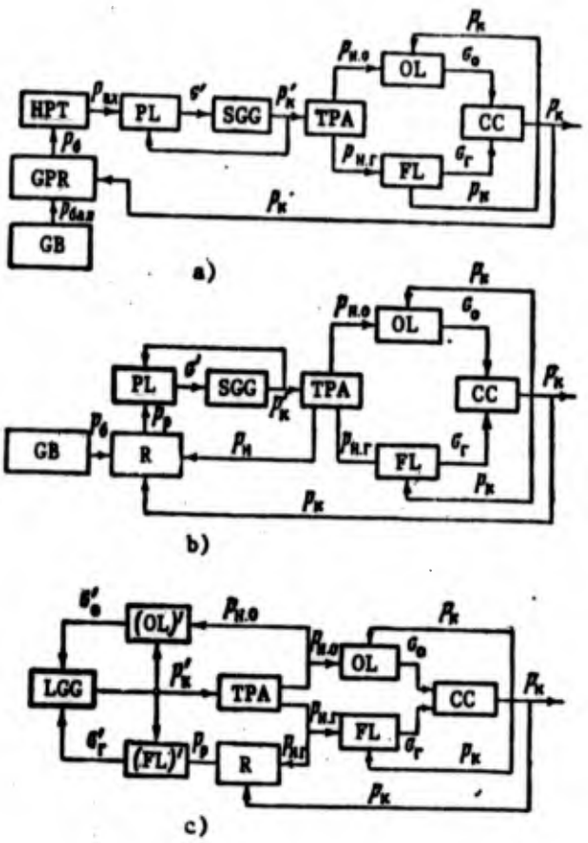

Figure 5.12. Possible automatic combustion chamber pressure regulation configurations:
a) scheme with gas generation and pressurized peroxide feed system; b) scheme with gas generation and pumped peroxide feed system; c) scheme with liquid gas generator; HPT - hydrogen peroxide tank; PL - peroxides line; SGG - gass generator; TPA - turbopump assembly; OL - oxidizer line; FL - fuel line; CC - combustion chamber; LGG - liquid gas generator; GPR - gas pressure reducer; GB - gas bottle; R - regulator.

reducer controlled by compressed gas pressure, and intthe third scheme a regulator of the type examined in Chapter 4 can be used.

We see that in all the schemes feedbacks are provided between the combustion chamber pressure (controlled parameter) and the flow rate

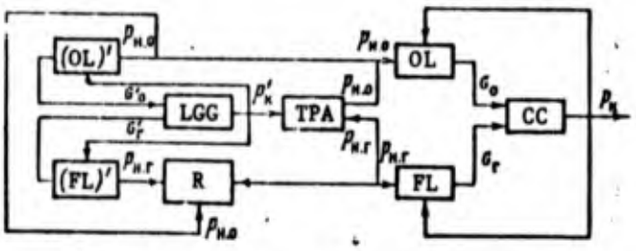

Figure 5.13. Automatic regulation of propellant ratio in LGG:
OL', FL' - gas generator oxidizer and fuel lines; OL, FL- main oxidizer and fuel lines; LGG - liquid gass generator; TPA - turbopump assembly; CC - combustion chamber; R - regulator

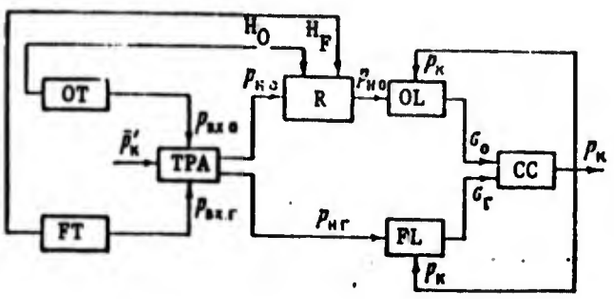

Figure 5.14 Propellant tank level regulation system:
OT - oxidizer tank; FT - Fuel tank; TPA - turbopump assembly; H_O - hydrostatic heads of oxidizer; H_F - hydrostatic heads of fuel; OL - oxidizer lines; FL - fuel lines; CC - combustion chamber; R - regulator

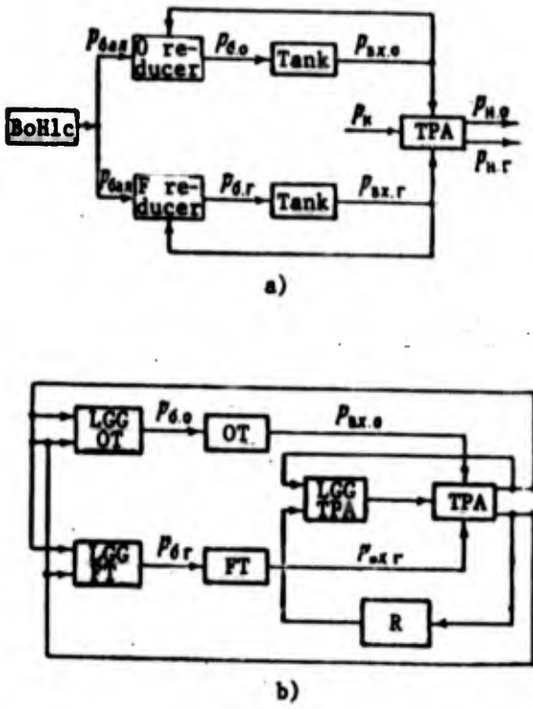

Figure 5.15. Pump inlet pressure regulation schemes:
a) scheme with bottle gas generator tank pressurization system;
b) scheme with special generators for pressurizing tanks; OT - oxidizer tank; FT - fuel tank; TPA - turbopump assembly; LGG - liquid gas generator; R - regulator.

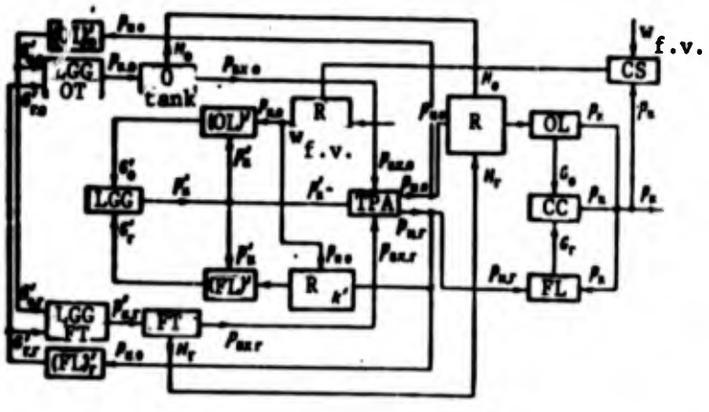

Figure 5.16. Possible system for controlling powerplant of a flight vehicle:
OT - oxidizer tank; FT - fuel tank; LGG - liquid gas generator; CS - control system; OL - main oxidizer line; FL - main fuel line; OL' - gas generator oxidizer lines; FL' - gas generator fuel lines; OL_0 - lines for pressurizing oxidizer tanks; FL_0 - lines for pressurizing fuel tanks; TPA - turbopump assembly; $w_{f.v.}$ - apparent flight vehicle velocity; R - regulator.

change of k' can lead to a marked change of the TPA operating regime and even to burnout of the LGG wall.

Another important parameter for reliable LRE operation is the value of the pressure p_{in} at the pump inlet. Therefore, a system to regulate p_{in} may be provided on the power plants.

The flight range of a flight vehicle depends basically on the terminal flight vehicle weight. Therefore, it is natural that designers wish to reduce the amount of propellant remaining in the tanks, which may occur as a result of engine operation with a mixture ratio differing from the nominal value.

A system for regulating the propellant component levels in the tanks is provided in order to reduce the residual component quantities.

In addition to these LRE automatic control systems, for multichamber power plants a system is provided to synchronize the thrust of the individual combustion chambers.

The combustion chamber pressure control system is in essence a system for regulating the absolute engine thrust. We know [6] that the combustion chamber pressure is determined by the propellant flow rate, and therefore, p_K can be regulated by varying the component flow rates. In turn, a change of the propellant flow rate is the result of a change of either the line hydraulic resistance or the flow rate of the working medium to the turbine, which defines the pump operating regime. Figure 5.12 shows some possible schematics of systems for regulating combustion chamber pressure. Figure 5.12a shows the basic interrelationships between the elements of a LRE with an expulsion system for feeding peroxide to the steam gas generator, Figure 5.12b shows a system with steam gas generation and a pump system for feeding the components, Figure 5.12c shows a system with a liquid gas generator. In the first scheme the regulator is a gas pressure reducer, which determines the pressure which expells the hydrogen peroxide from the tank, in the second scheme the regulator is a hydraulic pressure

reducer controlled by compressed gas pressure, and in the third scheme a regulator of the type examined in Chapter 4 can be used.

We see that in all the schemes, feedbacks are provided between the combustion chamber pressure (controlled parameter) and the flow rate of the working medium in the gas generator[6] in order to reduce the regulation errors. We note that the system for regulating p_K is coupled with the system for regulating the flight vehicle velocity: the sensor which measures the vehicle true velocity sends a signal indicating increase of this velocity to a computer which determines the deviation of the velocity from the programmed value, after which a signal indicating the magnitude of the difference with account for the sign is directed to the p_K regulator, which then alters the combustion chamber pressure (and therefore the thrust) in the required direction.

A system for regulating the mixture ratio in a liquid gas generator is shown in Figure 5.13. We see that the regulator is installed in one of the propellant lines through which the components flow (the fuel line in the present case) to the LRE. The mixture ratio is maintained within the required limits not only by the action of the regulated component (fuel) pressure, but also by the pressure of the second component (oxidizer). The design of a possible mixture ratio regulator was examined in Chapter 4.

Figure 5.14 shows in simplified form a possible scheme of a system for regulating the level of the propellants in the tanks. Proportional emptying of the tanks is accomplished as follows: the sensors determine the component levels in the tanks and alter the flow rate of one of the components as a function of the deviation of the ratio of the components in the tanks from the required value.

Figure 5.15 shows a schematic of a system for regulating the inlet pressures of the components through the pumps. This scheme is frequently termed a system for regulating the tank pressurization pressure p_t, which is connected with the pump inlet pressure as follows

---

Footnote (6) appears on page 189.

$$p_б = p_{вх.min} + \Delta p_{пот} - \rho H (j + g \sin \alpha).$$

where $p_{in.mix}$ is the minimal acceptable pump inlet pressure;

Δp_{loss} are the pressure losses from the tank to the pump inlet.

A possible system for controlling the entire power plant is shown in Figure 5.16, which indicates the interrelationship of all the systems mentioned above — regulation of the ratio of the mass flow rates of the components to the LRE, regulation of the level of the components in the tanks, regulation of the pump inlet pressures, and also the system for maintaining the required flight vehicle velocity.

Footnotes

1. on page 148 — With minimal energy losses, naturally.

2. on page 165 — With no losses in the gas feed line.

3. on page 166 — The effect of the pressure p'_K in the gas generator is accounted for by the proportional quantity G'.

4. on page 169 — We recall that here and hereafter ω is the circular frequency, and $\delta\bar{\omega}$ is the relative change of the angular velocity of rotation of the TPA rotor.

5. on page 176 — Obviously $K_{6a} = 0$ in the case of the monopropellant gas generator.

6. on page 187 — This is not entirely correct for the last scheme, since the mixture ratio must also change in the LGG, which has a significant effect on the work capacity of the working medium.

Trim
theoretic
tain the
tics of i
regulatin
results o
and pneum
also the

The
of paramo
self-cont
of the ta
sign with
trimming
thrust or
rates, i.e
ballistic

The
vided by
turbine.

CHAPTER 6

TRIMMING THE LRE

§ 1. Concept of LRE Trimming

Trimming of the LRE is the term used for the entire complex of theoretical and experimental operations which make it possible to obtain the specified engine parameters by determining the characteristics of its regulating elements. The required characteristics of the regulating elements are determined by computation with the use of the results of hydraulic cold flow tests, pneumatic tests of the engine, and pneumatic testing of the engine components and assemblies, and also the use of the results of preliminary tests of the complete engine.

The trimming of the LRE installed in pilotless flight vehicles is of paramount importance, since engine control during rocket flight is self-contained. Therefore, trimming must provide optimal satisfaction of the tactical and technical requirements imposed on the engine design with respect to the basic parameters. The ultimate goal of LRE trimming is to ensure nominal values of the basic engine parameters: thrust or propellant flow rates and the ratio of the component flow rates, i.e., those parameters of LRE operation which are used in the ballistic computation of the rocket trajectory.

The required value of the thrust of uncontrollable LRE is provided by maintaining a constant working medium flow rate through the turbine. This is accomplished either by controlling the pressure

reducers or by adjusting the diameters of the flow sections of the metering elements (injector diaphragms, and so on) which are installed in the lines which feed the propellants to the gas generator. The engine is trimmed to a given propellant component flow rate ratio by installing flow-control orifices in the oxidizer and fuel lines downstream of the pumps.

The trimming scheme is chosen with regard for the specific characteristics of the pneumatic and hydraulic systems, the mission, and the LRE operating and storage conditions. For example, if the LRE is used as a booster its trimming does not offer any particular problem, since in this case severe requirements are not usually imposed on the specified values of the engine parameters. If the LRE is installed on a ballistic rocket which must provide high target impact accuracy, then severe requirements are imposed on the LRE trimming, which is explained basically by two factors.

First, a large scatter of the propellant ratio leads to an increase of the residual propellant quantities which can be guaranteed in the tanks and consequently to an increase of the rocket launch weight, which leads to a reduction of the maximal flight range.

Second, if there is large scatter of the overall propellant flow rate and consequently of the thrust, control of the rocket is made difficult due to the appearance of additional disturbing factors acting on the rocket velocity control system.

§ 2. Trimming LRE For the Nominal and Required Values of TPA Shaft Angular Velocity (RPM)

The LRE can be trimmed for the nominal and required angular velocities (rpm) of the TPA shaft. Here, nominal TPA rpm means that rpm required to ensure the nominal engine operating regime in the case in which it is necessary to throttle both propellant lines to obtain the nominal value of the propellant mixture ratio k. However, if the nominal value of k is obtained by throttling only one of the propellant lines, then the nominal engine operating regime is obtained for a different TPA shaft angular velocity, termed the required rpm. In this

case both techniques for engine trimming are required in order to ensure that the specified value of k will be obtained.

1. Trimming the LRE for a Given Value of the Propellant Mixture Ratio

In both cases the same basic data can be used when trimming the engine for a given value of the mixture ratio k:

1) nominal pressures at the pump inlets $p_{in.o}$, $p^*_{in.f}$
2) nominal values of the component flow rates through the pumps and through the combustion chamber $G^*_н$, $G^*_к$;
3) nominal combustion chamber pressure $p^*_к$;
4) head-flow rate characteristics of the pumps at nominal rpm, obtained experimentally

$$p_н = p_н(G_н);$$

5) pressure losses in the oxidizer and fuel lines from the pump to the combustion chamber. The magnitude of these losses is determined from the results of cold flow tests (usually using water), with the liquid flow rate in the cold flow tests being specified to provide equality of the hydraulic resistance when using water and when using the propellant component, and is determined using the formula

$$G_в = G^*_к \sqrt{\frac{\rho_в}{\rho_к}},$$

where G_w and G^*_k are respectively the water and component flow rates;
ρ_w and ρ_k are respectively the densities of the water and the component.

Since to obtain a given k the deviations of the flow rates from the nominal values must equal zero, it is obvious that the following equalities must be satisfied when trimming the engine to the nominal value of the shaft rpm

$$p^*_{вх.о} + p_{н.о}(G^*_{н.о}) = p^*_к + \Delta p^*_{н.к} + \Delta p_{но.о};$$
$$p^*_{вх.г} + p_{н.г}(G^*_{н.г}) = p^*_к + \Delta p^*_{н.к} + \Delta p_{но.г},$$

where Δp_{or} are the pressure losses in the flow-control orifices which must be installed in the propellant lines during trimming.

Hence the required pressure differential across the flow control orifices is

$$\Delta p_{н.о} = p^{*}_{вх.о} + p_{н.о}(G^{*}_{н.о}) - p^{*}_{к} - \Delta p^{*}_{вх.о};$$
$$\Delta p_{н.г} = p^{*}_{вх.г} + p_{н.г}(G^{*}_{н.г}) - p^{*}_{к} - \Delta p^{*}_{вх.г}.$$

The engine must be trimmed as follows to obtain a given value of k at the required value of TPA rpm. We first determine the required pump head for the nominal propellant component flow rate

$$p^{**}_{н.о} = p^{*}_{к} + \Delta p^{*}_{вх.о} - p^{*}_{вх.о};$$
$$p^{**}_{н.г} = p^{*}_{к} + \Delta p^{*}_{вх.г} - p^{*}_{вх.г}.$$

As a result of the influence of various internal factors (see above) on the pumps, these required heads will not coincide for the nominal flow rates with the experimental heads, corresponding to ω^{*} and G^{*}, i.e., the quantities $p^{**}_{H.o}$ and $p^{**}_{H.f}$ will differ from $p^{*}_{H.o}$ and $p^{*}_{H.f}$ (see Figure 6.1). Thus, the required heads can be obtained for the nominal flow rates at different pump shaft rpm ω^{**}_{o} and ω^{**}_{f}.

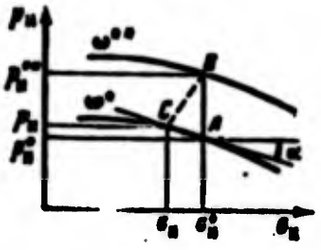

Figure 6.1. Diagram for determining pump speed change.

Let us use the experimental pump characteristics to determine ω^{**}_{o} and ω^{**}_{f} from the value of the difference $p^{**}_{н} - p^{*}_{к}$. We know (see Chapter 2) that for similar regimes we can write

$$p^{**}_{н} = p_{н}\left(\frac{\omega^{**}}{\omega^{*}}\right)^{2}; \qquad (6.1)$$

$$G^{*}_{н} = G_{н}\left(\frac{\omega^{**}}{\omega^{*}}\right). \qquad (6.2)$$

The required point B has its matching point on the line $\omega^{*} = \text{const}$ (point C). The similar regime line in Figure 6.1 is represented by the dashed curve CB. The pump head at the point C corresponds to some flow rate G_{H}, which is not equal to G^{*}_{H}. To move along the curve

ω^{**} = const to the nominal regime point we can use a linear approximation, which gives only a small error

$$p_n = p_n^* + (G_n^* - G_n)\operatorname{tg}\alpha. \tag{6.3}$$

Here we have assumed that

$$\operatorname{tg}\alpha = \left(\frac{\partial p_n}{\partial G_n}\right)^*$$

i.e., the slope of the tangent to the curve ω = const is taken from the experimentally obtained pump characteristic at the nominal regime point.

We substitute (6.3) into (6.1) with account for (6.2)

$$p_n^{**} = \left[p_n^* + \left(1 - \frac{\omega^*}{\omega^{**}}\right)\left(\frac{\partial p_n}{\partial G_n}\right)^* G_n^*\right]\left(\frac{\omega^{**}}{\omega^*}\right)^2 \tag{6.4}$$

It is obvious that in the linear approximation we can write in the vicinity of the point A

$$\delta p_n = \left(\frac{\partial p_n^{**}}{\partial \omega}\right)^* \delta\omega,$$

where $\delta p_n = p_n^* - p_n^{**}$;

$$\delta\omega = \omega^* - \omega^{**}.$$

The partial derivative $\partial p_n/\partial\omega$ is found from (6.4) for the nominal regime point, i.e., for $\omega^{**} = \omega^*$:

$$\left(\frac{\partial p_n^*}{\partial \omega}\right)^* = \frac{1}{\omega^*}\left[2p_n^* + \left(\frac{\partial p_n}{\partial G_n}\right)^* G_n^*\right],$$

where the derivative $\partial p_n/\partial G_n$ is found from the graph in Figure 6.2.

Thus,

$$\omega^{**} = \omega^*\left[1 - \frac{p_n^* - p_n^{**}}{2p_n^* + \left(\frac{\partial p_n}{\partial G_n}\right)^* G_n^*}\right].$$

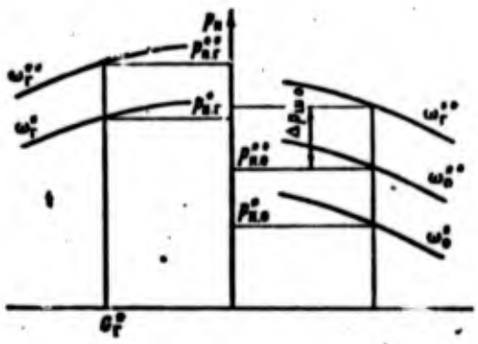

Figure 6.2. Diagram for determining required turbopump shaft speed.

It is not difficult to calculate rpm ω_o^{**}, and ω_f^{**} using this formula. Obviously the larger of the values ω_o^{**} and ω_f^{**} must be used. The pump for which the required value of the rpm is determined is called the unthrottlable pump, the other is called the throttlable pump. The head of the throttlable pump is found from (6.4) for the value of ω'', determined for the other pump.

The excess pressure (throttling effect) which is absorbed by the flow-control orifice is obviously equal to the difference between the throttlable pump head obtained and the pressure p_H^*, for example, if $\omega_f^{**} > \omega_o^{**}$, then

$$\Delta p_{\text{др.г}} = 0;$$
$$\Delta p_{\text{др.о}} = p_{\text{н.о}}^{\circ}(G_o^{\circ}, \omega_r^{\circ\circ}) - p_{\text{н.о}}^{\circ\circ}.$$

In this case the orifice diameter of the unthrottlable pump is assumed to be equal to the diameter of the line in which the flow-control orifice is installed.

The throttlable pump orifice diameter is found as a function of the required pressure loss across the orifice using the formula

$$d_{\text{др}} = 2\sqrt{\frac{G_{\text{н}}}{\pi K_t \mu \varepsilon \sqrt{2\rho\Delta p_{\text{др}}}}}$$

where K_t is a factor accounting for the thermal expansion of the orifice;

μ is the discharge coefficient;

ε is a factor accounting for the expansion of the flowing liquid;

ρ is the density of the flowing component;

$\Delta p'_{or}$ is the pressure drop across the flow-control orifice, connected with the orifice losses by the hydraulic formula

$$\Delta p_{or} = \Delta p'_{or}\left(1 - \frac{d_{or}^2}{D^2}\right) \tag{6.5}$$

D is the diameter of the line in which the orifice is installed.

Formula (6.5) is usually used to plot a curve of the relationship between orifice diameter and pressure loss (Figure 6.3). After trimming to a given value of the propellant component mass flow rates, the LRE is trimmed to a given value of the thrust (total propellant flow rate).

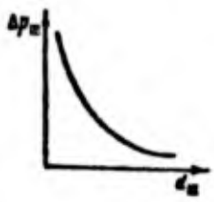

Figure 6.3. Pressure drop versus orifice diameter.

2. Trimming the LRE to a Given Value of the Propellant Component Flow Rate

We see from the discussion above that a given engine operating regime can be provided only for values of the TPA rpm which were determined in the calculation of the engine trimming to the specified propellant component mass flow rate ratio.

The following basic data are necessary in trimming the engine to the nominal value of the propellant component flow rates:

1) the values of the pressures at the points where the propellant components are tapped off for operation of the gas generator (if the power plant design includes a gas generator);

2) the power required by the pumps for the nominal values of the flow rate;

3) nominal flow rate of the propellant components through the gas generator;

4) the resistance of the propellant lines from the tapoff point to the gas generator combustion chamber, corresponding to the nominal flow rate of the components through the gas generator.

One basic requirement must be met when trimming the engine for the nominal value of the propellant component flow rates — the powers required by the oxidizer and fuel pumps must be balanced by the turbine power, i.e.:

$$N_{н.о}+N_{н.г}=N_{т}. \qquad (6.6)$$

The sequence for calculating engine trimming to the nominal value of the propellant component flow rates when using the scheme for tuning to the nominal value of the TPA shaft rpm may be represented as follows.

1. We plot from the results of water flow tests (or using theoretical computations) curves of the pump power as a function of the component flow rate for the nominal rpm

$$N_{н}=N_{н}(G_{н}).$$

We use these curves to find the values of the pump powers corresponding to the nominal propellant component flow rates.

2. We find the required turbine power from (6.6).

3. We find the turbine power as a function of the working medium pressure. Since engine trimming is accomplished for the condition $\omega=\omega^{*}=\text{const}$, the connection between the turbine power and the gas generator pressure $p_{К}^{'}$ can be written in the form [57]

$$N_{т}=cp_{к}^{'},$$

where c is a constant coefficient which depends on the geometric dimensions of the turbine flow passage, the energy losses in this part of the turbine, and the thermodynamic properties of the working medium.

4. Let us claculate the propellant component flow rate through the gas generator required to provide the given turbine power. We have the usual gasdynamic relationship between the working medium pressure ahead of the turbine and the medium flow rate through the turbine for critical pressure drop [2]

$$G'_г = \sqrt{n'\left(\frac{2}{n'+1}\right)^{\frac{n'+1}{n'-1}}}\frac{p'_г F_{кр} i}{\sqrt{R'_г T'_г}},$$

(6.6)

where n', $R'_г$, $T'_г$ are respectively the polytropic exponent, gas constant, and gas generator combustion product temperature;

F_{cr} is the turbine nozzle critical section area;

i is the number of turbine nozzles.

For a given ratio k' of the component mass flow rates in the gas generator the oxidizer and fuel flow rates through the LRE are defined by the known formulas [124]

$$G'_о = \frac{k'}{1+k'}G';$$

$$G'_т = \frac{1}{1+k'}G'.$$

5. Let us determine the required resistances of the gas generator lines from the tapoff point to the LRE firing chamber for $G'_о$ and $G'_т$:

$$\Delta p'_{о.т} = p'_{г.т.о.т} - p'_к.$$

We reduce these resistances to the nominal component flow rates through the generator

$$\Delta p''_{о.т} = \Delta p'_{о.т}(G''_{о.т})^2/(G'_{о.т})^2.$$

We find the required pressure differentials across the injectors from the equality

$$\Delta p_{инж.о.т} = \Delta p'_{о.т} - \Delta p''_{о.т},$$

where $\Delta p_{inj.o.f}$ is the required differential pressure across the injectors for the nominal component flow rates through the gas generator;

$\Delta p^{*'}_{o.f}$ is the overall resistance of the gas generator line for the nominal component flow rates.

Engine trimming to the nominal values of the component flow rates when using the scheme for trimming the engine to the required value of the TPA rpm differs fundamentally from the technique described above. The differences amount to the following:

— the given (nominal) values of the component flow rates and the required turbine shaft rpm determined in the calculation of the flow control orifice diameters are used to calculate the corresponding component flow rates

$$G_{\text{в}}=G_{\text{в}}^{\circ}\frac{\omega^{\circ}}{\omega^{\circ\circ}};$$

— the value of G_H along with the pump characteristics for the nominal rpm can be used to find easily the pump efficiency η_H, which then makes it possible to calculate the required pump powers

$$N_{\text{в}}=\frac{p_{\text{в}}G_{\text{в}}^{\circ}}{\varrho\eta_{\text{в}}};$$

— the component flow rate G_H through the pump is equated to the sum of the flow rates through the main combustion chamber G and that through the gas generator G';

— the required turbine power is found as the sum of these powers

$$N_{\text{т}}=N_{\text{в.о}}+N_{\text{в.г}};$$

— the dependence of the turbine power on the working medium pressure is found similarly.

The required resistances of the metering orifices are then found in the same sequence as used in trimming to the nominal value of the propellant component flow rates and in using the schemes for trimming to the nominal value of the TPA shaft rpm.

§ 3. Engine Retrimming Using the Results of Firing Stand Tests

1. General Information

The engines must be subjected to firing stand tests to verify functioning and that the basic parameters meet the requirements of the

specifications. After these tests the engine trim is corrected. Retrimming must be accomplished if the value of the overall component flow rate and the value of the mixture ratio k, reduced from the results of test stand measurements to the nominal conditions, do not correspond to the specifications.

It is obvious that in the first case the retrimming must involve a change of the magnitude of the hydraulic resistances of the LGG metering injectors; in the second case it involves a change of the flow-control orifice diameters.

The problem in retrimming lies in the fact that we must have sufficiently exact values of the relationship between the change of the overall propellant component flow rate and the change of the hydraulic resistances across the injectors ($G = G(\Delta p_{inj})$ and on the variation of the coefficient k as a function of the throttling effects in the flow-control orifices ($k = k(\Delta p_{or})$. These relationships can be calculated easily theoretically and then refined by experiment.

In deriving the relations

$$G = G(\Delta p_{\text{ж}}) \text{ and } k = k(\Delta p_{\text{ж}})$$

we must take account of the interrelationships between the LGG, TPA, and combustion chamber, all operating in a common loop, and also the disturbing factors which affect engine operation, i.e., the effect of both external and internal factors.

The external factors include:

a) the ambient temperature, which affects the change of the physical properties of the components (viscosity, density, thermal capacity, and so on);

b) the pressure at the inlets to the pumps.

The internal factors include:

a) variation of the hydraulic resistances of the combustion chamber and gas generator lines, which leads to change of the flow rates and therefore to a change of the basic engine operating parameters;

b) variation of the values of the combustion chamber throat diameter, which leads to a change of the propellant component flow rate through the chamber;

c) deviation of the values of the turbine nozzle throat diameters from their nominal values, which affects the power delivered by the turbine;

d) the quality of the finish of the engine components and detail parts, which determines the output parameters of the assemblies, for example, variation of the finish quality of the rotor blades and stator blades leads to a variation of turbine efficiency;

e) errors in determining the parameters in the water flow testing of the components and assemblies;

f) the difference between the engine component and assembly operating condition during the firing stand tests and the water flow testing conditions, and the differences between these values and the tests of the same components and assemblies in production.

This incomplete listing of the internal disturbing factors which affect engine operation shows that they cannot all be taken into account in the trimming process.

However, the variations of the geometric parameters and the errors made in the cold flow tests and production tests of the components and assemblies are small in practice in comparison with the absolute values of the parameters themselves, and therefore these deviations can be neglected. Therefore, we usually take into account only those disturbing factors which have the most significant influence on the engine operating regime and cannot be eliminated in the development process:

variation of the propellant component temperature, pump inlet pressure, and hydraulic resistances of the combustion chamber and gas generator lines, and so on.

2. Calculation of the Influence of External and Internal Factors on Engine Parameters

The basic data for calculating the influence of the external and internal factors are:

1) the nominal overall propellant flow rate G^* and the mixture ratio k^*;

2) the combustion chamber pressure p_K^*;

3) the overall propellant flow rate $G^{*\prime}$ through the gas generator and the LGG mixture ratio $k^{*\prime}$;

4) the gas generator pressure p_K';

5) the energy of the working medium at the inlet to the turbine stator $R_K'T_K'$;

6) the pressure dependence of the LGG propellant flow rate

$$G' = G'(p_K');$$

7) the densities ρ_O^* and ρ_f^* of the components at the nominal fueling temperature and their dependence on temperature T

$$\rho_T = \rho^* - \rho_1(T - T^*),$$

where ρ_1 is a constant coefficient;

8) the nominal pump inlet pressure p_{in}^*;

9) the hydraulic losses in the gas generator propellant lines $\Delta p_{M.K}^{*\prime}$ (from the pumps to the entrance to the LGG firing chamber) and the same for the combustion chamber $\Delta p_{M.K}^{*}$;

10) the variation of the turbine specific power as a function of its rotor rpm (see Chapter 2)

$$N_1 = \frac{N_T}{G'} = a_4 \sqrt{R_K' T_K'}\,\omega - a_6\omega^2 - \frac{a_5\omega^2}{\sqrt{R_K' T_K'}} - a_7 R_K' T_K'. \qquad (6.7)$$

11) the pump head and power characteristics as a function of pump rpm and component flow rates (see Chapters 2 and 3)

$$N_н = A_н Q\omega^3 + B\omega^2 G_н; \tag{6.8}$$

$$p_н = A_н Q\omega^2 + B_н \omega G_н + \frac{c_н}{Q} G_н^2. \tag{6.9}$$

We shall write the basic equation of engine operation in terms of deviations

Equations (6.7)—(6.9) become

$$\delta N_т = \frac{\partial N_т}{\partial G'} \delta G' + \frac{\partial N_т}{\partial \omega} \delta\omega + \frac{\partial N_т}{\partial (R_к' T_к')} \delta (R_к' T_к'); \tag{6.10}$$

$$\delta N_н = \frac{\partial N_н}{\partial G_н} \delta G_н + \frac{\partial N_н}{\partial \omega} \delta\omega + \frac{\partial N_н}{\partial Q} \delta Q; \tag{6.11}$$

$$\delta p_н = \frac{\partial p_н}{\partial G_н} \delta G_н + \frac{\partial p_н}{\partial \omega} \delta\omega + \frac{\partial p_н}{\partial Q} \delta Q. \tag{6.12}$$

The equation of pressure balance in the propellant lines from the pumps to the combustion chamber is

$$p_н + p_{вх} = p_к + \Delta p_{н.к}^{\circ} \left(\frac{G}{G^{\circ}}\right)^2 \frac{\rho^{\circ}}{\rho} + \Delta p_{тр},$$

hence

$$\delta p_н + \delta p_{вх} = \delta p_к + \frac{2\Delta p_{н.к}^{\circ}}{G^{\circ}} \delta G - \frac{\Delta p_{н.к}^{\circ}}{\rho^{\circ}} \delta Q + \delta \Delta p_{тр}. \tag{6.13}$$

The equation for the flow rate as a function of the combustion chamber pressure

$$G = G^{\circ} \frac{p_к}{p_к^{\circ}}$$

is written in variational form as

$$\delta G = \frac{G^{\circ}}{p_к^{\circ}} \delta p_к.$$

The dependence of the propellant flow rate into the combustion chamber on the component temperature for the nominal pressure is written in variational form as

$$\delta G = A_1 \delta T_0 + A_2 \delta T_r.$$

Therefore, in the general form we must obviously write

$$\delta G = \frac{G^*}{p_k^*} \delta p_k + A_1 \delta T_0 + A_2 \delta T_r. \tag{6.14}$$

The equation of pressure balance in the LGG propellant lines

$$p_n + p_{nc} = p_k + \Delta p_{n.k}^{**} \left(\frac{G'}{G^{*'}}\right)^2 \frac{\zeta^*}{\varrho} + \Delta p_m'$$

is written as follows in variational form

$$\delta p_n + \delta p_{nc} = \delta p_k' + \frac{2\Delta p_{n.k}^{**}}{G^{*'}} \delta G' + \frac{\Delta p_{n.k}^{**}}{\varrho^*} \delta \varrho + \delta \Delta p_m'. \tag{6.15}$$

The gas generator equation is

$$p_k' = \frac{\sqrt{R_k' T_k'}\, G'}{\sqrt{n' \left(\frac{2}{n'+1}\right)^{\frac{n'+1}{n'-1}} F_{kp}'}},$$

hence

$$\delta p_k' = \frac{\partial p_k'}{\partial G'} \delta G' + \frac{\partial p_k'}{\partial (R_k' T_k')} \delta (R_k' T_k'). \tag{6.16}$$

The equation of pump and turbine power balance in variational form is

$$\delta N_T = \delta N_{n.0} + \delta N_{n.T}. \tag{6.17}$$

The equation of propellant component flow rate balance through the pumps, combustion chamber, and gas generator in variational form is

$$\delta G_{\text{в}} = \delta G + \delta G'. \tag{6.18}$$

Solving the system of Equations (6.10)—(6.18) for the external and internal factors, we can obtain the following relations

$$\left.\begin{aligned}
\delta G_{\text{в}} &= f_1(\delta p_{\text{вх}}, \delta Q, \delta T, \delta\Delta p_{\text{ш}}, \delta\Delta p_{\text{к}});\\
\delta G &= f_2(\delta p_{\text{вх}}, \delta Q, \delta T, \delta\Delta p_{\text{ш}}, \delta\Delta p_{\text{к}});\\
\delta G' &= f_3(\delta p_{\text{вх}}, \delta Q, \delta T, \delta\Delta p_{\text{ш}}, \delta\Delta p_{\text{к}});\\
\delta p_{\text{к}} &= f_4(\delta p_{\text{вх}}, \delta Q, \delta T, \delta\Delta p_{\text{ш}}, \delta\Delta p_{\text{к}});\\
\delta p'_{\text{к}} &= f_5(\delta p_{\text{вх}}, \delta Q, \delta T, \delta\Delta p_{\text{ш}}, \delta\Delta p_{\text{к}});\\
\delta k &= f_6(\delta p_{\text{вх}}, \delta Q, \delta T, \delta\Delta p_{\text{ш}}, \delta\Delta p_{\text{к}});\\
\delta N_{\text{т}} &= f_7(\delta p_{\text{вх}}, \delta Q, \delta T, \delta\Delta p_{\text{ш}}, \delta\Delta p_{\text{т}});\\
\delta p_{\text{в}} &= f_8(\delta p_{\text{вх}}, \delta Q, \delta T, \delta\Delta p_{\text{ш}}, \delta\Delta p_{\text{к}}).
\end{aligned}\right\} \tag{6.19}$$

The relationships thus obtained between the basic engine parameters and the external and internal factors can be used to trim the first prototype engines which are destined for firing tests. The trimming relationships can be refined on the basis of the results of these and other special tests.

3. Technique for Recalculating Flow Control Orifice Diameter From the Results of Firing Stand Tests

We have mentioned previously that the diameters of the flow-control orifices are recalculated on the basis of the results of test stand firings in case the propellant component flow rate ratio does not correspond to the specification requirements and also if the hydraulic resistances of the lines (from the pumps to the combustion chamber) after the firing tests differ from their values prior to firing (as a result of replacement of components or variation of their hydraulic characteristics) by an amount greater than that allowed in the specifications.

In recalculating the orifice diameters, we must use the formulas which define the dependences of the basic engine operating parameters on the influence of the external and internal factors. To this end we must first determine the variation of the pressure drop across the oxidizer and fuel orifices as a function of the variation of the

coefficient k while maintaining a constant overall propellant flow rate through the engine (i.e., for $\delta G=0$ for $\delta k\neq 0$:

$$\delta\Delta p_{m.o}=A\delta\Delta p_{m.f}.$$

This expression together with the relations giving the effect of the external and internal factors makes it possible to find the connection between the change of the coefficient k and the change of the pressure differential across the orifices in the oxidizer and fuel lines

$$\delta\Delta p_{m.o}=B\delta k;$$
$$\delta\Delta p_{m.f}=C\delta k,$$

where δk is the deviation of the mixture ratio, obtained in the firing tests and reduced to nominal conditions, from its nominal (trim) value.

Thus, for the recalculation of the flow control orifice diameters from the engine test stand firing results, we can obtain equations which make it possible to determine the required pressure drops across the orifices as a function of the required variation of k and the hydraulic resistances of the propellant lines from the pumps to the combustion chamber.

These equations have the form

$$\Delta p_{m.o}^{(2)}=\Delta p_{m.o}+B\delta k+\Delta p_o-\Delta p_o^{(2)};$$
$$\Delta p_{m.f}^{(2)}=\Delta p_{m.f}+C\delta k+\Delta p_f-\Delta p_f^{(2)},$$

where $\Delta p_{or.o}$, $\Delta p_{or.f}$ and $\Delta p_{or.o}^{(2)}$, $\Delta p_{or.f}^{(2)}$ are the pressure differentials across the oxidizer and fuel flow control orifices, respectively, before and after testing; Δp_o, Δp_f and $\Delta p_o^{(2)}$, $\Delta p_f^{(2)}$ are the hydraulic resistances of the oxidizer and fuel lines respectively before and after testing.

The resistances of the automatic control elements (injectors, pressure reducers, regulators) which determine the magnitude of the overall propellant flow rate through the engine are recalculated on the basis of the results of test stand firings if the deviation from the nominal overall flow rate is greater in magnitude than the value

allowed in the specifications or if there is a change of the orifice diameters or of the hydraulic resistances of the elements forming part of the line which feeds the working gas to the turbine.

The relationships for the variation of the basic engine operating parameters as a function of the influence of the external and internal factors can be used to determine the variation of the pressure differentials Δp_{el} required across the regulating elements.

From the system of equations written out above, we can find the relationships for the variation of the required resistances of the regulating elements as a function of the change of the pressure differential across the flow-control orifices

$$\delta\Delta p_{e.o} = a_1 \delta\Delta p_{m.o} \text{ and } \delta\Delta p_{e.r} = a_2 \delta\Delta p_{m.r}$$

and the variation of the regulating element resistances as a function of the change of the overall flow rate if k' = const:

$$\delta\Delta p_{e.o} = a_3 \delta G; \quad \delta\Delta p_{e.r} = a_4 \delta G.$$

Thus the formulas for recalculating the required resistances of the regulating elements on the basis of the engine test stand firing results have the form

$$\Delta p_{e.o}^{(n)} = \Delta p_{e.o} + a_1 \delta\Delta p_{m.o} + a_3 \delta G_3 + \Delta p_0' - \Delta p_0'^{(n)};$$
$$\Delta p_{e.r}^{(n)} = \Delta p_{e.r} + a_2 \delta\Delta p_{m.r} + a_4 \delta G_3 + \Delta p_r' - \Delta p_r'^{(n)},$$

where a_1 - a_4 are numerical coefficients whose values are obtained as a result of solution of (6.19).

CHAPTER 7

OSCILLATORY PROCESSES IN LRE PLUMBING LINES

As a rule, the motion of a liquid (propellant component) or gas along the LRE lines is accompanied by periodic and aperiodic variations of the flow rate, velocity, and pressure. The sources of these variations may be: oscillations of valves, membranes, automatic control sensing elements, vibratory burning in the combustion chamber, abrupt actuations of cutoff and starting valves, and so on.

The time variation of the flow rate is associated with variation of the pressure. Sharp variations of the flow rate cause pressure waves whose magnitude depends to a considerable degree on the geometry and elastic properties of the pneumatic and hydraulic system lines. Under certain conditions the pressure may exceed the allowable limits and lead to failure of the plumbing lines.

In some cases the pressure oscillations in the lines may not necessarily lead to failure, but may have a significant effect on the engine dynamic properties. For example, if the frequency of the propellant component pulsation at the outlet of the pump coincides with the frequency of free oscillations of the component in the propellant lines, resonance is unavoidable and will lead to a considerable increase of the pressure oscillation amplitude, which in turn causes severe pulsations of the pressure in the engine combustion chamber.

A detailed theoretical study of the transient processes during engine startup cannot be performed without account for the wave

processes in the LRE propellant feed lines, i.e., in the general case it is not always possible to successfully identify the segments of the pneumatic and hydraulic systems in which the liquid or gas has only inertial or deformational elastic properties. In other words, it is not always possible to reduce the oscillations in a system with uniformly distributed mass to a system with lumped parameters without distortion of the quantitative and qualitative picture of the process.

The motion of the liquid (propellant) and gas in the plumbing lines of the LRE is unsteady during the period of both engine startup and engine shutdown. Disruption of the steady-state process is also observed in the process of engine functioning. In this case the deviation of the parameters from the steady state regime depends on the dynamic system properties, which are determined both by the dynamic characteristics of the automatic control elements and the feed system and also by the dynamic properties of the pneumatic and hydraulic systems.

Therefore, a very important step in the engine design process is the rational selection of the pneumatic and hydraulic systems, the proper positioning of the automatic control elements and the devices for damping the wave processes, which requires a detailed theoretical analysis of the influence of these factors on the unsteady liquid and gas flow through the system lines.

§ 1. Equations of Unsteady Liquid and Gas Motion in Lines

Even in the case of a constant line cross section the system of equations describing unsteady liquid motion (see Chapter 3) is nonlinear, therefore, its analytic solution is very difficult. Let us examine the linearization technique proposed by Charnyy [145].

In the case F = const the Equations (G) of Chapter 3 are easily transformed to the form

$$\left.\begin{aligned} -\frac{\partial p}{\partial x} &= \frac{1}{F}\frac{\partial Q}{\partial t} + \frac{k\omega}{2d_0F}G + \rho g \sin\alpha; \\ -\frac{\partial p}{\partial t} &= \frac{a^2}{F}\frac{\partial Q}{\partial x}. \end{aligned}\right\} \qquad (7.1)$$

We denote

$$\frac{\xi w}{2d_e} = 2b, \tag{7.2}$$

where d_e is the equivalent line flow section diameter.

In the general case the coefficient b is a variable quantity. Only in the laminar liquid flow regime does it remain constant, in view of the fact that

$$\xi = \frac{C}{Re} = \frac{C\nu}{wd_e}, \tag{7.3}$$

where C is constant;

ν is the kinematic viscosity.

Substituting (7.3) into (7.2), we obtain

$$2b = \frac{C\nu}{2d_e^2}. \tag{7.4}$$

We know that C = 64 for a circular tube. Then

$$2b = \frac{32\nu}{d_e^2}. \tag{7.5}$$

For turbulent liquid flow we must take an average value of the coefficient b, which is obtained by replacing the quadratic friction law by a linear law, which is equivalent to replacing a segment of the curve in some range of liquid motion velocity variation by a straight line (Figure 7.1).

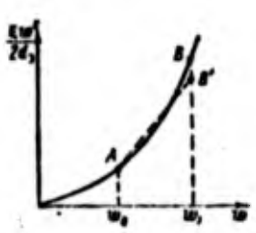

Figure 7.1. Diagram for deriving Equation (7.6).

In this case the straight line AB' is drawn so that the areas ABw_1w_0 and $AB'w_1w_0$ will be equal. This may be expressed mathematically as follows

$$\int_{w_0}^{w_1} \frac{\xi w^2}{2d_e} dw = \int_{w_0}^{w_1} \left[\frac{\xi w_0^2}{2d_e} + 2b(w - w_0)\right] dw.$$

Hence

$$2b=\frac{\xi}{3d_0}\,\frac{w_1^2+w_1w_0-2w_0^2}{w_1-w_0}, \tag{7.6}$$

where w_0 and w_1 are respectively the minimal and maximal value of the liquid motion velocity in the line.

For laminar gas flow

$$\xi=\frac{C\eta}{wd_0\varrho},$$

where η is the gas dynamic viscosity.

Since for a gas

$$\frac{p}{\varrho}=RT,$$

we obtain

$$2b=\frac{C\eta RT}{2d_0^2p_{cp}},$$

where p_{av} is the average gas pressure in the given unsteady flow.

For the quadratic resistance law we can also use (7.6). With account for the above analysis the system of Equations (7.1) takes the form

$$\left.\begin{aligned}-F\frac{\partial p}{\partial x}&=\frac{\partial Q}{\partial t}+2bG+fQF\sin\alpha;\\ -F\frac{\partial p}{\partial t}&=a^2\frac{\partial Q}{\partial x}.\end{aligned}\right\} \tag{7.7}$$

For a liquid ρ = const. Then, differentiating the first Equation (7.7) with respect to t, and the second with respect to x, we obtain

$$-F\frac{\partial^2 p}{\partial x\partial\tau}=\frac{\partial^2 G}{\partial\tau^2}+2b\frac{\partial G}{\partial\tau};$$
$$-F\frac{\partial^2 p}{\partial\tau dx}=a^2\frac{\partial^2 G}{\partial x^2}.$$

(7.6)

of the

Hence

$$\frac{\partial^2 G}{\partial\tau^2}-a^2\frac{\partial^2 G}{\partial x^2}+2b\frac{\partial G}{\partial\tau}=0. \tag{7.8}$$

For isothermal gas flow

$$\frac{p}{\varrho}=RT=a^2.$$

Then the first Equation (7.7) is written in the form

$$-F\frac{\partial p}{\partial x}=\frac{\partial G}{\partial\tau}+2bG+\frac{FJ\sin\alpha}{a^2}p=0. \tag{7.9}$$

Differentiating (7.9) with respect to τ and using the second Equation (7.7), we obtain for isothermal gas flow

$$\frac{\partial^2 G}{\partial\tau^2}+2b\frac{\partial G}{\partial\tau}-a^2\frac{\partial^2 G}{\partial x^2}-J\sin\alpha\frac{\partial G}{\partial x}=0. \tag{7.10}$$

Equations (7.8) and (7.9) are basic for studying unsteady liquid and gas flow in pipes.

ow.

With
akes

Let us examine a complex pneumatic-hydraulic system, consisting of lines, cavities, orifices, and so on. It is clear that any complex pneumatic-hydraulic system can be arbitrarily broken down into segments of simple lines, each of which has constant cross section geometry along its length, a constant elastic characteristic, and uniform liquid.

(7.7)

Equation
obtain

Assume that in the general case

$$F_1\neq F_2\neq\ldots\neq F_n;$$
$$l_1\neq l_2\neq\ldots\neq l_n;$$
$$a_1\neq a_2\neq\ldots\neq a_n,$$

where n is the number of simple lines making up the complex line;
F and l are the cross section area and the length of the simple line;
a is the elastic wave propagation velocity (sound speed) in the line.

The unsteady liquid flow in each simple line is described by the system of Equations (7.1). However, the effect of friction on the wave process can be neglected for liquid flow in short lines (which is valid for LRE propellant lines). For example, it is noted in [145] that it is necessary that b^2 be of the same order as $\left(\frac{\pi a}{2l}\right)^2$ to obtain a marked difference between the hydraulic impact of an ideal and viscous liquid.

Let $b=\frac{\pi a}{2l}$. According to (7.2) $b=\frac{\xi}{2d_0}w$, therefore, the friction effect can be neglected if

$$\frac{l}{d_0}w<\frac{\pi a}{\xi}. \tag{7.11}$$

It is not difficult to see that (7.11) is usually satisfied in LRE propellant feed lines. Therefore, in studying unsteady liquid flow in LRE lines we will use (7.7) (with b = 0). Moreover, for the pressures occurring in LRE in most cases we can neglect the effect of accelerations on the wave process. Then the computational equations take the form

$$\left.\begin{aligned}-\frac{\partial p}{\partial x}&=\frac{1}{F}\frac{\partial Q}{\partial \tau};\\ -\frac{\partial p}{\partial \tau}&=\frac{a^2}{F}\frac{\partial Q}{\partial x}.\end{aligned}\right\} \tag{7.12}$$

We differentiate the first equation with respect to x and the second with respect to τ. After simple transformation we obtain

$$\frac{\partial^2 p}{\partial x^2}=\frac{1}{a^2}\frac{\partial^2 p}{\partial t^2}; \tag{7.13}$$

$$\frac{\partial^2 Q}{\partial t^2}=a^2\frac{\partial^2 Q}{\partial x^2}. \tag{7.14}$$

Equations (7.13) and (7.14) describe the pressure and flow rate change in a simple line. Obviously, we need n Equations (7.13) or (7.14) in order to analyze the wave process in a complex line consisting of n simple lines:

$$\left.\begin{aligned}&\frac{\partial^2 p_1}{\partial x_1^2}=\frac{1}{a_1^2}\frac{\partial^2 p_1}{\partial t^2};\\&\cdots\cdots\cdots\\&\frac{\partial^2 p_n}{\partial x_n^2}=\frac{1}{a_n^2}\frac{\partial^2 p_n}{\partial t^2};\end{aligned}\right\} \tag{7.15}$$

$$\left.\begin{aligned}&\frac{\partial^2 Q_1}{\partial x_1^2}=\frac{1}{a_1^2}\frac{\partial^2 Q_1}{\partial t^2};\\&\cdots\cdots\cdots\\&\frac{\partial^2 Q_n}{\partial x_n^2}=\frac{1}{a_n^2}\frac{\partial^2 Q_n}{\partial t^2}.\end{aligned}\right\} \tag{7.16}$$

§ 2. Initial and Boundary Conditions. Methods for Integrating the Governing Equations

In order to solve the system of Equations(7.15)—(7.16) we must know the limiting conditions, which include the initial and boundary conditions.

The initial conditions define the distribution of the liquid flow rate and pressure along the length of the line at the initial time.

For our case the initial conditions have the form

$$\left.\begin{aligned}&p_1(x_1,\ 0)=f_1(x_1);\\&\cdots\cdots\cdots\\&p_n(x_n,\ 0)=f_n(x_n);\\&Q_1(x_1,\ 0)=F_1(x_1);\\&\cdots\cdots\cdots\\&Q_n(x_n,\ 0)=F_n(x_n).\end{aligned}\right\}$$

The flow rate and pressure distributions along the line at the initial time may also be uniform, i.e.,

$$\left.\begin{aligned} p_1(x_1, 0) &= p_{01} = \text{const}; \\ &\cdots\cdots\cdots \\ p_n(x_n, 0) &= p_{0n} = \text{const}; \end{aligned}\right\}$$

$$\left.\begin{aligned} G_1(x_1, 0) &= G_{01} = \text{const}; \\ &\cdots\cdots\cdots \\ G_n(x_n, 0) &= G_{0n} = \text{const}. \end{aligned}\right\}$$

The initial conditions are frequently found from the parameter distributions along the length of the line in the steady-state regime.

In view of the fact that, in the case of unsteady liquid flow along lines, the pressure and flow rate vary not only as a function of time but also as a function of the length, for the solution of the posed problem we must know the variation of the parameters at some certain sections of the system, which are determined by the boundary conditions.

For a simple line it is sufficient to know the parameter (pressure, flow rate) variation laws at the ends of the line. In the case of complex lines we must also establish the compatability conditions at the junctions of the simple lines.

The determination of the boundary conditions is a very complex problem, which can be solved only in certain particular cases in the corresponding approximation and under definite simplifying hypotheses and assumptions.

1. Boundary Conditions at the Junctions of Simple Lines (Compatability Conditions)

Consider two adjacent simple lines, for example, the (m - 1)st and the m^{th} (Figure 7.2). We assume that the pressures and flow rates are equal at the section where the lines join ($x_{m-1}=l_{m-1}$ and $x_m=0$), i.e.,

Figure 7.
stage l

We wi
lines in t

If th
conditions
assumption
that the i

Let t
Then we ha

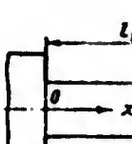

Figure 7.3
line.

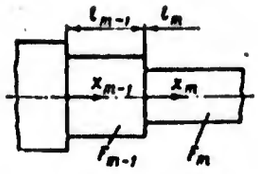

Figure 7.2. Three-stage line.

$$p_{m-1}(l_{m-1}, \tau) = p_m(0, \tau); \tag{7.17}$$

$$G_{m-1}(l_{m-1}, \tau) = G_m(0, \tau). \tag{7.18}$$

Differentiating (7.17) with respect to τ and using (7.12), we obtain

$$\left.\begin{aligned} \frac{a^2_{(m-1)}}{F_{m-1}} \frac{\partial G_{m-1}(l_{m-1}, \tau)}{\partial x_{m-1}} &= \frac{a^2_m}{F_m} \frac{\partial G_m(0, \tau)}{\partial x_m}; \\ G_{m-1}(l_{m-1}, \tau) &= G_m(0, \tau); \end{aligned}\right\} \tag{7.19}$$

$$\left.\begin{aligned} F_{m-1} \frac{\partial p_{m-1}(l_{m-1}, \tau)}{\partial x_{m-1}} &= F_m \frac{\partial p_m(0, \tau)}{\partial x_m}; \\ p_{m-1}(l_{m-1}, \tau) &= p_m(0, \tau). \end{aligned}\right\} \tag{7.20}$$

We will use the boundary conditions at the junction of two simple lines in the following.

If there are branched lines in the hydraulic system, the boundary conditions are found at the branching node on the basis of the same assumptions we used previously, i.e., that the pressures are equal and that the individual flow rates add up to the overall flow rate.

Let the j^{th} main line branch into r simple lines (Figure 7.3). Then we have at the branching node

$$G_j(l_j, \tau) = \sum_{k=1}^{k=r} G_k(0, \tau); \tag{7.21}$$

$$p_j(l_j, \tau) = p_1(0, \tau) = p_2(0, \tau) = \ldots = p_r(0, \tau). \tag{7.22}$$

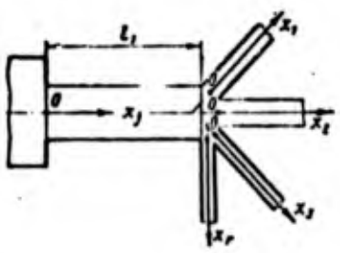

Figure 7.3. Branched line.

Using (7.12), the Equations (7.21) and (7.22) may be written in the form

$$G_j(l_j, \tau) = \sum_{k=1}^{k=r} G_k(0, \tau);$$

$$\frac{a_j^2}{F_j} \frac{\partial G_j(l_j, \tau)}{\partial x_j} = \frac{a^2}{F_1} \frac{\partial G_1(0, \tau)}{\partial x_1} = \ldots = \frac{a_r^2}{F_r} \frac{\partial G_r(0, \tau)}{\partial x_r}; \quad (7.23)$$

$$p_j(l_j, \tau) = p_1(0, \tau) = \ldots = p_r(0, \tau);$$

$$\frac{F_j \partial p_j(l_j, \tau)}{\partial x_j} = \sum_{k=1}^{k=r} F_k \frac{\partial p_k(0, \tau)}{\partial x_k}. \quad (7.24)$$

2. Boundary Conditions at the End Sections of a Hydraulic System

To solve the boundary value problem, in addition to the initial conditions and the compatability conditions at the junctions of the simple lines, we need to know the law of variation of the parameters (flow rate and pressure in our case) at definite points of the hydraulic system. As a rule, the values of these parameters are defined at the terminal sections of the hydraulic system.

In the majority of cases it is not possible to define the boundary conditions exactly, however, this problem is solvable under certain restrictions and assumptions. We shall examine some particular cases of the determination of the form of the boundary conditions.

In the hydraulic system there are lines which are open at the end sections. Assuming that the pressure at the end section of the line equals the ambient pressure, atmospheric for example, we obtain

$$p_j(l_j, \tau) = p_0 = \text{const}, \quad (7.25)$$

where j is the number of the terminal line;

p_0 is the ambient pressure.

Using the second Equation (7.12), the Condition (7.13) can be written in the form

$$\frac{\partial G_j(l_j, \tau)}{\partial x_j} = 0. \quad (7.26)$$

In the hydraulic system there are dead-end (closed) lines. In this case we can assume that the liquid motion velocity at the line end section equals zero and

$$G_j(l_j, \tau) = 0. \tag{7.27}$$

The pressure and flow rate are time functions:

$$\left.\begin{aligned} p_j(l_j, \tau) &= f(\tau); \\ G_k(l_k, \tau) &= F(\tau). \end{aligned}\right\} \tag{7.28}$$

There is an air damper at the line end section [145]. The change of the gas volume in the damper will be

$$\frac{d\Delta V_1}{d\tau} = \frac{G_j(l_j, \tau)}{\rho_j}, \tag{7.29}$$

where ρ_j is the density of the liquid entering the damper.

We assume that the air compresses isothermally. Then

$$p_0 V_0 = p(V_0 - \Delta V_1),$$

where p_0, V_0 are the average pressure and volume of the air in the damper.

Hence

$$p = \frac{p_0 V_0}{V_0 - \Delta V_1} \approx p_0\left(1 + \frac{\Delta V_1}{V_0}\right). \tag{7.30}$$

From (7.30) we find

$$\frac{d\Delta V_1}{d\tau} = \frac{V_0}{p_0}\frac{\partial p}{\partial \tau}(l_j, \tau).$$

Using (7.7) and (7.29), we obtain

$$G_j(l_j, \tau) + \frac{V_0 \rho_j a_j^2}{p_0 F_j}\frac{\partial G(l_j, \tau)}{\partial x_j} = 0. \tag{7.31}$$

There is an elastic damper at the line end section. Sometimes it is not possible to install a gas damper in the hydraulic system for

one reason or another. Then a damper with elastic walls is used, in which the walls increase the volume occupied by the liquid as they deform.

The damper volume increase due to elasticity is

$$d\Delta V = \frac{dp}{E_{np}} V_0,$$

where E_{red} is the reduced liquid bulk compression modulus, taking into account the elasticity of the damper wall;

V_0 is the liquid volume in the damper.

On the other hand

$$\frac{d\Delta V}{dt} = \frac{G_j(l_j, t)}{\rho_j} = \frac{\partial p(l_j, t)}{\partial t} \frac{V_0}{E_{np}}. \tag{7.32}$$

Using (7.7) and (7.32), we obtain

$$G_j(l_j, t) + \frac{\rho_j a_j^2}{F_j} \frac{V_0}{E_{np}} \frac{\partial G(l_j, t)}{\partial x_j} = 0.$$

In the more general case the boundary conditions at the end sections can be specified in the form

$$G_j(l_j, t) + \beta_j \frac{\partial G_j(l_j, t)}{\partial x_j} = f_j(t), \tag{7.33}$$

where the coefficient β_j is determined for each specific case.

Sometimes the form of the functions $f_j(t)$ is not known and is determined from the ordinary differential equations describing the motion of the automatic control elements installed at the end sections of the lines to regulate the flow rate or the pressure. In this case the problem becomes considerably more complicated, since we must integrate jointly the Equations (7.16) and the equations which define the form of $f_j(t)$.

3. Integra

The wa
ematical ph
devoted to

In the
operator me
although so
nique — th
paratively
equations f
This condit
must be hom
siderably m
eous. These
techniques

One suc
aid of which
homogeneous
tions the pa
(7.16) is of

where $X(x)$, T(

Substit
we obtain

3. Integration of the Equations of Unsteady Liquid Motion in Lines

The wave Equations (7.16) are among the linear equations of mathematical physics, and a considerable number of studies have been devoted to their integration.

In the solution of several problems some authors have used the operator method or the contour integration method [15]. Simplest, although somewhat cumbersome, is the separation of variables technique — the Fourier method. It permits obtaining the solutions comparatively simply in those cases in which the system of fundamental equations from which the general solution is composed is orthogonal. This condition depends on the form of the boundary conditions, which must be homogeneous in this case. However, the solution becomes considerably more complicated if the boundary conditions are not homogeneous. These complications can sometimes be avoided by using particular techniques which have been developed in mathematical physics.

One such technique is the introduction of new variables with the aid of which the nonhomogeneous boundary conditions are reduced to homogeneous conditions. In the case of homogeneous boundary conditions the particular solution of a system of equations of the type (7.16) is often sought in the form

$$\left.\begin{aligned} G_1(x_1, \tau) &= X_1(x_1)T(\tau); \\ &\cdots\cdots\cdots \\ G_n(x_n, \tau) &= X_n(x_n)T(\tau), \end{aligned}\right\} \tag{7.34}$$

where $X(x)$, $T(\tau)$ are functions which depend respectively on x and τ.

Substituting (7.34) into the basic system of Equations (7.16), we obtain

$$\left.\begin{aligned} &\ddot{X}_1(x_1) + \left(\frac{\omega}{a_1}\right)^2 X_1(x_1) = 0; \\ &\cdots\cdots\cdots\cdots \\ &\ddot{X}_n(x_n) + \left(\frac{\omega}{a_n}\right)^2 X_n(x_n) = 0; \\ &\ddot{T}(\tau) + \omega^2 T(\tau) = 0, \end{aligned}\right\} \tag{7.35}$$

where ω is the problem eigenvalue.

Further, integrating these equations we find

$$\left.\begin{aligned} X_1(x_1) &= A_1 \sin\left(\frac{\omega}{a_1}x_1+\varphi_1\right);\\ &\cdots\cdots\cdots\cdots\\ X_n(x_n) &= A_n \sin\left(\frac{\omega}{a_n}x_n+\varphi_n\right);\\ T(\tau) &= \sin(\omega\tau+\psi). \end{aligned}\right\} \qquad (7.36)$$

where $A_1, \ldots, A_n, \varphi_1, \ldots, \varphi_n, \psi$ are arbitrary constants which are determined from the boundary and initial conditions. Finally, the particular solutions of the system of Equations (7.16) have the form

$$\left.\begin{aligned} G_1(x, \tau) &= A_1 \sin\left(\frac{\omega}{a_1}x_1+\varphi_1\right)\sin(\omega\tau+\psi);\\ &\cdots\cdots\cdots\cdots\cdots\cdots\\ G_n(x_n, \tau) &= A_n \sin\left(\frac{\omega}{a_n}x_n+\varphi_n\right)\sin(\omega\tau+\psi). \end{aligned}\right\} \qquad (7.37)$$

It is not difficult to note from these solutions that ω is the natural frequency of the liquid oscillations in the hydraulic system lines and is one of the most important parameters characterizing not only the free oscillations, but also the other forms of unsteady liquid motion (for example, water hammer, steady periodic oscillations, and so on).

The possibility of constructing any time dependence by superposition of the Solutions (7.34) is retained if in place of the arbitrary functions $T(\tau)$ we consider only the functions which taken together form the complete system. Therefore, without loss of generality we can introduce in place of (7.34) the substitution corresponding to harmonic oscillations with amplitude and phase which vary from point to point. In this case, by virtue of the Fourier theorem any arbitrary space-time dependence can be obtained by superposition of oscillations of different frequencies.

It is convenient to describe the harmonic oscillations with the aid of complex functions of the form

$$\left.\begin{aligned} G_1(x_1, \tau) &= X_1(x_1)e^{i\omega\tau}; \\ &\cdots\cdots\cdots \\ G_n(x_n, \tau) &= X_n(x_n)e^{i\omega\tau}, \end{aligned}\right\} \tag{7.38}$$

where ω is the oscillation frequency;

X(x) is an initially unknown function of the x coordinate.

Substituting (7.38) into (7.16), it is not difficult to see that the functions $X_1(x_1), \ldots, X_n(x_n)$ have the same form as (7.37). Then the particular solutions of (7.16) will be

$$\left.\begin{aligned} G_1(x_1, \tau) &= A_1 \sin\left(\frac{\omega}{a_1}x_1 + \varphi_1\right)e^{i\omega\tau}; \\ &\cdots\cdots\cdots\cdots \\ G_n(x_n, \tau) &= A_n \sin\left(\frac{\omega}{a_n}x_n + \varphi_n\right)e^{i\omega\tau}. \end{aligned}\right\} \tag{7.39}$$

We obtain the general solutions in both the first and second methods by superposition of all the particular solutions found for the entire frequency spectrum $\omega_1, \omega_2, \ldots, \omega_k$, i.e.,

$$\left.\begin{aligned} G_1(x_1, \tau) &= \sum_{k=1}^{\infty} A_{1k} \sin\left(\frac{\omega_k}{a_1}x_1 + \varphi_{1k}\right)e^{i\omega_k\tau}; \\ &\cdots\cdots\cdots\cdots\cdots\cdots \\ G_n(x_n, \tau) &= \sum_{k=1}^{\infty} A_{nk} \sin\left(\frac{\omega_k}{a_n}x_n + \varphi_{nk}\right)e^{i\omega_k\tau}; \\ & k = 1, 2, 3, \ldots \end{aligned}\right\} \tag{7.40}$$

In many cases the liquid flow rate in a hydraulic system is a quantity which pulsates about its mean value with the definite frequency ω_0. In this connection the periodic solutions of (7.16), which correspond to steady flow rate oscillations, are of definite interest.

It is convenient to seek the periodic solutions of (7.16) in the Form (7.38). In this case the problem simplifies considerably, since the oscillation frequency ω_0 is known and the problem reduces to

determining the oscillation amplitudes at the required points of the hydraulic system.

The study of the simultaneous action of forced and free flow rate oscillations in hydraulic systems is of considerable theoretical and practical interest in the respect that under certain conditions these oscillations may be in resonance and thus may serve as the cause for severe vibrations of the liquid in these lines. These are undesirable from the viewpoint of strength and operational reliability of the system, instruments, automatic control elements, and so on.

In solving the water hammer problem it is sometimes convenient to represent the general solution of (7.12) in the form

$$\left.\begin{aligned} p_1 - p_{01} &= \rho_1 a_1 [\varphi_1(x_1 - a_1\tau) + \psi_1(x_1 + a_1\tau); \\ &\cdots\cdots\cdots\cdots\cdots\cdots \\ p_n - p_{0n} &= \rho_n a_n [\varphi_n(x_n - a_n\tau) + \psi_n(x_n + a_n\tau); \end{aligned}\right\} \quad (7.41)$$

$$\left.\begin{aligned} G_1 - G_{01} &= -\rho_1 F_1 [\varphi_1(x_1 - a_1\tau) + \psi_1(x_1 + a_1\tau); \\ &\cdots\cdots\cdots\cdots\cdots\cdots \\ G_n - G_{0n} &= -\rho_n F_n [\varphi_n(x_n - a_n\tau) + \psi_n(x_n + a_n\tau); \end{aligned}\right\} \quad (7.42)$$

where $(p-p_0)$ and $(G-G_0)$ are the pressure and flow rate deviations from their initial steady-state values;

$\varphi(x-a\tau)$ and $\psi(x+a\tau)$ are arbitrary functions of the arguments x and τ.

It is not difficult to show that (7.41) and (7.42) are the integrals of the differential Equations (7.12). To do this let us find the expressions for the corresponding partial derivatives (we drop the indices denoting the number of the simple line in the complex line, since the same proof can be carried out for a system of lines as well)

$$\frac{\partial p}{\partial x} = \rho a \left[\frac{d\varphi(x-a\tau)}{d(x-a\tau)} + \frac{d\psi(x+a\tau)}{d(x+a\tau)}\right];$$

$$\frac{\partial p}{\partial \tau} = \rho a^2 \left[-\frac{d\varphi(x-a\tau)}{d(x-a\tau)} + \frac{d\psi(x+a\tau)}{d(x+a\tau)}\right];$$

$$\frac{\partial G}{\partial \tau} = \rho F \left[-\frac{d\varphi(x-a\tau)}{d(x-a\tau)} + \frac{d\psi(x+a\tau)}{d(x+a\tau)}\right];$$

$$\frac{\partial G}{\partial \tau} = \rho F a \left[\frac{d\varphi(x-a\tau)}{d(x-a\tau)} + \frac{d\psi(x+a\tau)}{d(x+a\tau)}\right].$$

After substituting these expressions into (7.12) we obtain identities, which confirms the correctness of the solution obtained.

Let us analyze (7.41) and (7.42). Let the pressure in the line be described by the equation

$$p-p_0=\rho a[\varphi(x-a\tau)+\psi(x+a\tau)].$$

Let us examine the value of the function φ at the time τ_1 at the section x_1 and at the time τ_2. Obviously, the coordinate x_2 corresponding to the time τ_2 will be

$$x_2=x_1+a(\tau_2-\tau_1).$$

Then the value of the function $\varphi(x-a\tau)$ at the time τ_2 will be

$$\varphi(x_2-a\tau_2)=\varphi[x_1+a(\tau_2-\tau_1)-a\tau_2]=\varphi(x_1-a\tau_1).$$

This expression shows that the value of the function at the time τ_2 equals the value of the function at the time τ_1 at the section x_1. We can show similarly that

$$\psi(x_2+a\tau_2)=\psi(x_1+a\tau_1).$$

This shows that the values of the functions $\varphi(x-a\tau)$ and $\psi(x+a\tau)$ propagate along the line with the velocity a: the first in the direction of increasing values of x, the second in the direction of decreasing values.

The functions $\varphi(x-a\tau)$ and $\psi(x+a\tau)$ define only the connection between x and τ, but not their concrete form, which is defined by the form of the boundary conditions. In this case the form of the boundary conditions may be considerably more general than in the case of the solution of the wave equations by separation of variables.

We know that the solution of the water hammer problem also involves finding those functions which will satisfy completely the boundary conditions. Therefore, the solution of the wave equations in the form (7.41) and (7.42) makes it possible to solve several complex problems of unsteady liquid flow in pipes.

§ 3. Free Liquid Oscillations in a Complex Tanden Line

The natural frequency of elastic system oscillations is an important criterion characterizing the system dynamics. We note that oscillatory processes accompany the operation of any machine, beginning with the elastic oscillations of the very simplest mechanisms and terminating with the oscillatory processes in the hydraulic systems and combustion chamber of rocket engines. While in certain cases excessive oscillations can interfere with normal functioning, in other cases, particularly in the case of resonant phenomena, they can lead to structural failure. Moreover, the natural frequency is not simply of interest by itself, it is at the same time the problem eigenvalue, i.e., the parameter which is necessary in the solution of several other questions associated with unsteady liquid flow in LRE lines and test stand lines.

The primary problem in examining oscillatory processes in elastic mechanical systems becomes that of determining the system natural oscillation frequencies and this means clarification of the nature of the external and internal perturbing forces and the periodic nature of their action. Therefore, a large part of the published studies on oscillations, amounting to hundreds of titles [136], is devoted to the questions of the calculation of the natural frequencies of mechanical systems. As for the question of the calculation of the natural oscillation frequencies of liquid and gas in complex pipe lines, as far as we know in only a few studies [19], [48], [62] has this problem been examined for very simple hydraulic systems. It is true that the problem of determining the liquid natural oscillation frequencies has been solved in [11] in a somewhat more general formulation.

Let us examine a complex penumatic-hydraulic system consisting of lines, cavities, orifices, and so on, all connected in series. It is obvious that any complex penumatic-hydraulic system can be broken down into segments of simple lines and represented schematically in the form of a multistage line (Figure 7.4). We have in the general case

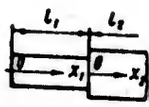

Figure 7.4. diagram f line.

The bou of the simpl

The init

We note cient to know

$$F_1 \neq F_2 \neq \ldots \neq F_n;$$
$$l_1 \neq l_2 \neq \ldots \neq l_n;$$
$$a_1 \neq a_2 \neq \ldots \neq a_n.$$

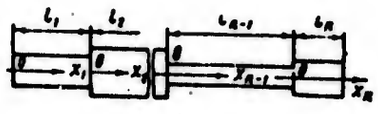

Figure 7.4. Computational diagram for multistage line.

We have noted previously that this problem reduces to the solution of the system of equations

$$\left.\begin{aligned} &\frac{\partial^2 G(x,\tau)}{\partial \tau^2} = a_1^2 \frac{\partial^2 G(x,\tau)}{\partial x^2};\\ &\ldots\ldots\ldots\ldots;\\ &\frac{\partial^2 G_n(x_n,\tau)}{\partial \tau^2} = a_n^2 \frac{\partial^2 G_n(x_n,\tau)}{\partial x_n^2}. \end{aligned}\right\} \qquad (7.43)$$

The boundary conditions at the end sections and at the junction of the simple lines have the form

$$\left.\begin{aligned} &a_1 \frac{\partial G_1(0,\tau)}{\partial x_1} + \beta_1 G_1(0,\tau) = 0;\\ &G_1(l_1,\tau) = G_2(0,\tau);\\ &\ldots\ldots\ldots\ldots\ldots\ldots\\ &G_{n-1}(l_{n-1},\tau) = G_n(0,\tau);\\ &\frac{a_1^2}{F_1}\frac{\partial G_1(l_1,\tau)}{\partial x_1} = \frac{a_2^2}{F_2}\frac{\partial G_2(0,\tau)}{\partial x_2};\\ &\ldots\ldots\ldots\ldots\ldots\ldots\\ &\frac{a_{n-1}^2}{F_{n-1}}\frac{\partial G_{n-1}(l_{n-1},\tau)}{\partial x_{n-1}} = \frac{a_n^2}{F_n}\frac{\partial G_n(0,\tau)}{\partial x_n};\\ &a_n \frac{\partial G_n(l_n,\tau)}{\partial x_n} + \beta_n G_n(l_n,\tau) = 0. \end{aligned}\right\} \qquad (7.44)$$

The initial conditions have the form

$$\left.\begin{aligned} &G_1(x_1,0) = F_1(x_1); \quad \frac{\partial G_1(x_1,0)}{\partial \tau} = \Psi_1(x_1);\\ &\ldots\ldots\ldots \quad \ldots\ldots\ldots\\ &G_n(x_n,0) = F_n(x_n); \quad \frac{\partial G_n(x_n,0)}{\partial \tau} = \Psi_n(x_n). \end{aligned}\right\}$$

We note that in determining the natural frequencies it is sufficient to know the form of the boundary conditions, since the frequency

is independent of the initial distribution of the flow rate or pressure in the line.

We know that the particular solution of (7.43) with the boundary Conditions (7.44) has the form

$$\left.\begin{aligned} G_1(x, \tau) &= A_1 e^{i\omega\tau} \sin\left(\frac{\omega}{a_1} x_1 + \varphi_1\right); \\ &\cdots\cdots\cdots\cdots \\ G_n(x_n, \tau) &= A_n e^{i\omega\tau} \sin\left(\frac{\omega}{a_n} x_n + \varphi_n\right). \end{aligned}\right\} \tag{7.45}$$

From (7.45) we obtain

$$\left.\begin{aligned} \frac{\partial G_1(x_1, \tau)}{\partial x_1} &= A_1 \frac{\omega}{a_1} e^{i\omega\tau} \cos\left(\frac{\omega}{a_1} x_1 + \varphi_1\right); \\ &\cdots\cdots\cdots\cdots \\ \frac{\partial G_n(x_n, \tau)}{\partial x_n} &= A_n \frac{\omega}{a_n} e^{i\omega\tau} \cos\left(\frac{\omega}{a_n} x_n + \varphi_n\right). \end{aligned}\right\} \tag{7.46}$$

From the boundary conditions at the junction of the simple lines we obtain the relations

$$\left.\begin{aligned} &\frac{F_1}{a_1^2} \frac{G_1(l_1, \tau)}{\dfrac{\partial G_1(l_1, \tau)}{\partial x_1}} = \frac{F_2}{a_2^2} \frac{G_2(0, \tau)}{\dfrac{\partial G_2(0, \tau)}{\partial x_2}}; \\ &\cdots\cdots\cdots\cdots\cdots \\ &\frac{F_{n-1}}{a_{n-1}^2} \frac{G_{n-1}(l_{n-1}, \tau)}{\dfrac{\partial G_{n-1}(l_{n-1}, \tau)}{\partial x_{n-1}}} = \frac{F_n}{a_n^2} \frac{G_n(0, \tau)}{\dfrac{\partial G_n(0, \tau)}{\partial x_n}}. \end{aligned}\right\} \tag{7.47}$$

After substituting (7.45) and (7.46) into (7.47) we obtain

$$\left.\begin{aligned} &\frac{F_1}{a_1} \operatorname{tg}\left(\frac{\omega}{a_1} l_1 + \varphi_1\right) = \frac{F_2}{a_2} \operatorname{tg} \varphi_2; \\ &\cdots\cdots\cdots\cdots\cdots \\ &\frac{F_{n-1}}{a_{n-1}} \operatorname{tg}\left(\frac{\omega}{a_{n-1}} l_{n-1} + \varphi_{n-1}\right) = \frac{F_n}{a_n} \operatorname{tg} \varphi_n. \end{aligned}\right\} \tag{7.48}$$

This system of transcendental equations defines the problem eigenvalues and in our case the liquid natural oscillation frequencies in complex multistage lines. Since the phase angles φ_1 and φ_n are found

from the boundary conditions at the end sections of the complex line, the system (7.48) is closed.

It follows from (7.48) that there is an infinite set (spectrum) of values of $\omega_1, \omega_2, \ldots, \omega_k$, which satisfy the solutions of the form (7.45). Therefore, the general solution of (7.43) with the boundary conditions (7.44) and with the previously indicated initial conditions consists of the sum of all the particular solutions and has the form (7.40), which we presented earlier without proof.

For known φ_1 and φ_n (7.48) defines the entire spectrum of natural frequencies. Let us show how the values of the phase angles φ_1 and φ_n are determined as a function of the boundary conditions.

Pipe line open at both ends. Then in accordance with (7.26) we have

$$\frac{\partial G_1(0, \tau)}{\partial x_1} = 0; \quad \frac{\partial G_n(l_n, \tau)}{\partial x_n} = 0. \tag{7.49}$$

Using (7.45) and (7.49), we obtain

$$\cos\varphi_1 = 0; \quad \varphi_{1k} = \frac{2k-1}{2}\pi, \quad k = 1, 2, 3, \ldots;$$

$$\cos\left(\frac{\omega}{a_n} l_n + \varphi_n\right) = 0; \quad \varphi_{nk} = \frac{2k-1}{2}\pi - \frac{\omega}{a_n} l_n.$$

Pipe line open at both ends. Then the liquid flow rates at the end sections equal zero, i.e.,

$$G_1(0, \tau) = 0; \; G_n(l_n, \tau) = 0.$$

In accordance with (7.46) we have

$$\sin\varphi_1 = 0; \quad \varphi_{1k} = (k-1)\pi; \quad k = 1, 2, 3, \ldots;$$

$$\sin\left(\frac{\omega}{a_n} l_n + \varphi_n\right) = 0, \quad \varphi_{nk} = (k-1)\pi - \frac{\omega}{a_n} l_n.$$

$$k = 1, 2, 3, \ldots$$

The formulas which define the angles φ_1 and φ_n, when one end is closed and the other is open are determined with the aid of the expressions presented in the two preceding cases.

An elastic element at the end of the line. There is considerable practical interest in the case in which elastic elements are installed at the end of a complex line: bellows, membranes, the disks of spring-loaded and pneumatic valves, and so on. In any case the elastic element can be represented in the form of a piston with mass m and a spring having the stiffness c (Figure 7.5).

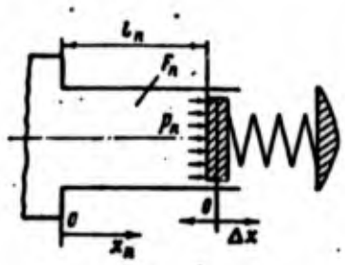

Figure 7.5. Typical elastic element scheme.

In the steady-state regime the piston of the elastic element is in equilibrium under the action of the liquid pressure and the spring force. At the moment a disturbance is applied, both the piston and the liquid in the line begin to perform an oscillatory motion about their equilibrium position.

The equation of the piston motion under the disturbing forces will be

$$m\Delta\ddot{x}+c\Delta x=\Delta pF_0, \tag{7.50}$$

where Δp is the deviation of the pressure from its steady value;
Δx is the piston displacement;
F_0 is the piston working area.

From (7.12) we have

$$-\frac{\partial p_n(l_n,\tau)}{\partial x}=\frac{a_n^2\partial G_n(l_n,\tau)}{F_n\partial x_n}. \tag{7.51}$$

After substituting in place of $G_n(l_n, \tau)$ its value from (7.40) and integrating (7.51), we obtain

$$-p_n(l_n,\tau)=\frac{a_n}{F_n}\sum_{k=1}^{\infty}A_{nk}l\cos\left(\frac{\omega_k}{a_n}l_n+\gamma_{nk}\right)e^{i\omega_k\tau}+c_1. \tag{7.52}$$

The arbitrary constant C_1 characterizes the magnitude of the steady pressure in the line, and the term consisting of the sum of the series is the deviation of the pressure from its steady value.

Then

$$\Delta p = \frac{a_n}{F_n} \sum_{k=1}^{\infty} A_{nk} l \cos\left(\frac{\omega_k}{a_n} l_n + \varphi_{nk}\right) e^{i\omega_k \tau}.$$

Let us assume that the liquid density changes only slightly. This is quite valid for a liquid. As for a gas, this assumption is acceptable if the amplitude of the pressure oscillation is much less than the mean pressure in the line.

Then the fluid velocity at the piston will be

$$w(l_n, \tau) = \frac{Q_n(l_n, \tau)}{\varrho_n F_n} = \frac{1}{\varrho_n F_n} \sum_{k=1}^{\infty} A_{nk} \sin\left(\frac{\omega_k}{a_n} l_n + \varphi_{nk}\right) e^{i\omega_k \tau}. \tag{7.53}$$

Since the piston motion velocity equals the fluid motion velocity at the section $x_n = l_n$, we have

$$\frac{d\Delta x}{d\tau} = w(l_n, \tau). \tag{7.54}$$

Using (7.53) and (7.54), the expressions for Δx and $\Delta \ddot{x}$ can be written in the form

$$\Delta \ddot{x} = \frac{dw(l_n, \tau)}{d\tau} = \frac{1}{\varrho_n F_n} \sum_{k=1}^{\infty} i A_{nk} \sin\left(\frac{\omega_k}{a_n} l_n + \varphi_{nk}\right) e^{i\omega_k \tau} \omega_k.$$

and

$$\Delta x = \int w(l_n, \tau) d\tau + C_2.$$

As in the case (7.52), $C_2 = 0$.

Then

$$\Delta x = \frac{1}{\varrho_n F_n} \sum_{k=1}^{\infty} \frac{A_{nk}}{i\omega_k} \sin\left(\frac{\omega_k}{a_n} l_n + \varphi_{nk}\right) e^{i\omega_k \tau}.$$

We substitute these expressions into (7.50). After simple transformations we obtain

$$\sum_{k=1}^{\infty}\left[\frac{m}{\varrho_n F_n}\sin\left(\frac{\omega_k}{a_n}l_n+\varphi_{nk}\right)-\frac{C}{\varrho_n F_n\omega_k^2}\sin\left(\frac{\omega_k}{a_n}l_n+\varphi_{nk}\right)-\right.$$
$$\left.-\frac{F_0\beta_n}{F_n}\cos\left(\frac{\omega_k}{a_n}l_n+\varphi_{nk}\right)\right]e^{i\omega_k t}=0.$$

Hence

$$\frac{m}{\varrho_n F_n}\sin\left(\frac{\omega_k}{a_n}l_n+\varphi_{nk}\right)-\frac{C}{\varrho_n F_n\omega_k^2}\sin\left(\frac{\omega_k}{a_n}l_n+\varphi_{nk}\right)-$$
$$-\frac{F_0\beta_n}{F_n\omega_k}\cos\left(\frac{\omega_k}{a_n}l_n+\varphi_{nk}\right)=0.$$

Thus the phase angle φ for a line having elasticity at the end section is determined from the equations

$$\operatorname{tg}\left(\frac{\omega_k}{a_n}l_n+\varphi_{nk}\right)=-\frac{\varrho_n F_0\beta_n}{\omega_k\left(\frac{c}{\omega_k^2}-m\right)}. \qquad (7.55)$$

Assuming that $\frac{c}{m}=f^2$ (f is the circular frequency of the free oscillations of the elastic element), (7.55) can be written in the form

$$\operatorname{tg}\left(\frac{\omega_k}{a_n}l_n+\varphi_{nk}\right)=\frac{\varrho_n F_0\beta_n}{\omega_k m\left(1-\frac{f^2}{\omega_k^2}\right)}. \qquad (7.56)$$

These relations have the same form for the case in which the elastic element mass is distributed uniformly along the length. Then (7.56) takes the form

$$\operatorname{tg}\left(\frac{\omega_k}{a_m}l_m+\varphi_{mk}\right)=\frac{\varrho_m F_0 f_k^2}{\omega_k c\left[1-\frac{f_k^2}{\omega_k^2}\right]}. \qquad (7.57)$$

where f_k is the k^{th} frequency of the elastic element free oscillations.

trans-

Damper at the end section of the line. We know that the boundary condition for a damper can be written as

$$G_j(l_j, \tau)+\beta_j \frac{\partial G_j(l_j, \tau)}{\partial x_j}=0, \tag{7.58}$$

where for a gas-filled damper

$$\beta_j=\frac{V_{00j}a_j^2}{p_0F_j}$$

for an elastic damper

$$\beta_j=\frac{\varrho_j a_j^2}{F_j}\frac{V_0}{E_{np}}.$$

end

Using (7.45) and (7.46), we obtain from (7.58)

$$\operatorname{tg}\left(\frac{\omega_k}{a_j}l_j+\varphi_{jk}\right)=-\frac{\omega_k}{a_j}\beta_j. \tag{7.59}$$

(7.55)

Grid installed at the end of a simple line. We represent the grid (Figure 7.6) in the form of open simple lines, of which there are s. Let the length of these lines (grid thickness) be l_{j+1}, and the flow section area be F_{j+1}.

ree
the

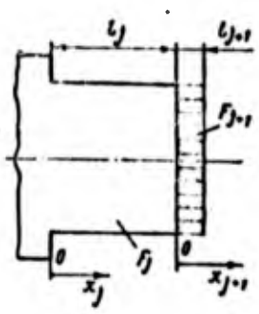

Figure 7.6. Diagram for deriving Equation (7.63).

(7.56)

The condition of equality of the pressures and flow rates is valid at the section $x_j=l_j$ i.e.,

$$\left.\begin{aligned} G_j(l_j, \tau)&=\sum_{k=1}^{k=s} G_k(0, \tau)=sG_{j+1}(0, \tau);\\ \frac{a_j^2}{F_j}\frac{\partial G_j(l_j, \tau)}{\partial x_j}&=\frac{a_{j+1}^2}{F_{j+1}}\frac{\partial G_{j+1}(0, \tau)}{\partial x_{j+1}}. \end{aligned}\right\} \tag{7.60}$$

Then

Using (7.45), (7.46), (7.60), we obtain

(7.57)

$$\frac{F_j}{a_j}\operatorname{tg}\left(\frac{\omega}{a_j}l_j+\varphi_j\right)=\frac{sF_{j+1}}{a_{j+1}}\operatorname{tg}\varphi_{j+1}. \tag{7.61}$$

ations.

Since the ports j + 1 are open, in accordance with (7.49) we have

$$\varphi_{(j+1)k}=\frac{2k-1}{2}\pi-\frac{\omega_k}{a_{j+1}}l_{j+1}.$$

Considering that

$$sF_{j+1}=F_g,$$

where F_g is the total port area, (7.61) may be written in the form

$$\operatorname{tg}\left(\frac{\omega}{a_j}l_j+\varphi_j\right)=-\frac{F_g}{F_j}\frac{a_j}{a_{j+1}}\operatorname{ctg}\frac{\omega_k}{a_{j+1}}l_{j+1}. \tag{7.62}$$

In view of the fact that $l_{j+1}\ll l_j$,

$$\operatorname{tg}\frac{\omega_k}{a_{j+1}}l_{j+1}\approx\frac{\omega_k}{a_{j+1}}l_{j+1}.$$

Finally, (7.62) can be written in the form

$$\operatorname{tg}\left(\frac{\omega}{a_j}l_j+\varphi_j\right)=-\frac{F_g a_j}{F_j\omega_k l_{j+1}}. \tag{7.63}$$

We note that (7.63) was obtained without account for the added mass, and therefore, it can be used only for calculations in the first approximation.

§ 4. Natural Oscillation Frequency of Fluid in Some Very Simple Pneumatic-Hydraulic Lines

The system of Equation (7.48) defines the natural frequency of the fluid oscillations in a multistage line. In deriving (7.48) the complex system was broken down into segments of simple lines. This division simplifies the mathematical apparatus significantly and makes it possible to solve the problem in general form.

We shall show that this simplification of the complex system does not in any way contradict the accuracy and broad generality of the computational relations obtained. Moreover, it is useful to use simple examples to show the qualitative influence of various factors on the frequency of the natural oscillations of the fluid in complex lines.

49) we have

he form

(7.62)

(7.63)

he added
n the first

ome

uency of the
) the com-
This divi-
d makes it

system does
of the
o use simple
rs on the
ex lines.

Cavity-open line. The fluid natural oscillation frequency in the system shown in Figure 7.7 is defined by the first Equation (7.48)

$$\frac{F_1}{a_1}\operatorname{tg}\left(\frac{\omega_1}{a_1}l_1+\varphi_1\right)-\frac{F_2}{a_2}\operatorname{tg}\varphi_2=0. \tag{7.64}$$

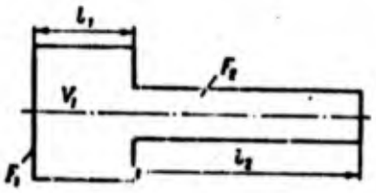

Figure 7.7. Diagram for deriving Equation (7.66)

For the system in question

$$\varphi_1=(k-1)\pi,\ \varphi_2=\frac{2k-1}{2}\pi-\frac{\omega l_2}{a_2},\quad k=1,\ 2,\ 3,\ldots \tag{7.65}$$

Then with account for (7.65), (7.64) takes the form

$$\frac{F_1}{a_1}\operatorname{tg}\frac{\omega}{a_1}l_1=\frac{F_2}{a_2}\operatorname{ctg}\frac{\omega}{a_2}l_2.$$

If the elastic wave propagation velocity is the same in the system lines, i.e., $a_1=a_2=a$ and $l_2\gg l_1$, then $\operatorname{tg}\frac{\omega}{a_1}l_1\approx\frac{\omega}{a}l_1$ and the last expression takes the form

$$\frac{V_1\omega}{aF_2}=\operatorname{ctg}\frac{\omega}{a}l_2. \tag{7.66}$$

Formula (7.66) was first obtained by Khailov [48] and also by Bodner [19] in studying the resonant supercharging of piston aircraft engines.

Cavity-line-second-cavity. The frequency of this system (Figure 7.8) is determined by two of the Equations (7.48)

$$\left.\begin{aligned}\frac{F_1}{a_1}\operatorname{tg}\left(\frac{\omega}{a_1}l_1+\varphi_1\right)-\frac{F_2}{a_2}\operatorname{tg}\varphi_2=0;\\ \frac{F_2}{a_2}\operatorname{tg}\left(\frac{\omega}{a_2}l_2+\varphi_2\right)-\frac{F_3}{a_3}\operatorname{tg}\varphi_3=0.\end{aligned}\right\} \tag{7.67}$$

Since the cavities are closed,

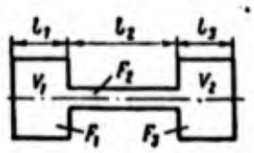

Figure 7.8. Diagram for deriving Equation (7.69).

$$\varphi_1=(k-1)\pi;\quad \varphi_3=(k-1)\pi-\frac{\omega}{a_3}l_3,\qquad k=1,\ 2,\ 3,\ldots \tag{7.68}$$

If $l_1 \ll l_2$, $l_1 \ll l_3$ and $(a_1=a_2=a_3=a)$, then with account for (7.68) the Equations (7.67) take the form

From the

$$\left.\begin{aligned}\frac{V_1\omega}{a}&=F_2\operatorname{tg}\varphi_2;\\ -F_2\operatorname{tg}\left(\frac{\omega}{a}l_2+\varphi_2\right)&=\frac{V_2\omega}{a}.\end{aligned}\right\}$$

After excluding φ_2 we obtain the familiar Schmidt formula [9]

from the

$$\operatorname{tg}\frac{\omega}{a}l_2=\frac{\frac{V_2\omega}{F_2a}+\frac{V_1\omega}{F_2a}}{\omega^2\frac{V_2V_1}{a^2F_2^2}-1}. \tag{7.69}$$

Cavity-line-second cavity-second line. The frequency of free oscillations of gas in this system (Figure 7.9) was first determined by Charnyy [145] in studying resonant supercharging of piston compressors.

Let us an
as lines of re
$l_1\to 0,\ l_3\to 0,\ F_1\to\infty$

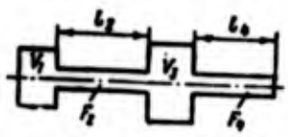

Figure 7.9. Diagram for deriving Equation (7.72).

We shall show that Charnyy's solution follows as a particular case from the characteristic Equation (7.48) of the system. The free oscillation frequency (for $a_1=a_2=a_3=a$) is determined by three equations of the System (7.48). In this case $\varphi_1=(k-1)$,

Then

and (7.70) and

$$\varphi_4=\frac{2k-1}{2}\pi-\frac{\omega}{a}l_4$$

and the computational equations take the form

$$\left.\begin{aligned} F_1 \operatorname{tg}\frac{\omega}{a} l_1 - F_2 \operatorname{tg}\varphi_2 = 0; \\ F_2 \operatorname{tg}\left(\frac{\omega}{a} l_2 + \varphi_2\right) - F_3 \operatorname{tg}\varphi_3 = 0; \\ F_3 \operatorname{tg}\left(\frac{\omega}{a} l_3 + \varphi_3\right) - \frac{F_4}{\operatorname{tg}\frac{\omega}{a} l_4} = 0. \end{aligned}\right\} \quad (7.68)$$

From the first and second equations of the system we have

$$F_3 \operatorname{tg}\varphi_3 = \frac{F_2 \operatorname{tg}\frac{\omega}{a} l_2 + F_1 \operatorname{tg}\frac{\omega}{a} l_1}{1 - \frac{F_1}{F_2} \operatorname{tg}\frac{\omega}{a} l_1 \operatorname{tg}\frac{\omega}{a} l_2}; \quad (7.70)$$

from the third equation,

$$F_3 \operatorname{tg}\varphi_3 = \frac{\frac{F_4}{\operatorname{tg}\frac{\omega}{a} l_4} - F_3 \operatorname{tg}\frac{\omega}{a} l_3}{1 + \frac{\operatorname{tg}\frac{\omega}{a} l_3}{F_3} \frac{F_1}{\operatorname{tg}\frac{\omega}{a} l_4}}. \quad (7.71)$$

Let us analyze (7.70) and (7.71). The cavities can be represented as lines of relatively small length and large diameter. In this case $l_1 \to 0$, $l_3 \to 0$, $F_1 \to \infty$, $F_3 \to \infty$, but $l_1 F_1 = V_1$, $l_3 F_3 = V_3$.

Then

$$\frac{\operatorname{tg}\frac{\omega}{a} l_3}{F_3} = 0, \quad F_1 \operatorname{tg}\frac{\omega}{a} l_1 \approx \frac{V_1 \omega}{a}$$
$$F_3 \operatorname{tg}\frac{\omega}{a} l_3 \approx \frac{V_3 \omega}{a},$$

and (7.70) and (7.71) can be written in the form

$$\left.\begin{aligned} F_3 \operatorname{tg}\varphi_3 = \frac{F_2 \operatorname{tg}\frac{\omega}{a} l_2 + \frac{V_1 \omega}{a}}{1 - \frac{V_1 \omega}{F_2 a} \operatorname{tg}\frac{\omega}{a} l_2}; \\ F_3 \operatorname{tg}\varphi_3 = -\frac{V_3 \omega}{a} + \frac{F_4}{\operatorname{tg}\frac{\omega}{a} l_4}. \end{aligned}\right\} \quad (7.72)$$

Equating Equations (7.72), after simple transformations we obtain an equation analogous to the equation derived by Charnyy [145]

$$\frac{V_1\omega}{F_2a}\left(\frac{F_2}{F_4}\cos\frac{\omega}{a}l_2\sin\frac{\omega}{a}l_4+\sin\frac{\omega}{a}l_2\frac{\omega}{a}l_4-\frac{V_3\omega}{F_4a}\sin\frac{\omega}{a}l_2\sin\frac{\omega}{a}l_4\right)=$$
$$=\cos\frac{\omega}{a}l_4\cos\frac{\omega}{a}l_2-\frac{F_2}{F_4}\sin\frac{\omega}{a}l_2\sin\frac{\omega}{a}l_4-\frac{V_3\omega}{aF_4}\cos\frac{\omega}{a}l_2\sin\frac{\omega}{a}l_2.$$

Cavity plus a line with an elastic element at the end section. Let the reduced mass of the moving parts of the elastic element be m, the stiffness c (Figure 7.10). The fluid free oscillation frequency in the system is defined by the first Equation (7.48)

$$\frac{F_1}{a_1}\operatorname{tg}\left(\frac{\omega}{a_1}l_1+\varphi_1\right)=\frac{F_2}{a_2}\operatorname{tg}\varphi_2, \tag{7.73}$$

where

$$\varphi=(k-1)\pi,\quad k=1, 2, 3,\ldots$$

From (7.56) we find

$$\operatorname{tg}\left(\frac{\omega}{a_2}l_2+\varphi_2\right)=-\frac{\varrho_2F_0a_2}{\omega m\left(\frac{f^2}{\omega^2}-1\right)}. \tag{7.74}$$

Excluding φ_2 from (7.73) and (7.74), we obtain

$$\frac{\operatorname{tg}\frac{\omega}{a_2}l_2+\frac{F_1a_2}{F_2a_1}\operatorname{tg}\frac{\omega}{a_1}l_1}{1-\frac{F_1a_2}{F_2a_1}\operatorname{tg}\frac{\omega}{a_2}l_2\operatorname{tg}\frac{\omega}{a_1}l_1}=-\frac{\varrho_2F_0a_2}{\omega m\left(\frac{f^2}{\omega^2}-1\right)}.$$

If the fluid in the system is homogeneous and $l_1\ll l_2$, this formula can be transformed to the form

$$\frac{\operatorname{tg}\frac{\omega}{a}l_2+\frac{V_1\omega}{F_2a}}{1-\frac{V_1\omega}{F_2a}\operatorname{tg}\frac{\omega}{a}l_2}=-\frac{\varrho F_0a}{\omega m\left(\frac{f^2}{\omega^2}-1\right)}. \tag{7.75}$$

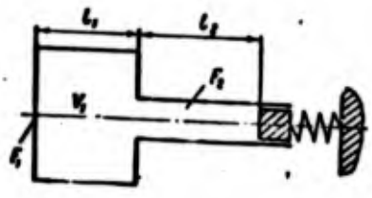

Figure 7.10. Diagram for deriving Equation (7.75).

It follows from (7.75) that for $f=\omega$ the frequencies of the free oscillations of the fluid and the elastic element coincide and the frequency is defined by the formula

$$\frac{V_1\omega}{F_2a}=\operatorname{ctg}\frac{\omega}{a}l_2, \tag{7.76}$$

which is identical to (7.66).

If the stiffness $c\to\infty$, i.e., the line is closed, then $f\to\infty$ and the system frequency is defined by the relation

$$\operatorname{tg}\frac{\omega}{a}l_2=\frac{V_1\omega}{F_2a_2}. \tag{7.77}$$

It is not difficult to show with the aid of (7.48) that (7.77) defines the fluid oscillation frequency in the "cavity-closed line" system. It follows from (7.77) that the presence of the cavity at the end of the line reduces the free oscillation frequency. To determine the degree to which the elasticity affects the frequency of the system in question we must analyze (7.76) and (7.77).

Assume $V_1=0$. Then from (7.66) we obtain the relation defining the fluid frequency in the line for which one end is open and the other is closed

$$\omega_k=\frac{2k-1}{2}\pi\cdot\frac{a}{l_2};\qquad k=1,\ 2,\ 3,\ldots$$

Equation (7.77) for $V_1 = 0$ defines the fluid-free oscillation frequency in a line of constant section with closed ends

$$\omega=k\pi\frac{a}{l_2},\quad k=0,\ 1,\ 2,\ 3,\ldots$$

After analyzing these equations we conclude that the presence of elastic elements in the pneumatic-hydraulic system reduces the fluid-free oscillation frequency. The minimal value of the frequency will occur in the case in which the frequencies of the fluid-free oscillations and elastic element frequencies coincide.

Cavity-line with throttling orifice at the end section (Figure 7.11). The fluid-free oscillation frequency in this system is defined by the system of equations

$$\left.\begin{aligned}\frac{F_1}{a_1}\operatorname{tg}\left(\frac{\omega}{a_1}l_1+\varphi_1\right)-\frac{F_2}{a_2}\operatorname{tg}\varphi_2=0;\\ \frac{F_2}{a_2}\operatorname{tg}\left(\frac{\omega}{a_2}l_2+\varphi_2\right)-\frac{F_3}{a_3}\operatorname{tg}\varphi_3=0,\end{aligned}\right\}$$

where

$$\varphi_1=(k-1)\pi,\quad \varphi_3=\frac{2k-1}{2}\pi-\frac{\omega}{a_3}l_3.$$

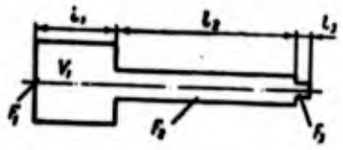

Figure 7.11. Diagram for deriving Equation (7.78).

Assuming that $\operatorname{tg}\frac{\omega}{a_3}l_3\approx\frac{\omega}{a_3}l_3$ (in view of the short throttle length l_3), it is not difficult to transform the system of equations to the form

$$\omega=\frac{F_3}{l_3}\frac{1-\frac{F_1a_2}{F_2a_1}\operatorname{tg}\left(\frac{\omega}{a_2}l_2\right)\operatorname{tg}\left(\frac{\omega}{a_1}l_1\right)}{\frac{F_2}{a_2}\operatorname{tg}\frac{\omega}{a_2}l_2+\frac{F_1}{a_1}\operatorname{tg}\frac{\omega}{a_1}l_1}.$$

If $l_2\gg l_1$, we can assume that $\operatorname{tg}\frac{\omega}{a_1}l_1\approx\frac{\omega}{a_1}l_1$ and then

$$\omega=\frac{F_3}{l_3}\frac{1-\frac{\omega V_1}{F_2}\frac{a_2}{a_1^2}\operatorname{tg}\left(\frac{\omega}{a_2}l_2\right)}{\frac{F_2}{a_2}\operatorname{tg}\left(\frac{\omega}{a_2}l_2\right)+\frac{\omega V_1}{a_1^2}}. \qquad (7.78)$$

With the aid of (7.48) we can obtain the theoretical relations which define the fluid-free oscillation frequency for other very simple pneumatic-hydraulic systems. But there is no advantage in doing this, since in the final analysis we obtain transcendental equations in terms of ω, whose solution is not much simpler than that of the system of equations in the form (7.48).

From the theoretical and practical viewpoint the examples analyzed above are quite sufficient. With their aid we have been able to explain the influence of the various elements in the system on the free

oscillation frequency and to show the quite broad generality of the theoretical computational equations obtained.

§ 5. Branched Multinode Lines

The actual pneumatic-hydraulic systems include branchings, parallel connections, return lines, which in the general case consist of fitting and line elements connected in series.

Suppose we have a multinode hydraulic system which includes branched lines (Figure 7.12). We break the system in question down into segments consisting of simple lines. We shall number the lines in a branch just as in the case of series-connected lines, adding to the nomenclature the branch number. The branch numbering sequence may be arbitrary but such that the number of a branch is not repeated. For example, the second simple line in the second branch will be denoted by 22.

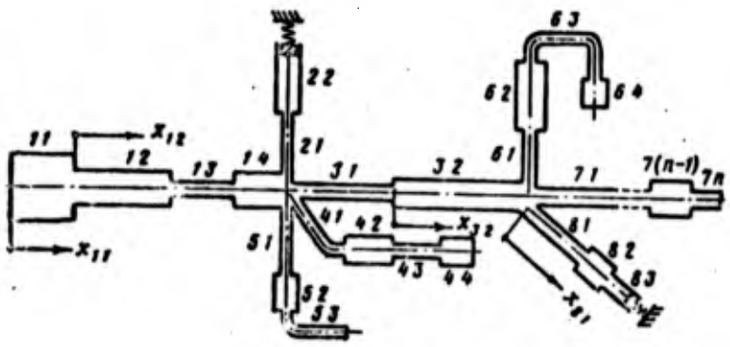

Figure 7.12. Schematic of complex hydraulic system.

As for the question of the choice of the origin of the x-axis, this problem must be approached very carefully. It is necessary that the end of the (n - 1)st simple line $x_{n-1}=l_{n-1}$ be the origin for the x_n axis of the n^{th} simple line, and so on.

The method for solving this problem is practically the same as that we have used previously. In the present case, we must add to the boundary Conditions (7.44) the Condition (7.23) at the branching nodes.

However, even at this stage we can write the equations describing in general form the frequency of each branch, considered as a multistage line.

For example, we can use (7.48) to find the following for the system in question.

First branch

$$\left.\begin{aligned}
&\frac{F_{11}}{a_{11}}\operatorname{tg}\left(\frac{\omega}{a_{11}}l_{11}+\varphi_{11}\right)-\frac{F_{12}}{a_{12}}\operatorname{tg}\varphi_{12}=0;\\
&\frac{F_{12}}{a_{12}}\operatorname{tg}\left(\frac{\omega}{a_{12}}l_{12}+\varphi_{12}\right)-\frac{F_{13}}{a_{13}}\operatorname{tg}\varphi_{13}=0;\\
&\frac{F_{13}}{a_{13}}\operatorname{tg}\left(\frac{\omega}{a_{13}}l_{13}+\varphi_{13}\right)-\frac{F_{14}}{a_{14}}\operatorname{tg}\varphi_{14}=0.
\end{aligned}\right\} \qquad (7.79)$$

Second branch

$$\frac{F_{21}}{a_{21}}\operatorname{tg}\left(\frac{\omega}{a_{21}}l_{21}+\varphi_{21}\right)-\frac{F_{22}}{a_{22}}\operatorname{tg}\varphi_{22}=0. \qquad (7.80)$$

Third branch

$$\frac{F_{31}}{a_{31}}\operatorname{tg}\left(\frac{\omega}{a_{31}}l_{31}+\varphi_{31}\right)-\frac{F_{32}}{a_{32}}\operatorname{tg}\varphi_{32}=0. \qquad (7.81)$$

Fourth and fifth branches

$$\left.\begin{aligned}
&\frac{F_{41}}{a_{41}}\operatorname{tg}\left(\frac{\omega}{a_{41}}l_{41}+\varphi_{41}\right)-\frac{F_{42}}{a_{42}}\operatorname{tg}\varphi_{42}=0;\\
&\frac{F_{42}}{a_{42}}\operatorname{tg}\left(\frac{\omega}{a_{42}}l_{42}+\varphi_{42}\right)-\frac{F_{43}}{a_{43}}\operatorname{tg}\varphi_{43}=0;\\
&\frac{F_{43}}{a_{43}}\operatorname{tg}\left(\frac{\omega}{a_{43}}l_{43}+\varphi_{43}\right)-\frac{F_{44}}{a_{44}}\operatorname{tg}\varphi_{44}=0;
\end{aligned}\right\} \qquad (7.82)$$

$$\left.\begin{aligned}
&\frac{F_{51}}{a_{51}}\operatorname{tg}\left(\frac{\omega}{a_{51}}l_{51}+\varphi_{51}\right)-\frac{F_{52}}{a_{52}}\operatorname{tg}\varphi_{52}=0;\\
&\frac{F_{52}}{a_{52}}\operatorname{tg}\left(\frac{\omega}{a_{52}}l_{52}+\varphi_{52}\right)-\frac{F_{53}}{a_{53}}\operatorname{tg}\varphi_{53}=0.
\end{aligned}\right\} \qquad (7.83)$$

We can also write in a similar fashion the equations for the lines leading to and from the second branching node. It is not difficult to see that there are more unknowns in the system (7.79)—(7.83) than there

bing in
ltistage

the sys-

are equations. To close the system we must use additional conditions which establish the connection between the parameters at the branching node. These additional conditions are the boundary conditions at the line branching nodes.

The boundary conditions (7.25) obtained for systems with branchings may be written in the form

$$\frac{F_j}{a_j^2}\frac{G_j(l_j,\tau)}{\frac{\partial G_j(l_j,\tau)}{\partial x_j}}=\sum_{k=1}^{k=r}\frac{F_k}{a_k^2}\cdot\frac{G_k(0,\tau)}{\frac{\partial G_k(0,\tau)}{\partial x_k}}. \tag{7.79}$$

Substituting in place of G and $\frac{\partial G}{\partial x}$ their values from (7.45) and (7.46), we obtain

$$\frac{F_j}{a_j}\operatorname{tg}\left(\frac{\omega}{a_j}l_j+\varphi_j\right)=\sum_{k=1}^{k=r}\frac{F_k}{a_k}\operatorname{tg}\varphi_k. \tag{7.84}$$

(7.80)

Equation (7.84) closes the system of equations of the type (7.79)—(7.83). Therefore, we must write equations of the type (7.84) for each branching node.

(7.81)

In solving certain practical problems it may be found that j_n pipe main lines come to a branching node, where they branch out into r_m branches (Figure 7.13). In this case (7.84) has the form

$$\sum_{k=j_1}^{k=j_n}\frac{F_k}{a_k}\operatorname{tg}\left(\frac{\omega}{a_k}l_k+\varphi_k\right)=\sum_{k=r_1}^{k=r_m}\frac{F_k}{a_k}\operatorname{tg}\varphi_k. \tag{7.85}$$

(7.82)

Equation (7.85) is presented without proof in view of the fact that the methods for obtaining it and (7.84) are analogous.

(7.83)

Thus the fluid natural oscillation frequency in complex branched lines is defined by a system of transcendental equations which are formulated with the aid of (7.48) and (7.85). Here the number of Equations (7.85) equals the number of branching nodes.

the lines
ficult to
than there

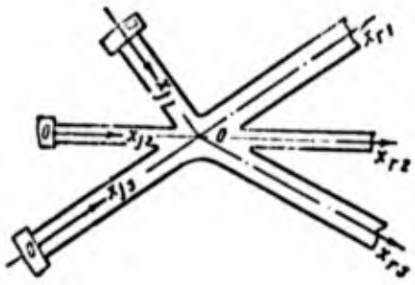

Figure 7.13. Diagram for illustrating Equation (7.84).

Of considerable practical and theoretical interest is the question of the study of the fluid natural oscillation frequency in pneumatic-hydraulic systems which have parallel connection of lines. The general solution of this problem essentially closes the question of determining the fluid-free oscillation frequency in complex piping systems.

Let us examine a complex branched system with lines connected in parallel (Figure 7.14). As before, we break the complex system down into segments with simple lines. The numbering of the simple lines will be accomplished in the same order used in the series and branched piping systems.

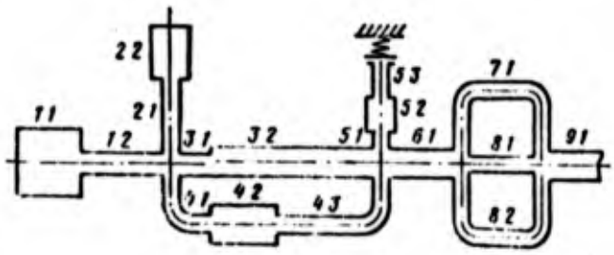

Figure 7.14. Schematic of complex hydraulic system with parallel connection of lines.

The branches and the parallel connections (return lines) consist of multistage lines. Using (7.48) and (7.85), we can write the system of equations defining the frequency of the system in question. In this case the number of computational equations will be less than the number of unknowns. Therefore, an additional equation must be written for each parallel connection.

Let us examine a system consisting of a single parallel connection. Each branch is a multistage line (Figure 7.15). The number of simple lines in the parallel branch I is μ, the number in branch II is ν.

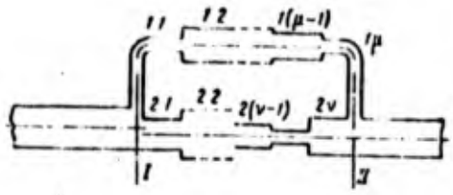

Figure 7.15. Diagram for deriving Equation (7.6).

The condition of equality of the pressures at the entrance to each simple line at the branching nodes is valid, i.e., the condition (7.3). Using this condition, we obtain

At node I

$$\frac{a_{11}^2}{F_{11}}\frac{\partial G_{11}(l_{11},\tau)}{\partial x_{11}}=\frac{a_{21}^2}{F_{21}}\frac{\partial G_{21}(0,\tau)}{\partial x_{21}}; \tag{7.86}$$

at node II

$$\frac{a_{1\mu}^2}{F_{1\mu}}\frac{\partial G_{1\mu}(l_{\mu},\tau)}{\partial x_{1\mu}}=\frac{a_{2\nu}^2}{F_{2\nu}}\frac{\partial G_{2\nu}(l_{2\nu},\tau)}{\partial x_{2\nu}}. \tag{7.87}$$

We express $\frac{\partial G_{1\mu}}{\partial x_{1\mu}}$ in terms of $\frac{\partial G_{11}}{\partial x_{11}}$, and $\frac{\partial G_{2\nu}}{\partial x_{2\nu}}$ in terms of $\frac{\partial G_{21}}{\partial x_{21}}$. We know that the pressure equality condition holds at the junction of the simple lines; this condition has the form

$$\left.\begin{array}{l}
\frac{a_{11}^2}{F_{11}}\frac{\partial G(l_{11},\tau)}{\partial x_{11}}\quad\frac{a_{12}^2}{F_{12}}\frac{\partial G_{12}(0,\tau)}{\partial x_{12}};\\
\frac{a_{12}^2}{F_{12}}\frac{\partial G_{12}(l_{12},\tau)}{\partial x_{12}}\quad\frac{a_{13}^2}{F_{13}}\frac{\partial G_{13}(0,\tau)}{\partial x_{13}};\\
\cdots\cdots\cdots\cdots\cdots\cdots\cdots\cdots\\
\frac{a_{1(\mu-1)}^2}{F_{1(\mu-1)}}\frac{\partial G_{1(\mu-1)}(l_{1(\mu-1)},\tau)}{\partial x_{1(\mu-1)}}\quad\frac{a_{1\mu}^2}{F_{1\mu}}\frac{\partial G_{1\mu}(0,\tau)}{\partial x_{1\mu}}.
\end{array}\right\} \tag{7.88}$$

From (7.88) we find

$$\frac{a_{11}^2}{F_{11}}\frac{\partial G(l_{11},\tau)}{\partial x_{11}}=\frac{a_{1p}^2}{F_{1p}}\frac{\prod_{k=2}^{k=p}\frac{\partial G_{1k}(0,\tau)}{\partial x_{1k}}}{\prod_{k=2}^{k=p}\frac{\partial G_{1k}(l_{1k},\tau)}{\partial G_{1k}}}. \tag{7.89}$$

Similarly, we can show that

$$\frac{a_{21}^2}{F_{21}}\frac{\partial G_{21}(l_{21},\tau)}{\partial x_{21}}=\frac{a_{2\nu}^2}{F_{2\nu}}\frac{\prod_{k=2}^{k=\nu}\frac{\partial G_{2k}(0,\tau)}{\partial x_{1k}}}{\prod_{k=2}^{k=\nu}\frac{\partial G_{2k}(l_{2k},\tau)}{\partial x_{2k}}} \tag{7.90}$$

We divide (7.86) by (7.87) and substitute the value of $\frac{\partial G}{\partial x}$ from (7.46)

$$\frac{\frac{a_{11}}{F_{11}}A_{11}\cos\varphi_{11}}{\frac{a_{1p}}{F_{1p}}A_{1p}\cos\left(\frac{\omega}{a_{1p}}l_{1p}+\varphi_{1p}\right)}=\frac{\frac{a_{21}}{F_{21}}A_{21}\cos\varphi_{21}}{\frac{a_{2\nu}}{F_{2\nu}}A_{2\nu}\cos\left(\frac{\omega}{a_{2\nu}}l_{2\nu}+\varphi_{2\nu}\right)}. \tag{7.91}$$

We substitute the value of $\frac{\partial G}{\partial x}$ from (7.46) into (7.89) and (7.90)

$$\frac{a_{11}}{F_{11}}A_{11}\cos\left(\frac{\omega}{a_{11}}l_{11}+\varphi_{11}\right)=\frac{a_{1p}}{F_{1p}}A_{1p}\frac{\prod_{k=2}^{k=p}\cos\varphi_k}{\prod_{k=2}^{k=p}\cos\left(\frac{\omega}{a_k}l_k+\varphi_k\right)}. \tag{7.92}$$

$$\frac{a_{21}}{F_{21}}A_{21}\cos\left(\frac{\omega}{a_{21}}+\varphi_{21}\right)=\frac{a_{2\nu}}{F_{2\nu}}A_{2\nu}\frac{\prod_{k=2}^{k=\nu}\cos\varphi_\nu}{\prod_{k=2}^{k=\nu}\cos\left(\frac{\omega}{a_k}l_k+\varphi_k\right)}. \tag{7.93}$$

Excluding the coefficients A_{11}, A_{21}, A_{1p}, in (7.91) with the aid of (7.92) and (7.93), we obtain

In branchin

It lines we sufficie (7.48) a may be w

or

Thus any branch transcende of (7.48)

$$\frac{\prod_{r=1}^{r=p}\cos\left(\frac{\omega}{a_{1r}}l_{1r}+\varphi_{1r}\right)\prod_{r=1}^{r=q}\cos\left(\frac{\omega}{a_{2r}}l_{2r}+\varphi_{2r}\right)}{\prod_{r=1}^{r=2}\cos\varphi_{1r}}=\frac{}{\prod_{r=1}^{r=q}\cos\varphi_{2r}}. \tag{7.94}$$

(7.89)

In the general case in which s parallel branches approach two branching nodes, (7.94) takes the form

$$\frac{\prod_{r=1}^{r=p}\cos\left(\frac{\omega}{a_{(s-1)r}}l_{(s-1)r}+\varphi_{(s-1)r}\right)}{\prod_{r=1}^{r=p}\cos\varphi_{(s-1)r}}=\frac{\prod_{r=1}^{r=q}\cos\left(\frac{\omega}{a_{sr}}+\varphi_{sr}\right)}{\prod_{r=1}^{r=q}\cos\varphi_{sr}}. \tag{7.95}$$

(7.90)

$\frac{\partial G}{\partial x}$ from

It follows from (7.95) that for a two-node parallel branching of lines we can obtain $(s-1)$ equations, which are the number necessary and sufficient to close the system of equations composed with the aid of (7.48) and (7.85). After simple trigonometric transformations (7.95) may be written in the form

(7.91)

$$\prod_{r=1}^{r=p}\left[\cos\frac{\omega}{a_{(s-1)r}}l_{(s-1)r}-\operatorname{tg}\varphi_{(s-1)r}\sin\frac{\omega}{a_{(s-1)r}}l_{(s-1)r}\right]=$$

nd (7.90)

$$=\prod_{r=1}^{r=q}\left[\cos\frac{\omega}{a_{sr}}l_{sr}-\operatorname{tg}\varphi_{sr}\sin\frac{\omega}{a_{sr}}l_{sr}\right],$$

(7.92)

or

$$\prod_{r=1}^{r=p}\cos\frac{\omega}{a_{(s-1)r}}l_{(s-1)r}\left[1-\operatorname{tg}\varphi_{(s-1)r}\operatorname{tg}\frac{\omega}{a_{(s-1)r}}l_{(s-1)r}\right]=$$

(7.93)

$$=\prod_{r=1}^{r=q}\cos\frac{\omega}{a_{sr}}l_{sr}\left[1-\operatorname{tg}\varphi_{sr}\operatorname{tg}\frac{\omega l_{sr}}{a_{sr}}\right]. \tag{7.96}$$

the aid

Thus, we conclude that the fluid natural oscillation frequency in any branched pneumatic-hydraulic system is defined by a system of transcendental algebraic equations which are formulated with the aid of (7.48), (7.85), and (7.96).

In calculating the fluid natural oscillation frequencies in complex lines, we encounter several serious difficulties associated with the fact that the equations which define the natural frequencies are transcendental. Therefore, it is not always possible to determine the entire frequency spectrum or even the laws governing the frequency distribution.

In most cases (7.48), (7.49) and (7.96) can be reduced to algebraic equations. To this end we must break the hydraulic system in question down into segments of simple lines so that the following relations are satisfied

$$\frac{l_1}{a_1}=\frac{l_2}{a_2}=\dots\frac{l_{n-1}}{a_{n-1}}. \tag{7.97}$$

It is obvious that such a division will sometimes be inexact; however, further breakdown into smaller segments leads to an increase of the number of simple lines and this means an increase of the number of computational equations.

Assume that it has been possible to break a multistage line down into n simple lines such that the satisfaction of the indicated conditions is possible. Then it follows from (7.48) that the natural frequencies in such a line will be defined by the following system of equations

$$\left.\begin{aligned}&\frac{F_1}{a_1}\operatorname{tg}\left(\frac{\omega}{a_1}l_1+\varphi_1\right)=\frac{F_2}{a_2}\operatorname{tg}\varphi_2;\\&\dots\dots\dots\dots\dots\dots\\&\frac{F_{n-1}}{a_{n-1}}\operatorname{tg}\left(\frac{\omega}{a_{n-1}}l_{n-1}+\varphi_{n-1}\right)=\frac{F_n}{a_n}\operatorname{tg}\varphi_n.\end{aligned}\right\}$$

Since $\frac{l_1}{a_1}=\frac{l_2}{a_2}=\frac{l_3}{a_3}=\dots=\frac{l_{n-1}}{a_{n-1}}$, after denoting $\frac{l_1}{a_1}\omega=z$ and expanding the tangent of the sum of two angles into the tangents of these angles, we obtain

$$\left.\begin{aligned}
&\frac{F_1}{a_1}\,\frac{\operatorname{tg} x+\operatorname{tg}\gamma_1}{1-\operatorname{tg} x\operatorname{tg}\gamma_1}=\frac{F_2}{a_2}\operatorname{tg}\gamma_2;\\
&\cdots\cdots\cdots\cdots\cdots\\
&\frac{F_{n-1}}{a_{n-1}}\,\frac{\operatorname{tg} x+\operatorname{tg}\gamma_{n-1}}{1-\operatorname{tg} x\operatorname{tg}\gamma_{n-1}}=\frac{F_n}{a_n}\operatorname{tg}\gamma_n.
\end{aligned}\right\}$$

Then, denoting $\operatorname{tg} x=y$, $\operatorname{tg}\gamma_1=y_1$, $\operatorname{tg}\gamma_2=y_2,\ldots,\operatorname{tg}\gamma_n=y_n$, we obtain

$$\left.\begin{aligned}
&\frac{F_1}{a_1}\,\frac{y+y_1}{1-yy_1}=\frac{F_2}{a_2}y_2;\\
&\cdots\cdots\cdots\cdots\\
&\frac{F_{n-1}}{a_{n-1}}\,\frac{y+y_{n-1}}{1-yy_{n-1}}=\frac{F_n}{a_n}y_n.
\end{aligned}\right\}\qquad(7.98)$$

If there are branchings in the system, then the equations which close the system (7.98) will have the form

$$\sum_{k=1}^{k=l}\frac{F_k}{a_k}\,\frac{y+y_k}{1-y_ky}=\sum_{k=1}^{k=r}\frac{F_k}{a_k}y_k.\qquad(7.99)$$

If there is a return line in the system we must use (7.96) after first expressing $\cos\frac{\omega}{a}l$ in terms of $\operatorname{tg}\frac{\omega}{a}l$:

$$\prod_{r=1}^{r=p}\frac{1}{\sqrt{1+\operatorname{tg}^2\left(\frac{\omega}{a_{(s-1)r}}l_{(s-1)r}\right)}}=\left[1-\operatorname{tg}\gamma_{(s-1)r}\operatorname{tg}\frac{\omega}{a_{(s-1)r}}l_{(s-1)r}\right]=$$
$$=\prod_{r=1}^{r=p}\left[1-\operatorname{tg}\gamma_{sr}\operatorname{tg}\frac{\omega}{a_{sr}}l_{sr}\right]\frac{1}{\sqrt{1+\operatorname{tg}^2\left(\frac{\omega}{a_{(s-1)r}}l_{(s-1)r}\right)}},$$

or, taking (7.97) into account, we obtain

$$\prod_{r=1}^{r=p}\frac{1}{\sqrt{1+y^2}}[1-y_{(s-1)r}y]=\prod_{r=1}^{r=p}\frac{1}{\sqrt{1+y^2}}[1-y_{sr}y].\qquad(7.100)$$

Thus, after breaking the hydraulic system down into segments of simple lines, for which the Condition (7.97) is met, we can reduce the transcendental Equations (7.48), (7.85) and (7.96) to algebraic equations. Then, knowing the roots of these equations, it is not difficult to define the frequency spectrum using the formula

$$\omega_k = \frac{a}{l} \operatorname{Arctg} y.$$

In conclusion we note that Equations (7.98)—(7.100) differ favorably from (7.48), (7.85), (7.96) and make it possible in certain cases to calculate quite quickly the natural frequencies. To this end we must first break the complex line down roughly into two simple lines and find the first root, and then find the exact solution by gradually increasing the number of segments.

CHAPTER 8

DYNAMICS OF LRE HYDRAULIC SYSTEM AND TEST STAND SYSTEMS

§ 1. Water Hammer in LRE Propellant Lines

Several studies [69] based on different techniques for integrating the wave equations have been devoted to the theory of water hammers in simple and complex pipe lines. We have noted previously that the integration of the wave equations in the case of complex lines involves several definite difficulties of a computational nature. Therefore, in the analysis of water hammer in complex lines recourse is made to certain simplifications [59], based primarily on reducing the complex line to an equivalent simple line. The latter permits the use of comparatively simple formulas to calculate the magnitude of the hydraulic impact and analyze its effect on the geometrical dimensions and elastic characteristics of the hydraulic system.

1. Wave Processes in a Simple Line with Instantaneous Valve Opening

Let us consider a segment of a LRE hydraulic system (Figure 8.1). The line is open at the section x = 0 and the pressure is held constant . At the time $\tau \geq 0$ the fluid flows at the section $x = l$ with the constant flow rate G_0.

The fluid equation of motion and boundary conditions have the form

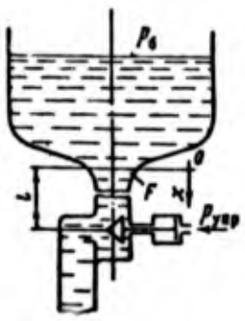

Figure 8.1. Diagram for calculating hydraulic shock with instantaneous valve closure.

$$\frac{\partial^2 G(x,\tau)}{\partial \tau^2}=a^2\frac{\partial^2 G(x,\tau)}{\partial x^2}; \tag{8.1}$$

$$p(0,\tau)=p_0; \tag{8.2}$$

$$G(l,\tau)=G_0. \tag{8.3}$$

We have noted previously that the Condition (8.2) can be written as

$$\frac{\partial G(0,\tau)}{\partial x}=0 \tag{8.4}$$

At the time $\tau = 0$ at any section of the line the fluid flow rate and its time derivative equal zero, i.e.,

$$G(x,0)=0; \tag{8.5}$$

$$\frac{\partial G}{\partial \tau}(x,0)=0. \tag{8.6}$$

Thus, to determine the fluid parameters, we must integrate (8.1) with the initial Conditions (8.5)—(8.6) and the boundary Conditions (8.3)—(8.4).

The Fourier method cannot be used in this case, since the boundary Condition (8.3) is not homogeneous.

We introduce the change of variables

$$G(x,\tau)=G_1(x,\tau)+G_0. \tag{8.7}$$

Then the problem in question reduces to integration of the equation

$$\frac{\partial^2 G_1(x,\tau)}{\partial \tau^2}-a^2\frac{\partial^2 G_1(x,\tau)}{\partial x^2}=0 \tag{8.9}*$$

*Translator's note: Equation (8.8) omitted in original document.

with the boundar

and the initial

In view of
the particular

where $X(x), T(\tau)$

We substit

where ω are the

After inte
tion of (8.9) i

where φ, ψ ar
itial and bound

It follows

with the boundary conditions

$$\left.\begin{aligned} G_1(l, \tau)&=0, \\ \frac{\partial G_1(0, \tau)}{\partial x}&=0 \end{aligned}\right\} \tag{8.10}$$

and the initial conditions

$$\left.\begin{aligned} G_1(x, 0)&=-G_0, \\ \frac{\partial G_1(x, 0)}{\partial \tau}&=0. \end{aligned}\right\} \tag{8.11}$$

In view of the homogeneity of the boundary conditions, we seek the particular solution of (8.9) in the form

$$G_1(x, \tau)=X(x)T(\tau), \tag{8.12}$$

where $X(x), T(\tau)$ are as yet unknown functions of x and τ.

We substitute (8.12) into (8.9)

$$\ddot{X}(x)+\left(\frac{\omega}{a}\right)^2 X(x)=0; \tag{8.13}$$

$$\ddot{T}(\tau)+\omega^2 T=0, \tag{8.14}$$

where ω are the problem eigenvalues.

After integrating (8.13) and (8.14) we find the particular solution of (8.9) in the form

$$G_1(x, \tau)=A \sin\left(\frac{\omega}{a}x+\varphi\right)\sin(\omega\tau+\psi), \tag{8.15}$$

where A, φ, ψ are arbitrary constants which are determined from the initial and boundary conditions.

It follows from the boundary conditions that

$$\cos\varphi=0; \quad \varphi=\frac{2k-1}{2}\pi; \quad k=1, 2, 3, \ldots$$

$$\cos\left(\frac{\omega}{a}l\right)=0; \quad \omega=\frac{2k-1}{2}\pi\frac{a}{l}, \quad k=1, 2, 3, \ldots$$

Then the general solution of (8.9) will be

$$G_1(x, \tau) = \sum_{k=1}^{\infty} (-1)^{k+1} A_k \cos\left(\frac{2k-1}{2}\pi \frac{x}{l}\right) \sin\left(\frac{2k-1}{2}\pi \frac{a}{l}\tau + \psi_k\right). \tag{8.16}$$

We find the arbitrary constants A_k and ψ_k from the initial conditions

$$-G_0 = \sum_{k=1}^{\infty} (-1)^{k+1} A_k \cos\left(\frac{2k-1}{2}\pi \frac{x}{l}\right) \sin\psi_k; \tag{8.17}$$

$$\sum_{k=1}^{\infty} (-1)^{k+1} A_k \frac{2k-1}{2}\pi \frac{a}{l} \cos\left(\frac{2k-1}{2}\pi \frac{x}{l}\right) \cos\psi_k = 0. \tag{8.18}$$

We multiply (8.17) and (8.18) by $\cos\left(\frac{2k-1}{2}\pi \frac{x}{l}\right)$ and integrate the equalities from 0 to l

$$-G_0 \int_0^l \cos\left(\frac{2k-1}{2}\pi \frac{x}{l}\right) dx =$$

$$= A_k \int_0^l (-1)^{k+1} \cos^2\left(\frac{2k-1}{2}\pi \frac{x}{l}\right) \sin\psi_k dx;$$

$$\cos\psi_k = 0; \quad \psi_k = \frac{2k-1}{2}\pi.$$

Hence

$$A_k = \frac{4G_0}{\pi(2k-1)}$$

Then

$$G_1(x, \tau) = \frac{4G_0}{\pi} \sum_{k=1}^{\infty} \frac{(-1)^{k+1}}{2k-1} \cos\left(\frac{2k-1}{2}\pi \frac{x}{l}\right) \cos\left(\frac{2k-1}{2}\pi \frac{a}{l}\tau\right). \tag{8.19}$$

Finally, converting to the old variables, we find

$$G(x, \tau) = G_0 + \frac{4G_0}{\pi} \sum_{k=1}^{\infty} \frac{(-1)^{k+1}}{2k-1} \cos\left(\frac{2k-1}{2}\pi \frac{x}{l}\right) \cos\left(\frac{2k-1}{2}\pi \frac{a}{l}\tau\right) \tag{8.20}$$

Equation (8.20) describes the variation of the fluid flow rate in the line at the time $\tau \geqslant 0$. Knowing G, we can find the pressure $p(x, \tau)$

(8.16)

$$p(x, \tau) = -\frac{1}{F}\int \frac{\partial G(x, \tau)}{\partial \tau}\, dx + p_1(\tau) \tag{8.21}$$

al

For $x=0$, $p(0, \tau) = p_0$,

(8.17)

$$p_0 + \frac{1}{F}\int \frac{\partial G(x, \tau)}{\partial \tau}\, dx\Big|_{x=0} = p_1(\tau) \tag{8.22}$$

(8.18)

Substituting (8.21) into (8.22), we obtain

te the

$$p(x, \tau) - p_0 = -\frac{1}{F}\int_0^x \frac{\partial G(x, \tau)}{\partial \tau}\, dx.$$

Thus, according to (8.20)

$$-p(x,\tau) + p_0 = \frac{4G_0 a}{\pi F}\sum_{k=1}^{\infty}(-1)^{k+1}\frac{1}{2k-1}\sin\left(\frac{2k-1}{2}\pi\frac{x}{l}\right)\times \\ \times \sin\left(\frac{2k-1}{2}\pi\frac{a}{l}\tau\right). \tag{8.23}$$

Equation (8.23) describes the pressure variation at any arbitrary section of the line at the time $\tau \geqslant 0$. It follows from this equation that at the time $\tau > 0$ the pressure at section $x = l$ will be

$$p(l, \tau) + p_0 = \frac{4G_0 a}{\pi F}\sum_{k=1}^{\infty}\frac{1}{2k-1}\sin\left(\frac{2k-1}{2}\pi\frac{a}{l}\tau\right) = \\ = \frac{4}{\pi}\varrho a w_0 \sum_{k=1}^{\infty}\frac{1}{2k-1}\sin\left(\frac{2k-1}{2}\pi\frac{a}{l}\tau\right). \tag{8.24}$$

(8.19)

Assuming that the infinite series in the right side of the equation is the Fourier series expansion of the function $p = \varrho a w_0$ in the

(8.20)

interval $0<\tau<\frac{2l}{a}$ and that $p=-\rho a\omega_0$ in the interval $\frac{2l}{a}<\tau<\frac{4l}{a}$, we obtain the familiar Zhukovskiy formula for water hammer

$$\Delta p_{уд}=\rho a\omega_0. \tag{8.25}$$

2. Water Hammer in a Simple Line With Linear Valve Closure Law

Although the valve closure time in the LRE is comparatively short, the formula obtained may not be suitable for calculating the magnitude of the water hammer. This is explained by the fact that (8.25) is valid only for direct impact, when

$$\tau_1<\frac{2l}{a},$$

where τ_1 is the valve closure time;
l is the line length from the valve to the tank;
a is the speed of sound in the line.

Therefore, in calculating water hammer in a LRE, we frequently must take into account the valve closure time. In the general case we need to know the equation of valve motion, which in turn depends on the fluid pressure in the line during valve closure. Joint solution of the wave equation and the valve equation of motion without recourse to numerical methods is very difficult and is only possible in certain particular cases. Therefore, in calculating water hammer, we assume the valve closure law to be linear, supposing the closure time known.

We assume a main line (see Figure 8.1) which is connected to the tank at the section x = 0 and to the valve at the section x = l. At the time $\tau\leqslant 0$ the fluid motion is steady with the flow rate G_0. At the time $\tau\geqslant 0$ the valve is closed so that the fluid flow rate at the section x = l varies linearly

$$G=G_0\left(1-\frac{\tau}{\tau_1}\right),$$

where G_0 is t
regi

Thus, to
tegrate the e

with the boun

and the initi

It is we

We intro

Then (8.

By virtu
we obtain the

where G_0 is the fluid flow rate through the line in the steady-state regime.

Thus, to determine the magnitude of the water hammer we must integrate the equation

$$\frac{\partial^2 G(x,\tau)}{\partial \tau^2} - a^2 \frac{\partial^2 G(x,\tau)}{\partial x^2} = 0 \tag{8.26}$$

with the boundary conditions

$$p(0,\tau) = p_0, \tag{8.27}$$

$$G(l,\tau) = G_0\left(1 - \frac{\tau}{\tau_1}\right) \tag{8.28}$$

and the initial conditions

$$G(0,x) = G_0, \quad \frac{\partial G(0,x)}{\partial \tau} = 0.$$

It is well known that (8.27) can be represented in the form

$$\frac{\partial G(0,\tau)}{\partial x} = 0. \tag{8.29}$$

We introduce the change of variables

$$G_1(x,\tau) = G(x,\tau) - G_0\left(1 - \frac{\tau}{\tau_1}\right). \tag{8.30}$$

Then (8.26), the boundary and initial conditions take the form

$$\frac{\partial^2 G_1(x,\tau)}{\partial \tau^2} - a^2 \frac{\partial^2 G_1(x,\tau)}{\partial x^2} = 0; \tag{8.31}$$

$$\left.\begin{aligned} \frac{\partial G_1(0,\tau)}{\partial x} &= 0; \\ G_1(l,\tau) &= 0; \end{aligned}\right\} \tag{8.32}$$

$$\left.\begin{aligned} \frac{\partial G_1(x,0)}{\partial \tau} &= \frac{G_0}{\tau_1}; \\ G_1(x,0) &= 0. \end{aligned}\right\} \tag{8.33}$$

By virtue of the homogeneity of the boundary Conditions (8.32), we obtain the function $G_1(x,\tau)$ in the form

$$G_1(x, \tau)=\sum_{k=1}^{\infty} A_k \sin\left(\frac{\omega_k}{a}x+\gamma_k\right)\sin(\omega_k\tau+\psi_k), \tag{8.34}$$

where A_k, γ_k, ψ_k are arbitrary constants which are determined from the initial and boundary conditions;

ω_k are the problem eigenvalues.

We have previously discussed the techniques for determining the arbitrary constants γ_k and the natural frequencies ω_k . Therefore, we shall find the arbitrary constants A_k and ψ_k, which are determined from the initial Conditions (8.33). Taking (8.34) into account, we have

$$0=\sum_{k=1}^{\infty} A_k \sin\left(\frac{\omega_k}{a}x+\gamma_k\right)\sin\psi_k; \tag{8.35}$$

$$\frac{G_0}{\tau_1}=\sum_{k=1}^{\infty} A_k\omega_k \sin\left(\frac{\omega_k}{a}x+\gamma_k\right)\cos\psi_k. \tag{8.36}$$

We know from mathematical physics that the eigenfunctions are orthogonal on the segment $0-l$, i.e.,

$$\int_0^l X_n(x)X_k(x)dx=\begin{cases}n\neq k=0\\ n=k=\text{const.}\end{cases}$$

Therefore, multiplying (8.35) and (8.36) by $\sin\left(\frac{\omega_k}{a}x+\gamma_k\right)$ and integrating the left and right sides of the equalities from 0 to l, we obtain

$$0=\frac{\int_0^l \sin\left(\frac{\omega_k}{a}x+\gamma_k\right)dx}{\int_0^l \sin^2\left(\frac{\omega_k}{a}x+\gamma_k\right)dx}A_k\sin\psi_k; \tag{8.37}$$

It fol

Thus, (8.37)—(8. viously, (8

Equati iation at a in practica magnitude o

Using

or with acc

After

(8.34)

rom the

$$\frac{G_0}{\tau_1}\frac{\int_0^l \sin\left(\frac{\omega_k}{a}x+\varphi_k\right)dx}{\int_0^l \sin^2\left(\frac{\omega_k}{a}x+\varphi_k\right)dx}=A_k\omega_k\cos\varphi_k. \tag{8.38}$$

It follows from (8.37) and (8.38) that

ning the
refore,
etermined
unt, we

$$\varphi_k=(k-1)\pi. \tag{8.39}$$

Thus, the arbitrary constants A_k and φ_k are determined from (8.37)—(8.39). With account for the replacement introduced previously, (8.30) may be given the form

(8.35)

$$G(x,\tau)=G_0\left(1-\frac{\tau}{\tau_1}\right)+\sum_{k=1}^{\infty}A_k\sin\left(\frac{\omega_k}{a}x+\varphi_k\right)\sin(\omega_k\tau+\varphi_k). \tag{8.40}$$

(8.36)

ns are

Equation (8.40) makes it possible to determine the flow rate variation at an arbitrary section of the line at the time $\tau\geqslant 0$. However, in practical calculations the need arises most often to calculate the magnitude of the pressure increase during valve closure.

Using the equation of motion in the Form (7.12), we obtain

$$-p(l,\tau)+p_0=\frac{1}{F}\int_0^l\frac{\partial G(x,\tau)}{\partial\tau}dx$$

and in-

or with account for (8.40)

to l,

$$\Delta p_{y\pi}=\frac{1}{F}\left[\frac{G_0 l}{\tau_1}+\sum_{k=1}^{\infty}aA_k\left[\cos\left(\frac{\omega_k l}{a}+\varphi_k\right)-\cos\varphi_k\right]\cos(\omega_k\tau+\varphi_k)\right] \tag{8.41}$$

After simple transformations (8.41) can be written in the form

(8.37)

$$\Delta p_{y\pi}=\frac{1}{F}\left[\frac{G_0 l}{\tau_1}-2\sum_{k=1}^{\infty}aA_k\sin\left(\frac{\omega_k l}{2a}+\varphi_k\right)\sin\frac{\omega_k l}{2a}\cos(\omega_k\tau+\varphi_k)\right] \tag{8.42}$$

Thus, the magnitude of the pressure rise at the valve for a linear valve closure law is defined by (8.42), in which the arbitrary constants A_k and ψ_k are found from (8.37)—(8.39), and the eigenvalues ω_k and φ_k are found from the boundary Conditions (8.32).

Let us find ω_k and φ_k. Using (8.34) and (8.32), we obtain

$$\left.\begin{aligned}\sin\left(\frac{\omega_k}{a}l+\varphi_k\right)&=0;\\ \cos\varphi_k&=0.\end{aligned}\right\}$$

Hence

$$\varphi_k=\frac{2k-1}{2}\pi; \qquad k=1, 2, 3,... \tag{8.43}$$

$$\omega_k=\frac{2k-1}{2}\frac{a}{l}\pi, \quad k=1, 2, 3... \tag{8.44}$$

We substitute φ_k and ω_k into (8.37)—(8.39)

$$A_k=-\frac{G_0}{\omega_k\tau_1\cos\psi_k}\frac{\int_0^l(-1)^{k+1}\cos\left(\frac{2k-1}{2}\pi\frac{x}{l}\right)dx}{\int_0^l\cos^2\left(\frac{2k-1}{2}\pi\frac{x}{l}\right)dx} \tag{8.45}$$

Finally, with account for (8.39) we find

$$A_k=\frac{8G_0l(-1)^{k+1}}{(2k-1)^3\pi^2a\tau_1} \tag{8.46}$$

We substitute (8.43)—(8.46) into (8.42). After suitable transformations we obtain

$$\Delta p_{y\pi}=\frac{1}{F}\frac{G_0l}{\tau_1}\left[1-\sum_{k=1}^{\infty}\frac{1}{(2k-1)^2\pi^2}\left(2\cos\frac{2k-1}{2}\pi\frac{a}{l}\tau\right)\right] \tag{8.47}$$

In the case of direct impact, i.e., when $\tau=\tau_1=\frac{2l}{a}$, we obtain in place of (8.47) the Zhukovskiy formula

$$\Delta p_{y\pi}=\rho a v_0.$$

r a linear
y con-
values

In fact, the sum of the series $\sum_{k=1}^{\infty} \frac{1}{(2k-1)^2\pi^2} = \frac{\pi^2}{8}$ and $G_0 = \rho\omega_0 F$ (w_0 is the fluid motion velocity in the line at the time $\tau \leqslant 0$).

in

In case of indirect impact the magnitude of the pressure rise at the valve is calculated using (8.47).

3. Approximate Technique for Calculating Water Hammer in Complex Lines

(8.43)

As a rule, LRE propellant lines consist of a complex network of branched or tandem-connected simple lines. Therefore, the solution

(8.44)

presented above for water hammer can be used only for certain particular cases.

The problem of hydrodynamic impact in a complex line is a very complex problem, and its analytic solution is extremely difficult, since

(8.45)

in this case we must integrate a system of differential equations of the type (8.1), which describe the unsteady fluid motion in each simple line.

For this purpose we can use, for example, the previously discussed separation of variables technique, which may be used to obtain the so-

(8.46)

lution in the form of sums of infinite series without any particular difficulty. However, serious difficulties do arise in determining

e trans-

the arbitrary constants. Moreover, the practical value of such a solution is very questionable, since in complex lines the magnitude of the impact depends on many factors, and therefore it is difficult to use finite relations for qualitative and quantitative analysis of the

(8.47)

process.

Therefore, in order to simplify the calculations the water hammer

ain in

problem in a series-connected complex line is replaced by the water hammer problem in a simple line which is equivalent to the complex one.

The length of the equivalent line is assumed to be

$$l=\sum_i l_i,$$

where l_i is the length of the simple line.

The elastic wave propagation velocity is computed from the formula

$$a=\frac{l}{\sum_i \frac{l_i}{a_i}},$$

where a_i is the elastic wave propagation velocity in the simple line.

The fluid motion velocity $w_0=\frac{G}{F\varrho}$ in the steady-state regime in the equivalent line is found from the equality

$$\frac{mw_0^2}{2}=\sum_i \frac{m_i w_{0i}^2}{2}$$

where m, m_i are the fluid masses enclosed in the equivalent and the i^{th} simple lines;

w_{0i} is the fluid motion velocity in the steady-state regime in the i^{th} simple line.

Considering that

$$m=\varrho lF=\frac{lG_0}{w_0};$$

$$m_i=\varrho l_i F_i=\frac{l_i G_0}{w_{0i}},$$

we obtain

$$w_0=\frac{\sum_i l_i w_{0i}}{l}$$

After determining l, a, and w_0 for the equivalent line, it is not difficult to use (8.47), for example, to calculate approximately the

magnitude
line with

Sever
pressure a
the most f
tween wave
problem wa
wave metho

1. Wave Pr

We co
a piston is
rate harmon
rate oscill
amplitude a

Figure 8.2
calculat
cess in

Since
oscillations
forces, the
on the natu
be a functi
the present

magnitude of the hydrodynamic impact in a complex tandem-connected line with linear valve closure law.

§ 2. Steady Periodic Propellant Flow in The Lines of LRE and Test Stands

Several studies have been made of the propagation of periodic pressure and flow rate oscillations in hydraulic systems [50, 145, 69], the most fundamental being those of Grizodub, based on the analogy between wave processes in electric lines and hydraulic lines. This problem was solved in the same formulation in [12] by the traveling wave method, which we shall examine in the following.

1. Wave Process in a Simple Hydraulic Line

We consider a line of constant cross section (Figure 8.2). Assume a piston is installed at the section $x = 0$, which changes the flow rate harmonically with the frequency ω_0. The amplitude of the flow rate oscillation at the section $x = 0$ is A_0. We shall determine the amplitude at an arbitrary section of the line.

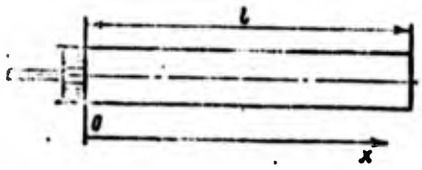

Figure 8.2. Diagram for calculating wave process in simple line.

It is well known that the wave process in a hydraulic line is described by the equation

$$\frac{\partial^2 G(x,\tau)}{\partial \tau^2} - a^2 \frac{\partial^2 G(x,\tau)}{\partial x^2} + 2b \frac{\partial G(x,\tau)}{\partial \tau} = 0. \qquad (8.48)$$

Since we are considering the fluid motion at a time when the free oscillations have decayed as a result of the action of the damping forces, the initial flow rate distribution in the line has no effect on the nature of the process. Therefore, the solution of (8.48) will be a function which satisfies only the boundary conditions, which in the present case may have the form

$$G(0, \tau) = A_0 e^{i\omega_0 \tau};$$
$$G(l, \tau) + \beta \frac{\partial G(l, \tau)}{\partial x} = 0. \qquad (8.49)$$

We seek the solution of (8.48), satisfying the Conditions (8.49), in the form

$$G(x, \tau) = A(x) e^{i\omega_0 \tau}, \qquad (8.50)$$

where A(x) is an unknown function of the coordinate, which describes the variation of the flow rate oscillation amplitude along the line.

We substitute (8.50) into (8.48), after first defining

$$\left.\begin{aligned} \frac{\partial G(x, \tau)}{\partial \tau} &= i\omega_0 e^{i\omega_0 \tau} A(x); \\ \frac{\partial^2 G(x, \tau)}{\partial \tau^2} &= -\omega_0^2 e^{i\omega_0 \tau} A(x); \\ \frac{\partial^2 G(x, \tau)}{\partial x^2} &= A''(x) e^{i\omega_0 \tau}. \end{aligned}\right\}$$

We obtain

$$a^2 A''(x) + A(x)(\omega_0^2 - 2b\omega_0 i) = 0. \qquad (8.51)$$

Thus, the function A(x) must satisfy the second-order ordinary differential Equation (8.51). We seek the particular solution of (8.51) in the form

$$A(x) = C' e^{kx}, \qquad (8.52)$$

where C' is an arbitrary constant.

After substituting (8.52) into (8.51), we obtain the characteristic equation for determining k

$$a^2 k^2 + \omega_0^2 - 2bi\omega_0 = 0.$$

Hence

$$k_{1,2} = \pm \frac{1}{a} \sqrt{-\omega_0^2 + 2b\omega_0 i}. \qquad (8.53)$$

We write (8.53) in the form

$$k_{1,2} = -|B| \pm i|D|.$$

After simple transformations we obtain

$$B = \frac{1}{a}\sqrt{\frac{\sqrt{\omega_0^4 + 16^2\omega_0^2} - \omega_0^2}{2}};$$

$$D = \frac{1}{a}\sqrt{\frac{\sqrt{\omega_0^4 + 16^2\omega_0^2} + \omega_0^2}{2}}.$$

Then it follows from (8.52) that

$$A(x) = Ce^{-Bx}\sin(Dx + \varphi), \tag{8.54}$$

where C and φ are arbitrary constants.

It follows from (8.54) that the magnitude of the oscillation amplitude along the line depends on the magnitude of the frictional damping forces, and also on the frequency which excites the oscillatory process.

Using the boundary conditions (8.49), we find

$$\left.\begin{aligned} C\sin\varphi &= A_0; \\ \sin(Dl + \varphi) + \frac{B}{D}\sqrt{B^2 + D^2}\sin\left(Dl + \varphi - \operatorname{Arctg}\frac{D}{B}\right) &= 0. \end{aligned}\right\} \tag{8.55}$$

It is not difficult to obtain from (8.55)

$$\varphi = \operatorname{Arctg}\left(\frac{-1 \pm \frac{B}{D}}{\frac{B}{D}}\right) - Dl.$$

Thus, after determining the arbitrary constant φ, it is not difficult to find the magnitude of the flow rate oscillation amplitude at any section of the simple hydraulic line.

In certain cases we need to know the amplitude of the pressure oscillations. It is obvious that (8.36) may be used to convert from flow rate to pressure.

2. Wave Process in Series-Connected Hydraulic Lines

Let us consider a multistage hydraulic line consisting of n simple lines. We note that just as in the case which we studied in examining free oscillations, the cavities, restricting orifices, and so on can be represented in the form of simple hydraulic lines (Figure 8.3).

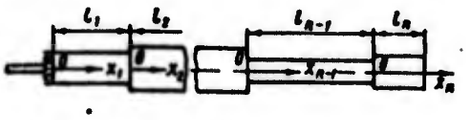

Figure 8.3. Diagram for calculating wave processes in series-connected lines.

In the general case

$$F_1 \neq F_2 \neq \ldots \neq F_n;$$
$$a_1 \neq a_2 \neq \ldots \neq a_n;$$
$$l_1 \neq l_2 \neq \ldots \neq l_n.$$

Assume that the fluid flow rate at the section $x_1 = 0$ of the first line varies according to the law

$$G_1(0, \tau) = A_{01} e^{i\omega_0 \tau}. \tag{8.56}$$

We wish to determine the amplitude of the flow rate oscillations at any intermediate section of the considered complex hydraulic line. As is known, this problem reduces to integration of the system of equations

$$\left.\begin{aligned}
&\frac{\partial^2 G_1(x_1, \tau)}{\partial \tau^2} - a_1^2 \frac{\partial^2 G_1(x_1, \tau)}{\partial x_1^2} + 2b_1 \frac{\partial G_1(x_1, \tau)}{\partial \tau} = 0;\\
&\ldots\ldots\ldots\ldots\ldots\ldots\ldots\ldots\\
&\frac{\partial^2 G_i(x_i, \tau)}{\partial \tau^2} - a_i^2 \frac{\partial^2 G_i(x_i, \tau)}{\partial x_i^2} + 2b_i \frac{\partial G_i(x_i, \tau)}{\partial \tau} = 0;\\
&\ldots\ldots\ldots\ldots\ldots\ldots\ldots\ldots\\
&\frac{\partial^2 G_n(x_n, \tau)}{\partial \tau^2} - a_n^2 \frac{\partial^2 G_n(x_n, \tau)}{\partial x_n^2} + 2b_n \frac{\partial G_n(x_n, \tau)}{\partial \tau} = 0.
\end{aligned}\right\} \tag{8.57}$$

with the boundary conditions

$$\left.\begin{aligned}
&G_1(0, \tau) = A_{01} e^{i\omega_0 \tau};\\
&G_1(l_1, \tau) = G_2(0, \tau);\\
&\ldots\ldots\ldots\\
&G_{i-1}(l_{i-1}, \tau) = G_i(0, \tau);\\
&\frac{a_1^2}{F_1} \frac{\partial G_1(l_1, \tau)}{\partial x_1} = \frac{a_2^2}{F_2} \frac{\partial G_2(0, \tau)}{\partial x_2};
\end{aligned}\right\} \tag{8.58}$$

Equation continued on next page

Equation continued

$$\left.\begin{array}{l} \cdots\cdots\cdots\cdots\cdots \\ \dfrac{a_{l-1}^2}{F_{l-1}}\dfrac{\partial G_{l-1}(l_{l-1},\tau)}{\partial x_l}=\dfrac{a_l^2}{F_l}\dfrac{\partial G_l(0,\tau)}{\partial x_l}; \\ \cdots\cdots\cdots\cdots\cdots \\ G_n(l_n,\tau)+\beta\dfrac{\partial G_n(l_n,\tau)}{\partial x_n}=0. \end{array}\right| \qquad (8.58)$$

Just as in the case of the simple line, we seek the solution of (8.57) with the boundary Conditions (8.58) in the form

$$G_l(x_l,\tau)=A_l(x_l)e^{i\omega\tau}. \qquad (8.59)$$

Substituting (8.58) into (8.57), we obtain

$$A_l(x_l)=C_le^{-\beta_l x_l}\sin(D_lx_l+\varphi_l), \qquad (8.60)$$

where

$$B_l=\frac{1}{a_l}\sqrt{\frac{\sqrt{\omega_0^4+16\beta_l^2\omega_0^2}-\omega_0^2}{2}};$$

$$D_l=\frac{1}{a_l}\sqrt{\frac{\sqrt{\omega_0^4+16\beta_l^2\omega_0^2}+\omega_0^2}{2}}.$$

In (8.60) the values of the arbitrary constants C_1 and φ_l are not known. For their determination we use the boundary conditions at the junction of the simple lines. It is not difficult to determine the constant C_1 from the boundary condition at the section $x_1 = 0$. In fact, at section $x_1 = 0$ we have

$$C_1\sin\varphi_1e^{i\omega\tau}=A_{01}e^{i\omega\tau},$$

hence

$$C_1=A_{01}\frac{1}{\sin\varphi_1}. \qquad (8.61)$$

Let us express C_l in terms of C_1. We can use the equality of the pressures at the junction of the simple lines for this purpose. However, it is preferable to use the last condition, since it has the same form as in the case of branched lines, i.e.,

$$\frac{a_{i-1}^2}{F_{i-1}}\frac{\partial G_{i-1}(l_{i-1},\tau)}{\partial x_{i-1}}=\frac{a_i^2}{F_i}\frac{\partial G_i(0,\tau)}{\partial x_i}, \tag{8.62}$$

where $i-1$ and i are two adjacent simple lines.

The Condition (8.62) is valid regardless of whether the lines are connected in series or emanate from a branch node.

It follows from (8.59) and (8.60) that

$$\frac{\partial G_i(x_i,\tau)}{\partial x_i}=-C_i e^{-\beta_i x_i}\sqrt{B_i^2+D_i^2}\times$$
$$\times\sin\left(D_i x_i+\varphi_i-\operatorname{arctg}\frac{D_i}{B_i}\right)e^{i\omega\tau}. \tag{8.63}$$

It follo
amplitude at

It is obvious that the Condition (8.62) is valid at the junction of simple lines. Then we can use (8.63) to write

$$\left.\begin{aligned}
&\frac{a_1^2}{F_1}C_1 e^{-\beta_1 l_1}\sqrt{B_1^2+D_1^2}\sin\left(D_1 l_1+\varphi_1-\operatorname{arctg}\frac{D_1}{B_1}\right)=\\
&=\frac{a_2^2}{F_2}C_2\sqrt{B_2^2+D_2^2}\sin\left(\varphi_2-\operatorname{arctg}\frac{D_2}{B_2}\right);\\
&\cdots\cdots\cdots\cdots\cdots\cdots\cdots\cdots\cdots\cdots\\
&\frac{a_{i-1}^2}{F_{i-1}}C_{i-1}e^{-\beta_{i-1}l_{i-1}}\sqrt{B_{i-1}^2+D_{i-1}^2}\sin\left(D_{i+1}l_{i-1}+\varphi_{i-1}-\right.\\
&\left.-\operatorname{arctg}\frac{D_{i-1}}{B_{i-1}}\right)=\frac{a_i^2}{F_i}C_i\sqrt{B_i^2+D_i^2}\sin\left(\varphi_i-\operatorname{arctg}\frac{D_i}{B_i}\right).
\end{aligned}\right\} \tag{8.64}$$

At the se

Excluding $C_2,\ldots,C_{i-1}$, we obtain from (8.64)

$$C_i=C_1\frac{\prod_{k=1}^{k=i-1}\sin\left(D_k l_k+\varphi_k-\operatorname{arctg}\frac{D_k}{B_k}\right)}{\prod_{k=1}^{k=i-1}\sin\left(\varphi_k-\operatorname{arctg}\frac{D_k}{B_k}\right)}e^{-\sum_{k=1}^{k=i-1}\beta_k l_k}\frac{a_1^2}{F_1}\frac{F_i}{a_i^2}\frac{\sqrt{B_1^2+D_1^2}}{\sqrt{B_i^2+D_i^2}} \tag{8.65}$$

In certai
oscillation am
section $x_i=0$,

Taking account of (8.59), (8.60), (8.61), and (8.65), we obtain the equation for determining the flow rate at an arbitrary section of the i^{th} line

$$G_i(x_i, \tau) = A_{0i}\frac{a_1^2}{a_i^2}\frac{F_i}{F_1}\frac{\sqrt{B_1^2+D_1^2}}{\sqrt{B_i^2+D_i^2}}e^{-\sum_{k=1}^{k=i-1}B_k l_k}\times$$

$$\times\frac{\prod_{k=1}^{k=i-1}\sin\left(D_k l_k+\varphi_k-\operatorname{arctg}\frac{D_k}{B_k}\right)}{\sin\varphi_1\prod_{k=2}^{k=i-1}\sin\left(\varphi_k-\operatorname{arctg}\frac{D_k}{B_k}\right)}e^{-B_i x_i}\sin(D_i x_i+\varphi_i)e^{i\omega t}$$

It follows from this expression that the flow rate oscillation amplitude at any section of the i^{th} line is defined by the relation

$$A_{0i} = A_{01}\frac{a_1^2 F_i}{a_i^2 F_1}\frac{\sqrt{B_1^2+D_1^2}}{\sqrt{B_i^2+D_i^2}}e^{-\sum_{k=1}^{k=i-1}B_k l_k}\times$$

$$\times\frac{\prod_{k=1}^{k=i-1}\sin\left(D_k l_k+\varphi_k-\operatorname{arctg}\frac{D_k}{B_k}\right)}{\sin\varphi_1\prod_{k=2}^{k=i-1}\sin\left(\varphi_k-\operatorname{arctg}\frac{D_k}{B_k}\right)}e^{-B_i x_i}\sin(D_i x_i+\varphi_i). \qquad (8.66)$$

At the section $x_i = l_i$ we have

$$A_{0i}(x_i=l_i) = A_{01}\frac{a_1^2 F_i}{a_i^2 F_1}\frac{\sqrt{B_1^2+D_1^2}}{\sqrt{B_i^2+D_i^2}}e^{-\sum_{k=1}^{k=i-1}B_k l_k}\times$$

$$\times\frac{\prod_{k=1}^{k=i-1}\sin\left(D_k l_k+\varphi_k-\operatorname{arctg}\frac{D_k}{B_k}\right)}{\sin\varphi_1\prod_{k=2}^{k=i-1}\sin\left(\varphi_k-\operatorname{arctg}\frac{D_k}{B_k}\right)}\sin(D_i l_i+\varphi_i). \qquad (8.67)$$

In certain cases we need to know the magnitude of the pressure oscillation amplitude. Assume the pressure variation is given at the section $x_1 = 0$, i.e.,

$$p_1(0, \tau) = p_{01} e^{i\omega_0 \tau}, \tag{8.68}$$

where p_{01} is the pressure oscillation amplitude at the section $x_1 = 0$.

Let us determine the amplitude of the oscillations at an arbitrary section of the i^{th} simple line. To do this we find the relationship between p_{0i} and A_{0i}.

As is known

$$\frac{\partial p_i(x_i, \tau)}{\partial \tau} = -\frac{a_i^2}{F_i} \frac{\partial G_i(x_i, \tau)}{\partial x_i}$$

Hence

$$p_i(x_i, \tau) = -\frac{a_i^2}{F_i} \int_0^{\tau} \frac{\partial G_i(x_i, \tau)}{\partial x_i} d\tau + C(x_i).$$

The function $C(x_i)$ characterizes the variation of the average value of the pressure along the line. The deviation of the pressure from the average value yields the amplitude of the oscillations. Since $p_i(x_i, \tau)$ represents the deviation of the pressure from its average value, the arbitrary function $C(x_i)$ may be dropped from consideration by equating it to zero, i.e.,

$$p_i(x_i, \tau) = -\frac{a_i^2}{F_i} \int_0^{\tau} \frac{\partial G_i(x_i, \tau)}{\partial x_i} d\tau. \tag{8.69}$$

We integrate (8.69), substituting in place of $\partial G_i/\partial x_i$ its value taken from (8.63)

$$p_i(x_i, \tau) = \frac{1}{i\omega_0} C_i \frac{a_i^2}{F_i} \sqrt{B_i^2 + D_i^2}\, e^{-B_i x_i} \sin\left(D_i x_i + \tau_i - \operatorname{arctg} \frac{D_i}{B_i}\right) e^{i\omega_0 \tau}. \tag{8.70}$$

Using (8.70) we find at the section $x_1 = 0$ of the first line

Equating (

We su
Then we e
simple tra
sure varia

It fo
at an arbi

The ar

(8.68)

ion $x_1=0$.

an arbitrary
ationship

$$p_1(0,\tau)=\frac{1}{i\omega_0}C_1\frac{a_1^2}{F_1}\sqrt{B_1^2+D_1^2}\sin\left(\varphi_1-\operatorname{arctg}\frac{D_1}{B_1}\right)e^{i\omega_0\tau}. \tag{8.71}$$

Equating (8.71) and (8.68), we obtain

$$p_{01}=\frac{1}{i\omega_0}C_1\frac{a_1^2}{F_1}\sqrt{B_1^2+D_1^2}\sin\left(\varphi_1-\operatorname{arctg}\frac{D_1}{B_1}\right) \tag{8.72}$$

We substitute into (8.70) in place of C_1 its value from (8.65). Then we express C_1 in terms of p_{01} using (8.72). Finally, after simple transformations we obtain the formula which defines the pressure variation at an arbitrary section of the i^{th} simple line

$$p_i(x_i,\tau)=-p_{01}e^{-\sum_{k=1}^{k=i-1}\beta_k l_k}\frac{\prod_{k=1}^{k=i-1}\sin\left(D_k l_k+\varphi_k-\operatorname{arctg}\frac{D_k}{B_k}\right)}{\prod_{k=1}^{k=i}\sin\left(\varphi_k-\operatorname{arctg}\frac{D_k}{B_k}\right)}\times \tag{8.73}$$
$$\times e^{-\beta_i x_i}\sin\left(D_i x_i+\varphi_i-\operatorname{arctg}\frac{D_i}{B_i}\right)e^{i\omega_0\tau}.$$

verage value
re from
Since
rage value,
n by

It follows from (8.73) that the flow rate oscillation amplitude at an arbitrary section of the i^{th} line will be

(8.69)

$$p_{0i}=-p_{01}e^{-\sum_{k=1}^{k=i-1}\beta_k l_k}\frac{\prod_{k=1}^{k=i-1}\sin\left(D_k l_k+\varphi_k-\operatorname{arctg}\frac{D_k}{B_k}\right)}{\prod_{k=1}^{k=i}\sin\left(\varphi_k-\operatorname{arctg}\frac{D_k}{B_k}\right)}e^{-\beta_i x_i}\times \tag{8.74}$$
$$\times\sin\left(D_i x_i+\varphi_i-\operatorname{arctg}\frac{D_i}{B_i}\right).$$

s value

The amplitude at the section $x_i=l_i$ will be

(8.70)

ne

$$p_{0i}(x_i=l_i)=-p_{01}e^{-\sum_{k=1}^{k=i}\beta_k l_k}\frac{\prod_{k=1}^{k=i}\sin\left(D_k l_k+\varphi_k-\operatorname{arctg}\frac{D_k}{B_k}\right)}{\prod_{k=1}^{k=i}\sin\left(\varphi_k-\operatorname{arctg}\frac{D_k}{B_k}\right)}. \tag{8.75}$$

Thus, (8.66) and (8.75) define the flow rate and pressure oscillation amplitudes at an arbitrary section of the i^{th} simple line which forms a part of a complex multistage hydraulic line. However, in this form they do not permit the calculation of the oscillation amplitude, since the arbitrary constants γ_A appearing in these expressions are not known a priori. To determine these constants we use the compatability conditions at the junction of the simple lines. As is known, these conditions have the following form for the (i - 1)st and i^{th} simple lines

$$G_{i-1}(l_{i-1}, \tau) = G_i(0, \tau); \tag{8.76}$$

$$\frac{a_{i-1}^2}{F_{i-1}} \frac{\partial G_{i-1}(l_{i-1}, \tau)}{\partial x_{i-1}} = \frac{a_i^2}{F_i} \frac{\partial G_i(0, \tau)}{\partial x_i}. \tag{8.77}$$

Substituting the values of G and $\partial G/\partial x$, taken from (8.60) and (8.63) into (8.76) and (8.77), we obtain

$$C_{i-1} e^{-B_{i-1} l_{i-1}} \sin(D_{i-1} l_{i-1} + \gamma_{i-1}) = C_i \sin \gamma_i; \tag{8.78}$$

$$\frac{a_{i-1}^2}{F_{i-1}} C_{i-1} e^{-B_{i-1} l_{i-1}} \sqrt{B_{i-1}^2 + D_{i-1}^2} \sin\left(D_{i-1} l_{i-1} + \gamma_{i-1} - \operatorname{arctg} \frac{D_{i-1}}{B_{i-1}}\right) =$$

$$= \frac{a_i^2}{F_i} C_i \sqrt{B_i^2 + D_i^2} \sin\left(\gamma_i - \operatorname{arctg} \frac{D_i}{B_i}\right). \tag{8.79}$$

We exclude from (8.78) and (8.79) the quantities C_i and C_{i-1}:

$$\frac{a_{i-1}^2}{F_{i-1}} \sqrt{B_{i-1}^2 + D_{i-1}^2} \frac{\sin\left(D_{i-1} l_{i-1} + \gamma_{i-1} - \operatorname{arctg} \frac{D_{i-1}}{B_{i-1}}\right)}{\sin(D_{i-1} l_{i-1} + \gamma_{i-1})} =$$

$$= \frac{a_i^2}{F_i} \sqrt{B_i^2 + D_i^2} \frac{\sin\left(\gamma_i - \operatorname{arctg} \frac{D_i}{B_i}\right)}{\sin \gamma_i}.$$

Considering that

$$\sin\left(Dl + \gamma - \operatorname{arctg} \frac{D}{B}\right) = \frac{B \sin(Dl + \gamma) - D \cos(Dl + \gamma)}{\sqrt{D^2 + B^2}},$$

we obtain

Since th
it can be exp

In this
knowns. The
the section x
ining $\varphi_{n-1}, \ldots,$
from the last
and so on.

We shall
already that
have used in
draulic lines
wave process,
erates into (

oscilla-
which
in this
itude,
are
mpata-
nown,
i^{th}

$$\frac{a_{i-1}^2}{F_{i-1}}[B_{i-1}-D_{i-1}\operatorname{ctg}(D_{i-1}l_{i-1}+\varphi_{i-1})]=\frac{a_i^2}{F_i}[B_i-D_i\operatorname{ctg}\varphi_i]. \tag{8.80}$$

Since the Condition (8.80) is valid for any two adjacent lines, it can be expanded into the following system of equations

$$\left.\begin{aligned}
&\frac{a_1^2}{F_1}[B_1-D_1\operatorname{ctg}(D_1l_1+\varphi_1)]-\frac{a_2^2}{F_2}(B_2-D_2\operatorname{ctg}\varphi_2)=0;\\
&\cdots\cdots\cdots\cdots\cdots\cdots\cdots\cdots\cdots\\
&\frac{a_{i-1}^2}{F_{i-1}}[B_{i-1}-D_{i-1}\operatorname{ctg}(D_{i-1}l_{i-1}+\varphi_{i-1})]-\\
&\quad-\frac{a_i^2}{F_i}(B_i-D_i\operatorname{ctg}\varphi_i)=0;\\
&\cdots\cdots\cdots\cdots\cdots\cdots\cdots\cdots\cdots\\
&\frac{a_{n-1}^2}{F_{n-1}}[B_{n-1}-D_{n-1}\operatorname{ctg}(D_{n-1}l_{n-1}+\varphi_{n-1})]-\\
&\quad-\frac{a_n^2}{F_n}(B_n-D_n\operatorname{ctg}\varphi_n)=0.
\end{aligned}\right\} \tag{8.81}$$

In this system of equations the quantities a, F, D, B, l are unknowns. The quantity φ_n can be found from the boundary conditions at the section $x_n=l_n$ of the i^{th} simple line. Then the process of determining $\varphi_{n-1},\ldots,\varphi_1$ does not present any particular difficulties. In fact, from the last Equation (8.81) we find φ_{n-1} from the next-to-last φ_{n-2}, and so on.

We shall examine the methods for determining φ_n later, but we see already that they do not differ essentially from the methods which we have used in studying the free oscillations of fluid in complex hydraulic lines. In fact, if we neglect the effect of friction on the wave process, i.e., if we set $b_1=b_2=b_3=\cdots b_n=0$, then (8.81) degenerates into (7.48), which was obtained in the study of free oscillations

$$\left.\begin{aligned}
&\frac{F_1}{a_1}\operatorname{tg}\left(\frac{\omega}{a_1}l_1+\varphi_1\right)-\frac{F_2}{a_2}\operatorname{tg}\varphi_2=0;\\
&\cdots\cdots\cdots\cdots\cdots\cdots\cdots\cdots\cdots
\end{aligned}\right\} \tag{8.82}$$

Equation continued on next page

Equation continued

$$\left.\begin{array}{l} \cdots\cdots\cdots\cdots\cdots\cdots \\ \dfrac{F_{l-1}}{a_{l-1}}\operatorname{tg}\left(\dfrac{\omega_0}{a_{l-1}}l_{l-1}+\varphi_{l-1}\right)-\dfrac{F_l}{a_l}\operatorname{tg}\varphi_l=0; \\ \cdots\cdots\cdots\cdots\cdots\cdots \\ \dfrac{F_{n-1}}{a_{n-1}}\operatorname{tg}\left(\dfrac{\omega_0}{a_{n-1}}l_{n-1}+\varphi_{n-1}\right)-\dfrac{F_n}{a_n}\operatorname{tg}\varphi_n=0. \end{array}\right\} \qquad (8.82)$$

The only difference is that in the case of free oscillations the quantities φ_1 and φ_n are known and ω_0 is to be determined.

Here, however, φ_n and ω_0 are known and we must determine $\varphi_1, \varphi_2, \ldots, \varphi_{n-2}, \varphi_{n-1}$.

We note that (8.81) can be used to determine the natural frequencies of fluid oscillation in complex lines under conditions with friction. However, the magnitude of the natural frequency depends very weakly on the friction; therefore, (7.48) may be used for its approximate determination.

In certain cases the effect of friction on the amplitude of the fluid oscillations can be neglected. Then (8.66) and (8.74) take the form

$$\left.\begin{aligned} A_{0l} &= A_{01}\frac{a_1F_l}{a_lF_1}\frac{\prod_{k=1}^{k=l-1}\cos\left(\frac{\omega_0}{a_k}l_k+\varphi_k\right)}{\sin\varphi_1\prod_{k=1}^{k=l}\cos\varphi_k}\sin\left(\frac{\omega_0}{a_l}x_l+\varphi_l\right), \\ p_{0l} &= p_{01}\frac{\prod_{k=1}^{k=l-1}\cos\left(\frac{\omega_0}{a_k}l_k+\varphi_k\right)}{\prod_{k=1}^{k=l}\cos\varphi_k}\cdot\cdot\cdot\cos\left(\frac{\omega_0}{a_l}x_l+\varphi_l\right). \end{aligned}\right\} \qquad (8.83)$$

3. Branched Hydraulic Lines

In view of the fact that the Condition (8.62) is valid both at the junction of series-connected hydraulic lines and at a branch node,

Formulas (8.66) and (8.74) may be used to calculate the amplitudes of the forced oscillations in branched hydraulic lines. In practice the problem reduces to finding the arbitrary constants φ_A, which appear in these equations. Therefore, in the present section we shall examine primarily the techniques for determining φ_A.

(8.82)

Before turning to the determination of the arbitrary constants φ_{A_i}, let us examine the specific peculiarities of the calculation of forced oscillation amplitudes in branched lines. Assume a line with two branches (Figure 8.4). The amplitude and frequency of the harmonic pressure oscillations are given at the section $x_1=0$ of line 1. We are required to determine the pressure oscillation amplitude in line 12.

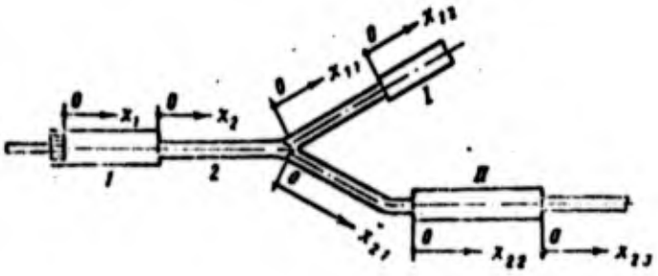

Figure 8.4. Branched hydraulic circuit.

Using (8.74), we find for the line 12

(8.83)

$$p_{12}=p_{01}e^{-(B_1l_1+B_2l_2+B_{11}l_{11})}\frac{\sin\left(D_1l_1+\varphi_1-\operatorname{arctg}\frac{D_1}{B_1}\right)}{\sin\left(\varphi_1-\operatorname{arctg}\frac{D_1}{B_1}\right)}\times$$

$$\times\frac{\sin\left(D_2l_2+\varphi_2-\operatorname{arctg}\frac{D_2}{B_2}\right)\sin\left(D_{11}l_{11}+\varphi_{11}-\operatorname{arctg}\frac{D_{11}}{B_{11}}\right)}{\sin\left(\varphi_2-\operatorname{arctg}\frac{D_2}{B_2}\right)\sin\left(\varphi_{11}-\operatorname{arctg}\frac{D_{11}}{B_{11}}\right)\sin\left(\varphi_{12}-\operatorname{arctg}\frac{D_{12}}{B_{12}}\right)}\times \tag{8.84}$$

$$\times e^{-B_{12}x_{12}}\sin\left(D_{12}x_{12}+\varphi_{12}-\operatorname{arctg}\frac{D_{12}}{B_{12}}\right).$$

The amplitudes of the pressure oscillations in the second branch can be determined similarly. However, the constants are the unknowns in the resulting equations. For example, in (8.84) $\varphi_1, \varphi_2, \varphi_{11}, \varphi_{12}$ are the unknowns. Therefore, these equations must be closed by using the boundary conditions at the branch node.

It is obvious that the Conditions (7.21) and (7.22) hold at the branch node. We substitute into these conditions the values of Q and $\frac{\partial Q}{\partial x}$, taken from (8.59) and (8.64)

$$C_j e^{-\beta_j l_j} \sin(D_j l_j + \varphi_j) = \sum_{k=1}^{k=r} C_k \sin \varphi_k; \tag{8.85}$$

$$C_j \frac{a_j^2}{F_j} e^{-\beta_j l_j} \sqrt{B_j^2 + D_j^2} \sin\left(D_j l_j + \varphi_j - \operatorname{arctg} \frac{D_j}{B_j}\right) =$$
$$= C_r \frac{a_r^2}{F_r} \sqrt{D_r^2 + B_r^2} \sin\left(\varphi_r - \operatorname{arctg} \frac{D_r}{B_r}\right). \tag{8.86}$$

We exclude the quantities C_j and C_r from (8.85) and (8.86).

After elementary transformations, we finally obtain

$$\frac{F_j}{a_j^2 [B_j - D_j \operatorname{ctg}(D_j l_j + \varphi_j)]} = \sum_{k=1}^{k=r} \frac{F_r}{a_r^2 (B_r - D_r \operatorname{ctg} \varphi_r)}. \tag{8.87}$$

It is not difficult to see that for $b_j = b_r = 0$ the Equation (8.87) takes the form

$$\frac{F_j}{a_j} \operatorname{tg}\left(\frac{\omega}{a_j} l_j + \varphi_j\right) = \sum_{k=1}^{k=r} \frac{F_k}{a_r} \operatorname{tg} \varphi_r. \tag{8.88}$$

Thus, in a branched hydraulic system the amplitudes of the flow rate and pressure oscillations are determined by (8.66) and (8.74), in which the arbitrary constants φ_k are calculated from equations obtained with the aid of (8.81) and (8.87).

We shall obtain the formulas for determining the arbitrary constants φ as a function of the boundary conditions at the end sections of the terminal lines of the hydraulic system. We note that the sequence in which these constants are determined is analogous to the case of free oscillations. The only difference is that in the case of forced oscillations the frequency is given, and the fluid friction on the line wall is taken into account.

We shall examine three cases.

A. In the hydraulic system there are lines which are open at the sections $x_1=0$ and $x_n=l_n$.

$$\frac{\partial G_1(0,\tau)}{\partial x_1}=0,\quad \frac{\partial G_n(l_n,\tau)}{\partial x_n}=0. \tag{8.89}$$

Using (8.63), we find

$$\sin\left(\varphi_1-\operatorname{arctg}\frac{D_1}{B_1}\right)=0;$$

$$\varphi_1=\operatorname{Arctg}\frac{D_1}{B_1};$$

$$\sin\left(D_1l_1+\varphi_1-\operatorname{arctg}\frac{D_1}{B_1}\right)=0;$$

$$\varphi_1=\operatorname{Arctg}\frac{D_1}{B_1}-D_1l_1.$$

B. The lines are closed at the sections $x_1=0$ and $x_n=l_n$.

$$G_1(0,\tau)=0,\ G_n(l_n,\tau)=0.$$

Using (8.60), we find

$$\varphi_1=(k-1)\pi,\ k=1,2,3,\ldots,$$

$$\varphi_n=(k-1)\pi-D_nl_n,\ k=1,2,3,\ldots$$

C. The terminal lines of the system have dampers at the sections $x_1=0$, $x_n=l_n$. Then in accordance with (7.33) the boundary conditions have the form

$$G_1(0,\tau)+\beta\frac{\partial G_1(0,\tau)}{\partial x_1}=0;$$

$$G_n(l_n,\tau)+\beta\frac{\partial G_n(l_n,\tau)}{\partial x_n}=0,$$

where the coefficient β characterizes the damper type.

Using (8.60) and (8.63), we obtain

$$\operatorname{ctg}\varphi_1=\frac{-1+\beta B}{\beta D},$$

$$\operatorname{ctg}(D_1l_1+\varphi_1)=\frac{-1+\beta B}{\beta B}.$$

Let us examine as an example the sequence for calculating the amplitude of the pressure oscillation in a two-node branched system (Figure 8.5). Assume the amplitude of the pressure p_{01} oscillation at the section $x_1=0$ is known. We determine the amplitude of the pressure oscillations at the section $x_1=l_1$ using (8.75)

$$\dot{p}_{01}(x_1=l_1)=\frac{p_{01}e^{-B_1l_1}\sin\left(D_1l_1+\varphi_1-\operatorname{Arc\,tg}\frac{D_1}{B_1}\right)}{\sin\left(\varphi_1-\operatorname{Arc\,tg}\frac{D_1}{B_1}\right)}. \tag{8.90}$$

Since there are no multistage lines in this system, then φ_1 is determined with the aid of (8.87) for each branch node, i.e.,

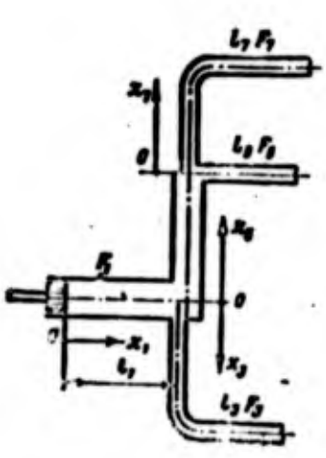

Figure 8.5. Binodal branching of hydraulic system.

$$\left.\begin{aligned}&\frac{F_1}{a_1^2[B_1-D_1\operatorname{ctg}(D_1l_1+\varphi_1)]}=\\&=\frac{F_3}{a_3^2(B_3-D_3\operatorname{ctg}\varphi_3)}+\frac{F_5}{a_5^2(B_5-D_5\operatorname{ctg}\varphi_5)}\\&\frac{F_5}{a_5[B_5-D_5\operatorname{ctg}(D_5l_5+\varphi_5)]}=\\&=\frac{F_7}{a_7^2(B_7-D_7\operatorname{ctg}\varphi_7)}+\frac{F_9}{a_9^2(B_9-D_9\operatorname{ctg}\varphi_9)},\end{aligned}\right\} \tag{8.91}$$

where φ_3, φ_7, φ_9 are determined by the boundary conditions at the sections $x_3 = l_3$, $x_7 = l_7$, $x_9 = l_9$.

It is not difficult to find φ_5, from the second equation (8.91) and φ_1 from the first equation. Substituting φ_1 and φ_5 into (8.90), we obtain the magnitude of the pressure oscillation at the section $x_1 = l_1$. In the particular case in which $F_1 = F_3 = F_5 = F_7 = F_9$, $b_1 = b_3 = b_5 = b_7 = b_9 = 0$, $a_1 = a_3 = a_5 = a_7 = a_9 = a$ and the branches l_7, l_9, l_3 are closed at the end sections, we obtain from (8.90) and (8.91)

$$p_{01}|_{x_1=l_1} = \left(1 - \operatorname{tg}\frac{\omega}{a}l_7 \operatorname{tg}\frac{\omega}{a}l_5 - \operatorname{tg}\frac{\omega}{a}l_9 \operatorname{tg}\frac{\omega}{a}l_5\right) \times$$
$$\times \left[\sin\frac{\omega}{a}l_1 \left(\operatorname{tg}\frac{\omega}{a}l_5 + \operatorname{tg}\frac{\omega}{a}l_7 + \operatorname{tg}\frac{\omega}{a}l_9 + \operatorname{tg}\frac{\omega}{a}l_3 - \right.\right.$$
$$- \operatorname{tg}\frac{\omega}{a}l_3 \operatorname{tg}\frac{\omega}{a}l_7 \operatorname{tg}\frac{\omega}{a}l_5 - \operatorname{tg}\frac{\omega}{a}l_3 \operatorname{tg}\frac{\omega}{a}l_5 \operatorname{tg}\frac{\omega}{a}l_9 \Big) -$$
$$\left. - \cos\frac{\omega}{a}l_1 \left(\operatorname{tg}\frac{\omega}{a}l_7 + \operatorname{tg}\frac{\omega}{a}l_5 + \operatorname{tg}\frac{\omega}{a}l_5 \operatorname{tg}\frac{\omega}{a}l_9 - 1\right)\right]^{(-1)} p_{01}.$$

§ 3. Some Questions of Test Stand Hydraulic System Dynamics

The design and production of LRE involve tremendous difficulties, whose solution is unthinkable without the use of specialized experimental studies. Test stand developmental work plays an important role in LRE design.

In the process of LRE testing the correctness of the geometric and layout decisions which form the basis of the LRE design is verified; the static and dynamic characteristics of the individual components, assemblies, and the engine as a whole are determined; a careful study is made of the reliability and functioning of the engine and its components under operational conditions. At the same time studies are made to refine and improve the test techniques.

These questions can be resolved most completely in the course of flight tests. However, flight tests can be only the culmination of the entire experimental development which is performed earlier during stand testing. The test stand results are verified during the flight tests.

At the present time definite success has been achieved in test stand simulation of altitude, transport, and climatic LRE operating conditions. Less well advanced is the question concerning the simulation under test stand conditions of the dynamic phenomena which take place in the engine hydraulic system during its functioning. This is explained by the fact that the hydraulic system of the test stand to which the engine is connected has an influence on the propellant dynamics in the LRE lines. Therefore, the stand pneumatic-hydraulic system (PHS) must be designed to minimize its influence.

On the other hand, the pneumatic-hydraulic automatic control components and the individual engine assemblies are subjected to tests on stands whose hydraulic system geometry, as a rule, differs from the corresponding components of the engine PHS. Therefore, it is necessary that the stand PHS be equivalent in the dynamic sense to the engine PHS.

All these questions can be resolved to some degree if we know the influence of hydraulic system geometry on the dynamics of the component being tested, which in turn requires a study of the wave processes in complex hydraulic plumbing systems.

Consider the following problem. Assume that assemblies of the same type are connected to PHS which differ in geometry and elastic characteristics (Figure 8.6). The PHS (a) corresponds to the engine, (b) corresponds to the test stand. We are required to determine under what criteria the dynamic load on the components in question will be the same in both cases.

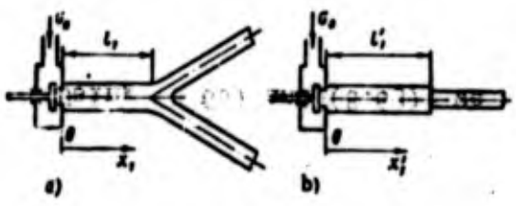

Figure 8.6. Diagram for deriving the conditions for dynamic similarity of test stand and engine pneumo-hydraulic systems.

We shall make the entire analysis for case (a) only, i.e., for the case in which the component functions in the engine hydraulic system. It is obvious that the analysis will be analogous for case (b).

Assume
mass flow r
as follows

We must
component i
solve this

In thi
the form (8.
the line bra
system, will
(7.23), (7.2
take into ac
simple line.
simple line
placing 2b f

where l_{eq} is
lo
l is

Then th

Find th

with the init

Assume that for $\tau \leqslant 0$ the fluid flow in the PHS is steady with the mass flow rate G_0. For $\tau \geqslant 0$ the flow rate at the section $x_1=0$ varies as follows under the influence of the component

$$G(0, \tau)=f(\tau). \tag{8.92}$$

We must determine the pressure variation at the section where the component is connected to the line, i.e., at the section $x_1=0$. To solve this problem we must integrate the system of Equations (8.57).

In this case the boundary condition at the section $x_1=0$ will have the form (8.92). The boundary conditions at the line junction and at the line branch nodes, and also at the end sections of the hydraulic system, will have the form obtained previously in Chapter 7 (see (7.19), (7.23), (7.25)—(7.33)). In (8.57) the coefficients $b_1, b_2 \ldots$ do not take into account the local resistances at the junction and within the simple line. Therefore, if there are local resistances along the simple line their effect can be accounted for approximately by replacing 2b from (7.2) by the following formula [145]

$$2b=\frac{\xi \bar{w}}{2d_0}\left(1+\frac{l_0}{l}\right), \tag{8.93}$$

where l_{eq} is the length which is hydraulically equivalent to all the local resistances;

l is the line length.

Then the posed problem is formulated as follows.

Find the solution of the system of equations

$$\left.\begin{aligned} &\frac{\partial^2 G_1(x_1, \tau)}{\partial \tau^2}-a_1^2 \frac{\partial^2 G_1(x_1, \tau)}{\partial x_1^2}+2b_1 \frac{\partial G_1(x_1, \tau)}{\partial \tau}=0; \\ &\ldots\ldots\ldots\ldots\ldots\ldots\ldots\ldots \\ &\frac{\partial^2 G_n(x_n, \tau)}{\partial \tau^2}-a_n^2 \frac{\partial^2 G_n(x_n, \tau)}{\partial x_n^2}+2b_n \frac{\partial G_n(x_n, \tau)}{\partial \tau}=0 \end{aligned}\right\} \tag{8.94}$$

with the initial conditions

$$\left.\begin{aligned} &G_1(x_1, 0)=0, \quad \frac{\partial G_1(x_1, 0)}{\partial \tau}=0; \\ &\cdots\cdots\cdots\cdots\cdots \\ &G_n(x_n, 0)=0, \quad \frac{\partial G_n(x_n, 0)}{\partial \tau}=0, \end{aligned}\right\}$$

the boundary conditions

$$G_1(0, \tau)=f(\tau); \tag{8.95}$$

the boundary conditions at the junction and branch nodes

$$\left.\begin{aligned} &G_{m-1}(l_{m-1}, \tau)=G_m(0, \tau), \\ &\frac{a_{m-1}^2}{F_{m-1}} \frac{\partial G_{m-1}(l_{m-1}, \tau)}{\partial x_{m-1}}=\frac{a_m^2}{F_m} \frac{\partial G_m(0, \tau)}{\partial x_m}; \\ &G_j(l_j, \tau)=\sum_{k=1}^{k=r} G_k(0, \tau), \\ &\frac{a_j^2}{F_j} \frac{\partial G_j(l_j, \tau)}{\partial x_j}=\frac{a_1^2}{F_1} \frac{\partial G_1(0, \tau)}{\partial x_1}=\ldots= \\ &\quad=\frac{a_r^2}{F_r} \frac{\partial G_r(0, \tau)}{\partial x_r}. \end{aligned}\right\} \tag{8.96}$$

and the boundary conditions at the end sections of the hydraulic line

$$G_n(l_n, \tau)+\beta \frac{\partial G_n(l_n, \tau)}{\partial x_n}=0. \tag{8.97}$$

Since the boundary Condition (8.95) is nonhomogeneous, we seek the solution of (8.94) in the form

$$\left.\begin{aligned} &G_1(x_1, \tau)=G_1^{\mathrm{I}}(x_1, \tau)+G_1^{\mathrm{II}}(x_1, \tau); \\ &\cdots\cdots\cdots\cdots\cdots \\ &G_m(x_m, \tau)=G_m^{\mathrm{I}}(x_m, \tau)+G_m^{\mathrm{II}}(x_m, \tau), \\ &\cdots\cdots\cdots\cdots\cdots \end{aligned}\right\} \tag{8.98}$$

where $G^{\mathrm{I}}(x, \tau)$ is the solution of (8.94) for the boundary conditions (8.96), (8.97) and $G_1^{\mathrm{I}}(0, \tau)=0$.

Then the initial conditions take the form

$$\left.\begin{aligned} G_1^{\mathrm{I}}(x_1, 0) &= -G_1^{\mathrm{II}}(x_1, 0) \\ &\cdots\cdots\cdots\cdots \\ G_m^{\mathrm{I}}(x_m, 0) &= -G_m^{\mathrm{II}}(x_m, 0), \end{aligned}\right\} \tag{8.99}$$

$$\left.\begin{aligned} \frac{\partial G_1^{\mathrm{I}}(x_1, 0)}{\partial \tau} &= -\frac{\partial G_1^{\mathrm{II}}(x_1, 0)}{\partial \tau}, \\ &\cdots\cdots\cdots\cdots \\ \frac{\partial G_m^{\mathrm{I}}(x_m, 0)}{\partial \tau} &= -\frac{\partial G_m^{\mathrm{II}}(x_m, 0)}{\partial \tau}. \end{aligned}\right\} \tag{8.100}$$

(8.95)

$G^{\mathrm{II}}(x, \tau)$ is the solution of (8.94) which satisfies only the boundary conditions (8.95), (8.96) and (8.97). We showed previously that the particular solution of (8.94) with the boundary Conditions (8.95), (8.96), (8.97) and the initial Conditions (8.100) may be sought in the form

(8.96)

$$\left.\begin{aligned} G_1^{\mathrm{I}}(x_1, \tau) &= A_1(x_1) e^{i\omega\tau}; \\ &\cdots\cdots\cdots \\ G_m^{\mathrm{I}}(x_m, \tau) &= A_m(x_m) e^{i\omega\tau}, \end{aligned}\right\}$$

where A(x) is defined by (8.60).

lic line

In studying steady periodic fluid oscillations in the hydraulic system, the oscillation frequency ω and amplitude at the entrance to the system were specified. In the present case the frequency ω must be selected so that the boundary conditions are satisfied.

(8.97)

e seek

To do this we must use the Condition (8.100) and the boundary conditions at the end sections of the hydraulic system to find from (8.81) and (8.87) the values of ω and ψ. Since (8.81) and (8.87) are transcendental, an infinite set of values of ω and ψ satisfy them. Therefore, the general solution of (8.94) with the boundary and initial Conditions (8.96), (8.97) and (8.99) will have the form

(8.98)

tions

$$\left.\begin{aligned} G_1^{\mathrm{I}}(x_1, \tau) &= \sum_{k=1}^{\infty} A_{1k}(x_1) e^{i\omega_k \tau}; \\ &\cdots\cdots\cdots\cdots \\ G_m^{\mathrm{I}}(x_m, \tau) &= \sum_{k=1}^{\infty} A_{mk}(x_m) e^{i\omega_k \tau}. \end{aligned}\right\} \tag{8.101}$$

With account for (8.60), after simple transformations we can write (8.101) in the form

$$\left.\begin{aligned} G_1^{\mathrm{I}}(x_1,\tau) &= \sum_{k=1}^{\infty} C_{1k} e^{-\beta_{1k}\tau_1} \sin(D_{1k}x_1 + \gamma_{1k}) \sin(\omega_k\tau + \psi_{1k}); \\ &\cdots\cdots\cdots\cdots\cdots\cdots\cdots\cdots \\ G_m^{\mathrm{I}}(x_m,\tau) &= \sum_{k=1}^{\infty} C_{1m} e^{-\beta_{mk}x_m} \sin(D_{mk}x_m + \gamma_{mk}) \sin(\omega_k\tau + \psi_{mk}), \end{aligned}\right\} \qquad (8.102)$$

where C_k and ψ_k are arbitrary constants which are determined from the initial conditions.

It follows from (8.100) that the initial conditions can be found by determining the form of the function $G^{\mathrm{II}}(x,\tau)$. Since in our case we are making a purely qualitative analysis of the wave processes in the system, it will be shown later that there is no need to find the function $G_1^{\mathrm{II}}(x,\tau)$.

Using the continuity Equation (7.12) and also taking (8.102) and (8.98) into consideration, we obtain for the line connected to the component

$$-\frac{\partial p_1(x_1,\tau)}{\partial\tau} = \frac{a_1^2}{F_1}\frac{\partial}{\partial x_1}\left[\sum_{k=1}^{\infty} C_{1k} e^{-\beta_{1k}\tau_1} \sin(D_{1k}x_1 + \right.$$

$$\left. + \gamma_{1k}) \sin(\omega_k\tau + \psi_k)\right] + \frac{\partial G_1^{\mathrm{II}}(x_1,\tau)}{\partial x_1}. \qquad (8.103)$$

On the basis of analogous arguments the same question can be obtained for the line connected to the component in the stand hydraulic system (b).

In (8.103) the arbitrary constants C_{1k} and ψ_k are determined from the initial conditions, which are the same in both hydraulic systems. The arbitrary constant γ_{1k} is determined from the boundary conditions at the section $x_1 = 0$, which are also the same in both the stand PHS and the engine cases. The function $G_1^{\mathrm{II}}(x_1,\tau)$ depends on the form of the function $f(\tau)$ and also in part on the dynamic properties of the hydraulic system. If the pressures in both hydraulic systems at the section

an write

8.102)

om the

found
se we
in the
e func-

2) and
the

8.103)

be ob-
raulic

ed from
stems.
itions
PHS and
ne func-
raulic
ion

$x_1 = 0$ change in accordance with the same law, then the equation of motion of the component regulating organs will have the same form, and this means that the fluid flow rates through the components will change in accordance with the same law.

After differentiation with respect to x, (8.103) takes the form

$$\frac{\partial p_1(x_1\tau)}{\partial \tau} = -\frac{a_1^2}{F_1}\sum_{k=1}^{\infty} C_{1k}[D_{1k}\cos(D_{1k}x_1+\gamma_{1k})-$$

$$-B_{1k}\sin(D_{1k}x_1+\gamma_{1k})]e^{-\beta_{1k}\tau_1}\sin(\omega_k\tau+\psi_k)+\frac{\partial G_1^{II}(x_1,\tau)}{\partial x_1}.$$

Hence, the pressure at the section $x_1 = 0$ varies as

$$\frac{\partial p_1(0,\tau)}{\partial \tau} = -\frac{a_1^2}{F_1}\sum_{k=1}^{\infty} C_{1k}[D_{1k}\cos\gamma_{1k}-B_{1k}\sin\gamma_{1k}]\times$$

$$\times\sin(\omega_k\tau+\psi_k)+\frac{\partial G_1^{II}(x_1,\tau)}{\partial x_1}. \qquad (8.104)$$

Based on the arguments presented above, we can with the aid of (8.104) determine under what conditions the action of the hydraulic system on the component will be the same on the stand and in flight. This requires that

$$a_1 = a_{1cr}, \qquad \text{(a)}$$

$$F_1 = F_{1cr}, \qquad \text{(b)}$$

$$\omega_k = \omega_{k\,cr}, \qquad \text{(c)}$$

$$D_{1k} = D_{1k\,cr}, \qquad \text{(d)}$$

$$B_{1k} = B_{1k\,cr}, \qquad \text{(e)}$$

where the subscript "st" denotes the parameters characterizing the stand PHS. It follows from (8.60) that

$$D_{1k} = \frac{1}{a_1}\sqrt{\frac{\sqrt{\omega_k^4+4\beta_1^2\omega_k^2}+\omega_k^2}{2}},$$

$$B_{1k} = \frac{1}{a_1}\sqrt{\frac{\sqrt{\omega_k^4+4\beta_1^2\omega_k^2}-\omega_k^2}{2}}.$$

Therefore, the conditions (a), (b), (c), and (d) can be represented as follows

$$b_1 = b_{1cr}, \quad \frac{a_1}{F_1} = \frac{a_{1cr}}{F_{1cr}}.$$

Thus, in order that the stand hydraulic system be dynamically equivalent to the engine hydraulic system it is necessary that

$$\left.\begin{aligned} &\frac{a_1}{F_1} = \frac{a_{1cr}}{F_{1cr}}; \\ &b_1 = b_{1cr}; \\ &\omega_k = \omega_{k\,cr}. \end{aligned}\right\} \qquad (8.105)$$

The condition of equality of the natural frequencies over their entire spectrum is seldom realizable, and therefore, it is desirable that this condition be satisfied at least approximately for the first few spectral frequencies. The satisfaction of this condition involves several difficulties associated with the calculation of ω_k or with the experimental determination of ω_k by recording the amplitude and frequency characteristics of the hydraulic systems.

In the particular case in which $b_1 = b_2 = \ldots = b$ and the hydraulic systems have similar geometry and consist of an equal number of simple hydraulic lines, the Conditions (8.105) are formulated somewhat more simply. This is explained by the fact that in this particular case the Equations (8.81) and (8.87), which define the natural frequency, will have a similar form, and the number of equations will be the same for both systems. Therefore, it follows from these equations that the condition $\omega_k = \omega_{st}$ will be satisfied if

$$\begin{aligned} &\frac{a_1}{F_1} = \frac{a_{1cr}}{F_{1cr}}; \quad \frac{l_1}{a_1} = \frac{l_{1cr}}{a_{1cr}}; \\ &\cdots\cdots\cdots\cdots \\ &\frac{a_n}{F_n} = \frac{a_{n\,cr}}{F_{n\,cr}}; \quad \frac{l_n}{a_n} = \frac{l_{n\,cr}}{a_{n\,cr}}. \end{aligned}$$

repre-

ically
at

(8.105)

er their
esirable
the first
n involves
r with the
and fre-

raulic sys-
simple
hat more
ar case
equency,
e the same
s that the

CHAPTER 9

INSTABILITY OF LRE OPERATION

§ 1. General Information on LRE Operational Instability

Instability of the LRE working process is characterized by uncontrolled pressure oscillations in the combustion chamber and in the feed system with increasing amplitude. We can also speak of the analogous oscillations of the thrust, propellant flow rate, mixture ratio, combustion product temperature, and other system parameters.

Observations show that if an engine is unstable pulsations of these parameters arise and develop either immediately after startup or under certain operating regimes. These pulsations usually lead to destruction of the chamber or components of the feed system, or to local burnout or melting of the combustion chamber, nozzle, and injector head. Even if the pressure oscillations in the chamber do not cause immediate failure, their appearance disrupts the normal engine operating process, degrades its basic parameters, and in particular reduces the specific thrust and service life.

Engine operation in the unstable regimes is accompanied by noise phenomena whose tone and timbre depend on the nature of the oscillations. It is obvious that instability of the LRE operating regime

is a very harmful phenomenon which must be combatted with all possible techniques.

Oscillographic recordings of the chamber pressure [78] have shown that even in a stably operating engine there may be some nonuniformity of the working process caused by various random factors. In this case the combustion chamber pressure and therefore the other parameters oscillate about some mean value, but the amplitudes of these oscillations are small and are not dangerous, since in a stable propulsive system they do not increase in the course of time.

Consequently, operating regime instability is one of the most important problems of rocket engineering. In this connection the designers and scientists have attempted to study the causes for the occurrence of instability in the LRE and to find ways to eliminate this instability. Systematic investigations of LRE stability began early in the fifties. Many studies have appeared since that time [3], [7], [38], [40], [78], [102], [120], [133], [148], [151], both in the Soviet Union and abroad, and these studies have made possible further development of the theoretical investigations in this field.

Most experimental studies have been devoted to the study of the influence of individual geometric and operating condition parameters on power plant stability. In the theoretical studies attempts have been made to explain the instability phenomenon from the viewpoint of some particular model of the working process, which was then used as the basis for proposing various computational methods and constructing the stability bounds.

We note that the achievements in applied LRE stability theory have been to a considerable degree the outgrowth of the fundamental studies of the outstanding Soviet Russian scientist A.M. Lyapunov on the stability of motion of dynamic systems [55].

1. Classification of unstable regimes.

The unstable LRE operating regimes are usually classified in terms

of the magnitude of the observed pressure oscillation frequencies in the combustion chamber. This criterion is used to identify three basic types of instability.

(1) Low-frequency instability is characterized by a comparatively low oscillation frequency (roughly less than 300 Hz); the oscillations of this type have been studied in considerable detail and they can be avoided or suppressed without any particular difficulty;

(2) Medium-frequency instability is characterized by an intermediate frequency band (on the order of 300-500 Hz). This instability is encountered most infrequently and has received very little study because of the absence of systematic experimental data. It has simply been remarked that medium-frequency instability is encountered in high-thrust engines and in gas generators [79].

(3) High-frequency instability is characterized by so-called acoustic oscillations of the pressure in the combustion chamber of comparatively high frequency (above 500 Hz). The oscillations of this type are most dangerous for the engine and it is very difficult to combat them, since they have not received adequate study because of the complexity of the problem.

This classification can not be considered entirely valid, since for a more precise identification of the unstable regimes of LRE operation the classsfication would have to be based on the mechanism which leads to self-excited oscillations of a particular type. However, the specific mechanisms or factors which give rise to the various forms of instability have not yet been definitely established. The inadequacy of this classification shows up in the fact that for certain power plant parameters the high-frequency oscillations can shift into the region of relatively low frequencies and vice versa. Therefore, the indicated frequency boundaries separating the different forms of LRE instability must be considered to be very approximate.

However, in spite of its drawbacks this classification is useful in that in most cases it identifies the LRE unstable operating regimes

correctly from the viewpoint of correspondence between the oscillation frequency and the nature of the unstable regime.

Theory and experience show that high-frequency pressure oscillations (pressure waves) can propagate in both the longitudinal and transverse directions in the combustion chamber. In this connection they are usually divided correspondingly into longitudinal and transverse acoustic oscillations. In turn, the transverse acoustic oscillations are subdivided into radial and tangential forms, depending on whether the pressure waves propagate along the radius or along a "traveling" tangent to an imaginary cylindrical surface located inside the combustion chamber.

Study of LRE instability in practice is complicated by the fact that several forms of pressure oscillations in the chamber are often realized, rather than one specific oscillation mode. However, the instability mode encountered most commonly in the development of the modern LRE is the transverse high-frequency vibration mode [81].

2. Qualitative picture of instability onset.

Analysis and correlation of experimental data on LRE instability [174], [175], [190], [172], [80], [79], [81], [9] make it possible to describe the most typical qualitative picture of the onset of instability of the working process in LRE. In a very rough approximation this picture can be described as follows. The kinetic process of propellant combustion can be characterized schematically by the time delay in the transformation of the liquid propellants into gaseous products after the propellants enter the combustion chamber. This temporal parameter, which plays such an important role in LRE stability theory, is encountered in the related technical literature under a briefer term: gasification delay time or transformation time.

This time obviously depends on the combustion process conditions and therefore varies with transition from one regime to another. Thus, it is natural to suppose that the vaporization rate increases monotonically with transition from the low engine operating regimes (for which low chamber pressures, low pressure drops across the injectors, and

coarse atomization are characteristic) to the high regimes (higher chamber pressures, high pressure drops across the injectors, and fine atomization), while the transformation time is reduced correspondingly. This also leads to a corresponding change of the burnup curve and to the onset of conditions which are favorable for the development of oscillations of increasingly higher frequency.

The low LRE operating regimes are usually accompanied by low-frequency pressure oscillations in the combustion chamber with frequencies not exceeding a few tens of Hertz. As the operating regime is intensified to a given degree these oscillations disappear, but at some operating regime oscillations start up which have a higher frequency, close to the natural frequency of one of the propellant lines. The frequency of these oscillations depends on the geometric dimensions of the lines and the speed of sound in the propellants, and lies in the range of about 100-300 Hertz.

Finally, further intensification of the engine operating regime, accompanied by increase of the chamber pressure, increase of the pressure drop across the injectors, and improvement of the efficiency of the atomization and mixing of the propellants, leads to stable operation in some range of variation of the operating regime parameters. The magnitude of this range varies over wide limits for different engines depending on their geometry, the nature of the propellants used, the arrangement and construction of the mixture formation organs, and other factors. The lower limit of this range is termed the lower LRE stable operation "threshold" while the upper limit is termed the upper stability "threshold."

Acoustic oscillations arise during engine operation at sufficiently forced operating regimes which lie above the upper stability threshold. As a rule, longitudinal acoustic oscillations develop first, and they then transition into transverse acoutic oscillations, which are extremely hazardous for the LRE as the engine operation is intensified still further or as the longitudinal modes continue to grow.

In accordance with the described picture of the phenomena which are observed in experimental investigations, the current ideas on the factors which lead to unstable LRE operating regimes are connected with certain specific factors.

The low-frequency instability develops either as a result of the vaporization lag factor or as a result of factors which are defined by the characteristics of the propellant feed system. The first low-frequency oscillation mode is independent of the feed system and therefore has been termed "intrachamber" instability [78]. The second low-frequency oscillation mode, conversely, is independent of the phenomena in the chamber and is therefore termed "line" instability.

The high-frequency oscillations arise as a result of nonuniformity of the physicochemical conditions in different regions of the combustion chamber, which leads to different local burning velocities. The latter then obviously lead to local oscillations of the combustion chamber pressure. As a result, pressure waves are formed and propagate in all directions in the intrachamber space in a fashion analogous to conventional sound (acoustic) waves. In the case of the stable chamber operating regime, these waves will decay as they are reflected from the walls and return to the region where they originated. Conversely, if the engine is prone to self-excited acoustic oscillations, the disturbances will be in phase with the reflected waves and there will be a rapid development of resonant local oscillations of the gas filling the chamber volume.

Let us examine the characteristic features of the low-frequency and high-frequency pressure oscillations in the combustion chamber. In the case of low-frequency oscillations the pressure is practically the same at all points inside the combustion chamber at every instant of time, since the pressure wavelength is much greater than the chamber geometric dimensions. In other words, in the low-frequency instability case the gas inside the chamber oscillates simultaneously throughout the entire volume. In the high-frequency instability case the wavelength is comparable with the chamber geometrical dimensions and therefore the pressure is not the same at different points of the

combustion chamber at every instant of time. Consequently, in the high-frequency oscillation case the pressure waves propagate through the combustion chamber volume.

While for low-frequency oscillations we can neglect the pressure wave propagation time, in the case of high-frequency oscillations the propagation time for this wave becomes commensurate with the oscillation period and it can not be neglected.

The most favorable conditions for excitation of the system are created in the case in which the pressure wave propagation frequency is close in magnitude to one of the natural frequencies of the gas oscillations in the combustion chamber. The principal characteristic of this oscillation mode is that as the combustion process is concentrated near the wave crests (i.e., at the points of maximal pressure) we would expect considerable deviations of the combustion velocities from their average values and the greatest probability of the unstable LRE operating regime.

In spite of the fact that this qualitative picture of the onset of instability may seem quite valid, in reality the nature and mechanism of the development of the oscillatory regimes in LRE are far more complex. Cases which are very difficult to explain may be encountered in the practice of experimental engine development work. This remark is particularly applicable with relation to the high-frequrency instability of the LRE working process.

§ 2. Results of Low-Frequency Instability Experimental Studies

1. Experimental observations.

A description of the phenomena observed in the low-frequency LRE instability region has been given in [174], [175], [190], [9], which present oscillographic recordings of the various engine parameters: pressure, temperature, and propellant component flow rates.

We noted previously that low-frequency instability arises in the low engine operating regimes, i.e., with low combustion chamber pressures and low pressure drops across the injectors. Just as all other periodic processes, the low-frequency oscillations are characterized by their amplitude, frequency, and form. Let us see how these characteristics vary as a function of the engine operating regime, i.e., as a function of the chamber pressure.

Oscillations with large amplitude are realized in the very low operating regimes (Figure 9.1a). In this case the pressure first rises sharply in the course of about one millisecond, and decreases exponentially (on the oscillogram the process proceeds in time from right to left). This abrupt and quite large pressure rise essentially blocks the entry of new batches of propellant and the combustion is terminated. Then as the combustion chamber is emptied of the combustion products the pressure falls off and propellent entry is renewed. However, the new ignition of the fresh batches of propellant does not take place immediately but rather after the end of the transformation time. When the propellants ignite a new pressure peak develops, and so on. The oscillogram of this instability mode is similar to that of the so-called relaxation oscillations, for which the defining parameter is the relaxation time, i.e., the time in the course of which the disturbance diminishes by a factor of e (e is the base of the natural logarithms).

Upon intensification of the operating regime as a result of increasing the supply pressure up to some definite value, the chamber pressure oscillation frequency increases, the amplitude decreases, and the oscillation approaches the sinusoidal form (see Figure 9.1b).

In addition to these typical low-frequency oscillations, in practice we sometimes observe more complex oscillation modes at the high chamber pressures, which are more difficult to define (see Figure 9.1c). It appears that in this case there is a superpositioning of various frequencies. More detailed analysis requires a study of the frequency spectrum to identify the principal harmonics.

Finally, Figure 9.1d shows still another low-frequency oscillation mode. Here oscillations develop after engine startup, which have an amplitude which builds up to some constant value and then the oscillations suddenly disappear. A possible cause of this phenomenon may be a random increase of the vaporization lag time, which leads to excitation of the low-frequency oscillations.

A similar pattern is also observed in analyzing the recordings of the temperature in the combustion chamber and at the nozzle exit. Oscillations with a large amplitude develop in the region of low chamber pressure (Figure 9.2a); with increase of the pressure the oscillation amplitude decreases while the frequency increase (see Figures 9.2b,c).

The same phenomena can be observed in the analysis of the propellant flow rate recordings.

Figure 9.3 shows a simultaneous recording of the pressure ahead of the oxidizer (nitric acid) and fuel injectors and the pressure in the combustion chamber at two different points. We see that small changes of the chamber pressure have no marked effect on the pressure variations ahead of the injectors (see Figure 9.3a): the pressures ahead of the injectors are constant and the pressure oscillations in the chamber are in phase. The variations of the chamber pressure with constant propellant flow rate are explained by the intrachamber instability, which is associated solely with the burning process.

In certain cases the pressure variations in the chamber are preceded by variations of the pressure ahead of the injectors of one or both components (see Figure 9.3b). These variations are obviously caused by the propagation of waves in the propellant system lines and gradually damp out.

2. Effect of various parameters on low-frequency oscillations.

The influence of certain operating conditions and geometric parameters on the nature of the engine working process behavior has been

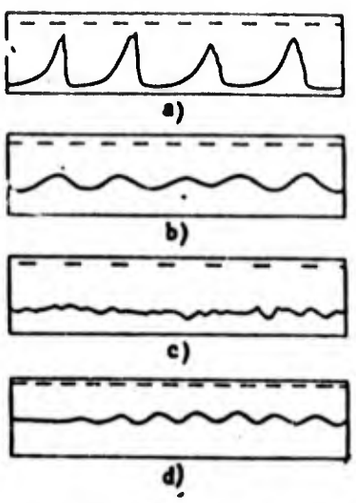

Figure 9.1. Low-frequency instability pressure oscillations (timing marks 100 Hz) [9].

established in the course of experimental studies of low-frequency instability. Such parameters include: combustion chamber pressure, pressure drop across the injectors and throttling orifices, type of propellant and its mixture ratio, the specific flow rate and residence time of the gases in the combustion chamber, the equivalent (or characteristic) chamber length, the length of the propellant lines, and the presence of elastic elements in the lines.

Effect of combustion chamber pressure p_K. With increase of p_K the system stability region becomes larger. This is explained by the reduction of the vaporization delay time τ_K in the case of high chamber pressures. Following Crocco [78], the variation of τ_K with p_K is expressed by the formula

$$\tau_K = \frac{a}{p_K^n},$$

where n is the interaction index;
a is a constant.

According to the experimental data [173], the interaction index has values $n > 1$ and increases with increase of p_K.

We see from Figure 9.4 that the oscillation frequency increases with increase of p_K. At the same time the oscillation amplitude decreases.

Effect of pressure drop across injectors and throttling orifices. Increase of the pressure drop Δp_{inj} across the injectors and the presence in the propellant lines of orifices with high differential

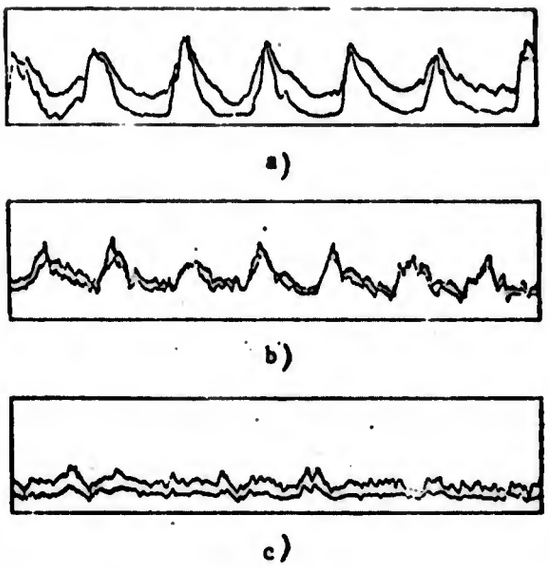

Figure 9.2. Low-frequency instability temperature oscillations [9].

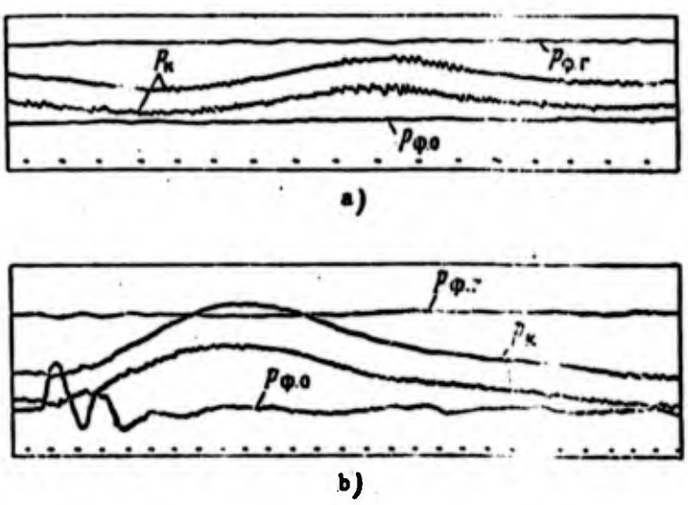

Figure 9.3. Simultaneous recording of pressure at two points of chamber and pressures ahead of oxidizer and fuel injectors.

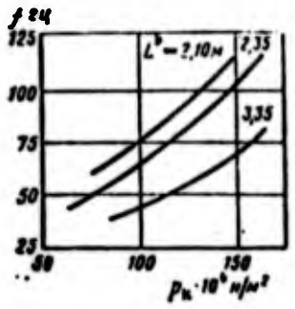

Figure 9.4. Frequency as a function of chamber pressure and characteristic length (fuel: nitric acid and furfuryl alcohol) [9].

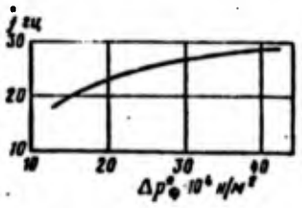

Figure 9.5. Oscillation frequency versus pressure differential across oxidizer injectors [9].

pressures lead to a broadening of the engine stable operating regime region. This technique is frequently used in practice to combat low-frequency instability.

We see from Figure 9.5 that the oscillation frequency increases as the pressure drop across the injectors increases.

Effect of propellant type and mixture ratio. The propellant type and ratio of the component mass flow rates play an important role in the development of low-frequency instability. This is explained by the fact that the transformation time τ_K depends significantly on the physical and chemical properties of the propellant. The more active components have a smaller value of τ_K and, consequently, are less prone to low-frequency instability. In most cases higher frequencies and lower oscillation amplitudes have been obtained for the hypergolic propellants.

As for the propellant mixture ratio k, a different effect for different propellants is observed in different ranges of variation of this parameter.

Effect of specific flow rate and residence time of the gases in the combustion chamber. The gas residence time θ_K in the combustion

chamber is d
chamber and

where V_K

F_{cr}
R_K, T_K

β

Consequ
and the smal
engine becom
tions. Conv
(F_K is the c
reduction of
region.

Effect
(equivalent)

More sta
quantity L*.
sions which d
that the osci
conditions re
pressure and
lation amplit

The effe
bility is ide
(9.1) there i
propellant

chamber is determined by the geometric dimensions of the combustion chamber and the nature of the propellants used

$$\theta_к = \frac{V_к \beta}{F_{кр} R_к T_к}, \qquad (9.1)$$

where V_K is the volume of the intrachamber space from the head to the throat;

F_{cr} is the critical section area:

R_K, T_K are the gas constant and temperature of the combustion products in the chamber;

β is the combustion chamber pressure specific impulse.

Consequently, for a given propellant θ_K is larger, the larger V_K and the smaller F_{cr}. It has been noted that with increase of θ_K the engine becomes more stable with relation to the low-frequency oscillations. Conversely, increase of the specific mass flow rate $g_F = \frac{G}{F_к \rho_к}$ (F_K is the combustion chamber cross section area), which leads to a reduction of θ_K, is accompanied by a narrowing of the LRE stability region.

Effect of chamber equivalent length. The chamber characteristic (equivalent) length L* is defined by the relations

$$L^* = \frac{V_к}{F_{кр}}.$$

More stable engine operation is observed with increase of the quantity L*. Figure 9.4 shows experimental data for three engine versions which differ in the characteristic chamber length L*. We see that the oscillation frequency decreases with increase of L*. Other conditions remaining the same, in particular for a constant chamber pressure and constant pressure drop across the injectors, the oscillation amplitude decreases somewhat with increase of the parameter L*.

The effect of the parameters θ_K and L* on engine operating stability is identical. This is understandable, since in accordance with (9.1) there is a direct proportionality between θ_K and L* for a given propellant

$$\theta_k = L^* \frac{\beta}{R_k T_k}, \qquad (9.2)$$

where the complex $\frac{\beta}{R_k T_k}$ depends only on the propellant type and mixture ratio and is practically independent of the combustion chamber pressure.

Effect of propellant line length. An increase of the line length leads to some stabilization of the engine operating regime along with a marked reduction of the oscillation frequency. For long lines there is an increase of the pressure drop in the feed system, which acts like an increase of the pressure drop across the injectors.

Effect of elastic elements. The presence of elastic elements in the propellant lines narrows the engine stability region. The presence of an elastic element immediately ahead of the engine injector head is particularly unfavorable with regard to stability.

§ 3. Analysis of Very Simple Low-Frequency Instability Model

Oscillations may develop in a LRE without any periodic external input. To understand the reason for the excitation of these oscillations we must make a detailed study of the dynamics of the transformation of the liquid fuel into the gaseous combustion products. However, at the present time such an analysis is not possible because of the complexity of the transformation process and the absence of sufficiently detailed information on the process.

In order to explain the instability of the engine operating process we represent the engine in simplified form (Figure 9.6). Several models of the instability phenomenon which explain the experimental data, at least qualitatively, can be established, depending on the degree of simplification or the source of the excitation for the pressure oscillations in the chamber [7], [78].

1. Basic assumptions. Oscillation excitation mechanism.

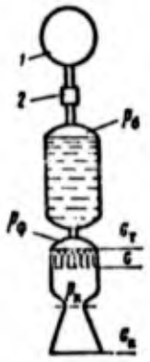

Figure 9.6. Simple arrangement of monopropellant LRE with short line: 1) high pressure gas bottle; 2) reducer

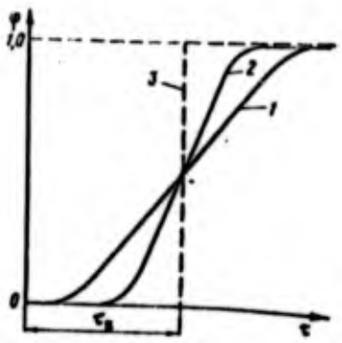

Figure 9.7. Schematic representation of burnup curve: 1) poorly mixed bipropellant; 2) monopropellant or well-mixed bipropellant; 3) step curve for instantaneous combustion process

The following assumptions form the basis for the very simple low-frequency instability model.

(1) Simplifications of the power plant arrangement (see Figure 9.6):

a. compressed gas feed system which provides constant propellant feed pressure and is not sensitive to pressure variations in the chamber;

b. engine operates on monopropellant;

c. propellant line is very short ("zero" length), therefore, we can assume that the injector inlet pressure equals the tank pressure $p_{inj} = p_t$.

(2) The actual time dependence of the propellant burnt fraction ("burnup curve") is replaced by a step process, in which each portion of liquid propellant entering the chamber does not burn but transforms into the gaseous phase in the course of the time τ_K, then it is transformed instantaneously into the final combustion products (Figure 9.7).

The actual $\varphi(\tau)$ curves (curves 1 and 2 in Figure 9.7) are characterized by a complex and gradual propellant burnup process, whose relationship is difficult to describe analytically with account for all

the details of the physical and chemical processes which take place in the preparatory period. From the moment of injection into the combustion chamber until complete transformation into the gaseous combustion products, the propellant goes through a complex sequence of transformations, including processes such as atomization of the liquid jets, warmup and vaporization of the droplets, diffusion and turbulent mixing of the vapors, thermochemical reactions, and so on. With the aid of the approximate replacement mentioned above, the unsolvable problem of describing the combustion process in terms of the quantitative characteristics of its intermediate stages is simplified considerably, since the only quantity which is necessary for the description of the process as a function of time is now only the time τ_K from the moment of propellant injection to the moment it is converted into the hot gases. This time is usually termed the transformation time or the gasification lag.

The existence of the transformation time means that the processes in the combustion chamber lag in comparison with the propellant feed processes. For example, if there is a change of the propellant flow rate the combustion chamber pressure does not take the value corresponding to the changed flow rate immediately, but only after the time τ_K.

(3) The propellant burns in the oscillatory process just as it does in the steady state regime. Consequently, oscillations of the operating regime parameters (p_K, G, Δp_{inj}) about their average values do not lead to any change of the transformation time.

(4) The pressure is practically the same throughout the entire combustion chamber at every moment of time, and the mass of the gases in the chamber oscillates as a whole about the average value.

(5) The temperature of the combustion products in the chamber is constant and independent of the pressure variations.

(6) The liquid is incompressible.

(7) There are no elastic elements in the lines.

We shall examine the mechanism of the development of self-excited oscillations in the engine under these assumptions. In the steady engine operating regime the working medium flow rates are the same at all sections of the chamber.

Now let us assume that the pressure in the combustion chamber suddenly increases as a result of some random disturbance, which corresponds to the creation in the chamber of an excess of gas in comparison with the gas content in the stable regime. This leads to an immediate increase of the gas flow rate G_K through the nozzle and a reduction of the propellant flow rate G_{in} through the injectors because of the reduction of the pressure drop Δp_{inj} across the injectors. The reduction of the propellant inlet flow rate G_{in} leads to a corresponding reduction of the gasification rate only after the end of the transformation time τ_K, which is required for the preparatory processes to take place, rather than immediately. At each moment the propellant portion burns which entered the chamber τ_K sec previously. Therefore, after a random increase of p_K the gas formation rate remains at its previous value for the time period τ_K.

Since the gas flow rate through the nozzle increased while the rate of gas formation remained at the previous level, p_K begins to decrease and after some time returns to its original value in the steady state regime. At this moment the gas influx and efflux equalize and the time has come for burnup of that propellant portion which entered the chamber at the time when the chamber pressure was high. Therefore, the gas influx rate decreases (in comparison with the steady state value), which leads to further reduction of the pressure in the combustion chamber. But reduction of p_K to values lower than the steady state value obviously leads to a corresponding reduction of the gas discharge rate from the chamber G_K and an increase of the propellant inflow rate through the injectors G_{in} because of the increase of the pressure drop Δp_{inj}. As a result the pressure in the chamber, after reaching some minimal magnitude, again begins to increase as a result of the arrival of the moment for combustion of the increased propellant portion which entered the chamber in the period of reduced p_K, and so on. This sequence of processes will obviously be repeated thereafter.

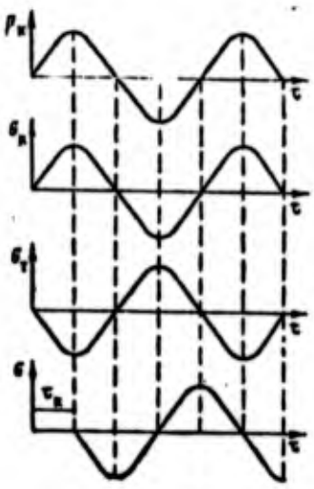

Figure 9.8. Relative positioning of curves of variation of different parameters as a function of time for onset of low-frequency instability.

Thus the random disturbance, once initiated, creates the necessary conditions for the oscillatory working process in the combustion chamber. The relative positioning of the curves for the variations of the different parameters in accordance with the self-excited oscillation mechanism just described is shown schematically in Figure 9.8. The very simple model of the phenomenon considered here was first formulated and studied by Natanzon in 1950 [7]. The described mechanism is not only of practical importance, it is also of historical value, since it was the first model used as the basis for a systematic study of LRE instability. A refinement of the described approximate model of the working process was made by Crocco in 1951. A further development and generalization of more complex theoretical models of the working process can be found in Crocco's monograph [78].

2. Analytic study and construction of the stability boundary.

The stability analysis can be conducted either for the purpose of determining the stability of a specific engine, all the parameters of which are known, or for the purpose of determining all possible values of the parameters for which the LRE dynamic system is stable. Such analyses are made with the aid of stability criteria, which define the necessary and sufficient conditions for all the roots of the characteristic equations of the system to have a negative real part. The D-partition, Satche, and other methods which also make it possible to construct the stability boundaries, have been widely used. We shall study the stability of the differential equation of combustion chamber

dynamics, which after linearization and reduction to dimensionless form is written as

$$\theta_к \frac{d\delta\bar{p}_к(\tau)}{d\tau} + \delta\bar{p}_к(\tau) - \delta\bar{G}_т(\tau-\tau_к) = 0, \tag{9.3}$$

where the overbar denotes dimensionless small deviations of the parameters from their steady state values, which have the superscript *

$$\delta\bar{p}_к(\tau) = \frac{p_к(\tau)-p_к^*}{p_к^*}; \tag{9.4}$$

$$\delta\bar{G}_т(\tau-\tau_к) = \frac{G_т(\tau-\tau_к)-G^*}{G^*}; \tag{9.5}$$

$$\theta_к = \frac{V_к p_к^*}{R_к T_к G^*}, \tag{9.6}$$

where θ_K is the mean working medium particle residence time in the combustion.

The notations such as $\delta\bar{p}_к$ and $\delta\bar{G}_т$ are sometimes termed the dimensionless variations of the corresponding parameters.

The absence of a feed line in the very simple model makes it possible to neglect the inertia of the liquid column and, therefore, to assume that the formula for the steady state liquid discharge from the injector is valid for the variable regime

$$G = \chi\sqrt{p_ф - p_к},$$

where χ is a coefficient which depends on the hydraulic characteristic of the system and the liquid density.

Substituting this expression into (9.5), we obtain

$$\delta\bar{G}_т(\tau-\tau_к) = \sqrt{\frac{p_ф - p_к(\tau-\tau_к)}{p_ф - p_к^*}} - 1 = \sqrt{1 + \frac{p_к^* - p_к(\tau-\tau_к)}{p_ф - p_к^*}} - 1.$$

Bearing in mind small deviations of the parameters from their steady state values, we replace the square root by its linear approximation

$$\delta\bar{G}_{\text{т}}(\tau-\tau_{\text{к}})=\left[1+\frac{1}{2}\,\frac{p_{\text{к}}^{\circ}-p_{\text{к}}(\tau-\tau_{\text{к}})}{p_{\text{б}}-p_{\text{к}}^{\circ}}\right]-1=-\frac{\dfrac{p_{\text{к}}(\tau-\tau_{\text{к}})-p_{\text{к}}^{\circ}}{p_{\text{к}}^{\circ}}}{\dfrac{2(p_{\text{б}}-p_{\text{к}}^{\circ})}{p_{\text{к}}^{\circ}}}$$

Introducing the notations (assuming that $p_t = p_{inj}$)

$$\delta\bar{p}_{\text{к}}(\tau-\tau_{\text{к}})=\frac{p_{\text{к}}(\tau-\tau_{\text{к}})-p_{\text{к}}^{\circ}}{p_{\text{к}}^{\circ}}, \tag{9.7}$$

$$\Delta\bar{p}_{\Phi}=\frac{2(p_{\text{б}}-p_{\text{к}}^{\circ})}{p_{\text{к}}^{\circ}}, \tag{9.8}$$

we obtain

$$\delta\bar{G}_{\text{т}}(\tau-\tau_{\text{к}})=-\frac{\delta\bar{p}_{\text{к}}(\tau-\tau_{\text{к}})}{\Delta\bar{p}_{\Phi}}. \tag{9.9}$$

With account for (9.9) the combustion chamber equation (9.3) takes the form

$$\theta_{\text{к}}\frac{d\delta\bar{p}_{\text{к}}\tau}{d\tau}+\delta\bar{p}_{\text{к}}(\tau)+\frac{1}{\Delta\bar{p}_{\Phi}}\delta\bar{p}_{\text{к}}(\tau-\tau_{\text{к}})=0. \tag{9.10}$$

The stability condition may be found by seeking the solution of (9.10) in the form of the sum of functions of the type

$$\delta\bar{p}_{\text{к}}(\tau)=Ce^{s\tau}, \tag{9.11}$$

where C is the constant of integration (in the general case a complex quantity)

s in the general case is also a complex quantity.

Substituting (9.11) into the differential equation (9.10), we obtain its characteristic equation

$$\theta_{\text{к}}s+1+\frac{1}{\Delta\bar{p}_{\Phi}}e^{-s\tau_{\text{к}}}=0. \tag{9.12}$$

We see that this equation is transcendental in the complex variable s and has an infinite set of roots. This implies that the parameters defining the stability of the system in question are the parameters

Δp_{inj}, θ_K a
roots s of t

Equatio
the course o
real part of
imaginary va
correspond t
the conditio
oscillations
ing the valu
the equation

which is tra
replace the e

Then we obtai

which breaks

We write

Here onl
relative pres
quantity.

Δp_{inj}, θ_K and τ_K, on the values of which the numerical values of the roots s of the characteristic equation depend.

Equation (9.11) shows that the disturbances $\delta\bar{p}_K$ will decrease in the course of time and consequently the system will be stable if the real part of all the roots s is negative, and vice versa. The purely imaginary values $s=i\omega$ (the real part of all the roots equals zero) correspond to the state of the system at the stability boundary, i.e., the condition of neutral equilibrium, in which the amplitude of the oscillations of p_K does not change with time. Consequently, substituting the value $s=i\omega$ into the characteristic Equation (9.12), we obtain the equation of the system stability boundary

$$\theta_K i\omega + 1 + \frac{1}{\Delta\bar{p}_\phi} e^{-i\omega\tau_K} = 0, \tag{9.13}$$

which is transformed as follows for convenience of calculation. We replace the exponential function using the Euler formula

$$e^{-i\omega\tau_K} = \cos\omega\tau_K - i\sin\omega\tau_K.$$

Then we obtain the equation

$$\Delta\bar{p}_\phi + \cos\omega\tau_K + i(\theta_K\Delta\bar{p}_\phi\omega - \sin\omega\tau_K) = 0,$$

which breaks down into the two following equations

$$\Delta\bar{p}_\phi + \cos\omega\tau_K = 0;$$
$$\Delta\bar{p}_\phi\omega\theta_K - \sin\omega\tau_K = 0.$$

We write them in final form as

$$\left.\begin{aligned} \Delta\bar{p}_\phi &= -\frac{1}{\sqrt{1+\omega^2\theta_K^2}}; \\ \operatorname{tg}\omega\tau_K &= -\omega\theta_K. \end{aligned}\right\} \tag{9.14}$$

Here only the plus sign on the square root is retained, since the relative pressure drop across the injectors is an essentially positive quantity.

We can use (9.14) to calculate and plot the stability boundary in the plane of any two parameters with the value of the third parameter fixed. If an analysis of the operating stability of a given engine is required in different regimes (for example, when regulating the thrust by throttling) it is better to plot the stability boundary in the plane of the parameters τ_K - $\Delta\bar{p}_{inj}$, since these parameters undergo the largest variations in the regulation process. As for the residence time θ_K, in accordance with (9.5) its magnitude is practically independent of the operating regime (since the ratio $p_к^*/G^* \approx \text{const}$ for a given engine), while variation of the quantity θ_K means either a change of the chamber volume V_K or replacement of the propellant in terms of a change of the product $R_K T_K$.

For computational convenience we write (9.14) in the form

$$\Delta\bar{p}_\Phi = \frac{1}{\sqrt{1+\omega^2\theta_к^2}}; \tag{9.15}$$

$$\tau_к = \frac{1}{\omega}(k\pi - \operatorname{arctg}\omega\theta_к), \tag{9.16}$$

where k is an infinite sequence of positive integers(k = 1, 2, 3,...) The zero value of k is eliminated from consideration, since it yields negative values of the obviously positive quantities τ_K and θ_K.

Each value of k corresponds to a particular curve on the plane $\Delta\bar{p}_{inj}$ - τ_K for θ_K = const. Consequently, the infinite sequence of values of k yields an infinite number of curves, each of which represents the corresponding stability boundary. Bearing in mind the qualitative nature of the stability theory presented here, we limit ourselves to examination of the simplest case with k = 1. In this case the Formulas (9.15) and (9.16) indicate that with variation of ω from 0 to ∞ the relative pressure drop Δp_{inj} can change correspondingly in the limits from 1 to 0 and the product $\omega\tau_к$ can change from π to π/2.

Giving the circular frequency various values from ω=0 to ω=∞, we can use (9.15) and (9.16) to calculate the parameters Δp_{inj} and τ_K for a constant (variational) value of θ_K and plot the corresponding curves (Figure 9.9). Each of these curves divides the $\Delta\bar{p}_{inj}$ - τ_K

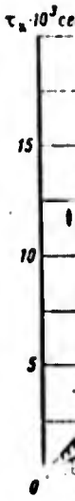

Figure 9.9.
in the pla
and $\Delta\bar{p}_\Phi$ fo

region is to
example, by
and solving

which confi
stability re

We see
respond to
of τ_K. The
θ_K. For an
has a more
large value
the engine
pressure dr
words, the

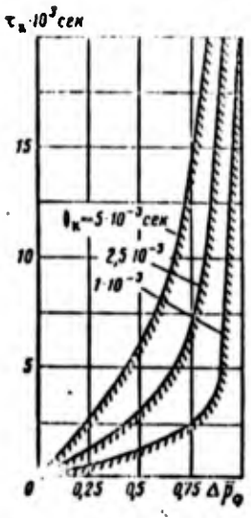

Figure 9.9. Stability boundaries in the plane of parameters $\tau_к$ and $\Delta\bar{p}_ф$ for $\theta_к$=var

plane into two parts: on one side of the curve there lie those combinations of the parameters $\Delta\bar{p}_{inj}$ and τ_K which yield negative real parts of the roots of the characteristic equation in question — this is the region of stability; on the other side lie the combinations of $\Delta\bar{p}_{inj}$ and τ_K corresponding to real values of the roots— this is the region of instability. Such curves are termed the stability boundaries, in the present case the boundaries in the plane of the two parameters $\Delta\bar{p}_{inj}$ and τ_K. In our example the region of stable regimes is located to the right and below the curve, while the instability region is to the left and above the curve. This is easily seen, for example, by taking some point on the $\Delta\bar{p}_{inj}$ axis, for which $\tau_к$=0 and solving (9.12) for s. We obtain a negative value of the root

$$s = -\frac{1+\Delta\bar{p}_ф}{\theta_к \Delta\bar{p}_ф} < 0,$$

which confirms what we have said relative to the location of the stability region.

We see from Figure 9.9 that stable engine operating regimes correspond to combinations of large values of $\Delta\bar{p}_{inj}$ and small values of τ_K. The stability region expands with increase of the parameter θ_K. For an engine with small values of $\Delta\bar{p}_{inj}$ and τ_K a change of θ_K has a more marked influence on its stability than for an engine with large values of these parameters. We also see from the figure that the engine will be stable for any values of τ_K and θ_K if the relative pressure drop across the injectors $\Delta\bar{p}_{inj} > 1$ is doubled. In other words, the condition for absolute engine stability can be written as

$\Delta\bar{p}_{inj} = \frac{2\Delta p_0}{p_k} \geq 1$. This condition is well known in the literature of LRE stability.

Thus, if we have a graph of the stability boundaries we can follow the behavior of the engine as we alter its operating conditions and geometric parameters. For example, in complete accord with the experimental data, on the basis of the theoretical analysis just made we can state that increase of $\Delta\bar{p}_{inj}$ (for example, by installing throttling orifices or different injectors), reduction of [illegible] (by using more active propellants), increase of the residence time θ_k (for example, by increasing the combustion chamber volume) all stabilize engine operation. Consequently, if an engine being studied is found to be unstable after a check, then by a suitable change of its parameters we can easily suppress the low-frequency oscillations. In conclusion we note once again that this theory, which yields a basically correct qualitative picture of the effect of the various parameters on the stability of the LRE operating regime, does not yield quantitative agreement with experimental data. This is quite understandable if we recall the major simplifications which are characteristic for the very simple model of the pnenomenon.

§ 4. Theory of Low-Frequency Stability of Monopropellant LRE Operation With Account for Feedline Length

The properties of the LRE feed system, in particular the propellant feed lines, have a major influence on engine operational stability. In actual LRE, which have feed lines of varying lengths, unstable operating regimes are due not only to the gasification lag but also to the wave processes in the propellant lines. Since the oscillation wave lengths are comparable with the line lengths, we must study the latter as a system with distributed parameters.

The time lag and the wave processes define several specific characteristics of LRE dynamics, which are examined in the following using the example of a monopropellant power plant with pressure feed, consisting of a propellant tank, a single uniform line, and an inelastic injector head (Figure 9.10). It is assumed that the inertia forces

Figure 9.1(with lon sure gas 3) tank; chamber

To de equations plant arra system are the form o usual, in equations. a step nat

where l is

For l pellant fl since this propellant

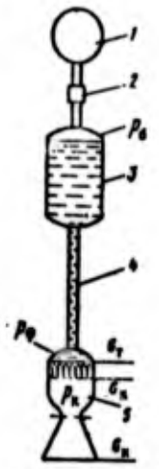

Figure 9.10. Monopropellant LRE with long line: 1) high pressure gas bottle; 2) reducer; 3) tank; 4) line; 5) combustion chamber

which arise during rocket acceleration have no effect on the liquid flow. The problem has been solved by Artamonov in this formulation in [7].

The effect of feed lines on LRE stability has also been analyzed in studies of American authors [191], [120], [40], but their results are obtained as a particular case from the more general solution of Artamonov. Therefore, the presentation of this section follows [7].

1. Basic equations of LRE dynamics. Determining the initial and boundary conditions of the problem.

To derive the stability conditions we write the differential equations of the dynamics of the elements of the considered power plant arrangement (see Figure 9.10). The dynamic elements of this system are the combustion chamber and the propellant feed system in the form of a single line which terminates with the injector head. As usual, in studying stability in the small we shall use the linearized equations. As before, the chamber equation is taken for the case of a step nature of the fuel burnup process (see curve 3 in Figure 9.7)

$$\theta_к \frac{d\delta\bar{p}_к(\tau)}{d\tau} + \delta\bar{p}_к(\tau) = k\bar{G}_т(\tau - \tau_к, l), \qquad (9.17)$$

where l is the feed line length.

For long feed lines it would be incorrect to express the propellant flow rate through the injectors using the formula $G_т = \chi\sqrt{p_б - p_к}$, since this formula is valid only for the steady state process in the propellant lines, when the liquid motion velocity follows the variations

of the pressure drop without any time lag. In the case in question this condition is not satisfied with account for the liquid compressibility, inertia of the motion, and finite propagation velocity of the pressure wave through the lines. Therefore, in order to express the propellant flow rate through the injectors with account for the length and elasticity of the line walls, we must make use of the equation of motion of the liquid in the line.

Liquid motion in a cylindrical straight line is defined by the Zhukovskiy equations (without account for the distributed friction)

$$-\frac{\partial p(\tau, x)}{\partial x}=\rho\frac{\partial w(\tau, x)}{\partial \tau};$$
$$\frac{\partial p(\tau, x)}{\partial \tau}=\rho a^2\frac{\partial w(\tau, x)}{\partial x}$$

where ρ is the constant liquid density;

a is the speed of sound in the liquid without account for the elasticity of the line walls.

Excluding the pressure p from these equations, we obtain the wave equation for the velocity

$$\frac{\partial^2 w(\tau, x)}{\partial \tau^2}-a^2\frac{\partial^2 w(\tau, x)}{\partial x^2}=0$$

or for the mass flow rate G_τ ($G_\tau=F\rho w$, where F is the line flow section area)

$$\frac{\partial^2 G_\tau(\tau, x)}{\partial \tau^2}-a^2\frac{\partial^2 G_\tau(\tau, x)}{\partial x^2}=0.$$

We introduce the notation for the relative deviation of the mass flow rate, i.e., its dimensionless variation

$$\delta\bar{G}_\tau(\tau, x)=\frac{G_\tau(\tau, x)-G_\tau^\circ}{G_\tau^\circ} \qquad (9.18)$$

Then we obtain

$$\frac{\partial^2\delta\bar{G}_\tau(\tau, x)}{\partial \tau^2}-a^2\frac{\partial^2\delta\bar{G}_\tau(\tau, x)}{\partial x^2}=0. \qquad (9.19)$$

question
compressi-
ity of the
press the
the length
uation of

d by the
riction)

for the

in the

low section

f the mass

(9.18)

(9.19)

For the complete problem formulation, in addition to the basic Equations (9.17) and (9.18) of the system dynamics, we must determine the initial and boundary conditions. The initial conditions are those of no flow rate or pressure variations in the system for $\tau=0$, $\delta\bar{G}_\tau=0$ and $\delta\bar{p}=0$ (the engine operating regime is steady state at the initial moment).

We obtain the boundary conditions from arguments concerning the entry of the liquid into the line and the discharge from the line.

(1) As a result of the comparatively large volume of the propellant tank and the presence of a gas "cushion" in the tank, we can assume that the pressure at the tank end (x = 0) of the line, and also the pressure in the tank itself, is constant in the oscillatory regimes $[\delta\bar{p}(\tau, 0)=0]$. Consequently, for x = 0

$$\frac{\partial\delta\bar{G}_\tau(\tau,0)}{\partial x}=0. \tag{9.20}$$

Neglecting the inertia of the liquid in the injector head cavity, we can assume that at any instant of time the propellant flow rate through the terminal section of a feed line of length l equals the flow rate through the injectors, i.e., for $x=l$

$$G_\tau(\tau, l)=G_\tau(\tau)=\chi\sqrt{\bar{p}(\tau, l)-\bar{p}_\kappa}.$$

Neglect of the inertia in the limits of the injector head simplifies the problem, since the propellant flow rate through the injectors can be expressed by the same formula as for a short feed line.

Linearization of the quadratic dependence of the flow rate on the pressure differential, performed using the same technique used in the preceding section, transforms this boundary condition to the following form:
for $x=l$, i.e., at the inlet to the injector head cavity,

$$\delta\bar{G}_\tau(\tau, l)=\delta\bar{G}_\tau(\tau)=\frac{\delta\bar{p}(\tau, l)-\delta\bar{p}_\kappa(\tau)}{\Delta\bar{p}_\phi}. \tag{9.21}$$

Here, as before $\Delta\bar{p}^{\circ}_{inj}$ denotes twice the relative pressure drop across the injectors in the steady state regime

$$\Delta\bar{p}^{\circ}_{\phi}=\frac{2\Delta p^{\circ}_{\phi}}{p^{\circ}_{k}}=\frac{2[p^{*}(l)-p^{\circ}_{k}]}{p^{\circ}_{k}}; \tag{9.22}$$

where the overbar denotes the dimensionless variations of the corresponding parameters. The pressure variation is

$$\delta\bar{p}(\tau, l)=\frac{p(\tau, l)-p^{*}(l)}{p^{\circ}_{k}} \tag{9.23}$$

where $p^{*}(l)$ is the value of the pressure at the end of the feed line attached to the injection head cavity, equal to the propellant pressure ahead of the injectors $(p^{*}(l)=p^{\circ}_{inj})$.

For the subsequent transformations it is better to differentiate the boundary Condition (9.21) with respect to time

$$\frac{\partial\bar{G}_{\tau}(\tau, x)}{\partial\tau}=1/\Delta\bar{p}^{\circ}_{\phi}\left(\frac{\partial\bar{p}(\tau, x)}{\partial\tau}-\frac{\partial\bar{p}_{k}(\tau)}{\partial\tau}\right)=0.$$

After this we make the change

$$-\frac{\partial\bar{p}(\tau, x)}{\partial\tau}=\frac{\varrho a^{2}w^{\circ}}{p^{\circ}_{k}}\frac{\partial\bar{G}_{\tau}(\tau, x)}{\partial x}.$$

Thus we have obtained the second boundary condition for $x=l$ in the final form

$$\frac{\partial\bar{G}_{\tau}(\tau, l)}{\partial\tau}+\frac{\bar{p}_{w}a}{\Delta\bar{p}^{\circ}_{\phi}}\frac{\partial\bar{G}_{\tau}(\tau, l)}{\partial x}+\frac{\partial\bar{p}_{k}(\tau)}{\Delta\bar{p}^{\circ}_{\phi}\partial\tau}=0, \tag{9.24}$$

where

$$\bar{p}_{w}=\frac{\varrho w^{\circ}a}{p^{\circ}_{k}}. \tag{9.25}$$

2. Derivation of stability boundary equation.

The combination of Equations (9.17), (9.19) and their boundary conditions (9.20), (9.24) constitutes a system of linear differential equations containing a time-lag term

$L[\delta\bar{p}_k(s)]$

ure drop

(9.22)

e corres-

$$\left.\begin{aligned}
&\theta_k \frac{d\delta\bar{p}_k(\tau)}{d\tau} + \delta\bar{p}_k(\tau) = \delta\bar{G}_\tau(\tau-\tau_k, l);\\
&\frac{\partial^2\delta\bar{G}_\tau(\tau,x)}{\partial\tau^2} - a^2\frac{\partial^2\delta\bar{G}_\tau(\tau,x)}{\partial x^2} = 0;\\
&\frac{\partial\delta\bar{G}_\tau(\tau,0)}{\partial x} = 0;\\
&\frac{\partial\delta\bar{G}_\tau(\tau,l)}{\partial\tau} + \frac{\bar{r}_\omega a}{\Delta\bar{p}_\phi^\circ}\frac{\partial\delta\bar{G}_\tau(\tau,l)}{\partial x} + \frac{\partial\delta\bar{p}_k(\tau)}{\Delta\bar{p}_\phi^\circ\partial\tau} = 0.
\end{aligned}\right\} \qquad (9.26)$$

(9.23)

feed line
the pro-
$_{ij}$).

We shall use the operator method to obtain the relationship between the defining parameters at the system stability boundary. Then the System (9.26) is written in transforms as

erentiate

$$(\theta_k s + 1)\, L[\delta\bar{p}_k(s)] = L[\delta\bar{G}_\tau(s,l)]\, e^{-s\tau_k}; \qquad (9.27)$$

$$s^2 L[\delta\bar{G}_\tau(s,x)] - a^2\frac{d^2L[\delta\bar{G}_\tau(s,x)]}{dx^2} = 0. \qquad (9.28)$$

$$\frac{dL[\delta\bar{G}_\tau(s,0)]}{dx} = 0; \qquad (9.29)$$

$$sL\left[\delta\bar{G}_\tau(s,l)\right] + \frac{\bar{r}_\omega a}{\Delta\bar{p}_\phi^\circ}\frac{dL[\delta\bar{G}_\tau(s,l)]}{dx} + \frac{s}{\Delta\bar{p}_\phi^\circ}L[\delta\bar{p}_k(s)] = 0. \qquad (9.30)$$

Thus the Laplace transform has converted the original basic partial differential equations into ordinary differential equations. The solution of (9.28) is obtained in the form

n the

$$L[\delta\bar{G}_\tau(s,x)] = Ae^{\frac{sx}{a}} + Be^{-\frac{sx}{a}}$$

(9.24)

which is easily verified by simple substitution.

Differentiating this equation with respect to x and using the boundary Condition (9.29), we obtain equality of the constants of integration

(9.25)

$$A = B.$$

undary
rential

Then

$$L[\delta\bar{G}_\tau(s,x)] = A\left(e^{\frac{sx}{a}} + e^{-\frac{sx}{a}}\right) = 2A\cosh\frac{sx}{a}. \qquad (9.31)$$

Excluding the variable ν from the chamber Equation (9.27) and the second boundary Condition (9.30), we obtain

$$sL[\delta\bar{G}_\tau(s,l)]+\frac{\bar{r}_w a}{\Delta\bar{p}_\phi^\circ}\frac{dL[\delta\bar{G}_\tau(s,l)]}{dx}+\frac{1}{\Delta\bar{p}_\phi^\circ}\frac{se^{-s\tau_\kappa}L[\delta\bar{G}_\tau(s,l)]}{t_\kappa s+1}=0. \tag{9.32}$$

We use (9.31) to find the values of the function $L[\delta\bar{G}_\tau]$ and its derivative for $x=l$:

$$L[\delta\bar{G}_\tau(s,l)]=2A\,\mathrm{ch}\,\frac{sl}{a};$$
$$\frac{dL[\delta\bar{G}_\tau(s,l)]}{dx}=2A\,\frac{s}{a}\,\mathrm{sh}\,\frac{sl}{a}.$$

Substituting these expressions into (9.32), we obtain

$$A\left[\Delta\bar{p}_\phi^\circ\,\mathrm{ch}\,\frac{sl}{a}+\bar{p}_w\,\mathrm{sh}\,\frac{sl}{a}+\frac{e^{-s\tau_\kappa}}{t_\kappa s+1}\,\mathrm{ch}\,\frac{sl}{a}\right]=0.$$

For the existence of a nontrivial solution ($A\neq 0$) it is necessary that the bracketed expression equal zero. We can finally write

$$\Delta\bar{p}_\phi^\circ+\bar{p}_w\,\mathrm{th}\,\frac{sl}{a}+\frac{e^{-s\tau_\kappa}}{t_\kappa s+1}=0. \tag{9.33}$$

This is the characteristic equation of the system. We obtain the equations for constructing the LRE stability boundary and for calculating the oscillation frequency ω on this boundary by substituting the value $s=i\omega$ into (9.33)

$$\Delta\bar{p}_\phi^\circ+\bar{p}_w\,\mathrm{th}\,\frac{i\omega l}{a}+\Delta\bar{p}_\phi^\circ t_\kappa i\omega+\bar{p}_w t_\kappa i\omega\,\mathrm{th}\,\frac{i\omega l}{a}+e^{-i\omega\tau_\kappa}=0 \tag{9.34}$$

Then we use the known relations

$$\left.\begin{aligned}\mathrm{th}\,\frac{i\omega l}{a}&=i\,\mathrm{tg}\,\frac{\omega l}{a}\\ e^{-i\omega\tau_\kappa}&=\cos\omega\tau_\kappa-i\sin\omega\tau_\kappa\end{aligned}\right| \tag{9.35}$$

and

on (9.27)

to write (9.34) in the form

$$\Delta\bar{p}_{\Phi}^{\circ}-\bar{p}_{\omega}\theta_{\kappa}\omega\operatorname{tg}\frac{\omega l}{a}+\cos\omega\tau_{\kappa}+i\left(\bar{p}_{\omega}\operatorname{tg}\frac{\omega l}{a}+\Delta\bar{p}_{\Phi}^{\circ}\theta_{\kappa}\omega-\sin\omega\tau_{\kappa}\right)=0. \tag{9.36}$$

(9.32)

Equating the real and imaginary parts of this equation to zero, we obtain the system of two equations

and its

$$\cos\omega\tau_{\kappa}=-\bar{p}_{\omega}\theta_{\kappa}\omega\operatorname{tg}\frac{\omega l}{a}-\Delta\bar{p}_{\Phi}^{\circ}; \tag{9.37}$$

$$\sin\omega\tau_{\kappa}=\bar{p}_{\omega}\operatorname{tg}\frac{\omega l}{a}+\Delta\bar{p}_{\Phi}^{\circ}\theta_{\kappa}\omega. \tag{9.38}$$

After elementary transformations this system reduces to the form

$$\Delta\bar{p}_{\Phi}^{\circ 2}=\frac{1}{\omega^{2}\theta_{\kappa}^{2}+1}-\bar{p}_{\omega}^{2}\operatorname{tg}^{2}\frac{\omega l}{a}; \tag{9.39}$$

$$\operatorname{tg}\omega\tau_{\kappa}=\frac{\Delta\bar{p}_{\Phi}^{\circ}\omega\theta_{\kappa}+\bar{p}_{\omega}\operatorname{tg}\frac{\omega l}{a}}{-\Delta\bar{p}_{\Phi}^{\circ}+\bar{p}_{\omega}\omega\theta_{\kappa}\operatorname{tg}\frac{\omega l}{a}}. \tag{9.40}$$

is necessary
rite

(9.33)

These formulas express the equations of the stability boundary for the case of a step-function propellant burnup law. In order to write these equations in dimensionless parameters, we select as the time scale the quantity l/a — the time for a sound wave to travel the length of the line. We introduce the following notations

obtain the
or calculat-
uting the

dimensionless circular frequency $\bar{\omega}=\frac{\omega l}{a}$ (9.41)

dimensionless transformation time $\bar{\tau}_{\kappa}=\frac{\tau_{\kappa}}{\frac{l}{a}}$ (9.42)

dimensionless residence time $\bar{\tau}^{\circ}=\frac{\theta_{\kappa}}{\frac{l}{a}}$ (9.43)

(9.34)

Then (9.39) and (9.40) may be written in the form

$$\Delta\bar{p}_{\Phi}^{\circ}=\pm\sqrt{\frac{1}{1+\bar{\omega}^{2}\bar{\tau}^{\circ 2}}-\bar{p}_{\omega}^{2}\operatorname{tg}^{2}\bar{\omega}}, \tag{9.44}$$

(9.35)

$$\operatorname{tg}\bar{\omega}\bar{\tau}_{\kappa}=\frac{\Delta\bar{p}_{\Phi}^{\circ}\bar{\omega}\bar{\tau}^{\circ}+\bar{p}_{\omega}\operatorname{tg}\bar{\omega}}{-\Delta\bar{p}_{\Phi}^{\circ}+\bar{p}_{\omega}\bar{\omega}\bar{\tau}^{\circ}\operatorname{tg}\bar{\omega}}. \tag{9.45}$$

3. Analysis and plotting of the stability boundary.

In accordance with (9.44) and (9.45), the stability of the operation of a LRE with feed lines is defined by the following four parameters: $\bar{\tau}_w$, $\bar{\tau}^*$, $\Delta\bar{p}^*_{inj}$ and $\bar{p}_w$. The dimensionless parameter $\bar{p}_w$, which is expressed by (9.25), is the ratio of the impact pressure which occurs with instantaneous retardation of the liquid to the pressure in the chamber.

For the same reasons discussed in the preceding section, it is advisable here again to plot the stability boundaries in the plane of the parameters $\Delta\bar{p}^*_{inj}$ $\bar{\tau}_w$ leaving the other two parameters ($\bar{\tau}^*$ and p_w as variable constants. Before turning to the construction of the stability boundary, we shall note some peculiarities of the system in question which result from an analysis of the derived equations. First of all, it can be shown that just as in the case of propulsive systems with short feed lines oscillations are impossible if

$$\Delta\bar{p}^*_\phi = \frac{2\Delta p^*_\phi}{p^*_w} > 1. \tag{9.46}$$

In fact, we have from (9.44)

$$\bar{\tau}^* = +\frac{1}{\omega}\sqrt{\frac{1}{\Delta\bar{p}^{*2}_\phi + \bar{p}^2_w \operatorname{tg}^2\bar{\omega}} - 1}.$$

Since the quantity $\bar{\tau}^*$ by definition can have only a real and positive value, the following inequality must be satisfied

$$\frac{1}{\Delta\bar{p}^{*2}_\phi + \bar{p}^2_w \operatorname{tg}^2\bar{\omega}} - 1 > 0,$$

which after obvious transformations takes the form

$$(1 - \Delta\bar{p}^{*2}_\phi)\operatorname{ctg}^2\bar{\omega} > \bar{p}^2_w.$$

This implies that for satisfaction of the inequality it is necessary that $\Delta\bar{p}^*_{inj} < 1$ and then oscillations are possible. Otherwise, i.e., for $\Delta\bar{p}^*_{inj} > 1$, the quantity $\bar{\tau}^*$ will be imaginary, which in

accordance with the Condi ion (9.46) for absolute engine stability means that oscillations are impossible for any values of the operating regime and geometric parameters.

We note that the limitations on the frequency of the excited oscillations can be derived from the same Equation (9.44). Since $\Delta\bar{p}'_{inj}$ is a real and positive quantity, frequencies either near $\bar{\omega}=0$, or near $\bar{\omega}=n\pi$ ($n = 1, 2, 3,....$) are possible. This is explained by the fact that $\operatorname{tg}\bar{\omega}$ is a periodic function, and for the indicated frequencies the reactance $\bar{p}_w \operatorname{tg}\bar{\omega}$ of the liquid column is close to zero. The value $\bar{\omega}=n\pi$ corresponds to the natural frequencies of acoustic oscillations of the liquid column in the line, i.e., to the frequencies $f=na/2\pi$. The value n = 1 corresponds to the fundamental tone, the values n = 2, 3,... correspond to its second, third, and so on harmonics.

Thus the integer n indicates the order of the harmonic of the free oscillations of the liquid in the line. As a rule, in practice we can restrict ourselves to the calculation of the first three harmonics, since as a result of the influence of friction the higher-order harmonics damp out quite rapidly.

Ir the case of a complex line, the natural frequencies of the liquid column oscillations are calculated using the formulas presented in Chapter 7.

For small values of an angle, not exceeding $\pi/6$ its tangent may be replaced by the angle itself. Then we obtain the approximate equality

$$\bar{p}_w \operatorname{tg}\bar{\omega}\approx\bar{p}_\kappa\bar{\omega}.$$

Replacing herein $\bar{p}_\kappa$ and $\bar{\omega}$ by their expressions from (9.25) and (9.41), we obtain

$$\bar{p}_w \operatorname{tg}\bar{\omega}\approx\omega\bar{l}_p$$

where $\theta_l = \frac{\varrho w^* l}{p_k^*} \cdot \frac{\varrho w^*}{p_k^*} \cdot \frac{l}{w^*}$ is a quantity which is proportional to the line length and has the dimension of time.

The product $\bar{p}_w \operatorname{tg} \bar{\omega}$ written in this form is defined by the single time dependent constant θ_l. We note that the same relation is obtained if we ignore liquid compressibility ($a \to \infty$ for an incompressible liquid)

$$\lim_{a \to \infty} \left[\bar{p}_w \operatorname{tg} \frac{\omega l}{a} \right] = \frac{\varrho w^* a}{p_k^*} \frac{\omega l}{a} \lim \frac{\operatorname{tg} \frac{\omega l}{a}}{\frac{\omega l}{a}} = \omega \frac{\varrho w^* l}{p_k^*} = \omega \theta_l$$

since $\lim_{\bar{\omega} \to 0} \frac{\operatorname{tg} \bar{\omega}}{\bar{\omega}} = 1$.

Consequently, liquid compressibility can be ignored up to values $\frac{\omega l}{a} \leqslant \frac{\pi}{6}$ or up to frequencies $f = \frac{\omega}{2\pi} \leqslant \frac{a}{12l}$ Hz. As an example, we take the propellant line length $l = 2$ m and the speed of sound as about $a \approx 1200$ m/sec. Then the limiting frequency up to which compressibility may be neglected is f = 40 Hz. Since the frequencies observed in practice usually exceed this value, in the majority of cases liquid compressibility may be neglected.

The stability boundaries in the plane of the parameters $(\bar{\tau}_k - \Delta\bar{\rho}_{inj})$ are calculated using (9.44) and (9.45) in the following sequence.

(1) We designate specific, constant values of the parameters $\bar{p}_k, \bar{\tau}^*$ and the harmonic order n.

(2) We take a series of values of the dimensionless frequencies $\bar{\omega}$ and for each of them we calculate the corresponding values of $\Delta\bar{p}^*_{inj}$ using (9.44).

(3) For the same values of $\bar{\omega}$ and the correspondingly calculated values of $\Delta\bar{p}^*_{inj}$ we find the quantities $\bar{\omega}\bar{\tau}_k$ using (9.45).

We note here that the quantity $\bar{\omega}\bar{\tau}_k$ is defined to within $2k\pi$ (k = 1, 2, 3,...). The value k = 0 drops out, since in this case we obtain negative values of the obviously positive quantity $\bar{\omega}\bar{\tau}_k$. In order to see this we transform (9.45) as follows.

We introduce the notations

$$\bar{\omega}\bar{\tau}^{\circ} = \operatorname{tg}\beta;$$

$$\frac{\bar{P}_{\omega}}{\Delta\bar{P}_{\phi}^{\circ}} = \operatorname{tg}\bar{\omega} = \operatorname{tg}\alpha.$$

With account for these notations (9.45) takes the form

$$\operatorname{tg}\bar{\omega}\bar{\tau}_{\kappa} = -\frac{\operatorname{tg}\beta + \operatorname{tg}\alpha}{1 - \operatorname{tg}\beta\operatorname{tg}\alpha} = -\operatorname{tg}(\alpha+\beta),$$

which implies that

$$\operatorname{tg}\bar{\omega}\bar{\tau}_{\kappa} + \operatorname{tg}(\alpha+\beta) = \frac{\sin(\bar{\omega}\bar{\tau}_{\kappa} + \alpha + \beta)}{\cos\bar{\omega}\bar{\tau}_{\kappa}\cos(\alpha+\beta)} = 0.$$

In order that this equality be satisfied, we must set

$$\bar{\omega}\bar{\tau}_{\kappa} + \alpha + \beta = 2k\pi.$$

Consequently,

$$\bar{\tau}_{\kappa} = \frac{2k\pi - (\alpha+\beta)}{\bar{\omega}}$$

Hence we see that the case k = 0 yields $\bar{\omega}\bar{\tau}_{\kappa} < 0$. For $k \neq 0$ oscillations are possible with the same dimensionless frequency $\bar{\omega}$ but for several values of $\bar{\tau}_{\kappa}$ differing from one another by the magnitude $\frac{2\pi}{\bar{\omega}}$.

(4) The computed points $(\Delta\bar{P}_{inj}^{\circ}, \bar{\tau}_{\kappa})$ are used to plot the stability boundary curve in the plane of these parameters.

Figure 9.11 shows the complete stability boundary in the plane of the parameters $\Delta\bar{P}_{inj}^{\circ}$ and $\bar{\tau}_{\kappa}$ for constant parameters $\bar{p}_{\kappa} = 2$, and for values n = 1, 2 and k = 1, 2. The stability region is located to the right of the curves, just as in the case of the very simple LRE scheme without feed lines. This region is bounded by the smooth upper curve, corresponding to the low frequencies, and the tooth-like curve for which the oscillation frequencies are close to the line natural frequencies.

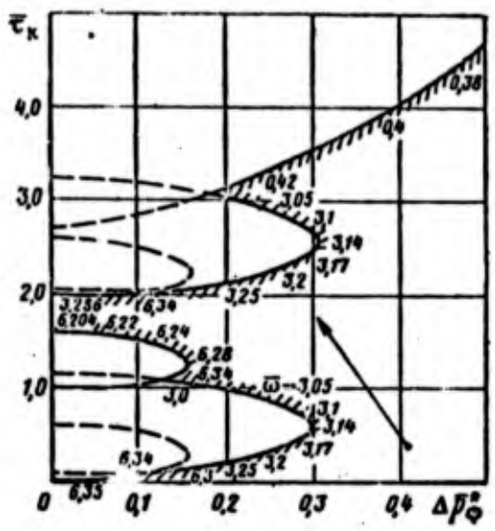

Figure 9.11. Complete stability boundary for monopropellant LRE with long line.

In this particular case, we see from the figure that the "teeth" corresponding to the values n = 1, k > 1, and n = 2, k > 2, do not alter the stability region.

As before, for the computational case being considered the operating point $(\Delta\bar{p}_{inj}, \bar{\tau}_к)$ moves to the left and upward as shown by the arrow in Figure 9.11 with reduction of the engine thrust by means of reduction of the pressure in the propellant tank. In this case the stable and unstable regimes may alternate. Here it is interesting, and at first glance unexpected, that in the figure there are regions within the limits of which stable operating regimes are possible even for $\Delta\bar{p}_{inj}=0$ i.e., for zero pressure drop across the injectors. This is a result of the favorable influence of the feed lines on engine low-frequency stability: for certain frequencies the lines play the role of such effective stabilizing elements that any oscillations which are excited are damped, even in the absence of a pressure differential across the injectors.

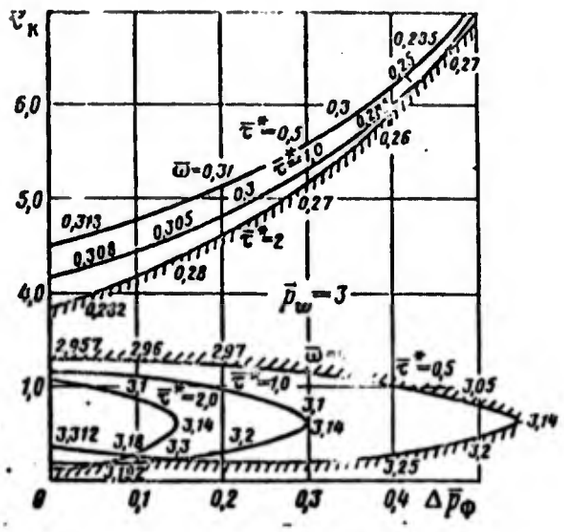

Figure 9.12. Effect of parameter $\eta_к$ (or $\frac{\tau}{T_к}$) on stability of operation of LRE with long line.

The influence of the parameters τ' and $p_к$ on the position of the stability boundary can be traced in Figures 9.11 and 9.12. Increase of $\bar{p}_w$ leads to narrowing of the teeth without altering their location and length, and also shifts the upper boundary markedly, thereby increasing the number of teeth (the value of k). In order to analyze the effect of the parameter l/a (the dimensional time for a sound wave to traverse the feed line) we turn to Figure 9.13. The influence of this parameter on LRE operating stability may be quite varied. On the one hand, increase of l/a leads to contraction of the stability region due to lengthening and broadening of the teeth; on the other hand, this increase leads to a considerable expansion of the stability region (movement of the upper boundary). In this process the tips of the teeth move upward; however, for large values of l/a we must take into account the location of the teeth corresponding to the harmonics of the fundamental. It is interesting to note that with a change of l/a in the case n = 1 the tips of the teeth move along the dashed curve ($l=0$)

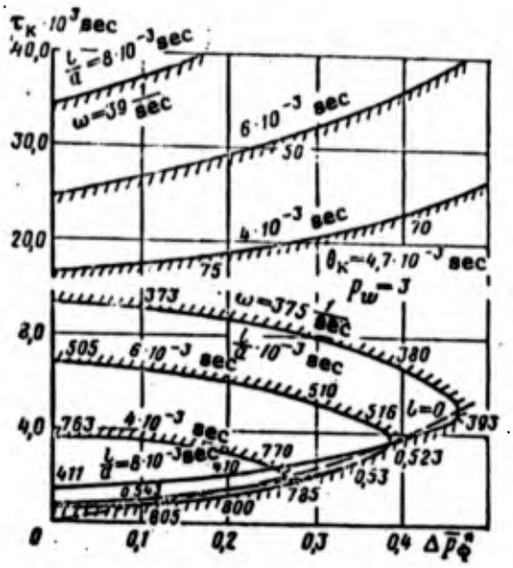

Figure 9.13. Effect of dimensional time l/a on stability of operation of LRE with long line.

In conclusion we note that the Equations (9.14), which express the analogous relation for the case of no feed line, are obtained as a particular case from Equations (9.44) and (9.45), which relate the parameters on the stability boundary of the power plant in question. In order to see this we must set $l=0$ and consider the notations for the dimensionless parameters (9.41), (9.42) and (9.43).

In spite of the fact that in comparison with the very simple LRE model in this case we have taken into consideration many favorable factors (feed line length, inertia of the motion, and liquid compressibility), which have a significant influence on LRE operating stability. Here again we must admit that the calculated results are very approximate and are not always in quantitative agreement with experimental data. However, this theory yields a correct qualitative picture of the influence of the basic operating condition and geometric parameters on LRE operating stability.

We have restricted ourselves to examination of the monopropellant LRE with pressure feed. The bipropellant LRE has two propellant lines operating in parallel. The introduction of the second line leads to

new dynamic qualities of the system. However, the examination of the problem in general form and the construction of the stability boundary in this case run into major difficulties even for the pressure feed system.

The pressure feed system with long feed lines is used primarily only for test stand LRE operations. The turbopump feed system with short lines has found extensive application in actual LRE [6], [70], [124], [9].

§ 5. "Intrachamber" Instability

It follows from the Crocco Equation [78]

$$\theta_{\kappa}\frac{d\,\delta\bar{p}_{\kappa}(\tau)}{d\tau}+\delta\bar{p}_{\kappa}(\tau)=\delta\bar{G}_{\tau}(\tau-\tau_{\kappa})+n\left[\delta\bar{p}_{\kappa}(\tau)-\delta\bar{p}_{\kappa}(\tau-\tau_{1})\right]$$

that low-frequency oscillations can arise even in the absence of dependence of the feed system operation on the combustion chamber pressure, i.e., without feedback between p_K and the propellant mass flow rate G_T through the injectors.

Actually, for a constant propellant flow rate G_T = const or $\delta\bar{G}_{\tau}=0$) low-frequency oscillations can appear as a result of the effect of variations of the physical parameters (pressure and temperature) on the burning velocity rate. This mechanism for the self-excitation of the oscillations, arising regardless of the feed system characteristics, was studied by Crocco [78] and termed "intrachamber" instability. The characteristic feature of this model of the working process in the LRE combustion chamber is that Crocco limits the overall transformation time to two components: the atmoization and mixing time, which is considered to be independent of the pressure and temperature variations in the chamber, and the time for heating-up, vaporization, and burning itself, which depends on the variations of these parameters of the combustion products.

We recall that in the Crocco equation τ_{κ} is the total transformation time, τ_1 is the variable part of the total transformation time,

n is the interaction index. The presence in this equation of time-delay functions with two different transformation times complicates markedly the theoretical study of the question. Therefore, and also because of the absence of reliable information on the magnitudes of these times, we take them to be equal to one another $\tau_1=\tau_K$ and dependent only on the combustion chamber pressure. For the case of small perturbations the change of the combustion temperature, and consequently the effect of this factor on the magnitude of τ_K, can be neglected. Then the chamber equation takes the form

$$\theta_K\frac{d\overline{\delta p}_K(\tau)}{d\tau}+\overline{\delta p}_K(\tau)=\overline{\delta G}_T(\tau-\tau_K)+n\left[\overline{\delta p}_K(\tau)-\overline{\delta p}_K(\tau-\tau_K)\right].$$

We first study this equation for the case of constant propellant flow rate through the injectors, i.e., for $\delta G_T=0$. In this case

$$\theta_K\frac{d\overline{\delta p}_K(\tau)}{d\tau}+(1-n)\overline{\delta p}_K(\tau)+n\overline{\delta p}_K(\tau-\tau_K)=0. \qquad (9.47)$$

The characteristic equation for (9.47) will be

$$\theta_K s+1-n+ne^{-\tau_K s}=0 \qquad (9.48)$$

Substituting $s=i\omega$ into (9.48) and separating the real and imaginary parts, we obtain two equations

$$\left.\begin{aligned} n\cos\omega\tau_K&=n-1;\\ n\sin\omega\tau_K&=\omega\theta_K,\end{aligned}\right\} \qquad (9.49)$$

which after obvious transformations can be written as

$$\left.\begin{aligned} \omega^2\theta_K^2&=2n-1;\\ \operatorname{tg}\omega\tau_K&=-\frac{\omega\theta_K}{1-n},\end{aligned}\right\} \qquad (9.50)$$

or

$$\left.\begin{aligned} \omega\theta_K&=\pm\sqrt{2n-1},\\ \omega\tau_K&=k\pi-\operatorname{arc}\operatorname{tg}\frac{\sqrt{2n-1}}{1-n}.\end{aligned}\right\} \qquad (9.51)$$

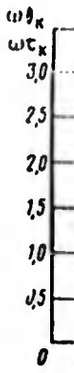

Figure 9.14.
and $\omega\tau_K$ on

case, in whi
lations in t
of the very
accordance w

Then (9

Its characte

Setting
to zero, we

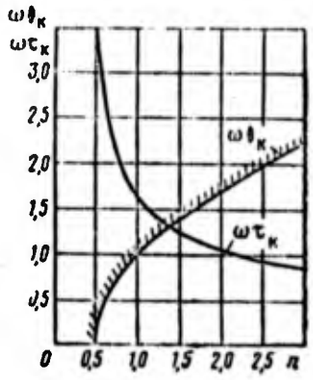

Figure 9.14. Dependence of $\omega\vartheta_к$ and $\omega\tau_к$ on interaction exponent n.

Curves of the dependences of $\omega\vartheta_к$ and $\omega\tau_к$ on the magnitude of the interaction index n, calculated using (9.51), are shown in Figure 9.14 for the fundamental harmonic (k = 1). Analysis shows that for $n < 1/2$ the system is always intrinsically stable, regardless of the magnitude of the variable transformation time. Increase of n leads to destabilization of the combustion chamber process.

Now let us examine another case, in which the propellant flow rate depends on the pressure oscillations in the chamber $(\delta\bar{G}_т \neq 0)$. We restrict this study to examination of the very simple LRE model without account for the feed lines. In accordance with (9.9) we have for this case

$$\delta\bar{G}_т(\tau-\tau_к)=-\frac{\delta\bar{p}_к(\tau-\tau_к)}{\Delta\bar{p}_ф}. \tag{9.48}$$

Then (9.47) transforms to the form

$$\vartheta_к\frac{d\delta\bar{p}_к(\tau)}{d\tau}+\delta\bar{p}_к(\tau)+\frac{1}{\Delta\bar{p}_ф}\delta\bar{p}_к(\tau-\tau_к)-n[\delta\bar{p}_к(\tau)-\delta\bar{p}_к(\tau-\tau_к)]=0. \tag{9.49}$$

Its characteristic equation will be

$$\vartheta_к s+1-n+\left(n+\frac{1}{\Delta\bar{p}_ф}\right)e^{-s\tau_к}=0. \tag{9.50}$$

Setting, as usual, $s=i\omega$ and equating the real and imaginary parts to zero, we obtain two equations defining the stability boundary

$$\left.\begin{aligned}\frac{(1-n)\Delta\bar{p}_ф}{n\Delta\bar{p}_ф+1}&=\sqrt{\frac{1}{1+\left(\frac{\omega\vartheta_к}{1-n}\right)^2}};\\ \operatorname{tg}\omega\tau_к&=-\frac{\omega\vartheta_к}{1-n}.\end{aligned}\right\} \tag{9.51}$$

We note that for n = 0 these equations become the equations (9.14), derived for the very simple model with a constant transformation time. In order to give these equations the form of the Equations (9.14), which were analyzed previously, we introduce the notations

$$\frac{(1-n)\Delta\bar{p}_\phi}{n\Delta\bar{p}_\phi+1}=(\Delta\bar{p}_\phi)_n;$$

$$\frac{\omega\theta_\kappa}{1-n}=(\omega\theta_\kappa)_n.$$

Applying these notations in (9.54), we obtain

$$\left.\begin{aligned}(\Delta p_\phi)_n&=\sqrt{\frac{1}{1+(\omega\theta_\kappa)_n^2}};\\ \operatorname{tg}\omega\tau_\kappa&=-(\omega\theta_\kappa)_n.\end{aligned}\right\} \qquad (9.55)$$

In studying the simplified LRE model — the Natanzon model — a criterion for unconditional stability was obtained, i.e., stability for any values of the transformation time constant τ_κ. This criterion has the form of the inequality $\Delta\bar{p}_{inj}>1$. In the present case we can write formally the analogous inequality $(\Delta\bar{p}_{inj})_n>1$, but it will represent stability only for n < 1/2. This means that for n > 1/2 it is not possible to achieve unconditional stability of the LRE even for very large pressure drops across the injectors. Consequently, for n > 1/2 the stable engine operating regimes will be found in a definite range of values of the transformation time τ_κ.

The results of this theoretical analysis are shown graphically in Figure 9.15, where the stability boundaries calculated using (9.54) are plotted in the plane of the parameters $\Delta\bar{p}_{inj}$ and τ_K for several values of n. Also shown are the stability boundaries for the very simple model (n = 0), plotted using Equations (9.14). We see that the stability region contracts with increase of the interaction index n.

Generalizing the results of this analysis of the Crocco equation, we can draw the following conclusion. For a constant propellant flow rate (G_T = const) or a constant pressure drop across the nozzle injectors (Δp_{inj} = const), low frequency oscillations may exist which are due to

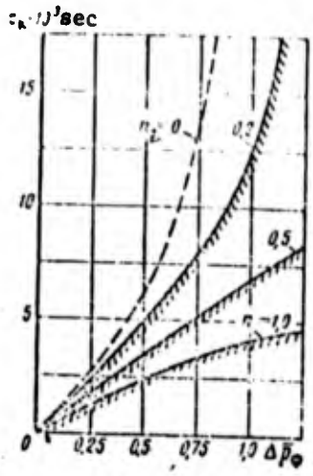

Figure 9.15. Effect of interaction exponent n on location of stability boundary of simple LRE model (for $\theta_k = 5 \cdot 10^{-3}$ sec)

the interaction index $n \neq 0$ (intrachamber instability). Account for the dependence of G_T or Δp_{inj} on the pressure oscillations in the chamber leads to still greater destabilization of the engine (see Figure 9.15).

§ 6. Low-Frequency Instability of Bipropellant LRE

1. Simplifying assumptions, basic equations, and characteristic equation of the system.

The bipropellant LRE has two feed lines connected in parallel. The introduction of the second line leads to the situation in which the system acquires new dynamic properties as a result of the mutual influence of the flow of the propellants in these lines.

In explaining the basic dynamic properties of the bipropellant engine, we shall limit ourselves to the examination of the pressure-fed engine arrangement (Figure 9.16). In addition, we introduce several simplifying assumptions.

(1) The burnup curve is a step function and the transformation time is constant, i.e., $\tau_k = \text{const}$.

(2) The temperature of the gas in the chamber and its physical constants are constant, i.e., the combustion chamber is considered a large capacitance without account for the variation of the thermal and

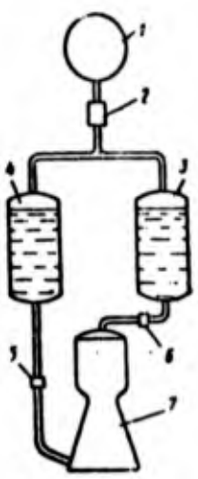

Figure 9.16. Bipropellant LRE with bottled gas feed system:

1) bottle; 2) reducer; 3 and 4) tanks; 5 and 6) valves; 7) combustion chamber

energetic properties of the gaseous stream due to variation of the propellant mixture ratio. If we have in mind the study of stability in the small, then for small deviations of the mixture ratio from its nominal value the gas temperature and composition vary only slightly, and in the first, although rough, approximation these variations can be neglected.

(3) The feed lines are inelastic, with lumped parameters, i.e., wave phenomena in the lines are not considered.

(4) The liquid propellants are incompressible.

(5) The inertia forces of the liquid in the injector head cavity are neglected.

The problem was studied in a similar formulation in [148]. We shall analyze a system (with lumped parameters) consisting of three dynamic elements: the combustion chamber and two feed lines. One element, namely the combustion chamber, is an element with time lag.

To study the combustion chamber stability, we write the system of linearized equations, including the equations of the dynamics of the indicated elements (see [9.10] and [5.83])

$$\left.\begin{aligned} \theta_{\kappa}\frac{d\overline{p}_{\kappa}}{d\tau}+\overline{p}_{\kappa}&=\overline{G}_{o}(\tau-\tau_{\kappa})+\overline{G}_{f}(\tau-\tau_{\kappa});\\ \theta_{M.o}\frac{d\overline{G}_{o}}{d\tau}+\overline{G}_{o}&=-K_{M.o}\overline{p}_{\kappa};\\ \theta_{M.f}\frac{d\overline{G}_{f}}{d\tau}+\overline{G}_{f}&=-K_{M.f}\overline{p}_{\kappa}. \end{aligned}\right\} \qquad (9.56)$$

The subscript "o" denotes oxidizer parameters, and "f" denotes fuel parameters.

Parameters which have a definite physical meaning appear in these differential equations. The parameters $\theta_к$, $\theta_{м.о}$ and $\theta_{м.ф.}$ have the dimension of time and characterize the inertia of the corresponding elements of the dynamic system. They are termed time constants and are defined by the following formulas

$$\left.\begin{aligned} \theta_к &= \frac{V_к}{F_{кр} R_к T_к}; \\ \theta_{м.о} &= \frac{l_{2o}}{2b_{1o}G_o^*}; \quad \theta_{м.ф} = \frac{l_{2г}}{2b_{1г}G_г^*}. \end{aligned}\right\} \tag{9.57}$$

The dimensionless coefficients $K_{м.о.}$ and $K_{м.ф.}$ are termed the gains of the corresponding lines and are defined as follows

$$K_{м.о} = \frac{P_{б.о}^* - P_к^*}{2b_{1o}G_o^{*2}}; \quad K_{м.г} = \frac{P_{б.г}^* - P_к^*}{2b_{1г}G_г^{*2}} \tag{9.58}$$

We see that the gains are inversely proportional to the parameter $\Delta\bar{p} = \frac{2\Delta p^*}{P_к^*}$ — twice the relative pressure drop in the line. In contrast with the parameter $\Delta\bar{p}_{inj} = \frac{2\Delta p_ф^*}{P_к^*}$ which was considered above, the parameter $\Delta\bar{p}$ is defined here in terms of the pressure drop in the corresponding lines from the tank up to and including the injectors. The parameter $\tau_к$ retains its previous meaning — the transformation time constant for a step function propellant burnup law.

The objective of the further analysis is to study the effect of the individual parameters in determining the conditions which are necessary and sufficient for the considered dynamic system, described by (9.56), to be stable. We write these equations in operator form with the aid of the Laplace transformation

$$\left.\begin{aligned} &L[\delta\bar{p}_к](\theta_к s + 1) - L[\delta\bar{G}_o]e^{-s\tau_к} - L[\delta\bar{G}_г]e^{-s\tau_к} = 0; \\ &L[\delta\bar{p}_к]K_{м.о} + L[\delta\bar{G}_o](\theta_{м.о}s + 1) = 0; \\ &L[\delta\bar{p}_к]K_{м.г} + L[\delta\bar{G}_г](\theta_{м.г}s + 1) = 0. \end{aligned}\right\} \tag{9.59}$$

To obtain the characteristic equation of this system we must exclude all the variables other than $L[\delta\bar{p}_к]$. But we can solve the problem more simply if we use the Cramer theorem, in accordance with which a system of homogeneous equations has a nonzero solution if the system

determinate equals zero

$$\Delta=\begin{vmatrix} \theta_к s+1 & -e^{-s\tau_к} & -e^{-s\tau_к} \\ K_{м.о} & \theta_{м.о}s+1 & 0 \\ K_{м.г} & 0 & \theta_{м.г}s+1 \end{vmatrix}=0. \qquad (9.60)$$

Expanding the determinant, we obtain

$$t_0 s^3+t_1 s^2+t_2 s+K_Σ(\theta_м s+1)e^{-s\tau_к}+1=0, \qquad (9.61)$$

where

$$t_0=\theta_к\theta_{м.о}\theta_{м.г};\quad t_1=\theta_к\theta_{м.о}+\theta_к\theta_{м.г}+\theta_{м.о}\theta_{м.г};\quad t_2=\theta_к+\theta_{м.о}+\theta_{м.г};$$
$$K_Σ=K_{м.о}+K_{м.г};\quad \theta_м=\frac{K_{м.о}\theta_{м.г}+K_{м.г}\theta_{м.о}}{K_{м.о}+K_{м.г}}. \qquad (9.62)$$

Equation (9.61) is the characteristic equation for the basic system with lumped parameters. It is transcendental, which is usually the case in systems with time lag. It may be simplified by expanding the exponential factor into a series and retaining the first two terms. Such a simplification was made in the studies [120] [78] of the American authors. It is quite approximate in the case in which the stability boundaries are being determined. It is better to use the D-partition method.

2. Analysis and construction of the stability boundary.

The characteristic equation shows that the parameters which define the stability of the bipropellant LRE system in question with lumped parameters are: $K_Σ$ the effective gain of the propellant lines; $\tau_к$ the time for transformation of the liquid propellant into the gaseous combustion products; τ_K the mean residence time of a gaseous particle in the combustion chamber; θ_K the effective value of the propellant line time constant; $\theta_{M.o.}$, $\theta_{M.f.}$ the propellant line time constants.

We shall derive the computational equations for contructing the stability boundary in the plane of the two parameters: $\tau_к$, $K_Σ$. Substituting the vllue $s=i\omega$ into the characteristic Equation (9.61) and separating the real and imaginary parts, we obtain the two equations

or after t
sides of t

Squar

After
transforma

We wr
in the for

Givin
to calcula
$\theta_м$ and a
then with
the gain K
from π to

Figur
considered
for $\theta_к$ = 0

$$-l_1\omega^2 + K_\Sigma \cos\omega\tau_K + K_\Sigma\theta_M\omega\sin\omega\tau_K + 1 = 0;$$
$$-l_0\omega^3 + l_2\omega + K_\Sigma\theta_M\omega\cos\omega\tau_K - K_\Sigma\sin\omega\tau_K = 0,$$

(9.60)

or after transferring the nontrigonometric functions into the right sides of the equations

$$K_\Sigma\cos\omega\tau_K + K_\Sigma\omega\theta_M\sin\omega\tau_K = l_1\omega^2 - 1;$$
$$K_\Sigma\omega\theta_M\cos\omega\tau_K - K_\Sigma\sin\omega\tau_K = l_0\omega^3 - l_2\omega.$$

(9.61)

Squaring both equalities and combining them, we obtain

$$K_\Sigma^2 = \frac{(l_0\omega^3 - l_2\omega)^2 + (l_1\omega^2 - 1)^2}{\omega^2\theta_M^2 + 1}.$$

(9.62)

After dividing one equality by the other and performing some transformations, we find

$$\operatorname{tg}\omega\tau_K = -\frac{l_0\omega^3 - l_2\omega - \theta_M l_1\omega^3 + \theta_M\omega}{l_1\omega^2 - 1 + \theta_M l_0\omega^4 - \theta_M l_2\omega^2}.$$

We write the final equation for calculating the stability boundary in the form

$$K_\Sigma = \sqrt{\frac{(l_0\omega^3 - l_2\omega)^2 + (l_1\omega^2 - 1)^2}{\omega^2\theta_M^2 + 1}}; \tag{9.63}$$

$$\tau_K = \frac{1}{\omega}\left[k\pi - \operatorname{arc\,tg}\frac{(l_0 - l_1\theta_M)\omega^3 + (\theta_M - l_2)\omega}{(l_1 - l_2\theta_M)\omega^2 + l_0\theta_M\omega^4 - 1}\right]. \tag{9.64}$$

Giving ω various values from 0 to ∞, we can use (9.63) and (9.64) to calculate the values of K_Σ and τ_K for constant values of θ_K, $\theta_{M.o.}$, $\theta_{M.f.}$, θ_M and a selected harmonic number k = 1, 2, 3,... If we take k = 1, then with variation of the circular frequency in the indicated limits the gain K_Σ varies in the range from 1 to ∞, and the product $\omega\tau_K$ varies from π to $\pi/2$.

Figure 9.17 shows the stability boundary for the operation of the considered bipropellant LRE in the plane of the parameters K_Σ and for θ_K = 0.003 sec, θ_M = 0.00222 sec, $\theta_{M.o}$ = 0.00166 sec, $\theta_{M.f.}$ = 0.0025

determinate equals zero

$$\Delta=\begin{vmatrix} \theta_к s+1 & -e^{-\tau_к s} & -e^{-\tau_к s} \\ K_{м.о} & \theta_{м.о}s+1 & 0 \\ K_{м.г} & 0 & \theta_{м.г}s+1 \end{vmatrix}=0. \qquad (9.60)$$

Expanding the determinant, we obtain

$$l_0 s^3+l_1 s^2+l_2 s+K_з(\theta_м s+1)e^{-\tau_к s}+1=0, \qquad (9.61)$$

where

$$l_0=\theta_к\theta_{м.о}\theta_{м.г};\quad l_1=\theta_к\theta_{м.о}+\theta_к\theta_{м.г}+\theta_{м.о}\theta_{м.г};\quad l_2=\theta_к+\theta_{м.о}+\theta_{м.г};$$
$$K_з=K_{м.о}+K_{м.г};\quad \theta_м=\frac{K_{м.о}\theta_{м.г}+K_{м.г}\theta_{м.о}}{K_{м.о}+K_{м.г}}. \qquad (9.62)$$

Equation (9.61) is the characteristic equation for the basic system with lumped parameters. It is transcendental, which is usually the case in systems with time lag. It may be simplified by expanding the exponential factor into a series and retaining the first two terms. Such a simplification was made in the studies [120] [78] of the American authors. It is quite approximate in the case in which the stability boundaries are being determined. It is better to use the D-partition method.

2. Analysis and construction of the stability boundary.

The characteristic equation shows that the parameters which define the stability of the bipropellant LRE system in question with lumped parameters are: $K_з$ the effective gain of the propellant lines; $\tau_к$ the time for transformation of the liquid propellant into the gaseous combustion products; τ_K the mean residence time of a gaseous particle in the combustion chamber; 0_K the effective value of the propellant line time constant; $0_{M.o.}$, $0_{M.f.}$ the propellant line time constants.

We shall derive the computational equations for contructing the stability boundary in the plane of the two parameters: $\tau_м$, $K_з$. Substituting the vllue $s=i\omega$ into the characteristic Equation (9.61) and separating the real and imaginary parts, we obtain the two equations

$$-l_1\omega^2 + K_\Sigma \cos\omega\tau_K + K_\Sigma\theta_M\omega\sin\omega\tau_K + 1 = 0;$$

(9.60)

$$-l_0\omega^3 + l_2\omega + K_\Sigma\theta_M\omega\cos\omega\tau_K - K_\Sigma\sin\omega\tau_K = 0,$$

or after transferring the nontrigonometric functions into the right sides of the equations

$$K_\Sigma\cos\omega\tau_K + K_\Sigma\omega\theta_M\sin\omega\tau_K = l_1\omega^2 - 1;$$

(9.61)

$$K_\Sigma\omega\theta_M\cos\omega\tau_K - K_\Sigma\sin\omega\tau_K = l_0\omega^3 - l_2\omega.$$

Squaring both equalities and combining them, we obtain

(9.62)

$$K_\Sigma^2 = \frac{(l_0\omega^3 - l_2\omega)^2 + (l_1\omega^2 - 1)^2}{\omega^2\theta_M^2 + 1}.$$

basic sys-
usually
expanding
t two terms.
of the
hich the
use the

After dividing one equality by the other and performing some transformations, we find

$$\operatorname{tg}\omega\tau_K = -\frac{l_0\omega^3 - l_2\omega - \theta_M l_1\omega^3 + \theta_M\omega}{l_1\omega^2 - 1 + \theta_M l_0\omega^4 - \theta_M l_2\omega^2}.$$

We write the final equation for calculating the stability boundary in the form

ry.

$$K_\Sigma = \sqrt{\frac{(l_0\omega^3 - l_2\omega)^2 + (l_1\omega^2 - 1)^2}{\omega^2\theta_M^2 + 1}}; \qquad (9.63)$$

which define
th lumped
lines; τ_K
he gaseous
s particle
ropellant
onstants.

$$\tau_K = \frac{1}{\omega}\left[k\pi - \operatorname{arc\,tg}\frac{(l_0 - l_1\theta_M)\omega^3 + (\theta_M - l_2)\omega}{(l_1 - l_2\theta_M)\omega^2 + l_0\theta_M\omega^4 - 1}\right]. \qquad (9.64)$$

Giving ω various values from 0 to ∞, we can use (9.63) and (9.64) to calculate the values of K_Σ and τ_K for constant values of θ_K, $\theta_{M.o.}$, $\theta_{M.f.}$, θ_M and a selected harmonic number k = 1, 2, 3,... If we take k = 1, then with variation of the circular frequency in the indicated limits the gain K_Σ varies in the range from 1 to ∞, and the product $\omega\tau_K$ varies from π to $\pi/2$.

acting the
K_Σ. Substi-
51) and
equations

Figure 9.17 shows the stability boundary for the operation of the considered bipropellant LRE in the plane of the parameters K_Σ and for θ_K = 0.003 sec, θ_M = 0.00222 sec, $\theta_{M.o.}$ = 0.00166 sec, $\theta_{M.f.}$ = 0.0025

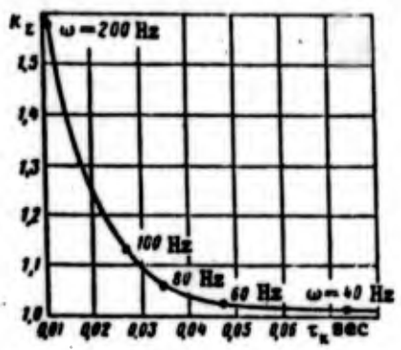

Figure 9.17. Bipropellant LRE stability boundary.

sec, and for the value K = 1, corresponding to the fundamental frequency. The zone lying below the curve is the region of stable engine operation, while the zone above the curve is the region of unstable operation.

The stability boundaries in the plane of the other parameters can be constructed similarly. Analysis shows that with increase of the pressure drop in the propellant lines the system stability increases, other conditions remaining the same. The lag time is not a physcochemical constant, but depends on the geometric and operating condition parameters of the engine. The stability also improves with reduction of this time.

Therefore, if a projected engine is found to be unstable, the low-frequency oscillations can be suppressed in any frequency range by suitable alteration of its parameters.

A more detailed qualitative examination of the dynamic stability of the bipropellant power plant has been carried out in specialized studies (for example, [3], [184]).

§ 7. Experimental Data on High-Frequency Axial Oscillations

1. Analysis of oscillograms.

To clarify the nature of the high-frequency oscillations in LRE we shall examine several types of oscillographic recordings of the combustion chamber pressure [9].

Figure 9.18a shows an example of the superpositioning of high-fre-

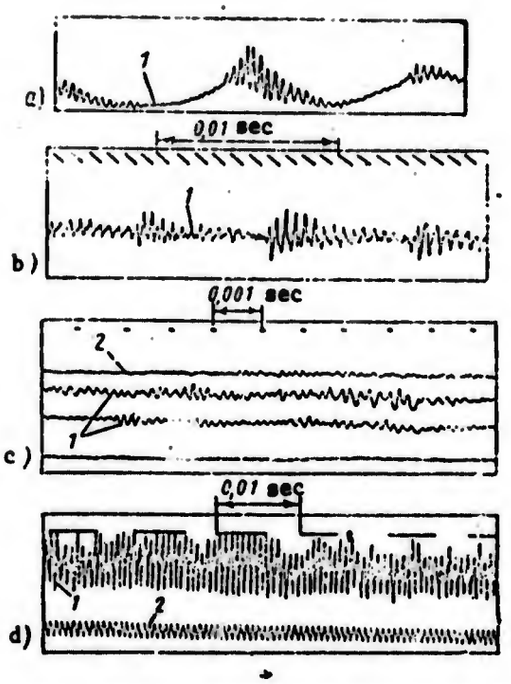

Figure 9.18. Oscillograms of pressure in combustion chamber during high-frequency instability:

1) chamber pressure; 2) pressure ahead of oxidizer injector

quency pressure oscillations on low-frequency oscillations, which usually occurs with low chamber pressures. Here the high-frequency instability corresponds primarily to the pressure peaks which develop in the low-frequency oscillations, i.e., amplification of the oscillations is observed for the high pressures. Figure 9.18b shows superpositioning of high- and low-frequency oscillations and their propagation through the chamber. We see that the superpositioning results in gradual amplification of the oscillations with subsequent rapid decay.

The high-frequency oscillations can sometimes have very large amplitudes, reaching $\pm$50 - 100% of the magnitude of the average combustion chamber pressure (see Figure 9.18d).

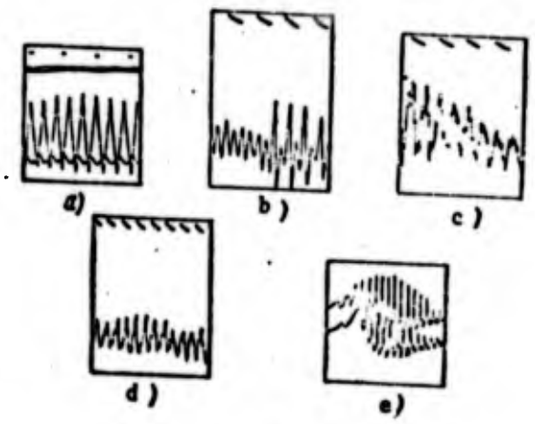

Figure 9.19. Pressure oscillations in chamber and frequency spectra for high-frequency instability (timing marks 10^{-3} sec).

As for the forms of the high-frequency oscillations, they can be quite varied. The most typical oscillation forms are shown in Figure 9.19. The oscillogram in Figure 9.19a corresponds to small amplitudes, for which approximately sinusoidal pressure oscillations are obtained with a clearly defined frequency. In other engine operating regimes or for a different location of the sensor these sinusoidal oscillations may be distorted as a result of the appearance of the second harmonic (see Figure 9.11b).

In longer combustion chambers, still more harmonics appear and the form of the oscillations becomes correspondingly more complicated (see Figure 9.19c). Finally, pressure peaks with very short duration with large amplitude (see Figure 9.19 d and e) may develop under certain quite well defined operating regimes. These peaks are formed as the shock waves pass the sensor. This type of oscillation is most hazardous because of the sudden and large pressure peak, which propagates through the entire chamber and usually leads to destruction of the chamber.

In order to obtain a more complete picture of the observed phenomenon, we must establish which engine elements are subject to high-

frequency oscillations. Simultaneous recordings of the pressure ahead of the oxidizer and fuel injectors and at two points of the chamber show that high-frequency oscillations are usually observed in the combustion chamber but occur only rarely in the liquid feed lines (see Figure 9.18c). The oscillograms shown in Figure 9.18c were obtained using four sensors of identical sensitivity. Consequently, the high frequency oscillations have practically no significant effect on the propellant feed pressures. This is explained, in particular, by the high inertia of the liquid propellants in the lines in comparison with the inertia of the gaseous combustion products.

Figure 9.20a and b show oscillograms of simultaneous recording of the pressures and temperatures at the nozzle exit at two points of the chamber. We note that while the two pressure sensors in the chamber indicate the same p_K oscillation frequency, the nozzle exit temperature varies in accordance with an entirely different law. Thus, the temperature oscillations at the nozzle exit and the pressure oscillations in the combustion chamber are not correlated. This means that the frequencies recorded in the combustion chamber have disappeared completely and have been replaced by different frequencies at the nozzle exit section, in spite of the very short gas residence time in the nozzle. The pressure waves which come from the combustion chamber and reach the throat are completely absorbed in the supersonic part of the nozzle. This implies a significant role of the convergent part of the nozzle in the propagation of the high frequency oscillations.

Measurements of the pressure distribution along the chamber show that in the case of high frequency instability the pressure waves which propagate both downstream and upstream are important. The nozzle cone angle has a strong influence on the system stability. Variations of this angle can lead to the high frequency oscillations either disappearing or developing.

Observations also show that the high frequency oscillations cause a marked increase of the thermal loading on the combustion chamber wall, nozzle, and engine head (greater by a factor of 1.5 - 2.5 times than for normal operation).

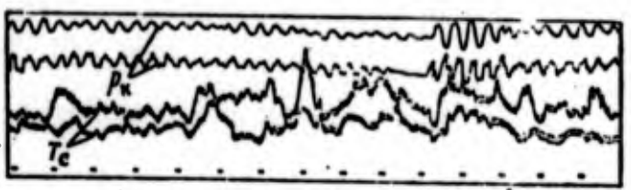

a)

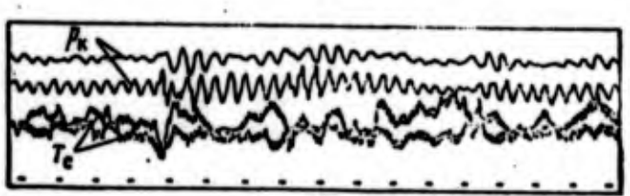

b)

Figure 9.20. Oscillograms of simultaneous records of pressures at two points of combustion chamber and temperature at nozzle exit (timing marks 10^{-3} sec).

2. Experimental data on the effect of certain parameters on high-frequency axial oscillations.

We shall examine the influence of certain operating regime and geometric parameters on high-frequency stability on the basis of experimental data published in [9], [175], [16].

Effect of injector pressure drop. The higher the pressure drop across the oxidizer and fuel injectors, the lower the chamber pressure at which axial high-frequency oscillations develop. Consequently, in contrast with the situation noted above for the low frequency oscillation case, and increase of Δp_{inj} leads to the opposite effect — a destabilization of the operating process, i.e., to the occurrence of LRE high-frequency operating instability.

Effect of propellant type and mixture ratio. The fuel type and mixture ratio affect the stability of the engine operating process as a result of the change of the chemical composition and temperature of the combustion products, which determine the local values of the speed of sound. However, this effect is small and the frequencies measured

for identical operating regimes differ very little with a change of propellant. The propellant type has a large influence on the amplitude of the oscillations. It has been noted that axial oscillations occur for a lower chamber pressure with reduction of the mixture ratio.

Effect of combustion chamber length. The geometric dimensions of the combustion chamber have a strong influence on the high-frequency instability. Specifically, not only the frequency and amplitude, but also the form of the axial high-frequency oscillations depend on the combustion chamber length. Figure 9.21 shows the axial oscillation frequency as a function of combustion chamber length from the data of [9]. In short chambers (for $\frac{L_r}{D_k} < 4$) the amplitude of the high-frequency oscillations is low and the oscillations usually have a sinusoidal form. With increase of the chamber length the amplitude increases progressively while the oscillations take on a form with a steep pressure rise front [9]. However, Crocco shows that increase of the chamber length beyond some definite limit leads to elimination of the axial instability phenomena. Thus there is a range of engine axial instability which is bounded by the two critical chamber lengths.

Effect of convergent part of nozzle. In many cases the intensity of the high frequency axial oscillations is determined by the dimensions of the converging part of the nozzle. According to [9], other conditions being the same, a longer converging section of the nozzle (i.e., with smaller cone angle) reduces the oscillation amplitude and, therefore, has a stabilizing action. Conversely, in chambers with a short convergent part, the axial oscillations arise from smaller chamber pressures. The short convergent part reflects practically all the pressure waves with a steep front. If the convergent part is long, it damps out the waves as they appear so that they will no longer be amplified. This is associated with distortion of the plane pressure wave front as it is reflected from the converging part of the nozzle.

In addition to the cone angle of the converging part of the nozzle, the form of the profile in the segment where the conical part of the nozzle joins the cylindrical combustion chamber has a significant influence on the high-frequency oscillations. A smoother junction favors stabilization of the operating process.

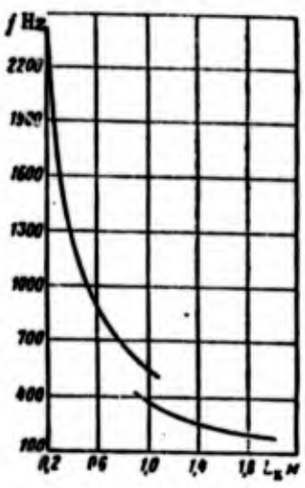

Figure 9.21. Oscillation frequency versus combustion chamber length [9].

Effect of combustion chamber diameter. The magnitude of the combustion chamber diameter has very little influence on the chamber pressure for which the axial oscillations are excited. Other conditions being the same, an increase of the combustion chamber diameter leads to an increase of the axial high-frequency stability.

This is associated with the fact that for a constant length of the cylindrical part of the chamber an increase of the diameter is associated with elongation of the converging part of the nozzle (for a given cone angle). In this case the wave reflected from the nozzle convergent cone will not be plane and, consequently, the intensity of the reinforcement of the oscillations at the head is reduced.

Effect of injection head construction. The role of the injector head and the technique for organizing the mixture formation process in the development of high-frequency oscillations in the LRE chamber is very important. First of all, the injector head plays the same role as the convergent part of the nozzle, since the pressure waves which are generated inside the combustion chamber are reflected from the head as well. The reflected waves can be weakened by nonuniform arrangement of the injectors in the head. Spherical and conical heads will be more effective and flat heads will be less effective from the viewpoint of damping of the pressure waves. Coarse and nonuniform atomization of the propellants also leads to damping of the pressure waves because of the fact they encounter the head zones which differ markedly in physical properties and velocity.

In the general case, elongation of the combustion burning zone along the length of the chamber by any technique (use of jet injectors or centrifugal injectors with small cone angles, the use of nonplanar injector heads, and so on) leads to improvement of the LRE stability characteristics with respect to the axial high-frequency oscillations.

These examples do not exhaust the entire list of factors which affect the development of axial high-frequency oscillations. In particular, an influence of the combustion chamber shape on the operating process stability has been noted. Combustion chambers of noncylindrical form (spherical, oval, conical) are more stable with regard to axial oscillations than are the cylindrical chambers.

§ 8. Theory of Axial High Frequency Instability

Since the high-frequency pressure oscillations in the chamber have a frequency which is close in magnitude to the natural frequency of gas oscillations in a closed pipe, they are termed acoustic oscillations.

We have emphasized above the importance of the geometric dimensions and shape of the individual chamber components. This is not simply accidental, since the geometric dimensions also play an important role in the acoustic theory of the gas-filled tube. For example, the natural frequency of gas oscillations in a closed tube depends directly on the tube length L [97]

$$f = \frac{1}{\tau_{ac}} = \frac{a}{2L}$$

where τ_{ac} is the complete oscillation period, equal to the time for a sound wave to travel twice the length of the tube;

a is the propagation velocity of sound in the gas filling the tube.

Therefore, before making the theoretical analysis of the high-frequency axial LRE instability we shall examine the qualitative picture of the development of acoustic oscillations in a closed cylindrical tube.

1. Qualitative picture.

The cylindrical LRE combustion chamber can be considered as a completely closed cylindrical tube: at one end it is closed by the injector head, at the other end by the converging part of the nozzle and by the imaginary surface where the gas stream transitions through the speed of sound at the throat.

Considering the gas flow to be one-dimensional, we assume that at some section of the combustion chamber at some instant of time there is a random disturbance, i.e., a deviation of the pressure from its steady state value. In the case of a pressure increase this perturbation has the nature of a compression wave, and in the case of pressure decrease it has the nature of an expansion wave.

The disturbance will propagate from the section in question in both directions with the speed of sound. The pressure waves (compression or expansion) are reflected after reaching the closed ends of the tube and begin to propagate in the opposite directions. As is known, after reflection the pressure waves reverse their nature; namely, the compression wave becomes an expansion wave, and the expansion wave becomes a compression wave. The combination of direct and reflected waves forms standing waves in the closed tube.

This pattern of the phenomenon is illustrated in Figure 9.22, which shows the variation of the pressure along the combustion chamber at sequential moments of time. It has been noted previously and is easily seen from Figure 9.22 that for a sufficiently high frequency of the gas oscillations in the combustion chamber the wavelength is commensurate with the chamber length, and the pressure at each given instant of time becomes different along the chamber length (see Figure 9.22b and c). The number of nodes, i.e., chamber sections at which there are no pressure oscillations, and the number of antinodes, i.e., sections at which the oscillation amplitude is maximal, depends on the order of the harmonic excited. The higher the order of the harmonic the higher the oscillation frequency: for example, in the case of

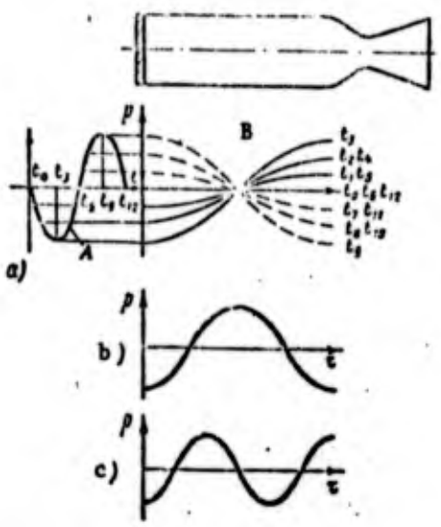

Figure 9.22. Standing wave formation during acoustic vibrations:

A) pressure variation in the plane of the head versus time; B) pressure distribution along combustion chamber

excitation of the second and third harmonics the frequency is two or three times higher than when the first harmonic is excited.

Thus, a random disturbance arising at any section of the combustion chamber gives rise to axial pressure oscillations with a definite frequency which depends on the engine geometric and other parameters. However, if these oscillations damp out in the course of time the engine operating regime will be stable with relation to axial acoustic oscillations. Otherwise, for unfavorable conditions or certain combinations of influencing factors, they do not damp out, rather they grow in time with progressively increasing amplitude, which indicates unstable engine operation.

For the development of randomly occurring oscillations, any system must have a sufficiently effective mechanism for the amplification of these oscillations. Under LRE conditions such a mechanism may be the resonance phenomenon, i.e., coincidence of the oscillations of the gas filling the intrachamber space, having the order $1/\tau_{ac}$, with the frequency of the propellant combustion oscillation, having the order $1/\tau_K$. This mechanism was examined in detail in the study of the low-frequency oscillations.

We note that the existence of the pressure wave nodes and antinodes (see Figure 9.22) introduces well-known difficulties into the experimental methods for detecting acoustic oscillations in the combustion chamber. In fact, while the locations of the sensors are not

of fundamental importance in the recording of the low-frequency oscillations, in the case of acoustic oscillations they must be located so that they are not at the sections where the nodes are located. If the sensors are located at the nodal sections they will not indicate any oscillations at all. Sometimes a chamber with longitudinal and transverse slits and high-speed movie photography (24,000 frames per second) are used in research work in order to determine the nature of the high-frequency oscillations [194]. In the case of axial oscillations photography through a longitudinal slit yields a graphic picture of the longitudinal pressure waves, while photography through a transverse slit yields records with only dark and light zones but the transverse waves are not shown (Figure 9.23).

2. Theory of longitudinal acoustic oscillations.

The actual picture of the origin of high-frequency oscillations in LRE is far more complex than that described above. In fact, just as in the case of the low-frequency oscillations, here there is a reverse influence of the gas pressure pulsations on the propellant flow rate through the injectors. This leads to corresponding oscillations of the gas influx rate, which in turn affects the pressure waves.

We must also bear in mind that the burning rate depends on the chamber pressure, so that the magnitude of this presure has a definite influence on the preparatory processes (atomization, heatup, vaporization of droplets). Consequently, oscillations of p_K near the head lead to corresponding oscillations of the basic characteristic of the combustion process — the transformation time. Thus, oscillations of the burning rate and pressure will affect one another.

Finally, we should not forget that the actual combustion products have properties which are quite nonuniform through the chamber volume. Inside the chamber there is always a definite fraction of liquid propellant and the presence of a protective, fuel-rich layer near the wall delays the propellant burnup process at the wall over the entire length of the chamber.

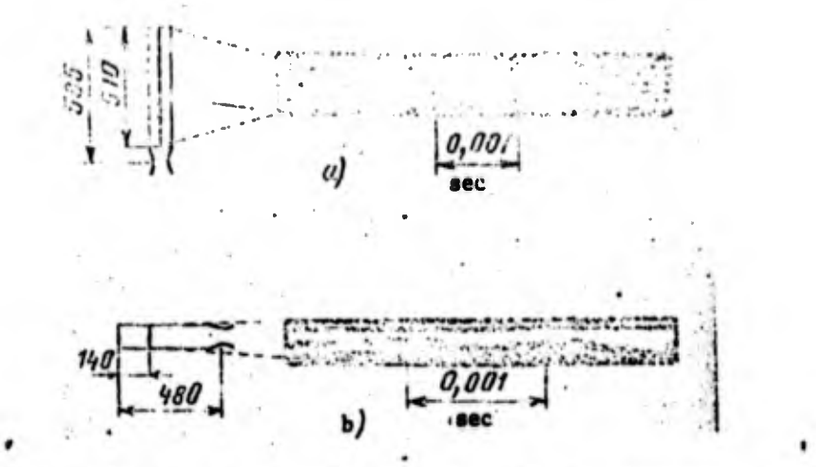

Figure 9.23. Luminous trails observed during high-frequency longitudinal instability [194]:

a) longitudinal slit (f = 990 Hz) b) transverse slit (f = 1140 Hz)

The theory of axial acoustic oscillations has been developed by Ackerman, Crooco, and others and is presented in the corresponding studies [78], [79], [80], [81] and others quite fully.

In view of the complexity of the actual picture of the phenomenon, it is not possible to examine high-frequency instability within the scope of the present book. Therefore, we shall limit ourselves to a discussion of the elementary theory of acoustic axial oscillations, which is based on several significant simplifications, the main ones being listed in the following.

(1) As the object of the study we take a monopropellant LRE with gas-tank pressure feed which provides a constant pressure in the propellant tank.

(2) The compressibility and inertia of the liquid in the head cavity are ignored. The pressure losses in the propellant feed line are also ignored, and the entire pressure drop from the tank to the combustion chamber is ascribed to the injectors (ν_{inj}).

(3) Uniform gas flow in the cylindrical combustion chamber is

assumed.

(4) Energy losses to friction and heat transfer are neglected; the gas flow is assumed to be isentropic.

(5) The transformation of the liquid propellant into the gaseous products takes place in a narrow zone adjacent to the head. Neglecting the extent of this zone, we assume that the burning combustion front coincides with the plane of the head, from which the longitudinal coordinate x is measured. The transformation law is assumed to be a step function.

(6) The converging part of the nozzle is assumed short in comparison with the wave length. Therefore, the gas motion in this region during oscillations can be assumed to be the same as for the steady state process at each given moment. This assumption permits the use of all the known gas dynamic relations for steady gas flow in a nozzle.

In studying high-frequency instability, the equation for the combustion chamber cannot be obtained from the mass balance, as was done in the case of low-frequency instability. Here, the phenomena associated with propagation of the pressure waves must be examined together with the burning process. Therefore, in the present case we use the following equations of gas dynamics for the unsteady one-dimensional motion of an ideal compressible gas:

equation of motion

$$\rho_K \frac{\partial w_K}{\partial t} + \rho_K w_K \frac{\partial w_K}{\partial x_K} = -\frac{\partial p_K}{\partial x_K}; \qquad (9.65)$$

equation of continuity

$$\frac{\partial \rho_K}{\partial t} + \frac{\partial (\rho_K w_K)}{\partial x_K} = 0; \qquad (9.66)$$

adiabatic equation

$$p_K \rho_K^{-k} = \text{const}. \qquad (9.67)$$

Here w_K, p_K, ρ_K are respectively the velocity, pressure, and density of the gas in the combustion chamber: x_K is the longitudinal

chamber co

The f
described

where x is

The bo
in the inje
(L_{cyl} is th

i.e., in ac
consider th
to the nozz
only by the
be constant
In other wo
is assumed

Finall
(9.69) as f

condit

i.e., the p
stant durin

chamber coordinate.

The flow of the inviscid liquid in the propellant feed line is described by the equations

$$\varrho\frac{\partial w}{\partial \tau}=-\frac{\partial p}{\partial x}; \tag{9.68}$$

$$n^2\varrho\frac{\partial w}{\partial x}=-\frac{\partial p}{\partial \tau}. \tag{9.69}$$

where x is the line longitudinal coordinate.

The boundary conditions for (9.65) - (9.67) are the conditions in the injection plane $x_K = 0$ and in the chamber exit plane $x_K = L_{cyl}$ (L_{cyl} is the length of the cylindrical part of the chamber)

$$x_к=0;\ G_в=c_т(\tau-\tau_в,\ t); \tag{9.70}$$

$$x_к=L_к;\ M=M^*=\text{const}, \tag{9.71}$$

i.e., in accordance with the assumptions made above (item 6) we can consider that at the end of the combustion chamber and at the entrance to the nozzle the Mach number, determined for the steady state process only by the dimensionless area of the combustion chamber F_K/F_{cr}, will be constant and equal to the Mach number in the steady state regime. In other words, the gas flow in the short entrance part of the nozzle is assumed to be quasi-steady.

Finally, we determine the boundary conditions for (9.68) and (9.69) as follows:

condition for the tank end of the feed line (see item 1)

$$x=0;\ p=p_т=\text{const}, \tag{9.72}$$

i.e., the pressure p_t in the propellant tank is considered to be constant during the pressure oscillations in the feed line;

condition for the end of the line adjacent to the head (see item 2)

$$x=l;\quad G_{\tau}=\gamma_{\tau}\sqrt{p_{\phi}-p_{\kappa}}. \tag{9.73}$$

where G_p is the liquid mass flow rate through the injectors;
p_{inj} is the liquid pressure ahead of the injectors.

As before, we write these equations and their boundary conditions in terms of dimensionless parameters. We retain the previously introduced notations, using an overbar to indicate dimensionless quantities, i.e.

$$p_{\kappa}=p_{\kappa}^{\circ}(1+\delta\bar{p}_{\kappa});\quad \varrho_{\kappa}=\varrho_{\kappa}^{\circ}(1+\delta\bar{\varrho}_{\kappa});$$
$$w_{\kappa}=w_{\kappa}^{\circ}(1+\delta\bar{w}_{\kappa});\quad p=p^{\circ}(1+\delta\bar{p});$$
$$w=w^{\circ}(1+\delta\bar{w});$$
$$G_{\kappa}=G_{\kappa}^{\circ}(1+\delta\bar{G}_{\kappa})=\varrho_{\kappa}^{\circ}w_{\kappa}^{\circ}F_{\kappa}(1+\delta\bar{\varrho}_{\kappa})(1+\delta\bar{w}_{\kappa})=$$
$$=G_{\kappa}^{\circ}(1+\delta\bar{\varrho}_{\kappa}+\delta\bar{w}_{\kappa})$$

since we have neglected a quantity of second order of smallness ($\delta\bar{\varrho}_{\kappa}\delta\bar{w}_{\kappa}\approx 0$).

$$G_{\tau}=G_{\tau}^{\circ}(1+\delta\bar{G}_{\tau})=\varrho w^{\circ}F_{\phi}(1+\delta\bar{w})=G^{\circ}(1+\delta\bar{w}).$$

Substituting these relations into (9.65) - (9.69) and the boundary conditions (9.70) - (9.73), and also taking account of the relations between the parameters in the steady state regime and neglecting terms of higher orders of smallness ($\delta\bar{w}^2$; $\delta\bar{w}\frac{\partial\delta\bar{w}}{\partial x}$ and so on), we obtain the following expressions:

for the gas in the combustion chamber

$$w_{\kappa}^{\circ}\frac{\partial\bar{w}_{\kappa}}{\partial\tau}+w_{\kappa}^{\circ 2}\frac{\partial\bar{w}_{\kappa}}{\partial x_{\kappa}}+a_{\kappa}^{\circ 2}\frac{\partial\bar{\varrho}_{\kappa}}{\partial x_{\kappa}}=0; \tag{9.74}$$

$$\frac{\partial\bar{\varrho}_{\kappa}}{\partial\tau}+w_{\kappa}^{\circ}\frac{\partial\bar{\varrho}_{\kappa}}{\partial x_{\kappa}}+\varrho_{\kappa}^{\circ}\frac{\partial\bar{w}_{\kappa}}{\partial x_{\kappa}}=0, \tag{9.75}$$

$$\bar{p}_{\kappa}=k\bar{\varrho}_{\kappa}, \tag{9.76}$$

where $a_k^* = \sqrt{k \frac{p_k^*}{\rho_k^*}}$ is the speed of sound in the combustion chamber in the steady state regime;

for the liquid in the feed line

$$\rho^* \frac{\partial \bar{w}}{\partial \tau} = -p^* \frac{\partial \bar{p}}{\partial x}; \tag{9.77}$$

$$a^2 \rho^* \frac{\partial \bar{w}}{\partial x} = -p^* \frac{\partial \bar{p}}{\partial \tau} \tag{9.78}$$

for the combustion chamber boundary conditions

$$x_k = 0; \quad \delta \bar{G}_k = \delta \bar{\rho}_k + \delta \bar{w}_k = \delta \bar{G}_1 (\tau - \tau_k); \tag{9.79}$$

$$x_k = l_k; \quad \delta \bar{w}_k = \frac{k-1}{2} \delta \bar{\rho}_k. \tag{9.80}$$

The Relation (9.80) is obtained as follows. We express the speed of sound in the combustion chamber in terms of the dimensionless parameters of the gas

$$a_k^2 = k \frac{p_k}{\rho_k} = k \frac{p_k^* (1 + \delta \bar{p}_k)}{\rho_k^* (1 + \delta \bar{\rho}_k)} = a_k^{*2} \frac{1 + \delta \bar{p}_k + \delta \bar{\rho}_k - \delta \bar{\rho}_k}{1 + \delta \bar{\rho}_k} =$$

$$= a_k^{*2} \left(1 + \frac{\delta \bar{p}_k - \delta \bar{\rho}_k}{1 + \delta \bar{\rho}_k}\right) \approx a_k^{*2} (1 + \delta \bar{p}_k - \delta \bar{\rho}_k),$$

since $\bar{\delta}_{\rho_k} \ll 1$.

Bearing in mind the smallness of the difference $(\bar{\delta} \bar{p}_k - \delta \bar{\rho}_k)$ we obtain

$$a_k \approx a_k^* \left[1 + \frac{1}{2} (\delta \bar{p}_k - \delta \bar{\rho}_k)\right]$$

or with account for (9.76)

$$a_k = a_k^* \left(1 + \frac{k-1}{2} \delta \bar{\rho}_k\right)$$

Then the Mach number in the combustion chamber can be represented as

$$M = \frac{w_k}{a_k} = \frac{w_k^* (1 + \delta \bar{w}_k)}{a_k^* \left(1 + \frac{k-1}{2} \delta \bar{\rho}_k\right)} =$$

$$= M^* \left(1 + \frac{\delta\bar{w}_x - \frac{k-1}{2}\delta\bar{Q}_x}{1 + \frac{k-1}{2}\delta\bar{Q}_x} \right) \approx M^* \left(1 + \delta\bar{w}_x - \frac{k-1}{2}\delta\bar{Q}_x \right).$$

We obtain (9.80) from this relation with account for (9.71).

Finally, the boundary conditions for the feed line take the following form after linearization

$$x = 0;\ \delta\bar{p} = 0, \tag{9.81}$$

$$x = l;\ \delta\bar{G}_\tau = \delta\bar{w}_\phi = \frac{p_\phi^*}{2\Delta p_\phi^*}\delta\bar{p}_\phi - \frac{1}{\Delta\bar{p}_\phi^*}\delta\bar{p}_\kappa, \tag{9.82}$$

where the previously introduced notations remain valid, namely

$$\Delta p_\phi^* = p_\phi^* - p_\kappa^*;\quad \Delta\bar{p}_\phi^* = \frac{2\Delta p_\phi^*}{p_\kappa^*}.$$

Then we use the Laplace transformation to solve the equations and satisfy the boundary conditions. As a result we obtain the characteristic equation relating the geometric and operating condition parameters of the engine with the complex frequency.

Applying the Laplace transformation to the chamber Equations (9.74) - (9.76), we find

$$w_x^* sL[\delta\bar{w}_x] + w_x^{*2}\frac{dL[\delta\bar{w}_x]}{dx_x} + a_x^{*2}\frac{dL[\delta\bar{Q}_x]}{dx_x} = 0; \tag{9.83}$$

$$sL[\delta\bar{Q}_x] + w_x^*\frac{dL[\delta\bar{Q}_x]}{dx_x} + w_x^*\frac{dL[\delta\bar{w}_x]}{dx_x} = 0; \tag{9.84}$$

$$L[\delta\bar{p}_x] = kL[\delta\bar{Q}_x]. \tag{9.85}$$

After the Laplace transformation the Equations (9.77) and (9.78) for the liquid in the feed line take the form

$$\rho w^* sL[\delta\bar{w}(s,x)] = -p^*\frac{dL[\delta\bar{p}(s,x)]}{dx}; \tag{9.86}$$

$$a^{*2}\rho w^*\frac{dL[\delta\bar{w}(s,x)]}{dx} = -p^* sL[\delta\bar{p}(s,x)]. \tag{9.87}$$

For the boundary Conditions (9.79) - (9.82) we obtain

Subst
$L[\delta\bar{w}(s,x)]$
line adjac

Hence

since

Subst
tain the t
between th

Befor
boundary C
$L[\delta\bar{G}_\tau(s)] = L[\delta$
nection be
liquid in
and (9.87)

$$x_k = 0;\quad L[\delta\bar{G}_k(s)] = L[\delta\bar{p}_k(s,0)] + \tag{9.88}$$
$$+ L[\delta\bar{w}_k(s,0)] = L[\delta\bar{G}_1(s)]\cdot e^{-\gamma x_k}.$$

$$x_k = L_k;\quad L[\delta\bar{w}_k(s,L_k)] = \frac{k-1}{2} L[\delta\bar{p}_k(s,L_k)] \ldots \tag{9.89}$$

.71).

$$x = 0;\quad L[\delta\bar{p}(s,0)] = 0 \ldots \tag{9.90}$$

the

$$x = l;\quad L[\delta\bar{G}_1(s)] = L[\delta\bar{w}_\phi(s)] = \frac{p_\phi^\circ}{2\Delta p_\phi^\circ} L[\delta\bar{p}_\phi(s)] - \tag{9.91}$$
$$- \frac{1}{\Delta p_\phi} L[\delta\bar{p}_k(s,0)].$$

(9.81) Substituting these expressions for the functions $L[\delta\bar{p}(s,x)]$ and $L[\delta\bar{w}(s,x)]$ into the boundary Condition (9.91) for the end of the feed

(9.82) line adjacent to the head, we find

ly

$$-\frac{1}{\Delta\bar{p}_\phi}\frac{L[\delta\bar{p}_k(s,0)]}{L[\delta\bar{w}_\phi(s)]} = 1 + \frac{p_\phi^\circ}{2\Delta p_\phi^\circ}\frac{\varrho w^{\circ 2}}{p_\phi^\circ}\operatorname{th}\frac{sl}{a}.$$

Hence

ations
the charac-
tion para-

$$L[\delta\bar{w}_\phi(s)] = L[\delta\bar{G}_1(s)] = -\frac{L[\delta\bar{p}_k(s,0)]}{\Delta\bar{p}_\phi^\circ + \bar{p}_w \operatorname{th}\frac{sl}{a}} \tag{9.92}$$

since

ations

$$L[\delta\bar{w}(s,l)] = L[\delta\bar{w}_\phi(s)];\quad p^\circ = p_\phi^\circ;\quad \bar{p}_w = \frac{\varrho w^{\circ 2}}{p_\phi^\circ}.$$

(9.83) Substituting (9.92) into (9.88) with account for (9.85), we ob-

(9.84) tain the transformed boundary condition which expresses the connection between the parameters at the combustion chamber head: for $x_K = 0$

(9.85)
and (9.78)
$$L[\delta\bar{p}_k(s,0)] + L[\delta\bar{w}_k(s,0)] = -\frac{kL[\delta\bar{p}_k(s,0)]e^{-\gamma x_k}}{\Delta\bar{p}_\phi + \bar{p}_w \operatorname{th}\frac{sl}{a}}. \tag{9.93}$$

(9.86) Before solving the combustion chamber equations we transform the boundary Condition (9.88) with the objective of replacing the function

(9.87) $L[\delta\bar{G}_1(s)] = L[\delta\bar{w}(s,x)]$ by the function $L[\delta\bar{p}_k(s,0)]$. We find the necessary connection between these functions if we solve the equations for the liquid in the feed line. Excluding the function $L[\delta\bar{w}(s,x)]$ from (9.86) and (9.87), we obtain

$$\frac{d^2L[\delta\bar{p}(s,x)]}{dx^2}=\frac{s^2}{a^2}L[\delta\bar{p}(s,x)].$$

The solution of this equation has the form

$$L[\delta\bar{p}(s,x)]=C_1e^{\frac{sx}{a}}+C_2e^{-\frac{sx}{a}}.$$

Using the boundary Condition (9.90) for the end of the line adjacent to the tank, we obtain $C_1 = -C_2$ and, consequently,

$$L[\delta\bar{p}(s,x)]=C_1\left(e^{\frac{sx}{a}}-e^{-\frac{sx}{a}}\right)=C\operatorname{sh}\frac{sx}{a}$$

where $C = 2C_1$.

Differentiating this expression with respect to x and substituting the result into (9.86), we find

$$L[\delta\bar{w}(s,x)]=-\frac{p^0}{\varrho w^0 a}C\operatorname{ch}\frac{sx}{a}$$

The second boundary condition for the combustion chamber is rewritten without change

$$x=L_к;\quad L[\delta\bar{w}_к(s,L_к)]=\frac{k-1}{2}L[\delta\bar{Q}_к(s,L_к)]. \tag{9.94}$$

Now we solve the system of Equations (9.83) and (9.84) for the gas with the boundary Conditions (9.93) and (9.94). Excluding the variable $L[\delta\bar{w}_к(s,x)]$ from this system, we reduce it to a single equation with a single unknown

$$(1-M^2)\frac{d^2L[\delta\bar{Q}_к]}{dx_к^2}-2M\frac{s}{a_к}\frac{dL[\delta\bar{Q}_к]}{dx_к}-\frac{s^2}{a_к^2}L[\delta\bar{Q}_к]=0. \tag{9.95}$$

This is a second-order ordinary differential equation whose solution may be written in the form

$$L[\delta\bar{p}_к(s,x)]=B_1e^{\frac{sx}{a_к^0(1-M)}}+B_2e^{\frac{-sx}{a_к^0(1+M)}} \tag{9.96}$$

where B_1 and B_2 are constants of integration.

To solv
with respect

Using t
$L[\delta\bar{Q}_к]$ from (9

This equatio

The con
conditions.
stituting th

or after obvi

Using th
into it the

The resu
(9.99) for de

To solve the system for the function $L[\delta\bar{w}]$ we differentiate (9.96) with respect to x

$$\frac{dL[\delta\bar{p}_K]}{dx} = -\frac{B_1 s}{a_K^*(1-M)} e^{\frac{sx}{a_K^*(1-M)}} - \frac{B_2 s}{a_K^*(1+M)} e^{-\frac{sx}{a_K^*(1+M)}}$$

Using this expression, and also (9.96), we exclude the quantity $L[\delta\bar{Q}_K]$ from (9.84) and divide it by a_K^*

$$M\frac{dL[\delta\bar{w}_K]}{dx} = -\frac{B_1 s}{a_K^*(1-M)} e^{\frac{sx}{a_K^*(1-M)}} + \frac{B_2 s}{a_K^*(1+M)} e^{-\frac{sx}{a_K^*(1+M)}}$$

This equation has the following solution

$$L[\delta\bar{w}_K(s,x)] = -\frac{B_1}{M} e^{\frac{sx}{a_K^*(1-M)}} + \frac{B_2}{M} e^{-\frac{sx}{a_K^*(1+M)}} \qquad (9.97)$$

The constants of integration B_1 and B_2 are found from the boundary conditions. Setting x = 0 in the solutions (9.96) and (9.97) and substituting them into the boundary Condition (9.93), we obtain

$$B_1 + B_2 - \frac{B_1}{M} + \frac{B_2}{M} = -\frac{k(B_1+B_2)e^{-s\tau_K}}{\Delta\bar{p}_\phi + \bar{p}_w \operatorname{th}\frac{sl}{a}}$$

or after obvious transformations

$$\left(\frac{M-1}{M} + \frac{ke^{-s\tau_K}}{\Delta\bar{p}_\phi + \bar{p}_w \operatorname{th}\frac{sl}{a}}\right)B_1 + \left(\frac{M+1}{M} + \frac{ke^{-s\tau_K}}{\Delta\bar{p}_\phi + \bar{p}_w \operatorname{th}\frac{sl}{a}}\right)\times B_2 = 0. \qquad (9.98)$$

Using the second boundary Condition (9.94), after substituting into it the same solutions for $x_K = L_{cyl}$ we obtain

$$\left(1 + \frac{k-1}{2}M\right) e^{\frac{sL_K}{a_K^*(1-M)}} B_1 - \left(1 - \frac{k-1}{2}M\right) e^{-\frac{sL_K}{a_K^*(1+M)}} B_2 = 0. \qquad (9.99)$$

The resulting system of two homogeneous Equations (9.98) and (9.99) for determining the constants of integration B_1 and B_2 can have

a nonzero solution if its determinant equals zero

$$\Delta=\begin{vmatrix} \frac{M-1}{M}+\frac{ke^{-s\tau_k}}{\Delta\bar{p}_\phi+\bar{p}_w\,\mathrm{th}\,\frac{sl}{a}}; & \frac{M+1}{M}+\frac{ke^{-s\tau_k}}{\Delta\bar{p}_\phi+\bar{p}_w\,\mathrm{th}\,\frac{sl}{a}} \\ \left(1+\frac{k-1}{2}M\right)e^{\frac{sL_k}{a_k^\circ(1-M)}}; & -\left(1-\frac{k-1}{2}M\right)e^{\frac{sL_k}{a_k^\circ(1+M)}} \end{vmatrix}= \\ =0 \qquad (9.100)$$

Then the sought values of B_1 and B_2 will be

$$B_1=\frac{\Delta_{B_1}}{\Delta};\qquad B_2=\frac{\Delta_{B_2}}{\Delta}$$

where Δ_{B_1} and Δ_{B_2} are the corresponding minors of the determinant.

With account for the determined values of the constants of integration, the Solutions (9.96) and (9.97) take the form

$$L[\delta\bar{Q}_k(s,x)]=\frac{\Delta_{B_1}e^{\frac{sx}{a_k^\circ(1-M)}}+\Delta_{B_2}e^{-\frac{sx}{a_k^\circ(1+M)}}}{\Delta}=\frac{F_{\bar{Q}}(s,x,a_k^\circ,M,\Delta_{B_1},\Delta_{B_2})}{\Delta};$$

$$L[\delta\bar{w}_k(s,x)]=\frac{\frac{\Delta_{B_1}}{M}e^{\frac{sx}{a_k^\circ(1-M)}}+\frac{\Delta_{B_2}}{M}e^{\frac{sx}{a_k^\circ(1+M)}}}{\Delta}= \\ =\frac{F_{\bar{w}}(s,x,a_k^\circ,M,\Delta_{B_1},\Delta_{B_2})}{\Delta}.$$

To return to the originals of the functions $\delta\bar{Q}_k$ and $\delta\bar{w}_k$, we must solve the following integral equations

$$L[\delta\bar{Q}_k(s,x)]=\frac{F_{\bar{Q}}}{\Delta}=\int_0^\infty e^{-s\tau}\delta\bar{Q}_k(\tau,x)\,d\tau;$$

$$L[\delta\bar{w}_k(s,x)]=\frac{F_{\bar{w}}}{\Delta}=\int_0^\infty e^{-s\tau}\delta\bar{w}_k(\tau,x)\,d\tau.$$

To solve these equations we write the originals $\delta\bar{Q}_k$ and $\delta\bar{w}_k$ in the form of the sum of the following functions

$$\left.\begin{aligned}\delta\bar{Q}_k(\tau,x)&=\sum_1^n C_{Q_i}e^{s_i\tau}\tau^m;\\ \delta\bar{w}_k(\tau,x)&=\sum_1^n C_{w_i}e^{s_i\tau}\tau^m,\end{aligned}\right\} \qquad (9.101)$$

where s_i are the roots of the denominator of the left side of the integral equations, i.e., the roots of the determinant Δ;

m is the index which accounts for the multiplicity of the roots s_i;

(9.100)

C_ρ and C_w are quantities which are independent of time.

The nature of the engine operating regime (stable or unstable) obviously depends on the sign of the real part of all the roots s_i of (9.100), which after expanding the determinant takes the form

$$\left(\frac{M-1}{M}+\frac{ke^{-s\tau_k}}{\Delta\bar{P}_\phi+\bar{P}_w\,\mathrm{th}\,\frac{sl}{a}}\right)\left(1-\frac{k-1}{2}M\right)e^{-\frac{sL_k}{a_k^0(1+M)}}+$$

$$+\left(1+\frac{k-1}{2}M\right)e^{\frac{sL_k}{a_k^0(1-M)}}\left(\frac{M+1}{M}+\frac{ke^{-s\tau_k}}{\Delta\bar{P}_\phi+\bar{P}_w\,\mathrm{th}\,\frac{sl}{a}}\right)=0; \tag{9.102}$$

The stability boundary is found if we set $s = i\omega$ in the last equation. However, in view of the complexity of (9.102) it is better to simplify it somewhat. Introducing the notation for simplifying the form of the equation

$$F(s)=\frac{ke^{-s\tau_k}}{\Delta\bar{P}_\phi+\bar{P}_w\,\mathrm{th}\,\frac{sl}{a}} \tag{9.103}$$

Equation (9.102) may be written in the form

$$\left[M-1+MF(s)-\frac{k-1}{2}M^2+\frac{k-1}{2}M-\frac{k-1}{2}M^2F(s)\right]e^{-\frac{sL_k}{a_k^0(1+M)}}+$$

$$+\left[M+1+MF(s)+\frac{k-1}{2}M^2+\frac{k-1}{2}M+\frac{k-1}{2}M^2F(s)\right]\times$$

$$\times e^{\frac{sL_k}{a_k^0(1-M)}}=0.$$

Limiting ourselves to the consideration of isobaric combustion chambers, for which $M \ll 1$, we neglect the terms containing M^2. Then we obtain

(9.101)

$$\left[M-1+\frac{k-1}{2}M+MF(s)\right]e^{-\frac{sL_н}{a_н^*}(1-M)}+$$

$$+\left[M+1+\frac{k-1}{2}M+MF(s)\right]e^{\frac{sL_н}{a_н^*}(1+M)}=0,$$

where

which after cancelling out the factor $e^{\frac{sL_{цил}}{a_н^*}M}$ may be written as

$$e^{\frac{sL_н}{a_н^*}}-e^{-\frac{sL_н}{a_н^*}}+\left[M+\frac{k-1}{2}M+MF(s)\right]\left(e^{\frac{sL_н}{a_н^*}}+e^{-\frac{sL_н}{a_н^*}}\right)=0.$$

Hence we the axial acc

Considering that

$$\frac{e^{\frac{sL_н}{a_н^*}}-e^{-\frac{sL_н}{a_н^*}}}{e^{\frac{sL_н}{a_н^*}}+e^{-\frac{sL_н}{a_н^*}}}=\text{th}\,\frac{sL_н}{a_н^*},$$

and also replacing F(s) using (9.103), we obtain

$$\text{th}\,\frac{sL_н}{a_н^*}+\frac{k+1}{2}M+\frac{kMe^{-s\tau_н}}{\Delta\bar{p}_ф+\bar{p}_ш\,\text{th}\,\frac{sl}{a}}=0. \qquad (9.104)$$

Comparin on the stabil cillations, w show that (9. as a particul can replace t

Recalling the known relation $\text{th}\,z=-i\,\text{tg}\,iz$ and setting $s=i\omega$, we rewrite the last equation as

$$i\,\text{tg}\,\frac{\omega L_н}{a_н^*}+\frac{k+1}{2}M+\frac{kMe^{-i\omega\tau_н}}{\Delta\bar{p}_ф+\bar{p}_ш i\,\text{tg}\,\frac{\omega l}{a}}=0. \qquad (9.105)$$

But the combustion ch quency oscill the combustio

As a result of separating the real and imaginary parts, this equation obviously breaks down into two equations

$$\frac{k+1}{2}M\Delta\bar{p}_ф-\bar{p}_ш\,\text{tg}\,\frac{\omega L_н}{a_н^*}\,\text{tg}\,\frac{\omega l}{a}=-kM\cos\omega\tau_н; \qquad (9.106)$$

$$\Delta\bar{p}_ф\,\text{tg}\,\frac{\omega L_н}{a_н^*}+\frac{k+1}{2}M\bar{p}_ш\,\text{tg}\,\frac{\omega l}{a}=-kM\sin\omega\tau_н. \qquad (9.107)$$

and Equations (9.45). Cons the previousl a more genera

Transforming the previously introduced Notations (9.41), (9.42), and (9.43), we obtain

$$\frac{k+1}{2}M\Delta\bar{p}_\phi - \bar{p}_\omega \operatorname{tg}\bar{\omega}_\kappa \operatorname{tg}\bar{\omega} = kM\cos\bar{\omega}\bar{\tau}_\kappa;$$

$$\Delta\bar{p}_\phi \operatorname{tg}\bar{\omega}_\kappa + \frac{k+1}{2}M\bar{p}_\omega \operatorname{tg}\bar{\omega} = kM\sin\bar{\omega}\bar{\tau}_\kappa,$$

where

$$\bar{\omega}_\kappa = \frac{\omega L_\kappa}{a_\kappa^*}$$

Hence we have the final equation for the stability boundary for the axial acoustic oscillations

$$\Delta\bar{p}_\phi = \sqrt{\frac{\left(\frac{2k}{k+1}\right)^2}{1+\left[\frac{2}{(k+1)M}\operatorname{tg}\bar{\omega}_\kappa\right]^2} - \bar{p}_\omega^2 \operatorname{tg}^2\bar{\omega}}; \tag{9.108}$$

$$\operatorname{tg}\bar{\omega}\bar{\tau}_\kappa = \frac{\frac{2}{(k+1)M}\Delta\bar{p}_\phi \operatorname{tg}\bar{\omega}_\kappa - \bar{p}_\omega \operatorname{tg}\bar{\omega}}{-\Delta\bar{p}_\phi + \frac{2}{(k+1)M}\bar{p}_\omega \operatorname{tg}\bar{\omega}_\kappa \operatorname{tg}\bar{\omega}}. \tag{9.109}$$

Comparing these equations with the Conditions (9.44) and (9.45) on the stability boundary, obtained in the study of low-frequency oscillations, we note that they are analogous in form. It is easy to show that (9.44) and (9.45) follow from the equations obtained above as a particular case. In fact, for the low-frequency oscillations we can replace the value of the tangent by the corresponding angle. Then

$$\frac{2}{(k+1)M}\operatorname{tg}\bar{\omega}_\kappa = \frac{2\bar{\omega}_\kappa}{(k+1)M} = \frac{2\omega}{(k+1)}\frac{L_\kappa}{a_\kappa}$$

But the ratio $\frac{L_{cyl}}{a_\kappa} = \vartheta_\kappa$ is the gas particle residence time in the combustion chamber. If we also further assume that for the low-frequency oscillations the process of pressure wave propagation within the combustion chamber is isothermal (k = 1) then

$$\frac{2}{(k+1)M}\operatorname{tg}\bar{\omega}_\kappa = \omega\vartheta_\kappa = \bar{\omega}\bar{\tau}^*$$

and Equations (9.108) and (9.109) become the Expressions (9.44) and (9.45). Consequently, the theory of acoustic oscillations generalizes the previously examined low-frequency oscillations, and, therefore, is a more general stability theory.

3. Analysis of stability boundary construction.

In accordance with (9.108) and (9.109) LRE operating stability is defined by the following parameters

$$\bar{\tau}_{\text{ж}},\ \Delta\bar{p}_{\phi},\ \bar{p}_{\text{ж}},\ M.$$

The stability boundary can be constructed in the plane of any two parameters, leaving all the other parameters constant, but for reasons discussed in the second section of the present chapter here again it is better to construct the stability boundary in the plane of the parameters $\Delta\bar{p}_{\text{inj}} - \bar{\tau}_{\text{ж}}$.

It is convenient to begin the construction of the stability boundary with the construction of the relation $\Delta\bar{p}_{\text{inj}} = \Delta\bar{p}_{\text{inj}}(\omega)$ defined by (9.108), which may be written in the form

$$\Delta\bar{p}_{\phi}(\bar{\omega}) = \sqrt{f_1(\bar{\omega}) - f_2(\omega)},$$

where

$$f_1(\bar{\omega}) = \frac{\frac{4k^2}{(k+1)^2}}{1+\left[\frac{2}{M(k+1)}\operatorname{tg}\bar{\omega}_{\text{ж}}\right]^2};$$

$$f_2(\bar{\omega}) = (\bar{p}_{\text{ж}}\operatorname{tg}\bar{\omega})^2.$$

In the case in which there is no feed line effect (system with short feed lines), the function $f_2(\bar{\omega}) = 0$ and the relation $\Delta\bar{p}_{\text{inj}} = \Delta\bar{p}_{\text{inj}}(\bar{\omega})$ is defined by the single function $f_1(\bar{\omega})$

$$\Delta\bar{p}_{\phi} = \sqrt{f_1(\bar{\omega})} = \sqrt{\frac{\frac{4k^2}{(k+1)^2}}{1+\left[\frac{2}{M(k+1)}\operatorname{tg}\bar{\omega}_{\text{ж}}\right]^2}}$$

In this case $\Delta\bar{p}_{\text{inj}} = \Delta p_{\text{inj}}(\bar{\omega}_{\text{ж}})$ will be a periodic function of $\omega_{\text{ж}}$ because of the periodicity of the term $\operatorname{tg}\bar{\omega}_{\text{ж}}$ and will vary periodically from the maximal value

$$\Delta\bar{p}_{\text{inj max}} = \frac{2k}{k+1}$$

obtained at the moment of equality

$$\bar{\omega}_k = k\pi,$$

to zero, obtained for the equality

$$\bar{\omega}_k = k\pi \pm \frac{\pi}{2}$$

where k = 1, 2, 3,.... (k = 0 corresponds to the low-frequency oscillations)

A plot of the relation $\Delta\bar{p}_{inj} = \Delta\bar{p}_{inj}(\bar{\omega}_k)$ is shown by curve 1 in Figure 9.24. The line effect is accounted for by the function $f_2(\bar{\omega})$ and amounts to the fact that of all the frequencies only the narrow band of possible frequencies for which the values of the quantities $\Delta\bar{p}_{inj}$ are positive are excited. These bands lie near the frequency of the harmonics of the free oscillations of the liquid in the lines, which are defined by the relation $\operatorname{tg}\bar{\omega} = 0$, which is satisfied if

$$\bar{\omega} = n\pi$$

n = 1, 2, 3,....

The plot of the relation $\Delta\bar{p}_{inj} = \Delta\bar{p}_{inj}(\bar{\omega})$ with account for the natural oscillations of the liquid in the lines is represented by the series of curves 2 in Figure 9.24.

After the limits of variation of $\Delta\bar{p}_{inj}$ have been found, we must calculate the corresponding values of the quantities τ_K. To this end we transform (9.109) to a somewhat more convenient form, dividing the numerator and denominator by $-\Delta\bar{p}_{inj}$

$$\operatorname{tg}\bar{\omega}\tau_k = \frac{\frac{2}{(k+1)M}\operatorname{tg}\bar{\omega}_k + \frac{\bar{p}_\infty}{\Delta\bar{p}_0}\operatorname{tg}\bar{\omega}}{1 - \frac{2}{(k+1)M}\frac{\bar{p}_\infty}{\Delta\bar{p}_0}\operatorname{tg}\bar{\omega}_k\operatorname{tg}\bar{\omega}}.$$

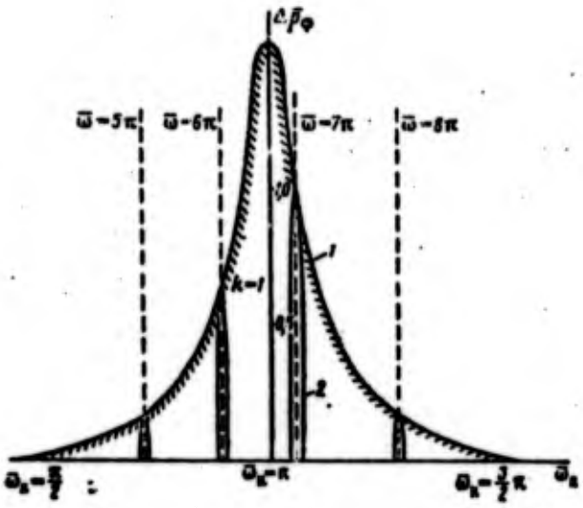

Figure 9.24. Dependence of $\Delta\bar{p}_{inj}$ on $\bar{\omega}_к$

1) without account for the line effect; 2) with account for the line effect

We introduce the notations

$$\operatorname{tg}\alpha=\frac{2}{(k+1)M}\operatorname{tg}\bar{\omega}_к;\quad \alpha=\operatorname{arctg}\left[\frac{2}{(k+1)M}\operatorname{tg}\bar{\omega}_к\right];$$

$$\operatorname{tg}\varphi=\frac{\bar{p}_ш}{\Delta\bar{p}_ф}\operatorname{tg}\bar{\omega};\quad \varphi=\operatorname{arctg}\left[\frac{\bar{p}_ш}{\Delta\bar{p}_ф}\operatorname{tg}\bar{\omega}\right].$$

In these Notations (9.109) will have the form

$$\operatorname{tg}\bar{\omega}\bar{\tau}_к=-\frac{\operatorname{tg}\alpha+\operatorname{tg}\varphi}{1-\operatorname{tg}\alpha\operatorname{tg}\varphi}=-\operatorname{tg}(\alpha+\varphi).$$

Further

$$\operatorname{tg}\bar{\omega}\bar{\tau}_к+\operatorname{tg}(\alpha+\varphi)=\frac{\sin(\bar{\omega}\bar{\tau}_к+\alpha+\varphi)}{\cos\bar{\omega}\bar{\tau}_к\cos(\alpha+\varphi)}=0.$$

This last equality is satisfied if

$$\bar{\omega}\bar{\tau}_к+\alpha+\varphi=2m\pi,\quad m=1,2,3\ldots$$

(m = 0 cannot be used, since in this case $\bar{\omega}\bar{\tau}_к<0$).

Of all t
ing to the st

Then

With cha
its sign. Th

α has a nega

α takes a po

The qua
for

and negative

Thus, s
into the exp

For sh
Then the fo
form

Of all the remaining values of m we must take m = 1, corresponding to the stability condition

Then

$$\bar{\tau}_{\kappa}=\frac{2\pi-(\alpha+\varphi)}{\bar{\omega}}$$

With change of the frequency the quantity α periodically alters its sign. Thus, for example, with variation of $\bar{\omega}_{\kappa}$ in the limits

$$k\pi>\bar{\omega}_{\kappa}>k\pi-\frac{\pi}{2}$$

α has a negative value, while with variation of $\bar{\omega}_{\kappa}$ in the limits

$$k\pi+\frac{\pi}{2}>\bar{\omega}_{\kappa}>k\pi$$

α takes a positive value.

The quantity φ also changes sign periodically; it is positive for

$$n\pi+\frac{\pi}{2}>\bar{\omega}>n\pi$$

and negative for

$$n\pi>\bar{\omega}>n\pi-\frac{\pi}{2}$$

Thus, substituting the absolute values of the angles α and φ into the expression for $\bar{\tau}_{\kappa}$, we finally obtain

$$\bar{\tau}_{\kappa}=\frac{2\pi-(\pm|\alpha|\pm|\varphi|)}{\bar{\omega}}$$

For short feed lines, when $\bar{p}_{w}$ = 0, the angle φ also equals zero. Then the formula for determining the quantity $\bar{\tau}_{\kappa}$ takes the simpler form

$$\bar{\tau}_{\kappa}=\frac{2\pi-(\pm|\alpha|)}{\bar{\omega}}$$

The formulas obtained for determining the dimensionless transformation time are convenient for calculating the stability boundaries, since in calculating the values of the angles α and φ there is no need to account for the signs of the angles themselves, which are easily found with the aid of the relations presented above.

Now let us construct the engine stability boundary. The basic data for construction of the curves is as follows.

The mean combustion chamber temperature is T_K = 3000° K. The gas constant R = 36 kgf·m/kgf °C. The combustion chamber pressure p_K = 40 kgf/cm^2. The adiabatic index k = 1.18. The gas velocity at the end of the cylindrical part of the combustion chamber w_K = 120 m/sec. The combustion chamber time constant $\vartheta_K = 5 \cdot 10^{-3}$ sec. With account for the nozzle entrance section, the length of the cylindrical part of the combustion chamber is L_{cyl} = 600 mm. The feed line length $l = 5$ m. The propellant specific weight γ = 1.4 g/cm^3. The propellant flow velocity in the lines w = 5 m/sec. The speed of sound in the liquid a ≈ 1400 m/sec.

To construct the engine stability boundary without account for the feed lines, we use the previously constructed plot of the relation $\Delta\bar{p}_{inj} = \Delta\bar{p}_{inj}(\bar{\omega}_x)$ (see Figure 9.24). Since for an engine with short lines $\Delta\bar{p}_{inj}$ varies from zero to a maximum and then back to zero, the stability boundary will have the form of a closed region.

This curve has the following characteristic points (in order of increasing frequency)

1. $\bar{\omega}_{x_1} = k\pi - \frac{\pi}{2}$;

$$\Delta\bar{p}_{\phi_1} = 0; \quad \alpha_1 = -\frac{\pi}{2}; \quad \bar{\tau}_{x_1} = \frac{\frac{5}{2}\pi}{\bar{\omega}_1}.$$

2. $\bar{\omega}_{x_2} = k\pi$;

$$\Delta\bar{p}_{\phi_2} = \frac{2k}{k+1}; \quad \alpha_2 = 0; \quad \bar{\tau}_{x_2} = \frac{2\pi}{\bar{\omega}_2}.$$

3. $\bar{\omega}_{x_3} = k\pi + \frac{\pi}{2}$;

$$\Delta\bar{p}_{\phi_3} = 0; \quad \alpha_3 = \frac{\pi}{2}; \quad \bar{\tau}_{x_3} = \frac{\frac{3}{2}\pi}{\bar{\omega}_3}.$$

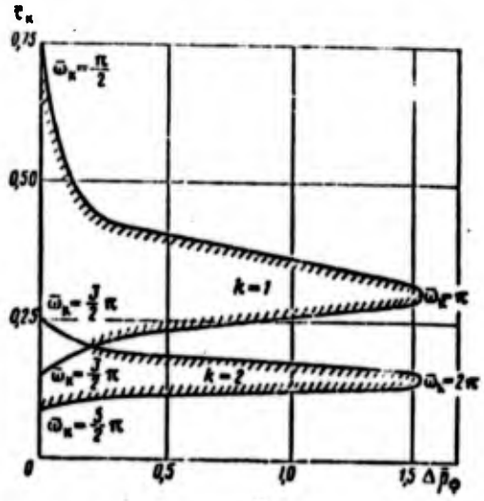

Figure 9.25. LRE stability boundary without account for the line effect.

Figure 9.25 shows the stability boundary for an engine with the parameters noted above, constructed for the two harmonics k = 1 and k = 2. The stability region is to the right of the curves.

Let us construct the engine stability boundary with account for the feed line effect. As noted previously, the line effect amounts to the fact that of all the possible frequencies only the narrow frequency bands lying near the harmonics of the natural oscillations of the liquid in the lines are excited. Thus, each harmonic of the free oscillations of the gas in the combustion chamber (k = 1, 2, 3,...) has a whole group of instability regions, corresponding to the harmonics (n = 1, 2, 3,...) of liquid free oscillations in the lines.

We see from Figure 9.24 that the quantity $\Delta\bar{p}_{inj}$ varies from zero to a maximum and then back to zero, even with account for the line effect. Consequently, the stability boundaries in this case will again have the form of closed regions which have three characteristic points, just as before.

The first point is characterized by the relation $\operatorname{tg}\bar{\omega}=0$ which is satisfied if $\bar{\omega}=n\pi$, where $\bar{\omega}$ is the frequency of liquid free oscillations in the line.

Then

$$\Delta\bar{p}_{\phi} = \sqrt{\frac{\frac{4k^2}{(k+1)^2}}{1+\left[\frac{2}{(k+1)\bar{M}}\operatorname{tg}\bar{\omega}_k\right]^2}}$$

Hence, we see clearly that for the frequencies corresponding to the natural frequencies of the liquid oscillations in the lines (different n) the line effect has no influence. It is convenient to determine the quantity $\bar{\tau}_k$ as follows: on the plot of the relation $\Delta\bar{p}_{inj} = \Delta\bar{p}_{inj}(\bar{\omega}_k)$, we note the dimensionless frequencies $\bar{\omega}$, corresponding to the values $\bar{\omega} = n\pi$ for the given harmonic k, and find from them the values of $\Delta\bar{p}_{inj}$. Then with the aid of the instability boundary in the absence of the feed line effect we find $\bar{\tau}_k$ drawing the straight lines $\Delta\bar{p}_{inj} = \text{const}$ to their intersection with the line bounding the instability region.

The other two points are characterized by the relation $\Delta\bar{p}_{inj} = 0$, which is possible near the frequency $\bar{\omega} = n\pi$. Thus, for each instability region related with the harmonic k there are the following characteristic points (in order of increasing frequency)

1. $\bar{\omega}_1 = n\pi - \Delta\bar{\omega}_1$;

$$\Delta\bar{p}_{\phi} = 0;\ \varphi = -\frac{\pi}{2};\ \bar{\tau}_{k_1} = \frac{\frac{5}{2}\pi - (\pm|\alpha|)}{\bar{\omega}_1}$$

2. $\bar{\omega}_2 = n\pi$;

$$\Delta\bar{p}_{\phi} = \sqrt{\frac{\frac{4k^2}{(k+1)^2}}{1+\left[\frac{2}{(k+1)\bar{M}}\operatorname{tg}\bar{\omega}_k\right]^2}};$$

$$\varphi = 0;\ \bar{\tau}_{k_2} = \frac{2\pi - (\pm|\alpha_2|)}{\bar{\omega}_2}.$$

3. $\bar{\omega}_3 = n\pi + \Delta\bar{\omega}_3$;

$$\Delta\bar{p}_{\phi} = 0;\ \varphi = \frac{\pi}{2};\ \bar{\tau}_{k_3} = \frac{\frac{3}{2}\pi - (\pm|\alpha_3|)}{\bar{\omega}_3}.$$

Calculations show that $\bar{\tau}_{n1}>\bar{\tau}_{n2}>\bar{\tau}_{n3}$; consequently the form of the stability boundary is the same as for the low-frequency oscillations.

Figure 9.26 shows the instability regions for the engine with the parameters noted above, corresponding to the harmonic of the free oscillations of the gas in the combustion chamber with k = 1. Here the possible frequencies are determined by the harmonics n = 5; 6; 7; 8 of the liquid free oscillations in the lines. The hatched curve shows the stability boundary in the absence of the feed line effect.

§ 9. Calculation of the Natural Frequencies of the Acoustic Oscillations of the Gas in a Combustion Chamber

We have previously emphasized the importance of the combustion chamber geometric dimensions in the development of high-frequency oscillations. Therefore, there is definite practical and theoretical interest in the method for calculating the natural acoustic oscillations of the gas in the combustion chamber.

Usually several assumptions and limitations which simplify the mathematical model of the oscillatory processes are used in the examination of this question. These simplifications include, first of all, the assumption that the gas mixture is uniform through the combustion chamber volume, low motion velocity, and small amplitudes of the oscillations of the gas in the chamber.

Under these assumptions the equation for the propagation of small pressure disturbances has the form

$$\frac{\partial^2 p}{\partial \tau^2}=a^2\left(\frac{\partial^2 p}{\partial x^2}+\frac{\partial^2 p}{\partial y^2}+\frac{\partial^2 p}{\partial z^2}\right) \tag{9.110}$$

where τ is time;

x, y, z are the rectangular coordinate axes;

a is the speed of sound.

In cylindrical Coordinates (9.110) transforms to

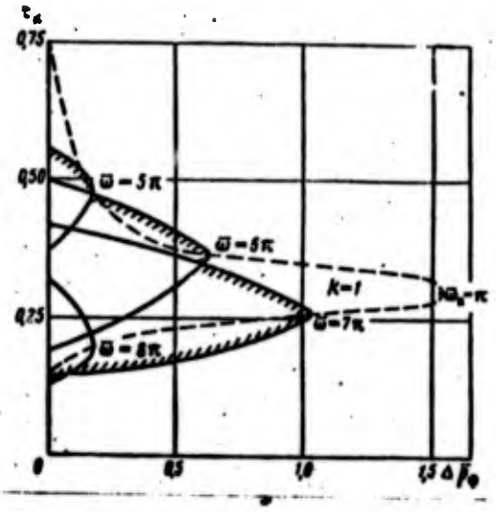

Figure 9.26. LRE stability boundary with account for the feed lines.

$$\frac{\partial^2 p}{\partial \tau^2} = a^2\left(\frac{\partial^2 p}{\partial x^2} + \frac{\partial^2 p}{\partial r^2} + \frac{1}{r}\frac{\partial p}{\partial r} + \frac{1}{r^2}\frac{\partial^2 p}{\partial \vartheta^2}\right) \tag{9.111}$$

The notations used in (9.111) are shown in Figure 9.27. The particular solution of (9.111) can be sought in the form

$$p(r, \vartheta, x, \tau) = R(r)\vartheta(\vartheta)X(x)T(\tau) \tag{9.112}$$

We substitute (9.112) into (9.111)

$$\frac{T''(\tau)}{T(\tau)} = a^2\left[\frac{X''(x)}{X(x)} + \frac{R''(r)}{R(r)} + \frac{1}{r}\frac{R'(r)}{R(r)} + \frac{1}{r^2}\frac{\vartheta''(\vartheta)}{\vartheta(\vartheta)}\right] \tag{9.113}$$

Hence

$$T''(\tau) + \omega^2 T(\tau) = 0; \tag{9.114}$$

$$X''(x) + \left(\frac{\xi}{a}\right)^2 X(x) = 0; \tag{9.115}$$

$$r^2R''(r) + rR'(r) + \left(\frac{\alpha}{a}\right)^2(r^2 - n^2)R(r) = 0; \tag{9.116}$$

$$\vartheta''(\vartheta) + n^2\vartheta(\vartheta) = 0; \tag{9.117}$$

where ω, ξ, a boundary co

It is

where A_1, A_2,

The se meaning of finite at a for r = 0,

Thus t

It fol which defin transverse from the co ends of the

$$\omega^2=\xi^2+a^2, \tag{9.118}$$

where ω, ξ, a are characteristic parameters, which are found from the boundary conditions.

It is obvious that the solution of (9.114) - (9.117) has the form

$$T(\tau)=A_1\sin(\omega\tau+\varphi_1); \tag{9.119}$$

$$X(x)=A_2\sin\left(\frac{\xi}{a}x+\varphi_2\right); \tag{9.120}$$

$$\Theta(\theta)=A_3\sin(n\theta+\varphi_3);$$

$$R(r)=A_4 I_n\left(\frac{a}{a}r\right)+A_5 Y_n\left(\frac{a}{a}r\right), \tag{9.121}$$

(9.122)

where $A_1, A_2, A_3, A_4, A_5, \varphi_1, \varphi_2, \varphi_3$ are arbitrary constants, defined by the initial and boundary conditions

I_n, Y_n are Bessel functions of the first and second kind.

(9.111)

The second solution $Y_n\left(\frac{a}{a}r\right)$ becomes infinite for r = 0. Since the

The meaning of the problem is such that the sought solution must remain finite at all points of the chamber, including the centerline, i.e., for r = 0, then we must set $A_5 = 0$ in (9.122).

(9.112)

Thus the particular solution of (9.111) has the form

$$p(r,\theta,x,\tau)=A\sin\left(\frac{\xi}{a}x+\varphi_2\right)\sin(n\theta+\varphi_3)I_n\left(\frac{a}{a}r\right)\sin(\omega\tau+\varphi_1). \tag{9.123}$$

(9.113)

It follows from these relations that α and ξ are the parameters which define the circular frequencies of the gas oscillations in the transverse and longitudinal directions. In particular, if we start

(9.114) from the condition that the gas velocity equals zero at the walls and ends of the cylinder (chamber), i.e.

(9.115)

$$\left.\frac{\partial p}{\partial x}\right|_{\substack{x=0\\x=L}}=0; \quad \left.\frac{\partial p}{\partial r}\right|_{r=R}=0,$$

(9.116)

(9.117)

then

$$\gamma_2 = k\pi; \quad \frac{\omega}{a} = \frac{a}{l} k\pi; \tag{9.124}$$

$$k = 1,2,3,4,\ldots$$

$$J_n'\left(\frac{\omega}{a} R\right) = 0. \tag{9.125}$$

Equation (9.125) has an infinite set of positive roots. In addition, the values of the roots depend on the order of the Bessel function. We denote

$$\frac{\omega}{a} R = \pi\beta_{nm}. \tag{9.126}$$

Table 3 presents the values of the roots β_{nm} for several oscillation modes.

TABLE 3. ROOTS OF THE EQUATION $J_n'(\beta_{nm}) = 0$

	Values of roots for various m			
n	0	1	2	3
0	0,000	1,220	2,233	3,238
1	0,586	1,697	2,714	3,726
2	0,972	2,135	3,173	4,192
3	1,337	2,531	3,611	4,633

Substituting (9.124) and (9.126) into (9.118), we obtain the formula for determining the natural frequencies of the acoustic oscillations of the gas in the chamber

$$f = \frac{a}{2} \sqrt{\left(\frac{k}{l}\right)^2 + \left(\frac{\beta_{nm}}{R}\right)^2}. \tag{9.127}$$

The indices m, n, k correspond to all possible oscillation modes:

$m \neq 0$, $n = 0$, $k = 0$	radial oscillations;
$m = 0$, $n \neq 0$, $k = 0$	tangential oscillations;
$m = 0$, $n = 0$, $k \neq 0$	longitudinal oscillations.

(9.124)

(9.125)

s. In addi-
essel func-

(9.126)

ral oscilla-

Figure 9.27. Cylindrical coordinate system.

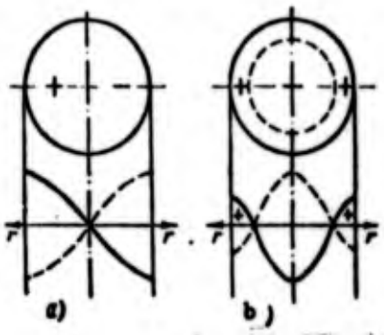

Figure 9.28. Acoustic wave forms for radial vibrations:

a) for $m=0,\ n=1,\ k=0,\ a_{01}=3,832$;
b) for $m=1,\ n=0,\ k=0,\ a_{10}=1,22$

It follows from Table 3, in particular, that the frequency of the first radial oscillation mode (n = 0, k = 0, m = 1) will be

$$f_r = 1{,}22\,\frac{a}{2R}\,.$$

For the first tangential oscillation mode (m = 0, k = 0, n = 1)

$$f = 0{,}586\,\frac{a}{2R}\,.$$

ain the form-
c oscilla-

Thus a low oscillation frequency corresponds to tangential transverse oscillations with a single nodal diameter (Figure 9.238a). The first radial oscillation mode is shown in Figure 9.28b.

(9.127)

The frequency of the longitudinal oscillations of the gas in the combustion chamber is described by (9.127) for n = 0, m = 0:

$$f = \frac{ka}{2L}\,.$$

tion modes:

Obviously, this formula yields very approximate results, since it was obtained with many simplifying assumptions and premises. A more exact method for calculating the natural frequencies of the

longitudinal oscillations of gas in lines of complex geometry is presented in Chapter 7.

10. Transverse High-Frequency Oscillations

The purely transverse modes refer to a large number of different regular high-frequency pressure oscillations which take place in the plane perpendicular to the combustion chamber axis. The transverse oscillations include tangential (standing and rotating), radial, and mixed modes (Figure 9.29). They represent one of the natural oscillation modes of the combustion chamber as a cylindrical resonator. It is well known that both radial and tangential oscillations can develop in the cylindrical resonator, along with the longitudinal oscillations.

Tangential oscillations of the first and second modes are observed most frequently in LRE combustion chambers. Radial oscillations are encountered less frequently. In the case of transverse oscillations, photography through a longitudinal window discloses dark and light zones (Figure 9.30). Radial waves are noted which reflect from the side walls of the combustion chamber; in this case oscillations are observed in the diametral plane. We can also observe rotation of the luminous traces as the incandescent particles travel toward the nozzle. The intensity of the pressure waves is such that erosion traces of spiral form may remain on the chamber walls.

At the present time instability in the form of the transverse high-frequency pressure oscillation modes is most frequently encountered during the experimental development of engines [80], [81]. After operating for a few seconds with these oscillations of large amplitude, the engine will be damaged beyond repair. In this case, on the firing surface of the head there are observed indentations as a result of detonation of the suspended propellant mixture or traces of fusion and burning, and also damage resulting from rotation of the incandescent gases in one direction.

The high frequency oscillations lead to heavy engine vibration, which may result in failure of welded joints and heavy components,

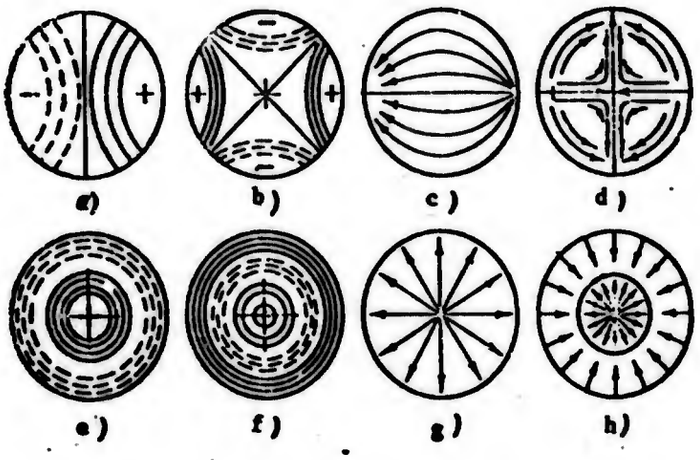

Figure 9.29. Nature of high-frequency transverse vibrations in LRE combustion chamber:

a,b,c,d) purely tangential modes;
e,f,g,h) purely radial modes

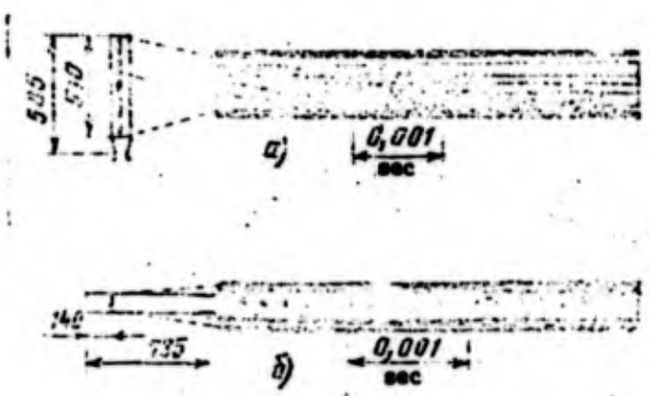

Figure 9.30. Luminous traces observed during high-frequency transverse instability [194]:

a) longitudinal slit (f = 6200 Hz);
b) transverse slit (f = 5860 Hz)

and propellant lines, welded to the chamber, are frequently torn loose together with pieces of the outer shell or at the very least cracks will develop in these areas.

It is clear that experimental investigation of the high-frequency transverse instability of the LRE operating process involves tremendous difficulties. In addition to the failures which are unavoidable in nearly every experiment involving the unstable engine operating regime, extensive material costs are involved because of the frequent nonreproducibility of the phenomenon if an attempt is made to obtain reliable experimental data.

It has been found that the transverse instability phenomenon, obtained at a definite pressure in the combustion chamber, may not be reproduced during the next test under the same operating conditions. The same engine with the same p_K and even in some range of variation of this pressure will operate stably, without pressure pulsations in the combustion chamber. Therefore, it appears that reliable experimental data on transverse oscillations can be obtained only by multiple repetition of the tests of several identical engines, which involves high costs. It appears that this factor, along with the multitude of types of transverse oscillations, is one of the reasons why these modes have received less study than the longitudinal modes.

Very few experimental data on transverse acoustic oscillations in LRE have been published to date [80], [81], [9]. These data indicate that the majority of the factors leading to the development of longitudinal oscillations are favorable for the development of transverse oscillations. It is probable that the mechanism for the onset and also the nature of the effect on the engine is the same for the transverse and longitudinal oscillations.

It has been established that increase of the combustion chamber diameter leads to the onset and development of transverse acoustic oscillations. As for the effect of chamber length, it is not possible at the present time to draw any firm conclusions. It is also known that the transverse acoustic oscillations are excited when the LRE is

boosted by in

All the
the core of t
the combustio
stability wit
It has been n
favorable eff

However,
combatting su
Further accum
the transvers
factor in the
nature of the
for the nonre
effective mea
of a new engi

To date
of the onset
theories base
or continuous
planation of
of suggesting
high-frequenc

A large
cesses taking
processes whe
Landau showed
instability d
made to apply
burning, the
tion, and oth
physical and
many question

boosted by increasing the combustion chamber pressure.

All the measures which lead to elongation of the burning zone in the core of the combustible mixture stream and to intensification of the combustion of the layer near the wall broaden the region of engine stability with respect to the high-frequency transverse oscillations. It has been noted that coarser atomization of the propellant has a favorable effect on this particular type of engine stability.

However, these few experimental data are far from adequate for combatting successfully the high-frequency transverse oscillations. Further accumulation of experimental data on the integrated study of the transverse acoustic oscillations in LRE is required. The primary factor in the problem of LRE stability is the explanation of the nature of the onset of the transverse acoustic oscillations, the reasons for the nonreproducibility of the phenomenon, and the development of effective measures or recommendations to prevent unstable operation of a new engine design.

To date we do not have a sufficiently complete physical picture of the onset of the transverse acoustic oscillations, and the existing theories based on simple models of the phenomenon with step-function or continuous burnup curve are not capable of even a qualitative explanation of the experimentally observed facts, nor are they capable of suggesting effective and reliable techniques for eliminating the high-frequency transverse instability of LRE operation.

A large number of investigations have been made to study the processes taking place in the burning zone and the stability of these processes when subjected to perturbations. Thus, as early as 1944 Landau showed that the plane flame front is unstable and that this instability depends on the acting accelerations. Attempts have been made to apply Landau's argument to explain the onset of turbulent burning, the mechanism of the transition from normal burning to detonation, and other phenomena. In view of the great complexity of the physical and chemical processes taking place in the burning zone, many questions associated with the stability of the working process

have not yet received adequate study. A review of the studies on LRE combustion can be found in the book [148] by Shaulov and Lerner.

es on
Lerner.

CHAPTER 10

LRE SHUTDOWN

In connection with the increasing range and flight velocity of the ballistic rockets there has been an increasing influence of various disturbing factors on their motion, and this means an influence on nose cone impact accuracy. These factors are determined by the errors in the operation of the engines and the guidance system, and also by the errors in fixing the target location [182].

The first group of errors leads to deviation of the velocity modulus and direction and variation of the rocket coordinates at the end of the powered portion of the trajectory from the calculated values. The downrange scatter is determined by the relationships between the parameters of the unpowered portion of the trajectory and the engine thrust after the shutdown command, whose impulse is called the thrust tailoff impulse (TTI). Moreover, the engine thrust decay law must be known for reliable separation of the stages and in order to prevent collision between the rocket body and the separated nose cone.

Several launches of the American Vanguard rocket were unsuccessful because of the fact that after separation the last stage of the rocket was again accelerated by the thrust tailoff impulse and collided with the satellite [44]. Analysis of flight tests [44] shows that combustion can continue in the LRE combustion chamber for several minutes and the resulting tailoff impulse is not so small that it can be neglected.

The operation of the rocket control system terminates simultaneously with the transmission of the command for engine shutdown, i.e., the further flight of the rocket becomes uncontrolled. As the command for nose cone separation is transmitted after the main command for engine shutdown, the tailoff process is very undesirable, since the existence of arbitrary and uncontrolled thrust leads to a significant increase of the downrange scatter. This scatter is determined by the deviation of the magnitude of the TTI from its nominal value, i.e., TTI variance.

§ 1. Concept of LRE Thrust Tailoff Impulse

We have already mentioned that the engine thrust does not disappear immediately upon transmission of the command for engine shutdown, rather the thrust continues to act in the course of some time. (Figure 10.1). The impulse of this thrust — the tailoff impulse — is expressed by the integral

$$I=\int_{\tau_{m.c}}^{\tau_0} P(\tau)d\tau, \qquad (10.1)$$

where $\tau_{m.c}$ is the time when the main command for engine shutdown is transmitted;

τ_0 is the time at which the pressure in the combustion chamber becomes practically zero;

$P(\tau)$ is the engine thrust during shutdown.

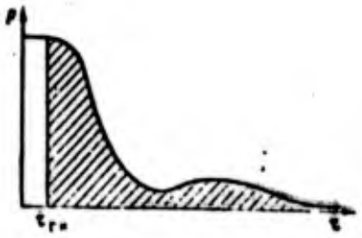

Figure 10.1. Typical curve of thrust variation versus time during LRE shutdown.

Denoting the tailoff impulse for any altitude by I_H and replacing the thrust at altitude P_H using the formula

$$P_H(\tau)=P_{i=}(\tau)G(\tau)-F_c p_H(\tau), \qquad (10.2)$$

we obtain

$$I_H=\int_{\tau_{r.n}}^{\tau_0} P_{i=}(\tau)G(\tau)d\tau-\int_{\tau_{r.n}}^{\tau_0} F_c p_H(\tau)d\tau \qquad (10.3)$$

From this we see that when the engine is shut down the magnitude of the TII in the general case is determined by the variation with time of the vacuum specific thrust and the propellant flow rate, and also by the ambient pressure.

Let us examine the first integral of the vacuum thrust

$$I_{\infty} = \int_{\tau_{p.c}}^{\tau_0} P_{1\infty}(\tau) G(\tau) d\tau. \tag{10.4}$$

Since under flight conditions the engine is usually shut down at high altitudes, where the atmospheric pressure is low (for example, at an altitude of 25 km the atmospheric pressure does not exceed 2% of the sea level pressure), it is the quantity I_{∞} which is of practical importance. We see from (10.4) that the vacuum TTI depends on the specific thrust $P_{1\infty}$, propellant flow rate G, and tailoff time τ_1. The parameters $P_{1\infty}$ and G may change significantly in the engine shutdown process.

The variation of the specific thrust is occasioned by the marked deviation of the oxidizer excess ratio α (the mixture ratio k) from its optimal value and deterioration of the process efficiency. The first factor is a result of uncontrolled variation of the propellant component flow rates in the tailoff period; the second is a result of the sharp dropoff of the pressure in the combustion chamber. The quality dropoff of the pressure in the combustion chamber. The quality of the working process in the LRE is usually evaluated by the specific thrust efficiency φ, which depends on the operating regime and is determined experimentally.

Thus, in the general case the vacuum specific thrust for a given engine can be represented as a function of two parameters

$$P_{1\infty} = P_{1\infty}(k, \varphi).$$

The change of the propellant flow rate is connected with the change change of the valve flow section area F_v and the discharge coefficient μ_v, and also depends on the possible change of the liquid pressure $P_{in.v.}$ ahead of the valve

The operation of the rocket control system terminates simultaneously with the transmission of the command for engine shutdown, i.e., the further flight of the rocket becomes uncontrolled. As the command for nose cone separation is transmitted after the main command for engine shutdown, the tailoff process is very undesirable, since the existence of arbitrary and uncontrolled thrust leads to a significant increase of the downrange scatter. This scatter is determined by the deviation of the magnitude of the TTI from its nominal value, i.e., TTI variance.

§ 1. Concept of LRE Thrust Tailoff Impulse

We have already mentioned that the engine thrust does not disappear immediately upon transmission of the command for engine shutdown, rather the thrust continues to act in the course of some time. (Figure 10.1). The impulse of this thrust — the tailoff impulse — is expressed by the integral

$$I=\int_{\tau_{т.к}}^{\tau_0} P(\tau)d\tau, \qquad (10.1)$$

where $\tau_{m.c}$ is the time when the main command for engine shutdown is transmitted;

τ_0 is the time at which the pressure in the combustion chamber becomes practically zero;

$P(\tau)$ is the engine thrust during shutdown.

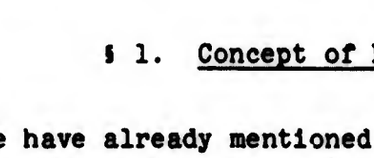

Figure 10.1. Typical curve of thrust variation versus time during LRE shutdown.

Denoting the tailoff impulse for any altitude by I_H and replacing the thrust at altitude P_H using the formula

$$P_H(\tau)=P_{1=}(\tau)G(\tau)-F_c p_H(\tau), \qquad (10.2)$$

we obtain

$$I_H=\int_{\tau_{т.к}}^{\tau_0} P_{1=}(\tau)G(\tau)d\tau-\int_{\tau_{т.к}}^{\tau_0} F_c p_H(\tau)d\tau \qquad (10.3)$$

From this we see that when the engine is shut down the magnitude of the TII in the general case is determined by the variation with time of the vacuum specific thrust and the propellant flow rate, and also by the ambient pressure.

Let us examine the first integral of the vacuum thrust

$$I_{\infty} = \int_{\tau_{\kappa}}^{\tau_1} P_{1\infty}(\tau) G(\tau) d\tau. \tag{10.4}$$

Since under flight conditions the engine is usually shut down at high altitudes, where the atmospheric pressure is low (for example, at an altitude of 25 km the atmospheric pressure does not exceed 2% of the sea level pressure), it is the quantity I_{∞} which is of practical importance. We see from (10.4) that the vacuum TTI depends on the specific thrust $P_{1\infty}$, propellant flow rate G, and tailoff time τ_1. The parameters $P_{1\infty}$ and G may change significantly in the engine shutdown process.

The variation of the specific thrust is occasioned by the marked deviation of the oxidizer excess ratio α (the mixture ratio k) from its optimal value and deterioration of the process efficiency. The first factor is a result of uncontrolled variation of the propellant component flow rates in the tailoff period; the second is a result of the sharp dropoff of the pressure in the combustion chamber. The quality dropoff of the pressure in the combustion chamber. The quality of the working process in the LRE is usually evaluated by the specific thrust efficiency φ, which depends on the operating regime and is determined experimentally.

Thus, in the general case the vacuum specific thrust for a given engine can be represented as a function of two parameters

$$P_{1\infty} = P_{1\infty}(k, \varphi).$$

The change of the propellant flow rate is connected with the change change of the valve flow section area F_v and the discharge coefficient μ_v, and also depends on the possible change of the liquid pressure $P_{in.v.}$ ahead of the valve

$$G = G(F_{\text{кл}}, \mu_{\text{кл}}, p_{\text{вх.кл}})$$

The pressure ahead of the valve may change as a result of reduction of TPA rmp after transmission of the engine shutdown command, change of the flight load factor, and as a result of the occurrence of water hammer as the valve is closed.

Entry of the propellants into the combustion chamber does not terminate after complete closure of the valves, since some definite amount of fuel and oxidizer remains in the lines from the valves to the injectors. Thus the qualitative picture of the phenomenon may be described as follows. After the propellant supply is cut off there is afterburning of the residual propellants and rapid emptying of the combustion products from the chamber. As a result the pressure in the combustion chamber reduces to tenths of a bar if the engine is operating in space or to normal atmospheric pressure if the engine is operating at sea level (on a test stand).

When the pressure of the liquid propellants decreases to the magnitude of their saturated vapor pressure, they begin to boil and evaporate; the result is the creation of a definite head which forces the propellants into the combustion chamber. Thus, the combustion process continues after the valves are closed until the supply of one of the components is completely exhausted. From that moment on only one of the propellants enters the combustion chamber — the propellant which is in excess — and the engine thrust is determined by the reaction of the exhausting jet of the vapors of this component or the products of thermal decomposition. The transient process from the moment the propellant feed supply is cut off to the initiation of the vaporization process sometimes leads to a dip in the chamber pressure curve (see Figure 10.1).

In certain cases pressure pulsations are observed after cut off of the propellant supply; these pulsations are most probably due to the intermittent nature of the component combustion process. We note that the intensity of the process of vaporization of the coolant component depends significantly on the heat influx from the hot chamber walls.

Finally, if the valves are located at a sufficient height above the injector head it may be necessary to take into account the increase of the liquid propellant head due to the effect of flight load factors. The magnitude of this part of the head is

$$\Delta p = \rho h j \tag{10.5}$$

where h is the height of the liquid column above the injector plane;
j is the rocket acceleration.

As for the second integral in (10.3), its magnitude depends only on the ambient pressure and therefore, shows up only during test stand LRE operation and provided the truss-like shock does not enter the nozzle. Otherwise the LRE thrust Formula (10.2) becomes invalid.

In any case, backpressure reduces the thrust tailoff impulse. On the basis of this analysis we can say that the LRE working process during the tailoff period depends on the conditions under which the engine is shut down — whether this is done on a test stand or in flight. This leads to a very important practical conclusion — the tailoff impulse measured on the test stand differs markedly in magnitude from its flight value.

Having analyzed the general expression for the TTI, let us list all the factors affecting its magnitude.

Gasification lag. This phenomenon is associated with the presence of liquid (or vapor) propellant components in the combustion chamber at any instant of time, in particular at the time when the main command is transmitted for engine shutdown. We shall denote the gasification lag by the time τ_1, which includes the time required for vaporization and mixing of the components, and the chemical induction time. During this time the engine does not react to the command; therefore, the entire process is essentially shifted to the right along the time axis (Figure 10.2). The lag time depends on the organization of the mixture formation process, the construction of the atomizing devices, and the nature of the propellant. This time is a quantity of the order of 0.001—0.01 sec.

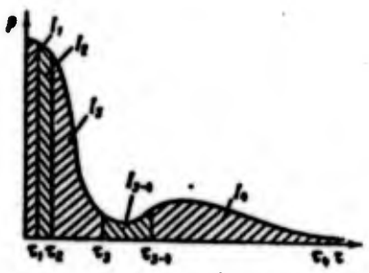

Figure 10.2. Primary components of LRE thrust tailoff impulse (time of each tailoff impulse segment measured from zero).

Propellant cutoff valve triggering lag. A definite time passes from the instant of transmission of the command for valve closure until the closure process begins; this time is called the triggering time τ_2. The valve triggering lag is a result of the inertia of the valve automatic control system. For pneumatic valves $\tau_2 \approx 0{,}05-0{,}15$ sec, for pyrovalves $\tau_2 \approx 0{,}001-0{,}015$ sec. During the time τ_2 the propellants will enter the combustion chamber in the same quantities as they did prior to the main cutoff command if the TPA rpm has not changed. In the general case the lag time τ_2 is different for the oxidizer and fuel valves.

Cutoff valve closure (actuation) process. We consider the valve closure time τ_3 to be the time from the initiation of motion of the valve disk until the disk is fully closed. The valve flow section area varies in time following some law which depends on the valve type and construction, and also on the law governing the control pressure rise in the pneumohydraulic valves (PHV) (for a system using pneumohydraulic valves). It is obvious that the cutoff valve closure law also affects the variation in time of the flow rates of the corresponding propellant components. For PHV $\tau_3 \approx 0{,}1-0{,}3$ sec, for pyrovalves this time is negligibly short ($\leq$0.001 sec). Since the pressure gradients in the chamber reach large values during valve closure, this segment of the process is termed the chamber pressure sharp tailoff segment.

Entry of propellants into the combustion chamber after complete valve closure. The reasons for this phenomenon have been mentioned previously. The vaporization process has the longest duration of all the factors which determine the tailoff period. The vaporization time may vary over wide limits, depending on the nature and amount of the

propellants in the lines between the valve and the injectors; this time varies from a few seconds to a few minutes[1]. We denote this time by τ_4.

Between the segment of sharp pressure drop in the chamber and the propellant vaporization segment, there is an intermediate segment which is defined by the transition time τ_{3-4}. In addition to these factors, the thrust decay law after transmission of the main shutdown command may also be affected somewhat by the transient processes in the components of the propellant supply system — the liquid-propellant gas generator (LGG) and the TPA.

The TPA does not shut down immediately after transmission of the command for engine shutdown, since there is a lag in the triggering of the valves which control the propellant flow to the LGG. The actuation of these valves is also not instantaneous. Therefore, the working fluid flow rate, and this means the shaft torque, diminishes gradually, i.e., the TPA rpm also changes gradually. The latter is also explained to a considerable degree by the inertia of the TPA rotating masses.

During the control valve triggering lag time the rpm remains constant; the rpm is also nearly constant in the course of the so-called transient lag time, which is inherent in dynamic systems with two or more elements connected in series. In the case in which the cutoff valves close before the TPA rpm begins to decay, this factor has no effect on the magnitude of the TTI. Otherwise the problem is complicated considerably by the necessity for taking into account the variation of the propellant pressures downstream of the TPA pumps, which determine the flow rates and therefore, the chamber pressure and the thrust.

Thus, the total tailoff time is represented by the sum

$$\tau = \tau_1 + \tau_2 + \tau_3 + \tau_{3-4} + \tau_4. \qquad (10.6)$$

Footnote (1), see page 453

Therefore, the total LRE vacuum tailoff impulse can be represented in the form of the sum of the following basic components (see Figure 10.2)

$$I_{\infty}=I_1+I_2+I_3+I_{3-4}+I_4. \tag{10.7}$$

We take as the zero point for measuring the duration of the process in a given segment the termination of the preceding segment. Then each component can be determined independently by the following expressions:

$I_1=P_{\infty}\tau_1$ is the TTI component due to gas formation lag in the combustion chamber. Here P_{∞} is the engine thrust at the moment of cutoff.

$I_2=\int_0^{\tau_2} P_{1-}Gd\tau$ is the TTI component due to valve triggering lag. If the TPA rpm does not change during the lag time τ_2, then the propellant flow rate remains constant. In this case $I_2=P_{\infty}\tau_2$.

$I_3=\int_0^{\tau_3} P_{1-}Gd\tau$ is the TTI component due to variation of the engine parameters in the valve closure period and the reduction of the fuel and oxidizer volumes in the lines as a result of the marked reduction of the pressure of the propellant components in these lines.

$I_{3-4}=\int_0^{\tau_{3-4}} P_{1-}Gd\tau$ is the TTI component which shows up during the transition from the sharp chamber pressure decay to propellant vaporization.

$I_4=\int_0^{\tau_4} P_{1-}Gd\tau$ is the TTI component due to discharge into the combustion chamber of the fuel and oxidizer which boil in their lines; in the general case this segment may in turn be broken down into periods of discharge of the fuel alone, joint discharge of the propellants, and discharge of the oxidizer alone.

While the I_1 and I_2 components can, as a rule, be calculated quite accurately, the determination of the other components involves serious difficulties as a result of the complexity of the physical processes taking place. We shall examine in greater detail the calculation of the components I_1, I_{3-4}, I_4.

§ 2. Transient Processes During Abrupt Combustion Chamber Pressure Decay After Transmission of Engine Shutdown Signal

1. Basic Equations

Depending on the arrangement of the projected LRE, propellant cutoff after the engine shutdown command is transmitted can be accomplished by pneumatic valves, pyrovalves, or with the use of a pneumatic valve in one line and a pyrovalve in the other.

We shall first write the complete system of differential equations which describe the transient process during engine shutdown for the general case (Figure 10.3). We first examine the process without considering the specific type of valve, and then present the solutions for individual particular cases.

We simplify somewhat the combustion chamber equation obtained in Chapter 3 by neglecting the lag. Then (3.13) may be written as follows

$$\frac{dp_к}{dt} = (G_o + G_г)\frac{R_к T_к}{V_к} - \frac{\mu_к F_{кр} \sqrt{R_к T_к}}{V_к} p_к. \qquad (10.8)$$

We use the equation of motion (3.50) of the propellants in the line from the valve to the combustion chamber in simplified form:

for the oxidizer line

$$p_{2,к} = p_к + b_{1,к} G_o^2 + b_{2,к} \frac{dG_o}{dt} + p_{н.к}; \qquad (10.9)$$

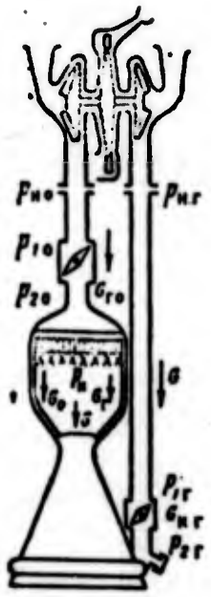

Figure 10.3. Typical LRE hydraulic flow diagram.

for the fuel line

$$p_{2r} = p_{\kappa} + b_{1r,\kappa} G_r^2 + b_{2r,\kappa} \frac{dG_r}{d\tau} - p_{r,z}, \qquad (10.10)$$

where p_2 is the pressure after the valve;

p_z is the pressure due to the difference of the height of the sections being considered (this quantity can usually be neglected);

G is the propellant flow rate into the combustion chamber.

The Bernoulli equation can be written in the form (4.18):

for the oxidizer valve

$$p_{1o} = p_{2o} + \left(\zeta_{1o} + \zeta_{2o} \frac{d_{co}}{x_o}\right) \frac{G_{\kappa.o}^2}{2\rho_o F_{io}^2 \mu_{io}^2}; \qquad (10.11)$$

for the fuel valve

$$p_{1r} = p_{2r} + \left(\zeta_{1r} + \zeta_{2r} \frac{d_{c.r}}{x_r}\right) \frac{G_{\kappa.r}^2}{2\rho_r F_{ir}^2 \mu_{ir}^2}. \qquad (10.12)$$

The equations of motion of the propellants in the line from the pump to the valve are written analogously to (10.9) and (10.10):

for the oxidizer line

$$p_{\kappa.o} = p_{1o} + b_{1o,\kappa} G_{\kappa.o}^2 + b_{2o,\kappa} \frac{dG_{\kappa.o}}{d\tau} - p_{oz\kappa}; \qquad (10.13)$$

for the fue

Since
short, we s
time functi

and

where p^*_{κ} i
d
θ_{κ} i

We sha
simultaneou
favorable f
the tailoff
to close be
plained by
the valve m
the instant
the pump ex
undesirable
of the TTI

Now we
masses in a

for the oxi

for the fuel line

$$p_{n.r} = p_{1r} + b_{1r.n} G_{n.r}^2 + b_{2r.n} \frac{dG_{n.r}}{dt} - p_{r2n}. \tag{10.14}$$

Since the time during which we must consider the TPA operation is short, we shall consider the pump exit pressure to be an exponential time function, i.e.,

$$p_{n.o} = p_{n.o}^* e^{-\frac{t}{\theta_a}} \tag{10.15}$$

and

$$p_{n.r} = p_{n.r}^* e^{-\frac{t}{\theta_a}}, \tag{10.16}$$

where p^*_n is the pump outlet pressure at the instant the engine shutdown signal is transmitted;

θ_a is the TPA time constant.

We shall also assume that the pump exit pressure decay begins simultaneously with the movement of the disks, since this case is most favorable from the viewpoint of reducing the magnitude and scatter of the tailoff impulse. In fact, the TTI increases if the valves begin to close before the pump exit pressure begins to decay. This is explained by the fact that the cutoff valve closure time increases, since the valve must overcome a constant pressure equal to the pressure at the instant the engine shutdown command is transmitted. However, if the pump exit pressure begins to decay before the valves begin to close undesirable pressure pulsations may develop, which leads to increase of the TTI scatter.

Now we write the equation of motion of the cutoff valve disk masses in accordance with (4.17):

for the oxidizer valve

$$m_o \frac{d^2 x_o}{dt^2} + c_{f.o}(F_{s.o} - P_{f.o} - p_y S_{y.o} - p_{2.o} S_{1.o}) \frac{dx_o}{dt} + c_o x_o + p_{1.o} F_{1o} - p_{2.o}(F_1 - F_{m.o}) - (p_y - p_H) F_{y.o} + P_{c0.o}; \tag{10.17}$$

for the fuel valve

$$m_r \frac{d^2x_r}{d\tau^2} \pm c_{fr}(P_{n.r} - P_{fr} - p_y S_{y.r} - p_{2r} S_{w.r}) \frac{dx_r}{d\tau} + \\ + c_1 x_r = p_{1r} F_{1r} - p_{2r}(F_1 - F_{w.r}) - (p_y - p_H) F_{y.r} \pm P_{c0r}. \quad (10.18)$$

If the cutoff valves block the lines rapidly, then in calculating the segment covering the rapid decay of the combustion chamber pressure we must take into account the elastic deformation forces which accompany the displacement of the propellants into the chamber from the volume between the valves and the injectors. Then, averaging the fluid pressure over the entire volume, we can write approximately:

for the oxidizer line

$$\frac{dp_{2o}}{d\tau} = (G_{n.o} - G_o - G_{o.s}) \frac{a_o^2}{V_o} \quad (10.19)$$

for the fuel line

$$\frac{dp_{2r}}{d\tau} = (G_{n.r} - G_r - G_{r.s}) \frac{a_r^2}{V_r} \quad (10.20)$$

where V is the volume of the line between the valve and the combustion chamber;

a is the speed of sound in the propellant;

G_{ve} is the propellant flow rate to the vent line (if the propellant flow system has this provision).

We obtain the equation defining the variation of the control gas pressure from the following considerations. In the simplest case we assume each cutoff valve has its own individual pneumatic line (Figure 10.4). Then we start from the following arguments to determine the relation $p_y = p_y(\tau)$. In the general case the control gas flow rate into the cavity above the cutoff valve piston is a variable quantity. The gas which is in the line between the pressure reducer and the electropneumatic valve (EPV) begins to flow into the cutoff valve gas line after the EPV is opened. The pressure reducer valve which lets gas flow from the high pressure line opens simultaneously.

(10.18)

calculating
ber pressure
ich accom-
rom the
ng the
nately:

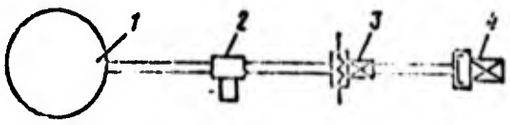

Figure 10.4. Block diagram of pneumatic line with a single main valve: 1) gas bottle; 2) reducer; 3) EPV; 4) pneu- hydraulic valve.

Making use of the fact that the line volume is small while the flow cross sections are comparatively large, we simplify the process scheme and represent it as follows. We assume that the EPV opens instantaneously after passage of the lag time τ_{epv}. After the EPV valve opens, the pressures in the lines and in the lines and in the gas cavity of the cutoff valve equalize rapidly. Then the pressure reducer valve opens and gas flows from the high-pressure lines into the low-pressure chamber. By low-pressure chamber we mean the entire segment after the pressure reducer valve, including the gas cavity. Neglecting heat transfer and gas leakage and assuming the low-pressure line volume small in comparison with the cutoff valve gas cavity volume, and assuming the pressure drop from the reducer valve small in comparison with the pressure in the low-pressure chamber, we write the equation for the pneumatic line in the form

(10.19)

$$\frac{dp_y}{d\tau} = -\frac{k}{V_m + V_{kn}} \left(R_0 T_0 G_p - p_y F_y \frac{dx}{d\tau} \right)$$

(10.20)

where V_m is the volume of the line from the pressure reducer to the cutoff valve;
V_v is the cutoff valve gas cavity volume;
G_{red} is the gas flow rate through the reducer;
T_b is the gas temperature in the bottle.

Neglecting the losses in the high-pressure line (from the high-pressure bottle to the reducer valve), since they usually constitute less than 5% of the bottle pressure, we assume that the pressure ahead of the reducer valve equals the pressure in the tank. Then the gas flow rate through the reducer is

$$G_{red} = A_{red} \frac{p_6 \mu_{red} F_{red}}{\sqrt{R_6 T_6}} q(\lambda_{red})$$

where $q(\lambda_{red})$ is the gasdynamic function of the velocity coefficient λ_{red}; since the reducer setting pressure is practically always less than the critical value, then $q(\lambda_{red}) = 1$;

μ_{red} is the discharge coefficient;

F_{red} is the minimal area for gas flow (in the reducer valve); it is determined by the reducer valve travel, which depends on the valve exit pressure p_{red}; usually in the process of cutoff valve closure p_{red} is such that the valve is fully open, i.e., $F_{red} = F_{red\ max}$.

In determining G_{red} we shall assume that the gas parameters in the bottle remain unchanged during the cutoff valve closure time. These assumptions facilitate considerably the determination of the relation $p_y = p_y(\tau)$ and are fully justified by the good agreement of calculation and experiment.

So far we have considered the case in which the gas flows from the pneumatic line to only a single cutoff valve. If there are two valves connected in parallel, the basic equation remains as before, since in the actual LRE pneumatic lines the pressure drops in the segments from the point where the main lines branch up to the main valve can be neglected, and therefore, the calculation of the relation $p_y = p_y(\tau)$ for the actual case differs only in that we take the volume V_v to mean the sum of the volumes of the low-pressure lines and the gas cavities of the oxidizer and fuel cutoff valves.

We finally write the pneumatic line equation in the form

$$\frac{dp_y}{d\tau} = \frac{k}{V_n + V_{k.o} + V_{k.r}} \left[A_{red} \mu_{red} F_{red} p_6 \sqrt{R_6 T_6} - p_y \left(F_{y.o} \frac{dx_o}{d\tau} + F_{y.r} \frac{dx_r}{d\tau} \right) \right]. \quad (10.21)$$

The equations defining the relationship between the propellant flow G_{ve} to the vent (if venting is provided in the design) and the flow rate G to the combustion chamber will be

$$G_{o.x} = \chi_o G_o; \tag{10.22}$$

$$G_{f.x} = \chi_f G_f. \tag{10.23}$$

The quantity χ can be determined as follows. If p_H is the ambient pressure into which the propellant is vented in order to reduce its flow rate into the chamber, then the connection between the pressure differential drop and the flow rate may be written as

$$G = \sqrt{\frac{p - p_H}{b_1}} \tag{10.24}$$

$$G_x = \sqrt{\frac{p - p_H}{b_{1x}}} \tag{10.25}$$

where the coefficient

$$b_{1x} = \frac{1}{2(\mu_x F_x)^2 \varrho} \tag{10.26}$$

and F_{ve} is the vent port area;

μ_{ve} is the flow rate through the vent.

In deriving this formula we have neglected any possible boiling of the propellant in the vent port. The coefficient $b_{1\ ve}$ will be found somewhat later for the exact calculations (with account for boiling). Now we write the expression for χ with the aid of (10.24) and (10.25)

$$\chi = \sqrt{\frac{b_1}{b_{1x}} \frac{1 - p_H/p}{1 - \frac{p_H}{p}}} \tag{10.27}$$

For the vacuum case we can take $p_H/p = 0$ in this formula. We see that χ depends on the pressure ratios p_H/p and p_H/p, which vary over only a small range and, moreover, appear under the radical. This permits determining χ from the parameters of the basic operating regime with adequate accuracy.

Since the combustion product work capacity $R_K T_K$ is a function of the mixture ratio $k = G_o/G_f$, we must supplement the equations written

above by the dependence of $R_K T_K$ on k, i.e.,[2]

$$R_K T_K = f\left(\frac{G_o}{G_f}, p_K\right) \tag{10.28}$$

or approximately

$$\frac{1}{R_K T_K} \approx a_1(p_K)\left(\frac{G_o}{G_f}\right)^2 + a_2(p_K)\frac{G_o}{G_f} + a_3(p_K) \tag{10.29}$$

where a_1, a_2 and a_3 are coefficients which depend on p_K.

The resulting system of 18 equations (10.8)—(10.23), (10.27), (10.28) contains 18 time-dependent quantities: x_o, x_f, p_{1o}, p_{1f}, p_{2o}, p_{2f}, $G_{H.o}$, $G_{H.f}$, G_o, G_f, $G_{o.ve}$, $G_{f.ve}$, p_K, p_y, $p_{H.o}$, $p_{H.f}$, R_K, T_K.

This system makes it possible in principle to find the time variation of these parameters. However, this is a system of nonlinear differential equations with variable coefficients, whose solution presents serious difficulties. These difficulties, which are associated with the numerical solution of the system, can be overcome with the aid of computers.

In application to specific LRE pneumohydraulic systems, this system can always be simplified without any loss of computational accuracy. In this connection it is advisable to solve the system which is simplified in accordance with the data of the particular case rather than the complete system of equations.

We shall examine possible combinations of cutoff valves in the main propellant feed lines.

Version I: pyrovalves installed in the oxidizer and fuel lines;

Version II; a pyrovalve in the oxidizer line and a pneumatic valve in the fuel line.

Footnote (2), see page 453

We shall study these two versions analytically.

2. Analysis of the Transient Process of Shutdown of LRE With Cutoff Pyrovalves (Version I)

We shall assume that the pyrovalves close instantaneously and simultaneously[3] (we neglect wave processes). Moreover, we make the following simplifying assumptions, which are justified in certain cases: a) the mixture ratio does not change during the time of the abrupt combustion chamber pressure decay; b) the quadratic dependence of the propellant flow rate on the pressure differential is linearized as follows

$$b_1 G^2 = \tilde{p} + BG \tag{10.30}$$

where $\tilde{p} = p - p^*$;

$$B = \left(\frac{p - p_к}{G}\right)^*$$

c) the piezometric head of the propellants in the lines is negligibly small.

Using these assumptions, the system of equations describing the transient processes in the engine after valve closure can be transformed to the form

$$\ddot{G}_г + 2a_3 \dot{G}_г + a_2 G_г = 0 \tag{10.31}$$

where $2a_3 = -\frac{kB_o - B_г}{kb_{2o} - b_{2г}}$.

Calculations show that usually $\lambda = \sqrt{a_2 - a_3^2} > 0$. Therefore, the solution of the second-order differential equation with constant coefficients (10.31) will be

$$G_г = e^{-a_3 t}(C_1 \cos \lambda t + C_2 \sin \lambda t)$$

Footnote (3), see page 453

where the constants C_1 and C_2 are found from the initial conditions[4]

$$C_1=\bar{G}_r^*;\ C_2=\frac{\dot{G}_r^*+a_3G_r^*}{\lambda}.$$

Since we are examining the case of constant k, there is no difficulty in finding the oxidizer flow rate variation law as a function of time. Solving (10.8), we determine the curve of the abrupt combustion chamber pressure decay (provided that for $\tau=0$ the value of $p_к=p_к^*$)

$$p_к=\frac{p_к^*}{e^{a_3\tau}}+$$

$$+\frac{[\lambda A_{к_2}+(A_{к_1}-a_3)A_{к_2}]\sin\lambda\tau+[(A_{к_1}-a_3)A_{к_2}-\lambda A_{к_2}](\cos\lambda\tau-1)}{e^{a_3\tau}[\lambda^2+(A_{к_1}-a_3)^2]}$$

where

$$A_{к_1}=\frac{A_к F_{кр}\sqrt{R_к T_к}}{V_к};\qquad (10.32)$$

$$A_{к_2}=\frac{(1+k)R_к T_к}{V_к}\bar{G}_r^*;$$

$$A_{к_3}=\frac{(1+k)R_к T_к}{V_к}\cdot\frac{(2\dot{G}_r^*+a_3G_r^*)}{2\lambda}.$$

Let us find the TTI component due to the abrupt pressure decay after valve closure (until evaporation of the propellants begins). As is known, the absolute vacuum thrust $P_{пу}$ can be expressed with account for the losses in the chamber and in the nozzle in terms of the pressure p_K by the formula

$$P_{пу}=m\varphi_{p_к}\varphi_c F_{кр}K_{пу}p_к, \qquad (10.33)$$

where m is the number of power plant chambers;
$\varphi_{p_к}$ is the combustion chamber pressure efficiency;
φ_c is the nozzle coefficient;
$K_{пу}$ is the vacuum thrust coefficient.

Now

where

Linear

when the i

can take,

tions, ove

where the

known engi

tions do n

The l

following

below the

the fuel)

to flow in

ical press

have seen

propellant

drop we ca

responding

end of the

If we

$b_2\dot{G}=0$ and

Footnote (4), see page 453

onditions(4)

is no dif-
a function
rupt com-
value of

Now

$$I_{3*} = m\tau_{p_*}\tau_{c_*}F_{*p}K_* \left\{ \frac{1 - e^{-a_3\tau_3}}{a_3}\left(p_*' - \frac{\tau_{2*}}{\tau_{3*}}\right) + \right.$$

$$\left. + \frac{e^{-a_3\tau_3}\sin\lambda\tau_3\,(\lambda\tau_{2*} - a_3\tau_{1*}) + (\lambda\tau_{1*} + a_3\tau_{2*})(1 - e^{-a_3\tau_3}\cos\lambda\tau_3)}{\tau_{3*}(a_3^2 + \lambda^2)} \right\}$$

where $\delta_1 = \lambda\Lambda_{K1} + (\Lambda_K - a_3)\Lambda_{K2}$;
$\delta_2 = (\Lambda_K - a_3)\Lambda_{K1} - \lambda\Lambda_{K2}$;
$\delta_3 = \lambda^2 + (\Lambda_K - a_3)^2$.

Linearization by means of (10.30) can be used for the calculations when the integration is made over time intervals $\Delta\tau$. But sometimes we can take, with a precision which is adequate for engineering calculations, over the entire abrupt pressure decay segment

(10.32)

$$b_1G^2 = BG, \tag{10.34}$$

where the coefficient B is determined from the parameters in some known engine operating regime. In this case the computational equations do not differ in any way from those presented above.

ure decay
begins).
ed with
terms of

The length τ_3 of the sharp decay segment may be found from the following considerations. When the combustion chamber pressure falls below the saturated vapor pressure of one of the propellants (usually the fuel) the latter boils (after the boiling delay time τ_{del} and begins to flow into the chamber. In practice, during the time τ_{del} the critical pressure drop will be established across the injectors, and we have seen previously that this pressure drop can be found from the propellant temperature ahead of the injectors. From this pressure drop we can find the propellant flow rate and therefore, the corresponding pressure in the combustion chamber, which defines τ_3 — the end of the sharp decay segment.

(10.33)

If we first assume the mixture ratio to be constant, then take $b_2\dot{G} = 0$ and linearize the quadratic dependence of the flow rate on the

pressure using (10.34), we can transform the original system of equations to the form(5)

$$\left.\begin{aligned}\dot{p}_0 &= -A_0 p_0 + A_0 p_K;\\ \dot{p}_r &= -A_r p_r + A_r p_K;\\ \dot{p}_K &= A_{K.0} p_0 + A_{K.r} p_r - A p_K\end{aligned}\right\} \qquad (10.35)$$

where A_0 and A_r are constant coefficients

$$A_{K.0} = \frac{1}{B_0}\frac{R_K T_K}{V_K}; \qquad A_{K.r} = \frac{1}{B_r}\frac{R_K T_K}{V_K}; \qquad A_0 = (1+\gamma_0)\frac{a_0^2}{B_0 V_0};$$

$$A = A_{K.0} + A_{K.r} + A_K; \quad A_r = (1+\gamma_r)\frac{a_r^2}{B_r V_r}.$$

Solving this system, we obtain

$$p = C_1 e^{\lambda_1 \tau} + C_2 e^{\lambda_2 \tau} + C_3 e^{\lambda_3 \tau}, \qquad (10.36)$$

where $\lambda_1, \lambda_2, \lambda_3$ are the roots of the characteristic equation;
C_1, C_2, C_3 are arbitrary constants which are determined from the initial conditions for $\tau = 0$; $p_0 = p_0^\circ$; $p_r = p_r^\circ$; $p_K = p_K^\circ$.

$$C_1 = \frac{(p_0^\circ - \alpha_{0.1} p_K^\circ)(\alpha_{r.2} - \alpha_{r.3}) + (p_r^\circ - \alpha_{r.2} p_K^\circ)(\alpha_{0.1} - \alpha_{0.2})}{(\alpha_{r.2} - \alpha_{r.3})(\alpha_{0.1} - \alpha_{0.3}) + (\alpha_{r.3} - \alpha_{r.1})(\alpha_{0.2} - \alpha_{0.3})}$$

$$C_2 = \frac{p_r^\circ - \alpha_{r.1} p_K^\circ + C_1(\alpha_{r.3} - \alpha_{r.1})}{\alpha_{r.2} - \alpha_{r.3}};$$

$$C_3 = p_K^\circ - C_1 - C_2;$$

$$\alpha_{0.1.2.3} = \frac{A_0}{A_0 + \lambda_{1.2.3}}; \qquad \alpha_{r.1.2.3} = \frac{A_r}{A_r + \lambda_{1.2.3}}.$$

The calculations show that the second root λ_2 of the characteristic equation

$$\lambda^3 + (A + A_r + A_0)\lambda^2 + [A_0(A_r + A_{K.r} + A_K) + A_r(A_K + A_{K.0})]\lambda + A_0 A_r A_K = 0.$$

is of decisive importance in the final results.

Footnote (5), see page 453

There
culate p_K
somewhat

Hence

For p
obtained f

Formul
but with c

In thi

where $A_{\lambda 1} = (1$

3. Analysis

For thi

em of equa-

Therefore, we can use the following approximate formula to calculate p_K with some loss of precision, obtaining a result which is somewhat low

$$p_к \approx C_2 e^{\lambda_2 \tau}. \tag{10.37}$$

(10.35)

Hence

$$I_{3к} = \bar{\tau}_{p_к} \bar{\tau}_c F_{кр} K_к C_2 \frac{(e^{\lambda_2 \tau_0} - 1)}{\lambda_2} \tag{10.38}$$

For preliminary calculations we can use the following formula, obtained for k = const and $b_2 \dot{G} = 0$:

$$p_к = p_к^* e^{-\Lambda_к \tau} + \frac{A_{к1}}{\Lambda_к}(1 - e^{-\Lambda_к \tau}) - \frac{B_к}{\Lambda_к^2}[\Lambda_к \tau - 1 + e^{-\Lambda_к \tau}]. \tag{10.39}$$

(10.36)

Formula (10.39) yields a result which is significantly too low, but with considerable simplification of the calculations.

rom the

In this case the magnitude of the TTI will be

$$I_{3к} = m \bar{\tau}_{p_к} \bar{\tau}_c F_{кр} K_к \left[\left(\frac{p_к^*}{\Lambda_к} - \frac{A_{к1}}{\Lambda_к^2} - \frac{B_к}{\Lambda_к^3} \right)(1 - e^{-\Lambda_к \tau_3}) + \right.$$
$$\left. + \left(A_{к1} + \frac{B_к}{\Lambda_к} \right) \frac{\tau_3}{\Lambda_к} - \frac{B_к}{2\Lambda_к} \tau_3^2 \right], \tag{10.40}$$

where $A_{к1} = (1 + k) \frac{R_к T_к}{V_к} G_т^*$;

aracteris-

$$B_к = \frac{(1 + k) R_к T_к a_1}{V_к};$$

$$a_1 = \frac{k(1 + \chi_0) a_0^2 / V_0 - (1 + \chi_т) \frac{a_т^2}{V_т}}{2(b_{1т} k^2 - b_{1т})}.$$

3. Analysis of LRE Shutdown Transient Process (Version II)

For this version we make the following assumptions.

For the fuel line with pneumatic cutoff valve: 1) $m_c\frac{d^2x_c}{d\tau^2}=0$ —

on the basis of the smallness of the inertia forces of the moving parts of the pneumatic valve in comparison with the pressure forces and the spring force;

2) on the basis of the relative smallness of the velocities of the propellants and the lengths of the lines from the pump to the valve, for today's pneumatic valve closure rates we shall assume that

$$b_{1r.n}G^2=0;\ b_{2r.n}\frac{dG_{n.r}}{d\tau}=0;\ p_{str}=0;$$

3) $\frac{dp_{\text{ж}}}{d\tau}=0$ — this assumption is equivalent to equality of the flow rates through the valve and the injectors, i.e., $G_{H.f.}=G_{f.}$, in other words, we neglect the accumulation of liquid in the fuel line due to its yielding and we also assume an arrangement without venting;

4) since the valve disk movement velocity changes over a very small range, we can neglect the dependence of the friction coefficient on velocity

$$P_f=\pm f(p_1S_1+p_2S_{\text{ш}}+P_{f\text{ж}}-P_{\text{п}})$$

For the oxidizer line with pyro cutoff valve: 1) since the pyrovalve actuation time is negligibly short [(1—3) · 10^{-3} sec], we can assume that the pyrovavle closes instantaneously and the hydraulic circuit can be examined directly. Consequently we can eliminate from the general system the equation of motion of the oxidizer pyrovalve disk and set

$$b_{1o.n}G^2_{n.o}=0;\ b_{2o.n}\frac{dG_{n.o}}{d\tau}=0;$$

$$\left(\xi_{1o}+\xi_{2o}\frac{d_{c.o}}{x_0}\right)\frac{G^2_{n.o}}{2\rho_n F^2_{1o}}=0;$$

2) $b_{2\kappa}\frac{dG_0}{d\tau}=0$ — as a result of the smallness of the coefficient $b_{2\kappa}$, which accounts for the mass of the fluid in the line downstream of the pyrovalve.

With account for these assumptions the basic system of equations is simplified and after some transformations takes the form

$$\frac{dp_\kappa}{d\tau}=(G_0+G_r)\frac{R_\kappa T_\kappa}{V_\kappa}-\frac{A_{\kappa p}F_{\kappa p}\sqrt{R_\kappa T_\kappa}}{V_\kappa}p_\kappa; \tag{10.41}$$

$$p^*_{m.r}e^{-\frac{\tau}{\theta}}=p_\kappa+b_{2r.\kappa}\frac{dG_r}{d\tau}+\xi_r(x)G_r^2; \tag{10.42}$$

$$\frac{dp_\kappa}{d\tau}+2b_{1o.\kappa}G_0\frac{dG_0}{d\tau}=-G_0\frac{a_0^2}{V_0}; \tag{10.43}$$

$$\begin{aligned}&\frac{dp_{m.r}}{d\tau}F_{1r}-(F_1-F_{m.r}\pm fS_m)\left(\frac{dp_\kappa}{d\tau}+2b_{1r.\kappa}G_r\frac{dG_r}{d\tau}+\right.\\&\left.+b_{2r.\kappa}\frac{d^2G_r}{d\tau^2}\right)-\frac{k(F_{y.r}\pm fS_y)}{V_m+V_{\kappa.r}}\left(A_{np}\mu_p F_p\right)\sqrt{R_6T_6}p_6-\\&-\frac{F_{y.r}}{F_{y.r}\pm fS_y}\left[p_{m.r}F_{1r}-(F_1-F_{m.r}\pm fS_m)(p_\kappa+b_{1r.\kappa}G_r^2+\right.\\&\left.+b_{2r.\kappa}\frac{dG_r}{d\tau}\right)-c_rx_r+p_aF_{y.r}+P_{i0r}\pm f(P_{f\kappa}-P_a)\Big]\frac{dx_r}{d\tau}-\\&-c_r\frac{dx_r}{d\tau}\Big\},\end{aligned} \tag{10.44}$$

where $\xi_r(x)=\left(\xi_{1r}+\xi_{2r}\frac{d_{c.r}}{x_r}\right)\frac{1}{2\rho_1F_{1r}^2}+b_{1r.\kappa}$.

The Equations (10.41)—(10.44) must be solved numerically. To do this we break the entire transient process down into quite short time intervals and calculate the curve $p_\kappa=p_\kappa(\tau)$ for these intervals. Let us begin with the examination of the first time interval, lying between 0 and the time τ_1. Within each interval certain variable quantities are replaced by constants (averages for the given interval). We introduce the following notations for these quantities

$$p_{u.r} = p^{\circ}_{u.r} e^{-\frac{t}{\theta}} = p^{\circ\circ}_{u.r}; \qquad 2b_{1u.k} G_{u} = B_2$$

for

Additionally, within each interval we linearize the quadratic dependence of the flow rate on the different pressure

$$\xi_r(x_r) G_r^2 = B_3 G_r + B_4',$$

where

$$B_3 = \frac{(\Delta p_r)_{l+1} - (\Delta p_r)_l}{G_{r(l+1)} - G_{rl}};$$

$$B_4' = \Delta p_{rl} - \frac{(\Delta p_r)_{l+1} - (\Delta p_r)_l}{G_{r(l+1)} - G_{rl}} G_{rl};$$

$$\Delta p_r = p_{u.r} - p_k.$$

Here,

to the reg

second der

For later convenience we denote

obtained f

$$p^{\circ}_{u.r} e^{-\frac{t}{\theta}} - B_4' = B_1.$$

The s

Then (10.41)—(10.43) can be reduced to a single nonhomogeneous third-order differential equation with constant coefficients

$$\dddot{p}_k + s_1 \ddot{p}_k + s_2 \dot{p}_k + s_3 p_k = s_4. \qquad (10.45)$$

where $\lambda_1, \lambda_2, \lambda_3$

The coefficients of (10.45) are defined by the following formulas

C_1, C_2, C_3

$$s_1 = \frac{a_0^2}{B_2 V_0} + \frac{B_3}{b_{2r.k}} + \frac{R_k T_k}{V_k}\left(A_{kj} + \frac{1}{B_2}\right);$$

$$s_2 = \frac{R_k T_k}{V_k}\left(\frac{a_0^2 A_k}{B_2 V_0} + \frac{1}{b_{2r.k}}\right) + \frac{B_3}{b_{2r.k}}\left[\frac{R_k T_k}{V_k}\left(A_k + \frac{1}{B_2}\right) + \frac{a_0^2}{B_2 V_0}\right];$$

$$s_3 = \frac{R_k T_k A_k a_0^2 \left(B_3 + \frac{1}{A_k}\right)}{V_k B_2 V_0 b_{2r.k}};$$

$$s_4 = \frac{B_1}{b_{2r.k}} \frac{R_k T_k}{V_k} \frac{a_0^2}{B_2 V_0},$$

where $B_1 = \frac{R_k T_k}{V_k}$; $B_2 = 2b_{1u.k} G_{u}$;

$$B_3 = \frac{(\Delta p_r)_{l+1} - (\Delta p_r)_l}{G_{r(l+1)} - G_{rl}}$$

Here t

the time in

To solve (10.45) we take the initial conditions in the form

The de

iation of t

for $\tau=0$; $p_к=p_к^*$; $G_т=G_т^*$; $G_г=G_г^*$;

$$\frac{dp_к}{d\tau}=\left(\frac{dp_к}{d\tau}\right)^*=0;$$

$$\frac{d^2p_к}{d\tau^2}=\left(\frac{d^2p_к}{d\tau^2}\right)^*=-\frac{B_1}{b_{2т.к}}-\frac{R_гT_к}{V_к}\frac{a_г^2G_г}{B_2V_0}-\frac{B_1}{b_{2т.к}}G^*-\frac{p_к^*}{b_{2т.к}}.$$

Here, and hereafter, the parameters with an asterisk (*) relate to the regime from which the shutdown begins. The expression for the second derivative of the pressure in the combustion chamber is easily obtained from the system written above for $\left(\frac{dp_к}{d\tau}\right)^*=0$.

The solution of (10.45) is obtained in the form

$$p_к=C_1e^{\lambda_1\tau}+C_2e^{\lambda_2\tau}+\frac{s_1}{s_3} \tag{10.46}$$

where $\lambda_1,\lambda_2,\lambda_3$ are the roots of the characteristic equation

$$\lambda^3+s_1\lambda^2+s_2\lambda+s_3=0;$$

C_1,C_2,C_3 are the constants of integration and are defined by the expressions

$$C_1=-\frac{\lambda_2\lambda_3\left(p_к^*-\frac{s_1}{s_3}\right)-\ddot{p}_к^{**}}{(\lambda_2-\lambda_1)(\lambda_3-\lambda_1)};$$

$$C_2=-\frac{\lambda_1\lambda_3\left(p_к^*-\frac{s_1}{s_3}\right)+\ddot{p}_к^{**}}{(\lambda_1-\lambda_2)(\lambda_3-\lambda_2)};$$

$$C_3=-\frac{\lambda_1\lambda_2\left(p_к^*-\frac{s_1}{s_3}\right)+\ddot{p}_к^{**}}{(\lambda_1-\lambda_3)(\lambda_2-\lambda_3)};$$

Here the parameters with (**) denote their average values within the time interval in question.

The dependence $p_к(\tau)$ makes it possible to determine the time variation of the other parameters of the transient process.

To find the valve disk displacement during the period from 0 to τ we must integrate (10.44). This is not difficult to do if we neglect the friction forces and average the spring force and the volume of the pneumatic valve air chamber.

The basic system of equations remains valid for any i^{th} time interval, but the initial conditions will be different: for the $(i + 1)$st time interval we must take as the initial conditions the parameters at the end of the i^{th} interval. For example, the initial conditions for the pressure in the combustion chamber are written as

$$p_к = p_к^l; \quad \dot{p}_к = \dot{p}_к^l = (G_0^l + G_т^l - A_к p_к^l)\frac{R_к T_к}{V_к};$$

$$\ddot{p}_к = \ddot{p}_к^l = \frac{B_1}{\theta_{гг.к}} - \left[\frac{R_к T_к a_0^2}{B_2 V_к V_0} + \left(\frac{R_к T_к}{V_к}\right)^2 \left(A_к + \frac{1}{B_2}\right)\right] G_0^l -$$
$$- \left[\frac{B_2}{\theta_{гг.к}} \frac{R_к T_к}{V_к} + \left(\frac{R_к T_к}{V_к}\right)^2 \left(A_к + \frac{1}{B_2}\right)\right] \dot{G}_т^l -$$
$$- \left[\frac{1}{\theta_{гг.к}} \frac{R_к T_к}{V_к} - A_к \frac{R_к T_к}{V_к}\left(A_к + \frac{1}{B_2}\right)\right] p_к^l.$$

The general solution of (10.45) for the time interval $\tau_i \leqslant \tau \leqslant \tau_{i+1}$ has the form

$$p_к = C_1 e^{\lambda_1(\tau-\tau_i)} + C_2 e^{\lambda_2(\tau-\tau_i)} + C_3 e^{\lambda_3(\tau-\tau_i)} + \frac{s_1}{s_3} \qquad (10.47)$$

where C_1, C_2, C_3 are the constants of integration

$$C_1 = \frac{\lambda_2\lambda_3\left(p_к^l - \frac{s_4}{s_3}\right) - (\lambda_2 + \lambda_3)\dot{p}_к^l + \ddot{p}_к^l}{(\lambda_2 - \lambda_1)(\lambda_3 - \lambda_1)};$$

$$C_2 = \frac{\lambda_1\lambda_3\left(p_к^l - \frac{s_4}{s_3}\right) - (\lambda_1 + \lambda_3)\dot{p}_к^l + \ddot{p}_к^l}{(\lambda_1 - \lambda_2)(\lambda_3 - \lambda_2)};$$

$$C_3 = \frac{\lambda_1\lambda_2\left(p_к^l - \frac{s_4}{s_3}\right) - (\lambda_1 + \lambda_2)\dot{p}_к^l + \ddot{p}_к^l}{(\lambda_1 - \lambda_3)(\lambda_2 - \lambda_3)}$$

For a quick calculation of the transient LRE shutdown process in order to obtain preliminary information on the variation of the main parameters of the working process, we must make one more assumption — we must neglect the inertial head in the fuel line, i.e., we assume that

$$\ldots \frac{dQ_r}{d\tau} = 0.$$

Then we obtain for the (i + 1)st time interval with account for the variation of the pressure downstream of the pump during the interval in question

$$p_{\kappa} = E_1 e^{\lambda_1(\tau-\tau_i)} + E_2 e^{\lambda_2(\tau-\tau_i)} + Re^{-\frac{\tau-\tau_i}{\theta}} \tag{10.48}$$

where λ_1 and λ_2 are the roots of the characteristic equation

$$\lambda_{1,2} = -\frac{r_1}{2} \pm \sqrt{\frac{r_1^2}{4} - r_2};$$

$$r_1 = \frac{R_{\kappa}T_{\kappa}}{V_{\kappa}}\left(\Lambda_{\kappa} + \frac{1}{B_2} + \frac{1}{B_3}\right) + \frac{a_0^2}{B_2 V_0};$$

$$r_2 = \frac{R_{\kappa}T_{\kappa}}{V_{\kappa}} \frac{a_0^2}{V_0 B_2}\left(\Lambda_{\kappa} + \frac{1}{B_3}\right);$$

$$r_3 = \frac{R_{\kappa}T_{\kappa}}{V_{\kappa}} \frac{p'_{\kappa.r}}{B_2 B_3}\left(\frac{a_0^2}{V_0} - \frac{B_2}{\theta}\right); \quad R = \frac{r_3\theta^2}{1 - r_1\theta + r_2\theta^2};$$

$$E_1 = \frac{\lambda_2(p'_{\kappa} - R) - \dot{p}'_{\kappa} - \frac{R}{\theta}}{\lambda_2 - \lambda_1}; \quad E_2 = \frac{\lambda_1(p'_{\kappa} - R) - \dot{p}'_{\kappa} - \frac{R}{\theta}}{\lambda_2 - \lambda_1}.$$

The calculation using this formula is considerably simpler but less accurate, since in certain hydraulic systems which have considerable le· ;th neglect of the inertial head leads to significant errors. Therefore, generally speaking, (10.48) is suitable only for rough preliminary calculations.

§ 3. Transient Processes in LRE During Evaporation of Propellants From Cooling Slot and Combustion Chamber Head

1. Physical Picture of Propellant Evaporation Process

Let us examine briefly the essence of the physical process which takes place in the cooling passage and in the combustion chamber head during the propellant evaporation period, where for the sake of

simplicity we shall consider the LRE scheme in which the chamber is cooled by the fuel.(6)

The physical essence of the evaporation process involves transformation of part of the liquid into vapor. This process begins at the moment when the pressure in the combustion chamber after actuation of the cutoff valves in the rapid decay period becomes equal to the saturated vapor pressure of the preheated fuel,(7) which leads to intense boiling of the fuel. The vapors which are formed maintain there a pressure equal to the saturated vapor pressure at the corresponding temperature.

Under the influence of this head the fuel flows through the injectors into the chamber.

As a result of the definite pressure differential across the injectors, the vapor content of the discharging emulsion(8) increases still further. Since the fuel temperature varies along the length of the cooling passage (Figure 10.5), the fuel layers which have not boiled will flow under the influence of the pressure of the vapors toward the vent channel and will discharge into the surrounding atmosphere. During the process of flow through the cooling slot the unboiled layers are warmed by the heat taken from the inner wall of the combustion chamber to the boiling point.

In the course of time the emulsion temperature decreases because of expansion and ejection of part of the emulsion into the chamber. This temperature reduction is compensated somewhat by the input of heat to the emulsion from the hot inner wall. The temperature decrease leads to boiling of new fuel layers. This increases the emulsion weight. After some time all the liquid in the cooling passage has boiled. From this moment all the heat from the wall goes into the emulsion and the work of expansion of the emulsion is expended on ejecting the liquid which is present in the lines.

Footnotes (6), (7), (8), see page 453

Figure 10
curve o
temperat
cooling
measure
combust
injecto

shown tha

The
chamber b
pressure
the oxidi
variation
small roc
will be s
emulsion

The
form of a
ment in t
the fact
chamber,
burning d
propellant
until the
moment on
charging
of whiche

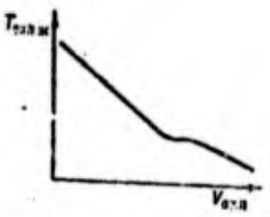

Figure 10.5. Typical curve of propellant temperature versus cooling slot volume, measured from the combustion chamber injector head.

When the entire cavity from the head up to the vent valve is filled, emptying of the fuel cavity begins as a result of discharge of the emulsion into the combustion chamber and into the surrounding atmosphere.

The oxidizer in the line from the cut-off valve to the injectors has the same temperature throughout the entire volume; this temperature is determined by the fueling temperature, since studies [24] have shown that preheating of the propellants in the pumps may be ignored.

The oxidizer boils at the moment when the pressure in the chamber becomes equal to the saturated vapor pressure (or the vapor pressure of the light fraction if there is one). We shall assume that the oxidizer boils throughout the entire volume, since the pressure variation along the height of the oxidizer column as a result of the small rocket accelerations during the period of propellant evaporation will be slight. Under the influence of the vapors the resulting emulsion is ejected into the combustion chamber.

The entry of the propellants into the combustion chamber in the form of a finely dispersed vapor-liquid mixture leads to an improvement in the efficiency of the mixture formation. If we also consider the fact that the fuel and oxidizer flow into the hot combustion chamber, then we obviously have all the conditions necessary for burning during the evaporation period, i.e., after cutting off the propellant flow in the supply lines. The combustion process continues until the supply of one of the propellants is exhausted. From that moment on the engine thrust is determined by the reaction of the discharging jet of vapor alone or the products of thermal decomposition of whichever component is present in excess.

2. Basic System of Equations

We shall first use the equation of material balance for the variable quantity of fuel emulsion present in the cooling passage. Considering that the emulsion mass changes as a result of efflux through the injectors and influx due to boiling[9], we can write

$$\frac{dm_f}{d\tau} = -G_{\phi} + G_{вк}. \qquad (10.49)$$

Since the emulsion volume increases as a result of discharge of part of the propellant into the vent line and its boiling,[10]

$$\frac{dV_f}{d\tau} = \dot{V}_{вк} + \dot{V}_{в}, \qquad (10.50)$$

where m_f is the mass of the fuel emulsion;
G_{inj} is the emulsion flow rate through the injectors;
G_{boil} is the emulsion influx rate due to boiling of the liquid;
V_f is the volume occupied by the emulsion;
V_{boil} is the boiled liquid volumetric influx rate;
V_{ve} is the fluid efflux rate into the vent line.

The increase of the internal energy of the emulsion is due to the addition of the heat Q and the energy input with the boiled liquid. On the other hand, the internal energy will be decreased as a result of emulsion efflux into the combustion chamber and because of the work expended in ejecting part of the fluid into the vent line

$$\frac{d(u_f m_f)}{d\tau} = \frac{dQ}{d\tau} - i_f G_{\phi} + i'_f G_{вк} - p_f \dot{V}_{в}, \qquad (10.51)$$

where u_f and i_f are the internal energy and enthalpy of the emulsion;
i'_f is the enthalpy of the liquid fuel at the boiling temperature;
p_f is the fuel saturated vapor pressure;
v' is the specific volume of the fluid on the saturation line;
G_{ve} is the mass flowrate into the vent line.

Footnotes (9) and (10) appear on page 453

The magnitude of the flow rates G_{inj} and G_{ve} and also the amount of heat Q added to the emulsion and the boiling liquid influx rate G_{boil} (or V_{boil}) are determined later [see (10.62), (10.65), (10.80), (10.85)]. At the moment we shall write out the equations describing the process of emptying of the oxidizer head.

The material balance equation has the form

$$\frac{dm_o}{d\tau} = -G_o, \tag{10.52}$$

where m_o is the mass of the oxidizer emulsion;

G_o is the oxidizer flow rate into the combustion chamber(11).

In the present case the energy equation can be written in a considerably simpler form

$$\frac{d(u_o m_o)}{d\tau} = -i_o G_o. \tag{10.53}$$

Since the oxidizer boils simultaneously throught the entire space, the emulsion volume V_o = const. We shall examine the method for calculating the oxidizer flow rate G_o later.

To the equations (10.49 - 10.53) we can add the equation of the combustion chamber

$$\frac{dp_к}{d\tau} = \frac{R_г T_к}{V_к}\left(G_o + G_ф - \frac{p_к}{A_к}\right). \tag{10.54}$$

where

$$A_к = \frac{\gamma\sqrt{R_г T_к}}{\mu_к F_{кр}}.$$

Footnote (11) appears on page 453

3. Determining the Liquid Boiling Rate at the Interface with the Emulsion

Assuming a considerable time lag of the inner wall of the combustion chamber, we shall consider that the amount of heat flowing into the emulsion and the cooling liquid is determined only by the heat removal from the surface of the wall: Moreover, since in our case the heat transfer is unsteady, generally speaking the formulas for calculating heat transfer in the steady regime are not suitable. However, Sidorov [123] has shown that the coefficient accounting for the unsteady nature of the process is << 1, and therefore for engineering calculations we can use the steady state heat transfer formulas.

Let us find the amount of liquid which boils per unit time. In so doing we must bear in mind that the liquid boiling is defined, on the one hand, by heating as a result of heat transfer from the combustion chamber wall and, on the other hand, by the reduction of the emulsion temperature and pressure of the saturated vapors.

Let us first find the liquid temperature rise. Assume that over an elementary segment dF_s of the cooling passage the difference between the temperatures of the side wall surface and the liquid is ΔT and the coefficient of heat transfer from the wall as a result of propellant flow to the vent channel is equal to α. Then the quantity of heat taken from the given wall segment will be

$$\frac{dQ}{d\tau} = \alpha \Delta T dF_{ст}.$$

On the other hand

$$\frac{dQ}{d\tau} = G_т c dT_{т.р.},$$

where c is the liquid specific heat;

$dT_{т.р.}$ is the liquid temperature rise in the given segment.

Then

$$\alpha \Delta T dF_{ох} = cG_ж dT_{ож}. \tag{10.55}$$

At a known engine operating regime the amount of heat removed by the cooling liquid will be

$$\frac{dQ}{d\tau} = \alpha^* \Delta T^* dF^*_{ох} = c^* G^*_ж dT^*_{ож}. \tag{10.56}$$

We divide (10.55) by (10.56)

$$\frac{\alpha}{\alpha^*} \frac{\Delta T}{\Delta T^*} = \frac{G_ж}{G^*_ж} \frac{c}{c^*} \frac{dT_{ож}}{dT^*_{ож}}. \tag{10.57}$$

Neglecting the variation of the temperature differential and the heat capacity in the regime from which the deviation begins, we find the value of the liquid temperature rise from the Expression (10.57)

$$dT_{ож} = \frac{G^*_ж}{G_ж} \frac{\alpha}{\alpha^*} dT^*_{ож}. \tag{10.58}$$

As is known [6], the heat transfer coefficient α can be calculated from the formula

$$\alpha = 0{,}021 \frac{1}{d_э^{0.2}} \left(\frac{G_ж}{F_ж}\right)^{0.8} Z_ж \left(\frac{Pr_ж}{Pr_{ст}}\right)^{0.25}.$$

The complex $Z_{liq} \frac{Pr_{liq.}}{Pr_w}^{0.25}$ is a weak function of the cooling liquid temperature. Therefore we can write

$$\frac{\alpha}{\alpha^*} = \left(\frac{G_ж}{G^*_ж}\right)^{0.8}.$$

Substituting this expression into (10.58), we obtain

$$dT_{ож} = \sqrt[5]{\frac{G^*_ж}{G_ж}} dT^*_{ож}. \tag{10.59}$$

Analysis of the cooling liquid temperature distribution as a function of the cooling cavity volume shows that with an adequate degree of accuracy we can write

$$T^* = T^*_\phi + k_T V, \qquad (10.60)$$

where k_T is an angular coefficient which is determined from the results of analysis of engine cooling in the shutdown regime[12];

V is the running volume of the cooling cavity, measured from the head

$$T^*_\phi = T^*_{head} - k_T V_\phi;$$

T^*_{head} is the cooling liquid temperature at the injector head in the shutdown regime;

V_{inj} is the injector head volume.

For engines in which the coolant is not supplied to the nozzle exit, the cooling liquid temperature distribution obeys the following relation

$$T^* = T_{\phi.noz} + k_T V,$$

where

$$T^*_{\phi.noz} = T^*_{coll} - k_T V_{coll};$$

T^*_{coll} is the cooling liquid temperature at its entry point (in the collector);

V_{coll} is the volume of the cavity from the head to the collector;

k_T is a coefficient which differs numerically from the coefficient k_T in (10.60).

We shall see later that this variation of T^*_{inj} and k_T is easily taken into account. Now, differentiating (10.60) we find

$$dT_{noz} = k_T dV$$

Footnote (12) appears on page 453

and substitute this value into (10.59)

$$dT_{\text{пол}} = k_T \sqrt[5]{\frac{G_1^*}{G_\Delta}}\, dV.$$

Considering that

$$dV = v' G_\Delta d\tau,$$

we finally obtain the expression for determining the magnitude of the liquid temperature rise

$$dT_{\text{пол}} = k_T \sqrt[5]{\frac{G_1^*}{G_\Delta}}\, v' G_\Delta d\tau.$$

Since the temperature at any section also changes as a result of the arrival of preheated liquid layers, the overall temperature change will be

$$dT' = dT_{\text{пол}} + dT_{\text{зад}} = k_T \sqrt[5]{\frac{G_1^*}{G_\Delta}}\, dV + k_T dV,$$

or

$$dT' = k_T \left(1 + \sqrt[5]{\frac{G_1^*}{G_\Delta}}\right) v' G_\Delta d\tau.$$

After integrating this expression we find the cooling liquid temperature variation law at any section with the volume V for any τ

$$T' = T_0^* + k_T V' + k_T \int_0^\tau \left(1 + \sqrt[5]{\frac{G_1^*}{G_\Delta}}\right) v' G_\Delta d\tau.$$

Now we can determine the volume of the fuel which boils as a result of heat input from the wall

$$V_{\text{кип}} = \frac{T_{\text{кип}} - T_0^*}{k_T} + \sqrt[5]{\frac{G_1^*}{G_\Delta}}\, v' G_\Delta d\tau.$$

During the time $d\tau$ the emulsion temperature changes by the magnitude dT, which leads to additional boiling of an amount of liquid equal to dT/k_T. The overall change of the emulsion volume as a result of

boiling is defined by the expression

$$dV_{boil} = \int \sqrt{\frac{G_v^2}{G_A}}\, v' G_A d\tau + \frac{dT}{k_T}.$$

Dividing both sides by $d\tau$, we obtain

$$\dot{V}_{boil} = \varepsilon v' G_A + \frac{1}{k_T}\frac{dT}{d\tau}, \qquad (10.61)$$

where

$$\varepsilon = \sqrt{\frac{G_v^2}{G_A}}.$$

Since calculations show that the quantity G_{ve} varies in a small range (G_{ve} changes at most by a factor of two by the time of complete boiling of the liquid in the cooling passage), this yields a change of $\varepsilon < \pm 5\%$. Therefore, in the following the value of ε can be determined for some average temperatue and we consider it to be independent of time. If the integration is performed over time segments, then the variation of ε is easily taken into account from the results of the preceding time interval. Knowing V_{boil}, it is easy to find the amount of liquid boiling per unit time

$$G_{boil} = \varepsilon G_A + \frac{\rho'}{k_T}\frac{dT}{d\tau}. \qquad (10.62)$$

We note that the values of the density ρ' and specific volume v' in (10.61) and (10.62) are defined by the emulsion temperature.

4. Determining the Amount of Heat Entering the Emulsion

The liquid boiling in the cooling passage takes heat intensively from the wall. The vapor content in the evaporation period is small (it increases markedly only toward the end of cavity emptying). Therefore we can assume that the heat transfer process takes place as a result of nucleate boiling. It has been shown in [5] that the vapor content has practically no effect on the heat transfer. It is true

that results were obtained in [131] which show a definite influence of the vapor content on the heat transfer, beginning with a value of the order of 0.3. However, neglect of this effect on α_{eq} does not lead to significant errors, since the portion of the process with a vapor content $\psi_s > 0.3$ is of very short duration in comparison with the entire vaporization time.

(10.61)

The process of heat transfer in the cooling passage is described most completely by Tolubinskiy's formula [132], which for the case of slots whose dimensions are comparable with the bubble size (0.003 m) was improved by Chernobyl'skiy and Tananayko [147]

$$\mathrm{Nu} = 26{,}1K^{0.6}\mathrm{Pr}^{-0.3}\mu^{0.66}, \tag{10.63}$$

where

$$\mathrm{Nu} = \frac{\alpha_0}{\lambda'}\sqrt{\frac{\sigma}{g'}}; \quad K = \frac{q}{r\rho'(\rho'-\rho'')p}; \quad \mathrm{Pr} = \frac{\nu'}{a'};$$

λ', ρ', ν', a' are respectively the thermal conductivity, density, kinematic viscosity, and thermal diffusivity of the liquid;

r is the heat of vaporization;

σ is the liquid surface tension;

ρ'' is the vapor density;

p is the variable pressure;

w_0 is the frequency of vapor bubble formation;

d_0 is the breakaway diameter of the bubbles;

h is a correction for the slot width, equal to the ratio of the wetted perimeter to the equivalent diameter $\frac{\Pi}{d_{eq}}$.

In (10.63)

$$\mu = 0{,}73\left(\frac{\rho_0^*}{\rho''}\right)^{1.1}\frac{w}{w_0},$$

where ρ_0^* is the vapor density at a pressure of 1 bar.

Tolubinskiy refined this quantity, suggesting that it be taken equal to $0{,}156\left(\frac{\rho'}{\rho''}\right)^{1.1}$. Then (10.63) will have the form

$$Nu = 0{,}0K^{0.6}Pr^{-0.7}\psi^{0.66}.$$

Substituting in place of Nu, K, Pr their values, we obtain the formula for determining the heat transfer coefficient

$$\alpha_0 = 0{,}0 \frac{(\lambda')^{1.3}(\rho')^{0.7}(\rho'')^{0.03}A^{0.66}}{\sigma^{0.5}r^{0.6}(\rho'')^{0.[illegible]}(\nu')^{0.3}(c')^{0.33}} q^{0.6}.$$

Generally speaking, this formula is valid only for low circulation velocities. MacAdams obtained a graph of the dependence of the heat transfer coefficient on the fluid velocity [72]. In the velocity range 4 - 10 m/sec we can consider that to within 8%

$$\alpha_0 \approx 0{,}52w^{0.4}.$$

Then the formula for determining the coefficient of heat transfer to the emulsion will finally have the form

$$\alpha_0 = A_T^{0.4}h^{0.45}w^{0.4}q^{0.6},$$

$$A_T^{0.4} = 20{,}8\frac{(\lambda')^{1.3}(\rho')^{0.2}(\rho'')^{0.06}}{\sigma^{0.5}r^{0.6}(\rho_0)^{0.16}(\nu')^{0.3}(c')^{0.33}}. \qquad (10.64)$$

The heat fluz q in some segment of the cooling passage is defined by the formula

$$q = \alpha_0 \Delta T,$$

where ΔT is the temperature difference between the wall and the liquid.

Substituting in place of α_{eq} its value from (10.64), we find the formula for the specific thermal fluxes on this segment

$$q = A_T h^{1.5} w \Delta T^{2.5} \frac{kcal}{m^2},$$

where A_T has the dimensions of $kJ/deg^{2.5}m^3$.

be taken

Averaging the value of the temperature difference ΔT, we can find the heat input to the entire emulsion per unit time

$$\frac{dQ}{d\tau} = A_1 i^{1.13} \omega \Delta T_{cp}^{2.5} F_{ohl},$$

tain the

where F_s is the lateral surface area of the combustion chamber wetted by the emulsion.

The emulsion velocity can be found approximately with the aid of the flow rate G_{inj} through the injectors

circula-
ce of the
he velocity

$$w = \frac{G_\phi}{F_{liq \cdot cr}} v,$$

where $F_{liq \cdot cr}$ is the averaged flow area of the cooling passage up to the section with the volume V.

Considering the relations presented above, we can finally write the expression for determining the heat input to the emulsion in the engine cooling passage

at trans-

$$\frac{dQ}{d\tau} = K_Q A_T v G_\phi, \qquad (10.65)$$

(10.64)

where

is defined

$$K_Q = \frac{A^{1.13} T_{cp}^{2.5} F_{ohl}}{F_{liq \cdot cp}} \rho a d^{2.5}.$$

5. Determining the Propellant Physical Parameters on the Saturation Line

the

Equations (10.49) - (10.53), which describe the state of the emulsion, contain the values of the various physical parameters of the liquid and the vapor on the saturation curve. Since the experimental determination of these parameters involves serious difficulties, we shall use an approximate technique for calculating them [109], [110], [23]. This technique, based on thermodynamic similarity theory, yields an accuracy which is quite satisfactory for engineering calculations.

find the

The idea of the method is that any physical parameter can be found by multiplying the coefficient A, characterizing the given liquid and the given property, by a function of the reduced temperature $\bar{T} = \frac{T}{T_{cr}}$ (or the reduced pressure $\bar{p} = p/p_{cr}$) which is universal for all thermodynamically similar substances, where T_{cr} and p_{cr} are the critical temperature and pressure of the given propellant, T and p are the instantaneous values of the temperature and pressure. The coefficient A depends on the critical parameters p_{cr}, T_{cr}, v_{cr}, molecular weight μ, and critical compressibility factor Z_{cr}. All the quantities required for determining the physical parameters of 25 propellants are presented in Table 4, calculated from the most reliable data available.

Preliminary calculations have shown that the possible range of variation of the dimensionless temperature $\bar{T}$ of the LRE propellants lies in the range 0.58 - 0.80. In this range we can with quite satisfactory accuracy approximate by formulas the universal functions obtained by Povarnin as a function of $\bar{T}$ and those obtained by Borishanskiy as a function of $\bar{p}$. The density of the liquid propellant on the saturation line can be determined to within 1% using the formula

$$\rho' = A_\rho (16{,}47 - 9\bar{T}). \tag{10.66}$$

The vapor density is expressed to within 3% by the formula

$$\rho'' = 1{,}77 A_\rho \bar{T}^{10}. \tag{10.67}$$

To within < 1% the liquid specific volume is

$$v' = A_v (0{,}0883 + 0{,}0341\bar{T}). \tag{10.68}$$

To within < 3% the vapor specific volume is

$$v'' = 0{,}565 A_v \bar{T}^{-9} \ (< 3\%). \tag{10.69}$$

TABLE 4. QUANTITIES FOR APPROXIMATE CALCULATION OF PROPELLANT PARAMETERS ON THE SATURATION LI

Component	Molecular weight	Gas constant kJ/kg·deg	T_{cr} °C	t_{cr} °C	Critical pressure $P_{cr} \cdot 10^{-5}$ N/m^2	Critical specific volume $v_{cr} \cdot 10^5$ m^3/kg	Critical specific density Q_{cr} kg/m^3	Critical compressibility factor Z_{cr}
Water	18	463	647,4	374,2	221,3	326	307	0,241
96% ethylalcohol	42	198	521,4	248,2	68,6	374	267	0,248
Methylalcohol	32	260	513,2	240	79,7	368	272	0,220
Isopropylalcohol	60	138,6	508	235	51,1	360	278	0,261
Ammonia	17	489	406	132,8	113	126	235	0,243
Diethylamine	73,1	113,9	497	223,5	35,5	406	246	0,255
UDMH $C_2H_8N_2$	60	138,6	307	234	49,6	372	269	0,262
Oxygen	32	260	155	−118,2	48,4	200	500	0,240
N_2O_4	92	90,4	431	157,8	98,1	107	934	0,268
Hydrogen	2,016	4190	33,1	−239,9	12,94	3226	30,9	0,2[illegible]
Nitric acid HNO_3	63	132	190,2	217	141,3	125	800	0,273
Aniline C_6H_7N	93,13	89,2	699,3	426,1	51,3	291	349	0,2[illegible]

*Numerator is value for liquid; denominator is value for vapor.

LLANT PARAMETERS ON THE SATURATION LINE

$P_{cr}\cdot10^{-5}$ N/m^2	Critical specific volume $v_{cr}\cdot10^5$ m^3/kg	Critical specific density Q_{cr} kg/m^3	Critical compressibility factor Z_{cr}	Parachor П	ρ_l kg/m^3	v_l m^3/kg	c_{p_l} kJ/kg °C	i' kJ/kg	r kJ/kg	$\lambda_l\cdot10^{-3}$, kJ/m·sec°C	$\mu_l\cdot10^{-4}$, N·sec/m^2	$\sigma_l\cdot10^{-4}$, N/m
3	326	307	0,241	54	83,4	1,199	8,16	529	607	226,7	18,54	31,4
6	374	267	0,248	120	70,9	1,410	0,636	332	230,3	73,25	17,96	11,78
7	368	272	0,220	93,2	71,1	1,406	0,5525	284	297,6	89,0	17,08	14,72
1	360	278	0,261	169	71,3	1,343	0,486	246,8	184,3	48,13	23,06	11,49
	126	235	0,243	64	60,8	1,615	0,396	361	367	169	13,74	16,7
5	406	216	0,255	211	62,8	1,592	0,42	208,7	111,9	40,3	22,85	8,78
6	372	269	0,262	171,4	70,3	1,422	0,518	262,7	162,8	44,6	23,18	11,17
4	200	500	0,240	40	101,5	0,9852	0,3524	54,6	71,25	48,35	9,8065	6,1
1	107	934	0,268	197,8	139,5*/86,84	0,7163*/1,1515	0,34	146,3	78,1	76,8	53,4	18,66
94	3226	30,9	0,2018	31,8	9,151	1,058	7,36	243,9	217,4	155	1,22	2,353
3	125	800	0,273	106	138,2	0,7226	0,318	170,5	202	89,5	49	25,5
3	291	349	0,2119	236,7	82,2	1,217	0,321	231,6	126,6	47,4	32,78	12,92

or vapor.

TABLE 4. QUANTITIES FOR APPROXIMATE CALCULATION OF PROPELLANT PARAMETERS ON THE SATURATION

Component	Molecular weight	Gas constant kJ/kg·deg	T_{cr} °C	t_{cr} °C	Critical pressure $p_{cr} \cdot 10^{-5}$ N/m^2	Critical specific volume $v_{cr} \cdot 10^5$ m^3/kg	Critical specific density Q_{cr} kg/m^3	Critical compressibility factor z_{cr}
Hydrazine N_2H_4	32,05	259,5	653,2	380	142,2	384	260	0,2632
Fluorine F_2	38	219	172,0	—100,8	55,7	187	534	0,2772
$HClO_4$	100,5	82,75	679	406,1	18,4	293	342	0,2521
Tetranitromethane	196	42,4	623,3	350,1	22,3	295	339	0,2190
Nitrogen trifluoride NF_3	71,01	117,2	243,1	—29,9	46,0	163	613	0,2636
Fluorine nitrate NO_3F	81,01	102,6	340,4	67,2	38,81	231	434	0,2563
Chlorine trifluoride ClF_3	9,172	90,0	447,2	174	56,9	155	645	0,2151
Fluorine monoxide OF_2	53,7	154	215,1	—57,9	47,76	194	515	0,2805
Methane CH_4	32,87	518	190,7	—82,5	45,0	617	162	0,2806
Ozone O_3	[illegible]	173,3	268,2	—5	61,6	186	537	0,272
Fluorine peroxide O_2F_2	70	118,9	379	105,8	56,2	208	481	0,2696
Methyl hydrazine CH_6N_2	46,07	181,6	530	256,8	73,6	343	292	0,2[illegible]
Benzene C_6H_6	78,11	106,4	562,1	288,9	46,8	329	304	0,2772

[a] Numerator is value for liquid; denominator is value for vapor.

LLANT PARAMETERS ON THE SATURATION LINE

$P_{cr}\cdot10^{-5}$ N/m^2	Critical specific volume $v_{cr}\cdot10^5$ m^3/kg	Critical specific density Q_{cr} kg/m^3	Critical compressibility factor Z_{cr}	Parachor II	A_ρ kg/m^3	A_v, m^3/kg	A'_ρ kJ/kg °C	i'_ρ kJ/kg	A_i kJ/kg	$A'_\lambda\cdot10^3$, kJ/m·sec°C	$A_\eta\cdot10^6$, N·sec/m^2	$A_\sigma\cdot10^4$, N/m
,2	384	260	0,2652	93,4	69,27	1,147	0,91	528	397	156,4	21,94	27,6
,7	187	534	0,2772	51,4	147,9	0,6761	0,435	74,6	71,1	76,9	13,04	9,81
4	293	342	0,2521	221	86,14	1,162	0,31	210,6	112	43,7	31,86	12,83
,3	295	339	0,2190	100,4	84,33	1,186	0,2009	130,8	53	20,9	36,3	7,34
0	163	613	0,2636	59,6	161,6	0,6243	0,293	71,9	55,2	42,6	19,55	9,22
81	231	434	0,2561	111,6	143,5	0,6969	0,3165	107,6	68,9	44,1	25,8	8,96
,9	155	645	0,2151	131,4	172	0,5814	0,2222	99,3	86,5	49,3	27,8	10,51
,78	194	315	0,2805	71,4	137,2	0,7289	0,365	78,4	62,3	59,4	15,94	9,66
,0	617	162	0,2806	73,2	45,46	2,206	1,216	237,6	186,2	107	8,61	8,91
,6	186	537	0,272	60,0	146,1	0,6845	0,365	97,6	89,0	74,3	16,78	12,75
,2	208	481	0,2896	91,4	128,3	0,7794	0,69	261,4	88,3	170,3	35,8	12,03
,6	343	292	0,2579	132,4	53,13	1,881	0,511	268,5	192,1	82,2	21,76	16
8	329	304	0,2572	207,1	78,2	1,279	0,391	221,6	117,8	49,3	27,12	12,02

or vapor.

The function $v''' = v'' - v'$ is very often encountered in calculations. Its dependence on $\bar{T}$ to within 1.5% is expressed by the formula

$$v''' = A_v 0{,}55\bar{T}^{-10{,}073}.$$

The specific heat of the liquid at constant pressure is determined to within < 1.5% by the relation

$$c'_p = A_{c'_p}(3 + 3{,}7\bar{T}). \tag{10.70}$$

This formula makes it possible to find the enthalpy of the liquid at the boiling temperature. In fact, in the general case the enthalpy is defined by the formula

$$i' = \int_{T_0}^{T} c'_p dT + \int_{T_0}^{T} v' \frac{dp}{dT} + i_0,$$

where i_0 is the enthalpy at the temperature T_0.

We take $T_0 = 0$ and $i_0 = 0$. The magnitude of the second integral is very small, for example, for kerosene it amounts to only 0.38% of the entire enthalpy. Therefore we can take

$$i' = \int_0^T c'_p dT.$$

Substituting (10.70) into this expression and converting to dimensionless temperature, we obtain

$$i' = A_i(3\bar{T} + 1{,}85\bar{T}^2). \tag{10.71}$$

The heat of vaporization r can be found from the formula

$$r = A_r(4{,}85 - 3{,}27\bar{T}). \tag{10.72}$$

As is known, the equation of state for the saturation line has the form

$$p=f(T)$$

This equation in our range of variation of $\bar{T}$ can be expressed by the formula

$$\bar{p}=a+b\bar{T}^{m_2} \tag{10.73}$$

where a, b, m_2 are constants for a given propellant (Table 5).

TABLE 5. VALUES OF THE CONSTANTS a, b, m_1, b_1, m_2 FOR CERTAIN COMPONENTS

Component	a	b	m_1	b_1	m_2
96% ethylalcohol	0	36,76	18,55	36,76	18,55
ADMH	−0,003433	1,46245	10,6425	1,7432	9,82
O_2	0,0039	1,25	8,52	1,2338	7,14
N_2O_4	0	1,57755	13,12	1,57755	13,12

Knowing the enthalpy i', the specific volume v', and the pressure p as functions of the temperature $\bar{T}$, we can use the known thermodynamic relation

$$u'=i'-p_{кр}\bar{p}v'$$

to find the temperature dependence of the internal energy

$$u'=A_1'(3\bar{T}+1{,}85\bar{T}^2)-$$
$$-A_0p_{кр}(a+b\bar{T}^{m_2})(0{,}03968+0{,}08445\bar{T}). \tag{10.74}$$

Thus the formulas presented above make possible an analytic calculation of the required physical parameters of the liquid and vapor on the saturation line.

6. Deter
Inj

The
examined
approxima
of the ga
fugal inj
nozzle is
without t

Stra
the flow
the vapor
10.6). T
formulas

where q(λ
tables us
drop q(λc

Figure 10
boiling
a centr

where the

6. Determining Flow Rates of the Boiling Propellants from the Injectors

The discharge of boiling liquids from centrifugal injectors was examined for the first time in [91], but the results obtained are approximate, since they are based on the assumption that the diameter of the gaseous vortex does not change along the length of the centrifugal injector and the axial component of the liquid velocity in the nozzle is independent of the radius. We shall examine the solution without these assumptions and obtain a more exact result.

Stratification of the light and heavy fractions takes place in the flow of a two-phase fluid in a centrifugal injector. Therefore the vapor and liquid discharge separately from the nozzle (Figure 10.6). The vapor flow rate may be determined from the gasdynamic formulas

$$G'' = \pi r_c^2 \sqrt{k\left(\frac{2}{k+1}\right)^{\frac{k+1}{k-1}} \rho_s \omega_s q(\lambda_c)},$$

where $q(\lambda_c)$ is a gasdynamic function which is found from graphs or tables using the value of the ratio $\frac{p_c}{p_s}$ (for the critical pressure drop $q(\lambda_c) = 1$.

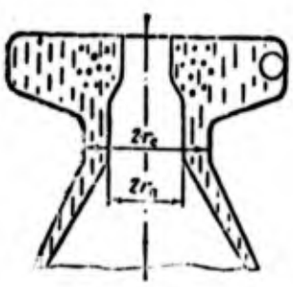

Figure 10.6. Flow pattern for boiling fluid discharge from a centrifugal injector.

Let us find the liquid flow rate. If the vapor content in the nozzle is such that for vapor flow an opening is required which is of larger diameter than the diameter of the vortex which is formed in the case of cold liquid discharge, then the flow rate G' in this case is found using the formula

$$G' = \int_{r_n}^{r_c} \rho_l \omega_a 2\pi r dr, \qquad (10.75)$$

where the axial velocity at the exit section is

$$w_a' = \sqrt{1-\mu^2A^2\frac{r_c^2}{r^2}}\sqrt{\frac{2\Delta p_\phi}{\varrho_c'}}; \qquad (10.76)$$

μ is the cold liquid discharge coefficient for the given centrifugal injector, having the geometric characteristic A and the nozzle radius r_c;

r is the instantaneous radius;

$\Delta p_{inj} = p_s - p_c$ is the pressure drop across the injector.

If μ'_{cen} is the fluid discharge coefficient for two-phase mixture flow, then

$$G' = \mu_{cen}'\pi r_c^2\sqrt{2\Delta p_\phi \varrho_c'}. \qquad (10.77)$$

Equating (10.75) and (10.77) with account for (10.76), after integration we obtain the following equation for finding μ'_{cen}

$$\mu_{cen}' = \sqrt{1-\mu^2A^2} - s_a\sqrt{s_a^2-\mu^2A^2} - \mu^2A^2\ln\left(\frac{1+\sqrt{1-\mu^2A^2}}{s_a+\sqrt{s_a^2-\mu^2A^2}}\right),$$

where

$$s_a = \frac{r_a}{r_c}.$$

In this equation, in addition to μ_{cen}, the value of s_p is also unknown; it may be found from the obvious relation

$$\frac{G'}{G''} = \frac{1-\psi_c}{\psi_c} = \frac{\mu_{cen}' r_c^2\sqrt{2\Delta p_\phi \varrho_c'}}{r_a^2\sqrt{k\left(\frac{2}{k+1}\right)^{\frac{k+1}{k-1}} p_s \varrho_s' q(\lambda_c)}}$$

where ψ_c is the vapor content of the emulsion in the injector nozzle. We denote

$$B = \frac{\psi_c}{1-\psi_c}\frac{C\sqrt{\Delta p_\phi}}{q(\lambda_c)} \qquad (10.78)$$

(10.76)

centrif-
nd the

(10.77)

ter
n

s also

nozzle.

(10.78)

$$C = \sqrt{2\frac{\rho_s\left(\frac{2}{k+1}\right)^{\frac{k+1}{k-1}}}{\rho_s p_s}}\cdot\frac{\cos\alpha^{\frac{1}{2}}}{\kappa z^{\frac{1}{2}}}$$

where $\frac{\cos\alpha^{\frac{1}{2}}}{\kappa z^{\frac{1}{2}}}$ is a quantity which depends only on the saturated vapor pressure p_s (or, equivalently, the boiling temperature T_s). The value of C can be found from precomputed graphs (Figure 10.7).

Then the additional equation for determining the value of s_p will be

$$\mu'_{cen} = \frac{A^2}{B} \tag{10.79}$$

The desired value of the fluid discharge coefficient μ'_{cen} is determined by joint solution of the transcendental Equation (10.78) and the quadratic Equation (10.79). The results of this solution are shown in Figure 10.8. We see from this figure that the curves for μ'_{cen} for different B intersect at certain points of the curve of μ versus A, calculated for the ideal fluid by Abramovich. If the centrifugal injector has a large value of the geometric characteristic A and the flow discharge conditions lead to a small value of the complex B, then $\mu'_{cen} = \mu$. This is explained by the fact that the vapor vortex which is formed in this case is sufficiently large to pass all the vapor. Therefore the vapors do not occupy the liquid flow section. The diameter of the flow section for the light phase will be equal to the diameter of the vortex which is formed with discharge of the cold liquid.

However, if the injector geometric characteristic A is quite small while the complex B is large, then the vortex section obtained in the case of cold liquid flow will not be adequate for passage of the vapor. Therefore, the vapor occupies part of the liquid flow section, thereby reducing the value of the discharge coefficient $\mu'_{cen} < \mu$. The value of the discharge coefficient μ'_{cen} determined from Figure 10.8 for the geometric characteristic A and the complex B makes it possible to calculate the liquid flow rate using (10.77) and therefore the entire flow rate of the two-phase mixture

$$G_{\text{ж}} = \frac{\mu'_{\text{ж}}}{(1-\varphi_c)}\pi r_c^2\sqrt{2\Delta p_{\text{ж}}\rho_{\text{ж}}} \tag{10.80}$$

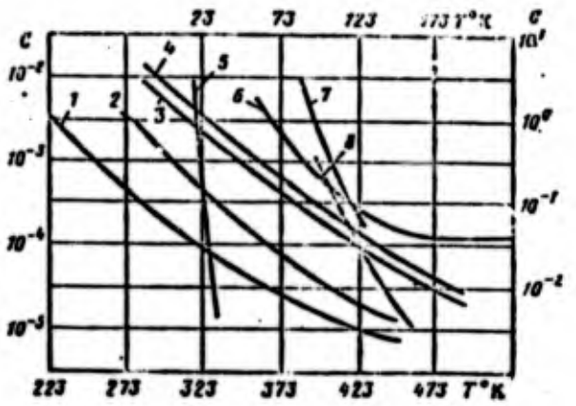

Figure 10.7. Variation of C with boiling point for several fuels: 1 - ammonia; 2 - nitrogen textroxide 5; 3 - UDMH; 4 - ethyl alcohol; 5 - liquid hydrogen; 6 - hydrazine; 7 - liquid fluorine; 8 - liquid oxygen (upper scale T° K and right scale C for curves 5, 7, 8).

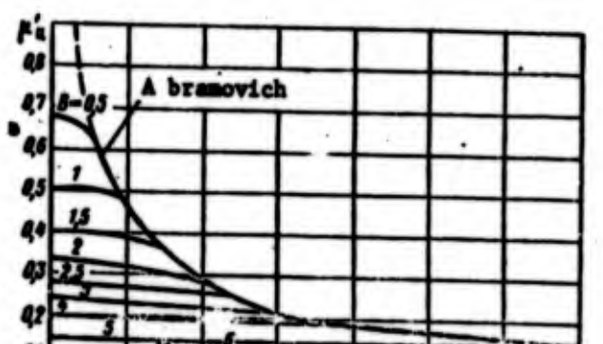

Figure 10.8. Variation of μ'_{cen} with injector geometric characteristic A and the complex B.

The centrifugal injector can be constructed so that the entrance port has somewhat smaller dimensions than the nozzle. In this case the emulsion flow rate through the injector may be determined by the entrance port. Let us find the condition under which this case holds. To do this we assume that the entire pressure drop is developed in the entrance channel. In order that the flow rate of the boiling liquid be determined by the injector nozzle, it is necessary that the

maximal pc
given conc
the nozzle

The c
orifices

where

μ'_c and μ'_c
the c
w'_c and w'_c
mined

Equat
for (10.82

The e
where R_K i
we can wri

Thus,
then in de
otherwise

For s
different

maximal possible flow rate through the entrance channel under the given conditions be greater than (or equal to) the flow rate through the nozzle, i.e., $G_{boil} = G_{cen}$.

The quantity G_{boil} can be found using the formulas derived for orifices [126] (and suitable for jet injectors)

$$G_{вх} = \frac{\mu'_ж}{(1-\gamma_c)} F'_{вх} \sqrt{2\Delta p_ф \rho'_ж}, \qquad (10.81)$$

where

$$F'_{вх} = \frac{F_{вх}}{1+\frac{\gamma_c}{(1-\gamma_c)}\frac{\mu'_c}{\mu''_c}\frac{\rho'_c}{\rho''_c}\frac{w'_c}{w''_c}} = \gamma F_{вх}; \qquad (10.82)$$

μ'_c and μ''_c are the liquid and vapor discharge coefficients through the orifice (or jet injector) (according to Soldatov [126] $\mu'_c = 1{,}05\,\mu''_c$);

w'_c and w''_c are the liquid and vapor velocities respectively (determined by the known formulas of hydromechanics).

Equating G_{boil} and G_{cen} from (10.80) and (10.81) with account for (10.82), we obtain

$$\frac{\mu'_c}{(1-\gamma_c)}\gamma F_{вх}\sqrt{2\Delta p_ф \rho'_ж} \geqslant \frac{\mu'_ж}{(1-\gamma_c)}\pi r_c^2\sqrt{2\Delta p_ф \rho'_ж}.$$

The entrance channel area $F_{boil} = \pi r^2_{boil}$, and $r_c = A\frac{r^2_{boil}}{R_K}$ where R_K is the jet swirl radius. Therefore, after transformations we can write

$$A \leqslant \frac{R_K}{r_{вх}}\sqrt{\frac{\mu'_c}{\mu'_ж}\gamma}. \qquad (10.83)$$

Thus, if the inequality (10.83) is satisfied for a given injector, then in determining the boiling liquid flow rate we must use (10.80), otherwise the flow rate must be calculated using (10.81).

For spiral injectors the inequality (10.83) has a somewhat different form

$$A \leqslant \sqrt{\varphi \frac{\mu'_{sp}}{\mu'_{sp}} \frac{\pi R_k^2}{F_\Sigma}}$$

where F_Σ is the spiral flow section;

μ'_{sp} is the liquid discharge coefficient through the spiral.

The magnitude of the vapor content at the injector nozzle exit appears in the formulas obtained above. This vapor content can be found from the formulas presented in [126], neglecting the kinetic energy of the vapor and liquid ahead of the injector:

$$\psi_k = \frac{g_1 (i'_s - i'_c) + \psi_s r_s}{r_c + \frac{w_c^2}{2}} \qquad (10.84)$$

where i'_s, i'_c, r_s and r_c are the enthalpy and heat of vaporization of the liquid ahead of the injector and in the nozzle;

ψ_s is the vapor content ahead of the injector;

g_1 is the mass fraction of the light fraction in the propellant (for a uniform substance $g_1 = 1$).

In conclusion let us examine the propellant discharge through the vent channels, which serve to remove the propellants downstream of the cutoff valves. Because of the fact that the power plants are shut down in what is practically a vacuum, the propellant boils in the vent port. The discharge of the fuel in this case has several characteristic singularities. Expulsion takes place under the influence of the saturated vapors of the propellant which boils in the head and in part of the cooling passage. Therefore we must take into account the losses from the section with the pressure p_s up to the vent port exit, where the pressure is approximately

$$p_{cs} = \left(\frac{2}{k+1}\right)^{\frac{k}{k-1}} p_{s.}$$

Here $p_{s\ fu}$ is the propellant saturated vapor pressure ahead of the vent port. Usually this pressure is found from the fueling temperature (if cold propellant is vented) or from the results of the cooling calculation (if preheated fuel is vented).

The magnitude of the velocity at the exit is determined by the formula

$$w'_{c.1} = \sqrt{2\frac{(p_s - \Delta p_{sep} - p_{c.1})}{\rho'_{c.1}}}$$

where the losses are

$$\Delta p_{sep} = b_{1.1} G_s^2.$$

The formula for calculating the boiling propellant flow rate has the form

$$G_s = \frac{\mu'_s \rho'_{c.1} w'_{c.1} F_1}{\psi_c \left[\frac{h}{\sqrt{p_s - p_{c.1} - b_{1.1} G_s^2}} + 1\right]}, \qquad (10.85)$$

where $h = \frac{\psi_c}{(1-\psi_c)} \frac{\mu'_s}{\mu'_s} \frac{\rho'_{c.1}}{\sqrt{\rho'_{c.1}}} \frac{w'_{c.1}}{\sqrt{2}}$.

This equation is solved by successive approximations.

In certain cases the discharge process is completely or partially nonequilibrium. In the case of the completely nonequilibrium discharge process the time during which the fluid with the velocity

$$w'_s = \sqrt{2\frac{p_s - p_{c.1}}{\rho'_{s3}\left[1 + 2b_{1.1}\mu'^2_s \rho'_{s3} F_1^2\right]}}$$

travels the distance from the section with the static pressure p_s fu (corresponding to the fueling temperature) to the valve exit must be no greater than the vapor formation delay time τ_{del}, i.e.,

$$\frac{l}{w'_s} \leqslant \tau_s.$$

In the case of a linear pressure distribution along the line, the condition for the nonequilibrium process has the form

$$p_{s3} \leqslant \frac{p_s \tau_s}{L} \sqrt{2\frac{p_s - p_{c.1}}{\rho'_{s3}\left[1 + 2b_{1.1}\mu'^2_s \rho'_{s3} F_1^2\right]}}$$

where L is the passage length from the section with the pressure p_s to the valve.

In this case the flow rate is found from the formula

$$G_{\text{ж}} = \mu_{\text{ж}} F_{\text{ж}} \sqrt{2 \frac{\varrho'_{\text{ж}} (p_{\text{ж}} - p_{\text{к}})}{1 + 2b_{\text{ж}} (\mu'_{\text{ж}})^2 \varrho'_{\text{ж}} F_{\text{ж}}^2}}$$

7. Solution of the Equations for the Oxidizer Line

The parameters in the oxidizer head (emulsion mass, vapor content, specific volume) depend only on the temperature which, in turn, is a function of time. This function is determined by the emulsion flow rate into the combustion chamber. Therefore we first find the connection between the vapor content (specific volume, mass) and the oxidizer temperature $\bar{T}_{\text{з.о}}$. To this end we examine the basic equations (10.49 - 10.51) for the oxidizer line

$$u_{\text{о}} \frac{dm_{\text{о}}}{d\tau} + m_{\text{о}} \frac{du_{\text{о}}}{d\tau} = -i_{\text{о}} G_{\text{о}};$$

$$\frac{dm_{\text{о}}}{d\tau} = -G_{\text{о}}.$$

The magnitude of the emulsion mass $m_{\text{о}}$ and internal energy $u_{\text{о}}$ depends only on the temperature. Therefore, dropping the subscripts for simplicity, we write

$$u \frac{dm}{d\bar{T}} \frac{d\bar{T}}{d\tau} + m \frac{du}{d\bar{T}} \frac{d\bar{T}}{d\tau} = i \frac{dm}{d\bar{T}} \frac{d\bar{T}}{d\tau}$$

Since $\frac{d\bar{T}}{d\tau} \neq 0$, dividing by $\frac{d\bar{T}}{d\tau}$, we obtain

$$(u - i) \frac{dm}{d\bar{T}} + m \frac{du}{d\bar{T}} = 0. \qquad (10.86)$$

It is known from thermodynamics that

$$i = u + pv$$

and, in addition, $v = \frac{V}{m}$. Therefore, (10.86) can be reduced to the form

$$\frac{di}{d\bar{T}} = v p_{\text{к}} \frac{d\bar{p}}{d\bar{T}}$$

We denote $v'' = v'' - v'$. Since $i = i' + \gamma r$ and $v = v' + \gamma v''$, it is easy to transform the resulting equation to the form

$$\frac{d\gamma}{d\bar{T}} + \vartheta_{\text{о.1}}(\bar{T})\gamma = \vartheta_{\text{о.2}}(\bar{T}) \qquad (10.87)$$

where

Curves
The solutio

. In the
be approxim

where
oxidizer (

The p
< 1%) by t

Here
on the nat
$s_{03} = -3{,}131$;

With
formed to

where

$$\theta_{v1} = \frac{1}{r}\left(\frac{dr}{d\bar{T}} - v''\frac{dp}{d\bar{T}}\right) = -\frac{6{,}54A_r\bar{T} + 0.55p_{kp}A_v bm_2\bar{T}^{m_2-11{,}675}}{A_r(4{,}85 - 3{,}27\bar{T}^2)};$$

$$\theta_{v2} = \frac{1}{r}\left(v'\frac{dp}{d\bar{T}} - \frac{dl'}{d\bar{T}}\right) =$$

$$= -\frac{p_{kp}A_v s_{v2}(0{,}03968 + 0{,}0811\bar{T})\bar{T}^{m_2-1} - (1 + 3{,}7\bar{T})A_l'}{A_r(4{,}85 - 3{,}27\bar{T}^2)}.$$

Curves of these functions for N_2O_4 are shown in Figure 10.9. The solution of (10.87) has the form

$$\psi = \exp\left(-\int \theta_{v1}d\bar{T}\right)\left(\int \theta_{v2}e^{\int \theta_{v1}d\bar{T}}d\bar{T} + C_1\right). \qquad (10.88)$$

In the possible range of variation of $\bar{T}$ the function $\theta_{v1}(\bar{T})$ can be approximated with good accuracy (error < 1%) by the relation

$$\theta_{v1} = s_{v1} + s_{v2}\bar{T} + s_{v3}\bar{T}^2,$$

where s_{v1}, s_{v2}, s_{v3} are coefficients which depend on the nature of the oxidizer (for N_2O_4 the coefficients $s_{v1} = -3{,}963$; $s_{v2} = 14{,}63$; $s_{v3} = -19{,}57$).

The product $\theta_{v2}\exp\left(\int \theta_{v1}d\bar{T}\right)$ can also be replaced (with an error < 1%) by the relation

$$\theta_{v2}\exp\left(\int \theta_{v1}d\bar{T}\right) = s_{v4} + s_{v5}\bar{T} + s_{v6}\bar{T}^2.$$

(10.86)

Here the values of the coefficients s_{v1}, s_{v5}, s_{v6} also depend only on the nature of the oxidizer (for N_2O_4 the coefficients $s_{v4} = -0{,}09936$; $s_{v5} = -3{,}131$; $s_{v6} = 2{,}985$).

With the aid of these formulas the Solution (10.88) is transformed to the form

$$\psi = \frac{\left(\frac{1}{2}s_{v4}\bar{T}^2 + \frac{1}{3}s_{v5}\bar{T}^3 + C_1\right)}{\left(-\frac{1}{2}s_{v1}\bar{T}^2 + \frac{1}{3}s_{v2}\bar{T}^3\right)}. \qquad (10.89)$$

(10.87)

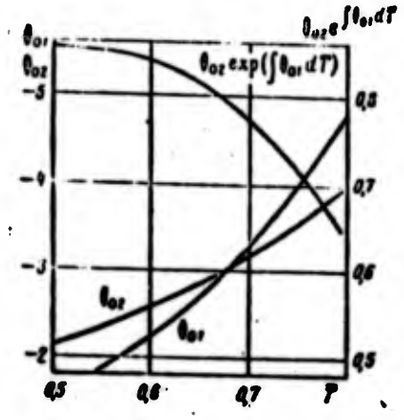

Figure 10.9. Curves of θ_{02}, θ_{02} and $\theta_{02}\exp(\int\theta_{01}d\bar{T})$ versus $\bar{T}$ for N_2O_4.

The constant C_1 is found from the initial conditions; for $\bar{T}=\bar{T}_0, \psi=0$

$$C_1 = -s_{02}\bar{T}_0 - \frac{1}{2}s_{03}\bar{T}_0^2 - \frac{1}{3}s_{04}\bar{T}_0^3.$$

The value of the second integration limit $\bar{T}_{boil}$ can be determined from (10.89), taking $\psi = 1$ in the limiting case. If the resulting value of the temperature is less than the freezing point of the given propellant $\bar{T}_{fr}$, then the second integration limit must be taken equal to $\bar{T}_{fr}$. Knowing the temperature dependence of the vapor content ψ in the head, it is easy to find the connection between $\bar{T}$ and the oxidizer emulsion weight m;

$$m = V\frac{\exp\left(s_{01}\bar{T} + \frac{1}{2}s_{02}\bar{T}^2 + \right.}{v'\exp\left(s_{01}\bar{T} + \frac{1}{2}s_{02}\bar{T}^2 + \frac{1}{3}s_{03}\bar{T}^3\right) + v''\left(s_{01}\bar{T} + \right.}$$
$$\left. + \frac{1}{3}s_{03}\bar{T}^3\right)$$
$$\left. + \frac{1}{2}s_{02}\bar{T}^2 + \frac{1}{3}s_{04}\bar{T}^3 + C_1\right)}.$$

The flow rate through the injectors for the critical pressure drop depends only on the vapor content ψ and the temperature ahead of the injectors (see Section 3, paragraph 6). If the pressure drop is less than the critical value the pressure in the combustion chamber also affects the flow rate. Therefore in the general case we can write

$$G(\psi,\bar{T},p_k) = -\frac{dm}{d\bar{T}}\frac{d\bar{T}}{d\tau},$$

hence

$$d\tau = -\frac{1}{G}\frac{dm}{d\bar{T}}d\bar{T}. \qquad (10.90)$$

Integrating (10.90), we obtain the dependence between the time and temperature

$$\tau = V \int_{\bar{T}_3}^{\bar{T}} \frac{\left[\frac{dv'}{d\bar{T}} + 0_{02}v'' + \frac{1}{2}\left(\frac{dv''}{d\bar{T}} - v''0_{01}\right)\right]}{(v' + \frac{1}{2}v')^2 G} d\bar{T}.$$

Using the formulas of Section 3, paragraph 5, we represent the integrand as a function of the temperature

$$\tau = V \int_{\bar{T}_3}^{\bar{T}} \frac{S_{0K}}{G} d\bar{T}, \tag{10.91}$$

where

$$S_{0K} = A_0 \frac{[0{,}550_{02}\bar{T} - 5{,}511(1 + 0{,}09960_{01}\bar{T}) + 0{,}0811\bar{T}^{11{,}075}]\bar{T}^{9{,}075}}{(0{,}03968\bar{T}^{10{,}075} + 0{,}08143\bar{T}^{11{,}075} + 0{,}55\bar{T})^2}.$$

In the case of critical oxidizer pressure drop across the injectors, the overall flow rate into the chamber can be expressed with high accuracy by the following formula, obtained from the results of calculation of the discharge of the boiling propellant through the head

$$G = [k_{01} + k_{02}\bar{T}^{\nu_{01}} + (k_{03} + k_{04}\bar{T}^{\nu_{02}})^2]^{-1}, \tag{10.92}$$

where $k_{01}, k_{02}, k_{03}, k_{04}, \nu_{01}, \nu_{02}$ are constant coefficients which depend on the injector parameters.

Approximating the integrand by the formula

$$\frac{S_{0K}}{G} = k_{05}\bar{T}^{\nu_{03}}, \tag{10.93}$$

we integrate (10.91)

$$\tau = V \frac{k_{05}}{(\nu_{03} + 1)} (\bar{T}^{\nu_{03}+1} - \bar{T}_3^{\nu_{03}+1})$$

where k_{05}, ν_{03} are constants for a given engine.

Hence we find the temperature as a function of time

$$\overline{T} = \sqrt[\nu_{ok}]{C_2 + k_{ok}\tau}, \tag{10.94}$$

where $C_2 = \overline{T}_2^{\nu_{o3}+1}$; $\nu_{ok} = \nu_{o3} + 1$; $k_{ok} = \frac{\nu_{o3}+1}{k_{o3}} \frac{1}{V}$.

Substituting (10.94) into (10.92), we obtain easily the time dependence of the flow rate, and substituting (10.94) into (10.89), we can also determine $\psi = \psi(\tau)$:

$$G = \left[k_{o1} + k_{o2}(C_2 + k_{ok}\tau)^{\frac{\nu_{o1}}{\nu_{ok}}} + \left[k_{o3} + k_{o4}(C_2 + k_{ok}\tau)^{\frac{\nu_{o2}}{\nu_{ok}}}\right]\psi\right]^{-1}$$

$$\psi = \frac{\sqrt[\nu_{ok}]{C_2 + k_{ok}\tau}\left[s_{o1} + \frac{1}{2}s_{o2}(C_2 + k_{ok}\tau)^{\frac{1}{\nu_{ok}}} + \frac{1}{3}s_{o3}(C_2 + k_{ok}\tau)^{\frac{2}{\nu_{ok}}}\right] + C_1}{\exp\left[s_{o1}\sqrt[\nu_{ok}]{C_2 + k_{ok}\tau} + \frac{1}{2}s_{o2}(C_2 + k_{ok}\tau)^{\frac{2}{\nu_{ok}}} + \frac{s_{o3}}{3}(C_2 + k_{ok}\tau)^{\frac{3}{\nu_{ok}}}\right]}. \tag{10.95}$$

These formulas make it possible to find the time dependence of the combustion chamber pressure for discharge of oxidizer only, since in this case these is usually the critical pressure drop across the injectors. To this end we use the combustion chamber equation in the form

$$\frac{dp_k}{d\tau} + A_k p_k = B_1 G, \tag{10.96}$$

where $A_k = \frac{F_{kp} R_k T_k}{V_k}$; $B_1 = \frac{R_k T_k}{V_k}$.

The coefficients A_K and B_1 will be practically constant because of the weak temperature variation of the discharging oxidizer.

The solution of (10.96) has the form[13]

$$p_k = e^{-A_k\tau}\left[B_1 \int G(\tau) e^{A_k\tau}\, d\tau + C_3\right]. \tag{10.97}$$

In the case of subcritical pressure drop across the injectors, the oxidizer flow rate can be approximated by the formula

Footnote (13) appears on page 454

$$\frac{1}{G} = k_{o7} + k_{o8}\left[p_K - p_{kp}(a + b\bar{T}^{m_2})\right]^{\nu_{o1}} + k_{o9}\left[k_{o10}\left[p_K - p_{kp}(a + b\bar{T}^{m_2})\right]^{\nu_{o5}}\right], \quad (10.98)$$

(10.94)

where k_{o7}, k_{o8}, k_{o9}, k_{o10}, ν_{o1} and ν_{o5} are constant coefficients which depend on the parameters of the combustion chamber head.

he time
(10.89),

In this case the combustion chamber pressure is found by joint solution of (10.97) and (10.98). To this end we must specify some time interval $\Delta\tau$ and magnitude of the pressure p_K (or the pressure drop $\Delta p_{inj.o}$). Substituting the value of p_K into (10.98), we can find the flowrate G through the injectors. Considering this value to be constant over the time segment $\Delta\tau$, it is easy to find from (10.97) the value of $p_{K\ I}$ in the first approximation. The constant C_3 is found from the initial conditions. Determining from p_{KI} the flow rate G and again solving (10.97). we find $p_{K\ II}$, and so on.

(10.95)

ndence of
only, since
cross the
tion in

We note that at normal fueling temperatures the oxidizers customarily used do not create a chamber pressure such that the pressure drop across the injectors becomes subcritical.

Using (10.33) for the engine thrust and considering that

$$I = \int_0^\tau P_{-}d\tau, \quad (10.96)$$

we can find the TTI component due to discharge of oxidizer alone (for one combustion chamber)

nt because
zer.

$$I = \tau_c F_{kp} \int_0^\tau \gamma_{p_K} K_{-} e^{-A_K \tau}\left[B_1 \int_0^\tau G e^{A_K \tau}\, d\tau + C_3\right] d\tau. \quad (10.97)$$

Here zero time is taken when the oxidizer alone begins to discharge.

njectors,

8. Solution of the Equations for the Fuel Line

The system of equations describing the process of fuel evaporation from the cooling passage can be written in the following form

(see Section 3, paragraphs 2-6) [111, 112]:

$$\frac{dm_r}{d\tau} = -G_\phi + G_{вк};$$

$$\frac{dV_r}{d\tau} = \dot{V}_{вк} + \dot{V}_A;$$

$$\frac{d(u_r \cdot m_r)}{d\tau} = \frac{dQ}{d\tau} - i_r G_\phi + i'_r G_{вк} - p_r \dot{V}_A;$$

$$G_{вк} = \varepsilon G_\phi + \varrho' \frac{T_{кр}}{k_T} \frac{d\bar{T}}{d\tau}; \quad (10.99)$$

$$\dot{V}_{вк} = \varepsilon v' G_\phi + \frac{T_{кр}}{k_T} \frac{d\bar{T}}{d\tau}; \quad (10.100)$$

$$\frac{dQ}{d\tau} = K_Q A_T \bar{v} G_\phi; \quad (10.101)$$

$$\dot{V}_A = v' G_A; \quad (10.102)$$

$$G_\phi = G_\phi(\psi, \bar{T}, p_к); \quad (10.103)$$

$$G_A = G_A(\bar{T}, \psi_{вх}, \bar{T}_{вх}, b_{1A}); \quad (10.104)$$

$$u_r = i_r - p_r v_r; \quad (10.105)$$

$$i_r = i'_r + \psi r_r; \quad (10.106)$$

$$v_r = v'_r + \psi v''_r. \quad (10.107)$$

The temperature dependence of the physical parameters i'_f, r_f, v'_f, v''_f, ϱ_f is presented in Section 3, paragraph 5.

We shall make some transformations, dropping the subscript "f";

(1) we substitute the values of V_{boil} and V_{ve} into (10.50)

$$\frac{dV}{d\tau} = (1+\varepsilon) v' G_A + \frac{T_{кр}}{k_T} \frac{d\bar{T}}{d\tau}; \quad (10.108)$$

(2) we

(3) in
(10.101), and

We examin
moment all the
integration me
sidering that

Substitut
(10.108) and

Using the
(10.109), (10.

where

Equating
relations for
$\frac{d\bar{T}}{d\tau}$:

(2) we substitute the value of G_{boil} into (10.49)

$$\frac{dm}{d\tau} = G_{\text{в}} - G_{\phi} + Q' \frac{T_{\text{ср}}}{k_T} \frac{d\bar{T}}{d\tau}; \tag{10.109}$$

(3) in (10.51) we replace G_{boil} using (10.99), $\frac{dQ}{d\tau}$ using (10.101), and V_{ve} using (10.102):

$$u \frac{dm}{d\tau} + m \frac{du}{d\tau} = (K_Q A_T v - i) G_{\phi} + (i' - pv') G_{\text{в}} + \\ + \frac{T_{\text{ср}}}{k_T} Q' i' \frac{d\bar{T}}{d\tau}. \tag{10.110}$$

(10.99)

(10.100)

We examine the solution of this system of equations up until the moment all the fuel has boiled. To this end we use the numerical integration method. We shall first make some transformations. Considering that $v = v' + v''' \psi$ and $v = \frac{V}{m}$, we find

(10.101)

$$\frac{dv'}{d\bar{T}} \frac{d\bar{T}}{d\tau} + \psi \frac{dv''}{d\bar{T}} \frac{d\bar{T}}{d\tau} + v''' \frac{d\psi}{d\tau} = \frac{1}{m} \left(\frac{dV}{d\tau} - v \frac{dm}{d\tau} \right).$$

(10.102)

(10.103)

Substituting in place of dV/dτ and dm/dτ their values using (10.108) and (10.109), after transformations we obtain the equation

$$m \frac{d\psi}{d\tau} = (v' Q''' - v'_{\text{ф}}) G_{\text{в}} + (v' Q''' + \psi) G_{\phi} - \left[\xi Q' \psi + m Q''' \left(\frac{dv'}{d\bar{T}} + \right. \right. \\ \left. \left. + \psi \frac{dv''}{d\bar{T}} \right) \right] \frac{d\bar{T}}{d\tau}. \tag{10.111}$$

(10.104)

(10.105)

Using the known thermodynamic relations, (10.105), (10.107) and (10.109), (10.110) can be written in the form

$$m \frac{d\psi}{d\tau} = \frac{1}{\theta_2} \left\{ (K_Q A_T - p) v G_{\phi} + [(\varkappa - 1) p v' - \varkappa' \theta_2] G_{\text{в}} + \right. \\ \left. + [\xi Q' (p v' - \varkappa' \theta_2) - m \left(\frac{d\theta_1}{d\bar{T}} + \psi \frac{d\theta_2}{d\bar{T}} \right)] \frac{d\bar{T}}{d\tau} \right\}. \tag{10.112}$$

(10.106)

(10.107)

where

$$\theta_1 = i' - p v'; \quad \theta_2 = r - p v'''; \quad \xi = \frac{T_{\text{ср}}}{k_T}.$$

$v'_{\text{ф}}$

Equating (10.111) and (10.112), we obtain with account for the relations for the physical parameters the expression for determining $\frac{d\bar{T}}{d\tau}$:

$n_{\text{ф}}$;

)

$$\frac{d\bar{T}}{d\tau} = \frac{\theta_2 G_{\phi} - \theta_{\text{ф}1} (G_{\phi} + G_{\text{в}}) + \varepsilon \theta_{\text{ф}2} G_{\text{в}} - \varkappa' \xi i_{\phi}}{m (\theta_{\text{ф}2} + \psi \theta_{\text{ф}1}) - \xi \rho_{\text{ф}} (\alpha + \delta \bar{T}^{m_1})} \tag{10.113}$$

(10.108)

where

$$\theta_{f1}=A_f\bar{T}^{10,075}(0,3503+0,7454\bar{T}-0,2362\bar{T}^2-0,5026\bar{T}^3)$$

$$\theta_{f2}=p_{up}A_v(a+b\bar{T}^{m_1})(0,03968+0,08445\bar{T});$$

$$\theta_{f3}=A_f'(3+3,7\bar{T})-A_vp_{up}m_2\bar{T}^{m_1-1}(0,03968+0,08445\bar{T})-$$
$$-0,1537A_f\bar{T}^{10,075}(4,85-3,27\bar{T}^2);$$

$$\theta_{f4}=-6,51A_f\bar{T}-0,55A_vp_{up}bm_2\bar{T}^{m_1-11,075}+A_f\left(\frac{48,86}{\bar{T}}-32,95\bar{T}\right)$$

$$\theta_q=K_QA_fA_v(0,03968+0,08445\bar{T}-0,55\bar{T}^{-10,075})$$

$$r=A_f(4,85-3,27\bar{T}^2).$$

Curves of the relations θ_{f1}, θ_{f2}, θ_{f3}, θ_{f4} and r for unsymmetrical dimethyl hydrazine are shown in Figures 10.10 and 10.11.

Writing the derivative $d\bar{T}/d\tau$ in terms of finite differences and specifying the magnitude of the interval $\Delta\tau_j$, we can find the temperature change $\Delta\bar{T}_j$. In so doing we assume that all the parameters in the right side of (10.113) remain constant for the time $\Delta\tau_j$ and equal to their values in the preceding $(j-1)^{st}$ interval.

Equations (10.108) and (10.109) make it possible to determine the incremental emulsion volume ΔV and mass Δm

$$\Delta V_j=(1+\varepsilon_j)A_v(0,03968+0,08445\bar{T}_j)G_{\Sigma j}\Delta\tau_j+\xi\Delta\bar{T}_j;$$

$$\Delta m_j=(\gamma_j G_{\Sigma j}-G_{\gamma j})\Delta\tau_j+A_0(16,47-9\bar{T}_j)\xi\Delta\bar{T}_j.$$

With the aid of these expressions we can find the magnitude of the emulsion specific volume after the time $\Delta\tau_j$

$$v_{j+1}=\frac{V_j+\Delta V_j}{m_j+\Delta m_j}=v'_{j+1}+\gamma_{j+1}v''_{j+1}.$$

Hence we can find the emulsion vapor content after the time $\Delta\tau_j$:

$$\gamma_{j+1}=1,82A_v(\bar{T}_j+\Delta\bar{T}_j)^{10,075}\left\{\frac{V_j+\Delta V_j}{m_j+\Delta m_j}-\right.$$
$$\left.-A_v[0,03968+0,08445(\bar{T}_j+\Delta\bar{T}_j)]\right\}. \qquad (10.114)$$

Figure 10.

Now w
for the di

The v
this formu
interval.

The v
determine
possible t
combustion
pressure d
Therefore,
of the var
ture $\bar{T}$ for
these curv

After
rise of th

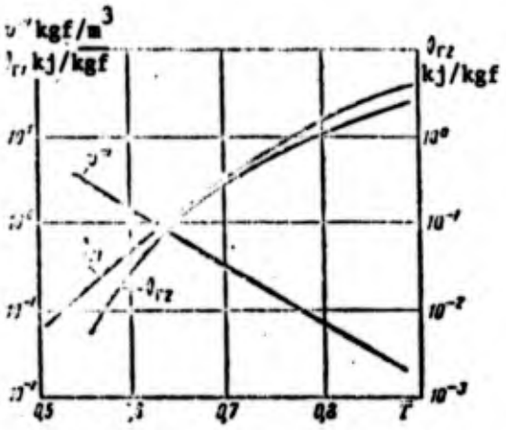

Figure 10.10. Variation of θ_{r1}, θ_{r2}, v''' with T.

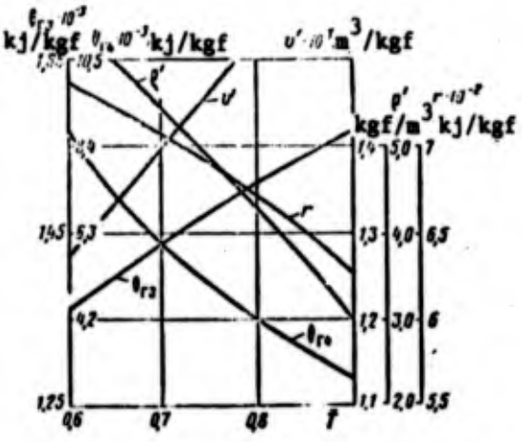

Figure 10.11. Variation of θ_{r2}, θ_{r1}, v', ϱ', r with T.

symmetrical

nces and
e temper-
ters in
and equal

ermine

tude

time $\Delta\tau_j$:

(10.114)

Now we shall determine the combustion chamber pressure, first for the discharge of fuel only. Solving (10.96), we obtain

$$p_{kj+1}=\exp\left(-\frac{F_{sp}R_kT_k}{\beta V_k}\Delta\tau_j\right)\left[\frac{\beta}{F_{sp}}G_{\phi j}\left(e^{\frac{F_{sp}R_kT_k\Delta\tau_j}{\beta V_k}}-1\right)+p_{kj}\right]. \tag{10.115}$$

The values of the specific impulse β and the product R_KT_K in this formula must be taken from the parameters of the j^{th} time interval.

The value of p_K calculated from (10.115) makes it possible to determine the injector pressure drop Δp_{inj}, which in turn makes it possible to find the flow rate of the boiling component into the combustion chamber in the next time interval. Usually the injector pressure drop is supercritical for the discharge of fuel only. Therefore, to simplify the calculations we can first plot a curve of the variation of the flow rates G_{inj} as a function of the temperature $\bar{T}$ for different ψ for the critical pressure drop and then use these curves.

After the cooling passage is filled with emulsion the temperature rise of the fluid terminates; therefore, from this moment on, we must

set $\varepsilon = 0$ in all the computational formulas.

After the fuel is forced out of the lines connecting the collector and the vent channel, the preheated propellant begins to discharge. In this case, to determine the flow rate G_{ve} we must know the propellant temperature ahead of the vent port. Therefore, we must find the amount of fuel which flows into the vent by the time

$$m_s = \sum_{j=1}^{c} G_{sj}\Delta\tau_j.$$

This quantity makes it possible to find the temperature $\bar{T}_{s\ ve}$ from graphs of the variation of the liquid mass and its temperature as a function of the emulsion volume.

Since the length of the path along which the preheated propellant is forced out is not extensive, the flow rate G_{ve} into the vent system is approximately

$$G_s = K_s \sqrt{\frac{p_{sj}\rho_1}{1+b_{1s}K_s^2}} \cdot \bar{T}^{\frac{m_s}{2}}$$

where $K_s = \mu_s' F_s \sqrt{2A_0(16{,}47 - 9\bar{T}_{ss})}$

Now we can also determine the increment of the thrust tailoff impulse during the time $\Delta\tau_j$:

$$\Delta I_j = \bar{\tau}_c \bar{\rho}_s \dot{K}_{s1} F_{s0} p_{sj}\Delta\tau_j.$$

After boiling of all the fuel in the cooling passage, the basic system of equations has the form

$$\left.\begin{aligned} &\frac{dm}{d\tau} = -G_\phi - G_s; \\ &m\frac{dw}{d\tau} + m\frac{du}{d\tau} = \frac{dQ}{d\tau} - iG_\phi - iG_s; \\ &\frac{dQ}{d\tau} = K_Q A_f \tau (G_\phi + G_s). \end{aligned}\right\} \qquad (10.116)$$

This s

where

Curves
shown in Fi

The so

In the
approximate

where s_{f1},
$s_{f1} = 0.19$;

The pr
quadratic p

The co
input to th
$s_{f4} = -1.67$

Footnote (1

This system reduces to the differential equation

$$\frac{d^2\varphi}{d\bar{T}^2} + \theta_{f5}\frac{d\varphi}{d\bar{T}} = \theta_{f6}. \qquad (10.117)$$

where

$$\theta_{f5} = \frac{\frac{dr}{d\bar{T}} - v'' \frac{dp}{d\bar{T}} - K_Q A_T \frac{dv''}{d\bar{T}}}{r - K_Q A_T v''} =$$

$$= -\frac{6{,}511\bar{T} + 0{,}55 A_v p_{kp} b m_3 \bar{T}^{m_3 - 11{,}075} - 5{,}511 K_Q A_T A_v \bar{T}^{-11{,}075}}{A_r(1{,}85 - 3{,}27\bar{T}^2) - 0{,}55 K_Q A_T A_v \bar{T}^{-10{,}075}};$$

$$\theta_{f6} = \frac{v' - \frac{dp}{d\bar{T}} - \frac{di'}{d\bar{T}} + K_Q A_T \frac{dv'}{d\bar{T}}}{r - K_Q A_T v''} =$$

$$= \frac{A_v p_{kp} b m_3 \bar{T}^{m_3 - 1}(0{,}05268 + 0{,}08415\bar{T}) - A_r'(3 + 3{,}7\bar{T}) + 0{,}08415 K_Q A_T A_v}{A_r(4{,}85 - 3{,}27\bar{T}^2) - 0{,}55 K_Q A_T A_v \bar{T}^{-10{,}075}}.$$

Curves of the quantities θ_{f5} and θ_{f6} for $K_Q = 0$ for UDMH are shown in Figure 10.12.

The solution of (10.117) has the form

$$\varphi = \exp\left(-\int \theta_{f5} d\bar{T}\right)\left[\int \theta_{f6} \exp\left(\int \theta_{f5} d\bar{T}\right) d\bar{T} + C_4\right].$$

In the range of possible variation of $\bar{T}$ the function θ_{f5} is approximated by the polynomial

$$\theta_{f5} = s_{f1} + s_{f3}\bar{T} + s_{f2}\bar{T}^2,$$

where s_{f1}, s_{f2}, s_{f3} are constant coefficients (for UDMH with $K_Q = 0$; $s_{f1} = 0.19$; $s_{f2} = -4.742$; $s_{f3} = -0.0029$).

The product $\theta_{f6}\exp\left(\int \theta_{f5} d\bar{T}\right)$ can also be approximated by the quadratic polynomial

$$\theta_{f6}\exp\left(\int \theta_{f5} d\bar{T}\right) = s_{f4} + s_{f5}\bar{T} + s_{f6}\bar{T}^2.$$

The coefficients s_{f4}, s_{f5}, and s_{f6} depend (if we neglect heat input to the emulsion[14]) on the nature of the propellant (for UDMH $s_{f4} = -1.67$; $s_{f5} = 0.9897$; $s_{f6} = -0.00459$).

Footnote (14) appears on page 454

Now the solution of (10.117) is written in the form

$$\psi = \frac{s_{10}\bar{T} + \frac{1}{2}s_{11}\bar{T}^2 + \frac{1}{3}s_{12}\bar{T}^3 + C_4}{\exp\left(s_{11}\bar{T} + \frac{1}{2}s_{13}\bar{T}^2 + \frac{1}{3}s_{14}\bar{T}^3\right)}. \qquad (10.118)$$

The constant C_4 is determined from the following condition: for the temperature $\bar{T} = \bar{T}_j$, corresponding to the instant the entire fuel cavity is filled with emulsion, the vapor content equals ψ_j.

Knowing $\psi = \psi(\bar{T})$, it is easy to find the dependence of the emulsion mass on $\bar{T}$:

$$m = \frac{V_{pa}}{v' + \psi v''},$$

where V_{pa} is the volume of the fuel cavity up to the vent valve. From (10.116) after transformations we obtain (measuring time from zero for simplicity)

$$\tau = V_{pa}\int_{\bar{T}_j}^{\bar{T}} \frac{S_\tau}{G_\phi + G_\alpha}\, d\bar{T}, \qquad (10.119)$$

where the function

$$S_\tau = A_\tau \frac{\bar{T}^{10,875}\left[0,08445\bar{T}^{11,875} + 0,554_{12}\bar{T} - 5,541\frac{1}{2}\left(1 + 0,009264_{12}\bar{T}\right)\right]}{\left[\bar{T}^{10,875}\left(0,03953 + 0,08445\bar{T}\right) + 0,55\frac{1}{2}\right]^2}$$

depends only on the fuel temperature. Calculating the integrand for different $\bar{T}$ and approximating the resulting relation by a power function of the form

$$\frac{S_\tau}{G_\phi + G_\alpha} = k_{12}\bar{T}^{n_{12}} \qquad (10.120)$$

we can integrate (10.119) and find the temperature as a function of time:

$$\bar{T} = \sqrt[n_{12}+1]{C_5 + K_{12}\tau}, \qquad (10.121)$$

where

$$n_{12} = n_{10} + 1;\ K_{12} = \frac{n_\tau}{k_{12}V_{12}};\ C_5 = \bar{T}^{n_{12}+1}.$$

Figure 10.
θ_{f6} with

of fuel al
To do this
analogous

in place
combustio

where the
of the va

The
the value

In c
oxidizer.
passage d
decreases
combustio
of the va
the combu
saturated
influence
the chamb

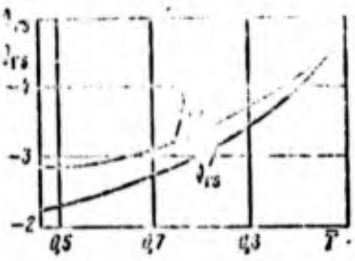

Figure 10.12. Variation of θ_{f5} and θ_{f6} with $\bar{T}$ for UDMH.

If the relation $S_f/G_{inj} + G_{ve}$ is difficult to approximate with adequate precision by a formula of the type (10.120), then the integral (10.119) must be calculated graphically or numerically.

Let us determine the combustion chamber pressure for the discharge of fuel alone and for the critical pressure drop across the injectors. To do this we must first substitute into the flow rate equation, analogous to (10.92)

$$G_\phi = [k_{r1} + k_{r2}\bar{T}^{r1} + (k_{r3} + k_{r4}\bar{T}^{r2})\gamma_1]^{-1} \qquad (10.122)$$

in place of $\bar{T}$ its value in terms of τ from (10.121). Integrating the combustion chamber equation, we obtain the formula for determining p_K:

$$p_K = \exp\left(-\int A_K d\tau\right)\left[\int B_1 G_\phi(\tau)\, e^{\int A_K d\tau} d\tau + C_0\right] \qquad (10.123)$$

where the coefficients A_K and B_1 also depend on the time as a result of the variation of β and $R_K T_K$.

The magnitude of the thrust tailoff impulse is easily found from the value of the pressure p_K.

In conclusion let us examine the joint discharge of fuel and oxidizer. Since the temperature of the emulsion in the cooling passage decreases in the course of time, the saturated vapor pressure decreases and this in turn reduces the emulsion flow rate into the combustion chamber. Moreover, G_{inj} is reduced as a result of increase of the vapor content ahead of the injectors. Therefore, at some time the combustion chamber pressure becomes less than the oxidizer saturated vapor pressure, the oxidizer then boils and, under the influence of the resulting pressure differential, begins to flow into the chamber. This leads to more intense burning in the chamber.

The pressure specific impulse increases, since the propellant ratio becomes nonzero. During this TTI interval the parameters of the emulsion must be calculated both in the oxidizer head and in the cooling slot. If the cooling passage and the supply lines are completely filled with emulsion at the moment oxidizer discharge begins, then the determination of the chamber combustion pressure at any instant (for critical pressure drop across the injectors) reduces to calculation of the integrals in an expression analogous to (10.123):

$$p_к = \exp\left(-\int A_к d\tau\right)\left[\int B_1(G_{ф.г} + G_0)\, e^{\int A_к d\tau}\, d\tau + C_1\right].$$

The quantities $R_K T_K$ and β can be approximated in a definite range of variation of k by the following formulas

$$\beta = \beta_1 + \beta_2\left(\frac{G_0}{G_{ф.г}}\right)^{\nu_3}\exp\left[-\nu_2\frac{G_0}{G_{ф.г}}\right];$$

$$R_к T_к = C_{к1} + C_{к2}\left(\frac{G_0}{G_{ф.г}}\right)^{\nu_3}\exp\left[-\nu_4\frac{G_0}{G_{ф.г}}\right],$$

where $\beta_1, \beta_2, C_{к1}, C_{к2}, \nu_1, \nu_2, \nu_3, \nu_4$ are constants for a given pair of propellants.

The magnitudes of the oxidizer G_o and fuel $G_{inj.f}$ flow rates are determined from Formulas (10.95) for the oxidizer and (10.122) with account for (10.121) for the fuel.

In practice it is more convenient to calculate p_K by numerical integration. If the injector pressure drop is subcritical or the cooling passage is not filled with emulsion, then p_K is found as follows. We select some time interval $\Delta\tau_j$ and combustion chamber pressure $p_{K\,j}$. If the fuel in the cooling passage has not all boiled, then we use (10.113) to find $\Delta\bar{T}_j$ and (10.114) to find the magnitude of the vapor content ψ_{j+1}.

If the entire passage is filled with emulsion, then $\Delta\bar{T}_j$ is calculated using (10.119) or (10.121) and the vapor content ψ_{j+1} is calculated using (10.118). These values make it possible to find the fuel flow rate into the combustion chamber. The temperature drop

in the oxidizer
(10.94). The o
presented in Se
critical inject
drop.

The flow ra
which can then
dynamic calcula
the formula

The result
the discrepancy
until the requi
discharge perio
pellants change
approximations
the combustion
fore, the calcu

The combus
possible to det
The end of join
fuel passage or
amount of remai
determined by t

where $m_{H.o.}$ is

in the oxidizer line during the time $\Delta\tau_j$ is found using (10.91) or (10.94). The oxidizer flow rate is computed either using the formulas presented in Section 3, paragraph 6 or using (10.95) in the case of critical injector pressure drop and (10.98) for subcritical pressure drop.

The flow rate values make it possible to find the mixture ratio, which can then be used to find β and $R_K T_K$ from graphs of the thermodynamic calculations. The combustion chamber pressure is found from the formula

$$p_{k\,j+1} = \exp\left(-\frac{F_{kp}(R_k T_k)_j}{\vartheta_j V_k}\Delta\tau_j\right)\left[\frac{\vartheta_j}{F_{kp}}(G_{\phi\,j}+G_j)\times\right.$$

$$\left.\times\left(e^{\frac{F_{kp}(R_k T_k)_j}{\vartheta_j V_k}\Delta\tau_j}-1\right)+p_{k\,j}\right].$$

The resulting value is compared with the assumed value. If the discrepancy is large we make a second approximation, and so on until the required accuracy is obtained. In practice, in the joint discharge period the temperature and vapor content of the two propellants change over only a small range. Therefore, the sequential approximations must be made only at the initial moment. Thereafter the combustion chamber pressure remains nearly constant, and therefore, the calculations are simplified considerably.

The combustion chamber pressure found in this way makes it possible to determine the magnitude of the TTI during this interval. The end of joint discharge is determined by complete emptying of the fuel passage or the oxidizer head. Therefore, we must estimate the amount of remaining liquid. In the oxidizer line this quantity is determined by the formula

$$m_{H} = m_{H.o.} - \sum_{j=1}^{n} G_{H}\Delta\tau_j,$$

where $m_{H.o.}$ is the initial oxidizer mass.

To determine the fuel mass in the cooling passage we must first determine the liquid flow rate into the vent system. Then the amount of ramaining liquid at any moment of time is found from the formula

$$m = m_{H.f.} - \sum_{j=1}^{n} (G_{\phi j} + G_{\text{г}j})\,\Delta\tau_j,$$

where $m_{H.f.}$ is the amount of fuel in the cavity from the head to the vent valve at the moment when oxidizer discharge begins.

§ 4. Calculation of the Transition Period Between Rapid Pressure Decay in the Combustion Chamber and Evaporation of the Propellants from the Cooling Passage

After closure of the cutoff valves, the combustion chamber pressure begins to decrease rapidly and at some instant of time becomes equal to the saturated fuel vapor pressure[15] $p_{s.f.}$ corresponding to the temperature of the liquid in the head. From this instant all the conditions for boiling of the propellants are created in the chamber head.

As is known, a definite time interval is necessary for the formation of vapor bubbles. Therefore, the fuel under the influence of the saturated vapors begins to be forced into the chamber only after the time τ_{del}, equal to the vaporization delay time. During this time the pressure p_K can decrease to some value which is easily determined from (10.32) if in place of τ we substitute τ_{del} and in place of p_K^* we substitute $p_{s.f.}$. Here we take as the zero reference time the instant corresponding to the equality $p_K^* = p_{s.f.}$. If

$$p_{K.del} > \left(\frac{2}{k+1}\right)^{\frac{k}{k-1}} p_{s.f.},$$

where k is the adiabatic index of the fuel vapors;

$p_{K.del}$ is the combustion chamber pressure after τ_{del},

---

Footnote (15) appears on page 454

then the pressure drop across the fuel injectors will be essentially subcritical. Otherwise, the discharge from the injectors will be critical.

The flow rate through the injectors can be found from the following considerations. Since the transient interval in question is short, the temperature $\bar{T}$ of the boiling fuel will be constant and the vapor content will be practically zero. Therefore, for the critical pressure drop, we can approximate with adequate accuracy the previously calculated curve of $G_{inj.f}$ versus $\Delta p_{inj.f} = p_{s.f.} - p_K$ for constant temperature and vapor content by the following formula

$$G_{\phi r} = B_r(p_{s.r} - p_k).$$

We shall examine, as being more general, the case of subcritical pressure drop across the injectors. To determine the pressure decay curve we must solve the following system of equations

$$p_0 = p_k + b_{10}G_0^2 + b_2\dot{G}_0;$$

$$\dot{p}_0 = -G_0\frac{a_0^2}{V_0};$$

$$\dot{p}_k = (G_0 + G_{\phi r} - G_k)\frac{R_k T_k}{V_k};$$

$$G_k = \frac{F_{kp}}{\beta}p_k.$$

The quadratic flow rate relation can be linearized as follows

$$b_{10}G_0^2 = \bar{p}_0 + B_0 G_0.$$

In addition, we make the replacement of variables

$$\tilde{p}_0 = p_0 - \bar{p}_0.$$

Now the relations above are easily transformed into a system of three linear differential equations

$$\dot{p}_0 = -A_1 G_0;$$

$$\dot{G}_0 = \frac{1}{b_{20}} p_0 - \frac{B_0}{b_{20}} G_0 - \frac{1}{b_{20}} p_k;$$

$$\dot{p}_k = B_0 G_0 - A_2 p_k + h,$$

where

$$A_1 = \frac{a_0^2}{V_0}; \quad B_0 = \frac{R_k T_k}{V_k};$$

$$A_2 = \frac{R_k T_k}{V_k}\left(B_r + \frac{F_{kp}}{\beta}\right);$$

$$h = p_{s.f.}\frac{\sqrt{R_k T_k}}{V_k} B_1.$$

The solution of this system of equations has the form

$$p_k = C_1 e^{\lambda_1 \tau} + C_2 e^{\lambda_2 \tau} + C_3 e^{\lambda_3 \tau} + \frac{h}{\lambda_1} r_1 - \frac{h}{\lambda_2} r_2 - \frac{h}{\lambda_3} r_3, \qquad (11.124)$$

where

$$r_1 = \frac{a_{12}}{a_{11}} r_2 + \frac{a_{13}}{a_{11}} r_3; \quad r_2 = \frac{a_{21}a_{13} - a_{23}a_{11}}{a_{22}a_{11} - a_{21}a_{12}} r_3;$$

$$r_3 = \frac{a_{11}(a_{22}a_{11} - a_{21}a_{12})}{(a_{21}a_{13} - a_{23}a_{11})(a_{11} - a_{12}) - (a_{13} - a_{11})(a_{22}a_{11} - a_{21}a_{12})};$$

$$a_{1k} = -\frac{A_1(A_2 + \lambda_k)\lambda_k}{\lambda_k B_0}; \quad a_{2k} = \frac{A_2 + \lambda_k}{B_0}; \quad a_{3k} = 1;$$

λ_K are the roots of the characteristic equation

$$\lambda^3 + \left(A_2 + \frac{B_0}{b_{20}}\right)\lambda^2 + \left(\frac{B_0}{b_{20}} + \frac{A_1}{b_{21}} + \frac{B_0}{b_{20}} A_2\right)\lambda + \frac{A_1}{b_{20}} A_2 = 0.$$

The arbitrary constants are determined from the following condition: at the initial moment the pressures in the chamber and in the oxidizer line and the oxidizer flow rate are defined by the formulas presented in Section 2, Chapter 10 for $\tau = \tau_{del}$.

When the chamber pressure becomes equal to $\left(\frac{2}{k+1}\right)^{\frac{k}{k-1}} p_{s.f.}$, the critical pressure drop is established across the injectors and the flow rate will be practically constant. In this case our basic system of equations is not altered externally, but some of the coefficients are replaced by the values

where $G_{inj.c}$
drop.

The sol
stants are d
period. The
initiation o
pressure bec

Thus, t
the combusti
rapid decay

§

It is d
TTI in vacuo
the results
area under t
multiply the
between thru
meters

where P_{∞}^{*} and
chamber pres

In certa
cant errors,
stand differs
The differen

$$A_2 = A_к = \frac{F_{кр}}{\beta} \frac{R_к T_к}{V_к}; \quad k = \frac{R_к T_к}{V_к} G_{ф\,кр},$$

where $G_{inj.cr}$ is the value of the fuel flow rate for critical pressure drop.

The solution is also found using (10.124). The arbitrary constants are determined by the closing conditions of the preceding period. The end of the transient segment from the rapid decay to the initiation of evaporation is determined by the instant when the chamber pressure becomes close to the value $p_K = \beta G_{inj}/F_{cr}$.

Thus, the formulas presented above make it possible to calculate the combustion chamber pressure in the period of transition from the rapid decay to the evaporation of the propellants.

§ 5. Conversion of TTI from Sea Level to Vacuum Conditions

It is desirable that the mean theoretical value of the engine TTI in vacuo, obtained in the design calculations, be corrected using the results of test stand results. To this end we can compute the area under the curve of the combustion chamber pressure decay and multiply the resulting value by the coefficient χ' of proportionality between thrust and pressure, obtained from the nominal regime parameters

$$\chi' = \frac{P_{\infty}^{*}}{p_K^{*}},$$

where P_{∞}^{*} and p_K^{*} are, respectively, the vacuum thrust and the combustion chamber pressure at the nominal engine operating condition.

In certain cases this determination of I_{∞} may lead to significant errors, since the engine shutdown transient process on the test stand differs markedly from shutdown under actual flight conditions. The difference amounts to the following.

1. In the case of a low fueling temperature the high-boiling oxidizers may not boil at all in the head (if the saturation vapor pressure for this temperature is less than 1 bar). Therefore, under test stand conditions there may not be any joint discharge of oxidizer and fuel at all.

2. Owing to the backpressure, the fuel flow rate into the vent system at sea level is less than that in space. Therefore, on the one hand, the work expended by the emulsion in the cooling passage on ejecting fuel into the vent system will be less under sea level conditions. This leads to an additional increase of the pressure in the combustion chamber. In addition, the amount of liquid discharged into the vent system during engine testing is less than under flight conditions. Therefore, the amount of the emulsion entering the combustion chamber on the stand is greater, which also leads to an increase of the pressure.

3. Under sea level conditions the pressure in the chamber, after values equal to 2 bar, decays more smoothly because of transition of chamber operation into the subcritical regime (under flight conditions there is always a critical section).

4. Discharge of the propellants and the products of their decomposition and combustion terminates under sea level conditions after values of p_K = 1 bar, while in vacuo this process may continue for a long time.

5. During the discharge of the products of decomposition of either propellant alone, under test stand conditions, the occurrence of condensation shocks is possible. The condition of the discharge of the products through the nozzle in this case also differs from vacuum conditions.

If in view of the peculiarities of the LRE design, joint discharge of the propellants does not occur (or is slight as a function of time) or if the oxidizer saturated vapor pressure is significantly

greater t
results t
following

Firs
coefficie
the nomin
between t
process i
F_c/F_{cr} de
index n.
propellan
nominal v
length.
estimate

Seco
the vent
chamber i
perature
time.

Third
result of
is lower t

The
conditions
created by

where G_{inj}
injector p

greater than 1 bar, then the results of the conversion of test stand results to full-scale conditions will exceed the true values for the following reasons.

First, the quantity $\chi' = \varphi_c F_{cr} K_\infty$ depends on the vacuum thrust coefficient, which in the shutdown period on the stand is less than the nominal value. This is the result of the considerable difference between the nozzle expansion process at sea level and the expansion process in space. In addition, the value of K_∞ for large area ratios F_c/F_{cr} depends to a marked degree on the variation of the polytropic index n. For discharge of the products of decomposition of a single propellant or for a mixture ratio which differs markedly from the nominal value, the average polytropic index increases along the nozzle length. Therefore, converting the TTI on the basis of χ' may overestimate I_∞ considerably, particularly for engines with large F_c/F_{cr}.

Second, as a result of the reduction of the fuel flow rate into the vent system the amount of propellant entering the combustion chamber is greater under sea level conditions and the propellant temperature is higher, which also increases p_K and lengthens the TTI time.

Third, for combustion chamber pressures less than 2 bar, as a result of chamber operation in the subcritical regime the pressure is lower than that obtained in space.

The TTI obtained on the test stand can be converted to flight conditions as follows. First we determine the chamber pressure created by the fuel alone. To do this we use the formula

$$p_{K\,inj} = \varphi_{p_K} \frac{G_{inj.cr}}{F_{kp}},$$

where $G_{inj.cr}$ is the fuel flow rate at the initial moment for critical injector pressure drop.

Using the value of this pressure, we determine from the decay curve the area up to the moment when $p_K = p_{K.cr}$. During this interval the parameters differ very little from the nominal values and therefore we can take $\chi' = \chi^{*}'$. This makes it possible to compute the magnitude of the TTI during the time of pressure decay to the value $p_{K.cr}$.

Now we examine the next segment, due to discharge of the fuel alone. If the saturated vapor pressure $p_{s\ o}$ of the oxidizer in the head is less than 2 bar, then this interval is terminated for $p_K \approx 2$ bar. However, if $p_{s\ o} > 2$ bar, then the end will occur for $p_K = p_{s\ o}$.

To calculate the magnitude of the TTI we must know the change of the vacuum thrust coefficient K_{∞} due to the dependence of the polytropic index on the fuel temperature ahead of the injectors. Therefore, we must use the calculated data obtained during design: we break the interval in question down into time intervals, find the corresponding temperatures $\bar{T}$ and the values of the index n, then calculate or find from a graph the value of K_{∞} (Figure 10.13). The value of K_{∞} then makes it possible to calculate χ' and the vacuum thrust for each time interval. Multiplying P_{∞} by the length of the interval and summing these products, it is easy to obtain the TTI for discharge of fuel alone.

If $p_{s\ o} > 2$ bar then for the segment with the pressure decay from the value $p_{s\ o}$ to 2 bar the TTI is found just as for the segment discussed above. But in this case the index n is taken from the results of the thermodynamic calculation of combustion for the corresponding mixture ratio and pressure.

We now need to find the difference between the amount of fuel discharging into the vent system in space and on the stand. To do this we first find from the results of the TTI calculation the quantities $b_{1\ ve}$ and $\bar{T}$ and the corresponding flow rate $G_{ve\infty}$ at any moment of time. From these values of $\bar{T}$ and $b_{1\ ve}$ we calculate G_{ve} on the stand using the formula

Figure 10.1
vacuum th
K_{∞} with p
values of
isentrope

bar, we fin
ditions as
system. Th
the end of
of the engi

The er
the segment
is obtained
the vent sy

If the
used in the
accounted

In co
is far fro
during the
can consid
from the r

Let u
velocity a

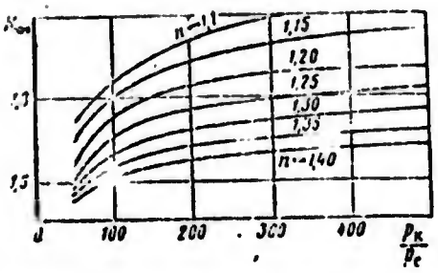

Figure 10.13. Variation of vacuum thrust coefficient K_∞ with p_K/p_c for different values of the expansion isentrope n.

$$G_{\text{ve}\infty} \simeq K_{\text{a}} \sqrt{\frac{p_{\text{kp}}}{1+b_{1\text{a}}K_{\text{a}}^2}\left(a + b\bar{T}^m - \frac{10^5}{p_{\text{kp}}}\right)}.$$

Then we determine at each moment of time the difference between $G_{ve\infty}$ and G_{ve0} and multiply this difference by the quantity $\varphi_c \varphi_{pK} K_\infty \beta\tau$. After summing the resulting values for all the time segments from the moment when the pressure equals $p_{K.cr}$ to $p_K = 2$ bar, we find that increase of TTI which is obtained under stand conditions as a result of the reduction of the flow rate to the vent system. The rest of the TTI from the moment when $p_K = 2$ bar until the end of the evaporation period can be found only from the results of the engine analysis in the preliminary design stage.

The entire TTI is obviously found by simple summation over all the segments examined, with subsequent subtraction of that part which is obtained as a result of the difference of the fuel flow rates into the vent system on the stand and in space.

If the propellant fueling temperature differs from the value used in the design by the magnitude $\Delta\bar{T}$, then this difference must be accounted for in making the conversion.

In conclusion, we note that for engines in which the vent valve is far from the collector, the fuel temperature changes very little during the evaporation period. Therefore, n may be averaged and we can consider that K_∞ = const. Then the determination of the TTI from the results of stand tests is simplified somewhat.

§ 6. Effect of TTI and its Scatter on the Impact Point Dispersion of Ballistic Rocket Nosecones

Let us relate the TTI and its scatter with the variation of the velocity at the end of the powered part of the trajectory [182].

To this end we examine the known equation

$$\Delta w_к = w_к - w_0 = P_{1-} \ln \frac{m_0}{m_к} - g \sin\gamma (\tau_{к} - \tau_0),$$

where Δw_K is the velocity change in the direction of the thrust vector in the engine shutdown process;

γ is the pitch angle (γ = const);

P_{1-} is the specific thrust, averaged over the shutdown time; the subscript "0" corresponds to the initiation of engine shutdown, while the index subscript "K" corresponds to the end of the shutdown process;

$\tau_{m.c.} - \tau_0$ is the duration of the shutdown period.

Since

$$P_{1-} = \frac{I}{\Delta m},$$

and since $\Delta m = m_0 - m_к \ll m_0$, then

$$\Delta w_к = \frac{I}{m_0} - g \sin\gamma (\tau_{к} - \tau_0).$$

The time variation in this formula for a change of the TTI by an amount δI has second order of smallness in comparison with $\frac{\delta I}{m_0}$. Therefore, we can take $\tau_{m.c}$, which makes it possible to determine the velocity variation when varying I:

$$\delta_I w_к = \frac{\delta I}{m_0}.$$

Denoting the relative change of TTI by $\delta \bar{I}$, we obtain

$$\delta_I w_к = \frac{I}{m_0} \delta \bar{I},$$

where $\delta \bar{I} = \delta I / I$.

Let us turn from the velocity variation in the thrust direction to the variation in the direction which is nominal for the velocity vector

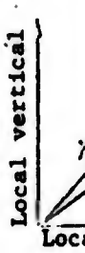

Figure 10
determi
nosecon

Assu
the veloc

The

The
of the en
nominal v

We f
tude of t

Prese
to variati
Therefore,
rocket mas
value of t

The
final mass

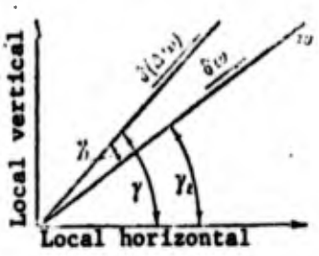

Figure 10.14. Diagram for determining ballistic rocket nosecone impat scatter.

$$\delta w_0 = \delta(\Delta w_k)\cos\gamma_{10},$$

where γ_{10} is the angle of attack (Figure 10.14).

The corresponding variation of the range L will be

$$\frac{\partial L}{\partial w_0}\delta w_0 = \frac{I}{m_0}\delta\bar{I}\frac{\partial L}{\partial w_0}\cos\gamma_{10}.$$

Assuming that $\delta w_0 \ll w_0$ and $\operatorname{tg}\delta\gamma_{20} \approx \delta\gamma_{20}$, we determine the change of the velocity vector direction $\delta\gamma_{20}$ with the variation Δw_K:

$$\delta\gamma_{20} = \frac{\sin\gamma_{10}}{w_0}\delta w_0.$$

The corresponding variation of the range L will be

$$\frac{\delta w_0}{w_0}\sin\gamma_{10}\frac{\partial L}{\partial\gamma_{20}} = \frac{I\sin\gamma_{10}}{m_0 w_0}\left(\frac{\partial L}{\partial\gamma_{20}}\right)\cos\gamma_{20}\delta\bar{I}.$$

The products $\partial L/\partial w_0$ and $\partial L/\partial\gamma_{20}$ are functions of the parameters of the end of the powered segment, which can be considered to be the nominal values.

We find the total range variation due to variation of the magnitude of the TTI

$$\delta L_1 = \frac{I}{m_0}\left(\frac{\partial L}{\partial w_0}\cos\gamma_{10} + \frac{\partial L}{\partial\gamma_{20}}\frac{\sin 2\gamma_{10}}{2w_0}\right)\delta\bar{I}.$$

Present-day radio-inertial and inertial guidance systems react to variation of the acceleration but not to variation of the thrust. Therefore, it is not possible to establish the variation of the final rocket mass, since it is not possible to determine the instantaneous value of the rocket mass.

The range deviation from the nominal value due to change of the final mass will be

$$\delta L_2 = -\frac{I}{(1+\delta\bar{m}_0)\,m_0}\left(\frac{\partial L}{\partial w_0}\cos\gamma_{10} + \frac{\partial L}{\partial \gamma_{20}}\,\frac{\sin 2\gamma_{10}}{2w_0}\right)\delta\bar{m}_0,$$

where

$$\delta\bar{m}_0 = \frac{\delta m_0}{m_0}.$$

Now let us find the partial derivatives $\partial L/\partial w_0$ and $\partial L/\partial \gamma_{20}$, assuming a spherical, nonrotating earth and neglecting atmospheric drag in the unpowered part of the trajectory. Since in accordance with elliptic theory the range from the point corresponding to the end of the powered part of the trajectory, measured along the arc of a great circle, will be

$$\Delta L = 6{,}371\cdot 10^6\left[3\arccos\frac{-2z_3z_2+z_1}{\sqrt{z_4^2+4z_3z_5}} - \arccos\frac{-2z_3z_2+z_4}{\sqrt{z_4^2+4z_3z_5}}\right],$$

where

$$z_1 = \frac{1}{R_0+H};\quad z_2 = \frac{1}{R_0};\quad z_3 = w_0^2 - \frac{2gR_0^2}{R_0+H}$$
$$z_4 = 2gR_0^2;\quad z_5 = [(R_0+H)\,w_0\sin\gamma_{10}]^2;$$

H is height above the spherical earth, then

$$\frac{\partial L}{\partial w_0} = \frac{1{,}2742\cdot 10^7}{w_0\left(z_4^2+4z_3z_5\right)}\left\{\frac{3\left[z_1\left(z_4^2+2z_3z_5-2z_5w_0^2\right)+z_3\left(z_1+w_0^2\right)\right]}{\sqrt{\frac{z_3}{z_5}+\frac{z_4}{z_5}z_1-z_1^2}} - \frac{z_2\left(z_4^2+2z_3z_5-2z_5w_0^2\right)+z_1\left(z_3+w_0^2\right)}{\sqrt{\frac{z_3}{z_5}+\frac{z_4}{z_5}z_2-z_2^2}}\right\};$$

$$\frac{\partial L}{\partial \gamma_{20}} = \frac{1{,}2742\cdot 10^7}{\lg\gamma_{20}\left(z_4^2+4z_3z_5\right)}\left\{\frac{3\left[\left(z_4^2+2z_1z_5\right)z_3+z_3z_4\right]}{\sqrt{\frac{z_3}{z_5}+\frac{z_4}{z_5}z_1-z_1^2}} - \frac{\left(z_4^2+2z_3z_5\right)z_2+z_3z_4}{\sqrt{\frac{z_3}{z_5}+\frac{z_4}{z_5}z_2-z_2^2}}\right\}.$$

The nominal values of the quantities appearing in these formulas are known; therefore calculation of δL_1 and δL_2 does not present any difficulty.

Figure 10.15.
$\bar{T}$ with $\delta\bar{m}_0$

The curv
Figure 10.15.

We see t
but is not sy
dispersion is

In conclu
TTI ($\delta I = 0$) the
same result m
δI and $\delta\bar{m}_0$).
range dispers
down is to re

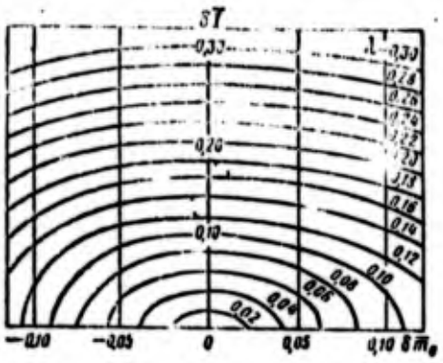

Figure 10.15. Variation of $\delta\bar{\lambda}$ with $\delta\bar{m}_0$ for various λ.

Assuming that δL_1 and δL_2 are independent random quantities, subject to the normal distribution law, we obtain the mean square variation

$$\sigma = \sqrt{\delta L_1^2 + \delta L_2^2} =$$

$$= \frac{l}{m_0}\left(\frac{\partial L}{\partial \omega_0}\cos\gamma_{10} + \frac{\partial L}{\partial \gamma_{20}}\,\frac{\sin 2\gamma_{10}}{2\omega_0}\right)\sqrt{\delta\bar{l}^2 + \left(\frac{\delta\bar{m}_0}{1+\delta\bar{m}_0}\right)^2}.$$

The curves of $\lambda = \lambda(\delta\bar{l}, \delta\bar{m}_0)$, where $\lambda = \sqrt{\delta\bar{l}^2 + \left(\frac{\delta\bar{m}_0}{1+\delta\bar{m}_0}\right)^2}$ are shown in Figure 10.15.

We see that the range dispersion is symmetric relative to δl, but is not symmetric relative to $\delta\bar{m}_0$, since for negative $\delta\bar{m}_0$ the dispersion is greater than for positive values.

In conclusion, we note that with absolutely no scatter of the TTI ($\delta l = 0$) the range dispersion is only reduced by one half. This same result may be obtained if we reduce I by one half (for fixed δl and $\delta\bar{m}_0$). Thus, the most effective technique for reducing the range dispersion of rocket nosecone impact points due to engine shutdown is to reduce the value of I and not the value of δl.

FOOTNOTES

1. on page 380 — The redidual thrust of the Vanguard rocket after engine shutdown continued for 2 minutes [44].

2. on page 389 — We neglect the variation of A_n.

3. on page 390 — The case of nonuniform closure of pyrovalves differs very little from the case examined.

4. on page 391 — Here the parameters with asterisk relate to the last stage engine operating regime, or to the main stage operating regime if there is no last stage.

5. on page 393 — Here we also assume that $R_*T_* \neq f(k)$.

6. on page 401 — In the case of mixed cooling of the combustion chamber or when the oxidizer is used as the coolant, the basic system of equations is not significantly more complicated.

7. on page 401 — For the known propellant pairs and for the usual engine schemes the saturated vapor pressure of the fuel preheated in the cooling passage is several times greater than the saturated vapor pressure of the oxidizer at the fueling temperature.

8. on page 401 — We assume the emulsion to be uniformly dispersed with vapor content which is constant throughout its volume.

9. on page 403 — After filling the entire cavity with the emulsion, the flow rate will be determined by the sum of the flow rates into the combustion chamber and the vent system, and $G_{boil} = 0$.

10. on page 403 — After filling the entire cavity the volume will not change, i.e., $\frac{dV_p}{dt} = 0$.

11. on page 404 — If a vent valve is installed in the oxidizer line, then in the right side of (10.52) we must add the value of the oxidizer flowrate into the vent system, which does not complicate the problem to speak of.

12. on page 407 — If the coefficient k_T changes along the length of the combustion chamber, this variation is easily accounted for.

13. on pa

14. on pa

15. on pa

13. on page 429

If it is difficult to approximate the integrand of (10.91) with sufficient accuracy by the Relation (10.93), then the Integral (10.91) must be found graphically or numerically. To simplify the calculation we can first use these results to construct a plot of the dependence of $\bar{T}$ on τ and use this plot in calculating the flow rates, combustion chamber pressure, and impulse.

14. on page 436

As a result of the low emulsion motion velocity through the cooling passage and the small temperature differential, the magnitude of the heat added to the emulsion can nearly always be neglected without any loss of computational accuracy but with considerable simplification in the calculations.

15. on page 441

Since in most cases the saturated vapor pressure of the preheated fuel is higher than the oxidizer vapor pressure.

REFERENCES

1. Abramovich, G. N. Gazovaya dinamika vozdushno-reaktivnykh dvigateley (Gasdynamics of Jet Engines). Izdatel'stvo BNT, 1947.
2. Abramovich, G. N. Prikladnaya gazovaya dinamika (Applied Gas Dynamics). GTTI (Gostekhizdat : State Publishing House of Technical and Theoretical Literature), 1953.
3. Artamonova, K. I. and I. G. Krutikova. Thermoacoustic Instability of Nonuniform Gas Flow. Izv. AN SSSR (Izvestiya akademii nauk SSSR : Newsletter of the Academy of Sciences, USSR), OTN (Otdeleniye tekhnicheskikh nauk : Division of Technical Sciences), Mekhanika i mashinostroyeniye, No. 3, 1962.
4. Ayzerman, M. A. Lektsii po teorii avtomaticheskogo regulirovaniya (Lectures on Automatic Control Theory). Fizmatgiz (Gosudarstvennoye izdatel'stvo fiziko-matematicheskoy literatury : State Publishing House of Literature on Physics and Mathematics), 1958.
5. Alekseyev, G. V., B. A. Zenkevich, and V. I. Subbotin. Study of Heat Transfer in Nucleate Boiling of Water in Tubes, Teploenergetika, No. 4, 1962.
6. Alemasov, V. Ye. Teoriya raketnykh dvigateley (Rocket Engine Theory). Oborongiz (Gosudarstvennoye izdatel'stvo oboronnoy promyshlennosti : State Publishing House for the Defense Industry), 1962.
7. Artamonov, K. I. LRE Operating Stability. Izv. AN SSSR, OTN, Mekhanika i mashinostroyeniye, No. 1., 1961.
8. Babikov, O. I. Ul'trazvuk i yego primeneniye v promyshlennosti (Ultrasound and Its Industrial Application). Fizmatgiz, 1958.
9. Barrere, M., A. Jaumotte, B. F. de Veubeke, and J. Vandenkerckhov. Raketnyye dvigateli (Rocket Propulsion). Oborongiz, 1962.
10. Bezhanov, B. N. Pnevmaticheskiya (Pneumatic Mechanisms). Mashgiz (Gosudarstvennoye nauchno-teknicheskoye izdatel'svo mashinostroitel'noy literatury : State Scientific and Technical Publishing House of Literature on Machinery), 1957.
11. Belik, N. P. On the Calculation of Liquid Natural Oscillation Frequencies in Complex Lines. Izv. VUZ, Aviatsionnaya tekhnika, No. 2, 1965.
12. Belik, N. P. On the Calculation of Wave Processes in Complex Lines with Periodic Discharge Variation. Izv. VUZ, Aviatsionnaya tekhnika, No. 3, 1965.
13. Belik, N. P., V. A. Makhin, and V. F. Prisnyakov. On the Calculation of Liquid Natural Oscillation Frequencies in Branched Lines. Mekhanika zhidkosti i gaza. Vol. 2, 1962.
14. Bergman, L. Ultrasonics. For. Lit. Press, (IL), 1957.
15. Bergeron, L. Ot gidravlicheskogo udara v trubakh do razryada v elektricheskoy seti (Water Hammer in Hydraulics and Wave Surges in Electricity). Mashgiz, 1962.
16. Berman, K. and S. Chini. VRT (Voprosy raketnoy teknhiki), No. 6, 1956.
17. Besser
(Voy
18. Blokh,
regu
GTTI
19. Bodner
Dize
20. Bodner
Cont
21. Bolgar
ZhRI
22. Borise
Engi
23. Borish
dvuk
of T
24. Bragg,
ture
1960
25. Burges
Voye
26. Ventze
27. VRT (V
28. VRT, N
29. VRT, N
30. VRT, N
31. VRT, N
32. VRT, N
33. VRT, N
34. VRT, N
35. VRT, N
36. Voronc
(El
37. Vostri
(Ai
38. Vulis
Comb
39. Gamyni
(Fur
40. Gunde
Mot
41. Gartma
VRT
42. Gerts
pnev
Powe
43. Gerts
priv
Auto
44. Goethe
Rake
45. Hydrau
Bla

* Translators N

17. Besserer, K. U. Missile Engineering Handbook. Voyenizdat (Voyennoye izdatel'stvo : Military Publishing House), 1962.
18. Blokh, Z. Sh. Dinamika leneynykh sistem avtomaticheskogo regulirovaniya (Dynamics of Linear Automatic Control Systems) GTTI, 1952.
19. Bodner, V. A. Increasing Internal Combustion Engine Power. Dizelestroyeniye, Nos. 9, 10, 11, 1939.
20. Bodner, V. A. Avtomatika aviatsionnykh dvigateley (Automatic Control of Aircraft Engines). Oborongiz, 1952.
21. Bolgarskiy, A. V. and V. K. Shchukin. Rabochiye protsessy v ZhRD (Working Processes in LRE). Oborongiz, 1953.
22. Borisenko, A. I. Gazovaya dinamika dvigateley (Gasdynamics of Engines). Oborongiz, 1962.
23. Borishanskiy, V. M. In: voprosy teplootdachi i gidravliki dvukhfaznykh sred (Problems of Heat Transfer and Hydraulics of Two-phase Media). Gosenergoizdat, 1961.
24. Bragg, S. Variation of Liquid Propellant Density and Temperature in Auxiliary Systems of Rocket Engines. VRT, No. 5, 1960.
25. Burgess, E. Long-range Ballistic Missiles. Fizmatgiz, 1958, Voyenizdat, 1963.
26. Ventzel, E. S. Probability Theory. Fizmatgiz, 1958.
27. VRT (Voprosy raketnoy tekhniki), No. 3, 1961.
28. VRT, No. 1, 1961.
29. VRT, No. 5, 1962.
30. VRT, No. 11, 1961.
31. VRT, No. 7, 1960.
32. VRT, No. 10, 1963.
33. VRT, No. 6, 1956.
34. VRT, No. 8, 1962.
35. VRT, No. 1, 1962.
36. Voronov, A. Elementy teorii avtomaticheskogo regulirovaniya (Elements of Automatic Control Theory). Voyenizdat, 1954.
37. Vostrikov, S. I. et al. Teoriya aviatsionnykh dvigateley (Aircraft Engine Theory), Parts 1, 2. Voyenizdat, 1960.
38. Vulis, L. A. Teplovoy rezhim goreniya (Thermal Regime of Combustion). Gosenergoizdat, 1954.
39. Gamynin, N. S. Osnovy sledyashchego gidravlicheskogo privoda (Fundamentals of Hydraulic Servodrive). Oborongiz, 1962.
40. Gunder, D. F. and D. R. Friant. Stability of Flow in a Rocket Motor. VRT, No. 1, 1951*
41. Gartman, H. Measurement of Rocket Model Thrust and Vibration. VRT, No. 4, 1951.
42. Gerts, Ye. V. and G. V. Kreynin. Teoriya i raschet silovykh pnevmaticheskikh ustroystv (Theory and Design of Pneumatic Power Devices). Izd-vo AN SSSR, 1960.
43. Gerts, Ye. V. and G. V. Kreynin . Dinamika pnevmaticheskikh privodov mashin-avtomatov (Dynamics of Pneumatic Drives for Automated Machines. Izd-vo Mashinostroyeniye 1964.
44. Goethert, B. H. Modeling Outer Space Conditions in Tests. Raketnaya tekhnika, No. 6, 1962.
45. Hydraulic and Pneumatic Power Control Systems, edited by D. Blackford, H. Ritkhof and D. L. Sherer. IL 1962 .

* Translators Note: The English version is in J. Appl. Mech., Vol. 17, Sept. 1950.

46. Gion, M. Issledovaniya i raschet gidravlicheskikh sistem (Hydraulic System Design and Analysis). Izd-vo Mashinostroyeniye, 1964.
47. Ginzburg, I. Sh. Prikladnaya gidrogazodinamika (Applied Hydrogasdynamics). LGU (Leningrad State University), 1958.
48. Gladkikh, P. A. and S. A. Khachaturyan. Vibratsii v truboprovodakh i metody ikh ustraneniya (Vibrations in Hydraulic Lines and Means for Their Elimination). Mashgiz, 1959.
49. Hoffman, S. K. Large Rocket Engines for Space Missiles. VRT, No. 2, 1962.
50. Grizodub, Yu. N. Study of the Variable Liquid Motion in Branched Hydraulic Systems of Machines and Automatic Control Devices. Avtomatika i telemekhanika, No. 1, 1952.
51. Gur'yev, V. P. and V. I. Shogorelov. Gidravlicheskiye ob'yemnyye peredachi (Hydraulic Drives). Mashgiz, 1964.
52. Dvukhsherstov, G. I. Hydraulic Impact in Noncircular Pipes and in Fluid Flow Between Elastic Walls. Uch. zap. MGU, Vol. II, Tekhanika, No. 122, 1948.
53. Davis, H. Design and Development of the XL-99 Rocket Engine. VRT, No. 10, 1963.
54. Dmitriyevskiy, A. and V. N. Koshevoy. Osnovy teorii poleta raket (Fundamentals of Rocket Flight Theory). Voyenizdat, 1964.
55. Duboshin, G. N. Osnovy teorii ustoychivosti dvizheniya (Fundamentals of Motion Stability Theory). MGU, 1952.
56. Esman, I. G. Nasosy (Pumps). Gostoptekhizdat (Gosudarstvennoye izdatel'stvo tekhno-teoreticheskoy literatury : State Publishing House of Technical and Theoretical Literature), 1954.
57. Zhiritskiy, G. S., V. I. Lokay, M. K. Maksutova and V. A. Strunkin. Gazovyye turbiny aviatsionnykh dvigateley (Aircraft Engine Gas Turbines). Oborongiz, 1963.
58. Zhmud, A. Ye. Gidravlicheskiy udar v gidroturbinnykh ustanovkakh (Hydraulic Impact in Hydraulic Turbine Installations). Gosenergoizdat, 1953.
59. Zhukovskiy, N. Ye. O gidravlicheskom udare v vodoprovodnykh trubakh (On Hydraulic Impact in Water Lines). GTTI, 1949.
60. Zucrow, M. J. Aircraft and Missile Propulsion. Fizmatgiz, Vol. 2, 1960.
61. Ivashchenko, N. N. Avtomaticheskoye regulirovaniya (Automatic Control). Mashgiz, 1962.
62. Inzel, L. I. Osnovy glusheniya shuma vykhlopa dvigateley vnutrennego sgoraniya (Fundamentals of Internal Combustion Engine Exhaust Noise Suppression). Mashgiz, 1949.
63. Kamenkov, G. V. On Motion Stability Over a Finite Time Interval. PMM (Prikladnaya matematika i mekhanika), Vol. 17, No. 5, 1953.
64. Kantorovich, Z. B. Osnovy rascheta khmmicheskikh mashin i apparatov (Fundamentals of the Design of Chemical Machines and Apparatus). Mashgiz, 1952.
65. Kampe-Nemm, A. A. Dinamika dvukhpozitsionnogo regulirovaniya (Dynamics of Two-position Control). Gosenergoizdat, 1955.
66. Kaplan, K. D. Selection of Expulsion Feed System for High-boiling LRE Propellants). Raketnaya tekhnika, No. 6, 1961.
67. Kar
68. Kar
69. Kar
70. Kva
71. Kry
72. Col
73. Kop
74. Korr
75. Kos
76. Krag
77. Kra
78. Cro
79. Cro
80. Cro
81. Kul
82. Kut
83. Cam
84. Loc
85. Mad
86. Mak

67. Karapet'yants, M. Kh. Khimicheskaya termodinamika (Chemical Thermodynamics). Goskhimizdat, 1953.
68. Kartvelishvili, N. A. Neustanovivshiyesya rezhimy v silovykh uzlakh gidroelektricheskikh stantsiy (Unsteady Regimes in Hydroelectric Station Power Components). Gosenergoizdat, 1951.
69. Kartvelishvili, N. A. Present Status of Hydraulic Theory of Unsteady Flows from Studies in the USSR, Izv. AN SSSR, OTN, Mekhanika i mashinostroyeniye, No. 3, 1961.
70. Kvasnikov, A. V. Teoriya zhidkostnykh raketnykh dvigateley (LRE Theory). Sudpromgiz (Gosudarstvennoye Soyuznoye izdatel'stvo sudostroite'noy promyshlennosti : State All-union Publishing House for the Shipbuilding Industry), 1959.
71. Krylov, Yu. V. Transactions of Moscow Higher Technical Institute. im. Baumana, No. 56, Oborongiz, 1955.
72. Collier, G. Survey of Studies on Two-phase Fluid Heat Transfer. IL, 1962.
73. Kopyrin, M. A. Hydraulics and Hydraulic Machines, Vysshaya shkola, 1961.
74. Kornfel'd, M. Uprugosti i prochnost' zhidkostey (Elasticity and Strength of Liquids). GTTI, 1956.
75. Koshlyakov, N. S., E. B. Gliner and M. M. Smirnov. Differentsial'nyye uravneniya matematicheskoy fiziki (Differential Equations of Mathematical Physics). Fizmatgiz, 1962.
76. Kragel'skiy, N. V. and I. E. Vinogradova. Koeffitsiyenty treniya (Friction Coefficients). Mashgiz, 1962.
77. Krassov, I. M. Gidravlicheskiye elementy sistem avtomatich-eskogo regulirovaniya (Hydraulic Components of Automatic Control Systems). Mashgiz, 1963.
78. Crocco, L., J. Grey, and D. Harrje. Theory of Combustion Instability in LRE. IL, 1958.
79. Crocco, L., D. Harrje and F. Riordan. Theory of Combustion Instability in LRE, and its Experimental Verification., VRT, No. 9, 1960.
80. Crocco, L., D. Harrje and F. Riordan. Transverse High-Frequency Oscillations in Liquid Rocket Engines. Raketnaya Tekhnika, No. 3, 1962.
81. Kulik, F. Stability of High-frequency Pressure Oscillations in Rocket Engine Combustion Chamber. Raketnaya tekhnika i kosmonavtika, No. 5, 1963
82. Kutateladze, S. S. and V. M. Borishanskii. Spravochnik po teplorperedache (Handbook on Heat Transfer). Gosenergoizdat, 1959.
83. Campbell, D. P. Dinamika protsessov khimicheskoy tekhnologii (Chemical Technology Process Dynamics). Goskhimizdat, 1962.
84. Locke, A. S. Upravleniye snaryadami (Missile Guidance). Fizmatgiz, 1958.
85. Madelung, E. Matematicheskiy apparat fiziki (The Mathematical Apparatus of Physics). Fizmatgiz, 1960.
86. Makkormak, P. D. The Driving Mechanism of High-frequency Instability Combustion in the LRE Chamber. VRT, No. 4, 1965.

87. Maksimov, D. G. Kurs elektrotekhniki (Course in Electrical Engineering). Voyenizdat, 1958.
88. Mamontov, M. A. Nekotoryye sluchai techeniya gaza (Certain Cases of Gas Flow). Oborongiz, 1951.
89. Mamontov, M. A. Voprosy termodinamiki tela peremennoy massy (Problem of Thermodynamics of a Body of Variable Mass). Oborongiz, 1961.
90. Markevich, N. M. Uch. zap. LGU, No. 27, Matematicheskiye nauki, No. 31, 1957.
91. Makhin, V. A., V. F. Prisnyakov, and I. F. Tokar. Theory of Boiling Fluid Discharge Through a Centrifugal Injector. Izv. VUZ, Aviatsionnaya tekhnika. Nos. 3. 4. 1962.
92. Mashinostroyeniye. Entsiklopedicheskiy spravochnik (Machine Design. Encyclopedic Handbook). Vol. 2, Mashgiz, 1948.
93. Mebus, G. G. Rocket Engine Design. IL, 1959.
94. Melik-Pashayev, N. I. Zhidkostnoy raketnyy dvigatel' (Liquid Rocket Engine). Voyenizdat, 1959.
95. Mikhaylov, I. G. Rasprostraneniye ul'trazvukovykh voln v zhidkostyakh (Propagation of Ultrasonic Waves in Liquids). GTTI, 1949.
96. Moles, G. Use of Rocket Engines for Aircraft. VRT, No. 1, 1952.
97. Morse, P. M. Kolebaniya i zvuk (Vibration and Sound). Gostekhizdat, 1949.
98. Morozov, I. I. Calculation of Gas Pressure in Automatic Control Pneumatic Elements. Avtomatika, No. 1, 1959.
99. Morozov, I. I. Approximate Calculation of Gas Vessel Emptying Process. IFZh, No. 12, 1959.
100. Mostkov, M. A. Gidravlicheskiy spravochnik (Hydraulic Handbook). State Press for Literature on Construction and Architecture, 1954.
101. Mostkov, M. A. Prikladnaya gidromekhanika (Applied Hydromechanics). Gosenergoizdat, 1963.
102. Moshkin, Ye. K. Dinamicheskiye protsessy v ZhRD (Dynamic Processes in LRE). Izd-vo Mashinostroyeniye, 1964.
103. Novikov, I. I. and K. D. Voskresenskiy. Prikladnaya termodinamika i teploperedacha (Applied Thermodynamics and Heat Transfer). Gosatomizdat, 1961.
104. Ovsyannikov, B. V. Teoriya i raschet nasosov ZhRD (Theory and Design of LRE Pumps). Oborongiz, 1960.
105. Aldrich, D. E. and D. D. Sanchini. Development of the F-1 Engine VRT, No. 11, 1961.
106. Osnovy avtomaticheskogo regulirovaniya (Fundamentals of Automatic Control,) edited by V. V. Solodovnikov. Mashgiz, 1954.
107. Peterson, J. B. Transient Processes During Startup of Rocket Engines Operating on Hypergolic Two-component Propellant, (In: Issledovaniya raketnykh dvigateley na zhikdom toplive (Study of LRE). Izd-vo Mir, 1964.
108. Pierce, K. V. Some Methods for Regulating Solid Rocket Engines. VRT, No. 6, 1962.
109. Povarnin, P.I. Application of the Thermodynamic Similarity Method to the Calculation of Liquid Surface Tension. In: Teploperedacha (Heat Transfer). AN SSSR, 1962.
110. Pova
He
Te
111. Pris
l,
112. Pris
Nc
113. Pris
So
te
114. Prisn
of
196
115. Prisn
Boi
sio
116. Prisn
IFZ
117. Desig
196
118. Rocke
nau
Sov
All-
of
for
No.
119. Lancas
120. Summer
121. Sutton
122. Semidu
Comp
123. Sidoro
Izv.
124. Sinyar
nyye
125. Skuchi
126. Soldat
diaf
meny
Taki
Chan
MEI,
127. Stepan
and
128. Stepan
Equat
izdat
ing
129. Stechki
Yu. N
dviga
130. Surin,
s nim
it).

110. Povarnin, P.I. Application of Thermodynamic Similarity to Heat Transfer Calculations of Liquid Surface Tension. In: Teploperedacha (Heat Transfer). AN SSSR, 1962.
111. Prisnyakov, V. F. IFZh, Vol. 14, No. 6, 1968, Vol. 16, No. 1, 1969.
112. Prisnyakov, V. F. Izv. VUZ, Energetika, No. 5, 1967; No. 2, 1969.
113. Prisnyakov, V. F. On the Determination of the Speed of Sound in Complex Hydraulic Lines. Izv. VUZ, Aviatsionnaya tekhnika, No. 1, 1965.
114. Prisnyakov, V. F. On the Exponent of the Thermodynamic Process of Gas Expansion with Heat Addition. IFZh, Vol. 10, No. 4, 1966.
115. Prisnyakov, V. F. Determining the Discharge Coefficient of a Boiling Liquid for Centrifugal Injectors. Izv. VUZ, Aviatsionnaya tekhnika, No. 4, 1966.
116. Prisnyakov, V. F. Analysis of the Process of Gas Vessel Filling. IFZh, Vol. 13, No. 3, 1967.
117. Design Studies of the Saturn Space Booster (Survey). VRT, No. 4, 1961.
118. Rocket Design, Abstract Journal. VINITI (Vsesoyuznny institut nauchnoy i tekhnicheskoy informatsii gosudarstvennogo komiteta Soveta Ministrov SSSR po nauke i tekhnike i adademii nauk SSSR; All-Union Institute of Scientific and Technical Information of the State Committee of the Council of Ministers of the USSR for Science and Technology and of the Academy of Sciences USSR), No. 9, 1963.
119. Lancaster, O. E. editor. Jet Propulsion Engines. Voyenizdat, 1962.
120. Summerfield, M. VRT. No. 3, 1952.
121. Sutton, G. P. Rocket Propulsion Elements. IL, 1958.
122. Semiduberskiy, M. S. Nasosy, kompressory, ventilyatory (Pumps, Compressors, Fans). Promstroyizdat, 1957.
123. Sidorov, E. A. Convective Heat Transfer in the Unsteady Regime. Izv. AN SSSR, OTN, No. 9, 1958.
124. Sinyarev, G. B., and M. V. Dobrovol'skiy. Zhidkostnyye raketnyye dvigateli (Liquid Rocket Engines). Oborongiz, 1957.
125. Skuchik, Ye. Fundamentals of Acoustics. IL, 1958.
126. Soldatov, N. N. Issledovaniya protsessov, proiskhodyashchikh v diafragmakh pri protekanii cherez nikh vody, chastichno menyayushchey agregatnoye sostoyaniye (Study of the Processes Taking Place in Diaphragms During Passage of Water Partially Changing Its State of Aggregation, Candidate Dissertation). MEI, 1952.
127. Stepanov, A. I. Tsentrobezhnnye i osevyye nasosy (Centrifugal and Axial Pumps). Mashgiz, 1960.
128. Stepanov, V. V. Kurs differentsial'nykh uravneniy (Differential Equations, 4th Edition). Gostekhizdat (Gosudarstvennoye izdatel'stvo tekhno-teoreticheskoy literatury; State Publishing House of Technical and Theoretical Literature), 1945.
129. Stechkin, B. S., P. K. Kazandzhan, L. P. Alekseyev, A. N. Govorov, Yu. N. Nechayev and R. M. Fedorov. Teoriya reaktivnykh dvigateley (Jet Engine Theory). Oborongiz, 1956.
130. Surin, A. A. Gidravlicheskiy udar v vodoprovodakh i bor'ba s ni- (Hydraulic Impact in Water Lines and Means for Combating it). Tranzheldorizdat (Vsesoyuznoye izdatel'skopoligraficheskoye

ob'yedineniye Ministerstva putey soobshcheniya SSSR; All-Union Publishing and Printing Association of the Ministry of Railroads USSR), 1946.
131. Tarasov, N. V., A. A. Armand, and A. S. Kon'kov. Study of Heat Transfer in a Tube During Boiling of Underheated Water and Water-Vapor Mixture, In: Teploobmen pri vysokikh teplovykh nagruzkakh, (Heat Transfer Under High Thermal Loads). Gosenergoizdat, 1959.
132. Tolubinskiy, V. I. On Boiling Heat Transfer Theory. Izv. VUZ, Energetika, No. 1, 1959.
133. Tsien, H. S. Servo-Stabilization of Combusion in Rocket Motors. VRT, No. 3, 1953.
134. Uginchus, A. A. Gidravlika i gidravlicheskiye mashiny (Hydraulics and Hydraulic Machines). KhGU (Khar'kov State University, 1960.
135. Feodos'yev, V. I., and G. B. Sinyarev. Vvedeniye v raketnuyu tekhniku (Introduction to Rocket Engineering). Oborongiz, 1960.
136. Filippov, A. P. Kolebaniya uprugikh sistem (Vibrations of Elastic Systems). AN USSR, 1956.
137. Frenkel', N. Z. Gidravlika (Hydraulics). Gosenergoizdat, 1956.
138. Hurden, D. Design of Rocket Engines Using Hydrogen Fuel. VRT, No. 8, 1962.
139. Humphries, J. Rocket Engines and Guided Missiles. IL, 1958.
140. Isai, D. H., and E. C. Cassidy. Trans. ASME, Ser. D, Journal of Basic Engineering, No. 2, 1961.
141. Tseyrov, Ye. M. Voprosy termogazodinamiki vozdushnykh vyklyuchateley (Thermogasdynamics of Air Circuit Breakers). Gosenergoizdat, 1963.
142. Tszi, Kh., and S. S'yu. Errors in Rocket Motion Parameters at End of Powered Segment. VRT, No. 7, 1965.
143. Tsypkin, Ya. Z. Stability of Systems with Lagging Feedback. Avtomtaika i telemekhanika, Nos. 2, 3; 1946.
144. Charnyy, I. A. Fundamentals of Gas Dynamics. Gostoptekhizdat, 1961.
145. Charnyy, I. A. Naustanoivivsheyesya dvizheniye real'noy zhidkosti v trubakh (Unsteady Pipe Flow of Real Fluids). GTTI, 1951.
146. Chernobyl'skiy, I. I. Vyparnyye ustanovki (Evaporators). KGU, 1960.
147. Chernobyl'skiy, I. I., and Yu. M. Tananayko. Heat Transfer During Liquid Boiling in an Annular Slot. ZhTF (Zhurnal Tekhnicheskoy Fiziki; Journal of Technical Physics), Vol. 26, No. 10, 1956.
148. Shaulov, Yu. Kh., and M. O. Lerner. Goreniye v zhidkostnykh raketnykh dvigatelyakh (Combustion in LRE). Oborongiz, 1961.
149. Shevelyuk, M. I. Theoretical Bases for Designing LRE. Oborongiz, 1960.
150. Shevyakov, A. A. Avtomatika aviatsionnykh i raketnykh silovykh ustanovok (Automatic Control of Aircraft and Rocket Power Plants). Izd-vo Mashinostroyeniye, 1965.
151. Shchelkin, K. I. Two Unstable Combustion Cases. ZhETF, Vol. 36, No. 2, 1959.
152. Ekspress-informatsiya "Aviadvigatelestroyeniye" (Express Information, Aircraft Engine Construction.) VINITI, No.42, 1958.
153. Ekspr
for
154. Ekspr
for
155. Exksp
Inf
No.
156. Ekspr
Roc
157. Ekspr
Roc
158. Ekspr
Roc
159. Ekspr
Roc
160. Ekspr
Roc
161. Ekspr
Roc
162. Ekspr
Roc
163. Ekspr
Roc
164. Ekspr
VIN
165. Ekspr
eni
VIN
166. Yavor
(Ha
167. Aerop
168. Allie
Ram
169. Ameri
170. Aviat
171. Aviat
172. Barre
195
173. Barre
195
174. Berma
175. Berma
176. Cople
Des
177. Dunni
Vol
178. Fligh
179. Flugw
180. Hurde
181. Jet P
182. Kelly
Dis

153. Ekspress-informatsiya "Aviadvigatelestroyeniye" (Express Information, Aircraft Engine Construction). VINITI, No.18,1959.
154. Ekspress-informatsiya "Aviadvigatelestroyeniye" (Express Information, Aircraft Engine Construction). VINITI, No. 19, 1959.
155. Exkspress-informatsiya "Avstronavtika i raketodinamika (Express Information, Astronautics and Rocket Dynamics). VINITI, No. 11, 1961.
156. Ekspress-informatsiya "Raketnaya Tekhnika" (Express Information, Rocket Technology). VINITI, No. 4, 1957.
157. Ekspress-informatsiya "Raketnaya Tekhnika" (Express Information, Rocket Technology). VINITE, No. 18, 1957.
158. Ekspress-informatsiya "Raketnaya Tekhnika" (Express Information, Rocket Technology). VINITI, No. 5, 1958.
159. Ekspress-informatsiya "Raketnaya Tekhnika" (Express Information, Rocket Technology). VINITI, No. 46, 1956.
160. Ekspress-informatsiya "Raketnaya Tekhnika" (Express Information, Rocket Technology). VINITI, No. 27, 1957.
161. Ekspress-informatsiya "Raketnaya Tekhnika" (Express Information, Rocket Technology). VINITI, No. 33, 1958.
162. Ekspress-informatsiya "Raketnaya Tekhnika" (Express Information, Rocket Technology). VINITI, No. 23, 1959.
163. Ekspress-informatsiya "Raketnaya Tekhnika" (Express Information, Rocket Technology). VINITI, No. 43, 1959.
164. Ekspress-informatsiya "Raketnodinamika i astronavtika". VINITI, No. 42, 1958.
165. Ekspress-informatsiya "Samoletostroyeniye i aviadvigatelestroyeniye" (Airplane Construction and Airplane Engine Construction). VINITI, No. 1, 1957.
166. Yavorskiy, B. M., and A. A. Deglaf. Spravochnik po fiziki (Handbook on Physics). Fizmatgiz, 1963.
167. Aeroplane. No. 25 IL, 1959.
168. Allievi, L. Theorie du coup de belier (Theory of the Battering Ram). Paris, 1921.
169. American Rocket Society, Prepr., No. 335, 1956.
170. Aviation Age. Vol. 79, No. 13, 1963.
171. Aviation Age. Vol. 25, No. 5, 1956.
172. Barrere, A. La Propulsion par fusees (Jet Propulsion). Paris, 1957.
173. Barrere, M., and A. Montef. Jet Propulsion. Vol. 26, No. 1, 1956.
174. Berman, F., and S. Logan. ARS. Vol. 22, No. 2, 1952.
175. Berman, K., and S. Cheney. ARS. Vol. 23, Nos. 3, 4; 1953.
176. Coplen, H. L. Realiability Concepts in Rocket Controls Design. Jet Propulsion, Vol. 25, No. 6, 1954.
177. Dunning, J. E. Journal of the Royal Aeronautical Society, Vol. 64, No. 600, 1960.
178. Flight and Aircraft Engineer, Vol. 70, No. 2479, 1956.
179. Flugwelt. No. 10, 1961.
180. Hurden, D. J. Brit. Interplant, Vol. 18, Nos. 5,6; 1961.
181. Jet Propulsion, Vol. 28, No. 12, 1958.
182. Kelly, A. J. Effect of Thrust Termination Process Upon Range Dispersion of a Ballistic Missil. ARS Journal, No. 6, 1959.

183. Lancaster, Otis E., and Carlton J. Bates. Gasturbine Progress Report Rocket Turbines, Paper. Amer. Soc. Mech. Engrs., A-46H, 1958.
184. Lee, J. C., M. P. Gore and C. Ross. IARS. Vol. 23, Nos. 4,5; 1953.
185. Lutz, O. Resonance Oscillations at the Exhaust in Exhaust Tubes of Series Motors. Vol. 16, Nos. 13, 14, 1939; Vol. 17, No. 4, 1940.
186. Miesse, C. C. Fifth Symposium on Combustion. London, 1955.
187. Missiles and Rockets. Vol. 3, No. 6, 1958.
188. Mulready, P. C. Astronautics, Vol. 6, Nos. 3, 26, 27, 85, 86; 1961.
189. Osborn, J. R. Unstable Burning in Solid and Liquid Propellant Rocket Motors. Reketen-technick und Raumfahrtforschung, Vol. VII, No. 2, 1963.
190. Ross, C. and P. Datner. Selected Combustion Problems, 1953.
191. Sabersky, R. Jet Prppulsion, Vol. 24, Nos. 5, 6; 1954.
192. The Aeroplane, Vol. 51, Nos. 2344, 2347, 2349; 1956.
193. The Engineer, Vol. 202, No. 5244, 1956.
194. Tischler, A. O., and T. Male. Oscillatory Combustion in Rocket Propulsion Engines. Gas Dynamics Symposium, Northwestern University, 1956.
195. Tischer, A. and D. Bellman. NACA TN, No. 2936, 1956.

RUSSIAN

К
С
КР
П
Г
ОБ
М
В
Н
ТР
В
УТ
К
Э
М
ВХ
ВЫ
К
ПР
Ф
О
Г
Г
Н
К
ОХЛ
Ж
ПОТ
В
Д
СП
КОН
УД
Ь
Р.О
М
Т
У
К
С
П
Ш
Э
ЭМ
Я
СФ
М
З
БАР
Н/М
Н.СЕ
М

SYMBOL LIST

RUSSIAN CHARACTER	ENGLISH MEANING	TYPED AS
К	chamber	K
С	nozzle	c
КР	critical	cr
П	blade	b
Г	hydraulic	h
ОБ	volumetric	v
М	mechanical	M
В	shaft	s
Н	pump	H
ТР	friction	fr
В	windage	w
УТ	leakage	le
К	end	K
Э	equivalent	e σ
М	local	M
ВХ	inlet	in
ВЫХ	outlet	out
К	rotor	K
ПР	inflow	inf
◆	injector	inj
О	oxidizer	o
Г	fuel	f
Г	corrugation	corr
Н	initial	in
К	final	K
ОХЛ	cooling	cool
Ж	liquid	liq
ПОТ	loss	loss
В	vortex formation	vf
Д	diffuser	d
СП	spiral	sp
КОН	conical	con
УД	shock	sh
Ь	tank	t
Р.О.	regulator	reg
М	line	M
Т	turbine	T
У	controlling	Y
К	valve	K
С	seat	c
П	piston	p
Ш	rod	r
Э	electro	e
ЭМ	electromagnetic	em
Я	armature	a
С◆	bellows	b
М	membrane	M
З	spool	s
БАР	bar	bar
Н/М	N/m	
Н.СЕК / М	H.sec / m	

RUSSIAN CHARACTER	ENGLISH MEANING	TYPED AS
Т	propellant	T
Н	tank (pressure)	H
ДВ	power plant	
С	combustion (products)	
БАЛ	bottle	
Л.А.	flight vehicle	f.v.
В	water	w
Ш	orifice	or
ОТБ	bleed	bl
Ж	injector	inj
Э	element	el
СР	average	av
ПР	reduced	red
УПР	control	cont
СТ	stand	st
АК	acoustic	ac
Ц	cylindrical	cyl
Г.К	main command	m.c.
КЛ	valve	v
А	assembly	a
Д	vent	ve
ЭПК	electropneumatic valve	epv
Р	reducer	red
Б	bottle	b
Р	discharge	dis
ЗД	delay	del
ОХЛ	coolant	cool
ВК	boiling	boil
БК	side	s
ПОД	temperature rise	t.r.
Ц	centrifugal	cen
СТ	wall	w
ГОЛ	head	head
Ш	spiral	sp
КОЛ	collector	coll
С.Д	vent exit	ve
З	fueling	fu
КОН	boiling	boil
ЗАМ	freezing	fr
ОК	oxidizer	o
КДЖ	kilojoule	kJ
КГ	kilogram	kg
СЕК	second	sec
ТР	passage	pa

UNCLASSIFIED

Security Classification

DOCUMENT CONTROL DATA - R & D

(Security classification of title, body of abstract and indexing annotation must be entered when the overall report is classified)

1. ORIGINATING ACTIVITY (Corporate author)

Foreign Technology Division
Air Force Systems Command
U. S. Air Force

2a. REPORT SECURITY CLASSIFICATION

UNCLASSIFIED

2b. GROUP

3. REPORT TITLE

DYNAMICS OF LIQUID ROCKET ENGINES

4. DESCRIPTIVE NOTES (Type of report and inclusive dates)

TRANSLATION

5. AUTHOR(S) (First name, middle initial, last name)

Makhin, V. A.; Prisnyakov, V. F.; Belik, N. P.

6. REPORT DATE	7a. TOTAL NO. OF PAGES	7b. NO. OF REFS
1969	465	195

8a. CONTRACT OR GRANT NO.	9a. ORIGINATOR'S REPORT NUMBER(S)
b. PROJECT NO. 6040104	FTD-HC-23-18-70
c.	9b. OTHER REPORT NO(S) (Any other numbers that may be assigned this report)
d. DIA TASK T65-04-18A	

10. DISTRIBUTION STATEMENT

Distribution of this document is unlimited. It may be released to the Clearinghouse, Department of Commerce, for sale to the general public.

11. SUPPLEMENTARY NOTES	12. SPONSORING MILITARY ACTIVITY
	Foreign Technology Division Wright-Patterson AFB, Ohio

13. ABSTRACT

This book discusses questions of the theory and calculation of certain dynamic processes which take place with variable parameters in liquid rocket engines and their major components. Primary attention is devoted to the description of the dynamic processes and the study of methods for the engineering calculation of these processes. The differential equations of motion of the working medium and of the moving parts of the individual components are used to describe the dynamic processes of liquid rocket engines (LRE). Theoretical LRE arrangements and their static characteristics are examined. Assuming the LRE to be potentially a dynamic system, the authors derive the equations of the dynamics of the powerplant primary components. The dynamics of the LRE automation elements are analyzed and the questions of automatic regulation, trimming, and retrimming of engines using the results of firing tests are studied. The oscillatory processes in the tubing lines are examined in detail; the influence of oscillations in the pneumatic and hydraulic lines on the stability of the LRE working process is determined. An analysis is given of the LRE startup processes and the effect of the thrust tailoff impulse (TTI) on the scatter of ballistic rockets. Original material used in the analysis of several engine elements and their control systems is presented. The book will be of interest for a wide range of specialists in rocket and aircraft engineering.

DD FORM 1 NOV 1473

UNCLASSIFIED

Security Classification

UNCLASSIFIED

Security Classification

DOCUMENT CONTROL DATA - R & D

(Security classification of title, body of abstract and indexing annotation must be entered when the overall report is classified)

1. ORIGINATING ACTIVITY (Corporate author)
Foreign Technology Division
Air Force Systems Command
U. S. Air Force

2a. REPORT SECURITY CLASSIFICATION
UNCLASSIFIED

2b. GROUP

3. REPORT TITLE
DYNAMICS OF LIQUID ROCKET ENGINES

4. DESCRIPTIVE NOTES (Type of report and inclusive dates)
TRANSLATION

5. AUTHOR(S) (First name, middle initial, last name)
Makhin, V. A.; Prisnyakov, V. F.; Belik, N. P.

6. REPORT DATE
1969

7a. TOTAL NO. OF PAGES
465

7b. NO. OF REFS
195

8a. CONTRACT OR GRANT NO.

b. PROJECT NO. 6040104

c.

d. DIA TASK T65-04-18A

9a. ORIGINATOR'S REPORT NUMBER(S)
FTD-HC-23-18-70

9b. OTHER REPORT NO(S) (Any other numbers that may be assigned this report)

10. DISTRIBUTION STATEMENT
Distribution of this document is unlimited. It may be released to the Clearinghouse, Department of Commerce, for sale to the general public.

11. SUPPLEMENTARY NOTES

12. SPONSORING MILITARY ACTIVITY
Foreign Technology Division
Wright-Patterson AFB, Ohio

13. ABSTRACT

This book discusses questions of the theory and calculation of certain dynamic processes which take place with variable parameters in liquid rocket engines and their major components. Primary attention is devoted to the description of the dynamic processes and the study of methods for the engineering calculation of these processes. The differential equations of motion of the working medium and of the moving parts of the individual components are used to describe the dynamic processes of liquid rocket engines (LRE). Theoretical LRE arrangements and their static characteristics are examined. Assuming the LRE to be potentially a dynamic system, the authors derive the equations of the dynamics of the powerplant primary components. The dynamics of the LRE automation elements are analyzed and the questions of automatic regulation, trimming, and retrimming of engines using the results of firing tests are studied. The oscillatory processes in the tubing lines are examined in detail; the influence of oscillations in the pneumatic and hydraulic lines on the stability of the LRE working process is determined. An analysis is given of the LRE startup processes and the effect of the thrust tailoff impulse (TTI) on the scatter of ballistic rockets. Original material used in the analysis of several engine elements and their control systems is presented. The book will be of interest for a wide range of specialists in rocket and aircraft engineering.

DD FORM 1 NOV 68 1473

UNCLASSIFIED

Security Classification

UNCLASS

Security

14.

Liquid ro
Dynamic s

UNCLASSIFIED

Security Classification

14. KEY WORDS	LINK A		LINK B		LINK C	
	ROLE	WT	ROLE	WT	ROLE	WT
Liquid rocket engines Dynamic system						

UNCLASSIFIED

Security Classification